Planetary and Space Science

Editor-in-Chief: MILTON GREENBERG

Regional Editors:

D. F. MARTYN — A. I. LEBEDINSKY
S. K. MITRA — W. W. KELLOGG
M. NICOLET — F. L. WHIPPLE

Volume 3, 1961

PROCEEDINGS OF THE CONFERENCE ON

PHYSICAL CHEMISTRY IN
AERODYNAMICS AND SPACE FLIGHT

PERGAMON PRESS, INC.

NEW YORK · OXFORD · LONDON · PARIS

Planetary and Space Science

NOTES FOR CONTRIBUTORS

1. Only papers not previously published will be accepted, and emphasis is placed upon originality of concept or observation. The text should be clear and concise, and a technical description of the methods used should be given in detail only when the methods are new.

2. The Editor-in-Chief requests that short *Research Notes* for which rapid publication is desired should be sent directly to him at Geophysics Corporation of America, 700 Commonwealth Avenue, Boston 15, Massachusetts, U.S.A. *Research Notes should be in English, without illustrations, and no longer than four double-spaced typewritten pages.*

3. Other contributions (Research Papers and Critical Surveys) should be sent initially to one of the other editors near the author: in the *Southern Hemisphere*, to Dr. D. F. Martyn, Radio Research Laboratories, CSIRO, Camden, New South Wales, Australia; in the *Far East*, to Prof. S. K. Mitra, F.R.S., Institute of Radiophysics and Electronics, University of Calcutta, India; in *Europe*, to Dr. M. Nicolet, c/o Service du Rayonnement, 3 Avenue Circulaire, Uccle, Belgium; in *Eastern North America*, to Dr. Fred L. Whipple, Astrophysical Observatory, 60 Garden Street, Cambridge 38, Massachusetts; in *Western North America*, to Dr. W. W. Kellogg, Head, Planetary Sciences, The Rand Corporation, 1700 Main Street, Santa Monica, California, U.S.A.; and in the *Soviet Union*, to Prof. A. I. Lebedinsky, Physical Department, Moscow State University, Moscow, U.S.S.R.

4. Submission of two typescripts (an original and a carbon copy) will facilitate refereeing; if one only is submitted, it should be the original. The author should retain a copy for his own use. The text should be ready for setting in type and should be carefully checked for errors. Scripts should be typed on one side of the paper with double or triple spacing.

5. Illustrations may accompany Research Papers and Critical Surveys but should be restricted to the minimum necessary, and must accompany the typescript mounted on separate sheets. Photographs should be enlarged sufficiently to permit clear reproduction (about 8 by 10 inches). If words or numbers appear in photographs, two copies should be sent, one with clear printing and the other without inscription. Line drawings which require redrawing should include all relevant details. Any lettering should be large and bold enough to be legible after the diagram has been reduced in size for printing. Captions or legends should be given on a separate sheet, and labelled to show which illustrations each is to accompany.

6. Proofs will be sent to authors for correction, and fifty free reprints of each paper will be provided. Additional reprints should be ordered when the proofs are returned by the author. Otherwise, it may not be possible to furnish them at a reasonable price. A reprint order form will accompany the proofs.

7. References are indicated in the text by superior numbers in parentheses, and the full reference should be given in a list at the end of the paper in the following form:

1. Y. TANAKA. *J. Chem. Phys.* **22**, 2045 (1954).
2. P. MOORE. *The Planet Venus*, p. 84. Faber and Faber, London (1957).

and should include the usual abbreviated title of the journal, the volume number, the page number and year, in that order.

Footnotes, as distinct from literature references, should be indicated by the following symbols—*, †, ‡, ‡‡, commencing anew on each page; they should *not* be included in the numbered reference system.

8. The language preferred is English, but papers may be published in other languages from time to time. An abstract of not more than 200 words, giving the essential contents of the paper should be provided by the author, if possible in English; but the abstract may be submitted in the language of the paper, for translation into English by the editorial staff.

9. To conserve space, authors are requested to mark the less important parts of the paper (such as records of experimental results) for printing in smaller type. For long papers (over 12 double-spaced typewritten pages) sections which could be deleted without destroying either the sense or the continuity of the paper should be indicated as a guide for the editors.

CONTENTS

PAGE

Foreword 1

I. SURFACE AND SOLID PHASE REACTIONS

JOHN L. MARGRAVE, *Session Chairman*: Introduction—Surface and Solid Phase Reactions at High Temperatures 3

J. M. BURGERS: The Boltzmann Equation for Flows with Chemical Reactions 4

R. J. ACKERMANN, R. J. THORN and G. H. WINSLOW: Systematic Trends in Vaporization and Thermodynamic Properties of Oxides 12

R. F. WALKER, J. EFIMENKO and N. L. LOFGREN: Rate of Vaporization of Refractory Substances 24

D. R. SCHRYER and J. L. MODISETTE: An Investigation of the Effects of Gaseous Diffusion on the Rate of Oxidation of a Metal Forming a Volatile Oxide 31

G. M. PROK: Nitrogen Atom Recombination on Surfaces 38

W. ZINMAN: A Study of the Interaction Between Carbon and Dissociated Gases 46

J. C. CUTTING, J. A. FAY, W. T. HOGAN and W. C. MOFFATT: A Non-Catalytic Surface for Dissociated Combustion Gases 53

L. S. NELSON and N. A. KUEBLER: Heterogenous Flash Pyrolysis of Hyrocarbon Polymers 61

S. RUBY, J. B. COHEN and F. K. WARD: Behavior of Plastic Laminates at Elevated Temperatures 68

P. H. SETTLAGE and J. C. SIEGLE: Behavior of "Teflon" Fluorocarbon Resins at Elevated Temperatures 73

R. SIMHA: Summary of Discussion on the Pyrolysis of Plastics in Ablation 82

P. J. FRIEL: The Ablation of Thermosetting Plastics 83

II. GAS PHASE REACTIONS AND KINETICS

S. S. PENNER, *Session Chairman*: Introduction—Gas Phase Reactions and Kinetics 85

R. MONSON, J. J. ALLPORT and F. ROBBEN: Comparative Studies of Vibrational Relaxation in Nitric Oxide 86

H. M. WIGHT: The Influence of Periodic Pressure Variations on Chain Reactions 94

M. H. BORTNER: Shock Layer Electron Densities Considering the Effects of Both Chemical Reactions and Flow Field Variation 99

M. A. BIONDI: Measurements of Electron Attachment, Recombination, Elastic and Inelastic Collisions in Atmospheric Gases 104

B. STEVERDING and L. WERNER: Thermodynamic Relaxation of Atmospheric Gases in Shock Waves 113

S. BAUER, N. ROL and J. KIEFER: A Survey of Methods for the Chemical Analysis of Transient Species, with Microsecond Resolution 118

B. KIVEL, P. HAMMERLING and J. D. TEARE: Radiation from the Non-Equilibrium Region of Normal Shocks in Oxygen, Nitrogen and Air 132

III. EXPERIMENTAL METHODS AND SIMULATION

MURRAY ZELIKOFF, *Session Chairman*: Introduction—Experimental Methods and Simulation 138

F. F. MARMO, J. PRESSMAN and L. M. ASCHENBRAND: Electron Clouds: A General Survey 139

W. WURSTER: Spectroscopic Measurement of the Temperature of Shock-heated Oxygen 158

G. S. HOLISTER, R. T. BRACKMANN and W. L. FITE: The Use of Modulated Atomic-Beam Techniques for the Study of Space Flight Problems 162

R. A. YOUNG and K. C. CLARK: Excitation of the Auroral Green Line in Nitrogen Afterglows 169

J. GOLDEN and A. L. MYERSON: Rate of Recombination of Atomic Oxygen Through Flash Spectroscopy in the Vacuum Ultraviolet 175

M. FINEMAN and A. PETROCELLI: Molecular Studies with a Lozier Electron Impact Apparatus 187

A. F. HILDEBRANDT, C. A. BARTH and F. B. BOOTH: Atom Concentration Measurements Using Electron Paramagnetic Resonance 194

IV. THERMODYNAMIC AND TRANSPORT PROPERTIES OF GASES

CHARLES CURTISS, *Session Chairman*: Introduction—Thermodynamic and Transport Properties of Gases 204

R. A. BUCKINGHAM: The Present Status of Intermolecular Potentials for Calculations of Transport Properties 205

A. DALGARNO: Intermolecular Potentials for Ionic Systems 217

R. E. WALKER, L. MONCHICK, A. A. WESTENBERG and S. FAVIN: High Temperature Gaseous Diffusion Experiments and Intermolecular Potential Energy Functions 221

I. AMDUR: An Experimental Approach to the Determination of Gaseous Transport Properties at Very High Temperatures 228

A. DALGARNO: Transport Properties of Atomic Hydrogen 236

R. S. BROKAW: Energy Transport in High Temperature and Reacting Gases 238

C. E. TREANOR and G. T. SKINNER: Molecular Interactions at High Temperatures 253

H. MYERS, J. H. BUSS and S. W. BENSON: Thermodynamic Effects of Coulombic Interactions in Ionized Gases 257

A. SHERMAN and F. MARTINEK: The Thermodynamic and Electrical Properties of Mercury Vapor at Pressures Below Atmospheric and High Temperatures 271

List of Participants 283

L.
61

FOREWORD

The intensive development of rocket power in the past decade has opened not only a new realm of technology, but also new facets to long established fields of research. By the spring of 1958, the establishment of a new régime of application of physical chemistry was apparent. This régime might well be called the physical chemistry of aerodynamic processes.

Under conditions of hypersonic flight, and especially in the case of vehicles re-entering the atmosphere, the heats generated induce chemical reactions and other interactions rarely met previously in terrestrial processes. Thus, the advent of space flight necessitates a thorough knowledge of physical chemical phenomena at very high temperatures over a wide range of physical conditions.

In answer to this need, increasing numbers of physical chemists have engaged in studies relative to hypersonic aerodynamics and space flight, these studies involving almost every branch of physical chemistry. The pertinent information evolving from these studies was reported in general either in limited distribution reports, or in the open physical chemistry literature in such form that the application to aerodynamics and space flight was not apparent.

To provide a centralizing medium for the exchange of information, and to enhance the interchange of ideas through personal contact, the Space Sciences Laboratory of General Electric's Missile and Space Vehicle Department, and the Air Force Office of Scientific Research organized a conference based on this new application of physical chemistry. The meeting took place on September 1, 2 and 3 1959 at the University of Pennsylvania. Two hundred participants aided in the successful accomplishment of the conference aims. Colonel A. P. Gagge, Commander, AFOSR, underscored the objective of the conference thus in his keynote address: " . . . by encouraging and engaging in such interdisciplinary activity as represented by this conference, we . . . can widen the frontiers of knowledge".

By incorporating in a volume the papers presented at the Conference on Physical Chemistry in Aerodynamics and Space Flight, we hope to accomplish more fully the purposes of the conference itself. We feel that a perusal of the proceedings will provide an insight into the present and future fundamental physical chemical problems of high speed aerodynamics and space flight.

The papers are subdivided into sections corresponding to the original sessions, with an introduction by the respective session chairmen. A short review is presented of the special session held to discuss the status of plastic pyrolysis in ablation.

We wish to extend our thanks to the authors, conference participants, conference committee members, the University of Pennsylvania and in particular to Mr. Milton Rogers, who acted as the Air Force liaison and whose efforts in helping to organize sessions and select the papers were most valuable.

A. L. MYERSON

A. C. HARRISON

Philadelphia, November 1959

SURFACE AND SOLID PHASE REACTIONS AT HIGH TEMPERATURES

J. L. MARGRAVE
Department of Chemistry, University of Wisconsin, Madison, Wisconsin

Accurate knowledge of chemical species, equilibrium constants and reaction rates over a wide range of temperatures is a basic requirement of the space research program if the safe launching and return of space vehicles is to be possible. The present state of high temperature research makes it clear that many unusual chemical species may be significant, if not predominant at temperatures above 1500°C. Non-stoichiometric solids and liquids, sub-oxides and sub-halides offer evidence that familiar oxidation states at room temperature are not the usual oxidation states at high temperatures.

One must also note that high temperature reactions may be primarily "entropy-controlled" rather than "enthalpy-controlled" since in the equation

$$\Delta F = \Delta H - T\Delta S$$

for a reaction at constant T, the second term likely becomes predominant as T gets very large. Thus molecular parameters as well as accurate heats of formation are needed for prediction of the behavior of complex systems at high temperatures.

Two methods of studying high temperature phenomena are common: (i) A large sample of material is heated slowly to the desired high temperature in a non-reactive container and changes are observed over a period of time long compared with 1 sec, or (ii) a very small sample of material is heated very quickly to a high temperature and observed (usually electronically) in a period of time short compared with 1 sec. Neither approach is completely satisfactory, since there are no truly non-reactive containers and since systems undergoing rapid changes may approach, but not attain, true equilibrium. It is hard to heat any sample, large or small, to a uniform temperature and it is hard to measure high temperatures with accuracy. Only by combination of these techniques is it possible to have a comprehensive understanding of chemical equilibria at high temperatures.

The fact that rapid heating or cooling of a system may not lead to the equilibrium state offers a chance to study high temperature kinetics, including the interaction of gaseous species with surfaces, and various techniques, especialy those utilizing shock waves, have been applied. Shock heating augmented by spectroscopic observations recorded electronically allows identification of species of transient existence and their rate of appearance or disappearance. The novel method for flash heating of small particles in a liquid or solid offers opportunity for new chemical studies.

The papers in this section of the Symposium offer information about chemical equilibria and the rates of reactions at high temperatures, and also discuss methods for attaining high temperatures. Of special importance are those efforts to generalize and formalize the observations of previous investigators for the prediction of the chemical behavior of unstudied systems at unattained conditions. Since the number of potential combinations of atoms is very large, only with the aid of such generalizations will it be possible for future researchers to produce a maximum understanding of chemical behavior in a minimum amount of time via carefully chosen experiments.

THE BOLTZMANN EQUATION FOR FLOWS WITH CHEMICAL REACTIONS*

J. M. BURGERS
University of Maryland, College Park, Maryland

Abstract—An extended form is presented of the Boltzmann equation for the effect of collisions upon the distribution function, in which account is taken of chemical reactions that may result from collisions and of spontaneous processes (spontaneous change of quantum state with emission of radiation). In order to prevent the scheme from becoming too complicated, a number of assumptions had to be introduced. A discussion is given of the various terms which must be written on the right hand side of the Boltzmann equation.

The extended form of the Boltzmann equation obtained in this way can be used for the deduction of continuity, momentum and energy equations, in which the production and the disappearance of molecular species finds a place along with diffusion. Lack of space makes it impossible to consider this part of the subject in the present paper. A Technical Note, to be published elsewhere, is in preparation in which these matters will be treated.

1. INTRODUCTION

The purpose of this lecture is an attempt to extend the Boltzmann equation of the kinetic theory of gases in such a way that collisions involving chemical reactions can be treated simultaneously with ordinary collisions. This gives a basis for the deduction of generalized flow equations in which the production and the disappearance of molecular species will find a place along with diffusion.

In order to fit in with the scheme of the Boltzmann equation, the processes occurring in reactive collisions must be schematized. In the original conception of the kinetic theory collisions are considered as instantaneous happenings, without duration of practical interest. Actually, each collision is a physical process evolving in time, and the duration may be of importance when collisions follow each other in rapid succession, so that one is forced to consider a process in which many particles are involved more or less simultaneously. In principle it must be possible to extend the Boltzmann equation in such a way that multiple collisions may be taken into account, but little has been done in this direction and in the following lines we shall restrict ourselves to binary collisions. A method will be indicated, however, which makes it possible to treat the effect of triple collisions in an approximate way.

Before coming to this it is necessary to observe that between the simple types of collisions which are considered in ordinary kinetic gas theory, where the molecules do not change during the process, and on the other hand chemical reactions in which molecules are broken up and atoms are re-arranged, there are those collisions in which the particles keep their chemical constitution, but where the quantum state of the internal motion changes. A change of quantum state may refer to a change of rotational motion, to the excitation of vibrations, or to the appearance of an electronic state different from the one which was found before. Such processes lead to an exchange of energy between the collision partners, which is superimposed upon the exchange of translational momentum and the exchange of energy connected with momentum.

A further point of importance is that in many cases a particle, which finds itself in a quantum state of high energy, can spontaneously pass into a quantum state of lower energy, with the

* The work reported in this paper was supported by the U.S. Air Force Office of Scientific Research of the Air Research and Development Command, under Contract Number AF 49(638)401.

emission of radiation. Our scheme therefore must include also *spontaneous* processes, occurring to a single particle.

By taking a proper account of the possibility of spontaneous reactions, a formalism can be developed which gives a representation of what otherwise is deduced from the notion of a three-body collision. To see this, consider a case where the co-operation of three particles, a, b and c, is needed to lead to a definite result. We assume the possibility that two of these particles, say a and b, can form a combination ab^* in a binary encounter, in such a way that the translational speed of ab^* is determined by the condition of conservation of translational momentum, while the excess energy connected with the relative motion of a and b together with potential energy is stored in a quantum state of ab^* at an appropriate high energy level. We now introduce the hypothesis that the particle ab^* can either spontaneously dissociate back into a and b, which would mean that ultimately nothing more has happened than what would have occurred in an ordinary, non-reactive collision; or that, before this happens, the particle ab^* encounters the particle c. Then, if circumstances are favorable, another reaction may occur, leading to the final product as is foreseen in the chemical description of the reaction between a, b and c. A particular case might be that ab^* simply passes into a stable configuration ab^0 of lower energy, while the excess energy is distributed over ab^0 and c as translational energy, in such a way that momentum again is conserved.

The supposed reaction between ab^* and c can occur only when the encounter takes place within the limited life of ab^*. A characteristic lifetime for a spontaneous process is defined by stating that the probability for the occurrence of a spontaneous reaction within the next interval of time dt is given by dt/τ, where τ is the "relaxation time" for the reaction. In the resulting formula this relaxation time plays an analogous role as the so-called "sensitive volume", within which the particle c should be present at the instant of a collision between a and b, in order that the reaction between a, b and c may take place according to the concepts of the usual theory. The scheme is not sufficient to represent more intimate details depending upon the order in time in which the particles approach each other, but it is helpful to treat a number of cases without introducing an explicit three-body encounter formalism.

It will be seen from this formalism that we use the term "molecules" for all entities which have a certain duration of existence, long enough to suffer collisions with other particles.

Along with "material particles" we must also give attention to the radiation field: radiation can be emitted as a result of a reaction, and radiation can stimulate reactions. Taking account of emission and absorbtion of radiation can be done formally by considering the radiation field to be made up of photons and to treat these on the same basis as material particles. For practical purposes photons can be left out when considering the conservation of mass (so long as we are not concerned about nuclear processes, where the mass of a photon plays a part in the result); but each photon has a definite energy $h\nu$ (or h/ν, if circular frequencies are used), and a momentum $h\nu/c$, in the direction of motion of the photon, which is the direction of the rays of radiation. When this is taken into account, all processes in which radiation is involved can be brought under the same formalism as serves for the description of reactions in which radiation does not enter.

It should be observed that while we are restricting our description to spontaneous processes, involving a single particle, and collisions involving only two partners at a time, the number of particles (including photons) which may result from any process is not limited and may have any value. In this respect our description is not based upon a reversible picture. The construction of a completely reversible picture brings too many complications; moreover, in the subsequent developments many probability assumptions will be introduced, which by their nature are irreversible in time. What we are doing here is nothing else than extending a method of treatment which has been applied in the kinetic theory of gases from its very beginnings.

2. "NUMBER OF COLLISIONS" AND COLLISION CROSS SECTIONS

In the formalism to be developed it is convenient to have an expression for the "*number of collisions*" which a given particle experiences during a given interval of time. Various rate quantities occurring in reaction equations can then be referred to this number. In the original form of the kinetic theory, devised for molecules which were considered as hard (elastic) spheres, collisions could be defined unambiguously and each collision brought about a definite change of translational velocity. For a given value g_{ab} of the relative velocity of the two collision partners, the number of collisions in unit time which a particle a would suffer from particles b, was then given by:

$$N_b g_{ab} S_{ab},$$

where N_b is the number density of the b particles per unit volume, and S_{ab} is the collision cross section or target area. In this case the target area was equal to the area of a circle, having as its radius the sum of the radii of the two colliding particles. The product written above has the dimensions of a reciprocal time.

The idea of a well-defined target area does not hold when hard spheres are replaced by force systems which in the usual descriptions extend to infinity. With such a picture the concept of a collision loses itself in vagueness. However, what really matters in the equations is the effect of the collision, as e.g. average rate of transfer of momentum, or of energy, or the chance that a molecule in the interval dt will suffer a specified reaction. Target areas therefore must be defined in an indirect way, by considering the effect of a collision upon some quantity connected with the motion of the particles, etc. In the classical kinetic theory this subject has been developed in great detail for molecules which are considered as spherically symmetric point centers of force. In the expressions obtained for transfer of momentum, occurring in the theory of diffusion; for the transfer of second order quantities as occur in the theory of viscous stresses; for the rate of transfer of energy which leads to heat conduction, various quantities occur which play the part of collision cross sections or target areas.

In our present topic we cannot make use of the classical method of calculation, since the assumption of spherically symmetric point centers of force is too restrictive for our purpose. Nevertheless we shall assume that a target area can be defined for transfer of momentum as it occurs in diffusion. For this target area we shall write:

$$S_{a,n;b,n'/0}$$

where the notation indicates that it refers to collisions between particles a and b, the former one being in a quantum state labeled n (see below), the other one being in a quantum state n'. The subscript $\ldots/0$ indicates that the target area is meant to refer to collisions in which no reaction will occur. There can be, however, a change of quantum state in one or in both of the collision partners. Collisions in which reactions will occur, will be considered further on.

To be precise a target area must be defined with reference to a definite value of the relative velocity between the colliding particles. However, we shall leave this complication aside in order not to overcharge the equations; we will assume, therefore, that the mean target area mentioned above can be used in combination with a mean value of the relative velocity of the two particles, for which we choose the expression $(g_{ab})_m = \{2k(m_b T_a + m_a T_b)/m_a m_b\}^{\frac{1}{2}}$. Here m_a, m_b are the masses of the particles a, b, respectively; T_a, T_b are the (translational) temperatures of the two kinds of particles.

With these definitions we shall henceforward use the following expression for the "number of collisions" which an a particle in quantum state n suffers from b particles in quantum state n', in unit time:

$$N_{b,n'}(g_{ab})_m S_{a,n;b,n'/0}. \tag{1}$$

Along with the collisions in which there are no reactions in the chemical sense, we shall find others leading to reactions of various kinds, which we label with subscripts $l \neq 0$ ($l=0$ being the case of no reaction). We assume that the probability of the occurrence of any reaction can be found, with the aid of quantum theory or, if the case may be, experimentally; we then

express this rate by means of a formula of similar type as above, having the same factors $N_{b,n}$ and $(g_{ab})_m$, but now involving a different target area $S_{a,n;b,n';l}$, referring to the reaction under consideration.

It is convenient to introduce a total target area

$$S_{a,n;b,n'} = \sum_l S_{a,n;b,n';l} \text{ (including } l=0), \quad (2)$$

and to write:

$$S_{a,n;b,n';l} = S_{a,n;b,n'} \cdot P_{a,n;b,n';l}, \quad (3)$$

with

$$\sum_l P_{a,n;b,n';l} = 1. \quad (3a)$$

Then $S_{a,n;b,n'}$ is the total target area for all kinds of collisions between particles a in quantum state n, and particles b in quantum state n', while $P_{a,n;b,n';l}$ gives the probability that such a collision shall lead to the reaction l.

The probability of the occurrence of a reaction is dependent upon the relative velocity of the reaction partners. Since we average over all relative velocities, the probability factors P introduced here will become functions of the mean relative velocities $(g_{ab})_m$. Hence they will be functions of the temperatures of the two reaction partners.

3. DISTRIBUTION FUNCTIONS AND THE BOLTZMANN EQUATION

For each type of particle a "distribution function" is introduced, which describes the distribution of the particles over the various states in which they can occur. The notion of "state" as used here embraces: (a) the values of the three components of the translational velocity ξ_{ax}, ξ_{ay}, ξ_{az}, for which we use classical (Newtonian) mechanics; (b) the state of internal motion, which we consider as a quantum state, specified by a quantum number n. In general the quantum state will require many parameters for its definition; hence the number n may stand for a group of component numbers, referring, say, to rotation, to various types of vibrations, and to the electronic state (which itself must be specified by several numbers). A more detailed notation can be introduced when this is felt to be desirable. We assume that the quantum state can be specified by integral numbers, keeping in mind that if there should be a parameter which can take all values of a continuous scale, an appropriate differential must be introduced as a factor of the distribution function.

Since the distribution of the particles over the various possible states can vary from region to region and can also change with time, the distribution function will be a function of the co-ordinates x, y, z and the time t. As a general notation for a distribution function we use:

$$F_{a,n}(\xi_{ax}, \xi_{ay}, \xi_{az};\ x, y, z, t)\, \mathrm{d}\Xi_a. \quad (4)$$

This function gives the number of particles of type a per unit volume, which are in quantum state n and which have translational velocity components between the limits ξ_{ax} and $\xi_{ax}+\mathrm{d}\xi_{ax}$, etc., the unit volume referring to the location x, y, z at the instant t.

In the classical kinetic theory of gases the dependence of the distribution function upon the velocity components is its most important feature. In the present considerations this point becomes of secondary importance; our main interest will be in the type of particle and in the quantum state. The velocity components ξ_{ax}, ξ_{ay}, ξ_{az} can be eliminated by integration. The first quantity which is obtained in this way is:

$$N_{a,n} = \int F_{a,n}\, \mathrm{d}\Xi_a, \quad (5)$$

giving the total number of particles of type a, per unit volume, which are in the quantum state n.

When we combine all quantum states, we arrive at the number

$$N_a = \sum_n N_{a,n}, \quad (6)$$

giving the total number of particles a per unit volume irrespective of translational motion and of quantum state.

Boltzmann's equation expresses that the change of the distribution function which is observed when we follow the motion of a group of particles through phase space (i.e. the six-dimensional space referring both to ordinary

co-ordinates and to the values of the velocity components), taking account of the possible effect of exterior forces f_{ah} producing accelerations (for instance gravity, or electric and magnetic forces in the case of charged particles), is equal to the change brought about by collisions and spontaneous reactions. This is expressed as follows:

$$\frac{\partial F_{a,n}}{\partial t}+\xi_{ah}\frac{\partial F_{a,n}}{\partial x_h}+\frac{f_{ah}}{m_a}\frac{\partial F_{a,n}}{\partial \xi_{ah}}= \tag{7}$$

$$=\left(\frac{dF_{a,n}}{dt}\right)_{\text{coll}}+\left(\frac{dF_{a,n}}{dt}\right)_{\text{spont. processes}}.$$

In the next sections we shall investigate which form must be given to the terms written on the right hand side.

4. COLLISION PROCESSES

Every collision changes the state of the particle in the sense in which we used this word before (there is always a change of the translational velocities, which may or may not be accompanied by change in internal state). Hence we can say that every collision throws a particle out of the group $F_{a,n}\,\mathbf{d}\xi_a$ to which it belonged. Consequently the number of particles a in quantum state n lost from the group $F_{a,n}\,\mathbf{d}\xi_a$ during unit time (and referred to unit volume), through collisions with particles b in quantum state n', will be given by:

$$F_{a,n}\,\mathbf{d}\xi_a N_{b,n'}(g_{ab})_m S_{a,n;b,n'}.$$

This quantity, with the omission of the factor $\mathbf{d}\xi_a$, must be entered upon the right hand side of equation (7) with the minus sign. It must be summed with respect to n' and with respect to all species b, including the case $b=a$ and $n=n'$.

We must next give attention to the particles coming out of a collision. This will form a separate problem for each type of reaction l. There is the possibility that we again shall find particles a; let the number of particles a produced by a reaction l be given by $\nu_{l/a}$. In the case of a collision with no reaction we shall have $\nu_{a/a}=1$, and also $\nu_{a/b}=1$, since both particles come out of the collision as they were before. The particles a, however, may have suffered a change of quantum state, say from n to n^* and they will have suffered a change of their translational velocities. A change of quantum state is a matter of chance, with a certain probability for its occurrence. As regards the change of translational velocity, classical kinetic theory gave precise calculations for point centers of force. However, since many molecules do not have spherical symmetry, and since, moreover, quantum states may be involved, precise formulas will not always hold. It is therefore appropriate to assume that the redistribution of the translational velocities of the particles a coming out of a collision can be represented by a Maxwellian function of the type:

$$\psi_{l/a,\,\mathrm{tr}}=\left(\frac{m_a}{2\pi kT_{l/a}}\right)^{3/2}\exp\left(\frac{-m_a(\boldsymbol{\xi}_a-\mathbf{u}_l)^2}{2\,kT_{l/a}}\right), \tag{8}$$

as proposed by Krook[1]. This formula gives an isotropic distribution of translational velocities around a mean flow velocity $\mathbf{u}_l$, governed by a translational temperature $T_{l/a}$.

The formula brings the problem how to determine the two parameters $\mathbf{u}_l$ and $T_{l/a}$. The collisions must satisfy the conditions of conservation of momentum and of energy. We consider it probable that all the material particles coming out of a collision have the same mean flow velocity. If radiation is involved in the process, we assume that on the average the photons are emitted in all directions (or absorbed from all directions) isotropically, so that they will not contribute to the mean momentum equation. The value of $\mathbf{u}_l$ will then be given by

$$\mathbf{u}_l=\frac{m_a\mathbf{u}_a+m_b\mathbf{u}_b}{m_a+m_b}, \tag{9}$$

where $\mathbf{u}_a$ and $\mathbf{u}_b$ are the mean flow velocities of the particles a and b in the gas.

With temperature the relation will be more complex, since exchange of internal energy may be involved. Moreover, the distribution of internal energy will not always be an equilibrium distribution corresponding to the translational temperature. It follows that the temperature problem cannot be considered without giving

attention to the distribution of the particles over the various quantum states. We assume that this distribution will be independent of the translational velocities. It can then be represented by a factor $\phi_{l/a,n}$ which acts as a multiplier of $\psi_{l/a,\mathrm{tr}}$.

We observe that the function $\psi_{l/a,\mathrm{tr}}$ defined in (8) is normalized in such a way that

$$\int \psi_{l/a,\mathrm{tr}} \mathbf{d}\xi_{\mathrm{a}} = 1. \tag{10a}$$

Similarly we require:

$$\sum_n \phi_{l/a,n} = 1. \tag{10b}$$

In certain cases of strong interaction—such as may occur in chemical reactions—there may result a complete equilibrium between all degrees of freedom. We then expect $\phi_{l/a,n}$ to be of the form

$$\phi_{l/a,n} = \alpha_{a,n} \exp \frac{-\varepsilon_{a,n}}{kT_{l/a}}. \tag{11}$$

Here $\varepsilon_{a,n}$ is the energy of the quantum state labeled n; the factor $\alpha_{a,n}$ is proportional to the multiplicity or weight of the state; $T_{l/a}$ is the same temperature as occurs in the function $\psi_{l/a,\mathrm{tr}}$. In such a case $T_{l/a}$ may be the same for all reaction products and can then be written T_l. It can then be calculated from the condition of conservation of energy.

When no reaction takes place (case $l=0$), the interaction in general must be termed weak. A considerable change of quantum state is then improbable. It may be that the only changes which are possible are those in which n (or rather, one of the component numbers of n) changes by a single unit either downward, or upward, while there is a big chance that n will not change at all. In the case of no reaction we shall often write

$$\phi_n^{n^*} \text{ for } \phi_{0/a,n}$$

so as to bring into evidence that n changes into n^*.

In order to avoid great complications we shall assume that the temperatures of all particles of a given molecular species coming out of a specified type of collision, will be independent of the quantum states of these particles. This is to say, it is assumed that the temperatures $T_{l/a}$ of the particles a coming out of a collision, although they will depend upon the quantum states of the particles before the collision, are the same for all a particles coming out of the collision. We further assume that the diffusion velocities of the various types of particles with respect to each other will be small compared with the mean molecular velocities; in that case the mean flow velocities drop out of the energy equation and we have to take account only of the random motions, the energy of which is expressed by means of the temperature. The equation for the conservation of energy in a collision between particles b in quantum state n', and particles c in quantum state n'', leading to the appearance of various species of particles, of which particles a are a typical example, can then be written:

$$\frac{3}{2}kT_b + \frac{3}{2}kT_c + \varepsilon_{b,n'} + \varepsilon_{c,n''} = \tag{12}$$

$$= \sum_a \nu_{l/a} \frac{3}{2} kT_{l/a} + \sum_{a,n} \nu_{l/a} \phi_{l/a,n} \varepsilon_{a,n}.$$

The left hand side gives the sum of the energies (random translational and internal) of the particles b and c before the collision; the right hand side gives the distribution of this sum over the particles resulting from the collision, using the average distribution of energy over the various quantum states which can result from the collision.

We can now form the following expression for the number of particles a, in quantum state n, which (in unit time and per unit volume) come out of collisions between, say, particles b in quantum state n' and particles c in quantum state n'', leading to a reaction l, while the a particles shall be in quantum state n and have acquired a translational velocities within the limits described by $\mathbf{d}\xi_{\mathrm{a}}$:

$$N_{b,n'} N_{c,n''} (g_{bc})_m S_{b,n';c,n''} P_{b,n';c,n''/l} \times$$

$$\times \nu_{l/a} \psi_{l/a,\mathrm{tr}} \phi_{l/a,n} \mathbf{d}\xi_{\mathrm{a}}. \tag{13}$$

In equation (7) this expression, divided by $\mathbf{d}\xi_{\mathrm{a}}$, must appear on the right hand side with the positive sign, summed with respect to b, n', c, n'', including the cases $b=a$ and $c=a$, and also summed with respect to l. A factor $\frac{1}{2}$ must

be inserted before the sum since otherwise every collision is counted twice.

5. SPONTANEOUS PROCESSES

With spontaneous processes relaxation frequencies $1/\tau$ take the place of collision frequencies.

We distinguish between processes leading to a change of the chemical state of the particle (this must be a spontaneous dissociation), to be labeled with i (or j) $=1, 2, \ldots$; and mere changes of quantum state for which we shall use $i=0$.

In the cases $i\neq 0$ we need factors $\nu_{i/a}$, $\psi_{i/a,\mathrm{tr}}$ and $\phi_{i/a,n}$ of similar nature as introduced before. We can assume that the total change of momentum in each process will be zero and consequently $\psi_{i/a,\mathrm{tr}}$ must be based upon a mean flow velocity equal to that of the particles which experience the spontaneous process.

For the case $i=0$ we define a frequency $1/\tau_0$ by the formula:

$$\frac{1}{\tau_0}=1-\sum_{i\neq 0}\frac{1}{\tau_i}. \tag{14}$$

We then introduce a function $\phi_n^{n^*}$, giving the probability for a spontaneous transition from a quantum state n to the state n^* of lower energy. Moreover we introduce

$$\phi_n^n(\text{probability of no change})=1-\sum_{n^*\neq n}\phi_n^{n^*}. \tag{15}$$

Again we assume that there is no change of momentum. It follows that the distribution of the translational velocities will not be altered, so that in this case we can write:

$$\psi_{0/a,\mathrm{tr}}=\frac{F_{a,n}}{N_{a,n}}. \tag{16}$$

The contribution of the spontaneous processes to the change of $F_{a,n}\mathbf{d}\xi_{\mathrm{tr}}$ can now be written:

$$\begin{aligned}-F_{a,n}\mathbf{d}\xi_{\mathrm{tr}}\Big(&\sum_{i\neq 0}\frac{1}{\tau_i}+\frac{1}{\tau_0}\sum_{n^*\neq n}\phi_n^{n^*}\Big)+\\&+\sum_{b\neq a,\,\text{all }n'/j\neq 0}\frac{N_{b,n'}}{\tau_j}\nu_{j/a}\psi_{j/a,\mathrm{tr}}\phi_{j/a,n}\mathbf{d}\xi_{\mathrm{tr}}+\\&+\sum_{n'\neq n}\frac{N_{a,n'}}{\tau_0}\phi_{n'}^{n}\frac{F_{a,n'}}{N_{a,n'}}\mathbf{d}\xi_{\mathrm{tr}},\end{aligned} \tag{17}$$

with τ_j in the second line for particles b in quantum state n'; τ_0 in the third line for particles a in quantum state n'.

The first and third lines of this equation can be transformed together into:

$$-F_{a,n}\mathbf{d}\xi_{\mathrm{tr}}+\sum_{\text{all }n'}\frac{F_{a,n'}}{\tau_0}\phi_{n'}^{n}\mathbf{d}\xi_{\mathrm{tr}}.$$

6. THE EXTENDED BOLTZMANN EQUATION

When all terms are collected, we arrive at the following extended form of the Boltzmann equation:

$$\begin{aligned}&\frac{\partial F_{a,n}}{\partial t}+\xi_{ah}\frac{\partial F_{a,n}}{\partial x_h}+\frac{f_{ah}}{m_a}\frac{\partial F_{a,n}}{\partial \xi_{ah}}=\\&\quad=-F_{a,n}\sum_{b,n'}N_{b,n'}(g_{ab})_m S_{a,n;b,n'}+\\&+\tfrac{1}{2}\sum_{b,n';c,n''/l}N_{b,n'}N_{c,n''}(g_{bc})_m S_{b,n';c,n''}\times\\&\qquad\times P_{b,n';c,n''/l}\nu_{l/a}\psi_{l/a,\mathrm{tr}}\phi_{l/a,n}\\&\quad-F_{a,n}+\sum_{\text{all }n'}\frac{F_{a,n'}}{\tau_0}\phi_{n'}^{n}+\\&+\sum_{b\neq a,\,\text{all }n'/j\neq 0}\frac{N_{b,n'}}{\tau_j}\nu_{j/a}\psi_{j/a,\mathrm{tr}}\phi_{j/a,n}.\end{aligned} \tag{18}$$

While the principles upon which this equation is based will be evident, its complication arises from the necessity to consider all types of particles which may play their part in a given reaction scheme, since for all these particles the various possible quantum states must be distinguished. At the same time the equation depends upon a large number of probability coefficients of the types $P_{b,n';c,n''/l}$ and $\phi_{l/a,n}$ which must be known before a calculation can be worked out. It is of great importance to make satisfactory guesses concerning states which may be left out of account without impairing too much the nature of the problem. There are many cases in which a large number of quantum states are not affected by the collision processes, or where they can be treated in a summary way. For instance, the rotation of molecules, at the high temperatures in which we are most interested, can be treated by means of classical formulas, the only datum of importance being the total amount of energy involved in the rotation, which will be a function of the same temperature as appears in the expression for the translational energy. Vibrational energy sometimes can be

treated in the same way, but there are important cases in which a more detailed treatment is needed. As to electronic states, it may often be possible to restrict the attention to only one or two of them.

The Boltzmann equation is essentially a tool to study the behavior of the distribution functions $F_{a,n}$. As mentioned before, in the study of reactions the velocity distribution usually is not of primary importance; the principal features are the number densities and the translational temperatures. The latter are determined, for each species of molecules, by the mean kinetic energy per unit mass of the random translational motion. The velocity components themselves will therefore be eliminated from the equation by integrating it with respect to $\mathbf{d}\boldsymbol{\xi}_a$ over all values of the three components from $-\infty$ to $+\infty$.

The integration can be performed either directly upon the equation as it is given above, or the equation can be multiplied through with a function of the velocity components before the integration is carried out. In this way one can derive a set of equations, the so-called "moments" of the Boltzmann equation. These equations form the basis of the usual treatment of flow problems. Those in common use are:

the *equation of continuity*, obtained by direct integration of both sides of the Boltzmann equation;

the *equations of momentum*, obtained by integration of the Boltzmann equation after both sides have been multiplied by the factor $m_a\xi_{ab}$, that is, by a component of the momentum of a particle;

the *energy equation*, obtained by integration of the Boltzmann equation after both sides have been multiplied by the factor $\frac{1}{2}m_a\xi_a^2+\varepsilon_{a,n}$, which is the sum of the kinetic energy of translation and the energy connected with the quantum state of the particle.

After the integration has been carried out the expressions found are usually summed with respect to n, so as to refer to particles a (say) in all quantum states together.

The forms obtained by the integration are not those ordinarily given in textbooks, but the latter can be derived by a suitable combination. For instance the most convenient form of the momentum equation is obtained when we substract $m_a(u_k+w_{ak})$ times the equation of continuity from the result first arrived at for the momentum equation. A similar procedure can be applied to derive the so-called thermodynamic equation of energy, from which the kinetic energy connected with the flow velocities is eliminated.

For the deduction of these equations and a discussion of the terms occurring in them the reader is referred to a Technical Note*.

REFERENCE

1. M. KROOK, *Phys. Rev.* **99**, 1896 (1955); E. P. GROSS and M. KROOK, *Phys. Rev.* **102**, 593 (1956). Some consequences of Krook's method of approximation have been considered by the present author in *Tech. Note Inst. Fluid Dynam. and Appl. Math., Univ. Maryland*, BN-103 (July 1957).

* This work is part of a larger paper which will be published as a *Technical Note of the Institute for Fluid Dynamics and Applied Mathematics, University of Maryland*, in the fall of 1960, and the reader must be referred to this Technical Note for the construction of continuity, momentum and energy equations and for various other details. The substance of Sections 1–6 has also been presented in a paper given at the *Dedication and Decennial Symposium of the U.S. Naval Ordnance Laboratory, White Oak, Maryland, 26 May 1959* ("Example I", Sections 1–3).

SYSTEMATIC TRENDS IN VAPORIZATION AND THERMODYNAMIC PROPERTIES*

R. J. ACKERMANN, R. J. THORN and G. H. WINSLOW

Argonne National Laboratory, Lemont, Illinois

Abstract—With the theoretical aspects of chemical bonding and the concepts of potential energy functions as guiding principles the sublimation behavior of refractory oxides is discussed. It is shown that for all processes in which the significant atomic and electronic configurations are the same in initial states and the same in final states the heat and entropy changes are intimately related so that to trace the trends in thermodynamic properties it is necessary to study the variation with atomic number of only one of these, preferably ΔH. Of the quantities determining the relative volatilities (i.e. relative stabilities of solid and gaseous oxides and metals) the molecular orbital theory successfully describes the trends by rows and groups in the dissociation energies of the gaseous monoxides for only the regular or B subgroups. Without the introduction of an additional factor the theory does not "explain" the increase in dissociation energies with increasing atomic number as observed in the pretransition group of calcium, strontium, barium and radium, and in the transition groups. This same factor determines the relative stabilities of the solid oxides and metals. The least volatile oxides in the respective A subgroups are lithium, calcium, yttrium, hafnium and perhaps protactinium oxides. The variation along and about this "diagonal" line in the periodic table is discussed as a resultant of two components which are manifested by variation from group-to-group and by changes within groups.

1. INTRODUCTION

The vaporization behavior of condensed phases and the thermodynamic properties of molecular gases are determined principally by chemical bonding energies. These energies are determined in part by the systematization of the elements which is reflected in the periodic table. Hence a discussion of the regularities in the vaporization behavior of the elements and compounds serves as an orderly framework about which one can organize inorganic chemistry. Since the ratio of molecules to atoms increases with pressure and since the highest pressure which one can achieve in a number of high temperature systems is the saturation pressure, equilibria between condensed and gas phases are optimum for the study of molecular species. Recent studies by various investigators have determined the thermodynamic properties of a number of gaseous molecules[1, 2]. Since molecules are the ideal starting point for studying chemical bonding, a renewed impetus has thus developed for investigating inorganic chemistry within the systematics of the periodic table. Trends in the thermodynamic properties have been discussed previously[3, 4], but principally from an empirical point of view. It is more fruitful to study them with theoretical aspects of chemical bonding and concepts of potential energy functions as guiding principles.

According to wave mechanical principles the problem of calculating chemical binding energies, dissociation energies or heats of sublimation requires knowledge of the appropriately restricted (eigen) solutions, ψ, of wave equations of the form,

$$\sum_i (1/m_i)\,\nabla_i^2\psi + (8\pi^2/h)\,(W-V)\,\psi = 0. \quad (1)$$

Here the m_i's are the masses of the particles involved, W is the eigenvalue of the total energy and V is the total potential energy of the system.

If it were generally possible to solve equations of this form for any complex system whatever, it would be found that the lowest eigenvalues

* Based on work performed under the auspices of the U.S. Atomic Energy Commission.

of the energy would be of a form conveniently describable as the combined result of the energies to be associated with various particles, combinations of particles, or processes. Corresponding identification of parts of the eigen solutions, ψ, would be possible. For instance, application to a molecule would yield results of such a form that one could extract an energy (and corresponding wave functions) describable as that required to dissociate the molecule into its constituent atoms in their normal states.

Unfortunately the solution of these equations is not easily accomplished. In fact, no molecular system has been solved exactly. In the case of H_2 approximation methods, which yield a satisfactory value for the dissociation energy, have been applied[5], but none of the many attempts to solve the equations for the next simplest molecule, diatomic lithium, has been entirely successful. (Recent studies by Arai and Sakamoto[6] have indicated some promise for semi-empirical methods.) Hence, in the past 26 years little if any progress has been made toward using these equations to obtain chemical binding energies which are satisfactory for thermochemistry.

On the other hand, some of the recent studies[7, 8] have recognized that for most cases of interest a total wave function or a complete solution of the wave equation is not needed. Recognition of the "separability" mentioned above suggests the possible fruitfulness of attempts to develop only those parts of interest. Thus, Hurley[8], with an electrostatic model, approaches the problem from another direction. The binding energy can be calculated "directly" starting from the equation

$$F_{ax} = -\int \psi^* \frac{\partial \mathcal{H}}{\partial X_a} \psi \, d\tau, \qquad (2)$$

in which F_{ax} is the force holding the nuclei together and $\mathcal{H}$ is the Hamiltonian for one aspect of the system. The ψ which appears in equation (2) has been integrated, in effect, over all core electrons.

It is partly with this sort of outlook that the discussion presented herein was initiated. It is possible that a correlative study employing wave mechanics as a guide will suggest ways in which well-established trends in one class of materials (subgroup B monoxides, for example) can be extrapolated to other groups and ways in which the more rigorous problem can be simplified by the use of models or procedures†. It may be argued that this has been accomplished by the electronegativity concept. However, one must remember that the electronegativity scale of Pauling[10] is based almost entirely on dissociation energies and hence is of value in studying trends only in that it reflects back the interrelations of these energies. More serious, however, is the fact that a property such as electronegativity cannot be a constant independent of atomic environment. Something somewhat more closely related to the present writers' views may be achieved by a consideration of the electronic radial distributions of atomic cores involved in chemical bonding. These are derivable from wave mechanics by the Hartree self-consistent field procedure[11]. This procedure is sufficiently far outside the field of thermochemistry that it should be easier to use these distributions without falling into the trap of the cyclic ingrown comparisons of energies which were used to derive the basis of the comparisons. This latter event frequently occurs as a result of forgetting the original source of the electronegativity scale. Even with the radial core distributions, however, it must still be remembered that the environment plays a role. That is, as shown at the end of this discussion, these (atomic) radial distributions are not entirely useful as they stand; knowledge of the deformation they undergo in molecules is required.

2. INTER-RELATIONS BETWEEN THERMODYNAMIC PROPERTIES

Before initiating a study of systematic trends in thermodynamic properties one should inquire whether it is necessary to study *both* the heat

† Coulson[9] expresses this viewpoint by stating, "It is not unfair to say that in this, as in practically the whole of theoretical chemistry the form in which the mathematics is cast is suggested, almost inevitably, by experimental results . . . . Our approximations to an exact solution ought to reflect the ideas, intuitions, and conclusions of the experimental chemist".

and entropy changes (or the counterparts such as depth and curvature of a potential energy curve). *A priori* there is no particular thermodynamic reason why one would expect the two to be related. Certainly it is possible to construct potential energy curves such that the depth and curvature at the minimum are not related, so that one must look further for such a relation. Accordingly, using the equation (2) derived from wave-mechanical principles, one can show easily that there is a very definite connection between the heat and entropy change of a chemical reaction. The arguments presented below are based essentially upon the dissociation of a diatomic molecule but, in principle at least, one can imagine other processes such as sublimation,

$$(1/n)\,M_n\,(c) \rightarrow M\,(g), \tag{3}$$

as being represented by a single potential energy curve and hence describable by the same equations. Since the dissociation energy (or heat of sublimation) is the total energy required to separate the atoms, one writes that

$$D_e = -\int_{r_e}^{\infty} F\,(r)\,dr, \tag{4}$$

which in view of equation (2) becomes

$$D_e = -\int_{r_e}^{\infty} dr \int \psi^* \frac{\partial \mathcal{H}}{\partial r} \psi\, dr. \tag{5}$$

Within the limits of the Born–Oppenheimer approximation one can express the entropy as the sum of translational, rotational and vibrational contributions. Clearly one can state that the first two are determined by atomic (or molecular) weights and interatomic distances which also determine in part the wave function. In the case of vibration one can show that the "frequency" is given by the equation,

$$\omega = \frac{1}{2\pi c} \sqrt{\left[\frac{(\partial F/\partial r)_{r=r_e}}{\mu}\right]}, \tag{6}$$

in which c is the velocity of light and μ is the reduced mass. Hence one can show that

$$S = S\,(m, r, F). \tag{7}$$

Since, however, for a given form of the Hamiltonian function the wave function is known if one can solve a differential equation, one can write that

$$D_e = D_e\,(m, r_e, \mathcal{H}), \tag{8}$$

and

$$S = S\,(m, r, \mathcal{H}). \tag{9}$$

(In these equations m and r are used as general indicators of masses and specialized distances.) Therefore both the heat and the entropy changes are determined by atomic constants and the form of the Hamiltonian function†. (Note for instance, that the Hamiltonian contains terms for each particle. Hence it "specifies" the number of quantum numbers as well as the form of the potential energy function.)

Because the arguments just presented are not detailed, one cannot be certain that the interrelations between ΔH and ΔS are not complex. Very probably they are. However, for those systems which have identical Hamiltonian functions (except for sizes of relatively inert atomic cores) well-behaved and traceable trends will occur as the numerical constants change. For example, to the extent that all of the alkali metals can be considered, either when free or when bound, to consist of atomic cores of inert gases plus an electron, one predicts systematic trends in properties on the basis of the equations cited above whenever the electron is in the same configuration (same form of Hamiltonian). One is quite familiar with the fact that the molecular constants such as D_e, r_e and ω_e of diatomic molecules in a given group vary smoothly with atomic number[12]. Perhaps the existence of similar trends in the equivalent constants, the heat of sublimation, the atomic radius and the Debye temperature of the con-

† After this manuscript was prepared, the July issue of Physical Review was received. In this issue (*Phys. Rev.* **115**, 249, 1959) G. Falk states: "The actual meaning of the third law (of thermodynamics) is a universal connection between the energy and entropy of any physical system". Independently the present writers have obtained the same conclusion, but in so doing have extended it. For instance Falk states, "Energy as well as entropy of any physical system each has a smallest value which can be normalized to zero". The present writers state that the entropy can be equated arbitrarily to zero when the energy is a minimum and if this is done then in the construction of any theory parameters will be introduced which uniquely determine not only the minimum energy but also the entropy in excess of zero.

densed phases have been less frequently referred to. These same trends are reflected through the equations given above into the heats and entropies of vaporization, so that at these quantities display an interdependency. At two points the relations between ΔH_v and ΔS_v are trivial. At 0°K ΔS_v is zero so that only ΔH_v

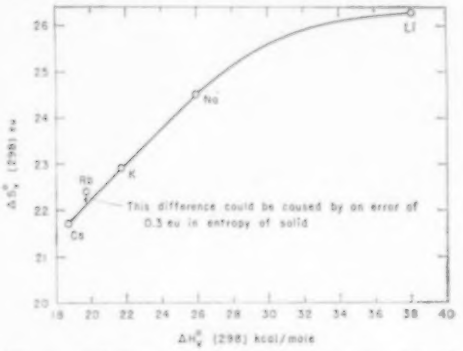

Fig. 1. Relation between heats and entropies of vaporization for alkali metals.. For data see ref. 24.

varies; at the critical temperature both are zero. At intermediate temperatures, however, ΔS_v is a monotonic function of ΔH_v as shown for one specific case in Fig. 1. As suggested previously the nature of this interdependence of ΔH and ΔS is determined in part by the fact that there is a definite relation between the depth and curvature at the minimum of the potential energy curve for all systems having similar

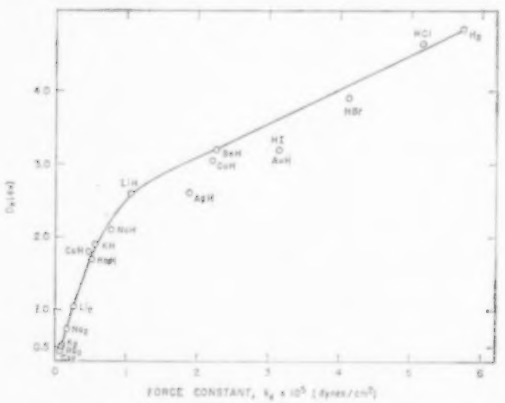

Fig. 2. Relation between force constants and dissociation energies of diatomic molecules having electron pair bonds.

configurations. Thus, there is a close relation between the heat of sublimation and the Debye temperature of the alkali metals. In a similar manner there is a very definite relation between the dissociation energy and the force constant, k_e, of all the electron pair bonded molecules as shown in Fig. 2. Numerous studies have been effected concerning the interrelations among the parameters D_e, k_e and r_e and empirical potential energy functions. These are of course interesting and in agreement with the discussion presented above. However, having once established the interrelations, one must then realize that trends in one are not caused by trends in another but rather they are symptoms of a common cause, and accordingly one must proceed to the essential or crucial problem as to what fundamental properties of atoms and molecules dictate these trends, rather than to search for one of these molecular parameters which "explains" the others.

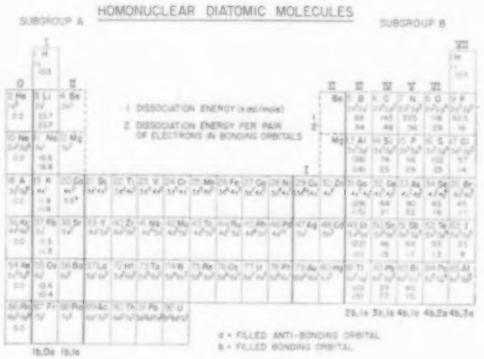
HOMONUCLEAR DIATOMIC MOLECULES
SUBGROUP A
SUBGROUP B
1. DISSOCIATION ENERGY (kcal/mole)
2. DISSOCIATION ENERGY PER PAIR OF ELECTRONS IN BONDING ORBITALS
a = FILLED ANTI-BONDING ORBITAL
b = FILLED BONDING ORBITAL

3. SYSTEMATIC TRENDS IN DISSOCIATION ENERGIES OF DIATOMIC MOLECULES

A tabulation (Table 1) of the dissociation energies[13, 14] of the homonuclear diatomic molecules reveals for the regular or B subgroup elements and the alkali elements the following relations: (1) In a given row the dissociation energies increase and decrease in a regular way so as to manifest maxima for atoms with ns and ns^2np^3 electronic configurations and minima for those with ns^2 and inert gas configurations. The value of the maximum at ns^2np^3 is the larger. (2) The dissociation energy per pair of electrons

from *p* atomic orbitals increases only slightly in groups IV, V and VI. This enables one to estimate dissociation energies for diatomic aluminum, gallium, iridium and thallium. (3) In each group the dissociation energies decrease with increasing atomic number. If one assumes that the chemical bonding is increased by the number of electrons in orbitals which are energetically lower in the united atom than in the separated atoms and decreased by the number in orbitals which are higher, then the molecular orbital theory, which was developed to investigate the electronic structure for the interpretation of spectra, describes the observed trends in the dissociation energies within a row in the periodic table[9, 15]. For the *ns* atomic configuration the *ns* molecular orbitals can be occupied by two electrons with opposite spins so that the alkali dimers contain a pair of electrons in bonding orbitals. For the ns^2 configuration the united atoms contain a bonding orbital and an antibonding orbital so that the alkaline earth dimers are not very stable. The ns^2np^3 configuration is such that all of the bonding orbitals are filled and hence the bonding is a maximum. This aspect of the molecular orbital theory is illustrated well by observing that the removal of an electron from a bonding orbital in N_2 to produce N_2^+ yields a *less* stable molecule whereas removal of an electron from an antibonding orbital in O_2 to produce O_2^+ yields a *more* stable molecule. The decrease in the dissociation energies within a group is undoubtedly related to an increase in the radii. To illustrate this one is tempted to cite the fact that the dissociation energy is a function of the spectroscopically measured bond length[15]. This observation, however, is a consequence of the interrelation between the parameters of the potential energy curve as discussed in Section 2 above. It is more satisfying to relate this trend to a quantity derivable from atomic properties by the use of the wave equation. Accordingly, one can suggest that the bond length is really a reflection of the more fundamental radial distribution function of the electronic density of the ion corresponding to the inert gas configuration. In the case of the alkali metals (and probably the other groups) the Hartree self-consistent field calculations yield distributions which indicate that the core "size" increases with increasing atomic number.

The same trends and principles apply to the stabilities of the monoxides of the regular or B subgroup elements so that one predicts (and observes, see Table 2) maximum dissociation energies at oxides of group IVB elements (CO,

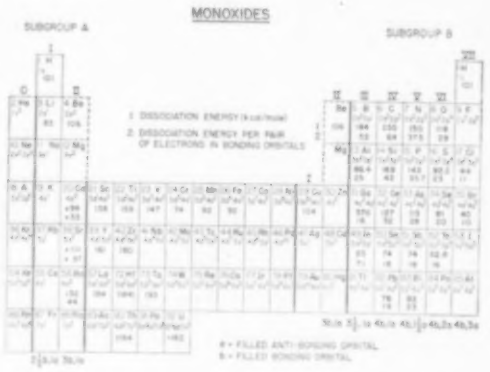

SiO, GeO, SnO and PbO) and minima at the inert gases because bonding orbitals are being filled between the alkali metals and group IVB inclusive and antibonding orbitals are being filled between group IVB and the inert gases. One can expect the same behavior with sulfides, selenides and tellurides. Similar trends will occur for the nitrides, phosphides, etc., except the maximum will occur at group VB.

The molecular orbital theory has been so successful in predicting these trends that one naturally wonders whether it can be as successful in tracing the relations in the transition groups. The problem of deriving correlation schemes for the transition elements may be more complicated because the energies of the 3*d*, 4*d* and 4*f* atomic orbitals are changing with respect to other orbitals. As an aid to the solution of this problem one can cite the trends which are revealed by an inspection of the known dissociation energies of the monoxides. This enables one to formulate the following statements: (1) Within a group the dissociation energies apparently increase with increasing atomic number so that some factor besides core radius is needed. (2) The dissociation energy

appears to be a maximum at group IVA indicating that bonding orbitals are completely filled with this group as occurs in monoxides of group IVB elements. (3) The factor which is operative in the transition elements is also present in group IIA, the alkaline earths calcium, strontium and barium, because in this group the dissociation energies increase with increasing atomic number in contrast to the behavior of the groups in the regular elements. In a manner of speaking the properties of compounds of the transition elements are anticipated by the properties of the compounds of calcium, strontium, barium and radium.

Group	Solid Phase	Gas Phase	Remarks
I-A	M_2O	$M + O_2, M_2O$	$Li_2O \longrightarrow \begin{cases} Li_2O \\ Li + O_2 \end{cases}$ Others $\longrightarrow M + O_2$ $MgO(s) \longrightarrow Mg(g) + O(g)$
II-A	MO	$M + O_2$, MO	$BaO \longrightarrow BaO(g)$
III-A	M_2O_3	$MO + O$, M	
IV-A	MO_2	MO_2, $MO + O$	
V-A	M_2O_5	$(M_2O_5)_n$ $MO_2 + MO + O$	$V_2O_5 \longrightarrow (V_2O_5)_2(g)$
VI-A	MO_3	$(MO_3)_n$	$n = 3, 4, 5$ $MoO_2 \longrightarrow \begin{cases} MoO_2(g) + Mo(s) \\ MoO_2(g) \end{cases}$
	MO_2	$(MO_3)_n, MO_2$	$WO_2 \longrightarrow (WO_3)_n(g) + W(s)$ $UO_2 \longrightarrow (UO)(g) + UO_2(g)$ small

4. SYSTEMATIC TRENDS IN THE SUBLIMATION OF OXIDES

Having failed to "explain" the trends observed in the stabilities of the simple molecules of the transition elements, one must seek "excuses" for extending the discussion to systematic trends in the sublimation of oxides of these elements. Accordingly, without detailed rationalization and in agreement with the initial intent the writers summarize the "excuses" as follows: In order to present an orderly picture of the general behavior of the sublimation of oxides so that persons less familiar with the field do not need to correlate isolated facts, it is desirable to organize a discussion within the background of a systematic framework. Certain trends more subtle than those previously discussed are apparent in the sublimation properties of oxides. One inquires what fundamental properties give rise to these. For example how do the stabilities of the gaseous oxides influence these trends? Is there any relation between the trends observed in the dissociation energies of the monoxides and those in the sublimation behavior of oxides?

Because the refractory oxides and the oxides which yield gaseous molecules are mainly those of elements contained in the A subgroups (see Table 2) plus those of beryllium, magnesium, boron, aluminum and silicon, only these oxides are discussed herein. Of all the possible oxides in these groups the sublimation behavior of only those listed in Table 3 is described. If sublimation occurs in a vacuum or in an effusion cell in an evacuated space (neutral conditions), then the predominant gaseous species in each group are those tabulated. By inspection one observes that gaseous molecules become more important with increasing group number and that gaseous polymers have been observed in the cases of beryllium, vanadium, molybdenum and tungsten oxides. At present the more complex molecules will not be discussed. In group IA the principal gaseous species at all temperatures are the elements. Only in the case of lithium have gaseous molecules been observed[116] and in this case the mole fraction of Li_2O is only one-tenth. In the alkaline earth group the mole fraction of the monoxide in the saturated vapor increases with increasing atomic number (beryllium excepted) to such an extent that with calcium (and magnesium) the vapor contains less than 1 per cent oxide whereas with barium the vapor is at least 99 per cent monoxide[1]. In group IIIA the predominate gaseous species observed in sublimation are the monoxide, atomic oxygen and, to a lesser extent, the gaseous metal[1]. To a certain degree, then, the stabilities of the gaseous monoxides will determine some of the vaporization properties of this group. The sublimation of the oxides of group IVA elements is characterized by the presence of both the gaseous dioxides and the monoxides, the latter being in general less abundant than the former[1].

The sublimation processes of the oxides of elements in groups VA and VIA are more complicated than the ones just discussed in two

respects. First, one observes that there are more than one condensed phases, some being non-stoichiometric. Second, the gaseous species are more complex. In certain instances the differences between some members are so pronounced that one might infer that the two are not even similar. For example vanadium pentoxide sublimes predominately to complex molecules[17] such as V_4O_{10}, V_4O_8, V_6O_{14}, V_6O_{12} and V_2O_4, whereas tantalum pentoxide sublimes to the gaseous dioxide and monoxide under reducing conditions[18] and most probably to gaseous dioxide and oxygen under neutral conditions; molybdenum[19] and tungsten[20] trioxides sublime to gaseous trimer, tetramer and pentamer of the trioxide, whereas uranium trioxide vaporizes to the monomer of the trioxide[21]; tungsten dioxide sublimes to polymers of the trioxide and metallic tungsten[22], whereas molybdenum dioxide sublimes to monomeric dioxide and trioxide[22]. These apparent contrasts illustrate the subtle nature of the trends in the sublimation properties. They are comprehended only when one recognizes that the behavior is determined by competing processes. The probable absence of complex molecules in the saturated vapor above tantalum oxide does not indicate that the chemical bonding in the gaseous tantalum oxides is different from that in vanadium oxides; nor does the absence of polymers of uranium trioxide indicate that uranium is not chemically related to tungsten. Rather, these differences are a consequence of the fact that higher temperatures are required in the cases of tantalum pentoxide and uranium trioxide to produce the saturated vapor. This depends mostly upon the relative values for the free energies of formation of the condensed phases. In a manner of phrasing one states that the tendency to produce polymers is competing with that to produce stable condensed phases. Or that the tendency to produce polymers becomes so great that a huge polymer, the condensed phase, is the result! A more favorable reaction then occurs such as sublimation to simple species.

If one examines the "vapor pressures" or volatilities of solid oxides at 2000°K (Fig. 3), one finds that the least volatile oxides in the respective groups as listed in Table 2 are those

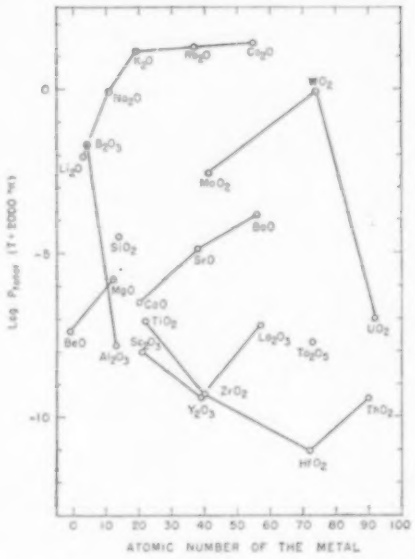

Fig. 3. Trends in the vapor pressures of oxides under neutral conditions at 2000°K.

of lithium, calcium, yttrium, hafnium and probably protactinium at the left, and beryllium and aluminum at the right. Of all these, hafnium oxide is the least volatile under neutral conditions. The question which immediately arises is that concerning the thermodynamic and fundamental atomic properties which "cause" this trend. The thermodynamic aspects can best be investigated by referring to a modified Born–Haber cycle as shown in Fig. 4. In this diagram the processes represented along the diagonal are the ones encountered when one measures "vapor pressures". This diagram

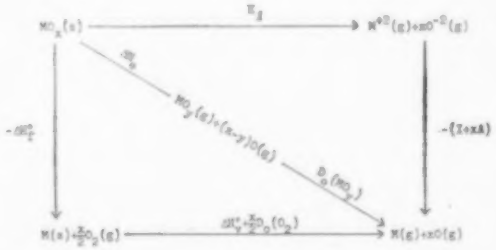

Fig. 4. Thermochemical cycle depicting the vaporization process.

shows that if the vapor contains gaseous molecules, then the volatility is greater than that calculated for decomposition to the gaseous elements. Therefore one would expect without further examination that the trends cited for the volatilities of the oxides are determined at least in part by the relative stabilities of the gaseous oxides. To ascertain the role of the molecules, one can calculate the trends expected for that part of the cycle involving the decomposition to the elements, compare this with the trends in volatilities and account for any differences by the presence of the gaseous oxides. If this were done rigorously, the free energies would be used. However, in the present case one can show that the principal determining quantities are the heats, provided comparisons are made for processes having similar entropy changes. This can be accomplished by calculating per mole of gaseous elements the heat of sublimation, ΔH°_{se}. Accordingly the quantity,

$$\frac{1}{1+x}[\Delta H^\circ_{ss}(\mathrm{M}) - \Delta H^\circ_{of}(\mathrm{MO}_x) + \tfrac{1}{2}D_0(\mathrm{O}_2)] =$$

$$= \frac{1}{1+x}[\Delta H^\circ_{s} + D_0(\mathrm{MO}_g)] = \Delta H^\circ_{se}\ , \qquad (10)$$

in which ΔH°_{ss} is the heat of sublimation of the metal, ΔH°_{of} is the heat of formation of the condensed oxide per gram atom of metal, and D_0 is the dissociation energy, is plotted as a function of atomic number in Fig. 5. (The quantities mentioned above are listed in Table 4.)

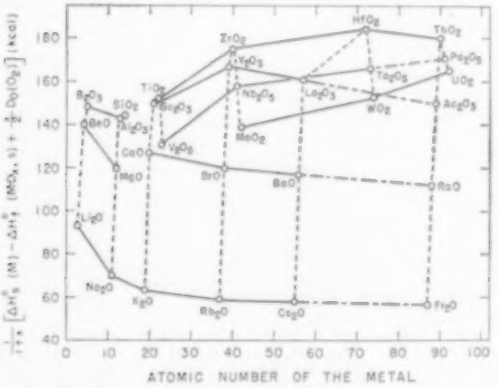

Fig. 5. Trends in the vaporization of oxides to the gaseous elements.

Comparing the relations in this figure with the trends found in the volatilities of the oxides, one observes that there is an extremely close correspondence. From comparisons within groups one writes the following statements:

(1) In group IA the volatilities increase and the heats of sublimation, ΔH°_{se}, to the gaseous elements decrease with increasing atomic number. Since molecules have been observed only in the case of lithium, it is surmised that the dissociation energies of the monoxides decrease with increasing atomic number so that the alkali metals behave like the B subgroup elements. The presence of the gaseous molecules has only a slight influence on the volatilities because of their relatively small concentration.

(2) In group IIA the volatilities increase and the heats, ΔH°_{se}, decrease with increasing atomic number. The dissociation energies of the monoxides increase with increasing atomic number, so that the trend is opposite from that observed in the alkali metal group and the B subgroups. The presence of gaseous molecules therefore supplements the volatilities to the gaseous elements. The alkaline earth elements, calcium, strontium, barium and possibly radium, appear to bridge the pronounced changes which occur between the alkali metals and the transition elements. In group IIA some of the properties such as the volatilities resemble those observed in the alkali metal group, while others such as the dissociation energies of the monoxides resemble the ones observed in the transition groups.

(3) In group IIIA the volatility is a minimum and the heat, ΔH°_{se}, is a maximum at yttrium oxide. The dissociation energies of the monoxides increase with increasing atomic number and consequently have little effect upon the trend in volatilities. It is essentially the heats of formation of the solid oxides which determine the trends in volatilities and ΔH°_{se}'s.

(4) In group IVA the volatility is a minimum and the heat, ΔH°_{se}, is a maximum at hafnium dioxide. The dissociation energies of the monoxides and probably the dioxides increase with increasing atomic number. For the most part the stabilities of the solid oxides determine the volatilities, but because the

Table 4. Heat Quantities Involved in the Process of Sublimation to the Gaseous Elements

Oxide	$-\Delta H_f^\circ$ (MO_x)*‡	ΔH_s° (M)†‡	$\frac{1}{1+x}[\Delta H_s^\circ(M) - \Delta H_f^\circ(MO_x) + \frac{x}{2} D_0(O_2)]$[25]
Li_2O	71	38	92
Na_2O	50	26	70
K_2O	43	22	63
Rb_2O	40	20	59
Cs_2O	38	19	57
BeO	143	78	140
MgO	144	36	120
CaO	151	42	126
SrO	141	39	120
BaO	134	42	118
B_2O_3	153	128[26]	
Al_2O_3	200	77	146
Sc_2O_3	(205)	(82)	150
Y_2O_3	228[27]	(102)	167
La_2O_3	214	100	161
SiO_2	210	105	144
TiO_2	226	113	152
ZrO_2	262	146	175
HfO_2	266	168	184
ThO_2	293	134[28]	183
V_2O_5	186	123	131
Nb_2O_5	228	178	158
Ta_2O_5	244	187	165
MoO_2	141[29]	158	139
WO_2	141[30]	200	153
UO_2	259	117	165

* Heat of formation per gram atom of metal at 298°K. Values taken from Ref. (23) unless otherwise specified.

† Heat of sublimation of the metal at 298°K. Values taken from Ref. (24) unless otherwise specified.

‡ The difference between the heats at 298°K and 0°K is not significant for the purposes of this discussion.

dissociation energies of the gaseous thorium oxides are sufficiently greater than those of gaseous hafnium oxides, thoria is more volatile than hafnia.

(5) In group VA the volatility is a minimum at either tantalum or protactinium oxide and the heat, ΔH_{sv}°, is a maximum at one or the other of these two. The dissociation energies of the monoxides and possibly the dioxides appear to increase with atomic number, and consequently may determine the relative volatilities of tantalum and protactinium oxides. Essentially, however, the behavior is determined by the heats of formation of the solid oxides. The presence of gaseous polymers in the case of vanadium oxide supplements the trend predicted by the stabilities of the condensed oxides.

(6) In group VIA the volatility is a maximum at tungsten dioxide—the volatility of chromium dioxide is not known—but the heat, ΔH_{sv}°, increases with increasing atomic number. The first is determined by the relative stabilities of gaseous polymers of tungsten and molybdenum

trioxides, whereas the second is determined principally by the heats of sublimation of the metals.

Across the rows one can observe the following relations:

(1) In the K row the volatilities decrease between lithium and beryllium oxides and then increase between beryllium and boron oxides. The heats, ΔH°_{sv}, of sublimation to the gaseous elements and the dissociation energies of the gaseous oxides increase across the row. The latter quantity in the case of boric oxide becomes sufficiently large to make boric oxide more volatile than beryllium oxide.

(2) In the L row the volatilities decrease between sodium and aluminum oxides and increase thereafter. The heats, ΔH°_{sv}, and the stabilities of the gaseous oxides increase across the row. The latter become sufficiently large to cause silica to be more volatile than alumina.

(3) In the M row the volatilities decrease between potassium and scandium oxides and increase between scandium and vanadium oxides. The behavior of the heats, ΔH°_{sv}, is similar in that a maximum value occurs at scandium oxide. The dissociation energies of the monoxides appear to attain a maximum at titanium oxide. Other gaseous oxides become more stable beginning with titanium so that the volatilities are even greater than those calculated for decomposition to the gaseous elements or to gaseous monoxides and oxygen.

(4) In the N row the volatilities decrease between rubidium and yttrium oxides and increase between yttrium and molybdenum oxides. The heats, ΔH°_{sv}, increase between rubidium and zirconium oxides and decrease between zirconium and molybdenum oxides. The dissociation energies of the monoxides appear to be a maximum at zirconium oxide. Other gaseous oxides, such as dioxides and trioxides, become more stable beginning with zirconium so that the volatilities are even greater than those calculated for decomposition to the gaseous elements or to gaseous monoxides and oxygen. Hence zirconium dioxide is slightly more volatile than yttrium oxide.

(5) In the O row the volatilities decrease between cesium and hafnium and increase between hafnium and tungsten. The heats, ΔH°_{sv}, behave similarly. The dissociation energies probably increase to a maximum value at hafnium monoxide.

(6) The trends in row P are probably the same as those observed in row O.

As a result of the behavior by groups and rows the quantity plotted in Fig. 5 increases in the series lithium, calcium, yttrium, hafnium oxides and the volatilities decrease in this same order. This diagonal line is the resultant of two components which are manifested by the variations from group-to-group and by the changes within groups. The variation from group-to-group is such that the heats of sublimation of the metals, the heats of formation of the solid oxides and the dissociation energies of the gaseous oxides increase. However, the heats of formation of the solid oxides increase to such an extent that they overshadow the tendency of the volatilities to increase because of increasing stabilities of gaseous oxides. One deduces that bonding orbitals or their equivalent are being filled from group-to-group in a manner similar to the behavior in the B subgroup elements. The sources of the changes within groups, however, are more elusive. In a given A subgroup the element having the most stable gaseous oxide is generally not the same as the one having the most stable solid oxide or metal. For example, in the second group the most stable gaseous monoxide is that of barium (or perhaps radium), whereas the most stable solid oxide is that of calcium, and in group IIIA the solid oxide of yttrium is the most stable, whereas the gaseous monoxide of lanthanum (or perhaps actinium) is the most stable; on the contrary, however, thorium forms the most stable gaseous oxides as well as solid oxide in group IVA. The subtle nature of the sublimation properties is best illustrated perhaps by pointing towards hafnium and/or thorium dioxides. In this region of the periodic table the heat of formation of the solid oxides is a maximum and the dissociation energy of the gaseous oxides is also a maximum. However, despite the latter and the fact that stable gaseous oxides tend to increase the volatility, the vapor pressure is a minimum in this region. It is apparent that

one single property of elements determines all these behaviors, but one must remember that combinations of these properties and/or environmental changes produce subtle trends.

It is not particularly astounding to demonstrate that the stabilities of the monoxides, the solid metals and the solid oxides are interrelated, for, as anyone versed in wave mechanics can point out, some combination of atomic wave functions does predict chemical bonding in molecules and solids. The more important point is that although the molecular orbital theory satisfactorily traces the trends in the dissociation energies of the B subgroup elements by a resolution into bonding and antibonding orbitals, and radial electronic distributions, the trends in the pretransition group of calcium, strontium, barium and radium, and the transition groups are not so readily explained. Other factors such as the relative deformation of atoms in molecules must, therefore, be introduced into the theory. It has been the secondary purpose of this discussion to show the need for a new, or more penetrating, approach to the problem of correlating and explaining the systematics of numbers of interest in thermochemistry, than is provided, for instance, by the electronegativity scale or the present form of the molecular orbital theory. Suggestions for answering this need have been made along the way. The authors lay claim to none of these, but only hope to encourage renewed activity by workers in the field.

DISCUSSION

S. H. BAUER: Your summary re-emphasizes the need to rationalize the observation that some metal oxides, as of the alkali metals, vaporize to produce metal atoms plus molecular oxygen, while others such as of some transition metals vaporize in the form of molecules in polymeric states. This must be due primarily to differences in the enthalpies of the vaporization process. As you have indicated, one should consider the competition for formation of the strongest bonds. In the first group, the M–O bond energy must be less than the O–O bond energy, while for the transition metal oxides, possibly because of the larger allowed O/M ratio, overall greater stability is achieved by forming M–O bonds rather than molecular oxygen.

REFERENCES

1. R. J. ACKERMANN and R. J. THORN, *Prog. Ceram. Sci.* **1**.
2. M. G. INGHRAM and J. DROWART, in *Proc. Internat. Symp. High Temperature Technology*. Stanford Research Institute (1959).
3. D. HART, *J. Phys. Chem.* **56**, 202 (1952).
4. B. LAKATOS, *Acta. Chem. Acad. Hung.* **8**, 207 (1955).
5. H. M. JAMES and A. S. COOLIDGE, *J. Chem. Phys.* **1**, 825 (1933).
6. T. ARAI and M. SAKAMOTO, *J. Chem. Phys.* **28**, 32 (1958).
7. P. O. LÖWDIN, *Phys. Rev.* **97**, 1474 (1955).
8. C. A. HURLEY, *Proc. Roy. Soc.* **A226**, 170, 179, 193 (1954); **A235**, 224 (1956).
9. C. A. COULSON, *Valence* p. 108-9. Oxford University Press (1952).
10. L. PAULING, *Nature of the Chemical Bond*. Cornell University Press, Ithaca, N.Y. (1939).
11. D. R. HARTREE, *Rep. Progr. Phys.* **11**, 113 (1946-7).
12. See for example Y. P. VARSHNI, *J. Chem. Phys.* **28**, 1078-81 (1958).
13. G. HERZBERG, *Molecular Spectra and Molecular Structure—I: Spectra of Diatomic Molecules*. Van Nostrand, New York (1950).
14. A. G. GAYDON, *Dissociation Energies*, Dover Publications, New York (1950).
15. L. PAULING, *J. Phys. Chem.* **58**, 662 (1954).
16. J. BERKOWITZ, W. A. CHUPKA, G. D. BLUE and J. L. MARGRAVE, *J. Phys. Chem.* **63**, 644 (1959).
17. J. BERKOWITZ, W. A. CHUPKA and M. G. INGHRAM, *J. Chem. Phys.* **27**, 87 (1957).
18. M. G. INGHRAM, W. A. CHUPKA and J. BERKOWITZ, *J. Chem. Phys.* **27**, 569 (1957).
19. J. BERKOWITZ, W. A. CHUPKA and M. G. INGHRAM, *J. Chem. Phys.* **26**, 842 (1957).
20. J. BERKOWITZ, W. A. CHUPKA and M. G. INGHRAM, *J. Chem. Phys.* **27**, 85 (1957).
21. R. J. ACKERMANN, R. J. THORN, C. ALEXANDER and M. TETENBAUM, *J. Phys. Chem.* **64**, 350 (1960).
22. P. E. BLACKBURN, M. HOCH and H. L. JOHNSTON, *J. Phys. Chem.* **62**, 769 (1958).
23. J. P. COUGHLIN, *Bull. U. S. Bur. Min.* 542 (1954).
24. D. R. STULL and G. C. SINKE, *Thermodynamic Properties of the Elements*. American Chemical Society, Washington, D.C. (1956).

25. P. Brix and G. Herzberg, *Canad. J. Phys.* **32**, 110 (1954).
26. W. A. Chupka, Argonne National Laboratory, private communication.
27. E. J. Huber, Jr, C. E. Holley, Jr. and E. L. Head, *J. Phys. Chem.* **61**, 497 (1957).
28. A. J. Darnell, W. A. McCollum and T. A. Milne, *J. Phys. Chem.* **64**, 341 (1960).
29. A. D. Mah, *J. Phys. Chem.* **61**, 1572 (1957)
30. A. D. Mah, *J. Amer. Chem. Soc.* **81**, 1582 (1959).

RATE OF VAPORIZATION OF REFRACTORY SUBSTANCES

R. F. WALKER and J. EFIMENKO
National Bureau of Standards, Washington 25, D.C.
and
N. L. LOFGREN
Chico State College, Chico, California

Abstract—Techniques and some preliminary data on the rate of vaporization of aluminum oxide and palladium are presented. Experimental techniques were based on the Langmuir method, using an induction furnace with a microbalance, and on a transpiration-type method using a solar furnace.

The vaporization of sapphire *in vacuo* and water vapor has been studied. The data obtained *in vacuo* could not be fitted to a linear extrapolation of the data of Brewer and Searcy, and possible causes for the discrepancy are discussed. No evidence for a reaction between solid alumina and water could be detected up to 1600°C. During the latter experiments an unexpected attack of platinum by the aqueous atmosphere was encountered.

The vaporization of liquid Al_2O_3 has been studied in the presence of 2-25 mm of H_2O and 0·1-1 mm of O_2. A marked reaction between liquid alumina and water vapor was observed. An attempt has been made to analyze the data in terms of the reaction:

$$\frac{1}{2}\,Al_2O_3\,(l)+\frac{x}{2}\,H_2O\,(g)=AlO_yH_x\,(g)+\left(\frac{3}{4}+\frac{x}{4}-\frac{y}{2}\right)O_2\,(g)$$

The data were not inconsistent with the formation of AlOH molecules.

A value of 103 kcal has been obtained for heat of vaporization of palladium. The equilibrium vapor pressure is higher than the estimated data of Brewer but lower than the value determined by Haefling and Daane.

1. INTRODUCTION

The Langmuir method for studying rates of vaporization is based on measurements of the rate at which mass vaporizes from unit area of a heated surface. If the vaporization takes place freely, that is in a vacuum and in some physical system which permits the condensation of the gaseous molecules without reflection back to the vaporizing surface, then the rate of vaporization is related to the equilibrium vapor pressure in accordance with the equation:

$$m=\alpha p\left(\frac{M}{2\pi RT}\right)^{\frac{1}{2}}$$

m = weight loss of the condensed phase in g/cm² sec
p = equilibrium vapor pressure
M = molecular weight of the vapor species
R = gas constant
T = absolute temperature.

The coefficient of evaporation, α, is the fraction of the gaseous molecules which would condense if they impinge on the vaporizing surface under equilibrium conditions. The need for such a coefficient arises because if, under equilibrium conditions, some of the molecules would not condense (i.e. $\alpha<1$), then a reduced rate of vaporization would be sufficient to maintain the equilibrium vapor pressure.

The Langmuir method has been used quite extensively for the determination of the vapor pressures of metals. The coefficients of evaporation of metals generally appear to be close to unity, and there is sufficient data on their emissivity to permit reasonable estimates of temperature. Furthermore, it is relatively simple to achieve the theoretical requirement of a freely evaporating surface with metals, because they can be readily heated electrically. With

nonmetals this requirement is very difficult to fulfill, and reliable values for coefficients of evaporation and emissivity are not commonly available. Nevertheless, the Langmuir method possesses some advantages which render attempts to extend its range of usefulness worthwhile.

This paper describes two approaches, based on the Langmuir method, which are being scrutinized for the investigation of rates of vaporization at temperatures above 1000°C. The techniques are illustrated by reference to studies of the vaporization of aluminum oxide and the platinum group metals.

2. MICROBALANCE WITH AN INDUCTION FURNACE

In principle, rates of vaporization can be measured with high precision by hanging a sample of known surface area from a microbalance and measuring the weight-loss *in situ*. Unfortunately, a number of practical difficulties have to be circumvented in order to make such measurements at high temperature. The apparatus used (Fig. 1) is based on induction heating using an r.f. generator, as this is the most generally applicable electric heating technique. Resistance or electron bombardment heating are also useful for this purpose, but have their own particular limitations.

Microbalance

The microbalance design follows closely that employed by Bradley for measuring the vaporization of sulfur[1] and by Gulbransen for studies of the oxidation of metals[2]. The balance (Fig. 2) consists essentially of a fused quartz beam mounted on an 0·002 in. dia. stretched tungsten wire, which acts as the central fulcrum. The central fulcrum is attached to a fused quartz frame. A secondary fulcrum of 0·001 in. dia. tungsten wire is stretched across the fork at each end of the beam. Short hang-downs terminating with a hook are attached to the secondary fulcrums and are used for suspension purposes.

Silver chloride has been used extensively to cement the tungsten to the fused quartz both in this and earlier investigations. However, it has been found that water vapor from the ambient atmosphere will penetrate along the interface between the silver chloride and the quartz, thus restricting the use of the balance. Gold-plating the balance after fabrication inhibits the penetration considerably, and permitted the experimental work described below, but the plating does not provide long term reliability.

The gold-plating was originally applied to drain static charge from the balance. During studies of the vaporization of metals, however, it has been found necessary to introduce an insulator in the suspensions of gold-plated balances. Otherwise, currents introduced by the induction coil travel up the suspensions, through the fulcrums and gold-plating, to ground. These currents are sufficient to soften the silver chloride, causing a slow creep of the fulcrums and, hence, a change in calibration of the balance.

The nonuniform r.f. field of the induction coil also causes oscillation of the load and displacement of the beam and its load. This is more serious with metal samples, for interaction between the sample and the field causes the balance beam to be displaced full scale to one of the beam rests, thus preventing continuous reading and making it necessary to read at room temperature with the field off. By suspending the sample just above the center of the field so that it is displaced upward, the balance is not subjected to undesirable stress. Displacement of the beam is not a serious problem with nonmetals, and continuous reading is possible providing the field strength is maintained constant. However, as discussed below, oscillations of the sample and suspension may cause difficulty. Periodic vibrations of the beam are damped magnetically with an aluminum counterweight (Fig. 3).

Oscillations of the sample and its suspension may also occur if they are not located at the center of a horizontal plane in the field. Location of the center has presented no problem with metal samples, but nonmetal samples suspended from 0·002 in. dia. platinum wires often oscillate prohibitively at high field strengths, probably due to distortion of furnace components and displacement of the field at

high temperature. This problem has now been solved by suspending nonmetal samples from a "chain" of 0·010 in. dia. sapphire rods, extending several inches above the induction coil. The upper portion of the suspension is 0·002 in. dia. platinum wire attached to the balance beam through a fused quartz pan. Interaction of the field with this portion of the suspension is eliminated by shielding externally with a coil of copper wire (Fig. 3).

The balance is designed to carry samples up to 4 g in weight (i.e. a total load of 8 g). Displacements of the beam are directly proportional to changes in weight and are measured with a cathetometer reading to 1 μ. The calibration of the balance is dependent on the load, but weight changes of about 1 μg are detectable.

Furnaces and samples

Nonmetals are heated by radiation from a seamless metal tube which is the susceptor of the induction coil. A 2 in. long × $\frac{1}{2}$ in. dia. platinum tube, the ends of which had been spun over leaving a $\frac{1}{8}$ in. dia. hole at the top and bottom, has been used *in vacuo* and in water vapor at temperatures up to 1600°C. A single crystal or a polycrystalline sample, $\frac{3}{4}$ in. long × 0·1 in. dia., was suspended within the tube. This arrangement facilitates accurate temperature measurement, but undesirably restricts the free vaporization of the sample. A more recent furnace, designed for temperatures up to 2000°C and employing a seamless molybdenum or tungsten tube, is currently being evaluated. These tubes are $5\frac{1}{2}$ in. long × 1 in. dia. and permit the use of samples of different shapes. By using such different shapes as a rod, a disk and a sphere, it is possible to obtain some indication of the extent to which the free vaporization and condensation of the molecules is impeded by the tube walls.

Metal samples, $\frac{3}{4}$ in. long × 0·080 in. dia., are heated directly, by induction. A water-cooled copper concentrator (Fig. 4) is inserted into the furnace chamber to increase the field intensity in the neighbourhood of the sample.

In all cases temperatures are measured with an optical pyrometer through a calibrated window which is protected with a magnetically-operated shutter.

Results

Sapphire single crystals. During experiments with the platinum furnace, a flame-polished sapphire single crystal, having its *c*-axis at approximately 45° to the axis of the sample, was suspended from an 0·002 in. dia. platinum wire. The system was evacuated to pressures in the range $(0{\cdot}7\text{–}1{\cdot}3) \times 10^{-5}$ mm Hg, as measured with an ionization gage.

Assuming for comparison purposes that AlO is the vapor species and the coefficient of evaporation is unity, the data given in Table 1 have been obtained. The weight loss due to sublimation of the platinum suspension was estimated from the data of Jones *et al.*[3].

Table 1. Weight Loss of Sapphire Single Crystal in a Platinum Furnace in Vacuo

Temp. (°K)	Weight loss (g/cm²/sec)	Vapor pressure atm (as AlO)
1493	$3{\cdot}43 \times 10^{-10}$	$4{\cdot}50 \times 10^{-11}$
1564	$1{\cdot}523 \times 10^{-9}$	$2{\cdot}06 \times 10^{-10}$
1614	$2{\cdot}445 \times 10^{-9}$	$3{\cdot}28 \times 10^{-10}$

The calculated vapor pressures are approximately 5 times higher than indicated by a least squares extrapolation of the Knudsen cell measurements of Brewer and Searcy[4]. There are two sources of error which could yield vaporization rates which are too high. The assumption that nearly black-body conditions exist within the furnace may be incorrect. More probably, the sapphire reacted with the platinum furnace through the vapor phase. No clear substantiation of these possibilities has been obtained, but calculated ΔH_0° values for the reaction forming AlO show a trend with temperature, and indicate that an undetected systematic error is involved.

A similar experimental technique was used to study rates of evaporation in 2–10 mm of water vapor. As discussed below, however, rapid vaporization of the platinum suspension prevented accurate measurements of the weight-loss of the sapphire *in situ*. A more conventional laboratory microbalance capable of ± 10 μg precision was, therefore, employed to measure the weight-loss of the sapphire alone,

Fig. 1. General view of the high temperature micro balance, with vacuum system, gas trains and 450 kc r.f. generator.

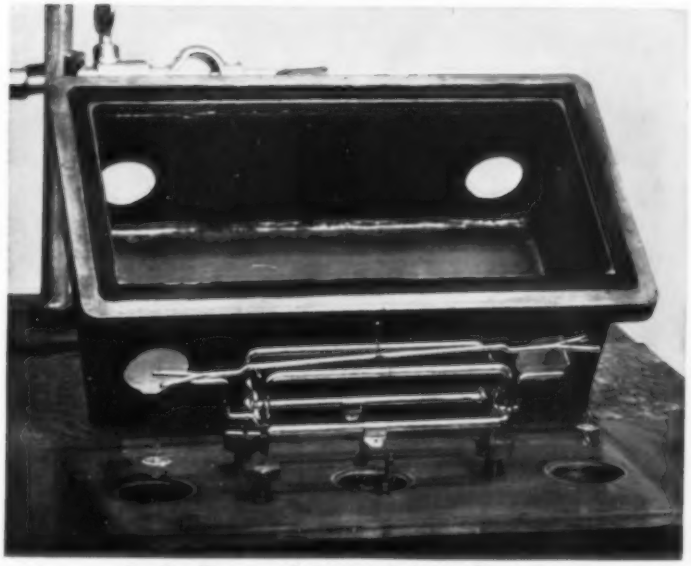

Fig. 2. Close-up of the microbalance. Easy access and viewing of the balance is permitted by removal of the brass box with flange and neoprene gasket, shown in the background.

(facing page 26)

Fig. 3. General view of furnace chamber, with balance and cathetometer mounted above.
(A) Copper wire shielding of platinum suspension.
(B) Magnetic damping of the balance.

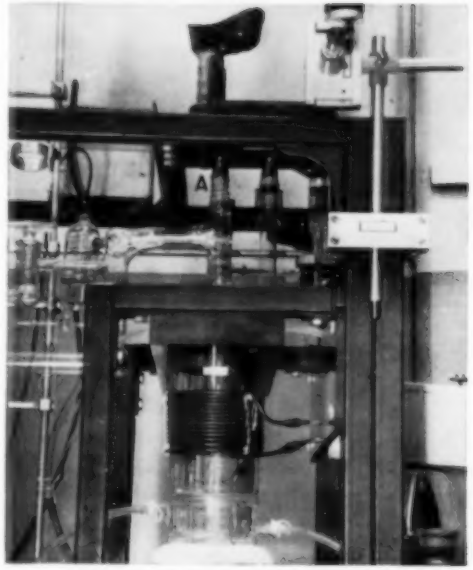

Fig. 4. Water-cooled copper concentrator used for heating small metal samples.

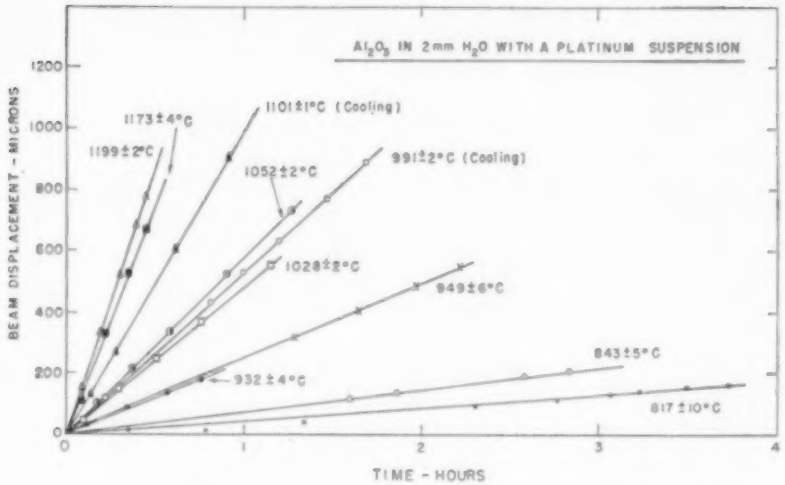

Fig. 5. Weight loss data for 0·002 in. dia. platinum wire suspending a sapphire single crystal in 2 mm H_2O atmosphere. Furnace temperatures were as given, but the wire was attacked most extensively outside the furnace (~2 in. length). Gradual withdrawal of the suspension from the furnace caused a twist in the wire to become exposed to atmosphere outside furnace; hence, the accelerated rate of weight loss for curves marked "cooling." Beam displacement corresponds to 0·377 μg weight loss/μ.

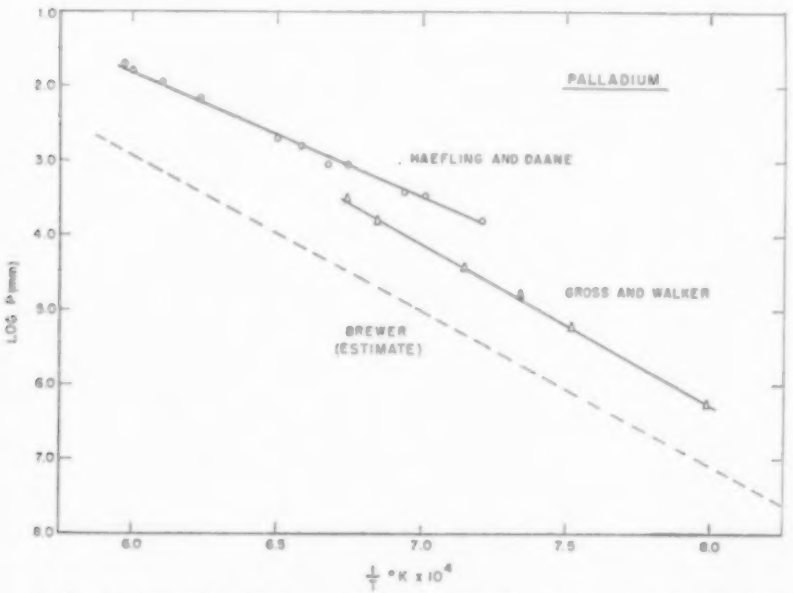

Fig. 6. Logarithm of the vapor pressure of palladium vs. reciprocal of absolute temperature compared with the experimental determination of Haefling and Daane and the estimated curve of Brewer.

after it had been removed from the high temperature apparatus. The weight-loss of the sapphire was negligible in comparison to the weight-loss of the platinum suspension. It was concluded that at temperatures up to 1600°C the rate of vaporization of the sapphire was not significantly greater than the rate attributable to vaporization *in vacuo*. The results were, therefore, in agreement with the results of Glemser and Volz[5], who were unable to detect a reaction between corundum and water vapor using a transpiration technique at temperatures up to 1700°C.

The evidence for the marked increase in the rate of vaporization of the platinum suspension is shown in Fig. 5. It is not possible to treat the data quantitatively, because the temperature of the suspension was not uniform over its reacted length. Furthermore, with gradual displacement of the balance beam the heated length of the suspension decreased. The data are not, however, in accord with any known reaction between platinum and water vapor. The observed reaction appeared to be associated with a convective stream of gas issuing from the furnace tube, because the platinum was most strongly attacked in this region. It is probable that a dissociation product of water vapor, perhaps ionized by the induction field, was one of the reactants.

Palladium. Vapor pressures calculated from the rate of vaporization of 99·9 per cent palladium rods are plotted in Fig. 6. The coefficient of evaporation is assumed to be unity. The data of Haefling and Daane, obtained with a Knudsen cell suspended from a microbalance[6] and the estimated curve of Brewer[7] are also shown in Fig. 6 for comparison purposes. The emissivity of palladium was taken as 0·33 at its melting point of 1828°K and was assumed to have a temperature dependence similar to that of platinum[8]. Heats of sublimation calculated from the slopes of the $\log p$ vs. $1/T$ plots are respectively 103, 80 and 94 kcal/mole for the present work, the data of Haefling and Daane, and the estimate of Brewer. However, using the free-energy functions of Stull and Sinke[9] values of ΔH°_{298} vary with the temperature of the experimental data for both sets of experimental measurements. Hence, unresolved systematic errors were involved in both investigations.

4. EXPERIMENTS WITH A SOLAR REFLECTOR

Studies of the rate of vaporization of aluminum oxide in aqueous atmospheres have been undertaken with a 60″ parabolic solar reflector, because of the ability to heat nonmetals by this method under well-defined chemical conditions. Accurate temperature measurements are very difficult to achieve, however; hence, the present studies were restricted to rates of vaporization of alumina in the region of its melting point.

In preliminary qualitative experiments a roughened sapphire disk was melted *in vacuo* in a spherical flask. Water vapor was then introduced into the flask up to a pressure of approximately 25 mm. The molten oxide was observed to "boil", then solidify almost immediately, and vaporize profusely. The flask was quickly covered with condensate which prevented further attainment of high temperatures.

An alternative procedure was, therefore, used, in which the spherical flask was filled with an inert gas. It was assumed that a boundary layer of gas above the heated surface was saturated with vapor. To a first approximation, it was further assumed that the rate of vaporization based on transport of vapor by a diffusion mechanism was proportional to the equilibrium partial pressure of the vapor.

A $\frac{1}{4}$ in. dia. rod of 99·9 per cent alumina was mounted in a cradle so that one end of the rod was just beyond the plane of the focal point of the solar reflector. The sample was contained in a pyrex flask. After evacuating the flask, the system was filled with appropriate pressures of water vapor and nitrogen. The nitrogen had been purified by passing over copper filings at 600°C, at which temperature the equilibrium oxygen pressure is calculated to be about 10^{-6} mm.

The end of the sample was slowly moved into the focus of the reflector and brought to its melting point. A molten drop was obtained having the same diameter as the rod.

The apparent temperature of the sample, $2055 \pm 10°C$, was not greatly affected by reflections from the sun into the pyrometer. The rate of vaporization was measured with a microbalance capable of ± 10 μg precision.

Results

In Table 2 are shown the weight loss rates, W, at various O_2 and H_2O pressures, together with estimated uncertainties. The uncertainty in the measurement of the oxygen pressure is about 10 per cent and of the water pressure less than 10 per cent except for the last two entries.

Table 2. Weight Loss Rate of Al_2O_3 in O_2-H_2O Atm

p_{O_2} (mm)	p_{H_2O} (mm)	W (μg/min)
0·92	24·9	0·81 ± 0·2
0·68	25·4	2·20 ± 0·2
0·35	24	4·14 ± 0·5
0·13	27·5	1·28 ± 0·15
0·38	3·03	1·78 ± 0·15
0·44	2·88	3·03 ± 0·6

In Table 3, the data is reduced to give the weight loss rates at a constant oxygen pressure of 0·40 mm and a constant water pressure of 24 mm. Small corrections have been applied by assuming $W \propto 1/\sqrt{p_{O_2}}$ or $\propto \sqrt{p_{H_2O}}$. In view of the fact that the corrections are small, the actual relation used is relatively unimportant as long as the direction of change is properly taken.

Table 3. Weight Loss Rate of Al_2O_3 in O_2-H_2O Atm

(mm) p_{O_2}	(mm) p_{H_2O}	W	Log p_{O_2}	Log p_{H_2O}	Log W
0·92	24	0·79	−0·036	—	−0·10
0·68	24	2·14	−0·167	—	0·33
0·35	24	4·14	−0·456	—	0·62
0·13	24	1·20	−0·89	—	0·08
0·4	3·03	1·74	—	0·482	0·241
0·4	2·88	3·17	—	0·459	0·501
0·4	24	3·87	—	1·380	0·59

By considering the equilibrium at the surface to be described by the reaction:

$$\tfrac{1}{2}Al_2O_3\,(l) + \frac{x}{2}H_2O\,(g) = AlO_yH_z\,(g) + \left(\frac{3}{4} + \frac{x}{4} - \frac{y}{2}\right)O_2\,(g)$$

an equilibrium constant, K, may be defined as

$$K = \frac{p_{(AlO_yH_z)} \cdot p_{O_2}^{\left(\frac{3}{4}+\frac{x}{4}-\frac{y}{2}\right)}}{p_{H_2O}^{\frac{x}{2}}}$$

This assumes that the Al_2O_3 (l) is in its standard reference state. The exponents of this relation may be found most conveniently by treatment of the log of the expression:

$$\log p_{(AlO_yH_z)} = \frac{x}{2}\log p_{(H_2O)} - \left(\frac{3}{4} + \frac{x}{4} - \frac{y}{2}\right)\log p_{O_2} + \log K - \log k.$$

If it is assumed that $p_{(AlO_yH_z)} = k \cdot W$, then:

$$\log W = \frac{x}{2}\log p_{H_2O} - \left(\frac{3}{4} + \frac{x}{4} - \frac{y}{2}\right)\log p_{O_2} + \log K - \log k$$

One may then evaluate $x/2$, since it is the slope of a $\log W$ vs. $\log p_{H_2O}$ plot at constant p_{O_2}. Likewise one may find $\left(\frac{3}{4}+\frac{x}{4}-\frac{y}{2}\right)$ from a plot of $\log W$ vs. $\log p_{O_2}$ at constant p_{H_2O}. With x evaluated previously, y may then be computed. In Figs. 7 and 8 are shown the experimental points with their expected uncertainties. On these plots are also shown the theoretical slopes of $\frac{1}{2}$ and $-\frac{1}{2}$, which correspond to x and y equal to one.

The point in Fig. 7 which is well above the drawn line could be explained partly in terms of a lack of adsorbed water in the sample after heating. Inasmuch as nearly 10 days were required for a dry sample to reach equilibrium with the air in the constant temperature and humidity room containing the balance and since this sample was weighed after only 4 days, one might expect a high result. In the other instance the weights were measured over several days to insure attainment of equilibrium.

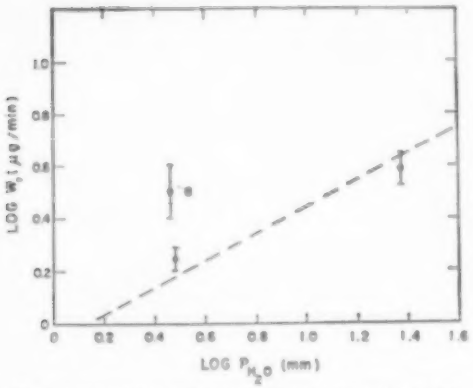

Fig. 7. Logarithm of the weight loss rate of Al_2O_3 (l) vs. logarithm of H_2O pressure at 2055 ± 10°C and 0-40 mm oxygen pressure. (a) Sample weighed before attaining equilibrium with atmosphere of balance room.

There are two points in Fig. 8 considerably below the constructed line. These could arise as a result of an air leak, which would inhibit volatilization. This is not unlikely because only 1 mm of oxygen would be needed to cause the largest observed effect.

Although there is a considerable amount of uncertainty in the conclusion because of some inconsistent data, there is a possibility that the vaporized molecule over Al_2O_3 (l) in the presence of H_2O (g) is AlOH (g). However, the measured values should be repeated until the statistical weight of the discrepancies can be eliminated.

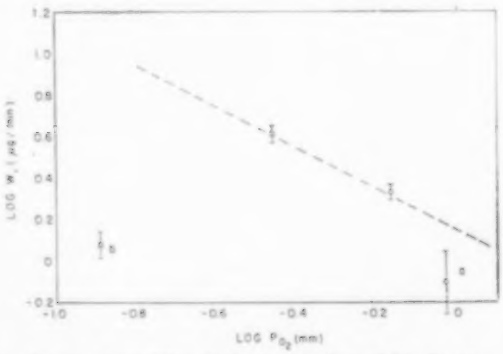

Fig. 8. Logarithm of the weight loss of Al_2O_3 (l) vs. logarithm of O_2 pressure at 2055 ± 10°C and 24 mm water vapor pressure. (a) Low sample weight loss, thus lower precision, (b) a 1-mm O_2 leak could have produced this lowering.

DISCUSSION

C. E. MAY: A recent report indicates that Brewer's work on Al_2O_3 may be in error. The vapor pressures given by him are probably too high and the true-valued curve might give better agreement with the present work.

J. EFIMENKO: It should be noted that Brewer and Searcy's data are on liquid alumina, while our data are on solid alumina. The extrapolation made for comparison purposes is very long and uncertain. For a more accurate comparison the heat of fusion of alumina should be included in the vapor pressure curve.

We feel that our data may need correction due to a possible reaction with platinum vapor. The extent to which Brewer and Searcy's data should also be corrected for the reaction between alumina and their tungsten Knudsen cell is uncertain. It is hoped that corrections for the reaction of alumina with tungsten can be made when the detailed mass spectrometric data of G. DeMaria, J. Drowart and M. Inghram at the University of Chicago are published. We are contemplating further work on the systems of alumina with platinum, tungsten, rhenium and molybdenum.

Acknowledgement—The able assistance of Mrs. Lucy M. Gross in determining the vapor pressure of palladium is gratefully acknowledged.

REFERENCES

1. R. S. BRADLEY, *Proc. Roy. Soc.* A**205**, 553 (1951).
2. E. A. GULBRANSEN, *Trans. Electrochem. Soc.* **81**, 327 (1942).
3. H. A. JONES, I. LANGMUIR and G. M. J. MACKAY, *Phys. Rev.* **30**, 211 (1927).
4. L. BREWER and A. W. SEARCY, *J. Amer. Chem. Soc.* **73**, 5308 (1951).
5. O. GLEMSER and H. G. VOLZ, repored at *Third International Conference on Reactivity of Solids, Madrid, April 1956.*
6. J. F. HAEFLING and A. H. DAANE, *Trans. Amer. Inst. Min. (Metall.) Engrs.* **212**, 115 (1958).
7. L. BREWER, in *The Chemistry and Metallurgy of Miscellaneous Materials* (edited by L. L. QUILL). McGraw-Hill, New York (1950).
8. R. E. STEPHENS, *J. Opt. Soc. Amer.* **29**, 158 (1939).
9. D. R. STULL and G. C. SINKE, *Thermodynamic Properties of the Elements.* American Chemical Society, Washington, D.C. (1956).

AN INVESTIGATION OF THE EFFECTS OF GASEOUS DIFFUSION ON THE RATE OF OXIDATION OF A METAL FORMING A VOLATILE OXIDE

D. R. SCHRYER and J. L. MODISETTE
NASA Langley Research Center, Langley Field, Virginia

Abstract—Data taken in flowing air and helium-oxygen mixtures have shown the oxidation rate of molybdenum to be dependent both on flow velocity and diffusivity in the temperature range 1945°–2959°R. An extension of the Arrhenius equation to include flow and diffusion effects was found to correlate the data quite well for temperatures above 2400°R, at which the oxide formed was gaseous. The results obtained for molybdenum should be applicable to other metals forming volatile oxides in the appropriate temperature ranges.

Molybdenum, tungsten, tantalum and niobium form a group of metals of particular interest in the field of high-speed, high-temperature flight. Each of these metals has its melting point above 4000°R and has acceptable strength properties at temperatures considerably above the limits of the commonly used iron–nickle–chromium–cobalt alloys. Unfortunately, each of these metals is subject to oxidation at elevated temperatures. The rate of the oxidation increases with temperature until it becomes so severe as to render the metal unfit for use even in relatively short-lived expendable structures at temperatures considerably below the useful limit as determined by strength considerations alone.

Since the metals under consideration possess such potential as high-temperature structural materials and since the need for such materials is so critical, much effort has been devoted to coping with the problem of oxidation. The present investigation began as one phase of this effort—specifically, an attempt to determine the nature and extent of the oxidation.

The oxidation of the metals under consideration is anomalous compared to the great majority of metals. Most metals form oxides which are solid at all temperatures below the melting point of the metal. The solid oxide then serves as a more-or-less protective coating through which, effectively, oxygen must diffuse in order for further oxidation to occur. The rate of diffusion of the oxygen through the solid oxide to the metal surface is usually so slow compared to any other steps involved that it is the sole rate-controlling factor.

However, molybdenum, tungsten, tantalum and niobium form oxides whose melting and boiling points lie below the melting point of the parent metal. It is to be expected that a liquid or, especially, a gaseous oxide would not afford the same measure of protection to a metal surface as a solid one, so that the oxidation mechanism involved under such circumstances need not at all be the normal one. In particular, at temperatures sufficiently high that the oxide vaporizes as rapidly as it is formed the metal surface would be essentially unprotected and vulnerable to direct attack by oxygen. In such a case the rate of oxidation would be a function of the concentration of oxygen in the gas just adjacent to the surface. But reaction of oxygen with the metal would tend to decrease its concentration in this region. If the reaction proceeded rapidly enough the depletion of oxygen would become significant and transport of fresh quantities of oxygen to the surface would become a rate-controlling factor.

The rate of transport of oxygen to the metal surface would be a function of the diffusivity of the oxygen in the gas mixture and, if the gas were flowing over the surface, of the flow velocity as well. In order to determine whether or not the two factors, flow velocity and

diffusivity, in actuality, do affect the rate of oxidation of a metal forming a volatile oxide a series of experiments were performed. The metal chosen as the subject of these experiments was molybdenum because its oxide volatilizes at temperatures conducive to laboratory investigation.

The experimental technique employed was to oxidize the specimens in a flowing gas stream taking weighings every 10–20 sec. During any given run gas composition, mass flow rate and temperature were maintained constant.

Fig. 1 shows the experimental facility employed which consisted essentially of a vertical tube furnace into which the molybdenum specimens were suspended by a platinum wire from the weighing arm of a torsion balance. The balance was situated on top of a water-cooled jacket placed between it and the furnace. The balance has a sensitivity of 0·1 mg.

Temperature was measured by a platinum, platinum–rhodium thermocouple placed immediately below the test specimen.

The specimens were sheared from 0·01 in. sintered molybdenum and were approximately 0·5 in. by 1 in. The molybdenum used for all tests reported herein was commercially pure. No analysis of the impurities present was available. A few tests were made with arc-cast molybdenum which was known to have about an order of magnitude more impurities than the sintered molybdenum but no difference was found in the oxidation rate. The specimens were not cleaned or treated in any way prior to testing.

The gas mixtures were introduced at the top of the tube through a perforated nozzle. Calculations showed the maximum Reynolds number in the tube to be 150 based on the tube diameter which was 1 in. and therefore the flow was assumed to be laminar. The gases were obtained from commercial cylinders and were metered by flowmeters.

The effect of flow rate on the oxidation rate was determined by carrying out three series of runs, all covering approximately the same temperature range, the mass flow rate being held constant for all the runs within a given series but being varied among the different series. The gas used for all three series was air.

Fig. 2 shows the results of the tests. This figure contains three curves, each representing a plot of the weight-loss rate or oxidation rate in lb-ft^{-2}-sec^{-1} vs. temperature in °R for one of the series of runs. For convenience and clarity, the mass flow rates have been expressed as flow velocities in ft-sec^{-1}. Since for a given mass flow rate the flow velocity is a function of temperature, the three values have been presented for a common temperature: 2600°R.

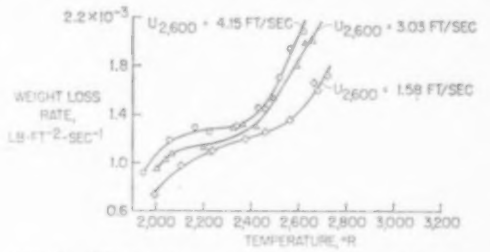

Fig. 2. Effect of flow velocity on rate of oxidation of molybdenum (air).

It can be seen from a comparison of the plots that the oxidation rate is not a constant at a given temperature but increases with increasing flow velocity.

It is of interest to note that three different oxidation regimes seem to exist for molybdenum with transition temperatures between the regimes at about 2100°R and 2400°R. These temperatures correspond roughly to the melting and boiling points of the trioxide which are 1922°R and 2560°R, respectively. We are primarily concerned with the upper regime where the oxide is entirely gaseous.

The effect of a variation in the diffusivity of the oxygen in the gas mixture on the oxidation rate was determined by utilizing mixtures of oxygen and helium in addition to air, which is essentially a mixture of oxygen and nitrogen. The diffusivity of oxygen in an oxygen–helium mixture is greater than in an oxygen–nitrogen mixture of the same relative composition.

Fig. 3 shows two plots of weight loss rate or oxidation rate in lb-ft^{-2}-sec^{-1} vs. temperature in °R. The two plots represent roughly equal flow velocities but different gas com-

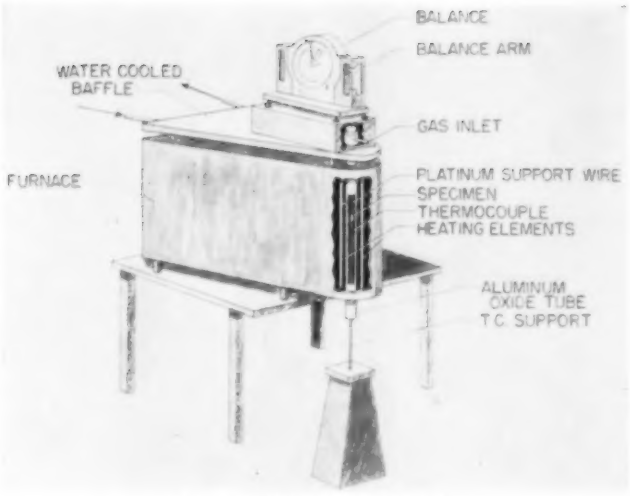

Fig. 1. Diagram of apparatus.

(facing page 32)

positions and, consequently, different diffusivities. The one gas was air and the other an oxygen–helium substitute of the same relative composition and about twice the diffusivity. It can be seen that at any given temperature the oxidation rate is greater for the oxygen–helium mixture.

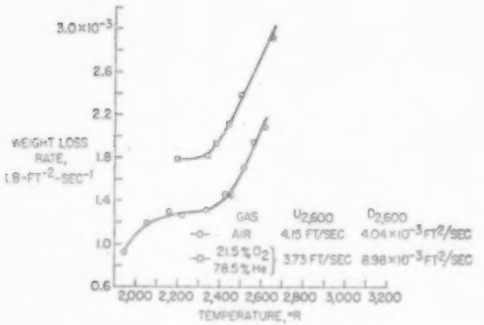

Fig. 3. Effect of diffusivity on rate of oxidation of molybdenum.

It is apparent from the data presented in Figs. 2 and 3 that the rate of oxidation of molybdenum in the temperature range considered is not constant at a given temperature but increases with increasing flow velocity and diffusivity, thus establishing that, in fact, gaseous transport of oxygen is a rate-controlling factor in the oxidation of a metal forming a volatile oxide.

A logical next step in the analysis of the experimental data for the oxidation of molybdenum is the determination of the activation energy. Activation energies are usually determined by means of the Arrhenius plot of $\ln k$ vs. $-1/RT$. A series of such plots for each of the regimes of the various experimental series were made and the values obtained for the activation energy from the plots are presented in Table 1. Within any given series there was found to be a sharp discontinuity in the slope of the Arrhenius plot, and consequently in the value of the activation energy obtained, between regimes. The values obtained for the middle regime are quite low and their physical significance is somewhat questionable. The magnitude of the variation among the different series of the values for each of the upper two regimes is rather large. Unquestionably, the results of the Arrhenius plots are rather disappointing and somewhat anomalous.

The anomalies of the results of the Arrhenius plot method are not so disconcerting if one recognizes the possibility that the Arrhenius equation from which the method is derived is not applicable to gaseous diffusion controlled reactions without suitable modifications being made.

The general nature of such modifications can be seen from an examination of the equation

$$k = A \exp(-E_a/RT) \qquad (1)$$

The right side of the equation may be thought of as the product of a physical factor, A—which is essentially the rate of collision of the reacting molecules—and a chemical factor,

Table 1. Activation Energy Values from Arrhenius Plots

Gas composition	U_{2600} (ft/sec)	E_a from Arrhenius Plot (B.t.u./lb-mole)		
		1900°–2100°R	2100°–2400°R	2400°–3000°R
Air	1·58	$22{\cdot}1\times10^3$	$7{\cdot}38\times10^3$	$20{\cdot}2\times10^3$
	3·03	$18{\cdot}1\times10^3$	$6{\cdot}64\times10^3$	$24{\cdot}3\times10^3$
	4·15	$19{\cdot}4\times10^3$	$5{\cdot}73\times10^3$	$29{\cdot}7\times10^3$
21·5% O_2 – 78·5% He	3·73		$3{\cdot}7\times10^3$	$19{\cdot}7\times10^3$
13·6% O_2 – 86·4% He	5·76			$31{\cdot}2\times10^3$
Mean value of E_a		$19{\cdot}9\times10^3$	$5{\cdot}88\times10^3$	$25{\cdot}0\times10^3$
Mean deviation		7·5%	19·2%	17·4%

$\exp(-E_a/RT)$—which is essentially the fraction of the collisions sufficiently energetic to result in reaction. The basic principles of activated reactions should still apply to the special case under consideration so the factor $\exp(-E_a/RT)$ will be retained unaltered. The factor A, however, warrants closer scrutiny. From the kinetic theory of gases the collision rate is given as

$$A = C_0 \frac{\bar{V}}{4} \tag{2}$$

The concentration of oxygen at any point is normally inversely proportional to the temperature. Since $\bar{V} \propto T^{1/2}$ then $A \propto 1/T^{1/2}$ and hence A is only a slowly varying function of temperature. On a logarithmic plot the variation of A with temperature would not be significant over reasonable temperature ranges. This makes possible the simplicity of the Arrhenius plot method of determining activation energies. However, as has already been demonstrated, the oxidation of a metal forming a volatile oxide may proceed rapidly enough to cause a depletion of the oxygen supply at the surface and hence C_0 may become a function the reaction rate and, through it, of the flow velocity and diffusivity. For such a case the factor A could no longer be safely regarded as a constant. In fact, it will now be demonstrated that the derivation of a rate equation applicable to the case under consideration results in a somewhat more elaborate expression for A which accounts for the effects of flow velocity and diffusivity.

The flow of a gas stream over a metal surface gives rise to an aerodynamic boundary layer. If the gas contains oxygen which is consumed at the surface there will also develop a concentration gradient and a concentration boundary layer. Assuming that the concentration gradient at the surface is proportional to the average gradient through the concentration boundary layer

$$\left(\frac{\partial C}{\partial y}\right)_0 = P_1 \left(\frac{C_\infty - C_0}{\delta_c}\right) \tag{3}$$

It will be further assumed that the concentration boundary layer is proportional to the aerodynamic velocity boundary layer:

$$\delta_c = P_2 \delta \tag{4}$$

Therefore

$$\left(\frac{\partial C}{\partial y}\right)_0 = \frac{P_1}{P_2}\left(\frac{C_\infty - C_0}{\delta}\right) = P\left(\frac{C_\infty - C_0}{\delta}\right) \tag{5}$$

If the oxide volatilizes as rapidly as it is formed, the oxidation rate will be very nearly equal to the rate at which oxygen diffuses through the gas to the surface so that

$$k \cong D\left(\frac{\partial C}{\partial y}\right)_0 \tag{6}$$

Combining equations (5) and (6)

$$k = DP\left(\frac{C_\infty - C_0}{\delta}\right) \tag{7}$$

The general form of the Arrhenius equation will be retained

$$k = A \exp(-E_a/RT) = \frac{C_0 \bar{V}}{4} \exp(-E_a/RT) \tag{8}$$

The common unknown C_0 may be eliminated between equations (7) and (8) yielding a new rate equation which should be applicable to the oxidation of a metal forming a gaseous oxide.

$$k = \left[\frac{PD}{\delta} \cdot \frac{\bar{V} C_\infty}{4} \Big/ \frac{\bar{V}}{4} \exp(-E_a/RT) + \frac{PD}{\delta}\right] \exp(-E_a/RT) \tag{9}$$

This equation and its derivation is similar to the work of Carpenter of England except for the inclusion of the concept of an activated reaction.

From a comparison of equations (1) and (9) it is obvious that

$$A = \frac{PD}{\delta} \cdot \frac{\bar{V} C_\infty}{4} \Big/ \frac{\bar{V}}{4} \exp(-E_a/RT) + \frac{PD}{\delta} \tag{10}$$

Although the flow velocity does not appear explicitly in this expression it appears implicitly through the aerodynamic boundary-layer thickness the expression for which is

$$\delta = 5\left(\frac{\mu x}{\rho U_\infty}\right)^{\frac{1}{2}} \tag{11}$$

Some insight into the physical significance

of the various terms in equation (9) may be gained by considering two limiting cases. If $\bar{V}/4\exp(-E_a/RT) \gg (PD)/\delta$ then $k \cong (PDC_\infty)/\delta$. This would represent a case where the rate of transport of oxygen molecules to the surface is so much slower than their reaction once there as to be the sole rate-controlling factor.

The second limiting case would occur if $\bar{V}/4\exp(-E_a/RT) \ll (PD)/\delta$. For this case $k \cong (C_\infty \bar{V})/4\exp(-E_a/RT)$. This is effectively the unmodified Arrhenius equation. This corresponds physically to the case where the transport of oxygen to the surface is so much faster than reaction can occur that it has no appreciable effect on the oxidation rate.

It would be convenient if all cases encountered in actual practice could be treated as one or the other limiting case but, of course, this is not possible. However, the ratio of the terms $\bar{V}/4\exp(-E_a/RT)$ and PD/δ does afford a useful criterion for determining when such simplifications may be made and when the full equation should be used.

Actually, the new rate equation cannot be applied directly to the experimental data obtained for molybdenum because it is applicable only to a point on a surface, since it contains the aerodynamic boundary-layer thickness, a parameter which varies from point to point on a given surface. Consequently, a specialized form of the new rate equation expressing the average oxidation rate of a thin flat plate is needed. Such an equation has been obtained by introducing the expression for the aerodynamic velocity boundary-layer thickness at a given point and then integrating over the surface of the plate. It is

$$k = 2PD \Big/ 5\left(\frac{\mu l}{\rho U_\infty}\right)^{1/2} \times$$
$$\times \left\{1 - 4PD \Big/ 5\left(\frac{\mu l}{\rho U_\infty}\right)^{1/2} V \exp(-E_a/RT) \ln \times \right.$$
$$\left. \times \left[1 + 5\left(\frac{\mu l}{\rho U_\infty}\right)^{1/2} V \exp(-E_a/RT) \Big/ 4PD\right]\right\} \tag{12}$$

This equation has been used to determine the activation energy for the oxidation of molybdenum. All the factors in the equation are known except P and E_a. Substitution of the values of the various factors at two different temperatures in the upper regime of each series of experimental runs yielded a pair of equations in P and E_a for each series. Each of the pairs of equations was then solved for P and E_a. The values of E_a obtained are given in Table 2. As can be seen they agree quite well among themselves with a mean deviation from the average of 3·6 per cent. This is in contrast to the deviation of 17·4 per cent among the values obtained from the Arrhenius plots.

It is of interest to note that as the flow rate increases among the three air series the Arrhenius plot values tend to approach the

Table 2. Comparison of Activation Energy Values (2400° R – 3000°R)

Gas composition	U_{3000} (ft/sec)	E_a from new rate equation (B.t.u./lb-mole)	E_a from Arrhenius plot (B.t.u./lb-mole)
Air	1·58	$36{\cdot}7\times10^3$	$20{\cdot}2\times10^3$
	3·03	$38{\cdot}7\times10^3$	$24{\cdot}3\times10^3$
	4·15	$39{\cdot}4\times10^3$	$29{\cdot}7\times10^3$
21·5% O_2–78·5% He	3·73	$36{\cdot}6\times10^3$	$19{\cdot}7\times10^3$
13·6% O_2–86·4% He	5·76	$40{\cdot}3\times10^3$	$31{\cdot}2\times10^3$
Mean value of E_a		$38{\cdot}3\times10^3$	$25{\cdot}0\times10^3$
Mean deviation		3·6%	17·4%

average value obtained from the new rate equation. This is consistent with the theoretical picture presented. As the flow rate increases the transport of oxygen to the surface should increase and the concentration of oxygen in the region just adjacent to the surface should approach the free-stream value. This would tend toward one of the limiting cases which we have already considered, namely, the one where gaseous transport of oxygen to the surface is sufficiently great as to exert no limitation on the oxidation rate, a case for which the unmodified Arrhenius equation should apply and give correct values for the activation energy. However, for circumstances where gaseous transport is not rapid enough and does affect the oxidation rate this effect is not taken into account by the unmodified Arrhenius equation and hence this equation cannot be expected to give correct values for the activation energy.

In addition to yielding self-consistent values for the activation energy the new rate equation is capable of correlating the experimental data obtained for molybdenum in the upper oxidation regime.

For example, comparing the upper two curves of Fig. 2 it can be seen that a 37 per cent increase in flow velocity produces an 8 per cent increase in oxidation rate at the same temperature. A 9 per cent increase is predicted by equation (12), the form of the new rate equation applicable to the data.

A comparison of the two curves in Fig. 3 shows that a 110 per cent increase in diffusivity produces a 38 per cent increase in oxidation rate. Equation (12) predicts a 44 per cent increase.

In general, the results of this study may be summarized in the statement that gaseous transport of oxygen to the surface of a metal which is oxidizing at temperatures at which its oxide is volatile can have a very significant effect on the rate of oxidation and failure to take this effect into consideration can bring about anomalous and even erroneous results.

DISCUSSION

C. TALLEY: I would like to point out for consideration that the important diffusing species may be the metal oxide rather than oxygen if the conditions are such that some oxide phase remains on the oxidizing metal surface. In this case, the rate limiting step could be the net evaporation rate of the oxide phase which would control the thickness of the protective oxide phase, and hence the oxidation rate.

D. SCHRYER: This is quite possible; this is why we have applied our theoretical work only to the temperature régime at which the oxide is completely volatized.

I. AMDUR: How sensitive are the calculated values of E_d to numerical values of the diffusion coefficient D?

D. SCHRYER: We have not checked this point.

I. AMDUR: How did you calculate numerical values of D?

D. SCHRYER: From a standard handbook formula.

I. AMDUR: The calculation of high temperature diffusion coefficients should be done with care. For example, errors as high as 50 per cent are possible if values are obtained by extrapolation from low temperatures.

D. SCHRYER: We believe that *relative* values of E_d would be essentially unchanged by errors in numerical values of D.

D. E. ROSNER: The data presented here reveal the fact that there is no single choice of "activation energy" characterizing the observed temperature dependence of the rate of oxidation. Thus, even if the time interfacial kinetics follow an Arrhenius type rate equation, owing to the effects of additional processes, the *observed* kinetics do not. One can recover the "true" activation energy of the interfacial reaction only if the temperature coefficient of these additional processes is estimated. This seems to have been attempted here. In the present case, however, it is not clear how the proposed mechanism of reactant diffusion to the surface followed by surface reaction alone can lead to a temperature coefficient which is not a monotonic function of the surface temperature. In connection with this, it is perhaps interesting to note that, for first order surface reactions, there is a special case for which the *observed* local kinetics can vary exponentially with the surface

temperature even in the presence of diffusion. This would be realized if the temperature dependence of the true reaction velocity and the diffusion velocity were each characterized by the *same* "activation energy". Of course, for gaseous systems, this is never encountered. Yet, this case is curious in that, upon examination of such data, one would be tempted to conclude that diffusion effects were absent!

Finally, I should like to call attention to the fact that generalizations of the Arrhenius rate law accounting for the effects of diffusion, date as far back as 1913. In that year Heymann outlined the basic method. About three decades later, the Russian investigator, D. A. Frank-Kamenetzkii elaborated upon this work, giving applications to flow systems. However, pitfalls arise in the straightforward application of this "quasistationary" method to diffusion layers developing on chemically active surfaces. These are due to the fact that the diffusional transfer coefficient itself is affected by the streamwise history of the chemical reaction. This problem has, in fact, been the subject of several recent theoretical papers in the chemical and aeronautical engineering literature.

D SCHRYER: It is quite true that our new rate equation, equation (12), is monotonic with respect to temperature and therefore cannot describe an oxidation rate which is not a monotonic function of temperature. It is also true that, considered over the entire temperature range for which we obtained data, the rate of oxidation of molybdenum is not a monotonic function of temperature under the conditions of flow rate, diffusivity, and oxygen concentration which we covered. However, at temperatures above about 2400°R the oxidation rate is a monotonic function of temperature and I must emphasize again that it is only at such temperatures that our theoretical treatment is meant to apply.

NITROGEN ATOM RECOMBINATION ON SURFACES

G. M. PROK
NASA Lewis Research Center, Cleveland, Ohio

Abstract—The efficiencies with which platinum, lithium chloride and lead monoxide surfaces catalyse the recombination of nitrogen atoms were determined. Energy due to nitrogen atom recombination was measured using commercial glass-bead thermistors placed in the stream of nitrogen atoms. Thermistors were coated with each of the test materials by vacuum evaporation. In addition, lithium chloride was coated on a thermistor by crystallization from a saturated solution. The total number of nitrogen atoms reaching the vicinity of the thermistor probes was determined by a gas titration using the reaction of nitrogen atoms with nitric oxide. The atoms were generated in a 1 in. diameter quartz tube by an electrodeless discharge at a pressure of 0·3 mm of mercury. The discharge was produced with a 125 W microwave diathermy generator, which has a frequency of 2450 Mc/sec.

Of the three test surface materials, lead monoxide was the best catalyst. Platinum was found to poison upon standing; however, several hours of atom bombardment would "clean up" this poisoning. Slightly more than 1 hr of atom bombardment of the lithium chloride surface was needed to remove water and to obtain a constant recombination coefficient. The results obtained are compared with those reported for oxygen in the recent literature.

1. INTRODUCTION

With the advent of the space age, increased interest has been shown in flight in the upper atmosphere. The gases of the upper atmosphere of the earth are partially dissociated due to solar radiation. The degree to which the dissociated gas recombines on the surface of a vehicle flying through these regions is important in heat-transfer and flow considerations. For example, a re-entering satellite can possibly use a noncatalytic surface to reduce the heat-transfer rates in continuum flow at low densities[1]. The recombination process is generally characterized by the heterogeneous recombination coefficient, which is defined as the ratio of the number of atoms recombining on the surface to the number of atoms striking the surface. The recombination coefficients of the various gases known to be in the atmosphere can also be used for upper atmosphere research. Work of this type is being done by sending catalytic surfaces into the upper atmosphere with balloons[2]. Surface recombination data may also be important in engine exhaust-nozzle design in which dissociated gases are present in the exhaust gases.

To date, most of the recombination work with gaseous atoms on surfaces has been with hydrogen and oxygen atoms. Some of the more recent work with hydrogen has been done by Katz *et al.*[3] and Wise *et al.*[4]. The history of work on oxygen recombination is not nearly as extensive as that for hydrogen, most of the work being done at the University of Oxford by J. W. Linnett *et al.*[5–7], beginning in 1955. Some work on oxygen recombination is also being done at the University of California[8]. Nitrogen atom recombination data are not as plentiful as those for hydrogen and oxygen; available data are mainly from the work of Roginsky and Schlechter[9].

This paper is concerned with measurement of the coefficients for nitrogen atom recombination on several types of surface. Three different test materials were used, namely: (1) a metal, platinum; (2) a salt, lithium chloride, and (3) an oxide, lead monoxide. These results are compared with those reported for oxygen atoms in the recent literature.

2. APPARATUS

A schematic drawing of the apparatus used for determining the heterogeneous recom-

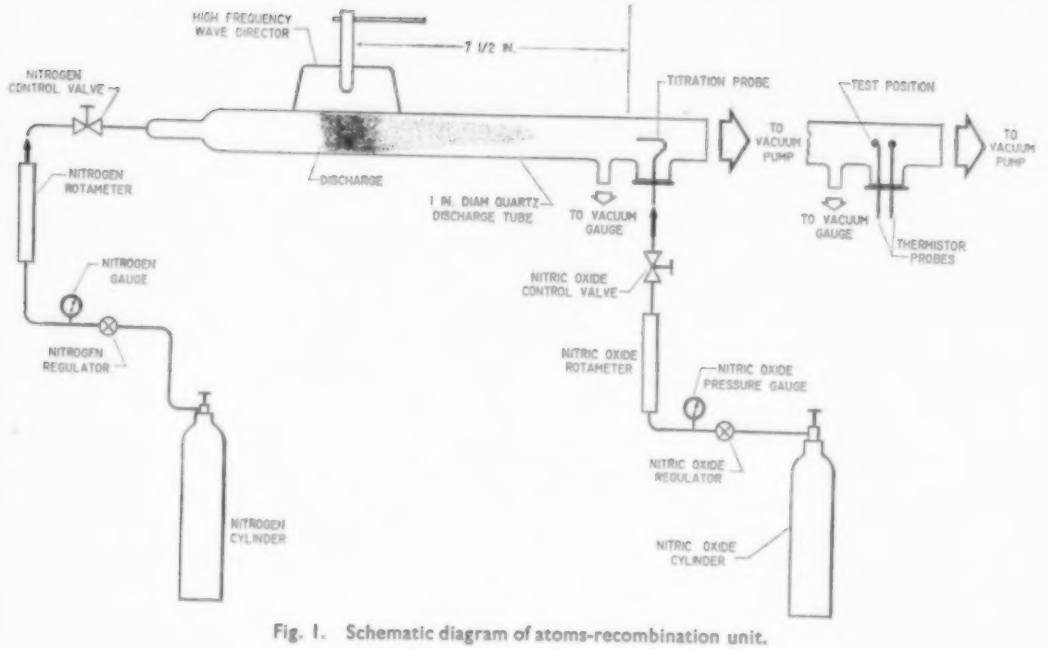

Fig. 1. Schematic diagram of atoms-recombination unit.

bination coefficient of various gases is shown in Fig. 1. The discharge tube was 14 in. long and was made of 1 in. O.D. quartz tubing. A 2450 Mc/sec, 125 W, variable power, microwave diathermy generator was used to produce the high-frequency discharge. With this diathermy generator, a vacuum spark tester was needed to initiate the discharge. The center of the discharge director was located 8 in. upstream of the probes. Water-pumped nitrogen, the gas used throughout the work, was metered by a small rotameter, flowed through the discharge and evacuated from the discharge tube by a 300 ft^3/min rotary piston vacuum pump. All glass-to-metal connections in the system were O-ring sealed.

The nitric oxide used in a gas titration was supplied from a gas cylinder and metered with a small rotameter (Fig. 1). A custom built, stainless steel, capillary-type valve was used for controlling the flow of the nitric oxide. The titration probe was made from a hypodermic needle. It was positioned at the axis of the discharge tube and directed into the main gas stream as shown in Fig. 1.

Two commercial, glass-bead thermistors, one coated and the other uncoated, were used to measure recombination heat transfer. These thermistor probes replaced the titration probe after the gas titration was completed. In Fig. 1, the section of discharge tube to the right of the main figure shows schematically the general location of the thermistor probes. The probe holder was easily rotated for proper location of each probe during a measurement. A modified Wheatstone Bridge circuit, which is

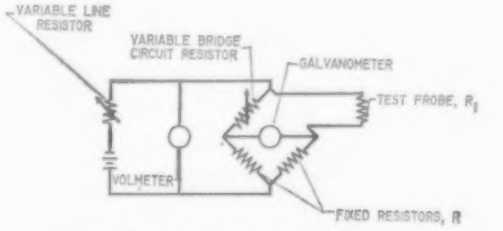

Fig. 2. Modified Wheatstone Bridge circuit.

shown schematically in Fig. 2, was used for measuring the resistance of and the power

through each thermistor. The power measurement was actually indirectly determined from the voltage across the bridge and the thermistor resistance. The bridge was balanced either by varying the current through the bridge, and thus the thermistor resistance, or with the variable resistance in the bridge. The themistor resistance is actually a measure of temperature as shown in Fig. 3 by a typical thermistor resistance–temperature curve.

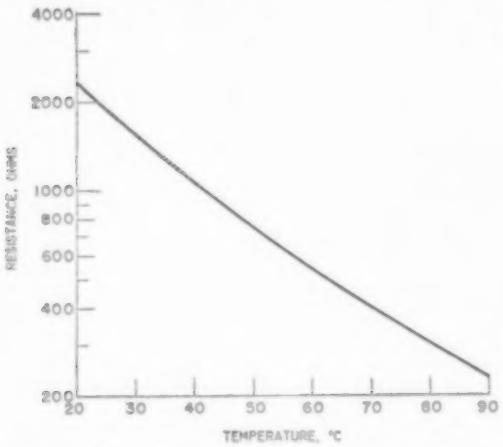

Fig. 3. Thermistor resistance–temperature curve.

The pressure in the discharge tube was measured with a Pirani type vacuum gage, which was calibrated against a McLeod gage.

3. PROCEDURE

Before each test, the proper probe was positioned and the entire system was evacuated and checked for leaks. After the system was vacuum tight, the nitrogen flow was adjusted to give the flow conditions listed in Table 1. The nitrogen rotameter range and the thermistors governed the selection of the flow conditions.

Table 1. Test Conditions

Nitrogen flow rate (g/min)	0·248
Discharge tube pressure (mm hg)	0·29
Nitrogen velocity (cm/sec)	1740
Temperature range of surfaces (°C)	47–81
Discharge tube cross-sectional area (cm^2)	5·71

For the present program no attempt was made to vary the flow conditions.

Titration of nitrogen atoms

One of the most important steps in determining the recombination coefficient of a dissociated gas on a surface is to measure the number of atoms in the gas at the position of the test surface. For dissociated nitrogen, the number of nitrogen atoms in the stream can be determined by a gas titration using nitric oxide[10]. When nitric oxide is added to a stream of nitrogen and nitrogen atoms, the following rapid reaction occurs:

$$NO + N \rightarrow N_2 + 0 \qquad (1)$$

With excess nitric oxide, a whitish afterglow will appear according to the following reaction:

$$NO + O \rightarrow NO_2 + h\nu \text{ (continuum)} \qquad (2)$$

With this gas titration as a tool for determining the number of nitrogen atoms, a titration probe was placed into the system, as shown in Fig. 1. After test conditions were obtained and measured, the discharge was initiated and the gas titration was performed. Only the power of the high-frequency generator was varied between titrations. Table 2 gives the data and results of the gas titration. Between the power limits of the diathermy generator, the number of nitrogen atoms reaching the vicinity of the probes varied between 2·5–3·4 per cent of the gas stream. The gas titration results were reproducible within 10 per cent.

Table 2. Gas Titration Data Results

Diathermy generator output (W)	Nitric oxide flow rate at end point (g/min)	Number of atoms reaching the vicinity of the probes (N-atoms/cm^2/sec)	Atoms in the stream reaching the vicinity of the probes (%)
37·5	0·0133	$0{\cdot}781 \times 10^{20}$	2·50
62·5	0·0151	$0{\cdot}888 \times 10^{20}$	2·84
87·5	0·0166	$0{\cdot}977 \times 10^{20}$	3·13
125	0·0181	$1{\cdot}060 \times 10^{20}$	3·40

Recombination heat measurements

Following the determination of the number of nitrogen atoms reaching the vicinity of the probe position, the number of atoms recombining on the various test surfaces was determined. The initial step was to replace the titration probe and probe holder with the thermistor holder containing two uncoated, glass-bead thermistors (Fig. 1). Since glass is almost noncatalytic[11], convective heat was measured with the uncoated glass-bead thermistors that was used as the test thermistor. The other uncoated thermistor was used as a reference. A measurement with a thermistor was made only when it was in the test position, obtained by rotating the thermistor holder. The test position, as shown in Fig. 1, is the upstream location with the thermistor at the discharge tube axis. With the proper flow conditions and the discharge off, the power required to hold each thermistor at a series of given temperatures was measured with a bridge circuit, which is schematically shown in Fig. 2. Then the discharge was turned on and, at various power settings of the diathermy generator, the power required to maintain various given temperatures with each thermistor was measured. At any given temperature for the uncoated thermistors, the difference between the power required with the discharge off and on is the increase in the convective heat input.

After this increase in convective heat transfer was determined, the test thermistor probe was removed and the bead of that thermistor was coated with one of the test surfaces. All test surfaces were vacuum evaporated on the thermistor bead except in one series of tests in which lithium chloride was crystallized from a saturated solution on to the test thermistor bead. When the test probe was properly coated with one of the test materials, it was replaced in the thermistor holder, and again the power required to maintain each thermistor probe at various given temperatures with the discharge off and on was measured. With the discharge on, measurements were made at several power settings of the diathermy generator. The difference between the power required with the discharge off and with it on to maintain any given temperature for the coated thermistor is the recombination plus convective heat. The reference thermistor measured any corrections necessary for the convective heat due to changes in ambient conditions. The energy due to surface recombination is the difference between the coated thermistor heat-transfer measurement and the corrected uncoated thermistor heat-transfer measurement.

Data from a typical run are shown in Table 3. Fig. 4 shows the heat transfer to a platinum coated and to an uncoated thermistor as a function of thermistor resistance, which is essentially temperature (Fig. 3), for a representative test.

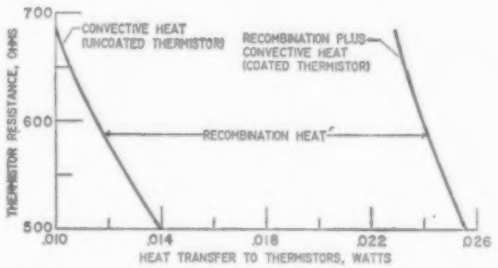

Fig. 4. Heat transfer to coated and uncoated thermistor.

4. CALCULATIONS

The equation used for calculating the recombination coefficient γ is

$$\gamma = \frac{G_1}{P\sqrt{\left(\frac{M_1}{2\pi RT}\right)\left(\frac{2m_s}{1+m_s}\right)}} \tag{3}$$

where

- G_1 mass of atoms recombining on the test thermistor per unit of coated area per second, g/cm²-sec
- P pressure in discharge tube
- M_1 molecular weight of atoms
- m_s mass fraction of atoms at the test surface

The quantity m_s is related to the mass fraction

Table 3. Sample Test Data for Platinum Coated Thermistor

Temperature (°C)	Coated thermistor			Uncoated thermistor			Recombination energy (W)	Recombination coefficient (γ)
	Resistance (Ω)	Voltage (discharge off) (V)	Voltage (discharge on) (V)	Resistance (Ω)	Voltage (discharge off) (V)	Voltage (discharge on) (V)		
60·8	640	13·81	1·29	522	14·06	10·85	$1{\cdot}62\times10^{-2}$	$2{\cdot}22\times10^{-2}$
52·4	845	12·25	1·29	685	12·31	9·64	$1{\cdot}44\times10^{-2}$	$2{\cdot}34\times10^{-2}$
61·0	625	13·93	1·29	521	14·07	10·76	$1{\cdot}64\times10^{-2}$	$2{\cdot}25\times10^{-2}$
53·3	820	12·44	1·29	665	12·53	9·82	$1{\cdot}47\times10^{-2}$	$2{\cdot}39\times10^{-2}$

of atoms in the stream m_∞ by the mass transfer Nusselt number correlation for spheres[12]:

$$Nu' = \frac{G_1 d}{\rho D_{12}(m_\infty - m_s)} = 2 + 0{\cdot}6\, Re^{1/2} Sc^{1/3} \quad (4)$$

where

Re = Reynolds number
Sc = Schmidt number
d test thermistor diameter, cm
ρ density of the gas in the discharge tube, g/cm³
D_{12} binary diffusion coefficient, cm²/sec (D_{12} estimated as 0·351 cm²/sec at 1 atm and 330°K)

The values for m_∞ were obtained from the gas titration results; G_1 was determined from the measured energy to the test thermistor due to nitrogen atom recombination with the equation

$$G_1 = \frac{WM_1}{QJA} \quad (5)$$

where

W energy to test thermistor due to nitrogen atom recombination, W
Q heat of nitrogen atom recombination, $113{\cdot}1\ 10^3$ cal/mole of nitrogen atoms[13]
J mechanical equivalent of heat, 4·186 J/cal
A thermistor coated area, cm²

Table 4. Recombination Coefficient of the Test Surfaces

Surface coating*	Number of measurements	Surface temperature range (°C)	Recombination coefficients (γ)		Reported recombination coefficient for oxygen
			Not corrected for diffusion	Corrected for diffusion	
Platinum (¼ of surface coated)	4	52–61	$2{\cdot}21\times10^{-2}$	$2{\cdot}30\times10^{-2}$	
Platinum (all of surface coated)	12	53–65	$2{\cdot}17\times10^{-2}$	$2{\cdot}22\times10^{-2}$	10×10^{-2}†
Lithium chloride	5	47–53	$7{\cdot}15\times10^{-3}$	$7{\cdot}21\times10^{-3}$	$1{\cdot}9\times10^{-3}$‡
Lithium chloride (crystallized coating)	6	57–60	$1{\cdot}37\times10^{-2}$	$1{\cdot}40\times10^{-2}$	$1{\cdot}0\times10^{-2}$**
Lead monoxide	4	76–81	$4{\cdot}18\times10^{-2}$	$4{\cdot}52\times10^{-2}$	$5{\cdot}8\times10^{-3}$‡

* All surfaces were vacuum coated unless otherwise noted.
† Ref. (14). ‡ At room temperature[7]. ** At 400°C[8].

The value of A was obtained by measuring the diameter of the thermistor bead and stem and calculating the thermistor surface area by assuming the thermistor bead was spherical. (The beads on the thermistors used were essentially spherical.)

5. RESULTS AND DISCUSSION

The recombination coefficients of nitrogen atoms on the various surfaces tested are listed in Table 4. The recombination coefficients for platinum and lithium chloride varied with time (Figs. 5 and 6). For platinum it took about 3 hr before γ reached a constant value, and for lithium chloride a constant value of γ was reached in slightly more than 1 hr. Table 4 compares the results obtained with those reported in the recent literature for oxygen.

In computing the absolute values of γ shown in this report, diffusion of nitrogen atoms to the

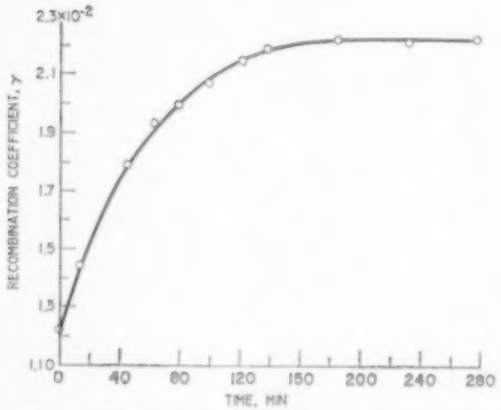

Fig. 5. The effect of atom bombardment on the recombination coefficient of platinum.

test surface was taken into account using equations (3) and (4). Also, values of γ neglecting this diffusion effect were computed by using equation (3) with m_s equal to m_∞. From Table 4 it can be seen that the diffusion correction is less than 10 per cent of the absolute value of γ; therefore, any uncertainty in the diffusion coefficient will have little effect on the results.

Initial experimental work showed that under the test conditions, the entire test surface of a thermistor would be effective for atom recombination. The value of γ for platinum covering approximately one-third of the surface of a themistor bead was $2{\cdot}30 \times 10^{-2}$. When the

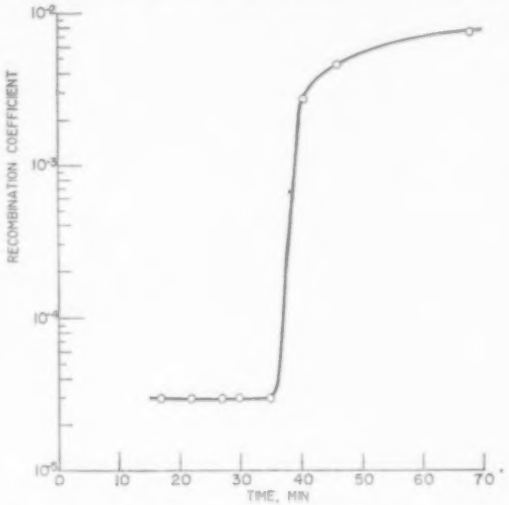

Fig. 6. The effect of atom bombardment on the recombination coefficient of lithium chloride.

entire thermistor head was covered, γ was $2{\cdot}22 \times 10^{-2}$. This difference in γ is within experimental error.

Platinum surface

The recombination coefficient of nitrogen atoms on platinum increased with time for several hours to a constant value (Fig. 5). After standing over night in an atmosphere of nitrogen, γ for the platinum surface dropped to a value of $1{\cdot}2 \times 10^{-2}$ but increased to its final value of $2{\cdot}22 \times 10^{-2}$ after 3 hr of atom bombardment. In[14], the authors find this surface clean-up effect with hydrogen atoms on platinum; they also find a clean-up effect with temperature up to 150°C with no variation of γ between 150° and 800°C. For oxygen recombination[15], reports that 10 per cent of the oxygen atoms hitting a platinum surface at low temperatures recombine, but at temperatures above 1000°C platinum is a very good catalyst for oxygen recombination. According

to[9], at high temperatures, platinum is 100 per cent efficient for the recombination of nitrogen atoms.

With the results reported herein and in the recent literature on platinum as a catalyst for atom recombination, it seems quite possible that adsorbed species on a platinum surface reduces its effectiveness as a catalyst. If adsorbed species do in fact reduce the catalytic effectiveness of platinum surfaces, then the surface available for recombination should be the total area of the active sites instead of the total coated area.

Lithium chloride

The value of γ for nitrogen atoms on lithium chloride increased to a constant value after more than 1 hr of atom bombardment (Fig. 6). For a vacuum coated lithium chloride surface, γ increased to an average value of $7{\cdot}2 \times 10^{-3}$. During the first 15 min, the value of γ was erratic and inconsistent. This was followed by a 15-min period where the value of γ was approximately equal to that for a glass surface; however, since glass was used to measure convective heat, these values might have a high per cent error. After 35 min of atom bombardment, γ rapidly increased to a value of $2{\cdot}6 \times 10^{-2}$ and then increased at a lesser rate to its final value. In[6] it is reported that γ of oxygen atoms on lithium chloride at room temperatures is about equal to γ of oxygen atoms on glass but increases to 1×10^{-2} as the temperature increases to 400°C. The authors of this reference suggest that the variation in γ is due partly to the removal of water from the lithium chloride as the temperature increases. The variation of γ of nitrogen atoms on lithium chloride can perhaps be explained in a similar manner except that the water removal is due to atom bombardment instead of heating.

Table 4 shows that the γ on vacuum coated lithium chloride is 50 per cent less than the γ on a crystallized lithium chloride surface. This large difference could be explained by the fact that the crystallized surface was not smooth like the vacuum coated surface; hence, the actual crystallized surface area could well be twice as large as the coated area of the thermistor bead.

Lead monoxide

The results for lead monoxide were rather surprising. From Table 4 it can be seen that γ of nitrogen atoms on this surface is much larger than the γ of oxygen atoms on the same surface[7]. Also, the results obtained show lead monoxide to be a better catalyst for nitrogen recombination than platinum. At present, no explanations can be offered for this high catalytic effect of a lead monoxide surface on nitrogen atom recombination.

6. CONCLUSIONS

Recombination of nitrogen atoms on platinum, lithium chloride and lead monoxide surfaces was measured. The following conclusions were drawn:

(1) Of the surfaces tested, a lead monoxide surface is the best catalyst for nitrogen atom recombination.

(2) A platinum surface, although a fairly good catalyst for nitrogen atom recombination, poisons upon standing. This poisoning of the platinum surface is cleaned up in about 3 hr by atom bombardment.

(3) Initially a lithium chloride surface is a very poor catalyst. After slightly more than 1 hr, the catalytic efficiency improved considerably. This may be due to the removal of water by nitrogen atom bombardment.

(4) The recombination coefficient of nitrogen atoms on a vacuum coated lithium chloride surface can be as much as 50 per cent less than for a crystallized coating of this surface probably because of the roughness of the crystallized surface.

DISCUSSION

G. M. PROK: In answer to the question of whether or not I observed luminescence on the test surfaces, the answer is that I did not observe any luminescence.

K. M. SANCIER: In response to the question from the floor as to whether luminescence was observed on these surfaces, I would like to comment that at Stanford Research Institute we are studying the transfer of the energy of the recombination of nitrogen atoms on phosphor. We had observed luminescence of pure nitrogen

atoms recombined on these surfaces to form molecules.

K. L. WRAY: In work done at this laboratory, it seems that at temperatures above 100°C the recombination coefficient for N atoms on Pt is near unity—as a detector made of platinum will indicate N concentrations of 10–50 per cent in a nitrogen discharge (electrodeless discharge).

G. M. PROK: Ref. (9) in my paper supports the indication that above 100°C the recombination coefficient for N atoms on bulk Pt is near unity. However, the results I reported are for thin evaporated films and are not necessarily the same as for the bulk material.

REFERENCES

1. N. H. KEMP and F. R. RIDDELL, *Jet Prop.* **27**, 132 (1957).
2. J. A. BROWN and G. I. LAVIN, *Preliminary Results Obtained with Catalytic Surfaces in the Upper Atmosphere During Balloon Flights*, Tech. Note No. 1230, Ballistic Res. Lab. (Dec. 1958).
3. S. KATZ, G. B. KISTIAKOWSKY and R. F. STEINER, *J. Amer. Chem. Soc.* **71**, 2258 (1949).
4. H. WISE, C. M. ABLOW and B. J. WOOD, *Surface-Catalyzed Atom and Free-Radical Reactions*, Project Squid Semi-Annual Report p. 57 (Oct. 1958).
5. J. W. LINNETT and D. G. H. MARSDEN, *Proc. Roy. Soc.* A**234**, 489 (1956).
6. J. W. LINNETT, F. R. S. MARSDEN and D. G. H. MARSDEN, *Proc. Roy. Soc.* A**234**, 504 (1956).
7. J. C. GREAVES and J. W. LINNETT, *Trans. Faraday Soc.* **54**, 1323 (1958).
8. S. A. HOENIG, *First Preliminary Report on the Oxygen Recombination Program*, Rep. HE-150-155, Univ. Calif. (Oct.-Dec. 1957).
9. S. ROGINSKY and A. SCHLECHTER, *Acta Physicochim. USSR* **6**, 401 (1937).
10. P. HARTECK, R. R. REEVES and G. MANNELLA, *J. Chem. Phys.* **29**, 608 (1958).
11. R. WENTINK, J. O. SULLIVAN and K. L. WRAY, *J. Chem. Phys.* **29**, 231 (1958).
12. W. E. RANZ and W. R. MARSHALL, Jr., *Chem. Eng. Progr.* **48**, 173 (1952).
13. G. B. KISTIAKOWSKY, H. T. KNIGHT and M. E. MALIN, *J. Chem. Phys.* **20**, 876 (1952).
14. J. W. FOX, A. C. H. SMITH and E. J. SMITH, *Proc. Phys. Soc., Lond.* **73**, 533 (1959).
15. R. R. REEVES, Jr. and P. HARTECK, *Utilization of Energy Stored in the Upper Atmosphere*, AFOSR TR 57-50, ASTIA No. AD 136-421 (July 1957).

A STUDY OF THE INTERACTION BETWEEN CARBON AND DISSOCIATED GASES*

W. ZINMAN†
General Electric Company, MSVD, Philadelphia, Pennsylvania

1. IMPORTANCE OF THIS STUDY

The reaction between dissociated gases and solids is of great technical interest to the astronaut for many reasons. For example, it is known that at the high altitudes of importance in satellite work, most of the residual atmosphere consists of dissociated gases. To determine accurately the trajectory of a satellite, it is undoubtedly necessary to understand the interaction of these gases with the satellite skin. Still another important technical application of this work is in the development of materials for rocket nozzles.

This problem is also of great scientific interest because very little is known about heterogeneous reactions in general. Therefore, considerable thought was devoted to the reaction to be studied first.

Carbon was chosen as the solid material for several reasons. It is physically stable at high temperatures; it is an element, and most of the conceivable products of reaction are gases which will not remain to contaminate the surface. It was also felt, that understanding of the reactions of carbon would lead to understanding of reactions of greater technical importance.

Nitrogen was chosen as the gas. Molecular nitrogen is inert at the temperature of the experiment and if a missile re-enters rapidly enough, dissociated nitrogen will be the predominant gas with which it comes in contact. From the scientists' point of view, it has been known for many years that active nitrogen can readily be prepared in the laboratory by subjecting nitrogen to an electric discharge, and it has been shown recently that the major reactive constituent in active nitrogen is atomic nitrogen in the ground state[1, 2]. Extensive studies (which have been reviewed elsewhere[3]) have been made of active nitrogen. It was felt that this work would be very helpful in planning and interpreting the projected experiments. This problem was considered to be particularly exciting because its solution might lead to understanding of the mechanism of the oxidation and combustion of carbon.

2. BACKGROUND

Work on heterogeneous reactions of carbon has been reviewed elsewhere[4]. For this reason, only work which the author considers most relevant will be discussed below.

Arthur[5] studied the reaction of carbon with oxygen containing small amounts of compounds known to inhibit the rapid homogeneous oxidation of carbon monoxide. In every case, he found that the oxidation rate of the carbon itself was lowered by the inhibitor. This finding has since been confirmed by others. Perhaps the most spectacular demonstration of this effect was the work of Day[6]. He maintained a burning carbon rod in a rapid flowing stream of oxygen. The reaction was quenched as soon as a small quantity of chlorine was added to the oxygen, even though the carbon rod was at 2000°C.

Many workers in the field feel that the inhibitors change the surface of the carbon, thereby preventing reaction. However, the author cannot help but wonder whether the hydrogen and hydroxl radicals which play an important part in the rapid oxidation of carbon monoxide also catalyse the oxidation of carbon itself, as suggested by Arthur[7]. This idea is

* This work was performed under the auspices of the U.S. Air Force, Ballistic Missile Division, Contract No. AF 04 (647)-269.

† Present affiliation: Republic Aviation Corporation, Farmingdale, L.I., New York.

corroborated by the strong effect of small amounts of hydrogen on the reaction between carbon and dissociated nitrogen which the author has found and will describe below.

Some studies have been made of the reactions of dissociated gases with carbon. Evidence has been obtained that finely divided soots prepared by pyrolysis of organic compounds will react with atomic hydrogen[8, 9] and atomic oxygen[10] at temperatures of the order of 100°C. In addition, Blackwood and McTaggart[11] reported that atomic oxygen reacts with natural graphite at room temperature but not with diamonds. None of the above workers attempted to degas either their vacuum system or carbon before initiating an experiment. As indicated below, this step was found to be crucial in this work. Finely divided carbon was used in all of the work cited except possibly that of Blackwood and McTaggart. Because of this, it cannot be established that reaction was not taking place on small hot spots, which were originally favored sites for atom recombination, rather than at room temperature.

An early study[12] indicated that active nitrogen does not react with carbon at room temperature. Stieber[13] has found that reaction between molecular nitrogen and carbon does not occur at an appreciable rate at temperatures as high as 2750°C.

2. APPARATUS

The apparatus used is shown in Fig. 1. Nitrogen at a velocity of 800 cm/sec and a pressure of 3 mm Hg was introduced into the vacuum through a flow-meter throttling valve[5]* and a cold trap containing liquid nitrogen. The nitrogen was pumped first through a quartz discharge tube (30 mm inner dia) where it was subjected to a 6 Mc/sec radio frequency field, and then over a carbon rod 25 cm from the discharge. The products condensible at the temperature of liquid nitrogen were collected in the liquid air traps. Eventually these products were transferred through the analytical manifold to an infrared cell.

Provision was made to leak small amounts of hydrogen into the nitrogen stream between stopcock[5] and the discharge tube. A standard leak made by the Veeco Vacuum Corporation (86 Denton Avenue, New Hyde Park, N.Y.) and rated 40 $\mu ft^3/hr$ with helium could be used for this.

The discharge tube could be connected to a liquid nitrogen trap and mercury diffusion

* The number refers to the valve number on Fig. 1.

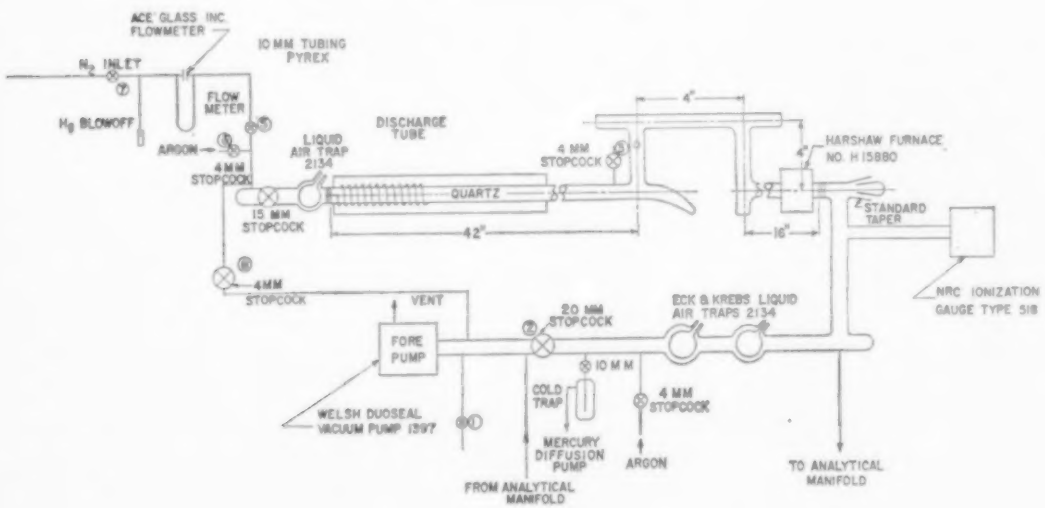

Figure 1.

pump for evacuation before initiating an experiment. As indicated on Fig. 1, an ionization gauge was attached to the apparatus to determine the degree of outgassing prior to initiating an experiment.

The carbon rod used in an experiment rested on the quartz tube and was heated by a resistance furnace. The temperature at the center and end of the rod was measured by chromel alumel thermocouples placed outside the quartz tube. The Bureau of Standards calibration was used[14].

3. MATERIALS USED

Regular grade spectroscopic carbon rods (6 mm dia and 15 cm long) manufactured by the National Carbon Company, New York, N.Y., were used. Before an experiment, these rods were dried at 150°C and weighed. The normal initial weight was about 6 g.

The following gases were used:

(1) Prepurified nitrogen and welding-grade argon obtained from Airco.

(2) Nitric oxide obtained from the Matheson Co., East Rutherford, N.J.

(3) Air Products Company water-pumped hydrogen. The manufacturer specified that this gas contained no detectable methane. This was verified by infra-red analysis. The hydrogen was purified by being passed through a Baker Company Deoxo unit.

All of the gases used in this work, except nitric oxide, were passed through a liquid nitrogen trap before used.

A piezon *T* was used as stopcock grease except in some preliminary experiments.

4. EXPERIMENTAL PROCEDURE

Several preliminary experiments were performed in which a carbon rod was heated overnight at about one micron pressure and then exposed to supposedly pure active nitrogen. The carbon rods treated in this way lost considerable weight; the major detectable products of reaction were N_2O and HCN. No effort was made to detect CO_2 or CO. It was felt that these results indicated that the nitrogen was being contaminated by water which outgassed from the discharge tube, dissociated in the discharge and then reacted with the carbon. Because of these results, the following procedure was used in the experiments reported below; considerable attention was given to the outgassing procedure used before the carbon was exposed to activated gases. The carbon rod was weighed and placed in the cold furnace. The system was then pumped on until the pressure indicated on the ionization gauge was less than 0·5 μ. The carbon was then heated to 800°C and outgassing was continued until a pressure of about 10^{-5} mm Hg was registered on the ionization gauge. Then, the liquid nitrogen trap nearest the forepump was filled and the system isolated from all pumps. A leakage rate of less than 10^{-5} mm/min was normally obtained using the ionization gauge. Argon at a pressure of about 150 mm Hg was introduced into the system. The discharge was ignited and maintained for 90 sec. After 60 sec, argon was introduced into the system so that its pressure was 1 atm when the discharge was extinguished. For 5 min argon was pumped through the system, passing first over the carbon, then through the discharge tube and finally through stopcock[15].

The procedure of ignition, etc., was then repeated. After this, all the liquid air traps between the nitrogen inlet (Fig. 1) and the forepump were filled with liquid nitrogen, the system was evacuated and the flow of the appropriate gas mixture was started. The carbon was exposed to active nitrogen for an appropriate time (the radio frequency generator was cycled 2–1/2 min on and 2 min off). At the end of this time, the carbon was cooled with nitrogen streaming over it. The condensible product was transferred to an infrared cell for analysis. The carbon was then removed from the apparatus and weighed. The change in weight was less than 5 mg in all experiments described here. A new carbon rod was used in each experiment.

Calibration of gas flows

The flow rates of gases were determined by permitting gas to flow into a known evacuated volume and monitoring the pressure.

Infrared analysis

All infrared analyses were performed with a Perkin–Elmer model 112 *U* infra-red spectroscope with a sodium chloride prism. The cell length was 7 cm. Although an IR was performed usually within about 2 hr after the experiment, it was found that holding a sample overnight did not change its spectrum. Unknowns were identified and quantitatively determined by direct comparison with known standards at about the same pressure as the unknown. Beer's law was used to make necessary interpolations.

Although cyanogen was not observed in these experiments, it is felt on the basis of this calibration, that 1 cm^3 (s.t.p.) of cyanogen could have been detected and identified.

Estimation of nitrogen atom concentration

The concentration of nitrogen atoms was estimated by titration with NO[15]. This titration was performed with the furnace at room temperature and no carbon rod in the furnace. The atom concentration was measured halfway down the length of the furnace where the center of the carbon rod normally lay.

5. RESULTS

Description of afterglows and discharge:

nitrogen atom concentration over the carbon.

The discharge with argon was normally sinuous. This discharge could be maintained even at a pressure of one atmosphere. Sometimes on the first cycle, a homogeneous discharge which could not be maintained at high pressure was obtained. It is believed that this indicated that impurities were present in the discharge tube.

The discharge was intense orange in color when pure nitrogen was used. Beyond this discharge, an intense violet glow extended about 10 cm. This was followed by an extremely weak nitrogen afterglow. Mr. R. Harner took an emission spectrum of this glow and found that the violet glow was due to the first negative band of N_2+ ion. The first positive band of N_2 characteristic of active nitrogen was observed also. No evidence of CN or NH bands was obtained. This is in agreement with the work of Broida *et al.*[22]. By adding appropriate amounts of oxygen to the nitrogen, all the afterglows described by Broida could be obtained.

Even though no nitrogen afterglow could be discerned at the point of titration, a green air afterglow could be excited by adding an excess of nitric oxide. With a total pressure of 3 mm Hg, the concentration of nitrogen atoms was found to be 0·05 mol. per cent.

When the hydrogen–nitrogen mixture was used, the violet afterglow was extinguished and the normal nitrogen afterglow appeared much stronger. However, the endpoint of the titration appeared to be the same whether pure nitrogen or the nitrogen–hydrogen mixture was activated. This was verified directly by setting the endpoint with pure active nitrogen and finding that it did not change when hydrogen addition was started. Therefore, the N : H ratio was about 10 : 1 when the nitrogen–hydrogen mixture was used.

Table 1. Product Obtained with Different Gas Mixtures

	Carbon and active nitrogen (cm^3/hr)	No carbon and active nitrogen (cm^3/hr)	Carbon and active nitrogen–hydrogen mixture (cm^3/hr)	No carbon and active nitrogen–hydrogen mixture (cm^3/hr)
HCN	0·12	none	1·1	0·13
C_2N_2	none	none	none	none
NH_3	none	none	0·9	1·0
N_2O	0·5	0·5	0·6	1·0

Reaction of carbon with active gases

Two series of experiments were performed. The object of the first series was to establish that the product HCN was coming primarily from the carbon rod, and that the hydrogen–nitrogen mixture had to be used to obtain significant amounts of HCN. The results are tabulated in Table 1. All of the experiments were conducted with the furnace at 800°C. Three experiments were performed with carbon and active nitrogen for a total time of 150 min,

as well as one without the carbon. The ones with the hydrogen–nitrogen mixture lasted 90 min. They verified the results found in several preliminary experiments which showed that a carbon rod had to be in the apparatus to obtain significant amounts of HCN.

The object of the second series of experiments was to establish the effect of time of the experiment on the yield of HCN and to obtain a material balance for the hydrogen.

Table 2. Effect of Time of Experiment on Product Yield

Time of experiment	%H as HCN	%H as NH_3	%H recovered
15 min	17*	86	103
60 min	21*	54	75
90 min	19*	51	70
5 min	55†	85	140
15 min	29†	86	115

* Determined from $J=1$; $J=2$ transition of the 712 cm^{-1} fundamental of HCN.

† Determined from the Q branch of the 712 cm^{-1} fundamental of HCN.

The furnace temperature in all of these experiments was 800°C. The yield of product is reported as equivalent to a certain per cent of hydrogen input. (The experiment of 90 min duration is tabulated in both Table 1 and Table 2.) Besides the products noted above, several unidentified products were obtained with measurable infra-red absorption at 774 cm^{-1}, 1220 cm^{-1}, 2840 cm^{-1} and 2920 cm^{-1} in different experiments including some with pure nitrogen, but without a carbon rod. It is believed that these contaminants were removed by the liquid air trap ahead of the discharge and later mixed with the reaction products.

6. CONCLUSIONS

The following results appear significant:

(1) Most of the hydrogen added to the nitrogen is recovered as condensable product.

(2) A carbon rod is necessary for the production of significant quantities of HCN.

(3) On experiments of 15 min or more, the yield of HCN is directly proportional to the time of the experiment.

At low temperature, it has been shown that H_2 is inert to atomic nitrogen[16]. The fact that most of the added hydrogen is recovered as condensable product is therefore evidence that it was completely dissociated under the conditions of the experiment. With this assumption, it can be seen that collision between N and H will be much more common than collision between two hydrogen atoms. However, as implied by Volpi and Kistiakowsky[16], the reaction $N+NH \rightarrow N_2+H$ will be highly exothermic and will rapidly decompose the NH radical in the presence of active nitrogen.

There are three possible explanations for the formation of HCN from carbon in the presence of the active nitrogen–hydrogen mixture.

(a) An organic contaminant on the carbon rod reacts with active nitrogen to form HCN, especially since Winkler[17,18] has shown that many organic compounds react in this way. It was felt that at 800°C any such organic contaminant would react extremely rapidly in this way and that the material balance of the hydrogen would show an excess hydrogen output. This may be the explanation for the hydrogen overbalance obtained in the experiment run for 5 min (Table 2). However, this table shows that HCN is produced at a constant rate after this time, indicating that another mechanism accounts for its production. Besides, this mechanism cannot explain why the production of HCN is augmented by the small addition of H while the N atom concentration over the carbon remains constant.

(b) Ammonia formed in the discharge reacts with carbon to form HCN. At 800°C, this reaction has been studied[19] and is several orders of magnitude too slow to account for the yield of HCN.

(c) The atomic mixture of hydrogen and nitrogen reacts directly with the carbon to form HCN. This appears to be the explanation of the above results. By assuming that the entire geometric surface of the carbon is exposed to the active gases, it is found that the formation of HCN occurs on at least one out of every thousand collisions between H and a carbon at 800°C. The standard formula[20] was used to

calculate the collision frequency between the hydrogen and carbon.

From the consistent failure to obtain cyanogen*, it is felt that the collision efficiency for reaction between atomic nitrogen and carbon is less than 10^{-4} at 800°C.

A plausible mechanism is that N becomes chemisorbed on the carbon and perturbs the adjacent C–C bands to an unknown extent. An H atom then reacts with the chemisorbed CN to form HCN. The anologous reaction between H atoms and cyanogen is known to be very rapid at 600°C[21].

It is known that when a plastic nose cone burns, a carbon char is left. This char probably contains considerable hydrogen. This work indicates that the above char would be very reactive.

DISCUSSION

S. Bauer

Acknowledgement—I would like to thank Mr. Eugene Engels who constructed most of the apparatus used in this work and assisted in conducting the experiments described above, Mr. James Graham for doing the more challenging glass blowing, Mrs. B. Moeller and Miss M. Weston for typing this manuscript and all of my colleagues for their considerable helpful criticism.

One might account for the lack of formation of a detectable amount of C_2N_2 by arguing that the surface of the graphite acts as a catalyst. Two adsorbed adjacent CN groups preferentially react to produce C_2 (which remains adsorbed and becomes part of the solid) and N_2. Instead of producing cyanogen, the thermodynamically more stable products are produced.

W. Zinman

Marshall and Norton* have shown that nitrogen outgasses from carbon at temperatures above 2,200°C. On the basis of this work, the author feels that chemisorbed nitrogen on carbon is stable at 800°C and that the reaction suggested by Dr. Bauer has too high an activation energy to occur at an appreciable rate at this temperature.

The author feels that it is more likely that a nitrogen atom from the gas recombines exothermally with an adsorbed nitrogen. This reaction probably has low activation energy and high collision efficiency.

* It was suggested in discussion that the cyanogen was lost as paracyanogen. The author checked this by dissolving the residue from the freezing trap in KOH and attempting to convert it to Prussian Blue. The results were negative.

In view of recent work (C. HAGGART and C. A. WINKLER, *Canad. J. Chem.* **38**, 329 (1960)) there is some question whether the consistent failure to collect cyanogen as a product is in itself proof that active nitrogen does not react with carbon. However, there were other pieces of evidence that this did not occur. First the black polymer which is reported to be a product of the reaction between cyanogen and active nitrogen was never observed. Secondly, when a mixture of about three parts of argon and one part of nitrogen with an unknown amount of oxygen from a leak was activited and passed over a carbon rod at 770°C, a normal yellow green active nitrogen afterglow was seen downstream from the carbon rather than the red or violet glow which accompanies the reaction of active nitrogen and cyanogen.

* Trans. Am. Inst. Mining & Met. Eng., Metal Division **156**, 3251 (1944).

REFERENCES

1. D. S. JACKSON and H. S. SCHIFF, *J. Chem. Phys.* **23**, 2333 (1955).
2. J. BERKOWITZ, W. A. CHUPKA and G. B. KISTIAKOWSKY, *J. Chem. Phys.* **25**, 457 (1956).
3. K. R. JENNINGS and J. W. LINNETT, *Quart. Rev.* **12**, 116 (1958).
4. P. L. WALKER, F. RUSINKO and L. G. AUSTIN, *Advances in Catalysis* Vol. XI, p. 133 [Edited by D. D. ELEY, P. W. SELWOOD and P. B. WEISZ]. Academic Press, Inc., New York and London (1959).
5. J. R. ARTHUR, *Trans. Faraday Soc.* **47**, 164 (1951).
6. R. J. DAY, *Pennsylv. State thesis* (1949). See also: R. J. DAY, P. L. WALKER, Jr., and C. C. WRIGHT in *Industrial Carbon and Graphite*, p. 348. Society of Chemical Industry, London (1958).
7. J. R. ARTHUR and J. R. BOWRING, *Industr. Engng. Chem.* **43**, 528 (1951).
8. L. J. AVRAMENKO, *Zh. fiz. Khim.* **20**, 1299 (1946).
9. A. W. TICKNER and G. N. HARRIS, *Nature, Lond.* **160**, 871 (1947).
10. T. STREZNEWSKI and J. TURKEVICHIN, *Proceedings of the Third Conference on Carbon*, p. 273. Pergamon Press, New York (1959).
11. J. D. BLACKWOOD and F. K. MCTAGGART, *Austr. J. Chem.* **12**, 114 (1959).
12. R. J. STRUTT, *Proc. Roy. Soc.* **A85**, 219 (1911).
13. H. C. STIEBER, unpublished communication (1959).
14. H. SHENKER, J. I. LAURIZEN, R. J. CORRUCCINI and S. T. LONBERGER, *Reference Tables for Thermocouples, Bur. Stand. Circ.* No. 561 (1955).
15. P. HARTECK, R. R. REEVES and G. MANNELLA, *J. Chem. Phys.* **29**, 608 (1958).
16. G. B. KISTIAKOWSKY and G. G. VOLPI, *J. Chem. Phys.* **28**, 665 (1958).

17. H. G. V. EVANS, G. R. FREEMAN and C. A. WINKLER, *Canad. J. Chem.* **34**, 1271 (1956).
18. B. DUNFORD, H. G. V. EVANS and C. A. WINKLER, *Canad. J. Chem.* **34**, 1074 (1956).
19. P. H. VAN DER LEY and J. P. WIBAUT, *Rec. Trav. chim.* Pays-Bas **51**, 1142 (1932).
20. J. JEANS, *An Introduction to the Kinetic Theory of Gases*, p. 191. Cambridge University Press (1946).
21. E. W. R. STEACIE, *Atomic and Free Radical Reactions*, 2nd Ed., p. 636. Reinhold, New York (1954).
22. U. H. KURZWEG, A. M. BASS and H. P. BROIDA, *J. Molec. Spectrosc.* **1**, 184 (1957).

A NON-CATALYTIC SURFACE FOR DISSOCIATED COMBUSTION GASES*

J. C. CUTTING, J. A. FAY, W. T. HOGAN and W. CRAIG MOFFATT
Massachusetts Institute of Technology, Cambridge, Massachusetts

Abstract—Heat transfer measurements have been made in a detonation tube using hydrogen-oxygen and acetylene-oxygen mixtures. A small diameter wire placed transverse to the tube axis is rapidly heated by the dissociated combustion products behind the advancing detonation front. Because of the high temperature (3000°K-4500°K) in a detonation wave, the combustible gases are appreciably dissociated, usually more than 50 per cent of the total enthalpy being in the form of dissociation energy. The variation of total heat transfer with composition and pressure was found to be close to theoretical expectations.

For wires coated with iodine, it was found that the total heat transfer could be reduced by about a factor of 3 in the oxy-hydrogen mixtures, and by a factor of 2 in an equi-molar acetylene-oxygen mixture at low pressure when compared with the uncoated wire experiments. Both these factors could be accounted for by assuming that the energy of dissociation and molecular vibration were not recovered at the cold wall. From separate measurements of the thickness of detonation waves in these same mixtures, it can be seen that for the conditions under which the coated wire substantially reduces the heat transfer, the aerodynamic boundary layer on the wire surface should be "frozen". Furthermore, theoretical arguments indicate that the effect of iodine evaporation on the net heat transfer should be much smaller than the experimentally observed reduction in heat transfer. Under these conditions, the surface recombination coefficient is estimated to be less than 10^{-2}.

1. INTRODUCTION

In considering the heat transfer to hypersonic vehicles, it was pointed out[1,2] that the energy transport to the cold wall could be considered to consist of two parts: first, the transport of kinetic, rotational and vibrational energy through collisions and secondly, the diffusion of dissociated particles carrying with them the potential energy of recombination. The dissociated particles diffusing toward the cold surface into regions of lower equilibrium concentration could recombine either in the gaseous boundary layer or on the surface of the wall. A principal result of the theoretical calculations[1] was the conclusion that the overall heat transfer was hardly affected by whether the recombination process was a gas phase or surface reaction. A third possibility, that recombination should fail to occur at all, would result in a substantial reduction in heat transfer since the recombination energy would not be delivered to the wall.

This third possibility has received some attention[1,2] since it obviously presents attractive possibilities for reducing the overall heat transfer. However, in order to achieve this situation, two requirements must be met. First, thermodynamic equilibrium must not subsist within the boundary layer. This is possible if the recombination time is very long compared to the time for a particle to diffuse through the boundary layer[1]. Secondly, the wall must be noncatalytic with respect to the recombination of the dissociated particles. The wall need not be absolutely noncatalytic, but should recombine particles much more slowly than they can diffuse through the boundary layer when the wall concentration is negligible. Up to the present time, there has been no clear experimental evidence of the achievement of either a

* This research was supported by the United States Air Force through the Air Force Office of Scientific Research of the Air Research and Development Command, under Contract Number AF 49 (638)-375.

nonequilibrium (or "frozen") boundary layer, or a noncatalytic surface. As a result of the experiments reported below, it is believed that both of these effects have been achieved for combustible mixtures.

The principal experimental technique for measuring heat transfer to models in shock tubes is the use of thin film resistance gages[4]. It is thus possible to measure local values of the heat transfer at various positions on the model. For the experiments reported below, the total heat transfer to a small diameter wire placed normal to a shock-tube axis was measured by determining the change in electrical resistance of the wire*. The combustion gases were those found in the wake of a detonation wave passing through a combustible mixture and enveloping the wire gage. The heat transfer to coated and uncoated wires were compared to determine the relative effects of various surface coatings.

2. HEAT TRANSFER THEORY

The heat flux (q) in a quiescent, partially dissociated gas mixture can be conveniently given by:

$$q = -k \operatorname{grad} T - \sum_i (h_i)(D_i\rho) \operatorname{grad} c_i \qquad (1)$$

where k is the thermal conductivity for transport of translational, rotational and vibrational energy, T is the temperature, h_i the total (including chemical) enthalpy, D_i the diffusion coefficient, ρ the density and c_i the mass fraction of species i. The first term of equation (1) is the transport of the energy of those degrees of freedom which are in equilibrium at the local temperature T, while the second term is the transport of potential energy of recombination, whether or not the species are in thermochemical equilibrium at the local temperature. If $D_i\rho c_p/k$ (Lewis number) is unity for all species, where c_p is the average constant pressure specific heat for the degrees of freedom included in k, then it is easily shown[1] that equation (1) may be written:

$$q = \frac{k}{c_p} \operatorname{grad} \left(\sum_i c_i h_i\right) \qquad (2)$$

Thus the gradient of total enthalpy determines the flux of heat. (In real cases where the Lewis number is not unity, there will be some modification of equation (2), but the principal result is still valid.)

The studies of aerodynamic heat transfer, such as the stagnation point heating of a blunt body[1, 2], can best be summarized by stating that the principal effects of the chemistry, when compared to a chemically inert but aerodynamically similar flow, are represented by equation (2). Thus the laminar heat transfer per unit length of a cylinder of diameter D, whose axis is normal to a flowing dissociated gas of velocity V, should be correlated by:

$$\frac{\text{(Nusselt No.)}}{\text{(Prandtl No.)}^{0.4}\,\text{(Reynolds No.)}^{1/2}} = \frac{Qc_p/\pi k\,(h_e - h_w)}{(\rho VD/\mu)^{1/2}\left(\frac{c_p\mu}{k}\right)^{0.4}} = \text{const.} \qquad (3)$$

where ρ is the density and μ is the viscosity of the free stream and $h_e - h_w$ is the enthalpy difference between the free stream and the wall. (For a more extensive discussion, see[5].)

If thermodynamic equilibrium exists at the wall as well as in the free stream, the heat transfer will be the same regardless of whether or not such equilibrium is achieved by gas phase recombination in the boundary layer or by catalytic recombination on the wall, for h_w is the same in either case. On the other hand, the heat transfer will be reduced only if recombination is prevented both in the gas phase and on the surface. The amount of reduction will be in proportion to the reduction in enthalpy difference between free stream and wall. By measuring the heat transfer, it is possible to deduce the enthalpy change and hence the nature of the chemical change, if any, of the hot free stream gases as they are cooled down to the low wall temperature.

A by-product of the heat transfer experiment is a measure of upper or lower limits for the gross recombination times. For gas phase recombination, a "frozen" reaction has a chemical time longer than the diffusion time

* To the author's knowledge, this technique was first applied by A. Vaughn, Avco Everett Research Laboratory, Everett, Mass.

D/V^*, while a reaction which achieves equilibrium has a shorter recombination time. For surface recombination, a noncatalytic surface has a recombination coefficient α which is less than the ratio of molecular diffusive to effusive flux at the wall:

$$\alpha \leqslant \frac{D_i\left(\frac{n_i}{\delta}\right)}{n_i \bar{c}_i} \tag{4}$$

where δ is the boundary layer thickness and $\bar{c}_i$ is the mean molecular speed. For laminar boundary layers, this ratio is about (Reynolds number)$^{-1/2}$. For the experiments reported below, the Reynolds number was in the range of 10^3 to 10^4, so that a surface with $\alpha < 10^{-2}$ would be noncatalytic.

The thermodynamic properties (velocity, density, enthalpy, composition and temperature) behind the detonation front can be obtained from a theoretical calculation of a normal detonation wave. Such calculations were available for the mixtures considered in these experiments†. The estimation of the transport properties used in the correlation of the heat transfer data is discussed in[5].

It is relatively simple to determine the stagnation enthalpy h_s from the detonation wave velocity and density ratio, which can be measured as well as calculated theoretically. If V_D is the velocity of the detonation wave moving into a stationary combustible mixture of density ρ_1, the equation of continuity requires that

$$\rho_1 V_D = \rho_2 (V_D - V_2) \tag{5}$$

where V_2 is the flow velocity behind the moving front. The conservation of energy also requires that

$$h_1 + \tfrac{1}{2} V_D^2 = h_2 + \tfrac{1}{2}(V_D - V_2)^2 \tag{6}$$

By combination of equations (5) and (6), the stagnation enthalpy is found to be:

$$h_s \equiv h_2 + \tfrac{1}{2} V_2^2 = $$
$$= h_1 + V_D^2\left(1 - \frac{\rho_1}{\rho_2}\right) \tag{7}$$

Thus the enthalpy difference between wall and free stream can be given by:

$$h_s - h_w = (h_1 - h_w) + V_D^2\left(1 - \frac{\rho_1}{\rho_2}\right) \tag{8}$$

Since the wall and initial temperatures are the same, the first term on the right-hand side of equation (8) is just the heat of combustion of the mixture, while the second term incorporates the kinetic energy of the flowing gases, which is small compared to the first term for detonation waves. This is an especially convenient way for determining how the enthalpy difference will vary if different possible products are formed at the wall.

The density ratio ρ_2/ρ_1 used in the subsequent calculations was taken to be 1·63, which is in agreement with the measurements of Duff[6].

3. EXPERIMENTAL APPARATUS AND HEAT TRANSFER GAGE CALIBRATION

The shock tube used in these experiments was a stainless steel tube, 21½ feet long, and with an inside diameter of 1½ in. Ionization probes were placed at intervals along the tube to enable velocity measurements to be taken. The tube was filled with premixed oxy–hydrogen and oxy–acetylene mixtures at various initial pressures, and a detonation wave was started at the end opposite from the heat gage by igniting with a hot wire. The velocity of the detonation wave was seen to be constant for most initial pressures and in good agreement with the wave speed predicted theoretically. Heat transfer measurements were taken only at pressures where the velocity remained constant.

The measurement of the heat transfer rate in detonation waves was obtained in the following manner. A very fine wire (0·004 in. diameter and 1 cm long) was suspended transversely in the shock tube and subjected to the high temperature detonation wave. The wire was fastened across two needle probes which held

* For the experiments reported, this time was about 10^{-7} sec.

† The authors are indebted to R. E. Duff of the Los Alamos Laboratory for making these calculations available.

the short length of wire in the tube. The probe and wire were placed in series with a large resistor, to ensure constant current, and a d.c. voltage supply. The change in voltage across the test specimen was displayed on an oscilloscope as the wave passed. The gage was so situated that no flow disturbances from downstream could reach the gage within the testing time of the experiments.

From the rate of change of wire resistance, the heat transfer could be found in either of two ways. From the known properties of the material (tungsten or platinum), the resistance versus heat capacity could be computed on the assumption that the wire temperatures were nearly uniform. Alternatively, a calibration of the wire gage could be determined by a sudden electrical heating of the wire. The results of both methods were in substantial agreement[8].

A comparison of the absolute value of the heat transfer with that expected theoretically is given in[5], which indicated that the measured values were low by about a factor of two (i.e. the constant of equation (3) was about one-half as great as would be expected from aerodynamic estimates). Subsequent experiments indicate that the gage response depends upon the magnitude of the measuring current, giving close to the theoretical heat transfer for very low currents. All the results reported herein were obtained for the same gage current, and the comparative effects appear to be independent of current.

4. HEAT TRANSFER EXPERIMENTS

Three series of experiments were performed; two to determine the dependence of heat transfer rate on initial pressure in stoichiometric hydrogen–oxygen and equimolar acetylene–oxygen mixtures, and the third to determine the dependence on composition in acetylene–oxygen mixtures at 1 atm initial pressure. In the first two series, additional experiments were performed to evaluate the effects on heat transfer produced by coating the gage with iodine.

In developing the heat transfer gage, it was necessary to evaluate the influence of wire diameter and wire material on the measured heat transfer rates at various pressures and in various mixtures. Experiments were performed with platinum and tungsten wires of various diameters between 0·004 in. and 0·010 in. For fixed initial conditions, the measured heat transfer rates were found to vary inversely as the square root of the wire diameter for both tungsten and platinum, as predicted by equation (3). For structural and signal strength considerations, wire diameters of 0·004 in. and 0·005 in. were selected for the actual heat transfer experiments. From Figs. 1 and 2, it may be seen that the data from tungsten and platinum gages differ by only 10 per cent or less, and that no difference exists in the trend of the data from the two types of gages. In stoichiometric hydrogen–oxygen mixtures, the tungsten gage

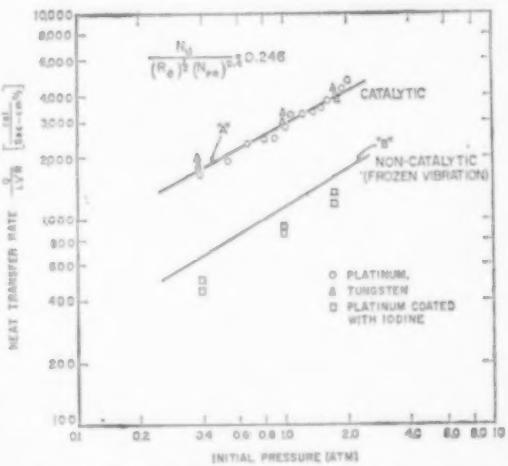

Fig. 1. The variation of heat transfer with initial pressure in stoichiometric oxy–hydrogen detonations. The solid lines are correlations of the type given by equation (3).

gives results about 10 per cent higher than the platinum gage; whereas in acetylene–oxygen mixtures the tungsten gives results about 6 per cent less than the platinum gage. In regard to the agreement between the two materials, it should be noted that for the same wire diameter, length and measuring current, the signal strength from a tungsten gage is only 0·45 times that from a platinum gage.

The iodine-coated gages were prepared by evaporating the iodine on to the wire to a

thickness somewhat greater than the final desired value. The coated wire was then passed rapidly through a flame so that the iodine melted and thereby formed a dense, smooth coating over the wire. By making successive passes through

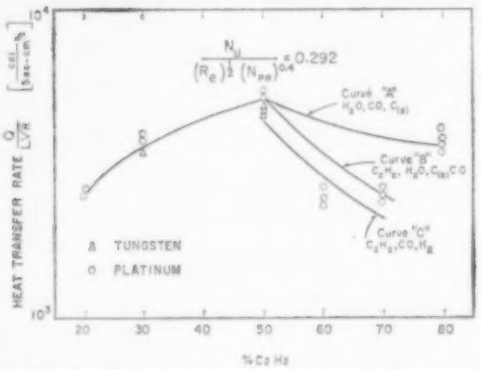

Fig. 2. The variation of heat transfer with composition in oxy—acetylene detonations at one atmosphere initial pressure. Curves A, B and C are correlations based on various assumptions as to free stream and wall composition.

the flame, the thickness of the coating was reduced to the desired value of 0·0005 in. as measured with a microscope within an accuracy of 20 per cent.

Fig. 1 shows the theoretical correlation and the experimental heat transfer rates for stoichiometric hydrogen–oxygen mixtures at various initial pressures. The theoretical curve is equation (3), with the constant chosen to be 0·246 in order to give the best fit. From curve *A* it is seen that the dependency on pressure predicted by the theory is in substantial agreement with the pressure dependency found by experiment. The theoretical curve *A* varies as the 0·6th power of the initial pressure*. Fig. 1 shows the heat transfer to an iodine coated gage to be approximately 0·28 times the heat transfer to the uncoated gage. The theoretical curve *B* is based on the assumption that the dissociated particles do not recombine either in the boundary layer or on the wall, and that the vibrational relaxation times are long enough so that the gas does not give up its vibrational energy to the gage.

Fig. 2 shows the correlation between experimental and theoretical heat transfer rates for various mixtures of C_2H_2–O_2 at 1 atm initial pressure. Again, the theoretical curve is determined from equation (3). Because of the uncertainty of the gas composition at the gage surface for rich mixtures, three theoretical curves are shown corresponding to three possible gas compositions. Curve *A* is based on the assumption that at the gage surface there is no C_2H_2 and that the available oxygen preferentially attaches first to the hydrogen to form H_2O, and upon depletion of the available hydrogen the oxygen then attaches to the carbon to form CO (or CO_2 if sufficient O_2 is available). Thus, for lean mixtures, the gas at the gage surface is composed of H_2O, CO_2 and O_2; whereas for rich mixtures the composition at the gage surface is H_2O, CO and solid C.

Curves *B* and *C* are based on the assumption that the decomposition of excess C_2H_2 in the free stream to form solid carbon is frozen. This assumption is based on the trend in velocity measurements reported by Kistiakowsky and Zinman[7], and in ionization measurements behind a detonation wave reported by Basu and Fay[8]. In addition, curve *B* assumes that the available oxygen at the surface preferentially attaches first to the hydrogen to form H_2O. Upon depletion of the hydrogen, the remaining oxygen attaches to the carbon to form CO, leaving a surplus of solid carbon. The composition at the surface is thus C_2H_2, H_2O, CO and $C_{(s)}$. For curve *C*, in addition to assuming the decomposition of C_2H_2 to be frozen, it is assumed that the available oxygen preferentially attaches first to the carbon to form CO, leaving a surplus of H_2. The composition at the surface is thus C_2H_2, CO and H_2.

Fig. 3 shows the effect of an iodine coating on a tungsten gage in an equimolar acetylene–oxygen mixture between 1 and 0·066 atm initial pressure. The upper solid curve is the theoretical correlation assuming complete equilibrium at the wall temperature, i.e. that the wall composition is $C_{(s)} + CO + H_2O$. The middle

* If there were no change in composition and temperature, the heat transfer would vary as the 0·5th power of the initial pressure.

curve assumes that the free stream composition (CO, H_2, H) is frozen with respect to the oxygen reattachment to the hydrogen, while the lowest curve assumes no chemical change and no vibrational equilibration. The difference between the two lower curves is the sum of the energy of dissociation of the hydrogen and the vibrational energy of all the molecules.

The feasibility of obtaining a noncatalytic gage surface by coating the wire with SiO_2 was explored. The coating was applied by passing the gage through a flame into which a silicone (Dow Corning No. 702 pump oil) was steadily introduced through a hypodermic tube. However, it was not possible to obtain a continuous coating of the desired thinness. As the thickness of the silica was increased to improve the continuity of the coating, the thermal insulating property of the silica rendered the gage ineffective. For the imperfectly coated gages, there appeared to be no reduction in heat transfer.

5. DISCUSSION

The analysis of the heat transfer tests is based upon the assumption that the combustion gases immediately behind the detonation front reach a state of thermodynamic equilibrium. That this is so is attested to by the fact that theoretical detonation wave velocities which are calculated under the assumption of thermodynamic equilibrium for the products are in very good agreement with experimentally measured values[9]. The thickness of the reaction zone, which determines the distance behind the shock front at which the gas reaches equilibrium, is in all cases small (of the order of a centimeter or less) compared with the length of gas traversed by the hot wire during the period of heat transfer measurement (about 30 cm). The comparison of the measured voltage rise across the heat gage with that computed under the assumption of a constant total heat transfer leads to the conclusion that the heat transfer is substantially constant for the first 150 μsec.

The variation of the heat transfer for the stoichiometric hydrogen–oxygen detonations, which is due to the change in density, temperature and composition of the combustion products with initial pressure is in excellent agreement with the theoretical variation using computed transport properties. Over the range of initial pressures tested, the principal variation in heat transfer is due to the change in density, with the change in transport properties accounting for about 25 per cent of the change.

A similar comparison (Fig. 2) for various acetylene–oxygen mixtures at 1 atm initial pressure also shows excellent agreement between theoretical and measured heat transfer with respect to the dependence upon composition (see Section 4 for a discussion of curves *A*, *B* and *C*). However, the variation of heat transfer is as much due to the variation in transport properties as it is due to the composition change.

The measurement at 60 per cent and 70 per cent acetylene in Fig. 2 deserve special comment. The measured heat transfer at 70 per cent acetylene is certainly in accord with the failure to achieve acetylene decomposition as indicated by the experiments of[7, 8]. That at 60 per cent seems somewhat low for only this effect and might be due to a failure to achieve complete equilibrium at the wall with respect to the preferential attachment of oxygen to hydrogen rather than to carbon. Why this might be so at 60 per cent acetylene but not at 70 per cent acetylene is not clear.

The reduction in heat transfer due to coating the wire gage with iodine is most striking in the oxygen–hydrogen mixture (Fig. 1). The measurements seem to agree fairly well with the reduction in heat transfer to be expected if no gas phase or surface recombination takes place, and if vibrational energy is assumed not to be transported to the wall. If the vibrational heat capacity were not frozen, then the theoretical heat transfer line would lie about 50 per cent higher than that shown in Fig. 2. Freezing the rotational heat capacity would lower the theoretical line about 40 per cent but this is not a likely hypothesis in view of the very short rotational relaxation times for most species. It might also be supposed that the evaporation of the iodine coating would reduce the heat transfer to the wire. In order for this effect to be appreciable, it is necessary that the partial pressure of the iodine vapor at the wire

surface should be an appreciable fraction of the total pressure. Since the wire surface did not exceed 200°C at the highest heat transfer rates over the testing times for which the heat transfer was measured, the effect of evaporation would at the most reduce the heat transfer by 5 per cent. There seems to be no other conclusion to be drawn from this drastic reduction in heat transfer other than that the iodine coating is noncatalytic for the recombination of the dissociated species.

In order for a noncatalytic surface to reduce the heat transfer, it is necessary that the boundary layer be "frozen". This latter condition will be achieved when the chemical recombination time is long compared with the time for a particle to diffuse through the boundary layer. Since this diffusion time for a boundary layer on a blunt body is also equal to the time for a free stream particle to flow around the body, it is about 10^{-7} sec for the experiments under consideration. From the measurements of the thickness of the reaction zone[10, 11], some idea of the recombination time may be obtained. Assuming that the time for the gas to flow through the reaction zone is about the same time as the recombination time, then the measurements indicate that the ratio of recombination time to diffusion time for the stoichiometric hydrogen–oxygen mixture is about 6 at 1 atm pressure and about 60 at 1/10 atm initial pressure. Thus, there is every reason to believe that the boundary layer is frozen for the oxy–hydrogen mixtures. For the acetylene–oxygen mixtures, this ratio is about 6 at 1/10 atm initial pressure and, assuming a recombination time inversely proportionate to the pressure, would be about 0·6 at 1 atm initial pressure. Thus, for acetylene–oxygen mixtures, the boundary layer would be frozen at the lower pressure, but near equilibrium at the higher pressure.

With reference to Fig. 3, which shows the variation of heat transfer to coated and uncoated gages for a 50 per cent acetylene mixture at reduced pressures, it can be seen that there is a tendency for the difference in heat transfer to become larger at lower pressures. The difference between coated and uncoated gages

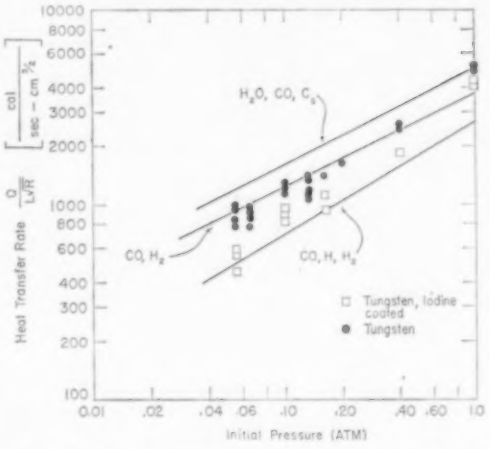

Fig. 3. The variations of heat transfer with initial pressure in equimolar oxy–acetylene mixtures. The three solid lines are correlations computed by assuming gas composition at the wall as indicated.

is less marked than in the oxy–hydrogen waves for two reasons. First, at the lower pressures the reaction*

$$2CO + \tfrac{1}{2}H_2 + H \rightarrow CO + H_2O + C_{(s)} \qquad (9)$$

fails to equilibrate in the gas phase as well as on the bare tungsten wire, as is to be inferred by the heat transfer measurements for the bare wire falling on the middle line of Fig. 3. Secondly, the energy of dissociation of the hydrogen and the vibrational energy of the molecules is not so large a fraction of the total as is the case for the more highly dissociated oxy–hydrogen mixture. Nevertheless, the trend is clear and it can be concluded that both the bare and coated surfaces are noncatalytic to the recombination of equation (9), while the coated wire is noncatalytic to H atom recombination.

The difference between the coated and uncoated wire heat transfer seems to be entirely in accord with the criterion discussed above as to whether or not the boundary layer is frozen or in equilibrium. At 1 atm pressure the boundary layer is nearly at equilibrium, and the noncatalytic coating of the wall has little effect

* The left side of equation (9) is the approximate free stream composition of the equimolar acetylene–oxygen mixture.

in reducing the heat transfer. At the lowest pressure, the boundary layer should be frozen and a marked reduction due to the noncatalytic wall is found.

It is possible to estimate an upper limit to the wall recombination coefficient (fraction of dissociated particles hitting the wall which are recombined on the wall) by comparing the maximum rate at which particles can diffuse to the wall with the rate of effusion when the dissociated particles have a wall concentration comparable to that in the free stream. Since this ratio varies inversely with the square root of the density, it will have its least value for the experiment at the highest initial pressure. Using the experimental results for the oxy–hydrogen mixture, it is found that the wall recombination coefficient must be much less than 10^{-2}; that is, about 10^{-3} or less. Such a value is not inconsistent with the best noncatalytic surfaces for hydrogen atom recombination, as given in[12].

REFERENCES

1. J. A. Fay and F. R. Riddell, *J. Aero. Sci.* **25**, 73 (1958).
2. L. Lees, *Jet Propulsion* **26**, 259 (1956).
3. R. Goulard, *Jet Propulsion* **28**, 737 (1958).
4. P. H. Rose and W. I. Stark, *J. Aero. Sci.* **25**, 86 (1958).
5. J. C. Cutting, J. A. Fay, W. T. Hogan and W. C. Moffatt, Final Report Air Force Office of Scientific Research, Contract No. AF49 (638)-375, AFOSR-TR-59-78 (1959).
6. R. E. Duff and H. T. Knight, *J. Chem. Phys.* **25**, 1301 (1956).
7. G. B. Kistiakowsky and W. G. Zinman, *J. Chem. Phys.* **23**, 1889 (1955).
8. S. Basu and J. A. Fay in *7th Symposium on Combustion*, p. 277. Butterworths, London (1959).
9. B. Lewis and G. von Elbe, *Combustion, Flames and Explosions of Gases*. Academic Press, New York (1951).
10. G. L. Opel, SM Thesis, Massachusetts Institute of Technology, Cambridge, Mass. (1959).
11. G. B. Kistiakowsky and P. H. Kydd, *J. Chem. Phys.* **25**, 824 (1956).
12. H. Wise, *J. Chem. Phys.* **29**, 1416 (1958).

HETEROGENEOUS FLASH PYROLYSIS OF HYDROCARBON POLYMERS

L. S. NELSON and N. A. KUEBLER
Bell Telephone Laboratories Inc., Murray Hill, New Jersey

Abstract—Pyrolysis takes place around minute particles suspended in a polymeric matrix when they are exposed to intense pulses of light. This method was used to study the pyrolysis of polyethylene and polypropylene in an exploratory fashion. Samples suspended in evacuated tubes were illuminated with a high-intensity flash discharge lamp, and the gaseous products analyzed by gas chromatography. The resulting analysis shows the presence of H_2, air, CO, CH_4, C_2H_6, CO_2, C_2H_4 and C_2H_2. It was noted that as a sample of polypropylene was exposed to a successively higher number of flashes the proportion of C_2H_2 formed decreased, while in the polyethylene pyrolysis, increasing the number of flashes increased the fraction of C_2H_2. The analysis, which was carried out only through C_3H_8 without detecting this component, accounted for approximately 50 per cent of the total gaseous products from polypropylene, while approximately 80 per cent of those from polyethylene were found. Proposals are made for improving the reproducibility of this type of experiment with more ideal suspensions for absorbing bodies.

1. INTRODUCTION

The degradation of polymers at high temperatures has become important recently in applications such as the re-entry of missiles into the atmosphere and the protection of clothing fibers against nuclear blast luminosities. In order to study such phenomena, new techniques are needed for inducing extreme temperatures in polymers in a rapid and controlled fashion. Hot flames[1], solar and arc image furnaces[1], water-stabilized arcs[1], dielectric breakdown[2] and hot filaments[2] are among the techniques which have been used previously.

The technique of heterogeneous flash heating described by Eggert[3] and in more detail by Nelson and Lundberg[4] provides a method of very rapidly and conveniently raising the temperature of light-transmitting materials easily to $\sim 2000°C$. This is done by using intense millisecond pulses of light with fluxes of the order of 4J cm^{-2}/msec (or 4 kW cm^{-2}) to illuminate small absorbing solid bodies (e.g. dust particles, fibers, thin foils) which are suspended in a transparent thermally insulating matrix such as a hydrocarbon polymer. The incident radiation is largely degraded into thermal energy which can heat both the absorber by inward conduction and the insulating matrix by outward conduction and cause black-body reradiation of some energy outward. If the smallest dimension of the absorber is approximately 1–100 μ, energy dissipation normally is low enough that its temperature will rise to very high levels. This induces degradation in the matrix immediately surrounding the absorber and produces materials characteristic of very violent pyrolytic decomposition. Most polymers, including polytetrafluoroethylene, degrade easily this way unless particular care is taken to exclude particulate impurities.

This paper describes a preliminary application of this technique to the degradation of polyethylene and polypropylene, both of which contain trapped absorbing particles, mainly dirt introduced during processing. Strips of these polymers were degraded by suspending in evacuated glass tubes inside the coil of a capacitor-powered spiral rare-gas discharge lamp. As the lamp was flashed one or more times, carbon and fluorescent materials were produced, accompanied by gaseous products which were analyzed by gas chromatography.

Since this work shows that absorbing spheres, cylinders and foils with dimensions 1–100 μ

trapped in a polymer are heated to pyrolysis temperatures when exposed to intense luminosities, the presence of such absorbers as impurities or reinforcements should be avoided when it is desirable to prolong polymer life toward luminous fluxes, for example in missile ablation. On the other hand, when primarily the cooling effects of degradation are desired in a poorly absorbing polymer, particles of just these shapes and sizes should be added as sensitizers, as in the case of protection against nuclear blast luminosities.

2. EXPERIMENTAL

The samples used were 0·060 in. × 0·25 in. × 2·50 in. strips of Esso 115 polypropylene and DYNK polyethylene, molded from commercial pellets in a heated press. Each strip was weighed, placed in a Pyrex tube behind a break-off seal and evacuated until the residual pressure was less than 10^{-5} mm of Hg. Since it was noted in early experiments that the degree of outgassing affected reproducibility somewhat, all samples of a given polymer were evacuated, sealed off and flashed at the same time.

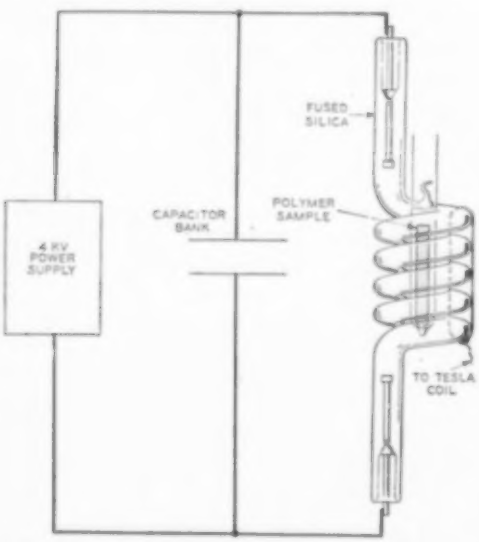

Fig. 1. Experimental arrangement for inducing heterogeneous flash heating.

Pyrolysis of the samples was accomplished by flashing them with a xenon-filled quartz lamp[5] as shown in Fig. 1. Samples were placed within the coil along the axis of the lamp which was flashed one or more times with capacitances of 216 and 324 μF (1728 and 2592 J/flash) for polyethylene and 396 and 468 μF (3168 and 3744 J/flash) for polypropylene. The capacitors always were charged to 4 kV. This resulted in formation of carbon-lined bubbles throughout the polymer, out of which pyrolysis gases burst explosively. A photograph of this type of degradation in polyethylene is shown in Figs. 2(a) and (b)*.

After illumination, the tubes were sealed on to a glass–mercury gas collection system where the gases formed during pyrolysis were pumped into a known volume and the pressure measured. This gas handling system consisted of a mercury diffusion pump, Toepler pump and a standard volume, all initially evacuated below 1×10^{-5} mm Hg. At the top of the standard volume was sealed a special glass gas sampling stopcock of the type described by Glew and Young[6].

Analysis of the products was carried out by injecting 0·099 cm^3 of the gases with this sampling stopcock directly into a Perkin–Elmer gas chromatograph, Model 154-*B*. Helium carrier gas at a flow rate of 33 cm^3 min^{-1}, a 2-m silica gel column at 50°C and a thermistor thermal conductivity detector were used. These conditions gave a chromatogram with optimum peak resolution and running time. The components observed were H_2, air, CO, CH_4, which were eluted in approximately 4 min, C_2H_6, CO_2, C_2H_4, which came through the column in approximately 30 min, followed by C_2H_2 at 55 min. Propane normally appears before C_2H_2, but never was observed here. The number of moles of any one component in the sample was obtained by comparing its peak area with that of the same component in a known mixture of the above eight gases used to standardize the system twice daily. A linear relation was assumed between peak area and partial pressure of the component.

* The authors are indebted to Dr. J. L. Lundberg for his assistance in preparing these figures.

3. RESULTS

It was found empirically that when samples of a given polymer are flashed multiply at low energies, the total number of moles of pyrolysis gas produced per gram of polymer is nearly linear with the square of the number of flashes to which it is exposed. This is shown in Figs.

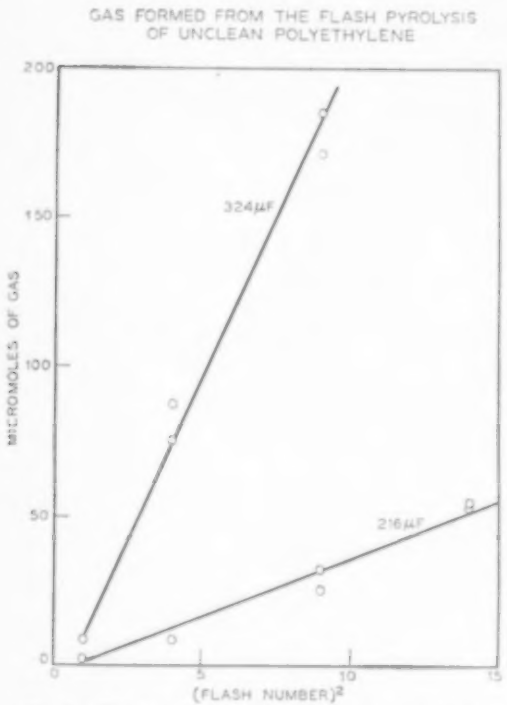

Fig. 3. Total volatiles produced by the flash pyrolysis of unclean polyethylene.

3 and 4. Linear plots other than those shown in Fig. 3 were obtained with the same polyethylene when flashed at somewhat different energies, but since analyses were not performed on the samples, they have not been included in this discussion. When the flash energies become considerably higher, near 5000 J/flash, considerable carbon is deposited on the inner walls of the tubes in which the polymer is flashed, which causes degradation on subsequent flashes to be greatly reduced with a marked departure from linearity. This is thought to be due to a diminution of the light which reaches the polymer by the opaque carbon deposit and also possibly to a reaction of the gases from earlier flashes with the heated carbon on the wall. We have avoided the heavy carbon deposits here by using flash energies low enough to produce at least three or four flashes without noticeable carbon formation on the walls of the container.

The degradation products observed are mainly hydrogen and small fragments of the hydrocarbon skeletons of the polymers, as shown in Figs. 5 and 6. In both polyethylene and polypropylene, methane was most prevalent,

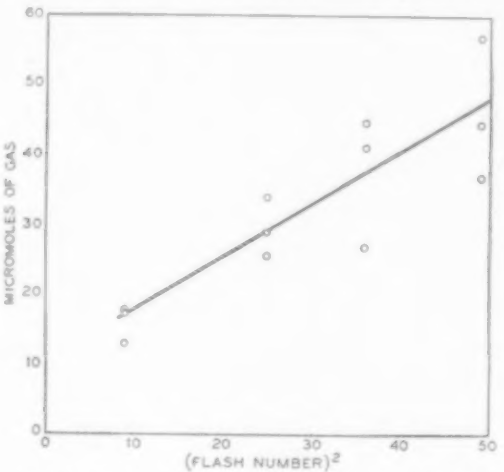

Fig. 4. Total volatiles produced by the flash pyrolysis of unclean polypropylene.

with almost as much hydrogen and considerably less of the C_2 hydrocarbons. No propane was ever observed from either polymer at our sensitivities, even though its peak would have appeared in our chromatograms. No analyses were carried further because of the very long appearance times necessary for the heavier gases on silica gel.

Acetylene did not appear to be a primary product of the degradation, since it was never detected until after more than one flash had occurred, unless the flash energy was so great that visible carbon was deposited during the first flash. It is thought that the methane reacts on subsequent flashes with the hot carbon deposited both in the polymer and on the walls of the tube to give acetylene and perhaps

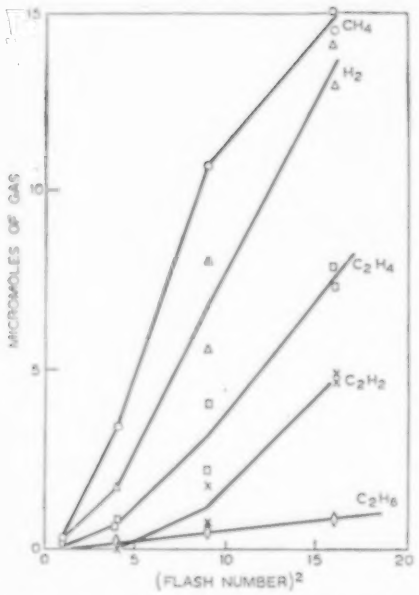

Fig. 5. Gases formed from flash pyrolysis of unclean polyethylene, 216 μF at 4 kV.

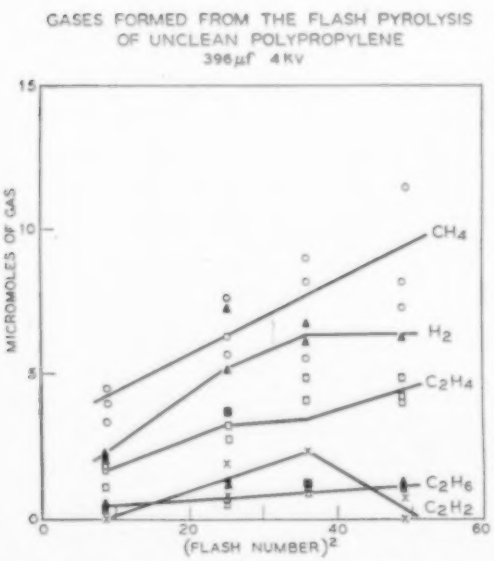

Fig. 6. Gases formed from flash pyrolysis of unclean polypropylene, 396 μF at 4 kV.

ethylene. Ethane did not seem to react similarly, however, since it formed in continually increasing amounts from both polymers as the flashing progresses.

Of the two polymers studied, the polyethylene sample formed carbon and gases at much lower flash energies than the polypropylene. From these experiments, where the absolute amounts and sizes of absorbing bodies trapped in the polymer are unknown, it is not possible to say whether the polyethylene is actually less stable thermally than the polypropylene or merely has more particles of the correct dimensions for energy transfer into the polymer. More reproducible methods of suspending the absorbing bodies will be needed before such information can be obtained. This will be discussed later.

The polyethylene gave a greater C_1 and C_2 fraction of the total volatile gaseous products than did the polypropylene. This was calculated by summing the number of micromoles of gas obtained by the chromatographic analyses of each experiment and comparing with the pressure-volume products of the total gases injected into the gas chromatograph. The fraction of C_2 hydrocarbons or lighter in the total volatiles is about 80 per cent in the case of polyethylene and about 50 per cent for

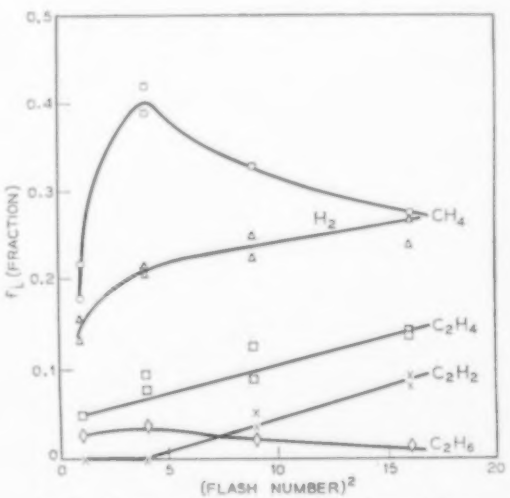

Fig. 7. Fraction of total volatiles formed from flash pyrolysis of unclean polyethylene, 216 μF at 4 kV.

Refer to page 62
(facing page 64)

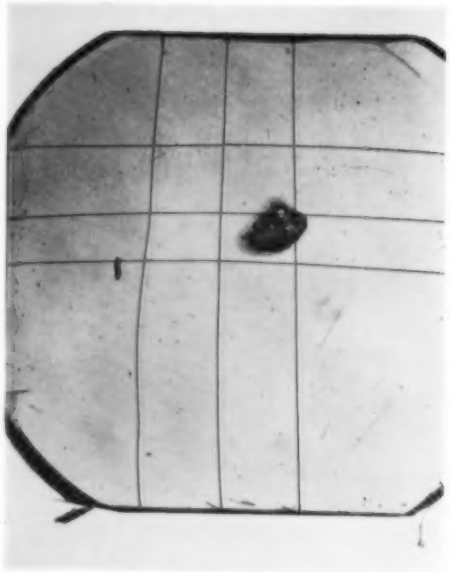

Fig. 2A

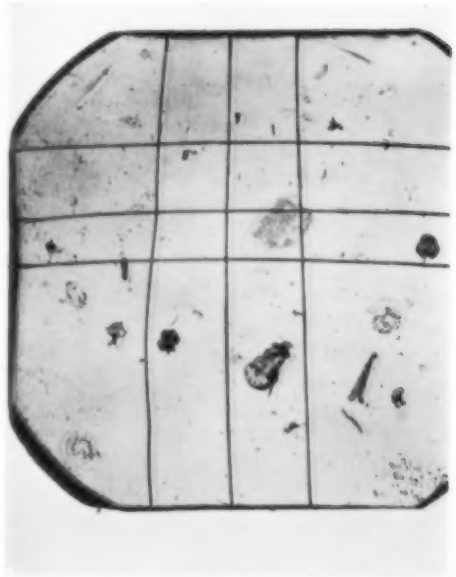

Fig. 2B

Fig. 2. Micrograph of heat-laminated polyethylene sandwich containing dust particles and 50 μ oxide-blackened tungsten wires spaced 1 mm apart; (a) before flash, (b) after two flashes at 5184 J/flash. Note cylindrical bubbles around wires and irregularly shaped bubbles around dust particles. Large spot is due to poor adhesion in laminate, and is not significant.

polypropylene in these experiments. When standardized against each other, the sums for our known mixtures of only the C_2 and lighter gases always were near 100 per cent. Experimentally, this means that we have carried out only partial analyses of the volatiles, since molecules more tightly adsorbed by the silica gel column packing than C_2 hydrocarbons remain in the column for several hours and emerge as a very broad peak which is corrected for as a small baseline drift. It is likely that the major product in the polypropylene is propylene, which was not analysed in these experiments.

In Figs. 7 and 8 are plotted the fractions of the total volatiles formed from the heterogeneous flash heating of polyethylene and polypropylene, respectively. It is evident that the decrease of the methane fraction with increasing flash number is quite similar for both polymers in the higher flash regions. Hydrogen in both polymers increases, then begins to decrease again. The fraction of ethane formed

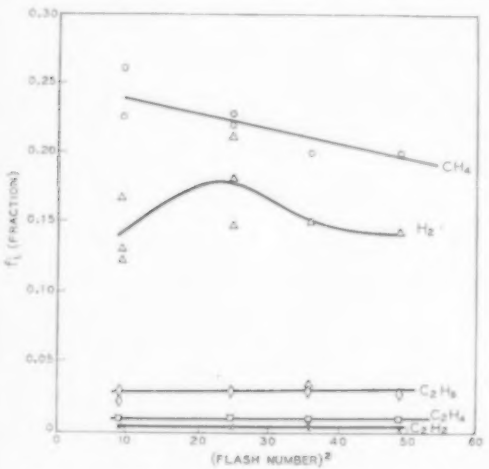

Fig. 8. Fraction of total volatiles formed from flash pyrolysis of unclean polypropylene, 396 μF at 4 kV.

is of nearly the same magnitude and constant in both polymers, suggesting that its formation may not be related to that of the other hydrocarbon fragments.

The fraction of C_2 unsaturates differs widely between the two polymers. In the case of the more easily degraded (under our conditions) polyethylene, the fraction of ethylene and acetylene increases with repeated flashing, while the same quantity for polypropylene is essentially constant.

Since these experiments are admittedly only preliminary studies of the application of the flash heating technique to polymer degradation, there are not enough data to interpret the results in a very quantitative fashion. Several patterns seem to emerge in the pyrolyses, however. The cleavage of polyethylene into small fragments, including carbon, seems quite consistent with lower temperature pyrolyses[7], where random chain scission predominates. The pyrolysis of polypropylene with its large fraction of high molecular weight volatiles, suggests that unzipping as well as random scission are both operative. More detailed studies of propylene formation would be desirable here.

The formation of the less saturated gases from methane in the presence of carbon heated by the flash seems to be quite well established also, especially from other pyrolyses at much higher flash energies (648 μF, 4 kV). Here the methane curve does not merely change slope as shown in Fig. 5, but actually drops nearly to zero when large amounts of carbon are present in the tube.

Thus we see the importance of not only the shape and size of the absorbing bodies suspended in the polymer[8], but also the contact between particle and polymer during the flash. As the flashing proceeds in a polymer, a bubble is blown which contains carbon, large polyenic and aromatic molecules and pyrolysis gases which react complexly on subsequent flashes.

The temperatures of pyrolysis are uncertain in these experiments, as in all the flash heating work done so far. Estimates of temperature rise can be made, however, by a simple energy balance equation from the characteristics of the flash, the thermal conductivity of the polymer, and the dimensions, absorptivity and thermal conductivity of the absorbing bodies[9]. If we use such a calculation, we find for particles with the properties of graphite spheres of diameters 1, 10 and 100 μ temperature rises of 200, 800 and 150 degrees centigrade. If it can be

assumed that the particles dispersed in the polymer have a wide distribution of sizes and about the same weight of particles of each dimension, the predominant reactions then will be those caused by the maximum temperature rise. The temperature dependence of a rate constant calculated for the optimum particle size, 10 μ, indicates a 56-fold increase in rate over 1 and 100 μ particles. This means that so long as there are particles with diameters near 10 μ present, the major fraction of our degradation products results from pyrolysis carried out at approximately 800°C. With higher-energy discharges and more ideal sample preparation, it should be possible to carry out pyrolyses at temperatures of the order of 2000°C.

4. CONCLUSIONS

These exploratory experiments have an overall reproducibility of about 10 per cent, even between samples taken from immediately adjacent positions in the original polymer sheets, which is greater than the combined instrumental errors of about 5 per cent. This was especially true of the polypropylene, which exhibited many fewer degradation centers than the polyethylene. This suggests that a poor distribution of absorbing particles in the original polymer matrix is causing the low reproducibility. (These light sources are extremely reproducible and used in certain instances as secondary illumination standards.) For this reason, we propose that further experiments be carried out with a more reliable dispersion of absorbers in the polymer matrix. Spherical particles of diameters in the 1–100 μ range are not easily dispersed in a viscous polymer without adding airborne solid contaminants also. On the other hand, cylindrical absorbers in the form of wires or fibers are quite easy to handle in this size range, are readily available commercially and have known shapes and dimensions. Some trial experiments with oxide-blackened tungsten wires of diameter 0·005 in. wound as a grid and imbedded in polyethylene have shown heavy degradation upon flash irradiation, but now with cylindrical bubbles the length of the wire. If the wires protrude from the surfaces of the polymer, there is the further advantage that these tubular bubbles allow the pyrolysis gases to leave the degradation sites more directly than by blowing out through the surface of the polymer as occurs with spherical particles. Perhaps the most reproducible technique for preparing samples would be to polymerize a freshly distilled dust-free liquid monomer in place around a precision-wound grid of metal, carbon or refractory oxide wires or fibers. This would minimize the effects of external dust contamination as well as give very intimate contact of the polymer with the absorber during the flash. There should be little restriction on the chemical nature of the polymer, as long as it transmits visible light.

It is felt that the preliminary experiments described in this paper demonstrate that flash heating is a usable technique for studying the behavior of polymers at high instantaneous thermal fluxes similar to solar furnaces[10] with simple commercial apparatus. Since the brightness temperatures of these flash sources are of the order of 5000°K, studies should be possible up to this limit with proper choice of flash energies and discharge times. In addition, it should be possible to surround samples easily with a variety of special atmospheres, such as plasmas, atomic species and hypersonic flows. Heterogeneous flash heating should have many applications to studies of degradation, protection and sensitization of polymers.

REFERENCES

1. See for example I. J. GRUNTFEST and L. H. SHENKER, *Mod. Plast.* **35**, 155 (1958).
2. R. S. LEHRLE and J. C. ROBB, *Nature, Lond.* **183**, 1671 (1959).
3. J. EGGERT, *J. Phys. Chem.* **63**, 11 (1959); *Phys. Bl.* **10**, 549 (1954).
4. L. S. NELSON and J. L. LUNDBERG, *J. Phys. Chem.* **63**, 433 (1959).
5. Similar to lamp III of M. I. CHRISTIE and G. PORTER, *Proc. Roy. Soc.* **A212**, 390 (1952).
6. D. N. GLEW and D. M. YOUNG, *Analyt. Chem.* **30**, 1890 (1958).
7. L. A. WALL, S. L. MADORSKY, D. W. BROWN, S. STRAUS and R. SIMHA, *J. Amer. Chem. Soc.* **76**, 3430 (1954).

8. See for example the temperature rise curves shown in Fig. 3 in the paper by J. L. LUNDBERG and L. S. NELSON, *Nature, Lond.* **183**, 1560 (1959).
9. J. L. LUNDBERG, L. S. NELSON and M. Y. HELLMAN in *Proc. 3rd Conf. on Carbon, Buffalo, N.Y., 1957.*
10. W. R. NULL and W. W. LOZIER, *Rev. Sci. Instrum.* **29**, 163 (1958).

BEHAVIOUR OF PLASTIC LAMINATES AT ELEVATED TEMPERATURES

S. RUBY, J. B. COHEN* and F. K. WARD
AVCO Corporation, Wilmington, Mass.

Abstract—"Charred" material from several plastic laminates have been analysed, chemically, by *x*-ray absorption and by activation analysis. Charring was caused either by exposure to a plasma jet or by re-entry. Some conclusions are drawn as to the mechanism of charring and the necessity for further work is outlined.

1. INTRODUCTION

When laminates consisting of a phenol–formaldehyde resin and glass are exposed to a plasma jet, they exhibit a "charred" layer. Visually, the charred layer is seen to consist of several separate layers having diffuse boundaries. The present program was instituted to characterize quantitatively these charred layers to determine whether changes in the physical form or fraction of glass had any effect on charring and to obtain information concerning the nature of charring and ablation.

There appear to be four mechanisms by which such a laminate might absorb heat. These are:

(1) The glass boils and absorbs heat of vaporization. The resin serves as a binder.

(2) The decomposition of the resin absorbs heat. The glass serves as reinforcement.

(3) Both the glass and resin absorb heat independently.

(4) The resin and glass interact. Silica and carbon react to form silicon carbide according to the equation:

$$SiO_2 + 3\,C \rightarrow SiC + 2\,CO$$

At 1400°C, the carbon monoxide pressure is about one atmosphere. Carbon or organic fragments resulting from the pyrolysis of the resin or perhaps even the resin itself might undergo similar reactions which would be endothermic. One purpose of the present work was to look for evidences of such reactions.

* Department of Metallurgy and Materials Science, North-Western University, Evanston, Illinois.

2. ORGANIC ANALYSIS

Three laminates, differing in the physical form of the reinforcing material and ratio of inorganic to organic fractions have been studied. Cylindrical specimens, $\frac{3}{4}$ in. in diameter and $1\frac{1}{2}$ in. long, were exposed to the jet of an air-stabilized arc. Fig. 1 represents the charred layers obtained with Material *A*. There were three fairly definite separate layers—the first was silver black, the second brown black and the third was light yellow. The original color of the material was brown. The charred layers on Materials *B* and *C* were somewhat different in that they were coated with a very thin layer of glass which appeared to be free of organic matter.

Samples were taken of the layers as shown in Fig. 1. Sample *E* was taken as representative of the uncharred material; and for Materials *B* and *C*, sample *D* was taken immediately beneath sample *C*. These samples were analysed by the usual method of quantitative microorganic analysis for hydrogen and carbon. The ash was weighed and the difference was taken as organic oxygen. The samples were burned under conditions which would not oxidize silicon carbide so that it, if any, would be found in the ash unchanged.

The resulting analyses for Material *A* are summarized in Table 1. The following points of interest may be noted:

(1) Layer *C*, though not black, was charred, i.e. altered.

(2) In the course of charring, the laminate loses a greater proportion of hydrogen than

Table 1. Material *A* (10 Samples)

Layer	% ash	% C	% H	% O	C/O	H/O	C/H	% C polymer	% H polymer	% O polymer
A	85·51 ± 4·14	14·46 ± 4·16	0·03 ± 0·09	0·19 ± 0·18	95·9	2·3	41·5	99·79	0·21	1·31
B	83·77 ± 5·48	14·65 ± 5·34	0·36 ± 0·11	1·26 ± 1·38	24·9	7·4	3·4	90·26	2·22	7·76
C	78·55 ± 8·18	17·21 ± 6·33	1·05 ± 0·50	3·19 ± 1·43	6·2	5·2	1·2	80·23	4·90	14·87
D	75·19 ± 9·17	18·84 ± 6·99	1·41 ± 0·53	4·55 ± 1·68	5·5	5·0	1·1	75·94	5·68	18·34
E	74·93 ± 7·52	19·04 ± 5·75	1·39 ± 0·46	4·68 ± 1·44	5·5	4·8	1·1	75·95	5·54	18·67

Table 2. Material *B* (18 Samples)

Layer	% ash	% C	% H	% O	C/O	H/O	C/H	% C polymer	% H polymer	% O polymer
B	91·70 ± 0·62	7·67 ±0·31	0·20 ±0·09	0·43 ±0·28	23·6	7·5	3·1	92·44 ± 3·68	2·44 ±1·07	5·23 ± 3·44
C	88·98 ± 0·86	8·81 ±0·54	0·49 ±0·09	1·72 ±0·45	6·8	4·6	1·5	80·01 ± 4·92	4·47 ±0·86	15·59 ± 4·12
D	86·94 ± 0·76	9·76 ±0·23	0·75 ±0·07	2·55 ±0·27	5·1	4·7	1·1	74·67 ± 1·79	5·75 ±0·54	19·54 ± 2·09
E	86·59 ± 0·89	9·89 ±0·19	0·83 ±0·07	2·69 ±0·20	4·9	4·9	1·0	73·73 ± 1·39	6·20 ±0·51	20·11 ± 1·48

Table 3. Material *C* (2 Samples)

Layer	% ash	% C	% H	% O	C/O	H/O	C/H	% C polymer	% H polymer	% O polymer
B	78·56 ± 0·13	20·86 ± 0·05	0·22 ±0·02	0·36 ±0·16	77·3	9·8	7·9	97·29 ± 0·23	1·03 ±0·09	1·68 ± 0·75
C	77·21 ± 0·20	20·49 ± 0·13	0·65 ±0·01	1·65 ±0·09	16·6	6·3	2·6	89·91 ± 0·57	2·85 ±0·04	7·24 ± 0·39
D	67·19 ± 0·20	24·30 ± 0·17	1·91 ±0·03	6·60 ±0·01	5·0	4·7	1·1	74·06 ± 0·52	5·82 ±0·09	20·12 ± 0·03
E	64·54 ± 0·29	25·43 ± 0·42	2·22 ±0·05	7·82 ±0·19	4·3	4·5	1·0	71·71 ± 1·18	6·26 ±0·14	22·03 ± 0·54

carbon and a still greater proportion of oxygen.

(3) The ratios given in the table are ratios of atoms. In both the *A* and *B* layers, the ratio of carbon atoms to oxygen and hydrogen atoms is so large that the organic residue in layer is practically free carbon and in layer *B* is largely carbon.

Tables 2 and 3 summarize data obtained for samples of Materials *B* and *C*. No analyses for the *A* layer are given since the samples were

Table 4. Material C Re-entered Vehicle (4 Samples)

Layer	% ash	% C	% H	% O	C/O	H/O	C/H	% C polymer	% H polymer	% O polymer
B	72·57 ± 0·48	26·34 ± 0·68	0·29 ±0·05	0·80 ±0·34	43·9	5·8	7·6	96·03 ± 2·48	1·06 ±0·18	2·91 ± 1·24
C	71·23 ± 0·47	25·04 ± 0·47	0·89 ±0·02	2·85 ±0·19	11·7	5·0	2·3	87·04 ± 1·63	3·09 ±0·06	9·87 ± 0·66
D	60·95 ± 1·00	29·15 ± 0·63	2·31 ±0·10	7·59 ±0·52	5·1	4·9	1·0	74·64 ± 1·61	5·92 ±0·26	19·44 ± 1·33
E	57·62 ± 1·05	30·31 ± 0·32	2·75 ±0·10	9·32 ±0·63	4·3	4·7	0·9	71·52 ± 0·76	6·49 ±0·24	21·99 ± 1·49

too small for analysis. Otherwise, the data lead to the same general conclusions.

Table 4 shows data for samples taken from a re-entered vehicle. The material was similar to Material *C* shown in the previous table. The data are quite similar to results obtained with samples exposed to the arc.

From the data shown, it can be concluded that charring consists of the loss of oxygen, hydrogen and carbon from the resin in decreasing amounts, finally leaving practically pure carbon.

3. VAPOR

The data already presented shows what is left but does not tell what fraction of the original material is left. Three approaches have been taken to obtain such data.

The first of these has been a material balance. By assuming that no glass was vaporized from the charred layers, that no reaction occurred in the charred layer between the glass and the resin, and that there was no volume change, it is possible to calculate the fraction of resin which vaporized from the layers and the composition of the vapor. The results of such a calculation for the data of Table 1 are shown in Table 5. The proportion vaporized is not large.

A second approach to this problem has been the determination of the density of charred layers by an X-ray technique. The intensity of an X-ray beam after traversing some material is given by

$$I = I_0 \exp\left[-\rho l \Sigma_i (\mu/\rho)_i X_i\right]$$

Table 5. Composition of Volatile Fraction of Char

Sample	% vaporized	Carbon (wt. %)	Hydrogen (wt. %)	Oxygen (wt. %)
A	12·5	51·1	10·9	35·8
B	10·7	55·9	10·0	32·9
C	4·7	57·0	8·3	33·9

where

I_0 is the flux of the incident radiation,
I is the flux of the transmitted radiation,
X_i is the weight fraction of each element in the laminate,
$(\mu/\rho)_i$ is the absorption coefficient of each element,
l is the thickness of the sample,
ρ is the density of the sample.

By using values of $(\mu/\rho)_i$ from the literature, values of the X_i from the chemical analyses and measuring I, I_0 and l, it is possible to compute values of ρ. The results of some determinations are given in Table 6. The data are for samples of Material *A*.

The gravitometer data were obtained by weighing in air and weighing in water. Such measurements cannot be made for charred samples because they absorb water. Agreement between these values and the X-ray data are excellent.

The geometry values were obtained by weighing and measuring. These values are low showing that the material is not fully dense.

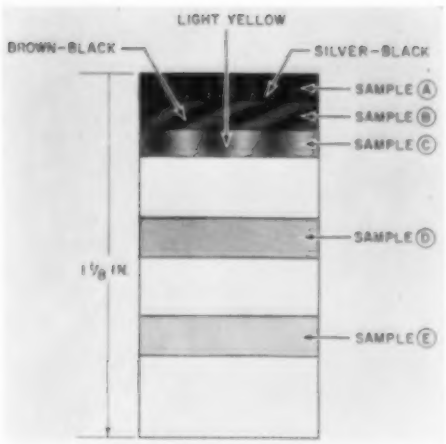

Fig. 1 Sampling of charred plastic laminate for analysis

Facing page 701

Table 6. Specific Gravity Change Upon Charring

Gravitometer*		Geometry*			*X*-ray absorption			Material balance	
Sample	ρg/cm^3	Sample	ρg/cm^3	% change in ρ	Sample	ρg/cm^3	% change in ρ	Sample	% change in ρ
2 uncharred	1·76	2 charred	1·35	20	2*B*	1·540	13·5	2*A*	11·4
								2*B*	10·0
		2 uncharred	1·69		2*E*	1·780		2*C*	4·8
7 uncharred	1·92	7 charred	1·41	19	7*B*	1·785	7·5	7*A*	7·9
								7*B*	8·2
		7 uncharred	1·74		7*E*	1·930		7*C*	3·9

* H. Seiger, personal communication.

The material balance data were obtained as were the data in the previous table. Agreement between these data and the X-ray data were quite good and tend to confirm the assumptions made in making the material balance calculations, i.e. (1) no glass is vaporized, (2) no volume change and (3) no reaction between glass and resin.

The third approach has been an analysis, by vapor phase chromatography and infra-red analysis, of the vapors evolved when laminates were pyrolyzed in a helium atmosphere at 900°C. Approximately 52 per cent of the resin remained in the residue after pyrolysis in the form of carbon. This represents approximately 67 per cent of the original carbon. These figures confirm what had already been found previously by density measurements and material balances, that the proportion of material which vaporizes on charring is relatively small.

This last work has led to some information on the nature of the gas which evaporates upon charring. Compounds which are solid or liquid at room temperature account for 32 per cent of the polymer and the remaining 16 per cent is gaseous. The liquid–solid fraction contains primarily water, phenol, cresols, toluene and benzene in decreasing amounts, with water about 50 per cent of the total. The gaseous fraction appears to be principally acetylene.

The front surface of a specimen recedes on exposure to the flame of an arc. This means that the charred layer is carried away either as solid, liquid, gas or mixtures and that charring continues into the specimen. Data have yet to be obtained on the composition of the vapor from the very surface of specimens. Further work upon the composition of vapors from plastic laminates is contemplated at temperatures higher than 900°C.

4. COMPOSITION OF THE ASH

X-ray diffraction studies of charred layers have given amorphous patterns except in one case where lines ascribed to β silicon carbide have been detected.

It seems reasonable from the studies already made that if chemical reactions are occurring between the resin and glass, such reactions must be taking place close to the surface of the specimen where the temperature is high enough. Samples for analyses of the ash must be taken from a very thin layer and these samples are very small.

Some work has been started at MIT to analyse these samples by activation analyses using deuterons in the MIT cyclotron. Examples of the nuclear reactions which occur are:

$$_8O^{17} + {}_1d^2 \longrightarrow {}_9F^{18} + {}_0n^1$$

$$_6C^{12} + {}_1d^2 \longrightarrow {}_7N^{13} + {}_0n^1$$

$$_{14}Si^{29} + {}_1d^2 \longrightarrow {}_{15}P^{30} + {}_0n^1$$

The resulting nuclides are all radioactive, decay by emission of positive beta rays. Their half-

lives, ranging from 2·55 min for the phosphorous to 1·87 hr for the fluorine, are sufficiently different for identification.

Samples of carbon and silica have been irradiated and the expected radioisotypes have been detected but quantitative results have yet to be obtained and the work is to be continued.

5. CONCLUSIONS

The purpose of this work was two-fold: (i) to quantitatively characterize the charred layer, and (ii) to determine whether reactions between the inorganic and organic parts of phenol–formaldehyde laminates occur.

Several conclusions can be drawn about the first part.

(1) Charring occurs by loss of oxygen, hydrogen and carbon, the fractions lost decreasing in that order.

(2) Only 33 per cent of the carbon is lost, the rest remaining as free carbon (in the *B* layer).

(3) Below the altered layer which can be discerned visually, the yellow layer, no chemical change in the resin has occurred.

(4) The fraction of original material lost on charring is relatively small, amounting to about 48 per cent of the resin (in the *B* layer).

The second part of the problem needs further work. It is unlikely that the resin and glass react anywhere but close to the surface and reactions there are unproven. It is hoped that the activation analysis and analyses of vapors produced at high temperatures will give an answer to this question.

BEHAVIOR OF "TEFLON" FLUOROCARBON RESINS AT ELEVATED TEMPERATURES

P. H. SETTLAGE and J. C. SIEGLE

E. I. du Pont de Nemours and Company, Wilmington, Delaware

Abstract—The rates of heating and of decomposition of TFE- and FEP-fluorocarbon resins under conditions of high thermal flux are discussed. Calculated heating curves and rates of ablation are presented, as well as values for thermal, thermodynamic, and kinetic properties on which the calculations were based. Experimental work on the decomposition of TFE- and FEP-fluorocarbon resins at 450 to 600°C, at higher temperatures in a solar furnace and at still more severe conditions in a plasma jet are described. Calculated and experimental results are compared.

1. INTRODUCTION

The outstanding thermal stability, chemical resistance and electrical properties of "Teflon"* TFE-fluorocarbon resins have been utilized in many applications. Heat has little effect on their chemical structure below 400°C. Above this temperature degradation begins to occur at appreciable rates. Thermal decomposition at 360 to over 600°C has been studied by various investigators[1, 6]. Recently, interest in the behavior of materials at higher temperatures and at high rates of thermal flux has increased markedly. TFE-fluorocarbon resins (polytetrafluoroethylene) and FEP-fluorocarbon resin (a copolymer of tetrafluoroethylene and hexafluoropropylene) might be expected to have interesting properties under those conditions. Accordingly, information concerning the behavior of both types of fluorocarbon resins at temperatures above 450°C will be the subject of this paper.

The pyrolysis of thin films of polytetrafluoroethylene in vacuum has been thoroughly studied at temperatures from 360 to 510°[2, 3, 5, 6] and will be reviewed only briefly. The gaseous products of pyrolysis are 94–97 per cent tetrafluoroethylene with small amounts of other fluorocarbons such as carbon tetrafluoride, hexafluoropropylene and octafluorocyclobutane [1–3, 5, 6]. The composition of the volatile products remains constant during the course of pyrolysis and at different temperatures. Rates of degradation are independent of molecular weight. The kinetics of depolymerization are first order[2, 3, 5, 6]. The rate of expression: $(dM)/(dt) = -3 \times 10^{19} M \exp(-83{,}000/RT)$ g/sec was derived from the data of Siegle and Muus which were in good agreement with that of Madorsky and coworkers[2]. The plot of half life vs. temperature, shown in Fig. 1, provides a convenient means for estimating the time required for TFE resins to decompose at various temperatures. The extrapolation to temperatures above 510°C was made assuming that the mechanism of degradation does not change.

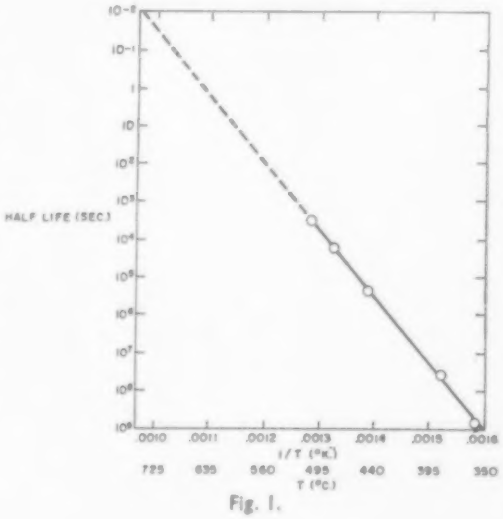

Fig. 1.

* du Pont registered trademark.

Measurements of rates of decomposition of thicker specimens of polytetrafluoroethylene have been made[5, 6], in vacuum and in the presence of various gases. Diffusion effects and temperature gradients in the sample make quantitative interpretation of these results difficult.

2. CALCULATIONS

The values for a number of properties of polytetrafluoroethylene over a range of temperatures are listed in Table 1. These quantities

Table 1. Properties of TFE Flourocarbon Resins

Density	
25–325°C	$\rho = 2{\cdot}333 - 7{\cdot}64 \times 10^{-4}\, T$ g cm^{-3} –
325°C	$\rho = 1{\cdot}985$ g cm^{-3} T = Temperature (°C)
325–450°C	$\rho = 1{\cdot}919 - 1{\cdot}16 \times 10^{-3}\, T$ g cm^{-3}
	Derived from data of Quinn, Roberts and Work, Ref. (7), and of Lupton, Ref. (8).
Specific heat	
25–300°C	$C_p = 0{\cdot}2227 + 2{\cdot}5 \times 10^{-4}\, T$ cal g^{-1} °C^{-1}
	Marx and Dole, Ref. (9).
Thermal conductivity	
25–325°C	$K = [1{\cdot}16 \times 10^{-2}\, T + 6{\cdot}05] \times$ $\times 10^{-4}$ cal cm^{-2} sec^{-1} °C^{-1} – cm
	Derived from data of Schultz and Wong[10].
Enthalpy of depolymerization	$\Delta H = 38{,}200 - 6{\cdot}67\,(T - 360)$ cal mole^{-1}
	Derived from data of Siegle and Muus[6].
Rate of depolymerization	$\frac{dM}{dt} = 3 \times 10^{-19}\, M \exp$ $(-83{,}000/RT)$ g sec^{-1}
	M = mass in grams

were used for the calculation, on an IBM 650 computer, of temperature gradients in slabs of TFE fluorocarbon resins when heat is applied to the surface.

Analytical solutions can be readily obtained from the Fourier conduction equation,

$$(dT)/(dt) = \alpha\,(d^2T)/(dx^2),$$

only when the thermal diffusivity α is constant. Since α is not constant for TFE resins over the range of temperatures of interest, the slab is considered as a series of laminae and the Fourier Conduction equation written in the difference form* is used.

$$T(x, t+\Delta t) = T(x, t) + \alpha \frac{\Delta t^2}{(\Delta x)} [T(x+\Delta x, t) - 2T(x, t) + T(x-\Delta x, t)]$$

where x = position, Δx = thickness of lamina, T = temperature, t = time.

The thermal diffusivity α is defined by the following equation

$$\alpha = \frac{K}{\rho C_p}$$

when K = thermal conductivity, ρ = density, and C_p = specific heat. Each of these quantities varies with temperature. The expression for heat capacity consists of the term for specific heat listed in Table 1 plus the following term to account for heat of fusion:

$$\frac{\Delta H_f \cdot \lambda}{\pi [\lambda^2 (T_f - T)^2 + 1]}$$

where

ΔH_f = heat of fusion = 14 cal g^{-1}
λ = parameter related to the melting range = 0·3
T_f = melting point = 327°C

In this term, the Cauchy approximation of the impulse function, λ was chosen so that 90 per cent of the heat of fusion would be taken up within 10° of the melting point. The curves calculated for temperatures within a slab with one surface maintained at 380°C are shown in Fig. 2. The temperatures at points at 0·04 in. intervals from the surface are shown as a function of time.

The heat of decomposition must be taken into account at temperatures above about

* The procedure for including thermal diffusivity, α, as a function of temperature in the Fourier equation, which ordinarily is discussed only for cases of constant α, was developed by Y. H. Pao, Polychemicals Department, E. I. du Pont de Nemours and Company.

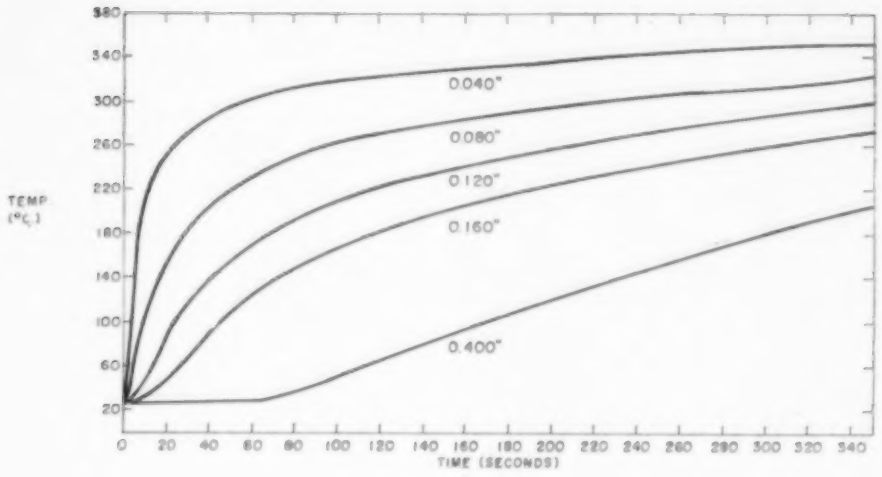

Fig. 2.

500°C. A third term involving rate of decomposition is included in the expression for heat capacity. This term is of the form

$$\frac{dH}{dt} = 1{\cdot}0 \times 10^{22} M \exp(-41{,}800/T) \text{ cal/sec.}$$

When the sum of the terms for a number of increments of time for the outermost lamina is equal to the total heat required to decompose it, the lamina is removed analytically. Rates of erosion are then determined from the intervals of time between analytical removal of successive layers.

Calculated results for a slab heated under conditions such that the boundary layer (the layer just above the surface of the polymer) is maintained at 700°C are shown in Fig. 3. The rate of erosion calculated for these conditions

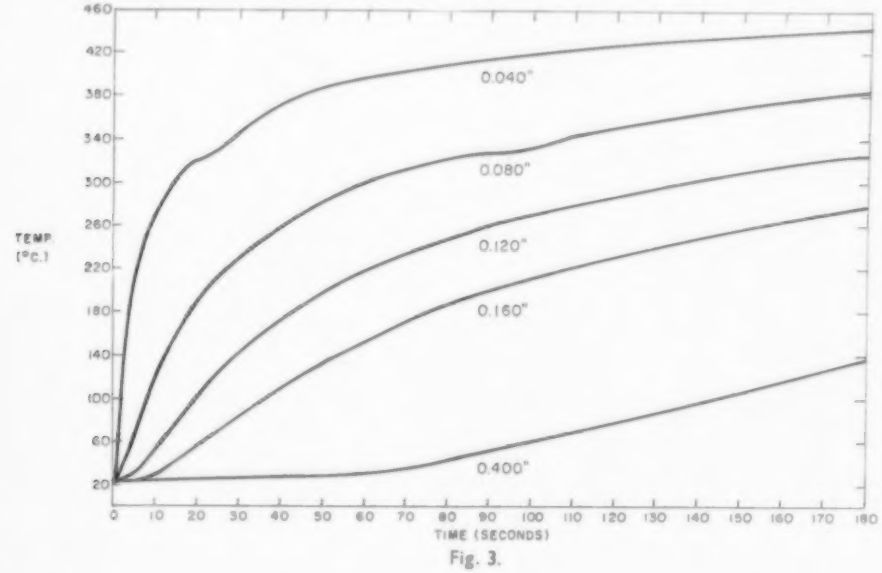

Fig. 3.

is 0·0005 in/sec. Under these conditions a large part of the thermal energy is used to raise the temperature of the bulk of the piece.

At higher temperatures conduction becomes less important. The calculated rate of ablation with a boundary layer temperature of 1800°C is 0·006 in/sec (Fig. 4). Points only 0·12 in. from the eroding surface are only about 25°C above their original temperature, a consequence of the low thermal conductivity of the resin and the relatively rapid rate of recession of the surface.

In this analysis only conditions at the surface of the polymer have been considered. The factors which influence conditions at the surface, such as coefficients of heat transfer and mass transfer into the boundary layer, must be taken into account in practice. Such an analysis, in which these and other factors were considered, was reported in a paper by Myers[11].

3. EXPERIMENTAL RESULTS

A thermogravimetric study* of the degradation of $\frac{1}{8}$ in. cubes of TFE and FEP fluorocarbon resins was made at temperatures from 420 to 620°C. Plots of weight loss in air are shown in Fig. 5. The kinetics of degradation do not appear to be first order as observed with thin films of TFE resins[6]. Diffusion of degradation products to the surface is rate

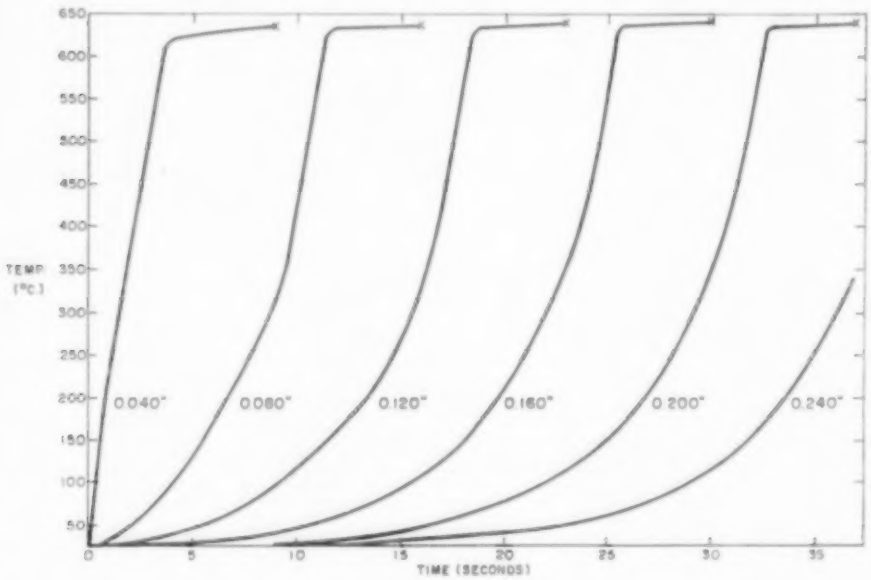

Fig. 4.

controlling for thicker samples. The surface area remains essentially unchanged over a considerable portion of the degradation and a relatively constant rate of degradation results.

The effects of nitrogen, air and oxygen atmospheres on the rate of decomposition were studied at 565°C. Differences in the rates of decomposition were observed (Fig. 6). A 200 mg sample of TFE fluorocarbon resin was completely degraded in less than 10 min in pure oxygen. In an atmosphere of nitrogen, less than 50 per cent of the sample had decomposed in 1 hr. The rate of decomposition in nitrogen is constant and characteristic of a diffusion controlled reaction. Similar behavior has been observed in vacuum for thick samples[6].

We believe that the differences in rates of decomposition in air, oxygen and nitrogen

* A Stanton thermobalance, model TR-1, was used.

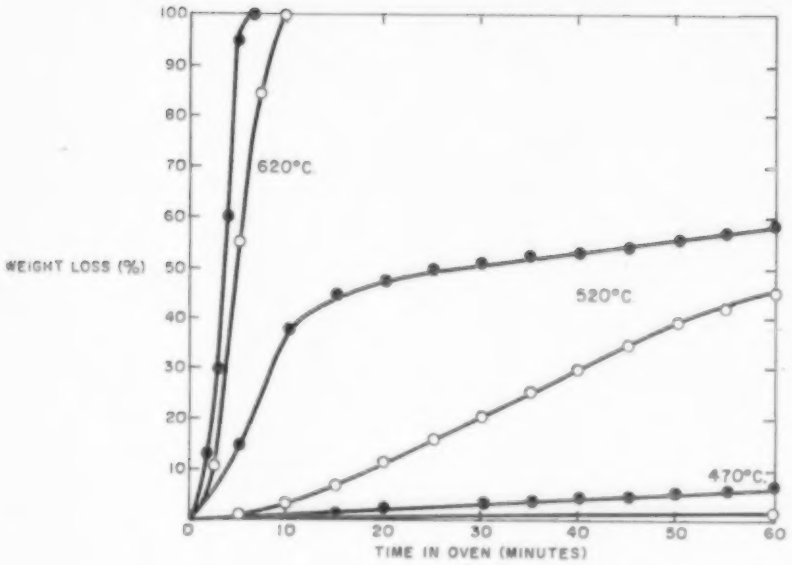

Fig. 5.

result from the exothermic reaction of oxygen and monomer within the sample. The heat of reaction is confined within the specimen increasing the rate of thermal decomposition. No such effect was observed for the pyrolysis of thin films in oxygen[6]. The rates of decomposition in atmospheres of air and oxygen are roughly proportional to the concentration of oxygen present.

The initial portion of the sigmoid shaped

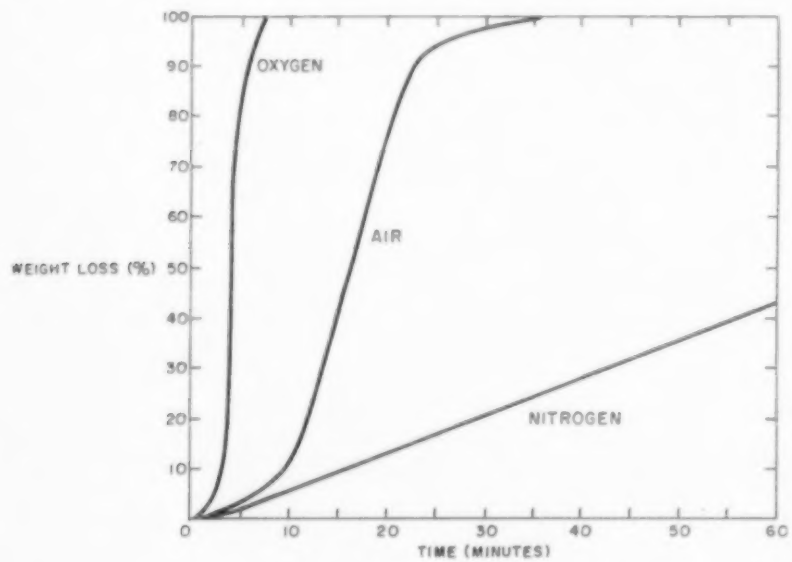

Fig. 6.

curve for the experiments in oxygen and air represents the time required to achieve steady state conditions of diffusion and heating.

The apparent reaction between oxygen and polymer is not self-sustaining. A visible flame appeared when heated air was passed over the surface of TFE fluorocarbon resin at ambient temperatures of 675°C or higher. The vapors above the surface ignited, but the flame was extinguished when the temperature was reduced a few degrees.

Specimens of TFE and FEP fluorocarbon resins, filled compositions of each and of filled phenolics were exposed in a solar furnace. The furnace consisted of a 60 in. searchlight which had been modified by replacing the electrode assembly with a mount for a sample holder. An adjustable cylindrical sleeve served as a diaphragm. The effective diameter of the reflector could be varied from 10 in. to 5 ft. The efficiency of the reflector was determined at each diameter used. Incident flux was measured with a normal incidence pyrheliometer* and a calorimeter was used to measure flux at the focal spot.

Specimens consisted of disks $1\frac{1}{2}$ in. in diameter and $\frac{1}{4}$ to $\frac{1}{2}$ in. The diameter of the central image was slightly more than $\frac{1}{4}$ in. thick. The run was 'tracked' during exposure to confine the area of the specimen exposed. Flux densities from 300 to 1100 W cm^{-2} were obtained. The surfaces of disks of TFE fluorocarbon resins were always smooth and showed no pits or cracks. Very small amounts of carbon were formed. With filled compositions, much larger quantities of carbon were formed. Bubbles were found in FEP resins, but no dripping was observed. The ablation rates for TFE resin are plotted in Fig. 7 and those for FEP resin in Fig. 8. In general, the rates of weight loss for 'Teflon' TFE resins, for filled compositions of TFE resins and asbestos or fiberglass and for filled phenolics were about the same. The rates for FEP resin were slightly higher than those for TFE resins, although the rates for FEP resin plus silica were lower than those of any other composition with fluorocarbon resins.

Cylindrical specimens, $\frac{1}{2}$ in. in diameter and $2\frac{1}{2}$ in. long were exposed in the jet from a plasma torch* under several conditions. Temperatures at the nozzle were estimated from curves of

* The Eppley Laboratory, Newport, R.I.

* Thermal Dynamics Corporation, Hanover, N.H.

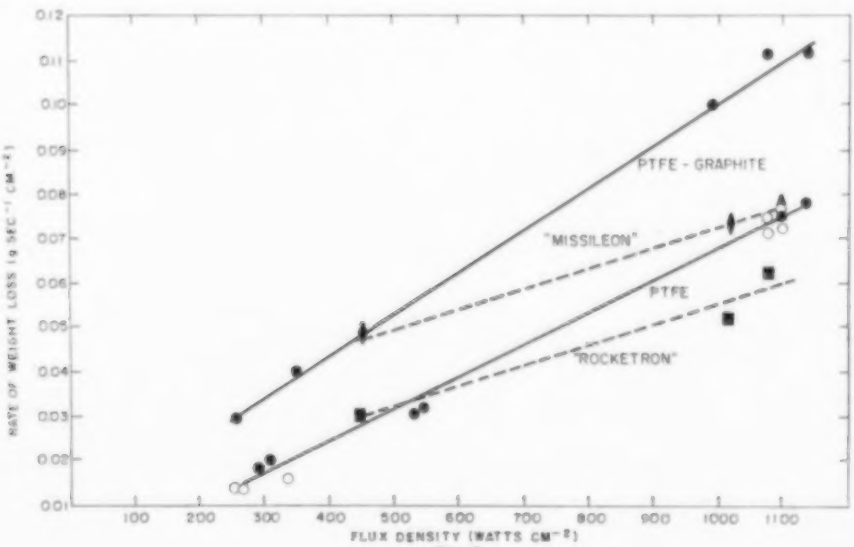

Fig. 7.

temperature vs. power input supplied with the apparatus. The jet was allowed to impinge on the end of the specimens which were located $1\frac{1}{2}$ in. from the nozzle. The results for each set of conditions can be compared, but comparison at different conditions probably are not valid. The results obtained are shown in Fig. 9 where weight loss is plotted against calculated temperature. The torch was operated with mixtures of nitrogen and hydrogen at the three

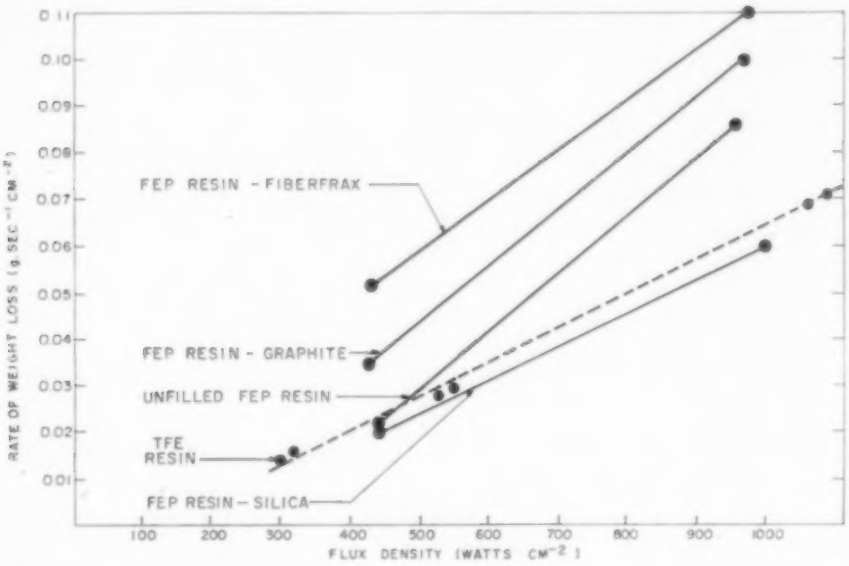

Fig. 8.

in the calculations described, is approximately 25 cal cm^{-2} sec^{-1}. An erosion rate of 0·006 in. sec^{-1} was observed in the solar furnace when the net rate of heat transfer to the surface of the TFE resin was 25 cal cm^{-2} sec^{-1}. The agreement between calculated and observed rates is not a rigid test of the procedure used in the calculations since the net rate of heat transfer to the polymer is not known precisely. It does indicate that the method of analysis is valid, and could be used for determining rates of ablation under conditions where other factors such as coefficients of heat transfer and effects of mass transfer into the boundary layer are known.

lower temperatures while a mixture of argon and hydrogen was used at the highest temperature. The rates of erosion for fluorocarbon resins were faster than those of the filled phenolics under all conditions. However, the great variability in the relative rates of erosion for the different materials under various conditions indicate that additional work must be done to define clearly the usefulness of various materials.

4. COMPARISON OF CALCULATED AND EXPERIMENTAL RESULTS

The flux density equivalent to a black body temperature of 1800°C, the temperature used

The sharp temperature gradient calculated (Fig. 4) for an eroding slab requires that the zone where the temperature is high enough to cause appreciable degradation be quite narrow. A photomicrograph of the cross section of a specimen exposed in the solar furnace (Fig. 10) shows that this is indeed the case. The zone of partially decomposed material, indicated by bubbles and crystalline areas of low molecular weight, has a thickness of less than 0·2 mm

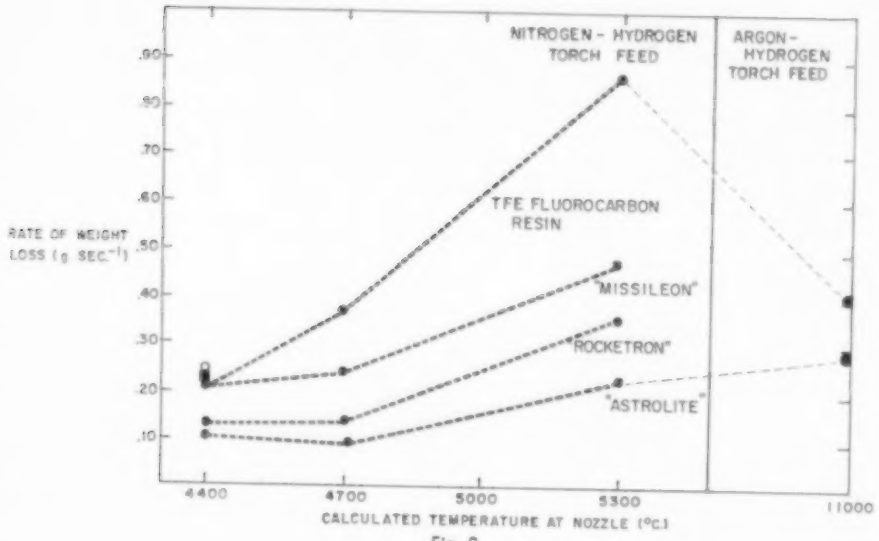

Fig. 9.

(about 0·01 in.). Additional evidence that degradation takes place only near the surface is furnished by infrared analysis. No evidence of degradation was observed in the interior portions of samples with eroded surfaces.

Calculations at various boundary layer temperatures indicate that the temperature within a slab of TFE resin does not exceed about 640°C regardless of the rate of heating. Above this temperature only pyrolysis products are present. Calculated values of maximum surface temperature as a function of the boundary layer temperature are plotted in Fig. 11. Experimental determinations of this maximum have given values of 550°–700°C. Recent work has indicated that the true value is probably close to 700°C. The experiments involve imbedding a thermocouple junction in a slab of TFE fluorocarbon resin, heating the surface with a flame and observing the temperature at the instant before there is a rapid rise to flame temperature.

The temperature of decomposition for reinforced phenolic and epoxy resins has been

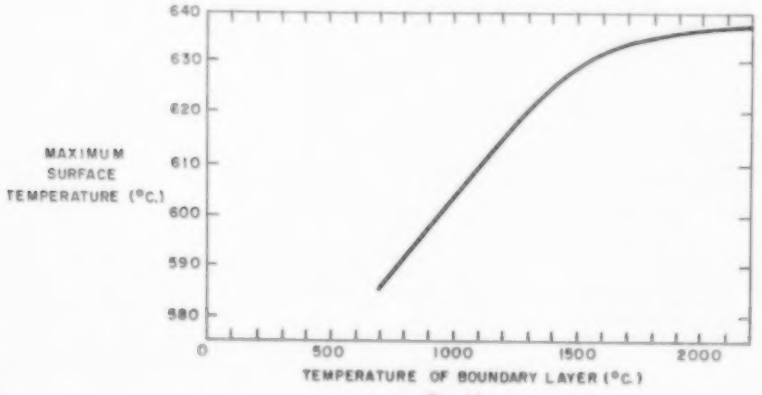

Fig. 11.

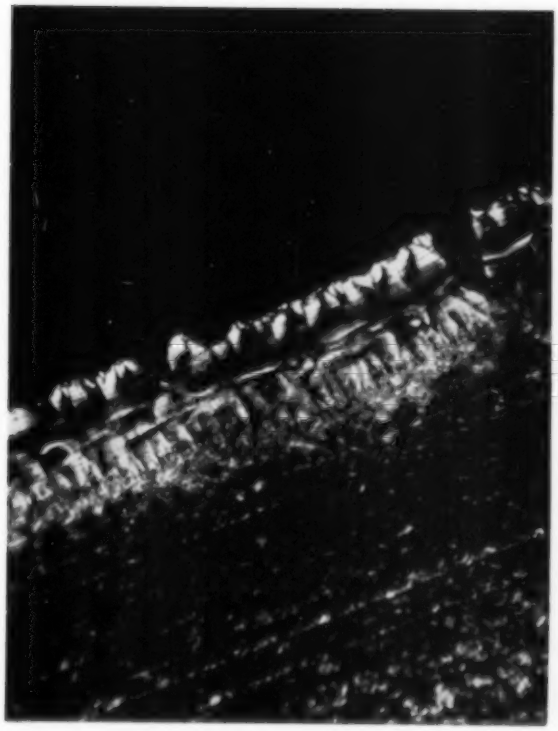

Fig. 16.

(facing page 80)

reported in the range of 1500–2000°C[12]. The relatively low temperature of decomposition of the fluorocarbon resins may be an advantage in applications involving relatively long exposures at low rates of ablation.

5. CONCLUSION

Thermodynamic and kinetic data for the decomposition of fluorocarbon resins are available. These data can be used to predict the behavior of these resins at temperatures exceeding 400°C since monomer is almost the exclusive decomposition product under a wide range of conditions. The good electrical properties, the low surface energy, and the low temperature of decomposition of the fluorocarbon resins make them attractive for applications where these properties, as well as good ablative behavior, are the important criteria of performance.

DISCUSSION

H. FRIEDMAN: The problem of predicting the ablation rate of Teflon has also been treated analytically by Sutton and Friedman (*Gen. Electr. Tech. Memo*, 113, March 1959) and also by Scala (*Gen. Electr. TIS Rep.* R59SD438, Sept. 1959). The above analyses were both for the quasi-steady state and included the effect of depolymerization in depth. The Sutton and Friedman analysis assigned the heat of depolymerization to the surface as does the present work by Settlage and Siegle. The work of Scala includes the effects of a spatially-dependent heat of depolymerization.

Recently, Troyanowsky (C. TROYANOWSKY, *Ann. Fals. Fraud.* **51,** 315, 1958) heated Teflon in a thermo-balance. Programmed heating was employed and the plastic was surrounded by an atmosphere of air. Up to 380°C the resin lost weight in a steady fashion. Between 390° and 400°C a weight gain was observed, while between 410° and 420° the plastic had regained and exceeded its initial weight. The weight gained passed through a maximum between 440° and 445°, but beyond this temperature the degradation exceeded the weight gain. Troyanowsky explained the gain in weight as being caused by oxidation by the air. In Fig. 5 you reported the results of heating a TFE resin in air at 450°C. Your work showed a steady weight decrease throughout the heating period. Troyanowsky's results suggested that a gain in weight might be expected at least in the early stages of your experiment. What are your feelings about this matter?

P. H. SETTLAGE: It is difficult to account for the very slight gain in weight reported by Troyanowsky because the details of his experiments are not available.

Our experiments were run in air at 50° intervals from 420 to 620°C. Small but continuous decreases in weight were observed on continuous automatic recording of weight vs. time at both 420 and 470°C. Assuming that temperatures were measured accurately, we have no explanation for the discrepancy between Troyanowsky's changes in the precise region of 440°C where he found the maximum weight gain.

REFERENCES

1. E. E. LEWIS and M. A. NAYLOR, *J. Amer. Chem. Soc.* **69,** 1968 (1947).
2. S. L. MADORSKY, V. E. HART, S. STRAUS and V. A. SEDLACK, *J. Res. Nat. Bur. Stand.* **51,** 327 (1953).
3. R. E. FLORIN, L. A. WALL, D. W. BROWN and J. D. MICHAELSON, *J. Res. Nat Bur. Stand.* **53,** 121 (1954).
4. D. R. HAGEMEYER and W. STUBBLEBINE, *Mod. Plast.* **31,** 136, 138, 141, 219 (1954).
5. L. A. WALL and J. D. MICHAELSON, *J. Res. Nat. Bur. Stand.* **56,** 27 (1956).
6. J. C. SIEGLE and L. T. MUUS, Paper presented at the *130th Meeting of the American Chemical Society, Atlantic City, N.J., 17 September 1956.*
7. F. A. QUINN, D. E. ROBERTS and R. N. WORK, *J. Appl. Phys.* **22,** 1025 (1951).
8. J. M. LUPTON, Paper presented at the *134th Meeting of the American Chemical Society.* Chicago, Illinois (12 September 1958).
9. P. MARX and M. DOLE, *J. Amer. Chem. Soc.* **77,** 4771 (1955).
10. A. W. SCHULZ and A. K. WONG, *Watertown Arsenal Lab., Tech. Rep.* 397/10 (1957).
11. H. MYERS, Paper presented at the *134th Meeting of the American Chemical Society.* p. 18M. Chicago, Illinois (12 September 1958).
12. H. A. PERRY and I. SILVER, Tech. Papers, Vol. 5, p. 70-I-5, presented at the *15th Annual Technical Conference of the SPE.* New York (January 1959).

A DISCUSSION OF THE PYROLYSIS OF PLASTICS IN ABLATION—SUMMARY*

R. SIMHA
University of Southern California, Los Angeles, California

It is very difficult to comprehend fully a phenomenon as complex as plastic ablation. For a full understanding, one must have a knowledge of aerodynamics, heat transfer, diffusion, chemical kinetics and the mechanical properties of plastics and of char produced during ablation. This discussion brought together about forty scientists and engineers who discussed various aspects of this problem. The discussion was lengthy and lively, and since the comments were not transcribed, they are not reported here. R. Simha started the program by presenting a summary of the kinetics and mechanisms of the degradation of vinyl polymers at moderate temperatures. It was pointed out that such degradation reactions are important for understanding the ablation of many types of plastics, since mechanisms of a similar nature probably occur behind char layers. Many participants contributed a description of experimental results and interpretations thereof. Also, theories were presented and discussed which have been used to explore the various aspects of the ablation problem. It was clear that the results of laboratory experiments were not always applicable to practical problems, and that very little is known about the basic chemical processes which occur during ablation. It was concluded that the results of industrial ablation tests also are very difficult to interpret. Several speakers voiced problems which they felt were in particular need of solution. In the following section, P. J. Friel outlines a number of these problems and surveys the physical chemical aspects of the ablation problem. It seemed clear, on the basis of the intense interest shown, that a conference devoted to this subject could be most profitable.

* This discussion and the related text were coordinated by Henry L. Friedman, General Electric Company, MSVD, Philadelphia, Pennsylvania.

THE ABLATION OF THERMOSETTING PLASTICS

P. J. FRIEL
General Electric Company, MSVD, Philadelphia, Pennsylvania

In order to predict the behavior of thermosetting resins in a re-entry hypersonic environment, it is necessary to know in some detail the physical and chemical properties of the char formed by the decomposition of the plastic and the virgin plastic. The virgin plastic decomposes a narrow region near the char–virgin plastic interface. By the proper formulation of the equation for transient heat conduction in the virgin plastic to include a "heat sink" term due to the endothermic heat of decomposition (and containing the kinetics of decomposition), it is possible to predict the rate at which the virgin plastic decomposes to form char and gas. Knowing the mass fraction of plastic converted to char and gas by an independent experiment, the gas evolution rate at the interface can be determined, and if the physical properties and porosity of the char are also known, the rate of gas injection into the hypersonic boundary layer can be calculated. Scala[1] has determined the reduction in the heat transfer rate across the boundary layer by mass injection and has developed a simple correlation formula for air-to-air injection which can be corrected for the injection of the gaseous decomposition products of the plastic by a molecular weight factor. Scala[1] has also shown that it is possible to consider the effect of combustion of the decomposition products in the boundary layer on the heat transfer rate. Thus, by simultaneously and continuously solving the equations describing the phenomena occurring in the hypersonic boundary layer and the transient heat conduction equation in the body (including in the analysis the heat capacity of the char and plastic, the energy absorbed by the gases flowing through the porous char and the energy re-radiated by the hot char surface), on an analog computer, the behavior of a thermosetting plastic can be predicted at any time during re-entry for a re-entry environment in which the principal process occurring in the body is the decomposition of the plastic to char and gas. By this we mean a re-entry environment in which no significant amount of char is removed by oxidation, vaporization, or mechanical "scrubbing" of the char surface, for example, a phenolic resin in a satellite re-entry (heat fluxes from 50 to 100 B.t.u/ft^2-sec and stagnation pressures not greater than about 1 atm). In the case of a ballistic re-entry, however, the conditions are much more severe (heat fluxes as high as 4000 B.t.u/ft^2-sec and stagnation pressures up to 100 atm) and char removal or ablation becomes quite significant. Scala[1] has shown that char oxidation is diffusion controlled, so that char removal by this mechanism can be predicted without a detailed knowledge of kinetics of the surface oxidation of the char. But surface oxidation of the char cannot account for the majority of the surface ablated during re-entry. Vaporization of the carbon-like char surface is unlikely since surface temperatures of the order of 7000°R would be required. Consequently, the principal mechanism by which the char is ablated is probably mechanical scrubbing. Therefore, in order to predict completely the behavior of thermosetting resins during a ballistic re-entry, it will be necessary to know the mechanical properties of the char and to formulate an analytical expression in terms of some flight parameter (e.g. dynamic pressure or boundary layer shear forces) and the char properties which will adequately describe the rate of char removal by mechanical scrubbing at various points throughout the re-entry trajectory. Information on the physical properties of char is, however, very sparse at this time.

In summary, the information required to

predict completely the behavior of thermosetting plastics during satellite and ballistic re-entry is as follows:

(1) Physical properties of the virgin plastic (thermal conductivity, density, heat capacity).

(2) The kinetics of decomposition of the virgin plastic to form char and gas.

(3) The validity of the assumption that the gas is evolved from a narrow region near the char–virgin plastic interface should be examined, i.e. it should be determined whether or not the char when formed is completely gasified.

(4) The mass fraction of virgin plastic converted to char and gas. Of course, some liquids are formed on pyrolysis, but for a first approximation, liquids can be assumed to be concentrated in the virgin-plastic–char interface and to be part of the virgin plastic.

(5) The energy absorbed in the pyrolysis reaction of the virgin plastic to form char and gas. This quantity can be determined from measurements of the heats of combustion of the char, gas and virgin plastics.

(6) The composition of the gases evolved by the plastic on pyrolysis.

(7) The effect of the injection of the decomposition gases into the hypersonic boundary layer, on the heat transfer rate to the body.

(8) The average temperature of the surface of the char during re-entry.

(9) The physical properties of the char, i.e. the thermal conductivity, heat capacity, density, porosity and particularly the mechanical properties. In addition it will be necessary to develop an analytical expression which adequately describes the mechanical removal of char as a function of some flight parameter.

A great deal or at least some information is available about items (1) to (8) and consequently a reasonable prediction of the behavior of a thermosetting plastic during a satellite re-entry can be made. However, very little information regarding the mechanical properties of the char formed by the various thermosetting plastics is available. Therefore, it is not possible at present to completely predict the behavior of thermosetting resins during a ballistic re-entry because an analytical expression has not been formulated to describe the mechanical ablation of the char surface. The method which has been used to avoid this difficulty has been to define an "effective heat ablation" which is the ratio of the aerodynamic heat transfer rate to a calorimeter divided by the mass loss rate which a model experiences during test in a high temperature facility. However, to obtain a more complete picture of the ablation of thermosetting plastics during a ballistic re-entry, the mechanism of char ablation will have to be formulated.

REFERENCE

1. S. Scala, *A Study of Hypersonic Ablation*, Gen. Electric Co., Techn. Inform. Ser. No. R59SD438 (September 1959).

INTRODUCTION TO THE PAPERS ON GAS-PHASE REACTIONS AND KINETICS

S. S. PENNER
California Institute of Technology, Pasadena, California

Probably no single topic is more vital to a quantitative understanding of Physical Chemistry in Aerodynamics and Space Flight than gas-phase chemical kinetics. With the advent of hypersonic flight, supersonic combustion and the coordinated increase in temperature, the principal errors in analytical treatments result directly from very large uncertainties in chemical reaction rates and in the rates of other relaxation phenomena.

Among the following papers we find shock-tube studies of vibrational relaxation rates, reaction rate measurements in high-temperature air, basic work on electron attachment, a survey of shock-tube techniques for studies of physico-chemical phenomena, and an analysis of radiation from the non-equilibrium region behind shock fronts. These interesting papers constitute an excellent sampling of current fundamental activities on gas-phase kinetics and associated phenomena relating to hypersonic flight.

COMPARATIVE STUDIES OF VIBRATIONAL RELAXATION IN NITRIC OXIDE

P. R. MONSON, J. J. ALLPORT and F. ROBBEN
Lockheed Aircraft Corporation, Sunnyvale, California

Abstract—Ultra-violet absorption and infra-red emission techniques have been used to follow the vibrational relaxation of nitric oxide after shock heating in a temperature range from 450°K to 1300°K. The infra-red technique yields a vibrational de-excitation probability, P_{10}, an order of magnitude or more below the ultra-violet results. A simultaneous experiment has also been performed with both methods at the same time, and it is found that the disagreement persists. Therefore, if the infra-red results represent the vibrational relaxation, then the ultra-violet light source has no effect. Possible interpretations of the experiments are offered and discussed with the purpose of removing the discrepancy. Suggestions for further experiments are also set forth.

1. INTRODUCTION

The study of vibrational kinetics, particularly the equilibration of vibrational modes after a sudden change in temperature, is of great interest. Knowledge gained in this area has many applications as for instance in gas flow through a shock wave or through a nozzle. There are likewise many methods used to study this phenomenon. Interferometry, stagnation pressure and ultrasonic absorption are but a few. In particular, here we are interested in the comparison of ultra-violet absorption and infra-red emission techniques for measuring the vibrational relaxation time after shock heating. From these measurements it is possible to infer the vibrational transition probability. The theory of low energy collisions is now becoming relatively well developed and such experiments form a valuable check.

Ultra-violet absorption methods were first used at this laboratory to follow the exchange of energy between translation and vibration in nitric oxide[1]. The results of this investigation have shown an anomalously large vibrational transition probability, which can be explained by modifying the shape of the intermolecular potential. With the advent of fast-response infra-red detectors it has become possible to do similar experiments using infra-red emission to monitor the population of vibrational levels[2]. After having been checked and found valid for N_2O and CO_2, this method has been used on nitric oxide, for which the transition probability seems to be one to two orders of magnitude smaller than previous results. The modified potential model is substantiated since the probabilities are still many orders of magnitude larger than existing theory predicted. The basic paradox is that two apparently valid experimental procedures differ so markedly.

The shock tube and theory of its use here have been described by Robben[1]. It is worthwhile, however, to discuss the spectroscopic methods more fully.

In the ultra-violet work the absorption of light in the γ_{01} band is assumed to be a measure of the population of the first vibrational level. The γ_{01} band represents transitions from the first vibrational level of the ground electronic state to the zero vibrational level of the first excited electronic state. In fact, the following relation is presumed and later demonstrated:

$$f = \alpha\rho', \tag{1}$$

where f is the fractional absorbance, α is an empirical constant and ρ' is the density in the first vibrational level. On the other hand, the infra-red technique involves the radiation of transitions within the ground electronic state from the first vibrational level to the zero vibrational level. We shall use the notation 1–0 to denote such transitions. An assumption

similar to equation (1) is made regarding the density in the first vibrational level and the observed intensity. Actually, radiation from transitions such as 2–1, 3–2, etc., is of approximately the same wavelength. The intensities of these transitions are, however, so small compared with the 1–0 transition that within the experimental error they may be neglected. It has also been found possible to monitor the forbidden 2–0 transition, where we have likewise omitted 3–1, 4–2, etc.

In Section 2 the experiments are described. Infra-red work is reported in greater detail than the ultra-violet because the former has not yet been published elsewhere, as has the latter. A brief account of a simultaneous experiment is also included. In Section 3 the evidence in favor of each method is reviewed and possible explanations of the anomaly are advanced. Finally recommendations are made for additional studies to resolve the problem.

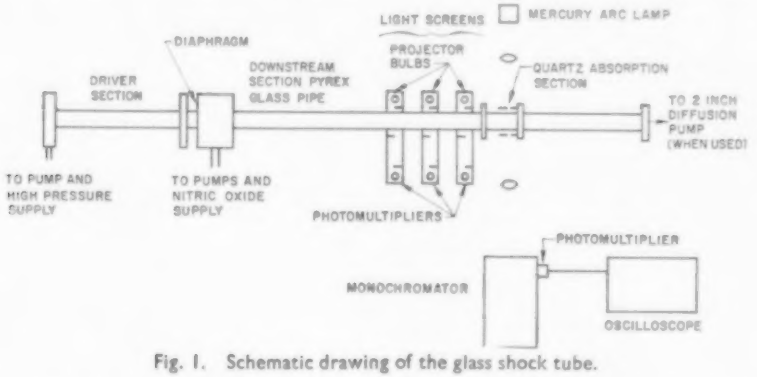

Fig. 1. Schematic drawing of the glass shock tube.

2. EXPERIMENTS

(*a*) *Ultra-violet method*[1]

Fig. 1 shows a diagram of the glass shock tube employed. The driver section is 3 feet of 1 in. stainless steel pipe. Twelve feet of Pyrex glass pipe forms the downstream portion. Three schlieren shock detectors have been used to determine shock velocity, and the test section is a 4 in. length of quartz tubing.

A typical time history of the γ_{01} absorption line appears in Fig. 2. The noise is rather large, but the trace clearly relaxes to equilibrium after passage of the shock. Long term traces under similar conditions show no increase in absorption after the plateau is reached.

To demonstrate that equation (1) holds, absorption measurements have been made on statically heated NO over a range of temperatures. Fig. 3 shows the density in first vibrational level plotted as a function of the resulting fractional absorbance. The same plot is shown for the equilibrium density behind the shock. Evidently both sets of points indicate a linear relationship. The results given as de-excitation probabilities, P_{10}, may be plotted against $T^{-1/3}$ (see Fig. 4). It is estimated that the error involved in reducing data from oscilloscope photographs was approximately ± 30 per cent. The scatter in P_{10}, though, indicates a larger margin, which suggests a possible dependence on an uncontrolled parameter. This suspected parameter is not the density, as a close examination has shown no correlation whatsoever of relaxation time with density[1].

(*b*) *Infra-red method*[2]

The infra-red emission experiments are performed in a 1 in. metal shock tube of approximately the same proportions as the glass tube. The experimental set-up is diagrammed in Fig. 5. Piezoelectric pressure pickups are used to time the shock and to mark its arrival at the slit.

The gas is viewed through a sapphire window and collimating slits by an indium antimonide infra-red detector. Filters in front of the

detector pass only radiation corresponding to the 1–0 vibrational transition at a wavelength of 5·34 μ. As pointed out previously, this also corresponds to 2–1 transitions, etc., but we have agreed that effects from higher order transitions are negligible here. Experiments have been also performed for the 2–0 transition. As will be seen, such investigations may clarify the interpretation of the transition histories. Fig. 6 shows some typical emission traces. Two of them, Fig. 6(a) and (b), are 1–0 transitions, and 6(c) is a 2–0 transition. Since the noise is relatively small in the emission work, the diagrams are smoothed.

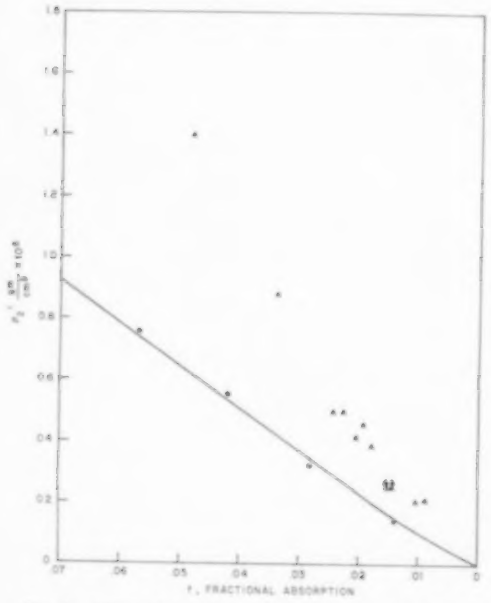

Fig. 3. Ultra-violet absorption of the γ_{01} band as a function of the density of the first vibrational level.
● Static head heated NO absorption measure-
▲ Shock tube NO absorption measurements.

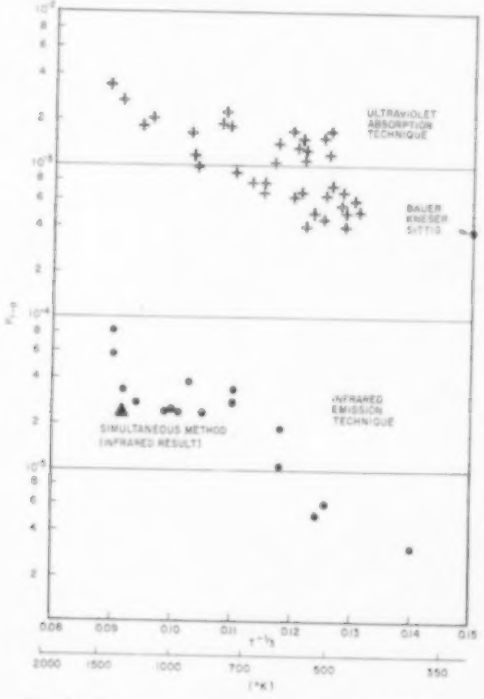

Fig. 4. Summary of vibrational de-excitation probabilities, P_{10}, as a function of $T^{-1/3}$

In order to obtain a transition probability or a relaxation time, a model for interpretation of the traces is necessary. From Fig. 6(a) and (b), it is evident that the 1–0 emission time histories may be divided into three principal regions for discussion. The first region contains a slow initial rise in radiation; the second is a near-linear faster rise; the third is a slow exponential-like relaxation to equilibrium. One of the theories for explanation of these regions is given below.

In this interpretation pre-radiation, or scattering, is thought to be responsible for the slow rise of the first region, i.e. the gas ahead of the shock receives and scatters radiation from behind the shock. In Region 2, compression of the scatterers as the shock crosses the viewing slit is supposed as the cause of the sudden linear increase in intensity. Further, in Region 3 we assume that vibrational equilibrium is not reached in a time comparable with the shock transit time, so that there is a rise in scattered intensity until emission from the relaxing gas takes over. The knee at the top of this region is taken as an increase in population of the first vibrational level. On this

basis Fig. 6(a) shows a vibrational relaxation time, τ, of about 10 μsec in laboratory co-ordinates, while in 6(b) which is for a run at higher temperature, the relaxation takes about 4 μsec.

Continuing with this explanation the last trace, Fig. 6(c) (2–0 transition), must be handled differently since apparently no pre-radiation is visible. It is assumed that only the radiation from thermally excited vibrational states is important. Therefore, Fig. 6(c) shows τ roughly the same as in Fig. 6(b), which is expected, as

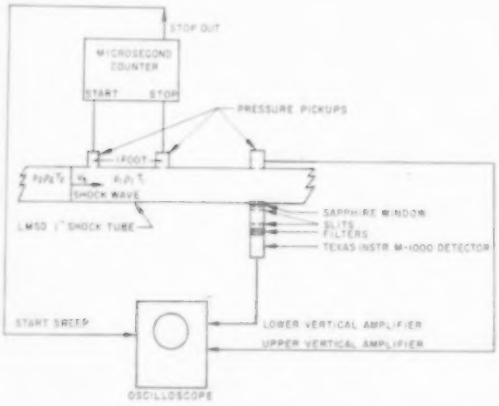

Fig. 5. Schematic drawing of the infra-red optics for the metal shock tube.

the temperatures are similar. The correspondence between relaxation times in Fig. 6(b) and (c) thus lends further credence to the explanation of 1–0 radiation pictures. More substantiation comes from traces where the shock is marked by a pressure gauge as arriving at the beginning of the linear rise of Region 2. The slow rise in Region 1 is then identified as pre-radiation or scattering, and also Region 3 may be said to correspond with the 2–0 traces.

Referring again to Fig. 4 we observe that with the above interpretive scheme the results of a number of runs show de-excitation probabilities, P_{10}, which are an order of magnitude or more below those obtained in the ultra-violet. There is evidently a discrepancy between the ultra-violet and infra-red experiments and some further explanation will be required. Although it is felt that this does not contribute to the disparity (see Section 2c) we should mention that the nitric oxide for the ultra-violet work was carefully distilled while only a refrigeration of the storage bottle to dry ice temperature was used for the infra-red investigations. In this manner all the common contaminants except N_2O are presumably removed.

Another point to make is that the emission technique has also been applied for CO_2 and N_2O vibrational relaxation and gives results commensurate with previously known rates.

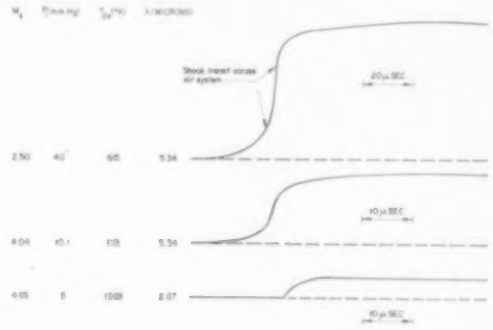

Fig. 6. Typical infra-red emission time histories.

(c) Simultaneous method

It was hoped that the wide divergence of the results from the two methods would be simply explained if the ultra-violet light had an accessory effect such as dissociating the NO or producing impurities which speed the relaxation. In this connection several runs have been simultaneously made with both methods.

The glass shock tube has been modified and set up as in Fig. 7. Since the quartz test section is opaque to 5 μ radiation, it is necessary to study the 2–0 transition.

Figure 8 gives the result of a typical run (1321°K). Although no pre-radiation is observed in previous work on the 2–0 transition, there is here a slight increase in radiation before shock arrival. Also from Fig. 8, it may be determined by the infra-red trace that the vibrational relaxation time is 11 μsec. The relaxation is too short to resolve on the ultra-

violet trace because of the slow sweep range, and no point representing the corresponding probability is plotted in Fig. 4. Presumably if the results could have been resolved, the probability would lie circa the previous ultra-violet points. The result for the probability derived from infra-red work is represented by the triangle of Fig. 4. Further, a series of several similar runs at nearby temperatures confirm the point plotted for 1321°K. Thus it is demonstrated that the ultra-violet light source has no observable effect on the vibrational relaxation of nitric oxide if, as has been interpreted, the infra-red measurements actually refer to the vibrational time. If, however, vibrational relaxation time is not what it is measured by the infra-red work then it should not be immediately concluded that the light has no effect.

As mentioned in Section 2(b), the present opinion is that contaminants have no significant effect. The following discussion supports this contention. It is true that the role of impurities, especially triatomic molecules, has generally been found important in shortening the relaxation time. Therefore, runs had been made with the ultra-violet method[1] in which the impurity level was less than one part in 10^{-4}. Conversely, the simultaneous experiment, previously run with impurities less than five parts in 10^{-3}, has been repeated using nitric oxide from the storage bottle. Surveying all the results it is found that there is no variance with impurities.

3. DISCUSSION

As shown in Fig. 3, ultra-violet absorption measurements on statically heated NO have indicated that assumption of equation (1) is justified. The divergence of the lines in Fig. 3 is however expected since the optical set-up for the oven is different from that on the shock tube. Absorption experiments have also been performed which demonstrate that the γ_{01} line is well separated from other interfering bands. Furthermore, for none of the shock tube runs is there any long term increase in absorption on the oscilloscope traces. On the basis of the above evidence it would seem that the initial decrease in transmitted ultra-violet intensity is actually due to relaxation into the first vibrational level.

On the other hand, the infra-red emission technique gives traces that are much easier to interpret because of the high signal to noise ratio. Also, the results have relatively small scatter, and if emission is assumed to be strictly proportional to the density of the first excited state, a much cleaner plot of the results is obtained (Fig. 4). Another advantage of the infra-red experiment is that the derived relaxation times are well out of the realm of shock transit times.

Independent measurements for the vibrational relaxation time have been made by Bauer *et al.*[3] with an ultrasonic technique. Their results, which are reproduced in Fig. 4, agree substantially with the ultra-violet work when an extrapolation is made to room temperature. A gas purity of one part in 10^{-3} is reported[4].

Although the work of Bauer *et al.* supports the ultra-violet study, the reason for the difference between the infra-red and ultra-violet results is still a nuisance. Two interpretations are offered below, one criticizing the ultra-violet experiments, and the other, the infra-red.

We may try to explain the ultra-violet work in another fashion. Since the relaxation times in absorption are so close to the shock transit time, the decrease in ultra-violet transmission may be due to compression of already excited gas. A simple increase in optical density is not sufficient for this interpretation, as the excitation at room temperature is too small for observation even after compression. Therefore, it appears necessary that there be pressure broadening of the γ_{01} rotational lines, which are absorbing at peak efficiency at room temperature. In this manner more energy may be removed from the ultra-violet beam without increasing the population of the first vibrational level.

Another explanation of the infra-red experiments is that the almost linear rise in Region 2 is actually caused by the vibrational relaxation as well as the shock transit. The "pre-radiation" or scattering hypothesis still applies except that

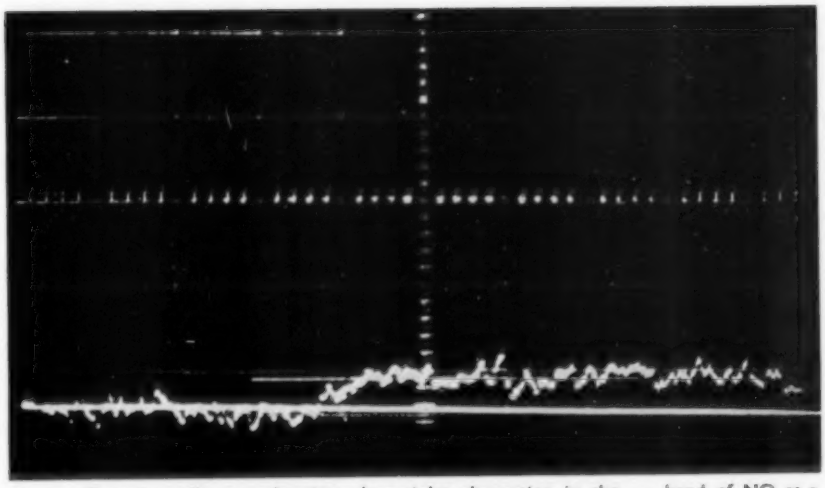

Fig. 2. Typical oscillogram showing ultra-violet absorption in the γ_{01} band of NO as a function of time. The sweep speed is 5 μsec/cm reading from left to right, and absorption increases upward. The temperature is 455°K.

Refer to page 88
(facing page 90)

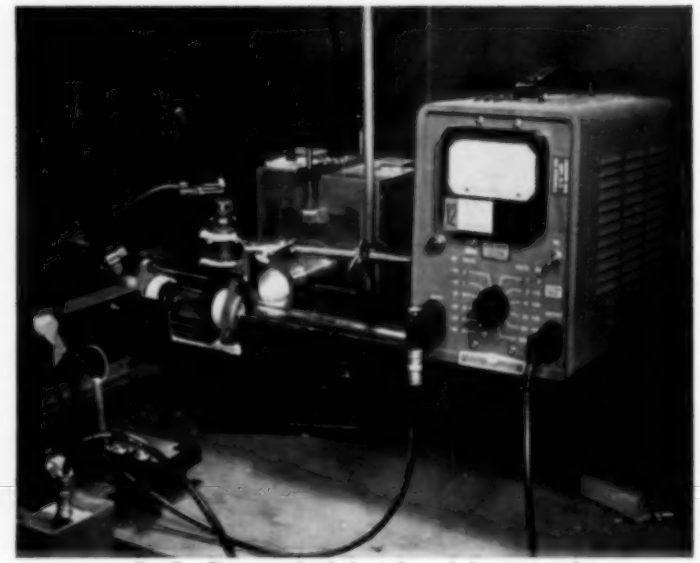

Fig. 7. Photograph of the infra-red detector and quartz test section.

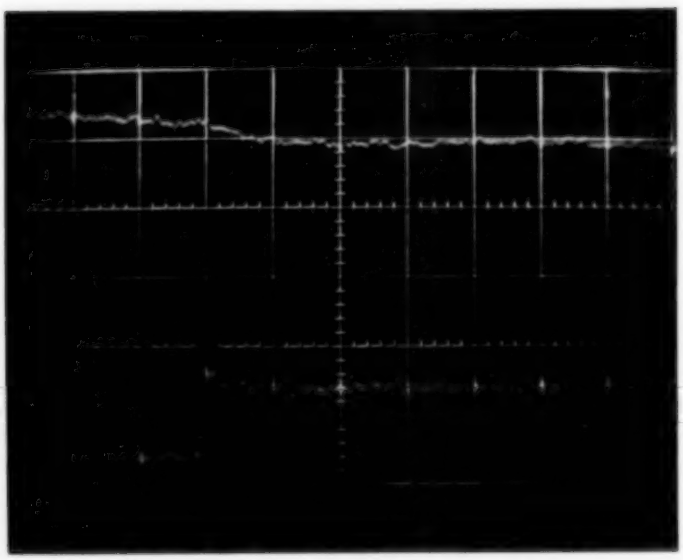

Fig. 8. Simultaneous time history of γ_{01} ultra-violet absorption and 1–0 infra-red emission. The upper trace shows infra-red emission with intensity increasing downward. Ultra-violet absorption is shown on the lower trace with absorption increasing upward. The sweep speed is 20 μsec/cm with time increasing from left to right. The temperature is 1321°K.

the knee at the top of the curve is now entirely attributable to scattering. "Pre-radiation" in a strict sense does not exist, as pre-excitation of the first vibrational level would have been observed in absorption studies. For the 2–0 traces, scattering is not apparent ahead of the shock because the optical path length is relatively long, whereas after the shock the density must have increased sufficiently to cause the noted scattering.

As further confirmation that "pre-radiation" does not exist, we may establish an upper limit on the population of the first vibrational level before shock arrival with the following analysis. It is assumed (1) that the gas behind the shock is radiating at maximum efficiency, i.e. black body; (2) that the entire flux is stopped by the downstream gas; (3) that no excited molecules drop to the ground state. Then, the vibrational excitation ahead of the shock is found to be 8×10^{-3} less than the equilibrium excitation behind the shock at 500°K, and 3×10^{-3} less at 1300°K.

We are still unable to determine which, if any, of the versions is correct. In order to clarify the infra-red results the scattering phenomenon should be studied in a static condition. Also, absolute emission measurements should be performed to show whether or not infra-red radiation intensity is proportional to the density of the first excited state. Further, a spectroscopic analysis of heated nitric oxide ought to be done in order to disclose the line shapes and possible interference with radiation from impurities such as N_2O_2. On the other hand, clarification of the ultra-violet work may result from static experiments in which the effect of pressure on line shapes is investigated.

There are at least two questionable points in the pressure broadening theory of our earlier criticism of the ultra-violet experiment. First, if the initial rise in absorption is a pressure effect then one should observe a much longer rise due to vibrational relaxation. Secondly, absorption has been shown experimentally (Fig. 3) to be linear with the density in the first vibrational state, which precludes a noticeable effect from line broadening unless there is a coincidental cancellation of effects.

It is hoped that research currently underway in our laboratory will definitely resolve the controversy.

Acknowledgement—We thank Dr. Henry Aroeste for his continuing interest and assistance during our investigations. Also, we appreciate the helpful discussions of Professor David B. Beard regarding scattering phenomena.

REFERENCES

1. F. Robben, *J. Chem. Phys.* **31**, 420 (1959).
2. J. J. Allport, to be published.
3. H. J. Bauer, H. O. Kneser and E. Sittig, *J. Chem. Phys.* **30**, 1119 (1959).
4. H. J. Bauer, H. O. Kneser and E. Sittig, private communication.

DISCUSSION

J. J. Allport: The infra-red emission technique has been extended to observe the formation of NO in strongly shocked air. The formation of NO is observed by monitoring radiation from the fundamental band (1875·9 cm^{-1}) as a function of time after shock passage. The experiments have been performed in the LMSD 3 in. tube for shocks in the Mach number range 8–14 and initial pressures of 10 mm and 5 mm dry, argon free air.

The experiments corroborate the recent theoretical investigations of Duff and Davidson[1, 2], wherein it is predicted that the transient NO concentration exceeds its equilibrium value. Following passage of a shock at Mach 8, the nitric oxide concentration grows slowly for 200 μsec, and no overshoot in concentration is observed. After passage of shocks at Mach 11 and 14, there are overshoots of 11 and 100 per cent, respectively, of the equilibrium concentration.

Absolute intensity measurements of radiation from the fundamental band are approximately 15 per cent higher than the calculations of Breene[3].

T. C. Peng: There are two ground states that are rather close together. Would you care to comment since only one ground level is mentioned in the paper?

P. R. MONSON: The reference here is to the ultra-violet absorption technique for monitoring vibrational relaxation. If transitions from both ground electronic states are observed, the only effect would be to lengthen the apparent vibrational relaxation time because of a long equilibration time for splitting. However, measurements have demonstrated that the relaxation time for splitting is much smaller than that for vibration (H. O. KNESER, *Ann. Phys.* **39,** 261 (1941)), whence no observable change in the vibrational relaxation should be observed. On the other hand, the splitting of the ground electronic state adds to the variation of the specific heat, and this is included in the calculation of conditions behind the shock (F. ROBBEN, *J. Chem. Phys.* **31,** 420 (1959)).

K. L. WRAY: We have been doing vacuum ultra-violet absorption experiments on shock heated air to observe the nitric oxide overshoot. The slide shows the experimentally obtained NO concentration as a function of time behind the shock front in a 20% air–80% argon mixture. The NO overshoot is clearly present.

The absorption coefficients for the wavelength radiation used (1270 Å) were obtained (as a function of temperature) by observing the signal (I/I_0) at a point where the state of the gas is known, e.g. following vibrational equilibration, but prior to the onset of dissociation.

S. H. BAUER: I wish to propagandize the use of a more reliable log τ vs. temperature dependence than that given by the Landau–Teller (L–T) theory. Dr. Ben Widom showed that by avoiding one of the serious approximations introduced by L–T, the dependence of log τ decreases linearly with T, rather than the $T^{-1/3}$ relation. However, one needs very precise data indeed, over a long temperature range, to show the difference between these. Blackman's data on O_2, barely show a slight curvature for the L–T plot and a straight line for Widom's relation.

With regard to the difference in relaxation time you found for NO based on the u.v. absorption and the i.r. emission, I feel a little uneasy about the latter. The gas sample may have been semi-black, and one should consider the radiation lifetime of the excited vibrational states. Have you considered these effects in your data reduction steps?

P. R. MONSON: Little can be said with regard to the correctness of either the Landau–Teller theory or the theory of Dr. Widom from the data obtained for NO thus far, inasmuch as the temperature range covered here is too small. The data when presented in a log τ vs. temperature plot forms as good a straight line as it does on the plot which is shown (Landau–Teller).

Concerning the radiation intensity, it is true that in some of the higher density experiments the NO radiation in the 1–0 i.r. band is semi-black. If the gas sample becomes black body, the intensity of the radiation no longer increases. Therefore, a point designated as in equilibrium on the intensity vs. time curve may merely represent a non-equilibrium black body with the interpretative scheme used. This would lead to a shorter apparent relaxation time, particularly at the lower temperatures (higher densities). Hence, the times thus obtained would in any event be lower limits, and the difference between the two experiments may not be further reduced on this basis. Indeed, the emission from the 2–0 transition yields the same results as the 1–0 transition. This tends to indicate that the black body effect is small, as presumably the gas sample is optically thin in this spectral region.

Radiative lifetimes for excited vibrational states are not significant in our problem, as they are very long compared to the observed vibrational relaxation times. Therefore, the depletion of excited levels by radiation is negligible compared to the excitation into such levels by collision processes.

F. KAUFMAN: The purification of nitric oxide is of obvious importance here and was carried out very successfully by the authors. We have been making quite pure NO for many years for a variety of investigations and want to point out that a product quite free of higher oxides of nitrogen is quickly obtained by passing the cylinder gas slowly through a long column of ascarite, through a dry-ice trap, and condensing at −195°C. This single procedure will reduce NO_2 to less than 0·01 per cent.

N_2O is then removed by slow distillation of the NO in which the middle fraction is collected. One such distillation reduces the N_2O content to about 1 part in 8000, and repeated distillation lowers it to less than 1 part in 20,000.

1. R. E. Duff and N. Davidson, *Bull. Am. Phys. Soc.* II, **4**, 195 (1959).
2. R. E. Duff and N. Davidson (to be published in *J. Chem. Phys.*)
3. R. G. Breene, Jr., *J. Chem. Phys.* **29**, 512 (1958).

THE INFLUENCE OF PERIODIC PRESSURE VARIATIONS ON CHAIN REACTIONS*

H. M. WIGHT
Aeronutronic, Newport Beach, California

Abstract—A theoretical study is made of the effect of simultaneous periodic variations in temperature and volume for chain reactions, with particular emphasis on the frequency dependence of the perturbation. If a kinetic mechanism is postulated for any given gas-phase chain reaction, a system of first order differential equations describing the time rate of change of the various species can be obtained by applying the Mass Action Law. This system of differential equations can be written to include explicitly the simultaneous temperature-volume perturbation.

Such a system of equations is generally nonlinear and can be integrated usually only by numerical successive approximation techniques. If this is to be done with any rapidity, a high-speed computer is required. It is shown, however, that the extreme cases of very low and very high perturbation frequencies can be treated analytically with regard to average rate of formation of product species.

Specific calculations are made for the low and high frequency cases for the HBr chain reaction. Numerical evaluation of the rate enhancement for the formation of HBr at intermediate frequencies is performed using an IBM-650 digital computer. A slow fall-off in the rate is predicted with increasing frequency. However, the high frequency rate is still significantly greater than the unperturbed rate.

1. INTRODUCTION

One of the many mechanisms which may contribute to resonance combustion instability (oscillating chamber pressure) in rocket motors is the interaction of the oscillating pressure and temperature with the gas-phase chain reaction combustion. The mean value of the oscillating chamber pressure is usually in excess of the unperturbed value. If oscillations occur, any small gaseous element of reacting material will be subjected to a periodic temperature and volume perturbation superposed on the unperturbed, non-oscillating temperature–volume history. The average reaction rate of such an element of gas will be increased due to the exponential temperature dependence of the rate constants. The enhancement in rate during compression more than offsets the diminution during rarefaction. The main interest of the present study is to investigate the frequency dependence of the rate enhancement for chain reactions.

Use of the steady state hypothesis with regard to chain carriers has been applied in the past to the high-temperature regions of flames[1]. The validity of steady state chain reaction chemical kinetics at elevated temperatures has been questioned by Benson[2]. Recently Levy[3] has experimentally established the adequacy of this assumption with respect to the gas-phase H_2–Br_2 reaction in the range of 600–1470°K. Levy's data are consistent with the classical[4–6] chemical kinetic explanation concerning the formation of HBr. Mathematical models of the H_2–Br_2 flame have been investigated by Hirschfelder and co-workers[7], von Kármán *et al.*[8], Gilbert and Altman[9], and Eyring and co-workers[10]. Studies[11–13] have also been made of the time required to approach steady state equilibrium in the dissociation of Br_2.

Our prime interest is concerned with the effect of simultaneous temperature–volume perturbations on disturbing the steady state concentrations of chain carriers. A general theoretical

* This paper presents the results of one phase of research carried out under Contract AF 49 (638)-311, Project 37510, Task 9751 with the U.S. Air Force, Office of Scientific Research.

analysis will now be presented of the effect of such perturbations with particular emphasis on the frequency dependence of the perturbation. This generalized treatment will then be applied to the H_2–Br_2 chain reaction.

2. GENERALIZED ANALYSIS

Assume that a mechanism has been postulated for a particular gas-phase chain reaction. By applying the mass action law to the various postulated elementary chemical processes, a system of first order ordinary differential equations describing the time rate of change of the various species is obtained.

$$\frac{d(A_i)}{dt} = f_i;\ i = 1,\ 2,\ \ldots,\ p \tag{1}$$

$$\frac{d(B_j)}{dt} = f_{j+p};\ j = 1,\ 2,\ \ldots,\ q \tag{2}$$

$$\frac{d(C_k)}{dt} = f_{k+(p+q)};\ k = 1,\ 2,\ \ldots,\ r \tag{3}$$

where

(A_i) = instantaneous number of mols of reactant species A_i,

(B_j) = instantaneous number of mols of chain carrier species B_j,

(C_k) = instantaneous number of mols of product species C_k.

The parenthesis notation, e.g. (A_i), will be used to denote numbers of mols rather than the more conventional concentration. The functions f_i, f_{j+p}, etc., are in general different functions of the elementary rate constants (and thereby of the instantaneous temperature) of the instantaneous system volume and of the number of mols of certain of the chemical species present. The total number of species is $(p+q+r)$. Now assume that the system is subjected to simultaneous periodic variations in temperature and volume of the form:

$$T = T_0(1 + a\sin\omega t) \tag{4}$$

$$V = V_0(1 - b\sin\omega t), \tag{5}$$

where perturbation constants a and b are related for an adiabatic process by

$$a = (\bar{\gamma} - 1)\, b. \tag{6}$$

The quantities T_0 and V_0 represent unperturbed values of temperature and system volume, ω is angular frequency of the perturbation (2π times the linear frequency), and $\bar{\gamma}$ is the effective specific heat ratio which will be assumed frequency independent. The perturbation constants a and b represent the fractional temperature and volume change amplitudes, respectively.

We desire to evaluate the effect of the temperature–volume perturbation described by equations (4) and (5) on the rate of formation of product species C_k. Specifically, the time average of $d(C_k)/dt$ over one complete perturbation period is desired. Assume that all perturbation periods $(2\pi/\omega)$ are much shorter than the half-time for changes of the major species.

If the functions f_i, f_{j+p} and f_{k+q} are written explicitly in terms of T and V given by equations (4) and (5), integration of the system of differential equations generally requires extensive numerical analysis. In practice the use of a high-speed computer is almost mandatory. However, two extreme cases can be treated analytically, namely the cases of very low and very high perturbation frequencies. In the low frequency case the system traverses a sequence of quasi-equilibrium states and use can be made of the steady state hypothesis for determining the instantaneous amounts of the chain carrier species. Treatment of the high frequency makes use of the fact that the chain carriers fail to respond significantly to the perturbation after the initial transients have damped out.

Low frequency perturbation

At extremely low frequencies application of the steady state hypothesis results in

$$\frac{d(B_j)}{dt} = f_{j+p} \cong 0. \tag{7}$$

The instantaneous number of mols of chain carrier (B_j) can be determined from equation (7) in terms of the major species. These values when substituted into $f_{k+(p+q)}$ in equation (3), permit an evaluation of the average value of $d(C_k)/dt$ for the low frequency case.

$$\overline{\left[\frac{d(C_k)}{dt}\right]}_{\omega\to 0} = \overline{[f_{k+(p+q)}]}_{\omega\to 0} \tag{8}$$

where the "bar" is used to designate a time average evaluated over one perturbation repetition period.

High frequency perturbation

By high frequencies, we mean those frequencies whose repetition period is much smaller than the adjustment time for any of the chain carriers. Interest will be focused on elapsed times after the initial transient effects have vanished. The character of (B_j) will then be as follows: (B_j) must be essentially periodic, having a period corresponding to that of the perturbation. Also (B_j) must be *nearly* constant in value. However, the instantaneous time derivative cannot vanish if the differential equations are to be satisfied. On the other hand, the time average value of the derivative over one complete period is zero, since (B_j) itself is assumed periodic. This is a consequence of the fact that for periodicity,

$$\overline{\left[\frac{d(B_j)}{dt}\right]}_{\omega\to\infty} = \frac{1}{P}\int_t^{t+P}\left[\frac{d(B_j)}{dt}\right]dt \qquad (9)$$

$$= \frac{1}{P}[(B_j)]_t^{t+P} \equiv 0,$$

where P is the perturbation repetition period. Applying equation (9) to equation (2) yields

$$\overline{[f_{t+P}]}_{\omega\to\infty} = 0. \qquad (10)$$

For very high frequencies (B_j) is essentially constant in value, and this permits solving equation (10) for (B_j) in a manner similar to that for the low frequency case. Substituting the resulting $(B_j)_{\omega\to\infty}$ into equation (3), allows an evaluation of the average rate of formation of the product species.

$$\overline{\left[\frac{d(C_k)}{dt}\right]}_{\omega\to\infty} = \overline{[f_{k+(p+v)}]}_{\omega\to\infty} \qquad (11)$$

We will now apply the preceding generalized mathematical structure to the case of the H_2–Br_2 chain reaction.

3. H_2-Br_2 CHAIN REACTION

The significant elementary reactions involved in the formation of gaseous HBr are as follows:

$$Br_2 + M \xrightarrow{k_1} 2Br + M$$
$$k_1 = 1{\cdot}44\times10^{18}T^{-1/2}\exp(-46{,}053/RT)\ \text{cm}^3/\text{mol-sec}$$

$$Br + H_2 \xrightarrow{k_2} HBr + H$$
$$k_2 = 3{\cdot}46\times10^{10}T\exp(-16{,}640/RT)\ \text{cm}^3/\text{mol-sec}$$

$$H + Br_2 \xrightarrow{k_3} HBr + Br$$
$$k_3 = 6{\cdot}43\times10^{12}T^{1/2}\exp(-1109/RT)\ \text{cm}^3/\text{mol-sec}$$

$$HBr + H \xrightarrow{k_4} H_2 + Br$$
$$k_4 = 7{\cdot}65\times10^{11}\exp(-1109/RT)\ \text{cm}^3/\text{mol-sec}$$

$$2Br + M \xrightarrow{k_5} Br_2 + M$$
$$k_5 = 10^{16}\ \text{cm}^6/\text{mol}^2\text{-sec}, \qquad (12)$$

where M represents any third body, and Br and H are the chain carriers. The values of rate constants are those of Campbell and Hirschfelder[14]. The pertinent elementary rate equations corresponding to the kinetic mechanism can be written as

$$\frac{1}{V}\frac{d(HBr)}{dt} = k_2\frac{(Br)}{V}\frac{(H_2)}{V} + k_3\frac{(H)}{V}\frac{(Br_2)}{V} - k_4\frac{(H)}{V}\frac{(HBr)}{V} \qquad (13)$$

$$\frac{1}{V}\frac{d(Br)}{dt} = 2k_1\frac{(Br_2)}{V}\frac{(M)}{V} - 2k_5\frac{(Br)^2}{V}\frac{(M)}{V} - k_2\frac{(Br)}{V}\frac{(H_2)}{V} + k_3\frac{(H)}{V}\frac{(Br_2)}{V} + k_4\frac{(H)}{V}\frac{(HBr)}{V} \qquad (14)$$

$$\frac{1}{V}\frac{d(H)}{dt} = k_2\frac{(Br)}{V}\frac{(H_2)}{V} - k_3\frac{(H)}{V}\frac{(Br_2)}{V} - k_4\frac{(H)}{V}\frac{(HBr)}{V}. \qquad (15)$$

In the HBr system the H atoms can certainly be expected to satisfy the steady state hypothesis[15, 16] (due to the extremely small concentration present at temperatures in the range of present interest) but this is not the case for the Br atoms. Under these conditions we obtain during the initial stage of the reaction

$$\frac{d(HBr)}{dt} = \frac{2}{V}[k_2(H_2)_0(Br)] \qquad (16)$$

$$\frac{d(\mathrm{Br})}{dt} = \frac{2(\mathrm{M})_0}{V}\left[k_1(\mathrm{Br}_2)_0 - k_5\frac{(\mathrm{Br})^2}{V}\right], \quad (17)$$

where the subscript 0 refers to the initial values.

Now consider a perturbation of the form described by equations (4) and (5). The cases of very low and very high frequencies can be treated in the manner previously developed in the generalized analysis. The case of intermediate frequencies is also of interest. Numerical integration of equation (17) was performed making use of an IBM-650 digital computer. The resulting (Br) was substituted into equation (16) and the right-hand member then averaged over a perturbation period.

By intermediate frequencies we mean perturbation frequencies whose repetition period is comparable to the adjustment time for (Br) to respond to a small step function in temperature. If such a step function is applied to the system described by equation (17) and the (Br) is initially at steady state corresponding to the lower temperature, the time constant for approach to the steady state corresponding to the elevated temperature can be shown to be given by

$$\tau = \frac{V^{3/2}}{4(\mathrm{M})_0[(k_1)_0(k_5)_0(\mathrm{Br}_2)_0]^{1/2}}, \quad (18)$$

where the 0 subscript again refers to initial values. The angular relaxation frequency ω_τ is given by

$$\omega_\tau \equiv 2\pi/\tau. \quad (19)$$

A computer program for intermediate frequencies was instituted for a sinusoidal perturbation having the following values:

$$b = 0{\cdot}10 \text{ and } 0{\cdot}20$$
$$T_0 = 600^\circ\mathrm{K}$$
$$V_0 = 1\ \mathrm{cm}^3.$$

The results of this program are depicted in Fig. 1. The fall-off with increasing perturbation frequency is monotonic in both cases. The results are accurate to within ± 5 per cent. Greater accuracy could have been obtained by tightening the error control for the solution of equation (17). However, the additional expense arising from the corresponding increase in "machine time" was not felt warranted. The

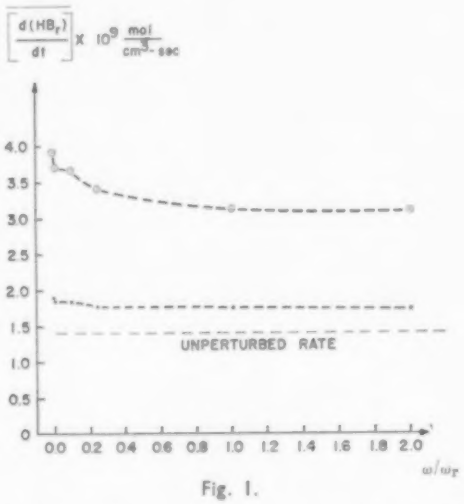

Fig. 1.

lack of smoothness in the line joining the low frequency data points arises due to small errors in the program and is not an intrinsic phenomenon. The analytical treatment predicts an enhancement fall-off of about 8 per cent for $b = 0{\cdot}10$ in going from extremely low to extremely high perturbation frequencies. For the case $b = 0{\cdot}20$, the fall-off is about 20 per cent. In neither of the cases does the high frequency averaged rate of formation approach the unperturbed value. An interesting result of the computer program was the observation that (Br) when averaged over a perturbation period actually *increased* slightly as the frequency was increased.

4. CONCLUSION

The major point of interest which has emerged from the present study is that a detailed knowledge of the chain mechanism does not appear necessary to evaluate the effect of temperature–volume perturbations. It would appear adequate to utilize a rate expression for product formation corresponding to the over-all reaction, since the enhancement fall-off with frequency is probably mild in most cases.

Acknowledgements—During the early stages of this program the author had many useful discussions with his colleagues at Aeronutronic, particularly Mr. H. Uyehara and Drs. D. Altman, W. Jones and J. Neustein.

REFERENCES

1. T. von Kármán and S. S. Penner, *Fundamental Approach to Laminar Flame Propagation, Selected Problems.* Butterworths London (1954).
2. S. W. Benson, *J. Chem. Phys.* **20,** 1605 (1952).
3. A. Levy, *J. Phys. Chem.* **62,** 570 (1958).
4. J. A. Christiansen, *Kgl. Dansk. Videnskab. Selsk., math.-fys. Medd.* **1,** 14 (1919).
5. K. F. Herzfeld, *Ann. Phys.* **57,** 635 (1919).
6. M. Polanyi, *Z. Elecktrochem.* **26,** 50 (1920).
7. J. O. Hirschfelder and C. F. Curtiss, *J. Chem. Phys.* **17,** 1077 (1949); Hirschfelder and Curtiss, *J. Phys. Chem.* **55,** 774 (1951); J. O. Hirschfelder, C. F. Curtiss, R. B. Bird and E. L. Spotz, *The Kinetic Theory of Gases and Liquids,* Wiley, New York (1954).
8. T. von Kármán, S. S. Penner and G. Millán, *Rep. Calif. Inst. Tech.* No. 16, (Aug. 1956).
9. M. Gilbert and D. Altman, *Sixth Intern. Symposium on Combustion.* Reinhold, New York (1957).
10. H. Eyring, J. C. Giddings and L. G. Tensmeyer, *J. Chem. Phys.* **24,** 857 (1956).
11. D. Britton and N. Davidson, *J. Chem. Phys.* **25,** 810 (1956).
12. F. A. Matsen and J. L. Franklin, *J. Amer. Chem. Soc.* **72,** 3337 (1950).
13. H. B. Palmer and D. F. Hornig, *J. Chem. Phys.* **26,** 98 (1957).
14. E. S. Campbell and J. O. Hirschfelder, *Rep. Univ. Wisconsin* No. CF 2108 (Nov. 17, 1953).
15. D. A. Frank-Kamenetskii, *J. Phys. Chem. U.S.S.R.* **14,** 695 (1940).
16. N. N. Semenov, *J. Phys. Chem. U.S.S.R.* **17,** 187 (1943).

SHOCK LAYER ELECTRON DENSITIES CONSIDERING THE EFFECTS OF BOTH CHEMICAL REACTIONS AND FLOW FIELD VARIATIONS*

M. H. BORTNER

General Electric Company, MSVD, Philadelphia, Pennsylvania

Abstract—A method for the calculation of the variation of electron density with time in a non-equilibrium shock layer of a re-entry vehicle has been developed. The method includes the effects of changes in both temperature and density. The temperature and the density are each changed by both chemical reaction and the expansion of the gas in the flow field. These changes in turn affect the rate of the chemical reactions. Calculations on a simplified system of four reversible chemical reactions were made along given streamlines by an iterative method on a set of simultaneous equations for the rate of change of concentrations of the various species.

An example is given for a calculation in which the electron density is far below the equilibrium value for a considerable time.

In the study of the properties and the effects of the gases in the flow field of a re-entering nose cone, it is desirable to be able to calculate the electron densities in the chemical system. Such data are needed not only for a system in equilibrium, but also for one not in equilibrium. Calculation of these quantities should include the effects of the most changeful quantities. Among these are the individual chemical species and their concentrations, the temperature and the density. The last two are affected both by the chemical reactions and by the expansion of the flow field as will be described later.

Previously[1], a system of chemical equations was used to determine times required to form equilibrium electron densities, assuming a simplified isothermal model. It was found that these times could be relatively long for certain sets of conditions. If the times required to form equilibrium electron densities are found by calculation to be short, equilibrium may be assumed. If these times are found to be long, it is dangerous to assume equilibrium values throughout the shock layer. The following discussion develops a method for making these calculations with the inclusion of temperature and density effects.

It is necessary to use a simplified model of the chemical system involved since the actual system obviously is made up of an unwieldy number of reactions. Since the calculation procedure could only include a limited number of reactions, only the most important chemical reactions in the over-all dissociation and ionization process could be included. The system of reactions which has been used is:

$$O_2 + X \underset{k_1'}{\overset{k_1}{\rightleftharpoons}} O + O + X \qquad (1)$$

$$O + N_2 \underset{k_2'}{\overset{k_2}{\rightleftharpoons}} NO + N \qquad (2)$$

$$O + NO \underset{k_3'}{\overset{k_3}{\rightleftharpoons}} O_2 + N \qquad (3)$$

$$N + O \underset{k_4'}{\overset{k_4}{\rightleftharpoons}} NO^+ + e \qquad (4)$$

where reaction (1) accounts for the formation of oxygen atoms, reactions (2) and (3) account for the formation of nitrogen atoms and involve NO, and reaction (4) accounts for ion formation. Other reactions, such as N_2 dissociation, NO dissociation, charge transfer and attachment

* This work was performed under the auspices of the U.S. Air Force, Ballistic Missile Division, Contract No. AF 04(647)-269.

may be important under some conditions but have been omitted from these calculations since they were thought to be less important than those included and to have no major effect on the over-all kinetics under the conditions of interest to this study.

It should also be noted that these include only species arising from an N_2–O_2 atmosphere. It does not include any "foreign" or "impurity" materials, no materials emitted from an ablating nose cone, no materials from boundary layer reactions, no minor components of air, etc.

In calculating the rates of the chemical reactions, a system of seven simultaneous equations was used. These are equations giving the variation with time of each of the species considered, N, N_2, O, O_2, NO, NO^+ and the total concentration of all species, X. These equations are:

$$\frac{d(\mathrm{N})}{dt} = k_2(\mathrm{N_2})(\mathrm{O}) - k_2'(\mathrm{N})(\mathrm{NO}) + k_3(\mathrm{NO})(\mathrm{O}) - k_3'(\mathrm{N})(\mathrm{O_2}) - k_4(\mathrm{N})(\mathrm{O}) + k_4'(\mathrm{NO^+})(e) \tag{5}$$

$$\frac{d(\mathrm{N_2})}{dt} = -k_2(\mathrm{N_2})(\mathrm{O}) + k_2'(\mathrm{N})(\mathrm{NO}) \tag{6}$$

$$\frac{d(\mathrm{O})}{dt} = 2k_1(\mathrm{O_2})(\mathrm{X}) - 2k_1'(\mathrm{O})^2(\mathrm{X}) - k_2(\mathrm{O})(\mathrm{N_2}) + k_2'(\mathrm{N})(\mathrm{NO}) - k^3(\mathrm{NO})(\mathrm{O}) + k_3'(\mathrm{N})(\mathrm{O_2}) - k_4(\mathrm{N})(\mathrm{O}) + k_4'(\mathrm{NO^+})(e) \tag{7}$$

$$\frac{d(\mathrm{O_2})}{dt} = -k_1(\mathrm{O_2})(\mathrm{X}) + k_1'(\mathrm{O})^2(\mathrm{X}) + k_2(\mathrm{O})(\mathrm{NO}) - k_3'(\mathrm{N})(\mathrm{O_2}) \tag{8}$$

$$\frac{d(\mathrm{X})}{dt} = k_1(\mathrm{O_2})(\mathrm{X}) - k_1'(\mathrm{O})^2(\mathrm{X}) \tag{9}$$

$$\frac{d(\mathrm{NO})}{dt} = k_2(\mathrm{N_2})(\mathrm{O}) - k_2'(\mathrm{N})(\mathrm{NO}) - k_3(\mathrm{O})(\mathrm{NO}) + k_3'(\mathrm{N})(\mathrm{O_2}) \tag{10}$$

$$\frac{d(\mathrm{NO^+})}{dt} = \frac{d(e)}{dt} = k_4(\mathrm{N})(\mathrm{O}) - k_4'(\mathrm{NO^+})(e) \tag{11}$$

where the terms in parentheses represent concentrations. The NO^+ and electron concentrations are assumed to be equal.

The rate constants (the k's in the above equations) and hence the rates of reactions are functions of temperature. The choices of values of these rate constants and their variations with temperature are a major problem and can introduce considerable variation and error. This problem is not to be considered here but was investigated in a succeeding study.

The rates of the reactions are also functions of density since a rate is proportional to the number density of each reacting species.

Consider the effects which cause temperature and density changes. First consider the chemical reactions. These, of course, cause a change in total number density (number of particles per unit volume) and in the number density of individual species since chemical reactions create some species by destroying others. The total number density in this chemical system is changed only by reaction (1), the oxygen dissociation, since this is the only reaction of those considered where the number of product particles is not equal to the number of reactant particles. The rates are, of course, proportional to the number densities of the individual reacting species. Concerning the temperature effect, the chemical reactions being considered are appreciably endothermic or exothermic. As written, the reactions proceeding from left to right are endothermic. In the initial stages of the reacting system until equilibrium is nearly reached, the over-all reaction system will be endothermic. Thus the reactions absorb energy from the flow field and lower the temperature. The temperature will vary according to

$$\Delta T = -\frac{\sum_i \Delta\eta_i \Delta H_i}{\sum_j N_j C_{P_j}}$$

ΔT = temperature change during time interval, Δt (°K)

C_{P_j} = molar heat capacity of species j (cal mole^{-1} deg^{-1})

N_j = total concentration of species j (molecules cm^{-3})

ΔH_i = heat of reaction i (cal mole^{-1})

$\Delta\eta_i$ = molecules cm^{-3} reacting by reaction i, in time Δt, that is

$$\Delta\eta_1 = (k_1\eta_{\mathrm{O_2}}\eta_{\mathrm{X}} - k_1'\eta_{\mathrm{O}}^2\eta_{\mathrm{X}})\,\Delta t \tag{13}$$

$$\Delta\eta_2 = (k_2\eta_{\mathrm{O}}\eta_{\mathrm{N_2}} - k_2'\eta_{\mathrm{N}}\eta_{\mathrm{NO}})\,\Delta t \tag{14}$$

$$\Delta\eta_3 = (k_3\eta_O\eta_{NO} - k_3'\eta_N\eta_{O_2})\,\Delta t \qquad (15)$$

$$\Delta\eta_4 = (k_4\eta_N\eta_O - k_4'\eta_{NO^+}{}^2)\,\Delta t \qquad (16)$$

In the calculation process, the values of ΔH_i and C_{P_j} are represented mathematically as functions of temperature.

The flow field expansion will, of course, affect both the temperature and the density. These effects have been represented mathematically. By a G.E. flow field method[2], the determination of temperature, density, and velocity variations along streamlines of constant entropy furnished the data for temperature-time and

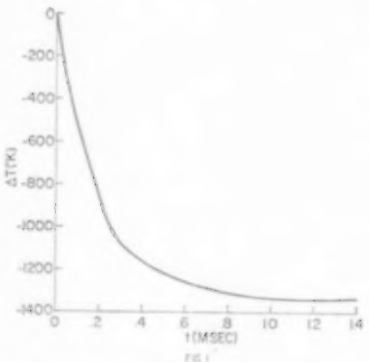

Fig. 1. Variation of flow-field temperature with time.

density-time curves for these streamlines. A typical curve is shown in Fig. 1. These data assume chemical equilibrium. Thus this furnishes only an approximate curve of temperature change vs. time because of the difference in chemical composition and absolute value of temperature, both of which effect the quantities which determine these curves. This effect (ΔT) is in the proper direction, however, and is a reasonable approximation, although a more involved coupling of the gas dynamics of the flow field with the chemical system would undoubtedly give more accurate results. The temperature change thus found is applied at each iteration by adding the temperature change since the last previous iteration.

Similarly, density (or density ratio) vs. time curves can be obtained. A typical curve is given in Fig. 2. Then at each iteration the individual

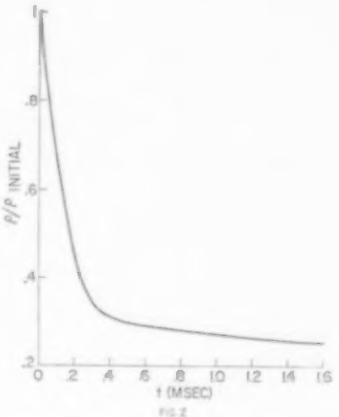

Fig. 2. Variation of flow-field density with time.

densities are multiplied by the ratio of the density at that time to the density at the time of the last previous iteration.

The effects of temperature and density on the rate are incorporated in the calculations as described above.

Calculations are made by an iterative method on the set of simultaneous equations for the rate of change of the various concentrations. The initial temperature is taken as that which the system attains immediately after passing through the shock front assuming instantaneous rotational and vibrational equilibrium.

The following is a summary of this method of calculating the rate of change of electron densities. The data which are needed are:

The rate constants and their variation with temperatures.

The initial concentrations of N, N_2, O, O_2, NO and NO^+.

The temperature.

The heat capacities and their variation with temperature.

The heats of reactions and their variation with temperature.

The steps of each iteration are:

1. Calculation of $\Delta\eta_i$ by equations (13)–(16).
2. Calculation of ΔT due to chemical reaction by equation (12).
3. Calculation of ΔT due to flow field expansion by a curve such as Fig. 1.

4. Calculation of total ΔT and new temperature.
5. Calculation of values of equilibrium constants for this temperature.
6. Calculation of values of rate constants for this temperature.
7. Calculation of density ratio by a curve such as Fig. 2.
8. Calculation of new values of concentrations by using equations (5)–(11).

A computation has been made using the foregoing method of incorporating temperature and density changes. The initial temperature was taken as 5000°K and the initial number density as $1 \times 10^{16}\,\mathrm{cm}^{-3}$. The data used were for an oblique shock.

The variations of concentrations of the various species in the flow-field are shown in a semi-log plot in Fig. 3. The solid lines are

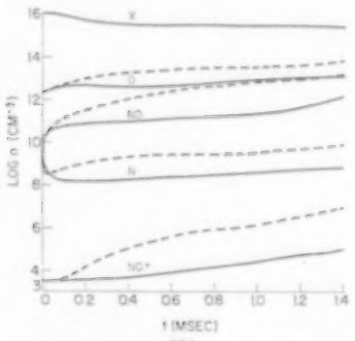

Fig. 3. Variations of flow-field concentrations with time.

for the case including the variation of T and density. The dotted lines do not include these effects. As would be expected, the concentrations change more slowly since the temperature and density are lower.

The computation was carried out to only a little over a millisecond because this section of the process was of the most interest. Some simpler (isothermal) calculations have been carried to much longer times.

This case is an example of extreme non-equilibrium. This is seen from the slow change in concentrations. The time involved here is a little over 1 msec. To see the extent of the

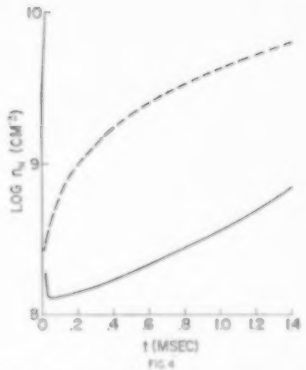

Fig. 4. Variation of N atom concentration with time.

non-equilibrium, the concentrations at the end of the time shown are compared in Table 1 with the equilibrium concentrations for the conditions of temperature and density at that time.

Table 1. Comparison of Calculated Number Densities with Equilibrium Number Densities after 1·4 msec

	Equilibrium	Calculated
(N)	$4{\cdot}4 \times 10^{13}\ \mathrm{cm}^{-3}$	$2{\cdot}0 \times 10^{9}\ \mathrm{cm}^{-3}$
(N_2)	$1{\cdot}7 \times 10^{15}$	$2{\cdot}0 \times 10^{15}$
(O)	$9{\cdot}2 \times 10^{14}$	$1{\cdot}5 \times 10^{13}$
(O_2)	$5{\cdot}2 \times 10^{11}$	$5{\cdot}4 \times 10^{14}$
(NO)	$7{\cdot}4 \times 10^{12}$	$1{\cdot}0 \times 10^{12}$
(NO^+)	$2{\cdot}7 \times 10^{10}$	$1{\cdot}0 \times 10^{5}$
Total	$2{\cdot}7 \times 10^{15}$	$2{\cdot}6 \times 10^{15}$

The system is still considerably different from equilibrium; the electron density is several orders of magnitude below equilibrium. Non-equilibrium must exist well back into the flow-field.

The conditions used here were ideal for non-equilibrium. The density was low and hence the rates would be expected to be low. For a two-body reaction, as most of these considered are, the rate is proportional to the square of the density. Also the temperature is comparatively low. This causes comparatively low rates, especially for the endothermic reactions which are the ones most important in approaching equilibrium.

In Figs. 4–7, the way in which the concentration of each of the several species—N atoms,

O atoms, NO molecules and NO^+ ions—change with time is shown. The solid line includes the temperature and density effects, the dotted lines do not.

The effects are obviously serious having an an effect of about two orders of magnitude in electron density. Thus such effects (which vary with trajectory and conditions thereon) must be included in calculations of electron density.

Thus it is concluded that non-equilibrium effects are important for certain conditions and that the temperature and density effects caused by flow-field expansion are large and should be included in calculations. The method developed may be used for calculating non-equilibrium shock layer electron densities including temperature and density effects.

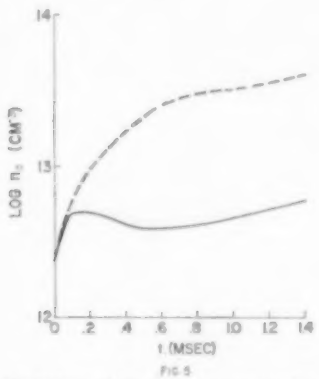

Fig. 5. Variation of O atom concentration with time.

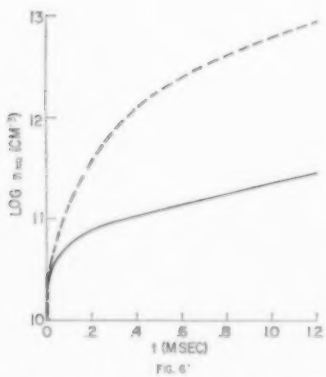

Fig. 6. Variation of NO concentration with time.

DISCUSSION

C. F. CURTISS: Could diffusion processes along a streamline act as an additional perturbation on the rate of change of composition?

M. BORTNER: It seems doubtful that diffusion along a streamline could be an important factor for such conditions as we have considered. However, it would certainly be good to make some calculations to check this.

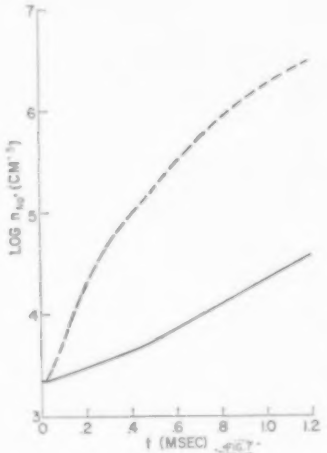

Fig. 7. Variation of NO^+ concentration with time.

R. L. CHUAN:

(*1*) What flight conditions are assumed in making calculations?

(*2*) What flow field is calculated? Inviscid or viscous?

(*3*) Are densities shown integrated averages through the flow field or for specific streamlines?

M. BORTNER:

(*1*) The data are those which correspond to an altitude of roughly 250,000 ft.

(*2*) Only the inviscid flow field was considered.

(*3*) Calculations are made along specific streamlines.

REFERENCES

1. M. H. BORTNER, *Bull. Amer. Phys. Soc.* **4**, 194 (1959).
2. F. G. GRAVALOS, *et al.*, *General Electric T. I. S.* Rep. No. R58SD245 (June 1958).

MEASUREMENTS OF ELECTRON ATTACHMENT, RECOMBINATION, ELASTIC AND INELASTIC COLLISIONS IN ATMOSPHERIC GASES*

M. A. BIONDI
Westinghouse Research Laboratories, Pittsburgh, Pennsylvania

Abstract—The present paper presents a brief summary of experimental and theoretical investigations by our Atomic Physics Group concerning the relevant atomic collision processes occurring in atmospheric gases. These include studies of electron attachment to oxygen molecules, dissociative recombination between electrons and molecular positive ions, and elastic and inelastic collisions of electrons in various gases.

1. ELECTRON ATTACHMENT STUDIES

Previously, experiments have been carried out using drift tubes[1–3] and microwave afterglow apparatus[4] to study the attachment of electrons in oxygen. The lowest electron energy reached with the drift tubes was $\sim 0{\cdot}2$ eV while the microwave afterglow studies were only carried out at thermal energies $T_e = T_{gas} = 300°\text{K}$ ($0{\cdot}04$ eV). In both cases the attachment was interpreted in terms of a *two*-body reaction over the pressure range studied ($\sim$3–30 mm Hg). The microwave studies yielded an apparent attachment cross section of $\sim 10^{-22}\,\text{cm}^2$ at $0{\cdot}04$ eV, while the drift tube studies yielded values of the order of $\sim 10^{-19}\,\text{cm}^2$ at a few tenths of an electron volt energy. The present results bridge the gap in energy between the two types of earlier measurements and show that, at low average electron energies, $\bar{u} < 1$ eV, the attachment occurs via a *three*-body reaction, in contradiction to the conclusions drawn from the earlier work.

A modified drift tube, similar in principle to that used by Doehring[2], has been used by Chanin *et al.*[5] to study the attachment over the range $0{\cdot}03 < \bar{u} < 3$ eV and pressures ranging from $\sim$5–50 mm Hg. The tube is shown schematically in Fig. 1. A pulse of electrons

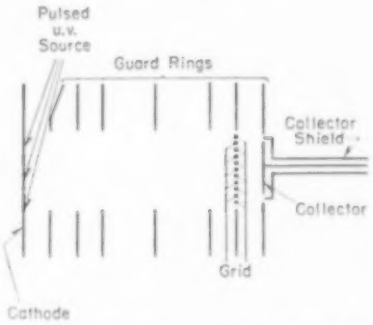

Fig. 1. Schematic representation of the electron drift tube used in attachment studies. The shutter grid is opened (made transmitting) by reducing the field between the grid wires to zero.

is liberated from the photocathode and drifts across the tube in a constant drift field. Some of the electrons attach to the oxygen molecules, leaving negative ions in the drift space. The time dependence of the arrival of ions at the shutter grid is determined by delaying the opening of the grid by variable amounts of time with respect to the photoelectron pulse. An electrometer is used to measure the charge reaching the collector. It can be shown that the ion arrival at the shutter grid approximately obeys the equation,

$$I_i = I_i(0) \exp(\alpha w_d t), \qquad (1)$$

for times less than or equal to the ion transit time across the drift space. I_i is the ion current, α is the attachment probability per unit drift

* This research was supported in part by the following contracts: AF 29(601)-1254 with the Air Force Special Weapons Center, ARPA 5-58 Task 1, Nonr-2584(00) with the Office of Naval Research and DA-36-034-ORD-2939 RD with the Office of Ordnance Research.

distance in the field direction and w_i is the ion drift velocity. The ion drift velocity is determined by a measurement of the transit time required for the ions formed near the cathode to reach the shutter grid.

Measurements of this type give us values of α as a function of E/p, the drift field to gas pressure ratio, as shown in Fig. 2. A knowledge of the values of average electron energy and electron drift velocity, w_e, as functions of E/p is required to reduce these measurements to the physically more interesting quantities of two- and three-body attachment coefficients as functions of electron energy.

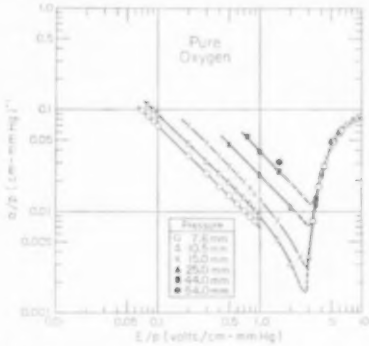

Fig. 2. Measured attachment coefficients in pure oxygen at a gas temperature of 300°K displayed as curves of α/p vs. E/p for a number of gas pressures.

The time rate of change of electron density, n_e, depends on the attachment frequency, $\nu_a = \alpha w_e$, which may be further characterized by a two-body coefficient, β, and a three-body coefficient, K, through the relation

$$\frac{dn_e}{dt} = -\nu_a n_e = -\alpha w_e n_e = -(\beta n + Kn^2)\, n_e, \qquad (2)$$

where n is the gas density. Consideration of equation (2) suggests that at a given electron energy (E/p value) a two-body process will exhibit values of α/p independent of the gas pressure. Thus, the data for $E/p > 4$ are characteristic of a two-body attachment process. The data for $E/p < 3$ indicate that α/p is proportional to p at constant energy, which from equation (2) may be seen to indicate dominance of a *three*-body attachment reaction at low energies.

The data of Fig. 2 were converted to values of β and K as functions of energy by use of an average of available data concerning electron energy[6] and drift velocity[7] as functions of E/p. The results are shown in Figs. 3 and 4.

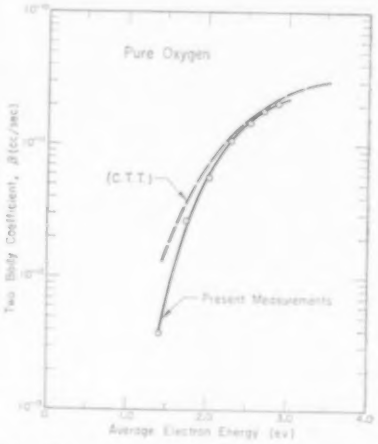

Fig. 3. The energy dependence of the two-body attachment coefficient, β. The dashed curve was obtained by averaging the attachment data of Craggs, Thorburn and Tozer (CTT) over a Druyvesteyn electron energy distribution for various average energies.

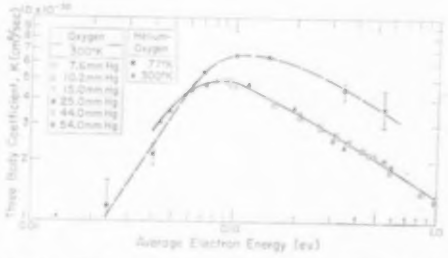

Fig. 4. The energy dependence of the three-body attachment coefficient, K, at 300°K and 77°K. The solid points were obtained from measurements of attachment coefficients in oxygen–helium mixtures containing 1–5 per cent of oxygen.

In Fig. 3 are shown the two-body coefficients deduced from our "swarm" experiments in comparison with the beam experiment results of Craggs *et al.*[8] (CTT). The beam experiments, which apply to electrons of narrow

energy spread, showed a sharply peaked dissociative attachment cross section, resulting from the reaction

$$O_2 + e \longrightarrow O + O^-, \qquad (3)$$

which had a threshold energy of $\sim 3{\cdot}5$ eV, reached a maximum value at $\sim 6{\cdot}7$ eV and then decreased again with increasing energy. The dashed curve of Fig. 3 represents β values obtained by averaging the measurements of CTT over a Druyvesteyn electron energy distribution for various average energies. The agreement between the two curves suggests that the high energy process observed in the swarm experiments is evidently the two-body dissociative attachment process. Recently, at our laboratories, Schulz[9] has used his electron beam apparatus to study attachment reactions in oxygen and has essentially verified CTT's results.

At low average electron energies ($\bar{u} < 1$ eV) and pressures in the range 5–50 mm Hg the attachment is predominantly a three-body process. The values of the three-body coefficient K obtained from our experiments are shown in Fig. 4. By use of oxygen–helium mixtures it was possible to extend the measurements to lower electron energies. In this case, however, care must be taken to determine the contribution of the helium atoms acting as the third body in stabilizing the attachment process.

It will be seen that at a gas temperature of 300°K the maximum value $K = 5 \times 10^{-30}$ cm^6/sec occurs at an average electron energy of $\sim 0{\cdot}09$ eV. At thermal energy ($T_e = 300$°K) the value has fallen to $\sim 2{\cdot}8 \times 10^{-30}$ cm^6/sec. In the upper atmosphere somewhat lower gas temperatures occur; thus our measured laboratory values at 77°K are of interest. Here the maximum value $K \simeq 7 \times 10^{-30}$ cm^6/sec occurs at $\sim 0{\cdot}1$ eV and an extrapolation of the data to determine the thermal value ($T_e = 77$°K) appears to give a K value substantially less than 1×10^{-30} cm^6/sec, although there are large uncertainties in these values, as indicated by the extent of the symbols.

At 300°K the energy and pressure dependences of the low energy three-body process have been verified by Schulz[9] using the electron beam method. A disadvantage of this method lies in the fact that, in order to obtain a reasonable attachment rate, the tube must be operated at rather high gas pressures, and consequently the electron beam suffers scattering collisions in traversing the measuring chamber. However, it was possible to calibrate the apparatus by comparing the low energy process with the high energy (dissociative) process in the high pressure range (the dissociative process had first been studied at low gas pressures, where the beam tube operated normally).

The advantage of the beam tube in studying this reaction is that for energies $> 0{\cdot}1$ eV the electron energy distribution is narrower in the beam tube than in the drift tube experiment. Schulz has obtained preliminary evidence that the curve of K vs. energy exhibits structure, indicating secondary maxima occurring at intervals of $\sim 0{\cdot}3$ eV above the energy of the main maximum. This observation may have some bearing on the nature of the three-body attachment process, as discussed below.

Bloch and Bradbury[10] suggested that the low energy attachment process in oxygen occurred in two stages. First, a short-lived vibrationally *excited* negative ion state (lying above the ground vibration state of the neutral molecule) was formed. This excited ion reverted to the initial state of neutral molecule and free electron (i.e. auto-detached) unless it underwent a stabilizing "collision" which removed its excitation energy. A specific case for this two-stage reaction may be represented by

$$(O_2)_{v=0} + e \rightleftharpoons (O_2^-)_{v=1}, \qquad (4a)$$

and

$$(O_2^-)_{v=1} + (O_2)_{v=0} \longrightarrow (O_2^-)_{v=0} + (O_2)_{v=1} \qquad (4b)$$

where $v = 0, 1$ refer to the ground and first excited vibration states, respectively. In this example, the excited negative ion is stabilized by a transfer of vibration energy to the neutral molecule. This vibration transfer may be real, or it may be "virtual" in the sense that a charge transfer takes place in which the electron jumps from the ion to the neutral molecule in the ground vibration state.

An alternate reaction, equally capable of

describing a three-body attachment process, is based on a modification of the Thomson theory of recombination. In this process, an electron passes in the vicinity of two oxygen molecules which statistically happen to be close together (~ 2 Å). The system of electron plus two oxygen molecules may be thought of as an unstable state of O_4^- which begins to dissociate. If the configuration can separate a sufficient distance before the electron wanders out of range we are left with O_2^- and O_2. The energy given up by the electron in forming the negative ion appears as kinetic energy of motion between the oxygen molecule and negative ion. Thus we may write

$$O_2 + O_2 + e \longrightarrow (O_4^-)_{\text{unstable}} \longrightarrow O_2^- + O_2 + \\ + \text{kinetic energy} \qquad (5)$$

The present experimental data give some preliminary evidence that equation (4), in modified form, is the actual process observed. First of all, the attachment exhibits a maximum K value at $\sim 0{\cdot}1$ eV energy. This is consistent with the existence of a threshold energy, such as would be required to excite the first vibration state of the negative ion, which is assumed to lie *above* the $v=0$ state of the neutral molecule. On the other hand, a "dissociative" attachment reaction of the type given in equation (5) might also require a positive electron energy to achieve a repulsive state of the O_4^-.

The preliminary observation by Schulz of secondary structure in the attachment curve at intervals of $\sim 0{\cdot}3$ eV beyond the first maximum can be accounted for by assuming that the oxygen negative ion in equation (4a) is excited to the higher vibration levels, $v=2$, 3, etc. In contrast, for this case equation (5) has no apparent mechanism to explain the structure in the K curve.

A rather important consequence of the present drift tube results is the demonstration that the three-body attachment reaction does not "saturate", i.e. go over to an apparent two-body pressure dependence, at ~ 5 mm Hg as assumed by Bloch and Bradbury from Bradbury's[1] experiments. This saturation pressure had required the assumption of a combination of a very long autodetachment time ($\sim 10^{-10}$ sec) and a remarkably large stabilizing cross section ($\sim 10^{-14}$ cm^2) for equation (4). The present drift tube results give no indication of a deviation from the three-body dependence to pressures in excess of 50 mm Hg, which permits us to assume more reasonable values for the autodetachment and stabilization rates.

2. ELECTRON MOBILITIES AND COLLISION FREQUENCIES

Pack and Phelps[11] have employed a special electron mobility tube capable of operating at very low values of drift field/gas pressure, i.e. $E/p < 0{\cdot}001$, to obtain electron mobilities at thermal energy and above in nitrogen. These studies have been carried out at gas temperatures of 77°K, 300°K and 373°K.

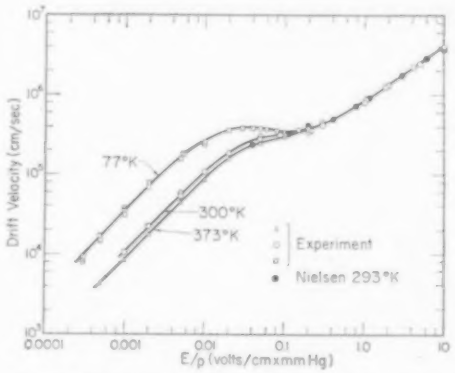

Fig. 5. Electron drift velocity in nitrogen as a function of E/p.

The observed values of electron drift velocity, w_e, as a function of E/p for nitrogen are shown in Fig. 5. The data are in good agreement with the results of Nielson[12] at room temperature, who was, however, unable to obtain measurements below $E/p \sim 0{\cdot}04$. At low values of E/p the drift velocity becomes directly proportional to E/p indicating that the electrons are in thermal equilibrium with the gas*. In order to obtain the energy dependence of the collision

* This proportionality between w_e and E/p would also occur when the electrons were *not* in equilibrium with the gas if the collision frequency, ν_c, were independent of electron energy. In the case of nitrogen this is shown not to be the case.

frequency, ν_c, it is represented by an expansion in powers of the electron velocity v[13, 14], i.e.

$$1/\nu_c = \sum_i a_i v^i, \tag{6}$$

where a_i are coefficients to be determined and use is made of the relation[15]

$$w_e/E \equiv \mu_e = \frac{4\pi}{3}\frac{e}{m}\int_0^\infty \frac{d}{dv}\left(\frac{v^3}{\nu_c}\right) f_0 dv. \tag{7}$$

For the thermal equilibrium data, f_0 is a Maxwellian distribution and the indicated integrations can be carried out to give the electron mobility μ_e in terms of the coefficients a_i and powers of temperature. By fitting the observed thermal mobility vs. temperature data, the collision frequency or the related quantity, the momentum transfer cross section shown in Fig. 6, was deduced ($\nu_c = n\sigma_m v$, where σ_m is the momentum transfer cross section and v is the electron velocity corresponding to an energy u). The temperatures on the energy axis are located at such points that $u = kT/e$. It will be seen that the drift velocity measurements are in rather good agreement with the results obtained by Phelps *et al.*[14] by determinations of the complex conductivity of the electrons in microwave afterglow experiments. They are, however, at variance with the results of microwave experiments of Anderson and Goldstein[16], which give values 5 times larger. Over the energy range of Fig. 6 an approximate expression for the collision frequency in nitrogen is:

$$\nu_c = 1{\cdot}3 \times 10^{-7} nu \ (\text{sec}^{-1}), \tag{8}$$

when the gas density, n, is expressed in cm^{-3} and u in eV.

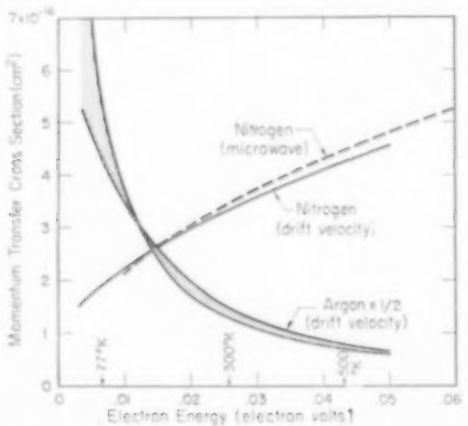

Fig. 6. The deduced energy dependence of the momentum transfer cross section for nitrogen and for argon. The temperatures on the abscissa are located at points such that $u = kT/e$.

To illustrate the sensitivity of the method in determining the energy dependence of momentum transfer cross sections from thermal mobility data, the results for argon are also included. Here the rapid variation of σ_m as the result of the Ramsauer effect has been determined at very low energies, where beam experiments have not been at all reliable. The indicated uncertainty in the determination is the result of two somewhat different choices of power series to fit the data. The present results on nitrogen have been used to calculate upper atmospheric collision frequencies and are in good agreement with measurements obtained from rocket data[17].

3. STUDIES OF LOW ENERGY INELASTIC COLLISIONS IN DIATOMIC GASES

A "trapped-electron" method has been developed by Schulz[18] for measuring those electrons which have undergone an inelastic collision and thereby lost an appreciable amount of their initial kinetic energy. A simplified schematic diagram of the experimental tube and the potentials at the axis of the tube is given in Fig. 7. A static magnetic field B is applied in the direction of the primary electron beam. Electrons from the filament pass through the elements of a gun which employs the retarding potential difference (RPD) method[19] to observe the effects of electrons of very narrow ($<0{\cdot}1$ eV) energy spread. The collision chamber consists of flat end plates and a cylindrical grid at ground potential. A positive potential applied to the cylinder M partially penetrates to the axis of the tube; the result is an electrostatic potential well in the axial direction. Thus, an electron which has suffered an inelastic collision with a corresponding loss of energy cannot reach the primary beam collector, E, nor the collision chamber electrodes, such as G. It oscillates in the well,

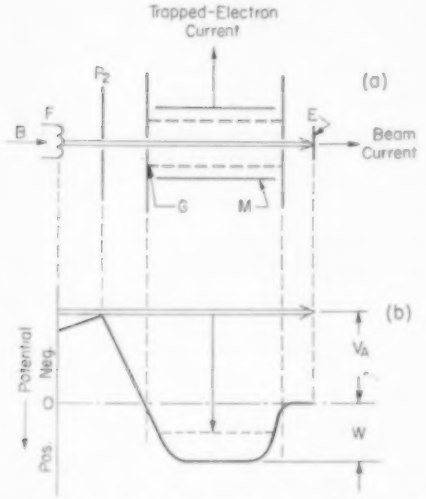

Fig. 7. Schematic representation of (a) the electrode configuration and (b) the potentials at the axis of the trapped electron tube. The double line in (b) indicates the electron energy and the arrow indicates the trapping of an electron which loses enough energy in an inelastic collision to drop into the well, W.

making collisions, and therefore diffusing across the magnetic field until it reaches the trapped electron collector, *M*.

This technique has been used to study inelastic collision processes in such gases as hydrogen, nitrogen and carbon monoxide. In addition to the usual inelastic collisions corresponding to electronic excitation of the molecules, a low energy ($\sim$ 1–2 eV) inelastic process has been observed[20] in N_2 and in CO. The relative shapes of the excitation curves for a particular well depth in each case are shown in Figs. 8 and 9. The inelastically scattered electrons observed at primary energies of >6 eV are the result of the excitation of the usual electronic states lying above the ground state of the molecule. The peaks at $\sim$2 eV, however, have been interpreted in terms of an unstable (virtual) negative ion state lying above the electronic ground state of the neutral molecule.

This process is illustrated schematically for nitrogen in Fig. 10. An incident primary

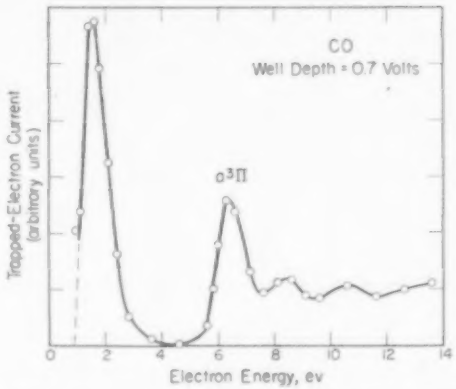

Fig. 9. Excitation spectrum of carbon monoxide at a well depth of 0·7V.

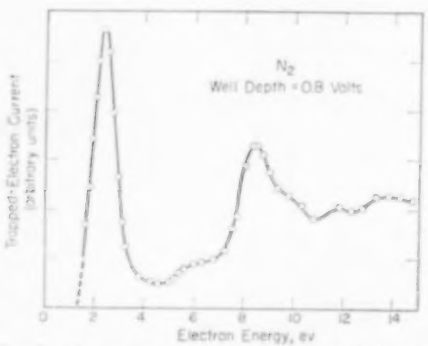

Fig. 8. Excitation spectrum of nitrogen indicating the inelastically scattered electrons trapped in a well of 0·8 V. depth. The large peak at $\sim$2 eV occurs at a much lower electron energy than is required to cause electronic excitation of the molecule.

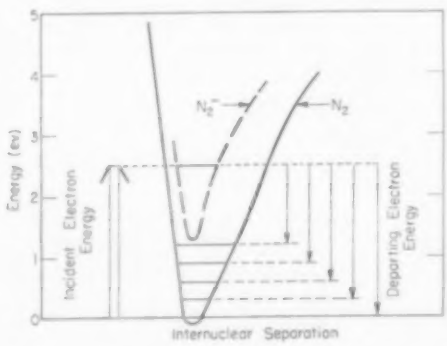

Fig. 10. Hypothetical energy level diagram indicating a virtual N_2^- state lying above the ground state of N_2.

electron of the proper energy is captured temporarily to form a state of N_2^-. After a short time autodetachment takes place; the electron is re-emitted, and the molecule returns to its ground electronic state. However, the molecule may be left in various states of vibrational excitation. If the molecule returns to the ground ($v=0$) vibration state, the overall collision process appears as an elastic scattering event. On the other hand, if the molecule ends up in a $v=1$, 2, 3, etc. state, the departing electron's energy is smaller than its incident energy (see Fig. 10) and an inelastic collision has resulted. Schulz's technique is sensitive in principle only to the inelastic part of this process.

If one is concerned with electron energy loss rates in the atmosphere, the present inelastic process provides a loss mechanism at electron energies substantially below the usual threshold for electronic excitation of the molecule. In addition, the cross section for the process, which leads to vibrational excitation of the molecule, is more than an order of magnitude larger than the inelastic collision cross section for direct excitation of vibration levels.

4. DISSOCIATIVE RECOMBINATION BETWEEN ELECTRONS AND MOLECULAR POSITIVE IONS

Microwave afterglow studies[21] have demonstrated the existence of an unusually large recombination rate between thermal electrons and positive ions. It has been suggested that the process responsible is the same one involved to explain recombination loss of electrons in the ionosphere, i.e. dissociative recombination:

$$X_2^+ + e \longrightarrow (X_2^*)_{\text{unstable}} \longrightarrow X^* + X + \text{kin. energy} \qquad (9)$$

The system of electron plus molecular positive ion, X_2^+, forms an unstable excited state of the molecule, which dissociates into two atoms, one of which may be in an excited electronic state. The energy given up by the electron in going into a bound state appears as kinetic energy of dissociation of the fragments. This reaction should be very efficient in electron capture, giving rise to recombination coefficients several orders of magnitude larger than the values for radiative recombination, where the electron capture is effected by an optical transition from a free to a bound state. It was, therefore, desirable to establish the exact mechanism of the recombination process observed in our laboratory measurements in order to permit conclusions to be drawn concerning recombination rates for positive ions occurring in the upper atmosphere.

From equation (9) it is clear that, if the laboratory process is indeed the dissociative reaction, it can only occur when *molecular* rather than atomic ions are present. Experiments were made using noble gases (where complicated positive ion formation should not occur) under conditions in which first molecular positive ions, then atomic ions were expected[22]. In pure argon at pressures ~ 10 mm Hg, it is expected that the ions in a microwave afterglow should be predominantly A_2^+. Studies of the electron loss under these conditions indicated the dominance of recombination as the removal mechanism. The recombination coefficient α (defined by the relation $dn_e/dt = -\alpha n_e n_+$, where n_+ is the positive ion density) was found to be large, $\sim 10^{-6}$ cm^3/sec, in this case.

In helium containing 10^{-3} parts of argon at total pressures of ~ 5 mm Hg, the predominant ion during the afterglow should be A^+. In this case the electron removal was characteristic of ambipolar diffusion loss, with no evidence of recombination loss to the limit of accuracy of the experiment (if recombination were present, α was less than 10^{-9} cm^3/sec). Thus, these experiments demonstrated that the large recombination required the presence of molecular positive ions, which is consistent with equation (9).

A much more conclusive proof that the dissociative process is indeed the recombination mechanism would be through the detection of the kinetic energy of dissociation of the atoms formed by the recombination process. This study can be carried out if the excited atom is formed in a radiating state and emits a quantum of radiation while the atom still has its additional kinetic energy. The resultant doppler shift of the radiation can be detected by techniques of high resolution spectroscopy. In this

case, helium afterglows were studied by means of a high speed Fabry–Perot interferometer[23–25]. The particular reaction studied was

$$He_2^+ + e \longrightarrow (He_2^*)_{\text{unstable}} \longrightarrow He + He^*(3^3D) \quad (10a)$$

$$He^*(3^3D) \longrightarrow He^*(2^3P) + h\nu\,(\lambda\,5876) \quad (10b)$$

Those recombination events which led to the formation of excited helium atoms in the 3^3D state were detected by means of the λ 5876 line emitted. When the various other afterglow processes were taken into account, it was shown that the radiation arising from recombination exhibited a doppler broadening appreciably in excess of the thermal width.

Thus, the mechanism responsible for the large recombination observed in laboratory experiments is most probably the dissociative process, and we can now turn our attention to measurements of the recombination coefficients of the molecular ions believed to be present in the upper atmosphere, e.g. N_2^+, O_2^+, etc. Unfortunately we immediately run headlong into the difficulty, encountered in various experiments in gases such as H_2, N_2 and O_2, that the positive ions present often are rather complex types, e.g. H_3^+, possibly N_1^+, etc. Therefore, previous measurements of recombination coefficients in gases such as nitrogen[26] have had the difficulty that the identity of the ion responsible for the observed recombination is not known. At the present time we are extending our microwave afterglow studies to the atmospheric gases; however, we are first rebuilding the apparatus to include mass analysis of the ions taking part in the afterglow reactions. In this manner we hope to obtain the recombination coefficients for various ions, such as O_2^+, O_3^+, N_2^+, N_4^+, to provide the fundamental data for calculations of upper atmosphere recombination rates.

DISCUSSION

A. DALGARNO: Can you exclude the possibility that your postulated N_2 is in a metastable state rather than a virtual state, the autodetachment being forbidden by some selection rule?

M. BIONDI: The apparatus used in the nitrogen studies is capable of detecting any negative ion whose lifetime is longer than 10^{-7} sec. A careful check for the presence of negative ions was made, without success; therefore, we conclude that no long-lived metastable state of N_2^- occurs.

REFERENCES

1. N. E. BRADBURY, *Phys. Rev.* **44**, 883 (1933).
2. A. DOEHRING, *Z. Naturf.* **79**, 253 (1952).
3. P. HERRENG, *Cah. Phys.* **38**, 7 (1952).
4. M. A. BIONDI, *Phys. Rev.* **84**, 1072A (1951); E. HOLT, *Bull. Amer. Phys. Soc.* Ser. 2, **4**, 112 (1959); M. C. SEXTON, private communication.
5. L. M. CHANIN, A. V. PHELPS and M. A. BIONDI, *Phys. Rev. Letters* **2**, 344 (1959).
6. These curves are an average of the data of R. H. HEALY and J. W. REED, *The Behaviour of Slow Electrons in Gases* p. 94 ff: Amalgamated Wireless, Sydney (1951); H. L. BROSE, *Phil. Mag.* **50**, 536 (1925); and R. W. CROMPTON, private communication. We have taken the average energy to be equal to 1·5 times the experimentally determined values of D/μ.
7. These curves are an average of the data of H. L. BROSE, *Phil. Mag.* **50**, 536 (1925); R. A. NIELSEN and N. E. BRADBURY, *Phys. Rev.* **51**, 69 (1937); R. W. CROMPTON, private communication; and P. HERRENG, Ref. (3).
8. J. D. CRAGGS, R. THORBURN and B. A. TOZER, *Proc. Roy. Soc.* A**240**, 473 (1957).
9. G. J. SCHULZ, private communication.
10. F. BLOCH and N. E. BRADBURY, *Phys. Rev.* **48**, 689 (1935).
11. J. PACK and A. V. PHELPS, *Bull. Amer. Phys. Soc.* Ser. 2, **4**, 317 (1959).
12. R. A. NIELSEN, *Phys. Rev.* **50**, 950 (1936).
13. A. V. PHELPS, private communication.
14. A. V. PHELPS, O. T. FUNDINGSLAND and S. C. BROWN, *Phys. Rev.* **84**, 559 (1951).
15. W. P. ALLIS in *Encyclopedia of Physics* Vol. 21, p. 413, Springer, Berlin (1956).
16. J. M. ANDERSON and L. GOLDSTEIN, *Phys. Rev.* **102**, 388 (1956).
17. J. A. KANE, *J. Geophys. Res.* **64**, 133 (1959).
18. G. J. SCHULZ, *Phys. Rev.* **112**, 150 (1958).
19. R. E. FOX, W. M. HICKAM, D. J. GROVE and T. KJELDAAS, *Rev. Sci. Instr.* **26**, 1101 (1955).
20. The low energy inelastic process in nitrogen has previously been reported by R. HAAS, *Z. Phys.* **148**, 177 (1957).
21. See, for example, M. A. BIONDI and S. C. BROWN, *Phys. Rev.* **76**, 1697 (1949) and R. B. HOLT, JOHN M. RICHARDSON, B. HOWLAND and B. T. MCCLURE, *Phys. Rev.* **77**, 239 (1950).

22. M. A. Biondi, *Phys. Rev.* **83,** 1078 (1951).

23. W. A. Rogers and M. A. Biondi, *Phys. Rev.* **99,** 1657 (1955).

24. W. A. Rogers and M. A. Biondi, *Bull. Amer. Phys. Soc.* Ser. 2, **2,** 87 (1957).

25. W. A. Rogers and M. A. Biondi, *Bull. Amer. Phys. Soc.* Ser. 2, **4,** 113 (1959).

26. A C. Faire, O. T. Fundingsland, A. L. Aden and K. S. W. Champion, *J. Appl. Phys.* **29,** 928 (1958); A. C. Faire and K. S. W. Champion, *Phys. Rev.* **113,** 1 (1959).

THERMODYNAMIC RELAXATION OF ATMOSPHERIC GASES IN SHOCK WAVES

B. STEVERDING and L. WERNER
Army Ballistic Missile Agency, Redstone Arsenal, Alabama

Abstract—This paper applies the thermodynamic theory of relaxation to shock waves. Soft shock waves, which are nearly adiabatic, show a simple exponential relaxation mechanism, which agrees with results obtained from the kinetic gas theory. For strong shock waves, deviations occur which increase as the disturbance of the thermal equilibrium increases.

1. INTRODUCTION

The historical development of the theory of shock waves started with the consideration of only the compressibility of gases and the assumption of an adiabatic "energy law", like in sound propagation. This gave satisfactory results as long as the shock velocity was relatively small and did not appreciably exceed the sound velocity. A step forward was made when the complete energy equation was stated. This revealed general information concerning the increase in entropy and the variables of state in front of and behind the shock front. Next, the structural shape of the shock front itself was revealed by the simultaneous solution of the continuity equations for mass, momentum, and energy and an equation of state.

At this time, heat conductivity and internal friction were considered as being responsible for the shape of the shock front; however, with increasing shock velocities, it became obvious that the physical chemistry of certain high-energy reactions that take place at the high temperatures encountered also control the shape of the shock front; thus, in shock wave investigations it is important to include the excitation of vibrational energy, dissociation and ionization. The theory of gas dynamics is commonly applied to these phenomena in investigating shock fronts, but this paper will show that the same results may be derived by the application of the theory of irreversible thermodynamics.

The energy absorption of the gas in the front of a shock wave, due to friction, vibration, dissociation, etc., is in general a very complicated process; however, it is possible to divide a shock wave front into steps that can be treated almost independently of each other. The shape of the first step is determined by internal friction and heat conductivity. The second step, by the excitation of vibrational energy; and the third, by the activation of dissociation, ionization, etc. The basic physical reason for step separation is because only translation and rotation energy are transferred in the first step, and these within a few mean free paths only. The subsequent steps are caused by the delayed energy transfer to vibration and dissociation. (Fig. 1 is a schematic cross section through the front of a shock wave.) The actual separation into the different steps is mainly caused by the large differences between the energy levels of vibration, dissociation and ionization and, to a

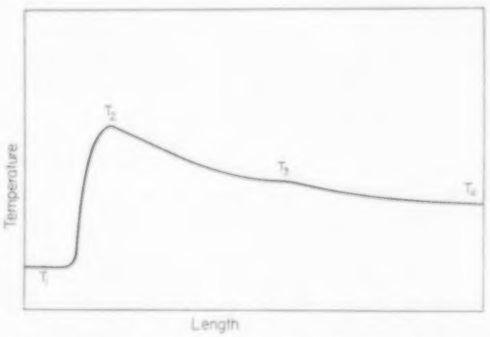

Fig. 1. A schematic cross section through the front of a shock wave.

lesser extent, the low density of the gas. The density can never exceed its initial value more than 8 times. In an adiabatic compression, the density approaches infinity as the pressure and temperature go to infinity but the high entropy production in a shock wave leaves the density small.

The first stage of a shock front, in contrast to the subsequent stages, cannot be considered a relaxation process since there is no conversion from kinetic to potential energy, even though mathematically a relaxation-type formula can be obtained for this part of the shock front. Heat conductivity and internal friction, determining factors of the shape of the first stage, have a small influence on the relaxation processes. The internal friction influence is small since $\partial\rho/\partial x$ is small, and the heat conductivity is a third order effect.

2. RELAXATION THEORY

The thermodynamic relaxation theory will be defined only as it is related to the physical chemistry of gases. For explanation purposes, think of a thermodynamic system in which chemical and physical internal variables—like excitation of vibrations, dissociation, ionization and formation of chemical compounds—can be caused by changing external variables, temperature, pressure, etc. A continuous slow change of the external variables allows the internal variables time to follow correspondingly. But, because the internal variables need time to establish the thermal equilibrium, a sudden change will cause a time lag. The relaxation theory determines the time law that defines how the thermal equilibrium is approached under the influence of external disturbances.

If there is only one internal variable and the deviation from the equilibrium is not too large, the reaction rate dn/dt can be expressed by

$$\frac{dn}{dt} = \varepsilon(T, v, n) \cdot A(T, v, n) \qquad (1)$$

The rate is proportional to the distance from equilibrium. The term $A(T, v, n)$ is the affinity (similar to the thermodynamic potentials) and is defined by the formula

$$dE = TdS - pdv - Adn$$

This formula also holds for the irreversible processes. The term $\varepsilon(T, v, n)$ is a proportional factor. If the equilibrium value n_0 replaces n, equation (1) is limited to small deviations from the equilibrium, and its expansion in a Taylor series yields

$$\frac{dn}{dt} = \varepsilon \left(\frac{\partial A}{\partial n}\right)_{T,v} (n - n_0) + \ldots$$

The term n_0 is a unique function of T and v but not n. Integration yields

$$n = n_0(T, v) + C \exp \frac{t}{\tau_{T,v}} \qquad (1')$$

Where C is an integration constant and $\tau_{T,v} = 1/\varepsilon (\partial n/\partial A)_{T,v}$ has a time dimension, it is called relaxation time at constant T and v. The variables T and v can be replaced by other variables of state: entropy, pressure, etc., allowing other relaxation times to be defined. Among these are the following relations:

$$\tau_{Sv} \leqq \tau_{Tv} \leqq \tau_{pT}$$
$$\tau_{Sv} \leqq \tau_{Sp} \leqq \tau_{Tp}$$

The equation of state is

$$p = p(T, v, n)$$

This equation expanded in a power series with the equilibrium state as a reference point gives

$$p - p_0 = \left(\frac{\partial p}{\partial T}\right)_{vn} (T - T_0) + \left(\frac{\partial p}{\partial v}\right)_{Tn} (v - v_0) + + \left(\frac{\partial p}{\partial n}\right)_{Tv} (n - n_0) + \ldots .$$

Applying the same procedure to equation (1) results in

$$\frac{1}{\varepsilon}\frac{d}{dt}(n - n_0) = \left(\frac{\partial A}{\partial T}\right)_{vn} (T - T_0) + + \left(\frac{\partial A}{\partial v}\right)_{T,n} (v - v_0) + \left(\frac{\partial A}{\partial n}\right)_{T,v} (n - n_0) \qquad (2)$$

The term $n - n_0$ can be eliminated from these last two equations, supplying an equation that may be called the dynamic equation of state

$$p - p_0 + \tau_{Tv}\dot{p} = \left(\frac{\partial p}{\partial T}\right)_{vA} (T - T_0 + \tau_{pv}\dot{T}) + + \left(\frac{\partial p}{\partial v}\right)_{TA} (v - v_0 + \tau_{pT}\dot{v}) \qquad (3)$$

The factors τ_{pT}, τ_{Tv}, etc. can be defined as mentioned above.

3. SHOCK WAVE EQUATIONS

Now the theory of relaxation will be applied to the one dimensional and steady state shock wave equations. These are the equations for the continuity of mass, momentum and energy. They are

$$\operatorname{div}(\rho u) = 0 \tag{4}$$

$$u\frac{\partial u}{\partial x} + \frac{1}{\rho}\frac{\partial p}{\partial x} - \frac{1}{\rho}\mu\frac{\partial^2 u}{\partial x^2} = 0 \tag{5}$$

Since the temperature gradient vanishes at the metastable points 2, 3 and 4 on Fig. 1, the static equation of state may be applied and the system of equations solved by simple integrations. (The temperature and velocity gradients become zero at the same location.) The knowledge of the variables of state at these points is important, since they are the initial values for the relaxation process. The location of the metastable points and the shape of the temperature curve are obtained by solving the shock wave equations and the dynamic equation of state simultaneously.

$$\rho\frac{\partial u}{\partial x}u = p\frac{\partial p}{\partial x}\frac{u}{\rho} + \lambda\frac{\partial^2 T}{\partial x^2} + u\sigma\frac{\partial T^4}{\partial x} \tag{6}$$

where

u = velocity

$\mu = \frac{4}{3}\eta$; η = internal friction coefficient

λ = heat conductivity

The last term of the last equation represents heat loss by radiation, which usually can be neglected. As a fourth equation, the dynamic or static equation of state is used, depending on the required objective.

The entropy production can be calculated by determining the entropy values in front of and behind the shock front from the other known variables of state or by integrating over the energy dissipating processes of friction, heat conduction and relaxation. Inserting $E_2 = \frac{5}{2}RT_2$ in the energy equation yields the peak value of temperature, which is attained when the whole internal energy is restricted to the translational and rotational degrees of freedom. At this stage, the molecules are overburdened with energy, but in the subsequent relaxation steps, new degrees of freedom are activated, decreasing the temperature[3]. The maximum density obtainable in this case is 6 times the initial density.

For complete vibration, $E_3 = \frac{7}{2}RT_3$ can be inserted in the energy equation, in a similar manner. This yields a density ratio of 8. For complete dissociation, $E_4 = \frac{3}{2}RT_4 + E_d$ is inserted, E_d being the dissociation energy.

This paper is limited to vibrational relaxation; although, using the initial conditions for dissociation and replacing the vibration relaxation times by the corresponding dissociation times, this method can also be applied for dissociation.

By denoting the state before the shock wave with the suffix 1 and the metastable states, which correspond to the activation of the translation and rotation degrees of freedom, the excitation of vibration, dissociation, etc., with 2, 3, 4, ..., the following system of equations is obtained

$$u_1\rho_1 = u_2\rho_2 = u_3\rho_3 = M \tag{7}$$

$$u_1^2\rho_1 + p_1 = u_2^2\rho_2 + p_2 = u_3^2\rho_3 + p_3 = I \tag{8}$$

$$E_1 + \frac{u_1^2}{2} + \frac{p_1}{\rho_1} = E_2 + \frac{u_2^2}{2} + \frac{p_2}{\rho_2} = E_3 + \frac{u_3^2}{2} + \frac{p_3}{\rho_3}$$

$$\frac{p_1}{\rho_1 T_1} = \frac{p_2}{\rho_2 T_2} = \frac{p_3}{\rho_3 T_3} \tag{9}$$

From these equations, the velocities u_1 and u_2 can be calculated. The energy equation simplifies to

$$E_2 - E_1 = \tfrac{1}{2}(p_1 + p_2)(v_1 - v_2) \tag{10}$$

where v = specific volume.

A comparison with the first law of thermodynamics

$$dE = TdS - pdv$$

shows that only soft shocks, where Δp and Δv are small, are adiabatic and not entropy producing.

4. RELAXATION IN SOFT SHOCK WAVES

Since soft shock waves are nearly adiabatic, it is advantageous to transform the dynamic equation of state to

$$p = p(S, v, t)$$

Near the equilibrium value this may be transformed to

$$p-p_0+\tau_{Sv}\dot{p}=\frac{\partial v}{\partial p}_{SA}(v-v_0+\tau_{Sp}\dot{v})+$$

$$+\frac{\partial p}{\partial S}_{vA}(S-S_0+\tau_{pv}\dot{S}) \qquad (11)$$

The last term on the right-hand side may be neglected.

The basic equations for the steady-state shock wave are

$$u\frac{\partial \rho}{\partial x}=-\rho\frac{\partial u}{\partial x}$$

$$u\frac{\partial u}{\partial x}=-\frac{1}{\rho}\frac{\partial p}{\partial x}$$

From this follows

$$\frac{\partial v}{\partial x}=-\frac{1}{\rho^2}\frac{\partial \rho}{\partial x}+=\frac{1}{u\rho}\frac{\partial u}{\partial x}=-\frac{\partial p}{\partial x}\frac{1}{\rho^2u^2}$$

and from equation (4) is obtained

$$v-v_3=-\frac{v_1^2}{u_1^2}(p-p_3)$$

If the values of these last two equations are inserted in the dynamic equation of state, the following is obtained

$$p-p_3\left(1-\frac{1}{\rho_1u_1^2k}\right)+\frac{\partial p}{\partial x}u\left(\tau_{Sv}-\tau_{Sp}\frac{1}{\rho_1u_1^2k}\right)=0$$

where

$$k=\frac{1}{v_1}\left(\frac{\partial v}{\partial p}\right)_{SA}$$

After defining

$$\alpha=1-\frac{1}{\rho_1u_1^2k} \quad \text{and} \quad \beta=\tau_{Sv}-\tau_{Sp}\frac{1}{\rho_1u_1^2k}$$

the integration yields a typical relaxation process

$$p-p_3=K\exp-\frac{\alpha}{\beta x}$$

The value for the constant K may be obtained by setting $x=0$. At this point, only translational and rotational degrees of freedom are excited; therefore, the pressure and the temperature reach extreme values. These values would be permanently retained if no vibration energy were produced in the later relaxation process. The value of the constant then is

$$K=p_2-p_3$$

The term p_2 can easily be obtained from the basic equations. Since the relaxation process is almost isobar, this relaxation curve is very flat. The choice of temperature as a variable would be much more characteristic.

As long as the shock wave is relatively soft, a linear relation exists

$$E-E_3=a(T-T_3)=b(p-p_3)$$

where a and b are constants.
As a consequence, the relaxation times for internal energy, temperature and pressure are equal.

It is interesting to compare this result with a work of Bethe and Teller, based on a completely different theory[45]. The same dependency is obtained; comparison of the coefficients yields

$$\frac{\alpha}{\beta}=-\frac{\mu+1}{\mu\tau}$$

with the definition $\mu=dE_3/dE$.

5. RELAXATION IN STRONG SHOCK WAVES

Since the relaxation process in shock waves is nearly isobar and isenthalpic, the dynamic equation of state is derived with the variables T, h and p. The term h is the enthalpy.

Because it is advantageous to write the basic equations in a dimensionless form, the following are defined as

$$\omega=v\frac{M^2}{I^2}$$

$$\theta=\frac{RTM^2}{I^2}$$

$$\lambda^1=\frac{\lambda}{C_vM}$$

$$\partial=\frac{R}{2C_v}$$

$$\left.\begin{aligned}\bar{\theta}&=\theta-\theta_3\\ \bar{\omega}&=\omega-\omega_3\end{aligned}\right\}\text{deviations from equilibrium}$$

Subscript 3 represents the equilibrium value,

while M and I are the integration constants from the continuity and momentum equation (see equation 4). The energy equation and the dynamic equation of state then attain the form

$$\bar{\theta} - \partial(\varpi^2 + 2\varpi(\omega_0 - 1) = \lambda \frac{d\bar{\theta}}{dx} \qquad (12)$$

$$\bar{\theta} + \tau_{ph} \cdot C\varpi \cdot \frac{d\theta}{dx} = 0$$

where C is a constant equal to u_1/ω_1.

Elimination of ω from equations (12) and (13) yields

$$\bar{\theta} \cdot \left(\frac{d\bar{\theta}}{dx}\right)^2 - \frac{\partial}{\tau^2 C^2}\bar{\theta} - \frac{2\partial(\omega_0 - 1)}{\tau C} \cdot \bar{\theta} \cdot \frac{d\bar{\theta}}{dx} = \lambda^1 \left(\frac{d\bar{\theta}}{dx}\right)^3$$

Inside the relaxation area, $\lambda^1 (d\bar{\theta}/dx)^3$ for low Mach numbers is, on the average, comparatively small. Therefore, it can be neglected and the equation divided by $\bar{\theta}$. The integration of this differential equation can be written

$$x = -\frac{1}{b}(2\xi + a \ln \xi + C)$$

$$\xi = -\frac{a}{2} - \sqrt{\left(\frac{a^2}{4}\right) - \theta b}$$

$$a = -\frac{2\partial(\omega_0 - 1)}{\tau C}; \qquad b = -\frac{\partial}{\tau^2 C^2}$$

This may be transformed to

$$\exp - \left(\frac{xb}{a}\right) = K \cdot \xi \exp\left(\frac{2\xi}{a}\right); \qquad K = \exp\left(\frac{C}{a}\right)$$

The constant K is determined by the condition that when $x = 0$, $\xi = \xi_0$; ξ_0 being the difference between stage 2 and stage 3.

$$K = \frac{1}{\xi_0} \exp - \left(\frac{2\xi_0}{a}\right)$$

$\xi_3 - \xi_2 = \xi_0$ can be computed by assuming that the enthalpy is constant in the relaxation interval

$$\tfrac{7}{2} RT_2 = \tfrac{7}{2} RT_3 + R \frac{h\nu}{K}\left[\exp \frac{h\nu}{KT_3} - 1\right]^{-1}$$

From this equation, ξ_0 and θ_3 may be calculated; thus, the final equation for vibrational relaxation becomes

$$\exp - \left[\frac{x}{2\tau u_1 \left(1 - \frac{1}{\omega_1}\right)}\right] = \frac{\xi}{\xi_0} \exp\left[\partial \frac{\tau u_1}{\omega_1(\omega_1 - 1)}(\xi - \xi_3)\right]$$

If $\xi - \xi_3$ approaches zero, a simple relaxation type formula is obtained. It is interesting, that the relaxation time is multiplied by the factor $(1 - 1/\omega_1)$ where $\omega_1 \leqslant 1$; ω_1 becomes 1 as the shock velocity increases to infinity. This means the effective relaxation time is always smaller than the corresponding static time. This is caused by the density increase in shock waves.

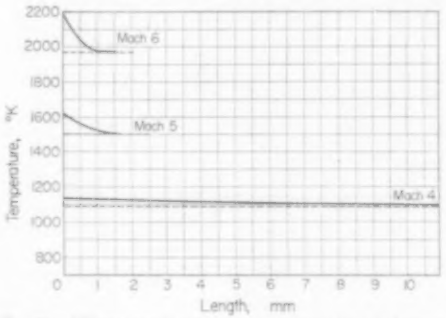

Fig. 2. Vibrational relaxation curves for different shock waves.

Fig. 2 illustrates several relaxation curves for different shock waves in nitrogen.

6. CONCLUSION

The application of the relaxation theory of irreversible thermodynamics to shock waves reveals two points. For soft shock waves, a simple relaxation type function is obtained. For strong shock waves that remain within the validity limits of the linearized theory, deviations from the exponential function occur and enlarge as the shock velocity increases.

Acknowledgement—Acknowledgement is made to Mr. E. A. Braunlich who performed the numerical computations for this paper.

REFERENCES

1. J. Meixner; *Ann. Phys.* **43**, 244 (1943).
2. J. Meixner; *Z. Phys.* **53**, 235 (1943).
3. W. Döring; *Ann. Phys.* **49**, 133 (1949).
4. Bethe and Teller, *Deviations from Thermal Equilibrium in Shock Waves.* Cornell University, Ithaca, N.Y.

A SURVEY OF THE METHODS FOR THE CHEMICAL ANALYSIS OF TRANSIENT SPECIES WITH MICROSECOND RESOLUTION

S. H. BAUER, N. C. ROL and J. H. KIEFER
Cornell University, Ithaca, New York

Abstract—Chemical kinetics at elevated temperatures has recently become an exciting field of research as a consequence of the application of shock tube technology; one may thus readily heat a gas very rapidly and homogeneously to a predetermined high temperature. The full exploitation of this powerful tool depends on the development of analytical procedures which have short response times compared to the half-times of the very fast reactions being studied and are not only specific for the chemical species which are generated in appreciable concentrations under these conditions but also for their states of excitation. Determination of the time dependence of a gross variable, such as the temperature or density, gives kinetic information which is generally useful only as a limiting condition.

In this paper, we shall first outline the variety of procedures which have been developed in other laboratories for the measurement of gross variables and suggest two methods for the direct estimation of temperatures. We shall then discuss the utility of absorption measurements in the infrared. In many respects, this is a desirable portion of the spectrum for investigation since practically all substances (except homatomic diatoms) have bands in that region. Several restricted configurations have been tested, and we have completed a feasibility analysis for a much more versatile arrangement. To this end, we developed a large infrared source (6×12 mm) which operates at an effective temperature of about 5000°K. Interference filters and a grating monochromator will permit the isolation of band widths of approximately 18 cm^{-1} to be incident on a cooled gold-doped germanium detector (response time, 1 μsec) and will operate at a signal/noise ratio of 40/1, over the spectral range 1·5–7 μ. Additional discrimination can be provided by a double-path geometry, whereby the sensitivity toward specified components may be either enhanced or greatly reduced by the insertion of extra absorption cells.

A very useful analytical procedure for estimating concentrations of reaction intermediates is measurement of the absorption of characteristic radiation by diatomic species. The essential feature of the method is the use of an intense source of radiation emitted by the species under study, as excited by a condensed discharge in a suitable gas. Of course, one must select bands (with a monochromator) of which the final state is that in which the species to be measured is present in the shocked gas. One thus avoids the need for a high resolution, high aperture spectrograph and a continuous source of very high intensity. The disparity in the rotational line widths between the electrically excited source and the shocked gas proved less troublesome than had been anticipated. Examples of the analysis for OH, CN and C_2 will be cited.

1. INTRODUCTION

Analysis for the concentration of chemical species as a function of time constitutes the essential measurement of chemical kinetics. In comparing various methods of analysis, one should characterize each with respect to the following desirable features:

(*a*) sensitivity,
(*b*) reproducibility and accuracy,
(*c*) extent of interference with the progress of the reaction,
(*d*) a high degree of specificity, and
(*e*) for shock tube application, the minimum useful time constant for response.

Specificity generally implies the identification of the chemical constitution of each of the species. Currently, information is also desired on the distribution of populations among energy states of the chemical entities if they are generated in excited states.

Since not all of the desirable features listed above are compatible, in the design of an experiment one must select the instrument within the limitations of the apparatus available which will provide answers to the questions posed. One should not forget that for rapid reactions, such as occur at high temperatures in shock tubes, the usual chemical identifications of those species recognized as stable under ordinary conditions are insufficient. Indeed, the dominant species at high temperatures may be molecular fragments which are thought of as transients by conventional kineticists. This presents an additional problem; the properties of these highly reactive transients are not well established, and, hence, methods for their identification have not been developed, so that in many instances their very identity can only be surmised rather than directly proven. Therefore, for shock tube application, it is necessary to extend the established techniques to new ranges in time and sensitivity as well as to develop new and subtle methods for the identification of these significant transients.

For shock tube applications, an essential classification of methods is based on whether the measurement gives information on a gross gas dynamic parameter or on the concentration of a specific chemical species. In the shocked gas, the total enthalpy and the pressure may be considered fixed. However, because very few chemical reactions are thermo-neutral, the temperature and density are generally functions of the time when a chemical rate process occurs. Only in very simple cases can one determine from the time variations of these gross variables the rates of the corresponding chemical changes. Relations between the changes in density or temperature and the chemical composition of the mixture can be uniquely established when not only the mechanism of the reaction is fully known but also the ratios of all the rate constants to the one being determined. Then, it is advantageous to follow the time dependence of the temperature or the density, because these variables can be measured on an absolute scale and with precision.

2. MEASUREMENT OF TEMPERATURE

The shock tube equations permit the computation of the *terminal* temperature from the measured shock speed, the initial composition, temperature and pressure, assuming thermodynamic equilibrium is attained in the system for specified selected end products. It is essential that the thermodynamic functions of these selected species be known for the temperature range covered. Of course, lack of knowledge of the composition precludes the estimation of the corresponding temperature. The transient temperature can be measured in one of two ways. J. G. Clouston and coworkers[1,2] have extended the NaD line-reversal technique for determining the rapidly changing temperature of the shocked gas. Although this method is capable of high precision when long measuring times are available as in steady state conditions for flames[3], it is accompanied by considerable difficulties when the data must be recorded with microsecond resolution. To obtain a sufficiently dense suspension of sodium salt particles in the gas to be shocked, these investigators had to pass the incoming gas through a hot tube ($\sim 800^\circ$C) containing sodium chloride (NaI requires a lower temperature). Small droplets of the molten salt were picked up by the gas in the form of "smoke" which was stable for over a minute, as long as the initial pressure was 6 mm Hg or higher. Very few gases of chemical interest can be inoculated with NaCl in this manner. Depending on the manner of introducing the salt, the NaD line emission lags more or less behind the shock wave due to the vaporization, dissociation, and excitation steps (several microseconds). Care must be taken in making corrections for reflection losses and for the difference in emissivity between the reference source and the emitting gas, as viewed by the spectrograph and detector. Their upper temperature limit is set at about 300° above the operating temperature of the reference

source. In spite of these difficulties, Clouston *et al.* have developed an interpolation method[2] which they claim gives temperatures to better than $\pm 20°K$, over the temperature range 2000°K–3000°K. They found that, in argon, $T_{measured} < T_{shock}$, possibly because of the low efficiency of excitation of sodium atoms by collisions with monatomic gases. However, the ^2P states of Na apparently rapidly attain thermal equilibrium with the vibrational states of N_2 and the condition of dissociation in O_2, since they were able to measure the relaxation time for vibration equilibration in the former and to obtain a clear indication of the expected delay in the latter gas.

Summarized below are the results of a feasibility analysis of a method for measuring relative "atomic" temperatures. These can be reduced to absolute values by calibration in a shock tube with computed temperatures obtained under nearly ideal conditions. To avoid the difficulty of working with droplets of a non-volatile material, we propose using the resonance emission lines of chromium at $\lambda 4290$ and $\lambda 5206$, and of manganese at $\lambda 4033$. The metals can be readily introduced at known concentrations into the gas to be shocked in the form of $Cr(CO)_6$ and $Mn_2(CO)_{10}$ vapors. Flame spectra (temperatures 2200–3200°K) indicate that the "spectral sensitivities" of these lines are of the order 10^{-2}, that for NaD. However, the amounts of Cr and Mn in the shock front can be made 10^2–10^3 times that of Na derived from suspended crystallites of NaCl and still be negligible relative to the chief constituent. In order to convert the ratio of intensities of two lines emitted at different wave lengths, one must correct for their relative f numbers, for the phototube sensitivity and relative effective spectral transmission of the dispersing system. It is also likely that their intensities will be reduced by varying amounts of self-absorption, for which corrections will have to be made.

The estimation of a temperature from the ratio of intensities of two lines either in emission or absorption is based on the equation

$$T = \frac{\Delta E}{\ln R - \ln K}$$

where ΔE is the energy difference between the two upper excited levels of the two emission lines involved, K is the calibration constant and $R_e = I_a/I_b$ for emission is the ratio of the line intensities, while $R_a = \ln(J_a^\circ/J_a)/\ln(J_b^\circ/J_b)$ is the ratio of the extinctions of the absorbing lines. Analysis shows that an error in R produced by an error of specified magnitude in the measured intensities may be 16 times as large in absorption measurements suitable for T estimations, compared to that for emission measurements. In addition, an indeterminate error is introduced when one integrates the equation $-dJ_\nu = J_\nu \alpha_\nu dx$ for finite band width and finite spectrograph resolution in order to evaluate $\int \alpha_\nu d\nu$.

In Table 1, we have listed the relative intensities of several resonance lines and computed the expected errors in the estimated temperature on the assumption that the intensity ratio of two lines can be measured to ± 2 per cent. It is worth noting that the *change* in temperature (and hence the corresponding chemical relaxation time) for any particular shock would be obtained with much better than the indicated precision. An experiment is currently in progress to test this method. To calibrate the system, shocks will be run in mixtures of 90 per cent Ar and 10 per cent N_2, and varying amounts of the tracer gases will be added to determine the minimum useful pressure.

As yet, we have no information as to the time lags which will be encountered in the use of the chromium and manganese carbonyls. Some interval will elapse before dissociation occurs to metal atoms and CO. The resulting chromium atoms should then be in equilibrium with the translational temperature. An additional lag may appear before the metal atoms become electronically excited to attain temperature equilibrium with either the vibrations or the translations of the ambient gas. However, since both the cromium and manganese emission is sufficiently intense to permit use of these lines for flame analysis, it is expected that they are comparable in their excitation characteristics to the emission from alkali metal atoms.

The estimation of rotational temperatures of heated gases from the relative emission inten-

Table 1.

Relative intensity at:		4000°K	2000°K
Cr λ {4254·3, 4274·8, 4289·7}	$z,\ ^7P^\circ \longrightarrow a,\ ^7S$	1	1
Cr λ {5206}	$z,\ ^5P^\circ \longrightarrow a,\ ^5S$	0·029	0·008
Mn λ {4033}	$z,\ ^6P^\circ \longrightarrow a,\ ^6S$	—	0·032

(Cr resonance line is roughly 10^{-2} of NaD intensity.)

Errors: Assume intensity ratio known to ±2 per cent,

$$\Delta T = \begin{cases} \pm 1{\cdot}6\% \text{ for Cr/Cr} \\ \pm 3{\cdot}5\% \text{ for Cr/Mn} \end{cases} \text{ at } 4000^\circ\text{K}; \qquad \begin{cases} \pm 0{\cdot}4\% \text{ for Cr/Cr} \\ \pm 0{\cdot}9\% \text{ for Cr/Mn} \end{cases} \text{ at } 2000^\circ\text{K}.$$

sities of the rotational lines in a resolvable band is a well-known procedure. Sufficient intensity (or time) must be available to permit recording of the spectrum with the necessary resolution. This method has been adequately described in connection with the estimation of flame temperatures. The problem of self-absorption is ever present[4], so that care must be taken to introduce the necessary corrections. It has yet to be demonstrated that even diatomic gases, shocked to temperatures of interest to chemists, emit with an intensity sufficient to be recorded under the necessary spectral dispersion and with microsecond time resolution.

Determination of the rotational temperature by absorption presents a problem which is no less difficult. Spectrographs of high resolving power and large aperture must be used in conjunction with intense light sources. The accurate recording of absorption line shapes with microsecond resolution is under current development in at least one laboratory[5].

In one of the contributions to this symposium, Wurster[6] reported on a method for measuring vibrational temperatures. He selected four narrow spectral regions (10–15 Å wide) at which the characteristic Schumann–Runge absorption bands of oxygen involving a range of vibrational levels in the ground $^3\Sigma_g^-$ electronic state just miss intense NO absorption bands. The relative absorption intensities were measured and calibrated against temperatures computed from shock speeds in pure oxygen. Thus, in systems in which small amounts of molecular oxygen will not prove disturbing, measurement of the relative intensities of absorption at these spectral regions (involving the same optical arrangement) will permit estimation of the vibrational temperature (to ±30°). Such a calibration procedure is necessary. Although the relative *f* numbers for these vibrational transitions have been computed[7], the results are of undetermined accuracy, and the individual spectral bands generally involve a superposition of several transitions.

We propose to sample the vibrational temperature of a shocked gas by means of a tracer *emitter*. In the absence of strong oxidizing agents, CN can be produced in sufficient amounts by the addition of traces of CH_4 and NH_3 (or of CO_2 and N_2, when the temperatures are high enough) to provide useful emission bands. Only moderate spectral resolution is needed, but it is essential that for the temperature measurements the spectrographs view the identical portions of the two band heads which were used in the calibration. An error analysis shows that were one to determine to ±1 per cent the intensity ratio of the (0, 0) band for the

red system ($A^2\Pi_i \longrightarrow X^2\Sigma^+$) to that of the (0, 0) band for the violet system ($B^2\Sigma^+ \longrightarrow X^2\Sigma^+$) the temperature could be estimated to about 7°K.

Finally, in some systems, it may be possible to estimate temperatures spectroscopically by means of tracer chemical equilibria. This technique has been developed extensively by Sugden and co-workers[8] in their studies of equilibria involving metals, their halides, hydrides and hydroxides.

In the above, no mention was made of limitations on resolving times. Since the intensities are measured photoelectrically, the minimum useful time will be set by the acceptable noise/signal, which will be determined statistically by the number of photons which reach the photosurface per unit time interval and by the stability of the light source.

3. MEASUREMENT OF GAS DENSITY

For determining rapid changes in the thermodynamic state of a shocked gas, the density has proved most useful. The variety of techniques which have been developed are described by Ladenburg and collaborators[9]. In the following, we shall refer to selected investigations of particular chemical interest to illustrate the range in sensitivity and time resolution.

The structure of shock waves in polyatomic gases has been studied by Griffith *et al.* by means of an interferometer[10]; they reported on vibration-translation relaxation times in a variety of polyatomic gases. Recently, Byron[11] utilized this technique for measuring the rates of dissociation of O_2. Assuming that fringe displacements can be measured to 1/20 fringe, the smallest increment in gas density which may be detected is 10^{-6} g/cm^3 ($\approx \pm 10^{-5}$ atm, NTP); time resolutions of about 0·5 μsec have been attained.

An "integrated schlieren" technique for measuring gas densities has been proposed by Resler[12]. Preliminary data have thus been obtained on the vibrational relaxation time for CO_2. The potential of the method in terms of sensitivity ($\pm \Delta\rho \approx 10^{-6}$–$10^{-9}$ g/cm^3) and time resolution has yet to be demonstrated. The optics must be set up with care, particularly with regard to parallelism of the light rays used; the windows must be free of strains, and other optical disturbances must be minimized since these introduce an effective "noise".

X-ray densitometers have been set up in several laboratories to measure both kinetic and equilibrium shock densities. Kistiakowsky and Kydd[13] determined the density profile of the rarefaction wave which follows detonations in acetylene–oxygen mixtures. In this study, subsequent experiments indicated that the high intensity of X-rays incident on the gas sample may have sufficiently activated the mixture to cast doubt on the density profile deduced. Knight and Rink[14] determined the heat of sublimation of carbon and the dissociation energy of CO from the ratio of the equilibrium gas density behind the reflected shock to the initial density in CO/Kr mixtures (13 per cent/87 per cent, respectively). For an initial total pressure of about 30 mm Hg, ρ/ρ_0 was measured to ± 2 per cent (i.e. to $\pm 10^{-3}$ atm, NTP) with a laboratory time resolution of 1 μsec. The latter is limited essentially by the width of the slits required to give a sufficient statistical count of X-ray photons. For reactions with $t_{1/2} \approx 30$ μsec, this technique would permit an estimate of the rate by following the over-all density which, of course, is another measure of the heat release in the system. Various investigators have suggested the use of soft X-rays, perhaps of the order of 13 Å. These permit the determination of ρ/ρ_0 of 2 per cent at 0·01 of an atmosphere. However, the indicated resolving times are of the order of 1 sec and, hence, cannot be used for rapid analyses.

Xenon resonance absorption is being utilized by Kistiakowsky and co-workers[15] to measure rates of density changes in Xe–H_2 mixtures due to dissociation of the latter by rapid heating in a shock. The inert gas acts as a sensor, the concentration of which is determined from the percent absorption of incident resonance radiation (λ 1470). The limits of precision attainable for time resolutions of 1 μsec have yet to be determined. One may argue that the method is of limited applicability since practically all polyatomic species have broad absorption bands in the vacuum ultraviolet, in the region of λ 1470.

Density profiles across shock waves propagating in gases at very low densities can be observed from changes in the transmission of a 30–50 kV electron beam[16]. Laboratory time resolution of the order of 0·1 μsec and a sensitivity for increments in density of the order of 10^{-7} g/cm^3 are attainable. An electron beam probe for measuring gas densities by means of the induced fluorescence has been described[17].

4. INFORMATION REQUIRED FOR CHEMICAL KINETICS

The curves in Fig. 1[18] illustrate the need in chemical kinetics investigations of data on the specific composition of shocked gaseous mixtures, obtained with microsecond resolution. These are microphotometer records of a sequence of absorption spectra taken of the mixture 95 per cent Ar+5 per cent C_2N_2, heated to about 4030°K in a back-reflected shock. The top trace is the spectrum of the light emitted by an Ar flash lamp*, $t_{1/2} \approx 10$ μsec duration. Note the absorption by silicon, due to slight decomposition and vaporization of the quartz envelope. In the lower traces of spectra taken through the gas at increasing intervals after passage of the shock, characteristic absorptions due to CN, C_2 and C_3 are clearly evident as is also the fact that their concentrations are rapidly changing with time. The intensity of the continuum absorption is also increasing from the visible toward the ultraviolet progressively with time. However, independent studies indicate that after about 25 μsec the density changes little, possibly because the over-all complex of reactions is thermoneutral, even though none of the reactions had reached a steady state.

To date, the use of light emitted from shocked gases for the analysis of the transient com-

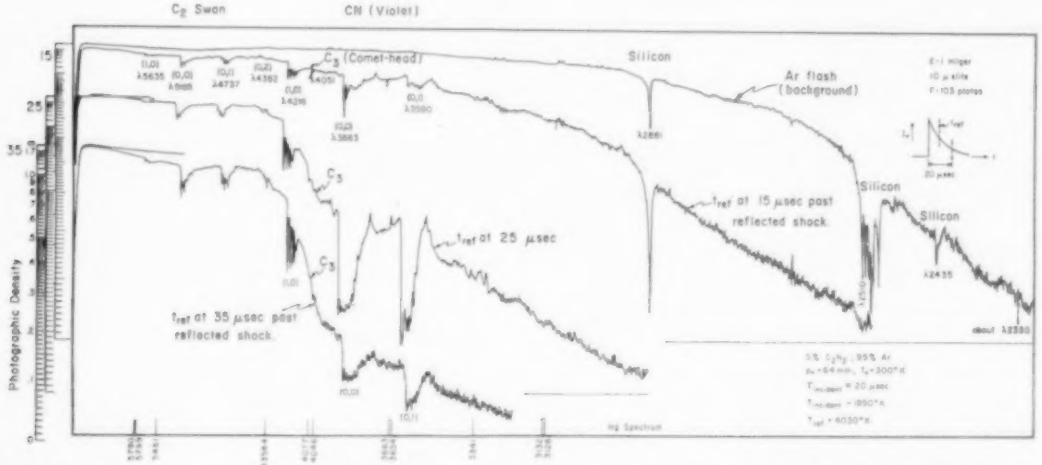

Fig. 1. Microphotometer records of absorptions in the visible and ultra-violet regions by shock heated C_2N_2, at various times after passage of the reflected shock through the sample.[18]

positions has not proven quantitatively useful. A variety of species have been identified, the time of their initial appearance in excited states noted, and their relative growth and decay recorded[19], but significant kinetic constants have not been determined from the intensity of characteristic emitted radiation. However, kinetic spectroscopy based on absorption measurements have been exploited by Norrish and co-workers[20] in their flash photolysis investigations.

Absorption spectra permit characterization of the chemical species (wave length) and

* See Fig. 6 for a description of this lamp.

estimates of the population in the lower state (intensity). One could, of course, use time resolved photographic spectra and thus obtain in a single experiment a time scale, a wave length scale and a measure of intensity. Such a three-dimensional recording would prove most advantageous were it not for severe limitations in the operation of the available instruments. Generally, it is possible to obtain either a fast response time but short recording time and poor spectral resolution *or* moderate resolution for a relatively long response time and accompanying long recording time. Another limitation appears in the processing of the photographic film and the reduction of the photographic density to a quantitative measure of light intensity. It is not only time consuming but very difficult to obtain with sufficient resolution in wave length the desired accuracy for the determination of concentrations of the interesting species. For intensity measurements, phototubes are superior, in that circuitry is available which provides linear response characteristics. Thus, it is relatively easy to obtain rough relative intensities as a function of the wave length at specified intervals by using a flash lamp of short duration triggered to emit at a given time after passage of the shock. Also, at a given wave length, one may evaluate precise intensities as a function of time, from the voltage output of a photodetector displayed on an oscilloscope. The adaptation of "direct reading" spectrometers for shock tube kinetics studies is an exciting possibility. Grating spectrographs of relatively low aperture with multiple slits (≈ 20) and phototube detectors are available. Instruments with large apertures have been designed, but multiple recording devices with fast response times (perhaps magnetic drum recorders) still have to be developed.

5. ABSORPTION SPECTROSCOPY IN THE INFRA-RED

A relatively small number of simple molecules have useful absorption spectra in the visible and ultraviolet regions; there are many more compounds of kinetic interest which in their stable configurations do not absorb either. Therefore, we have looked into the possibility of using infra-red radiation to determine the rate of disappearance of the original reactants and the rate of appearance of the final product, since all substances except the homoatomic diatoms have typical absorptions in that region. A serious limitation is the relatively small magnitude of the absorption coefficients. Also, one might anticipate a signal to noise ratio which is unfavorable because of the low intensity of conventional infra-red sources.

For a preliminary test of the utility of infrared spectra for analysis, we set up the experiment shown in Fig. 2. Relatively broad band filters were used for selecting portions of the i.r. spectrum. To simulate the pulse operation of the shock tube, a rapid chopper was placed in

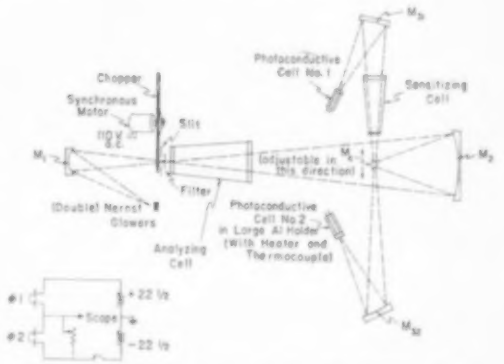

Fig. 2. Schematic optical layout for rapid analysis by infra-red.
PbS 500 μsec at 30°C } Noise ≃ 500 μV
PbS 150 μsec at 90°C }
PbSe 25 μsec at 30°C Noise ≃ 4 mV.

front of the analysing cell, which gave a scan time of the order 10^2 μsec. The lead sulfide and lead selenide photoconducting detectors were run above room temperature to reduce their response time constants; it was also possible in this way to smooth over short time temperature fluctuations. As is indicated in Fig. 2, a selectively sensitized balanced system was initially tested. After filling the absorption cells, the bridge was balanced for the dark resistance by means of the variable resistor in parallel with one of the photoconducting cells and for the resistance at full illumination by moving M_4. Then, a change in the concentration

of any chemical species present in the analyser cell will cause no unbalance in the bridge unless an appreciable amount of that species is also present in the sensitizing cell. The theory for this procedure is as follows.

Suppose the analysing cell is γ_1 cm long and contains n_A, n_B, n_C ... moles cm^{-3} of A, B, C ..., while the sensitizing cell of length γ_2 cm contains N_A only. Allow the filter to transmit the spectral interval $(\lambda_2-\lambda_1)$. *Imagine* that one can divide this interval into a sequence of strips $\Delta\lambda$ such that $\Sigma\Delta\lambda=(\lambda_2-\lambda_1)$ and of such narrow width that at each strip one and only one substance absorbs appreciably. These strips may be as narrow as 0·01 Å for diatomic species which exhibit fine-line rotational structure. One may then group all spectral regions absorbed by A as a sum over $\Delta\lambda^i$, by B as a sum over $\Delta\lambda^j$, etc. The intervals which are not absorbed by any substance will be summed over $\Delta\lambda^m$. Then, detector number 2 sees

$$I_2=\sum_i I_0(\lambda^i)\exp(-n_A\gamma_1\mu_A^i)\Delta\lambda^i+\sum_j I_0(\lambda^j)\exp(-n_B\gamma_1\mu_B^j)\Delta\lambda^j+\sum_k I_0(\lambda^k)\exp(-n_C\gamma_1\mu_C^k)\Delta\lambda^k+\ldots+\sum_m I_0(\lambda^m)\Delta\lambda^m \quad (1)$$

where the μ's are the corresponding absorption coefficients. However, detector number 1 sees less

$$I_1=\sum_i I_0(\lambda^i)\exp[-(n_A\gamma_1+N_A\gamma_2)\mu_A^i]\Delta\lambda^i+\sum_j I_0(\lambda^j)\exp(-n_B\gamma_1\mu_B^j)\Delta\lambda^j+\sum_k I_0(\lambda^k)\exp(-n_C\gamma_1\mu_C^k)\Delta\lambda^k+\ldots+\sum_m I_0(\lambda^m)\Delta\lambda^m \quad (2)$$

The difference recorded is

$$\Delta=\sum_i I_0(\lambda^i)\exp(-n_A\gamma_1\mu_A^i)\{1-\exp(-N_A\gamma_2\mu_A^i)\}\Delta\lambda^i \quad (3)$$

Clearly, one can determine n_A as a function of time, since all other parameters which appear in the expression for Δ do not change during the experiment and can be determined independently. The time resolution available is limited only by the time constant of the detectors, assuming that $I_0(\lambda)$ does not fluctuate, and by the total energy required to give a sufficient signal/noise ratio.

In systems wherein true overlap of the spectra occurs due to the broadness of the absorption regions, the mathematical formulation becomes more complicated than that indicated by equations (1)–(3). However, the method is still applicable, if the concentration of the interfering material, say Q, remains constant. Then, equation (3) becomes

$$\Delta_Q=\sum_i I_0(\lambda^i)\exp(-\gamma_1[n_A\mu_A^i+n_Q\mu_Q^i])\{1-\exp(-N_A\gamma_2\mu_A^i)\}\Delta\lambda^i.$$

When no such restriction can be imposed on the concentration of the interfering material, but it has been established that the substance of interest has an appreciably larger absorption coefficient over the selected interval $(\lambda_2-\lambda_1)$, transmission, data must be obtained over two spectral regions concurrently and reduced by the solution of simultaneous equations. The maximum sensitivity for the arrangement shown in Fig. 2 is obtained when $d\Delta/dn_A$ is maximised. Thus, one should operate with N_A as large as possible. Because the instrument integrates over various μ_A^i's one should anticipate the usual departure from Beer's law.

For satisfactory operation of the above scheme, the response times of the two detectors must be identical; otherwise, the bridge is not balanced dynamically. With the cells available to us, a complete dynamic balance could not be achieved even though the detectors were kept at slightly different temperatures. The analytical sensitivities shown in Fig. 3 were obtained with the light to cell 2 blocked. Then, the gas cell in path 1 operates as a "desensitizer", since the light which reaches detector number 1 is modulated by changes in concentrations of those species present in the analysing cell which are not present in the desensitizing cell in appreciable amounts. These curves show that C_2H_4 does not appreciably interfere with C_2H_6 nor does C_2H_2 with C_2H_4; there is a moderate interference by C_2H_4 in the calibrating curves for CH_3OH and C_2H_2, due to overlap of portions of the CH bands as selected by the i.r. filters available. Dimethyl ether and ethane show complete mutual interference in this region

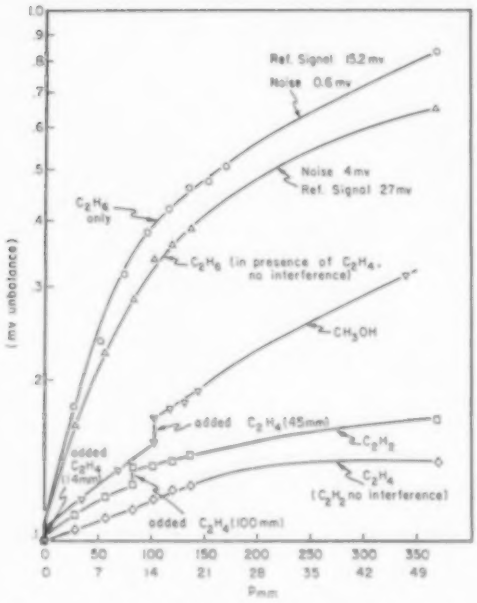

Fig. 3. Bridge unbalance voltage (in mV) as a function of pressure of the gas being analysed. The optical filters isolate various bands in the neighbourhood of 3000 cm^{-1} (C–H stretch). Note that the upper pressure scale (abscissa) applies to all the gases except CH_3OH, for which the lower scale should be read.
Pb Se detectors $\tau_{total} \sim 50$ μsec. Chopping frequency = 1·25 kc/s.

of the spectrum. The average response time was of the order of 50 μsec; this could have been reduced to about 30 μsec by further modifications in the electronics.

6. FEASIBILITY STUDY OF A RAPID RESPONSE TIME I.R. ANALYSER

As a consequence of the encouraging results obtained in the preceding experiment, a design was undertaken of an infrared analyser for practical use with a shock tube. Throughout, commercially available items were utilized except as indicated below. Also, specifications were written for an optical instrument which would not be difficult to construct and which would provide a much better performance than can be achieved with the units now purchasable. In Table 2, we have listed the characteristics and specifications for the instrument being assembled in our laboratory. Note that a grating instrument has been selected and interference filters used to isolate the various orders. Only about $\frac{1}{2}$ per cent of the useful light reaches the detector; this could be raised by a factor of 5 and possibly by a factor of 10 in a somewhat larger spectrograph. In the computations, the response time was set at 1 μsec. The spectral resolution attained is fully adequate for resolving the common gases and materials[21]. One could trade higher resolution for a better signal to noise ratio or for a shorter time constant. The signal/noise ratio was estimated for a gold-doped germanium photoconducting detector at 65°K, on the basis of studies reported by Beyen and co-workers[22]. We assumed that the noise was independent of the "chopping" frequency (their Fig. 8) and was directly proportional to the amplifier band width. If it were demonstrated that the effective noise were inversely

Table 2. Specifications for I.r. Analyzer

		2μ	4μ	6μ
Power (in the band pass given below) accepted by external optics (6×12 mm source, at 5000°K):		$2{\cdot}02\times10^{5}\mu w$	$7{\cdot}32\times10^{4}\mu w$	$5{\cdot}20\times10^{4}\mu w$
Slit (12 mm high) widths:		1000μ	2000μ	4000μ
Power transmitted by filter, spectrograph (P-E 98G) and detector optics:		988μw	736μw	972μw
Spectral band pass (0·0072μ):		18 cm^{-1}	18 cm^{-1}	24 cm^{-1}
"Spectracoat" filter band pass:		2·1 → 2·5μ	2·5 → 4μ	4 → 7μ
Grating order used:		3	2	1
Signal/noise at 65°K				
White noise assumed, ampl. band width 10^6 c/s:		40	40	40
	C_2H_2	C_2H_4	C_2H_6	CH_4
Typical absorption band widths:	0·16μ	0·26μ	0·25μ	0·04μ (Q)

proportional to the chopping frequency, a very large gain in signal/noise would result, and the spectral resolution attained in this design would be correspondingly increased.

The instrument is shown schematically in Figs. 4 and 5. In the top view, note the external optics (the manner of getting the light from the source through the tube to the entrance slit) and the detector optics. An adequate source

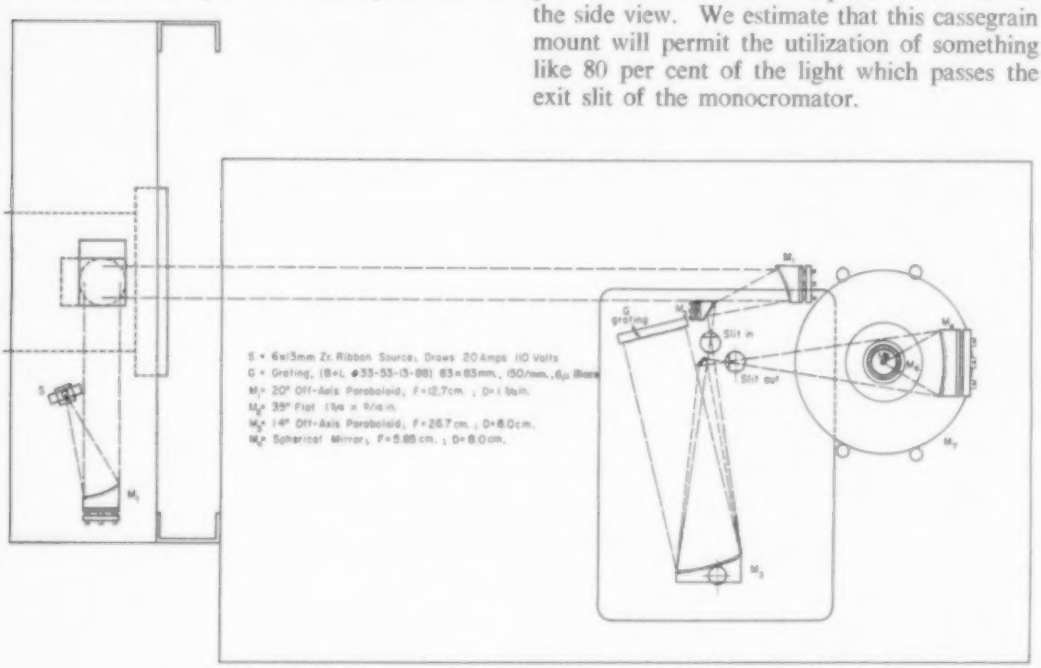
S = 6x13mm Zr. Ribbon Source, Draws 20 Amps 110 Volts
G = Grating, (B&L #33-53-(3-88) 83×83mm., 150/mm., 6μ Blaze
M1 = 20° Off-Axis Paraboloid, F=12.7cm. ; D=1 9/16in.
M2 = 35° Flat 1¾a × 9/16in.
M3 = 14° Off-Axis Paraboloid, F=25.7cm. ; D=8.0cm.
M4 = Spherical Mirror, F=5.85cm. ; D=6.0cm.
S
M1
G grating
M2
Slit in
Slit out
M3
M4
M5

Fig. 4. Top view of infra-red optics for analyzer being constructed.

developed so far is a strip of zirconium (6 × 12 mm, 0·002 in. thick) through which an a.c. current somewhat in excess of 20 A is passed. The discharge through the strip of a much larger current does not produce more useful radiation. In fact, we believe that a major portion of the light is due to the combustion of the zirconium by the surrounding air. We plan to test a high current density discharge through a suitable gas; this might provide a more convenient and possibly more intense source of smaller dimensions. To fill the spectrograph slits, a 6/1 90° off-axis ellipsoidal mirror will be used to transfer the radiation to the off-axis paraboloids. The shock tube windows are $1\frac{1}{2}$ in. in diameter.

The grating and the collimating mirror of the Perkin–Elmer 98G instrument were changed to provide an increase of about 50 per cent in the amount of light transmitted and altered to permit full opening of 4 mm; however, an instrument with 10 mm slits would have been preferable. The detector optics is best seen in the side view. We estimate that this cassegrain mount will permit the utilization of something like 80 per cent of the light which passes the exit slit of the monocromator.

Modifications of a Bausch and Lomb 33-86-45 grating monochromator would provide a faster spectrograph with greater dispersion. In addition to replacement of the grating by a Bausch and Lomb 33-53-15-88, changes would have to be made in the grating tilt mechanism and in the slits to allow scanning of a larger range in wave lengths and to permit adequate precision and reproducibility of settings for wave length calibration and band pass control.

7. RAPID SPECTROPHOTOMETRIC ANALYSES IN THE VISIBLE AND U.V.

The analytical procedures which to date have

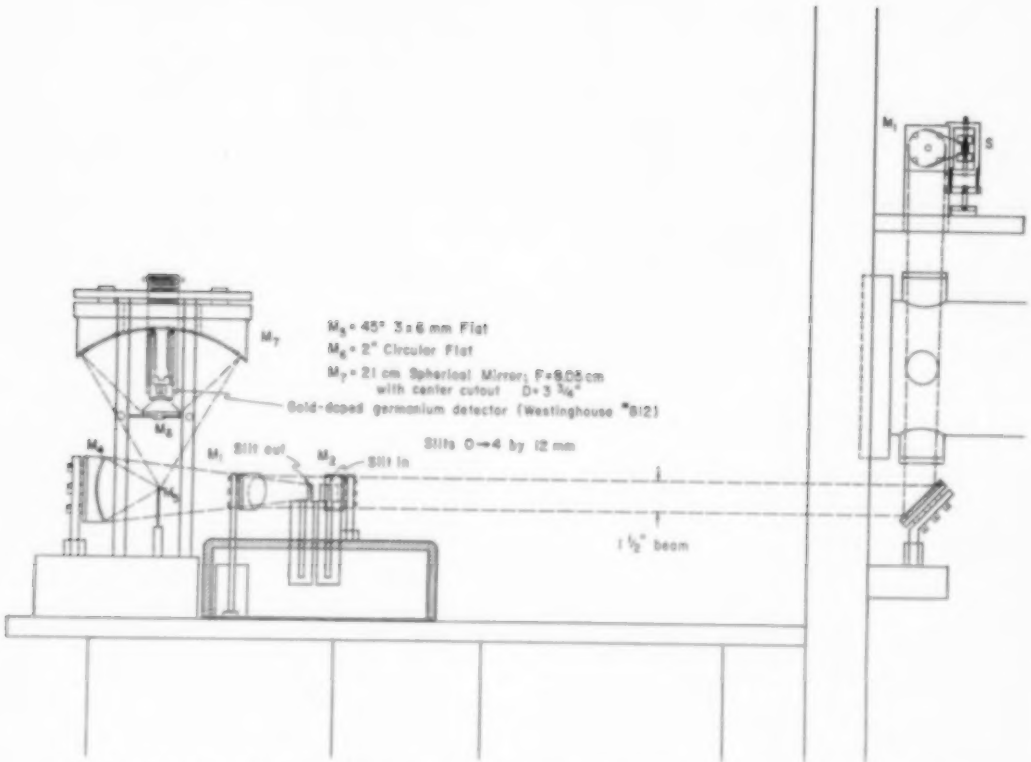
M5 = 45° 3 x 6 mm Flat
M6 = 2" Circular Flat
M7 = 21 cm Spherical Mirror; F=8.05 cm
with center cutout D=3 3/4"
Gold-doped germanium detector (Westinghouse "8121)
Slits 0→4 by 12 mm
M1 Slit out
M2 Slit in
1½" beam
M1
S

Fig. 5. Side view of infra-red optics for analyser being constructed. All mirrors are front surface.

been successfully utilized for the estimation of chemical rate constants involve either short duration flashes photographed with moderate spectral dispersion, the flashes being set-off at successively increasing intervals after initiation of the experiment, or the monitoring of light intensity by monochromators fitted with phototubes, so that radiation of specified wave lengths, covering finite spectral intervals, was measured as a function of time. Studies of the explosive combustion of acetylene by Norrish and co-workers[23] are typical of the first procedure. These investigators initiated the reaction by flash photolysis of a mixture of acetylene, oxygen and nitrogen dioxide which acted as the initiator. The analysing short duration flashes were set-off by a high voltage, low inductance discharge through argon in a capillary tube. The continuum was sufficiently intense to be photographed with a Littrow instrument (Hilger E478). This type of lamp, as further developed by Ramsay[24], is shown in Fig. 6.

Measurements in the visible and ultraviolet regions with phototubes possess two attractive features: (a) the detectors (photomultipliers) inherently have a short time constant and high sensitivity, and fast response circuitry is readily available; (b) the absorption bands generally have large coefficients, since electronic excitations are involved. A disadvantage appears when it is necessary for identification and selectivity in analyses to work with high resolution. The first applications of spectrophotometric analyses to chemical kinetics in shock tubes were extended to species with broad absorption bands. The rates of dissociation of bromine, nitrogen, tetroxide, ozone and oxygen,

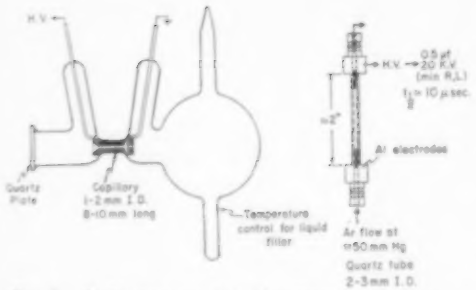

Fig. 6. Light sources. (a) Characteristic radiation source. Power 8–15 kV; 2 μ F; selected (R, L) for 2 msec duration.

Fill with H_2O (liquid) → OH

C_6H_6 20 mm, Ar 10 mm → C_2

C_4H_{10} 10 mm, N_2 10 mm → CN

CS_2 20 mm, Ar 10 mm → CS

(b) Continuum source:
2300A → longer than 7000 A.

in the vacuum ultraviolet, were thus determined. Currently, we are studying the rates of the cis–trans interconversion of 1,2-dichloroethylene and its concurrent dehydrohalogenation by measuring the absorption by shocked samples of 5 Å wide bands in the 2650–2700 Å region. The high temperature decomposition of $(CH_3)_2N_2$ will be measured similarly.

To estimate the concentrations of diatomic molecules which have narrow line absorptions, special techniques had to be introduced. For such species as OH, NH, CH, C_2, CN and CS, the limitation is often the resolution of the available spectrograph. When the slit width is several times wider than the absorption line widths, incorrect absorptions (if any is detectable) will be recorded. The difficulty is circumvented by using, instead of a continuum, a characteristic sharp line emitter which is of the same species as the absorber. Thus, the wave length resolution is built into the source. Of course, the emission selected must involve the ground level, or one close to it, as the final state of the transition. An effective lamp design is shown in Fig. 6. There is a difficulty in reducing per cent absorptions to absolute concentrations, except for one or two of these species, because the f values for the absorptions involved are not known. However, relative rate constants can be obtained with ease and activation energies deduced therefrom.

The utility of specific radiation absorption measurements for the study of kinetics of a chemical reaction in a shock tube is illustrated by the dissociation of water[25] and the combustion of hydrogen[26]. Both types of experiments were performed in the back-reflected shock region utilizing the OH emission $[^2\Sigma^+ \longrightarrow {}^2\Pi\,(0,0]$ from an electrical discharge in water vapor (Fig. 6). A monochromator limited the region of the spectrum viewed by the photomultiplier to 8 Å (3090–3098 Å). This spectral window (Fig. 7) was selected so that lines with

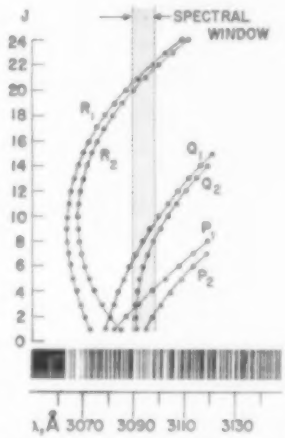

Fig. 7. Fortrat diagram for the OH emission band and the lines selected by the monochromator for the absorption measurements. (From Ref. 25).

the lowest J values will be included and the absorption from the ground state would be least subject to changes in population as a function of temperature; nevertheless, corrections were made for the effect of temperature on the overall absorption coefficient. In order to convert the observed absorptions into absolute concentrations of OH, we plotted the terminal absorptions against the computed equilibrium concentrations. That this condition was reached could be ascertained from the appearance of the oscilloscope traces and further verified when points from $H_2O \longrightarrow OH + \text{products}$ and $O_2 + H_2 \longrightarrow OH + \text{products}$ fell on the same curve. The computed equilibrium con-

dition thus permitted a calibration of the absorption for the particular spectral window used on the assumption that the heat of formation of the OH radical was known. The first calibration[25] curve was based on the assumed value of +6 kcal. A more recent calibration curve[26] is now available, based on the currently acceptable value of $+9{\cdot}27 \pm 0{\cdot}3$ kcal[27].

In the second illustration of the use of characteristic radiation absorbtimetry, relative rate constants for the production of C_2, rather than absolute concentrations, were plotted to estimate an activation energy. In these studies[25], ethylene (diluted 8/92 with Ar) was pyrolysed with back reflected shocks at temperatures in the range 3200°K–4000°K. The experimental arrangement is shown in Fig. 8.

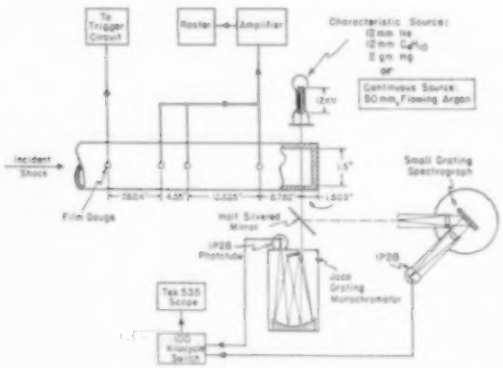

Fig. 8. Schematic of the shock tube and optics used in the study of the rate of production of C_2 during the pyrolysis of ethylene. Replacement of the exit collimator and phototube in the right-hand spectrograph by a lens and plate holder permitted the recording of the absorption over a range in wave lengths, using a short duration Ar flash instead of the characteristic radiation discharge.
For continuous absorption spectra a $3\frac{1}{4}$ in. $\times 4\frac{1}{4}$ in. camera is substituted for the phototube.

We found it advantageous to observe concurrently the percent absorption at the (0, 0) C_2 band head (λ 5165, $^3\Pi_g \rightarrow {}^3\Pi_u$) and at some other wave length where very little characteristic absorption takes place, say at the Hg, λ 5460 line. For this purpose, the transmitted light was split, sent to two monocromators, and the output signals displayed on the same oscilloscope photograph. The decrement of intensity of the Hg line due to a continuum background absorption was subtracted from that which appeared at the C_2 band head. In our case, such a correction had to be made only for absorptions taking place 100 μsec or more after passage of the reflected shock; in general, this technique permits the identification and analysis of a characteristic emission superposed on a broad background. The emission spectrum produced by the butane discharge lamp is shown in Fig. 9, as is the spectral window used for the analysis of C_2.

The initial rate of production of C_2 was found to be first order in the reflected shock density. After correction for the effect of temperature on the population of the $v''=0$ level, a plot of

$$\log\left[\frac{1}{\rho_2}\frac{d}{dt}(\log I_0/I)_{\text{initial}}\right] \text{vs. } 1/T$$

gave a reasonably straight line with a slope equal to about 68 kcal. The population of C_2 radicals does reach a steady state level which is well below the equilibrium concentration, as estimated from rough f values for this Swan band head. In addition, the pyrolysis of ethylene produces a broad range of polyaromatic fragments which are responsible for the broad background absorption.

The final example is an extension of the cyanogen problem mentioned previously (Fig. 1 and Ref. 18). When mixtures of C_2N_2 and argon (5/95) are shocked to temperatures in the range 1600–2000°K, dissociation of the cyanogen takes place; the instantaneous relative concentration of CN can be estimated from the amount of characteristic absorption at the (0, 0) band of the ultraviolet system (λ 3883). In the incident shock region, the reaction appears to be second order. A plot of

$$\log\left[\frac{1}{\rho_2^2}\frac{d}{dt}(\log I_0/I)_{\text{initial}}\right] \text{vs. } 1/T$$

gave a good straight line with a slope equal to 108 ± 8 kcal. This we believe is a reliable value for the dissociation energy of the NC–CN bond:

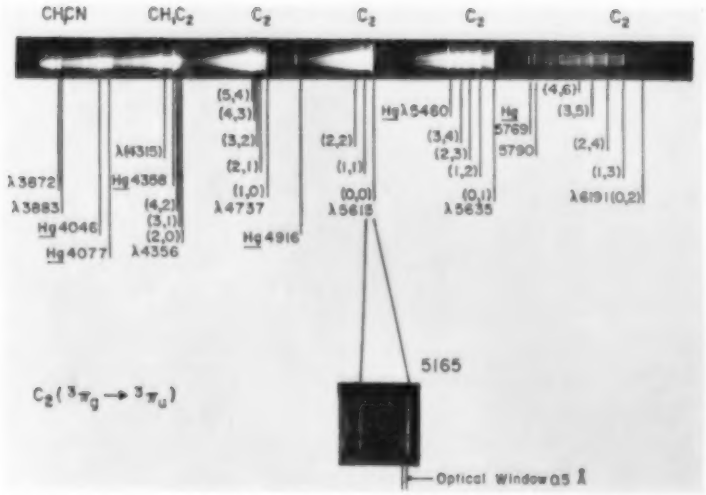

Fig. 9. Spectrum emitted by a discharge through butane, argon and mercury. Note the very strong C_2 bands and the spectral window selected by the monochromator.

(facing page 130)

it is consistent with a large amount of circumstantial data.

8. RECENT DEVELOPMENT IN MASS SPECTROMETRY

A list of the available methods for the specific analysis of gaseous mixtures with response times in the microsecond range would be incomplete without mention of mass spectrometry. To date, two units have been developed commercially, but the range in masses, the lower limits on response times, the relation between sensitivity and response time, scan rates, etc., have yet to be fully explored. That mass spectrometry will prove to be a powerful tool there is no doubt. Expansion of the gases heated by a back reflected shock through a small divergent nozzle in the reflecting end of the shock tube will provide a rapidly quenched sample in the form of a fine jet, suitable for injection into a mass spectrometer.

Kistiakowsky and Bradley[29] have modified a Bendix "time-of-flight" spectrometer and used it for the determination of the nature and relative abundance of chemical species produced in the pyrolysis of acetylene. The cycloidal-focusing mass spectrometer described by Robinson and Hall[30] has been recently modified to allow for rapid scanning of selected m/e ranges. The relative merits of these two types of instruments for the rapid estimation of shock tube products require further investigation.

Acknowledgement—This work is supported by ARDC under contract AF33(616)-3839 and by the ONR under project NR051-242 to whom acknowledgement is gratefully made.

REFERENCES

1. J. G. Clouston, A. G. Gaydon and I. I. Glass, *Proc. Roy. Soc.* **A248,** 429 (1958).
2. J. G. Clouston, A. G. Gaydon and I. R. Hurle, *Proc. Roy. Soc.* **A252,** 143 (1959).
3. H. M. Strong and F. P. Bundy, *J. Appl. Phys.* **25,** 1521, 1527 (1954).
4. H. J. Kostkowski and H. P. Broida, *J. Opt. Soc. Amer.* **46,** 246 (1956).
5. P. E. Rouse and H. M. Peek, Los Alamos Scientific Laboratory, private communication.
6. W. Wurster, *AFOSR-GE* (Sept. 1959). *This volume.*
7. R. W. Nicholls, *Proc. Phys. Soc.* **A69,** 741 (1956).
8. T. M. Sugden, *Trans. Faraday Soc.* **52,** 1465 ff (1956); **54,** 830 (1958).
9. R. Ladenburg *et al. Physical Measurements in Gas Dynamics and Combustion,* Vol. 9 of *High Speed Aerodynamics and Jet Propulsion.* Princeton University Press, Princeton, N.J. (1954). Eds.: R. W. Ladenburg, B. Lewis, R. N. Pease and H. S. Taylor. Authors: F. J. Weyl, J. W. Beams, R. W. Ladenburg and Eva Winkler.
10. W. Griffith, D. Brickl and V. Blackman, *Phys. Rev.* **102,** 1209 (1956).
11. S. R. Byron, *J. Chem. Phys.* **30,** 1380 (1959).
12. E. L. Resler, Jr., and M. Scheibe, *J. Acoust. Soc. Amer.* **27,** 932 (1955).
13. G. B. Kistiakowsky and P. H. Kydd, *J. Chem. Phys.* **23,** 271 (1955).
14. H. T. Knight and J. P. Rink, *J. Chem. Phys.* **29,** 449 (1958).
15. G. B. Kistiakowsky, private communication.
16. D. Venable and R. E. Duff, Los Alamos Scientific Laboratory, private communication.
17. B. W. Schumacher and E. O. Gadamer, *Canad. J. Phys.* **36,** 659 (1958).
18. Data recorded by W. Tsang and M. Cowperthwaite, Cornell University.
19. D. F. Hornig, *Ann. N.Y. Acad. Sci.* **67,** 463 (1957).
20. R. G. W. Norrish and B. A. Thrush, *Chem. Soc. Quart. Rev. London* **10,** 149 (1956).
21. For typical spectra, refer to R. H. Pierson, A. N. Fletcher and E. St. Clair Gantz, *Anal. Chem.* **28,** 1218 (1956).
22. W. Beyen *et al.* paper presented at IRIS meeting in Boston, Sept. 17, 1958, issued as *Appendix Report No. 103-6* by Syracuse University Research Institute.
23. R. G. W. Norrish, G. Porter and B. A. Thrush, *Proc. Roy. Soc.* **A216,** 165 (1953).
24. D. A. Ramsay, NRC, Canada, private communication.
25. S. H. Bauer, G. L. Schott and R. E. Duff, *J. Chem. Phys.* **28,** 1089 (1958).
26. G. L. Schott and J. L. Kinsey, *J. Chem. Phys.* **29,** 1172 (1958).
27. R. F. Barrow, *Ark. Fys.* **11,** 281 (1956).
28. Unpublished data by F. Waelbroeck and W. Tsang, Cornell University.
29. G. B. Kistiakowsky and J. N. Bradley, private communication.
30. C. F. Robinson and L. G. Hall, *Rev. Sci. Instr.* **27,** 504 (1956).

RADIATION FROM THE NON-EQUILIBRIUM REGION OF NORMAL SHOCKS IN OXYGEN, NITROGEN AND AIR*

B. KIVEL, P. HAMMERLING and J. D. TEARE
Avco-Everett Research Laboratory, Everett, Massachusetts

Abstract—Radiation from N_2, N_2^+, NO and O_2 molecules in shock fronts in O_2, N_2 and air is discussed. We elaborate on the difference between the several band systems which result in only some of them overshooting their equilibrium values in the high temperature front.†

Luminous spikes were observed at the front of normal shocks in noble gases[1] by Kantrowitz and co-workers at Cornell University and LaPorte and co-workers at the University of Michigan. These investigators soon learned that the radiation spike was due to impurity molecules such as CN and C_2. This radiation disappears when the impurity molecules are dissociated. Since this was not an important aerodynamic discovery they did not pursue the problem further. The luminous spike provides an opportunity to learn about physical-chemical processes.

It is just this kind of spike which is important in the non-equilibrium radiation in air[2]. The radiation rises from zero at the shock front as the electronic temperature is increased by collisions. Measurements of the rate of increase of radiation intensity provide a source of information about the collisional mechanisms for exciting the electronic states of molecules. The radiation peak occurs when the electronic temperature reaches the value of the local kinetic temperature. The radiation after this time can be characterized by local thermodynamic equilibrium properties. It reduces to the equilibrium value as the molecules are dissociated and as the non-equilibrium temperature relaxes to the lower equilibrium value. As a consequence, after the luminous peak, it is possible to determine the rate of dissociation by measuring the rate of decrease in radiation intensity.

In order to ascertain that the non-equilibrium radiation was indeed a property of air and not of impurity molecules, it was necessary to obtain spectrographic records of this radiation[3]. Fig. 1 shows a typical spectrograph of radiation from nitrogen. While CN is a dominant radiation in the spectrogram it is mostly in the boundary layer at the tube wall. Prominent molecular band characteristic of air in this spectrum are the first negative bands of N_2^+ and the second positive band of N_2.

The radiation intensity (I) is in direct proportion to the density of radiating molecules (N^*), and the energy radiated in a radiative transition ($h\nu$), and in inverse proportion to the mean radiation time (τ_r).

$$I = N^* h\nu / \tau_r$$

This simple expression gives the essential part of the radiation story. A more difficult but somewhat secondary consideration is how the radiation is distributed throughout the spectrum. It is not necessary for our discussion to understand the spectral distribution since it is not very sensitive to temperature.

From the simple expression one sees that the important changes throughout the non-equilibrium region are determined by the density of radiating molecules. This density can be related to the density of the ground state molecules (N)

* This work was sponsored jointly by Ballistic Missile Division, ARDC, USAF, under contract AF-04(647)-278, and Army Rocket and Guided Missile Agency, AOMC, USA, under contract DA-19-020-ORD-4862 under ARPA order 39-59 Task 6.

† We are in debt to Dr. F. R. Gilmore of Rand Corporation, Santa Monica, California, for unpublished notes on the potential wells of O_2, N_2 and NO.

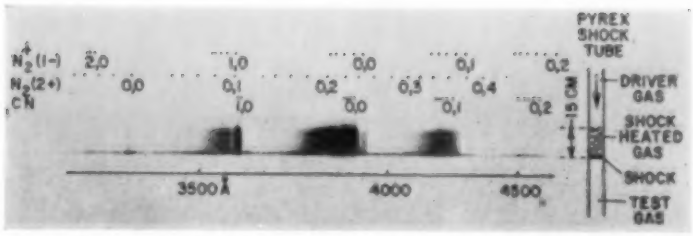

Fig. 1. A spectrogram of a shock wave in nitrogen (equilibrium conditions: $T = 6600°K$; $\rho/\rho_0 = 0{\cdot}02$). (Courtesy Camm and Keck [3]). This slide was first presented at a meeting of the American Physical Society in New York City, January 1959. At the front of the shock a bright spike of luminous intensity appears which is almost continuous throughout the spectrum. In addition to very strong bands of CN which is due to impurities in the boundary layer at the wall of the shock tube, there are bands from N_2 and N_2^+.

(facing page 132)

according to

$$N^* = \frac{g^*}{g} N \exp(-E^*/kT_e)$$

where g and g^* are statistical weights, E^* is the excitation energy with respect to the ground state, and T_e, which is defined by this relation, can be thought of as an electron temperature (i.e. a temperature for the bound and not for the free electrons). This temperature may be expected to rise monotonically as excitation is produced by inelastic molecular collisions, until it reaches the local gas kinetic temperature. The population of radiating molecules may then be considered in local thermodynamic equilibrium. Following this time the electronic temperature will decay as the chemical relaxation proceeds. Except for a slight perturbation because of changes in the density of the ground molecular state, the peak in the radiation intensity will occur when the electronic temperature becomes equal to the kinetic temperature.

In order to illustrate the magnitude of radiation intensity, let us consider a simple example. The radiation lifetimes for the molecules of interest vary between 10^{-6} and 10^{-8} sec; we will use 10^{-7} in our example. For the density of radiating molecules, let us consider an initial gas density of 10^{-3} atmospheres ($\rho/\rho_0 = 10^{-3}$), a compression at the shock of about a factor 10 and since Loschmidt's number is 3×10^{19}, a particle density of 3×10^{17}; the molecule O_2 when it is 50 per cent dissociated so that the fraction of O_2 molecules in air is 10 per cent; an excitation energy of 70,000°K and a temperature of 10,000°K so that $\exp(-E^*/kT) = 10^{-3}$; the ratio statistical weights $g^*/g = 1$; for this case $N^* = 3 \times 10^{13}$. The energy radiated ($h\nu$) is taken to be 5 eV. It should be noted that this value is not necessarily equal to E^*, since the final state of the radiative transition is not necessarily the ground state of the molecule. The excitation energy E^* will be greater than or equal to $h\nu$. In this case our simple radiation expression tells us that $I \doteq 2 \times 10^2$ W/cm^3, where we have converted from eV to J with the factor $1{\cdot}6 \times 10^{-19}$.

Before proceeding to examples of the non-equilibrium radiation, we would like to review some information about the rate of radiation excitation observed under equilibrium conditions. At very low densities the radiation will fall below the equilibrium value because the rate of exciting collisions is not sufficiently fast to maintain the equilibrium density which is being depleted by radiation emission. A factor to be appended to our expression for the radiation intensity (I) which delineates this fact is

$$\frac{\tau_r}{\tau_r + \tau_e}$$

where τ_r is the mean radiation time and τ_e is a mean excitation time. At high densities τ_e goes to zero and this factor becomes one. At low densities this expression reduces to τ_r/τ_e which is proportional to the density. Thus at low densities the radiation decreases as with an extra power of density, a situation we have called "collision limited". Measurements by Keck and Camm have indicated that at initial pressures of $p_1 = 1$ mm Hg both the Schumann-Runge bands of O_2 and the first negative of N_2^+ are not "collision limited" so that for these bands there is evidence of a fast mechanism for exciting the radiating states. We will use this fact when discussing the non-equilibrium radiation of these band systems.

To obtain the time history of the radiation at a given wave length we use a grating monochromator and photo cells. As the shock flows past a slit in the shock tube wall the radiation signal is focused on the monochromator and dispersed into different wave length channels.

In Fig. 2 we see oscillograms from the normal shocks in air as a function of increasing Mach number. It is seen that the overshoot of intensity increases rapidly with Mach number and that the relaxation time decreases.

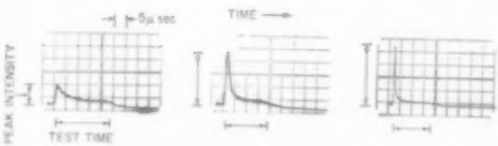

Fig. 2. Oscillograms of radiation at the front of normal shocks as a function of Mach number in air from Avco-Everett RR 22. Peak intensity increases rapidly with increasing shock speed and relaxation time decreases with increasing speed. (a) $V_\infty =$ 12,600 ft/sec, $T = 3{,}600$°K; (b) $V_\infty = 14{,}100$ ft/sec, $T = 4{,}400$°K; (c) $V_\infty = 16{,}000$ ft/sec, $T = 5{,}200$°K.

In Fig. 3 the non-equilibrium radiation at two different pressures but at the same Mach number are compared. In making this figure we have scaled the oscilloscope sensitivity to radiation intensity in inverse proportion to the

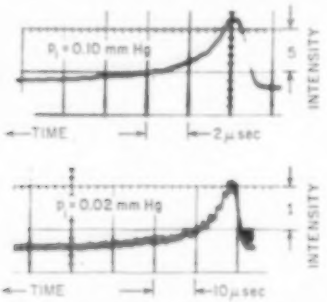

Fig. 3. Oscillograms of non-equilibrium radiation in air for two different pressures (Courtesy Camm and Keck, unpublished). The figure illustrates the density dependence in the non-equilibrium region. The sensitivity has been scaled up as the initial pressure is reduced while the sweep speed is reduced with pressure. To a reasonable approximation this results in the same oscillogram trace as expected. $\lambda = 4300$ Å ($N_2^+ + CN$); $U_s = 5{\cdot}8$ mm/μ sec.

density and we have adjusted the sweep speed in proportion to the density. Since the collisional processes in the front of the shock are all binary we expect the two radiation curves to be identical. Indeed they are, or at least almost, the same. The slight differences are attributed tentatively to lack of resolution and impurities.

In the shock front in oxygen in the Schumann–Runge region no overshoot in radiation intensity is observed[4]. In Fig. 4 is an oscillograph of the radiation from this band system published by Keck *et al.* in *J. Chem. Phys.* The equilibrium conditions for this example are 4100°K and $\rho/\rho_0 = 0{\cdot}19$. The top trace is of the monitor signal with sweep speed of 5×10^{-6} sec/division; the bottom trace is of the monochromator channel at $\lambda = 3914$ Å and sweep speed of 10^{-6} sec/division.

By comparing the equilibrium level of intensity from this and other traces at different pressures it is determined that the radiation is not "collision limited" at $p_1 = 1$ mm Hg and consequently that there is a very fast mechanism for excitation of the radiating electronic state.

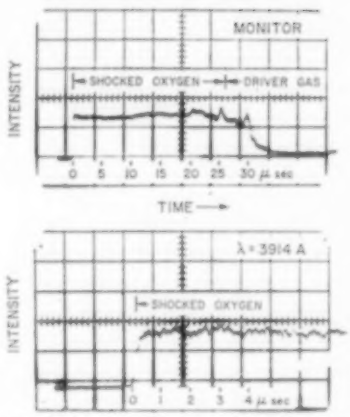

Fig. 4. A photo multiplier record of the luminous front in oxygen taken from Keck, Camm and Kivel[4]. The upper trace is the radiation received by the monitor. The lower one is the record made at 3194 Å. Note that the time scale is different on the two traces. The signal goes to zero in the upper trace when the cold driver gas arrives. Note that in these traces there is no overshoot in luminous intensity.

The path is readily recognized as the coupling of the radiating state with two free ground state atoms (Fig. 5). This path brings the radiating state into equilibrium with the density of free atoms. Since the free atom density increases monotonically to equilibrium and since the radiating state is at about the same energy level as the free atoms, this coupling will explain the absence of the luminous overshoot. If a strong

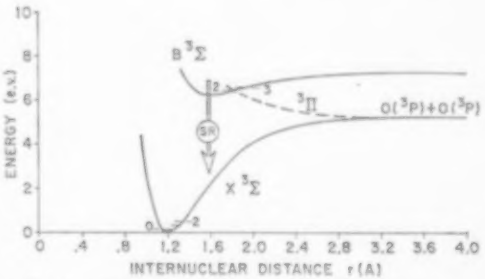

Fig. 5. Molecular diagram for O_2 Schumann–Runge radiation. In addition to the initial ($B\,^3\Sigma$) and the final ($X^3\Sigma$) states for the radiation we have included the repulsive $^3\Pi$ potential. The $^3\Pi$ level acts as a drain via dissociation of molecules from the $B^3\Sigma$ state. As a result of this drainage, the absence of an overshoot in the Schumann-Runge radiation can be understood.

coupling occurred between the ground molecular state and the radiating state, then a strong radiation overshoot would have occurred. The absence of a strong overshoot tells us that the collision cross-section for exciting the ground molecular state to the radiating state of the Schumann–Runge band is indeed very small.

Figure 5 shows three of the important potential wells for determining the oxygen radiation. The Schumann–Runge bands correspond to the electronic change $B^3\Sigma \rightarrow X^3\Sigma$. The repulsive $^2\Pi$ state is thought to cross near the minimum of the $B^3\Sigma$ well*.

In Fig. 6 are calculated results for the Schumann–Runge radiation. The two solid curves are for extreme equilibrium assumptions.

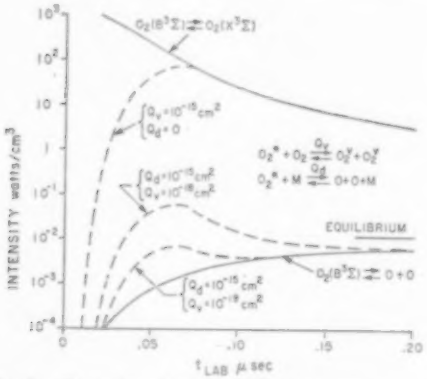

Fig. 6. Typical predictions of O_2 Schumann-Runge radiation in oxygen at $U_s = 4{\cdot}49$mm/μsec and $p_1 = 1$ mm Hg. The solid lines correspond respectively to equilibrium of the radiating state with the ground state or with two free atoms as indicated. The dashed curves correspond to different assumptions about the mechanism of excitation. A strong coupling between the ground state and the radiating state leads to a large overshoot ($Q_v = 10^{-15}$ cm²). Dissociating of the radiating state by collisions reduces the overshoot ($Q_d \gg Q_v$).

The upper corresponds to an infinitely fast excitation from the ground state to the radiating state. Because of the high non-equilibrium temperature and the high concentration of O_2 this leads to a strong overshoot. At the other extreme of fast coupling between the radiating state and free atoms there is no radiation overshoot. Three intermediate situations are delineated by dashed lines. The first assumes an excitation mechanism in which molecules give their vibration energy to excite the electronic state. If the rate for this path is sufficiently fast to explain the absence of "collision limiting" then a large overshoot is predicted. The lower two dashed curves are constructed assuming that the cross-section for dissociating the radiating state is sufficiently large to prevent collision limiting and the vibration excitation cross-section is sufficiently small so as not to produce a marked overshoot.

Fig. 7 is an energy diagram for the electronic states of N_2 and N_2^+. The important bands from these molecules in experimental results are the first and second positive of N_2

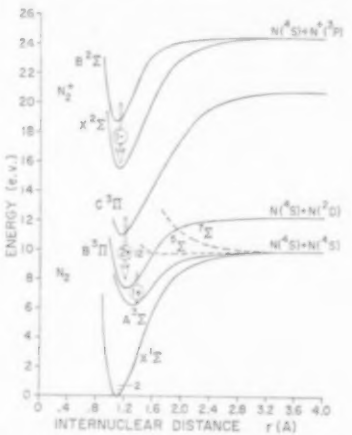

Fig. 7. Molecular diagram for N_2 and N_2^+. The important radiating bands for these molecules are illustrated in the figure; they are N_2^+ (1−) and N_2 (1+ and 2+). Even though N_2^+ is formed from atoms, the first negative bands can overshoot because of its high energy and consequent sensitivity to temperature.

and the first negative of N_2^+. All of these bands overshoot in the non-equilibrium region although the experimental data on the first positive system is only preliminary.

An interesting problem in calculating the radiation from $N_2^+(1-)$ and the ionization in pure nitrogen has arisen[5,6]. We have found two paths which can explain the radiation which give different ionization predictions. Until the ionization measurement is made the choice between the two is arbitrary. The problem

arose when we assumed that the rate for dissociative recombination of nitrogen ($N_2^+ + e$) measured by Sayers could be detail balanced by two ground state atoms. We also knew there was a large cross-section for excitation in equilibrium. We were forced to the complex excitation mechanism of transfer of vibration energy to electronic which would change from a small to a large excitation rate as the vibration temperature rose from 300° to local equilibrium. Otherwise, we predicted too strong a radiation overshoot. Professor D. R. Bates pointed out that the dissociative recombination might go to $N + N^*$. The production of ions then requires an additional step $N \longrightarrow N^*$ which can be very slow. This choice reduces the electron overshoot and the somewhat contrived vibration excitation path is not required.

In Fig. 8 we give the predictions for the electronic density for the two paths behind a normal shock in nitrogen with $p_1 = 4$ mm Hg and a shock speed of 6·6 mm/μsec. It is seen

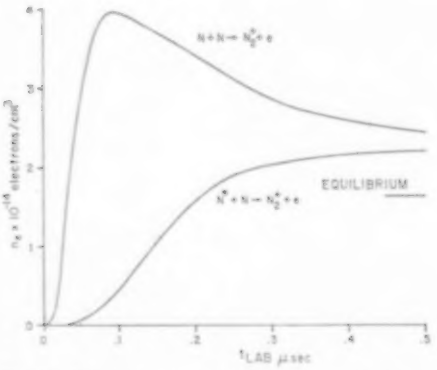

Fig. 8. Electron density predictions behind a normal shock in nitrogen at $U_s = 6{\cdot}6$mm/μsec and $p_1 = 4$mm Hg. The electron overshoot predicted on the basis of ground state atoms recombining to form the molecular ion is much larger than when an excited atom is required.

that when the ions can be produced from two ground state atoms that the electron density overshoots its equilibrium value by an appreciable factor. The production of N^* by collisions is sufficiently slow so that only a slight overshoot occurs in this case.

The molecular diagram for nitric oxide (NO) is shown in Fig. 9. Two radiation bands which are important in equilibrium radiation from air at ~ 8000°K are the β and γ. The transitions which give rise to these band systems are illustrated in Fig. 9. The structure of the potential

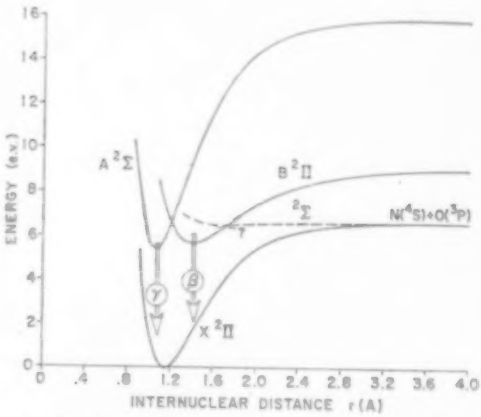

Fig. 9. Potential energy diagram for NO. This molecular diagram shows the γ and β band transitions. Also shown is the repulsive $^2\Sigma$ state which intersects the $B^2\pi$ at the $v' = 7$. The drainage by dissociation is not expected to be as good as in O_2 where the crossing occurs at $v' = 2$ (see Fig. 5).

levels for the β band system are very similar to that of the Schumann–Runge system of O_2. The important property which gives rise to the similarity is the displacement of the minimum in the potential well of the excited state with respect to that of the ground state. As was noted, the Schumann–Runge bands in oxygen do not overshoot their equilibrium value. This is not necessarily so for the NO β system. An important difference is that the $^2\Sigma$ repulsive state intersects the upper level of the β system at a high vibration level ($v' = 7$), which would lessen the drainage by dissociation. Another difference is that the NO ground state density is initially zero and overshoots its equilibrium value while O_2 decays monotonically. Preliminary experimental results indicate that the NO radiation does overshoot its equilibrium value.

In summary, we note that the radiation overshoots occur when the density of radiating

molecules in the non-equilibrium region exceeds their equilibrium density. In the case of oxygen, the radiation population did not overshoot and we concluded that this resulted from a strong coupling between the radiating state and the free atoms. In the case of N_2^+ where the radiating state was also coupled to the atoms an overshoot is observed. The difference is that the N_2^+ radiating state has a large excitation energy with respect to the free atom state and consequently is very sensitive to temperature. The N_2 (1+ and 2+) bands and the NO (β and γ) bands show overshoots in preliminary experiments. This indicates that for these band systems, the coupling to the ground molecular state is sufficiently faster than the drainage by dissociation so that the radiating state density overshoots the corresponding equilibrium value.

Acknowledgement—We are in debt to J. C. Keck and J. C. Camm for use of their experimental results and to A. R. Kantrowitz, the director of the Avco-Everett research program.

REFERENCES

1. H. E. Petschek, *Phys. Rev.* **84**, 614A (1951). E. B. Turner, *Phys. Rev.* **99**, 633A (1955). R. J. Rosa, *Phys. Rev.* **99**, 633A (1955).
2. M. Camac, J. C. Camm, S. Feldmann, J. C. Keck and C. C. Petty, *Chemical Relaxation in Air, Oxygen and Nitrgen*. Institute of the Aeronautical Sciences, 26th Annual Meeting, New York (1958).
3. J. C. Camm and J. C. Keck, *Bull. Amer. Phys. Soc.* Series 2, **4**, 19 (1959).
4. J. Keck, J. Camm and B. Kivel, *J. Chem. Phys.* **28**, 723 (1958).
5. P. Hammerling, J. D. Teare and B. Kivel, *Theory of Radiation from Luminous Shock Waves in Nitrogen RR 49*, Avco-Everett Research Laboratory, Everett, Mass. (1959). *Phys. Fluids* **2**, 422 (1959).
6. P. Hammerling, J. D. Teare and B. Kivel, *Non-Equilibrium Electrical and Radiative Properties of High Temperature Air, Nitrogen and Oxygen RN 152*, Avco-Everett Research Laboratory, Everett, Mass. (1959). Presented at International Conference on Ionization Phenomena in Gases, Uppsala, Sweden (1959).

INTRODUCTION TO THE SESSION ON EXPERIMENTAL METHODS AND STIMULATION

M. ZELIKOFF
Geophysics Corporation of America, Boston, Massachusetts

In the past few years, it has become evident that many of the problems encountered by workers in aerodynamics and space flight fall into the fields covered by physical chemists and spectroscopists. The critical lack of all types of cross-section data has placed emphasis on work in recombination coefficients, electron attachment processes, charge exchange, transition probabilities and absorption coefficients. Many of these data are so difficult to obtain in the laboratory that only theoretical techniques are feasible. An equally large amount of information is subject to experimental and simulation methods and this section is devoted to these.

During this period of intense interest in molecular physics, several powerful techniques of experimental study have received much attention. One of these is the excellent work in shock tubes. Here it becomes possible to study rapid reactions at high temperatures. The application of absorption and emission spectroscopic methods together with advanced electronics has enhanced our ability to perform time-resolved observations. Flash photolysis and spectroscopy are other examples of the useful application of advanced electronics.

One of the most difficult problems to study is that involving reactions between unstable species since these generally recombine or deactivate themselves on the walls of the containing vessel. In order to obviate this difficulty, the use of atomic beam methods has provided much valuable support. While this technique is experimentally very difficult, recent advances in high vacuum technology together with sophisticated electronics give rise to a growing body of meaningful data in this area.

It is important to note here that a recently developed experimental method using chemical releases from rockets at high altitudes gives much promise in the solution of problems not otherwise attainable. This method eliminates completely the problem of wall reactions and enables one to study processes taking place in their atmospheric environment. At present, although by laboratory standards only a few experiments have been performed, the general field of chemical releases shows potentially the development of a type of upper atmospheric chemical research which will have unique value.

It appears that we can now expect a re-birth of interest in the classical fields of spectroscopy and chemical kinetics. One may hope that new workers will be attracted to the field and that many of those who have left it will return to it.

ELECTRON CLOUDS: A GENERAL SURVEY

F. F. MARMO, J. PRESSMAN and L. M. ASCHENBRAND
Geophysics Corporation of America, Boston, Massachusetts

Abstract—This paper summarizes the results and analysis of seven rocket experiments designed and performed to study systematically the physics of the generation of artificial electron clouds in the upper atmosphere.

The several experiments can be discussed in four phases. For example, the first involved the daytime Aerobee rocket release of potassium at 121 km and served to establish the feasibility of solar photoionization generation of artificial electron clouds. The second phase was the Nike–Cajun night-time release of cesium at 101 km to establish the role of thermo-chemical generation of electron clouds. The third phase was designed to study the correlation of optical and radio-radar data as obtained from a visible, photographic electron cloud. This was accomplished by the morning twilight releases of cesium and sodium at 128 km and 116 km, respectively. The final phase of this series reported here involved three releases of cesium at 91 km, 82 km and 69 km, in order to determine the altitude below which long-lived, dense artificial electron clouds cannot be generated by the techniques employed here. The results of this last phase yield valuable physical data pertinent to several of the electron decay processes dominant in the lower altitudes.

The overall analysis of the extensive optical and radar data has yielded information on the following physical parameters: (a) chemical yield of contaminant, (b) thermal ionization efficiency, (c) upper atmospheric wind velocity, (d) wind shear, (e) optical and Gaussian half-width of cloud with time, (f) ambipolar diffusion, (g) neutral diffusion, (h) photoionization cross-sections, (i) mutual neutralization processes and (j) rate of chemical consumption of alkali by atmospheric oxygen.

Finally, the role that artificial electron clouds can assume for practical utilization for radio-radar propagation is emphasized with some discussion indicating the extent of the available potential for this engineering purpose.

1. INTRODUCTION

Since March 1956 a series of upper atmosphere rocket experiments has been performed to study the formation of artificial electron clouds and some of the processes associated with their production. These exploratory experiments established the foundation of a new technique of study of physical and chemical processes associated with the earth's upper atmosphere. A substantial amount of qualitative and quantitative data has been obtained from these experiments pertinent to the studies of upper atmospheric winds, diffusion, microscopic cross-section values (electron attachment, ion-electron recombination, charge exchange, etc.), chemical consumption, expansion of high-pressure gases into an attenuated atmosphere, electromagnetic propagation research and implications, ionospheric research and thermo-chemical and explosive effects, to name but several. To date, eight successful experiments have been conducted and are reported here with a brief survey of the data and the results of analysis upon these data.

Artificial electron clouds are formed by the ejection of a suitable chemical contaminant at preselected altitudes with the generation of the electrons due to photoionization and/or thermal ionization. The first experiment, in which 18 lb (275 moles) of nitric oxide gas was released from high-pressure containers at an altitude of 95 km has been previously reported[1]. The success of this experiment, whereby an artificial electron cloud with an initial average density of about 4×10^6 electrons/cm^3 was detected for more than 10 min by radar techniques, indicated

that it would be feasible to use other contaminants to create artificial electron clouds at various altitudes with a wide range of densities, time durations, sizes, shapes and other parameters.

Examination of the photoionization cross-section data of various constituents, the character of the solar flux and other parameters indicated that the alkali metal elements as a family offered a particularly high potential for obtaining high density, long-lived electron clouds at altitudes between 70 and 200 km with presently available techniques. It was decided to utilize only the alkali metals, cesium, potassium and sodium, throughout these initial experiments.

Alkali metal vapors characteristically have very low ionization potentials (2400 to 3200 Å) which fall into the spectral region where the solar photon flux averages about 5×10^{12} photons/Å cm²-sec. Fig. 1 shows the average

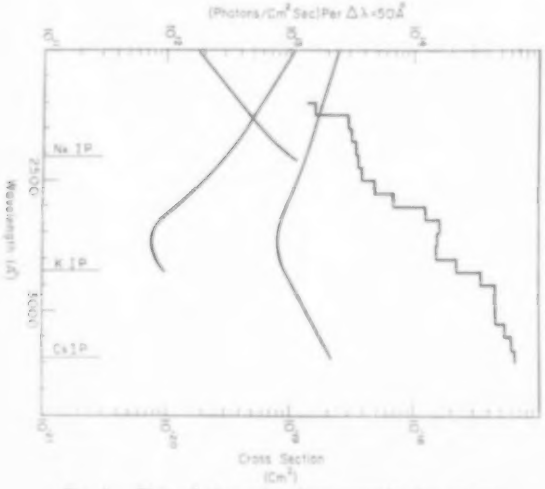

Fig. 1. Plot of the solar flux outside the atmosphere in units of $\Delta\lambda = 50$ Å, photons/cm² sec and photoionisation cross-sections of the alkali metals between 2000 and 3200 Å. The ionisation potentials are included.

($\Delta\lambda = 50$ Å) available photoionizing solar flux, I, throughout the spectral range 2000 Å to 3200 Å and the photoionization cross-sections, σ, of these alkali metals. For determining the probability of photoionization per particle, k, the sum of the $(\Delta\sigma \cdot \Delta I)$ products was taken over the 2200–3000 Å interval. Then the deduced or extrapolated values in the wave length region 1600 Å–2200 Å were obtained wherever applicable to a particular element and added to the larger wave length contribution. The k-values for Cs, K and Na were calculated to be $6{\cdot}5 \times 10^{-4}$ sec^{-1}, $1{\cdot}9 \times 10^{-5}$ sec^{-1} and $1{\cdot}0 \times 10^{-5}$ sec^{-1}, respectively. Since cesium possesses the highest solar photoionization probability of the family, an Aerobee rocket experiment was performed in September 1957, in which 110 moles of cesium compound was scheduled to be released at an altitude of about 120 km. The experiment was unsuccessful due to mechanical failure of both the primary and back-up release mechanisms, thus preventing release of the material.

Previous scheduling had called for a release of potassium vapor during the month of November 1957. There was no opportunity to reschedule the unsuccessful cesium experiment due to relatively difficult delivery problems; therefore, it was decided to continue the original schedule. A successful release of a payload containing 153 moles of K was accomplished from an Aerobee at 121 km. This flight occurred at about 0932 MST on 19 November 1957; it is represented by entry number 1 in Table 1. The electron cloud formed as a result of this experiment was readily detected by conventional radar techniques.

Interpretation of the results pertinent to the ionized cloud which was formed in this experiment suggested that some additional process to photoionization was responsible for the initial electron production. The chemical nature of the experimental method indicated that the effect could be due to thermal ionization. In order to examine this important effect, an experiment was devised in which atomic cesium would be released during the night-time hours to eliminate the role of solar photoionizing flux. The choice of this element arose from the consideration that, at a given temperature within the range considered, cesium should produce considerably more thermal electrons than other constituents of the alkali metal family; thus, a maximum-type effect could be anticipated. In

Table 1. Summary of Upper Atmospheric Artificial Ionization Experiments Conducted at Holloman Air Force Base in New Mexico

Flight No.	Date	Study constituent	Moles	Approximate release time (MST)	Release altitude (km)	Vehicle
1	19 Nov. 1957	Potassium	153	0932	121	Aerobee
2	20 May 1958	Cesium+10% sodium	Cs-43	0245	101	Nike–Cajun
3	21 May 1958	Cesium+2% sodium	Cs-46	0434	128	Nike–Cajun
4	22 May 1958	Sodium	61	0432	116	Nike–Cajun
5	15 Sept. 1958	Cesium	27	0934	82	Nike–Cajun
6	16 Sept. 1958	Cesium	28	0933	69	Nike–Cajun
7	18 Sept. 1958	Cesium	30	0953	91	Nike–Cajun
The following experiment was performed but was unsuccessful due to mechanical failure:						
A	19 Sept. 1957	Cesium	110	0930	—	Aerobee
The following was the initial experiment previously reported:						
B	12 March 1956	Nitric oxide	300	1415	95	Aerobee

addition, since this was to be a night-time release, it was considered feasible to produce a cloud easily visible and, therefore, easily photographed.

Some of the obvious advantages gained by optical detection are: accurate determination of release altitudes by triangulation optics, correlation of radar returns as a function of cloud size and shape, determination of yield and chemical rates, wind and diffusion data, and spectral characteristics of the emission. The method employed for rendering the cloud visible was to "dope" a cesium 100-km release with about 10 per cent sodium so that the latter would react in a chemiluminescent manner with the ambient atomic oxygen in the upper atmosphere (maximum number density at about 100 km). Of equal importance was the fact that results of the 17 November Aerobee flight suggested the desirability of utilizing the smaller Nike–Cajun two-stage rocket. Known advantages of using the smaller rocket included lower cost, ease of handling at launching, solid fuel and superior trajectory characteristics. However, it was recognized that, for the production of maximum-type electron clouds, such utilization would incur the sacrifice of larger payload. (The Aerobee's instrumented payload is capable of carrying aloft about three times more constituent.) In spite of this, the decision was made to utilize the Nike–Cajun vehicle whenever feasible.

The successful release of this Cs–Na mixture was accomplished from a Nike–Cajun rocket at an altitude of 101 km at the pre-dawn hour of 0245 MST on 20 May 1958. The electron cloud created was detected by radar; the cloud was assumed to be due to thermal ionization. It was clearly visible to the naked eye, the photographic and spectral data were obtained for as long as 6 min. Interpretation of the optical data presents the possibility of a study of the cloud dynamics versus time, as well as information pertaining to chemical consumption, kinetics of the reactions involved and some of the physical processes previously mentioned.

The next group of experiments of the series were primarily concerned with the correlation

of optical and radar data from ionized clouds as formed by solar ionization of alkali metal vapor. This could conveniently be accomplished by creating a light-emitting photographic cloud, preferably one that emits in the visible. The method of rendering the released contaminant visible is based upon the detectability of sodium resonance radiation against a morning-twilight-sky background[2]. Again, if we merely "doped" the chemical payload of cesium compound with a small amount of sodium, an easily observable cloud would be formed. A morning-twilight release was adopted since it was essential that the cloud be solar-illuminated for an extended period and that a reduced intensity sky background for the early part of the experiment exist. Two different experiments were performed as part of this phase of solar-induced ionization. A release of a mixture of cesium and sodium (2 per cent) was conducted at 128 km on 21 May 1958 and, following that, a payload consisting entirely of sodium compound was released at 116 km on 22 May 1958. Both experiments were successful in that they afforded the opportunity of providing good photographic and spectral coverage for over 8 min.

The radar results from the former release provided positive results for as long as 19 min, resulting in valuable correlated radar and optical data. The results of the sodium release were uniform in that all operating stations reported negative radar results. This negative result appears to be in agreement with the deduced relative photoionization probabilities of cesium, potassium and sodium. This further indicates, as expected, that thermal ionization does not play an important role for sodium as far as production of a detectable artificial electron cloud is concerned.

The last series of experiments in this program were conducted during September 1958 and were concerned with the study of the effect of altitude upon ionized cloud formation. The purpose of these flights was to determine the altitude below which the generation of a detectable, high-density, long-lived solar-induced artificial electron cloud is precluded due to the rate of photoionization electron production, recombination, electron attachment processes and chemical consumption of the contaminant. The approach next described was taken.

The first experiment was to be conducted at 80 km. Should positive radar detection results be obtained, a similar release at 70 km would be attempted. If results of the latter were positive, then a release at 60 km would be performed. If, however, the results of the 70 km release proved to be negative, a release at 90 km would be attempted in order to complete this investigation of altitude dependence upon generation of artificial electron clouds. The actual releases were performed in succession at 82, 69 and 91 km, respectively, since a negative result was obtained with the 69 km release of cesium.

The basic engineering technique concerning these releases of alkali metal vapors involved a stainless steel canister so designed and constructed as to be within the requirements of payload, configuration of nose cone, high acceleration and, finally, adaptability to the rocket body and instrument package.

The alkali metal compounds used for the experiments were all nitrates which were intimately mixed with aluminum granules: the chemical mix was then sealed in the steel canister. Actuation of the release mechanism was accomplished by an accurate timer which ignited two squibs imbedded in an igniter mix. The altitudes of release were determined by several independent techniques including optical triangulation, slant-range radar measurements, rocket-borne timer in conjunction with trajectory data, etc. In all cases, the altitude determinations were in excellent agreement.

The pertinent details of the performed experiments to be reported in this paper are summarized in Table 1 for ready reference. A series of papers which reported all the experimental data in detail, theoretical considerations, evaluation and interpretation, etc., have already been published[3–8].

2. EXPERIMENTAL RESULTS

2.1. *Radio-radar probes and results*

An extensive and elaborate network of radar-type equipment was located throughout the southwestern part of the United States. The

Fig. 2. Location and description of ground-based instrumentation used for ionisation detection of artificial electron clouds. Arrows designate either transmitting and/or receiving station.

map and index depicted in Fig. 2 shows the location of all the ground-based radar equipment together with a brief description of performance capabilities. The list is divided into categories, this is, equipment used to study back-scatter effects and those used to test forward-scatter results.

The descriptive details of the radar probes in Fig. 2 are described elsewhere[5, 6, 7]. Finally, Table 2 presents a summary of results for the radio-radar detection networks to provide a precise reference which can be applied in the following sections.

2.2. *Optical probes and results*

The methods employed for rendering visible both the night-time and twilight experiments have been described earlier. Here again, the optical instrumentation data are presented in tabulated form for ready reference in later discussions. Descriptions of the instrumentation have been provided in previous publications[6, 7, 8].

Table 3 provides a brief description of the optical equipment used and the respective geographic locations. Table 4 provides the information pertinent to the maximum time duration that gave positive results using optical techniques listed in the previous Table 3. Calibrated exposure times were obtained and fast film was used wherever applicable.

3. DATA ANALYSIS AND INTERPRETATION

In addition to their use as a powerful radar propagation tool, the scientific uses of electron clouds are varied in that the scientist is given a valuable research tool for the investigation of physical and chemical processes of the upper atmosphere. Several of the more prominent areas of investigation associated with this program include:

(*a*) a study of winds and wind shear obtained by radar responses and suitable optical techniques through proper "doping" of the chemical release,

(*b*) diffusion processes as applicable to both the determination and relative importance of ambipolar diffusion, diffusion associated with neutrals and the resultant effective diffusion coefficient,

(*c*) atomic and molecular cross-section evaluation of the processes of photoionization, photodetachment, recombination, electron attachment, chemical reactivity, etc., and their respective interdependence as a function of altitude of release, payload, mechanics of release, night-time versus daytime release, etc.,

(*d*) ionospheric structure as it is applied to information relative to existing electron density gradients, and use of this information towards subsequent observable ionospheric modifications created by the release of a high density electron cloud. The correlation of optical and radar data reveals the dynamic changes in cloud size, shape, and motion of these possible effects with changes in radar cross-section, scattering and other propagation aspects,

(*e*) expansion of high pressure gases into an attenuated atmosphere in a "limitless laboratory" over a varying range of mean free paths, and

(*f*) thermochemical phenomena associated with the chemical release process provide data pertinent to the thermal-ionization efficiency, chemical yield of the contaminant and other parameter data of similar value.

While some of the areas of investigation outlined above are discussed in this article, the reader is referred to the series of papers[3–8] in which not only are discussed all of these

Table 2. Summary of Results by Detection of Ionization Characteristics of Electron Clouds

The times refer to the maximum positive identification time reported. M = min, S = sec.
Neg. = no detection during proper equipment performance
— = equipment not in operation
X = no detection due to mechanical failure or lack of communication
All designations pertinent to equipment conforms with tabulation in Fig. 3

	Detection equipment results																		Remarks
	1A	1B	1C	2A	2B	3A	4A	4B	4C	4D	4E	5A	5B	5C	6A	6B	6C	7A	8A	
1	29S —	—	X	30M	X X	—	2½S	—	—	—	—	—	X	—	—	—	X	—	—	1A: 23·1 Mc/s 1A: 49·9 Mc/s
2	90S —	2½M	X	3M	60S 9S 6S Neg	—	—	7S	9S	—	—	2S Neg	Neg Neg	—	8M	4S	4M	Neg	Neg	1B: 6 Mc/s 5A–5B: 810 Mc/s 5A–5B: 13·56 Mc/s
3	— 20S	Neg	X	19M	10S 4S 2S Neg	—	—	3S	2S	—	—	1S Neg	2S Neg	—	15S	3S	Neg	Neg	Neg	Same as flight two
4	Neg —	Neg	X	Neg	2S Neg Neg Neg	—	—	Neg	Neg	—	—	Neg Neg	Neg Neg	—	Neg	Neg	Neg	Neg	Neg	Same as flight two
5	Neg 4·3S	Neg Neg Neg	—	24M	X	20M	—	—	—	—	—	Neg	—	Neg	Neg	Neg	Neg	—	—	1A: 23·1 Mc/s at Tucson 1A: 40·7 Mc/s
6	Neg 1½S	Neg Neg Neg	—	Neg	X	X	—	—	—	Neg	2S	Neg	—	Neg	Neg	Neg	Neg	—	—	Same as flight five
7	2M 54S	Neg 4M Neg	—	7M	X	2M	—	—	—	3·5S	3·5S	1S	—	Neg	Neg	Neg	Neg	—	—	Same as flight five

Note: Column 1B is split into 3 sections for flights 5, 6 and 7 (100 kc, 6 Mc/s, 20·8 Mc/s).
Column 2B is split into 4 sections for flights 2, 3 and 4 (36·94 Mc/s, 73·88 Mc/s, 132·48 Mc/s, 264·96 Mc/s).

scientific uses, but which report in detail the analysis and interpretation of each experiment.

3.1. *Basic equations and definitions*

For the data analysis associated with time behavior of the electron and/or contaminant cloud, the following model was employed.

Time zero is taken as the instant that the contaminant, released at very high pressure, assumes a pressure of the order of ambient—or

Table 3. Location (from Launch Site) of Ground-based Optical Detection Equipment

Flight No.	Location from launch site	Equpment
1	(A) 29·7 mi N—0·6 mi E (B) 0·4 mi N—0·6 mi E (C) 33·5 ni S—1·5 mi W	Three sites, each having two astro ballistic cameras (*f*/2·5 lens) located on HAFB-WSPG range
2	35 mi SW	Baker-Nunn satellite tracking camera (*f*/1 20 in. aperture)
3	20 mi E	Light amplifying unit (Lumicon) used with an 85 mm *f*/1·4 lens
4	15 mi E	Multicamera spectrograph consisting of 6 each 35 mm cameras fitted with appropriate narrow band pass and other filters
5	(A) 30 mi N—50 mi W (B) 7 mi N—25 mi E (C) 80 mi N—57 mi W	Three sites, each having a 4 in. × 5 in. press camera (*f*/2·8 lens)
6	15 mi E	Photometer with ½ degree field of view appropriately fitted with filter and sensitive phototube
7	15 mi E	Beattie-Coleman Varitron 35 mm recording camera
8	15 mi E	Spectrograph equipped with Schmidt optical system

Table 4. Summary of Results of Optical Data Obtained for May 1958 Series of Nike–Cajun Experiments

M = min S = sec — = equipment not in use.

All designations pertinent to equipment conform with tabulation in Table 3.

Flight No.	Detection equipment results								Remarks
	1	2	3	4	5	6	7	8	
2	6M	25S	40S	6M	6M	4½M	—	6M	1, 4, 6: time exposure
3	X	2S	6M	3½M	15S	—	2M	—	1: insufficient data provided 2: used yellow filter 3: used narrow band filter
4	X	45S	12M	6M	15S	—	4M	—	Same remarks as flight 3

Note: Photometer and spectrograph could not be used in flights 3 and 4 due to hour of firing and subsequent sky background intensity.

very low—pressure. At this time the contaminant distribution is considered to be Gaussian. Thereafter, cloud expansion is due to the concentration (or turbulent) diffusion mechanism.

This concept ignores the complex, initial, very fast "burst" or forced expansion which, in these experiments, occurred within a fraction of one second. Thus, at both time zero and thereafter, the following dynamic equations shall be applied to define the electron generative and decay processes of interest and to describe their time behavior.

$$\frac{dn_e}{dt} = q - \alpha_r n_e N^+ - \beta n_e + \delta N^- + \gamma N^- \qquad (1)$$

where d_{n_e}/dt is the net rate of production of electrons. Other definitions on a term-by-term basis are as follows:

$$q = \int \sigma n I d\nu \qquad (a)$$

where

n = number of contaminant particles per cm^3;
I = flux of ionizing radiation (photons/cm^{2}sec) per wave; and
σ = atomic photoionization cross-section (cm^2);
q thus represents the production rate of free electrons due to solar photoionization (cm^3/sec).

Recombination is indicated as

$$\alpha_r n_e N^+ \qquad (b)$$

α_r = ion electron recombination coefficient—here taken as radiative—(cm^3/sec),
n_e = density of electrons cm^{-3},
N^+ = positive ion density cm^{-3}.

The electron attachment term is

$$\beta n_e \qquad (c)$$

where

$$\beta = \eta_1 n_1 \text{ or } \eta_2 n_1 n,$$

and

η_1 = coefficient of attachment of electron to O (two-body in cm^3/sec),
η_2 = coefficient of attachment of electron to O_2 (three-body in cm^6/sec),
n_1 = particle density of neutral species (O_2 or O cm^{-3}),

thus β is the electron attachment probability per electron (sec^{-1}). The photodetachment contribution is indicated by

$$\delta N^- \qquad (d)$$

where

$\delta = \rho B$, and
$\int \rho B d\nu$ = photodetachment probability of electrons from negative ions (O_2^- and O^-) (sec^{-1}),
B = solar radiation intensity involved in the photodetachment processes,
N^- = negative-ion density (cm^{-3});
δ then represents the photodetachment probability per negative ion/sec.

The final term is for collisional detachment

$$\gamma N^- \qquad (e)$$

where

$\gamma = K n_2$,
K = coefficient of collisional detachment of electrons from negative ions (O_2^- and O^-) (cm^3/sec),
n_2 = particle density of constituents which may detach electrons from negative ions by collision (cm^{-3}).

Thus, γ, is the collisional detachment probability per negative ion/sec.

We can also write

$$\frac{dN^-}{dt} = -\alpha_i N^+ N^- + \beta n_e - \delta N^- - \gamma N^- \qquad (2)$$

α_i = coefficient of mutual neutralization by negative and positive ions (cm^3/sec).

We assume the net space charge as zero at all times so that

$$N^+ = n_e + N^- \qquad (3)$$

3.2. *Analysis of thermal release: Chemical yield and thermal ionization efficiency*

A sodium-doped cesium payload was released at 101 km during a night-time experiment (see Table 1, flight number 2) to determine the magnitude of thermochemical effects upon the production of artificial electron clouds. Subsequent analysis of radio-radar and optical data pointed towards the fact that it was indeed possible to ascribe to thermal processes the generation of an ample number of electrons to account for the observed electron cloud. A thermochemical treatment of these data with application of the Saha relationship suggested that values for the total number of electrons and thermal ionization probability could best be obtained from conditions wherein the temperature of reaction would be in the vicinity of

3000°K and with the canister-bursting pressure range between 300–500 atm.

Fig. 3 was derived from the Saha relationships as applied to the specific system employed. It relates the moles reacted to the temperature of the reactants for different bursting pressures. With the aid of this figure it can be shown[6] that a chemical yield of less than 10 per cent

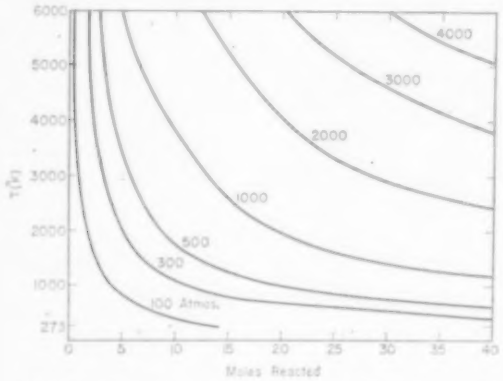

Fig. 3. Pressure within canister as a function of moles reacted and temperature of the reactants.

was to be expected. This fact was further substantiated by optical and radar data from subsequent experiments in the series in which yields of between 2–5 per cent have been determined in an independent manner.

An initial cloud optical radius of about 300 m and an initial electron density of the order of 10^7 cm^{-3} were determined from an analysis of optical and radar data, respectively. From these determinations it was experimentally concluded that the total electron content of the cloud, N_e, was of the order of 3×10^{21}. Theoretical evaluation of $N_e=1\times10^{21}$ was determined from subsequent cesium releases; a discussion will be found in another section of this paper. Therefore, an N_e value of between $1–3\times10^{21}$ is considered reasonable.

For cesium a value of 10^{-3} for the thermal efficiency, c, was determined from the results of this experiment in thermal release. Further, through utilization of the cesium data it was possible to extend these findings to other members of the metal alkali family. It was thus that a corresponding value of 5×10^{-4} was estimated for potassium. These c-values are employed in later data analysis.

3.3. *Analysis of C-3 radar data: Diffusion, chemical yield, ionization efficiency*

This section will outline some of the analysis methods which were employed for radar data, the results of which yielded values for several important parameters.

Of all the radar data obtained, the C-3 ionosonde data was considered the most compatible to analysis. The analysis is restricted to experiments 1 and 3 in Table 1, namely the potassium and cesium releases at 121 and 128 km, respectively. It has previously been demonstrated[5, 6] that for these cases, the only significant factor causing a decrease in the electron concentration is diffusion. Decay processes such as attachment, recombination and others are not sufficiently fast, for the time constants of the effects under discussion to materially affect electron concentration. Thus considerable simplification is possible; in particular, the governing equations are given by

$$\frac{dn_0}{dt}=D_n\nabla^2 n-kn \tag{4}$$

$$\frac{dn_e}{dt}=D_a\nabla^2 n_e+kn \tag{5}$$

where

n_0 = concentration of neutrals/cm^3,
n_e = concentration of electrons/cm^3,
D_n = neutral diffusion coefficient, cm^2/sec,
D_a = ambipolar diffusion coefficient, cm^2/sec,
k = photoionization probability, sec^{-1}.

In order to ascertain the magnitude of the photo-electrons which are solar-generated during the initial blast phase, we replace the D_n and D_a by D_x thus representing a forced expansion identical in nature for both ion–electrons and the neutral species. If t_1 represents the duration of the blast we select D_x so that

$$4D_x t_1=r_0^2 \tag{6}$$

where r_0 represents the Gaussian half-width of the cloud at time t_1. The initial conditions for the second and diffusive phase, represented by the original equations, are represented by the solution of these modified equations. In parti-

cular, the center point blast solutions for $t=t_1$ are

$$n(r,t_1)=\frac{N\exp(-kt_1)}{\pi^{3/2}r_0^3}\exp\left(-\frac{r^2}{r_0^2}\right) \tag{7}$$

$$n_e(r,t_1)=\left\{\frac{N[1-\exp(-kt_1)]+N_e}{\pi^{3/2}r_0^3}\right\}\exp\left(-\frac{r^2}{r_0^2}\right) \tag{8}$$

where

N = the total number of atoms at $t=0$,

$N_e=cN$ total number of electrons at $t=0$,

where

c = thermal ionization efficiency.

All the other symbols remain the same. The expression $N[1-\exp(-kt)]$ represents the photo-electrons created during the rapid expansion phase whereas N_e represents the thermal electrons. If we put $N=1\times10^{24}$ for the cesium case as determined by optical data (and, later, the fit to these data) and deduce that $N_e=1\times10^{21}$ for a thermal efficiency of ionization of 10^{-3} as indicated from thermochemical arguments presented in Section 3.2, we find that photo-electrons represent about one-third of the total for t_1 taken as about 0·5 sec and as experimentally estimated from the Lumicon photographs of the expanding cloud (8 frames/sec). This estimated expansion time is also in agreement with that expected from thermal velocity arguments. Analogous treatment of the potassium data indicated that as expected, an insignificant fraction of the initial electrons are due to solar photo-electrons.

These solutions now represent the initial conditions which apply for determining the center point solutions for the normal diffusion phase. These are given for a t' scale for which $t'=0$ when $t=t_1$.

$$n_e(0,t')=n_{e_0}\frac{r_0^2}{m^{3/2}}+$$
$$+\frac{kN\exp(-kt_1)}{2\pi^{3/2}(D_n-D_a)}\left[\frac{1}{m^{1/2}}-\frac{\exp(-kt')}{p^{1/2}}\right]+$$
$$+\frac{N}{4\pi}\left(\frac{k}{D_n-D_a}\right)^{3/2}\exp\left[\frac{km}{4(D_n-D_a)}\right]$$
$$\left\{\operatorname{erf}\left[\frac{kp}{4(D_n-D_a)}\right]^{1/2}-\operatorname{erf}\left[\frac{km}{4(D_n-D_a)}\right]^{1/2}\right\} \tag{9}$$

where

$$m=(r_0^2+4D_at')$$
$$p=(r_0^2+4D_at')$$
$$n_{e_0}=\frac{N[1-\exp(kt_1)]+N_e}{\pi^{3/2}r_0^3}$$

and is the initial electron center density.

It may appear that a large degree of flexibility is available for proper fitting in view of the several parameters involved. It is suggested that this is not the case; in fact, the requirement of utilizing several reasonable values simultaneously for proper fit can serve to make it highly restrictive. This seems to be the case here. For example, it was shown earlier that approximate N-values for the cases of the Nike–Cajun cesium and Aerobee potassium releases should be about 1×10^{24} and 3×10^{24}, respectively. Further, it was ascertained that thermal ionization efficiencies (c-values) of cesium and potassium are about 10^{-3} and 5×10^{-4}, respectively, for the chemical release system employed here.

Estimation of the r_0 values to be employed will now be described. Optical width data were available from the Nike–Cajun cesium and sodium twilight releases at altitudes of 128 and 116 km, respectively. These data were then correlated theoretically to the corresponding Gaussian half-width, r_0. At this point the r_0-value of 300 m deduced for cesium was applied directly. For the potassium case an intermediate optical width was deduced after proper adjustment for different payload. Again, the corresponding Gaussian half-width of 200 m was deduced.

Thus the r_0-value employed for fitting equation (9) are 300 m for the cesium 128-km release and 200 m for the potassium 121-km release.

Some uncertainty exists in the use of this method for estimating the proper Gaussian half-width. It is fortunate, therefore, that this parameter is not too sensitive to fitting.

The solar photoionization values of $6{\cdot}5\times10^{-4}$ $\sec^{-1}$ for cesium and $1{\cdot}9\times10^{-5}$ $\sec^{-1}$ for potassium were derived from published experimental data[9]. These values are considered to be the most reliable of the several parameters

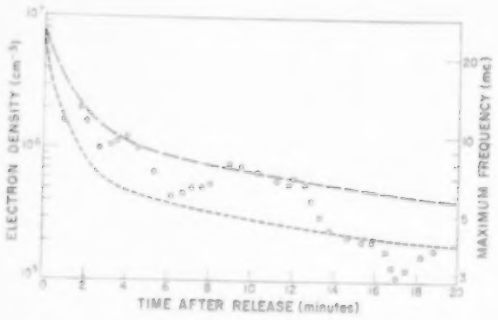

Fig. 4. Plot of the *C*-3 experimental data for the release of cesium at 128 km depicting the best fit values of D_n and D_a and illustrating the sensitivity of the technique.
— — $D_n = 2{\cdot}0 \times 10^8$ cm²/sec } where $D_n/D_a = 6$
- - - - $D_n = 3{\cdot}5 \times 10^8$ cm²/sec }

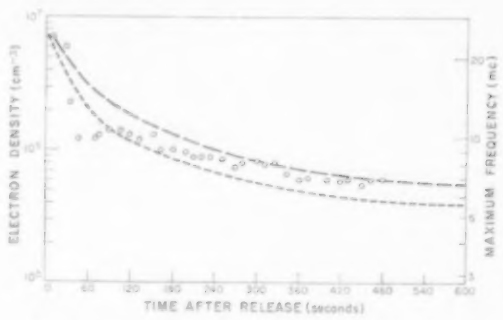

Fig. 5. The best fit values of D_n and D_a to the experimental *C*-3 data obtained from the experiment whereby potassium was released at 121 km are plotted.
— — $D_n = 5{\cdot}5 \times 10^7$ cm²/sec } where $D_n/D_a = 6{\cdot}7$
- - - - $D_n = 6{\cdot}9 \times 10^7$ cm²/sec }

employed and, as such, are not subject to variation, thereby imposing an additional restriction upon the available flexibility for proper curve fitting. There now remains the problem of determining the degree of agreement achievable between the theoretical and experimental values; application of various reasonable values of D_a and D_n, the ambipolar and neutral diffusion coefficients respectively, were used towards this end. Indeed, it was found that in both cases, D_a and D_n-values and the ratio of D_n/D_a were in close agreement with theory[10]. The best fit values for the cesium and potassium experiments are summarized in Table 5. The resultant fit to experimental data using these values is indicated in Figs. 4 and 5, which include the appropriate *C*-3 radar experimental data. In these figures two closely spaced sets of D_a and D_n-values are shown to illustrate the sensitivity of the technique.

3.4. *Optical data: Diffusion and chemical yield*

For obtaining diffusion and chemical yield determinations it is assumed that the initial, very rapid, explosive expansion occurring at release leads to a Gaussian cloud of half-width r_0. It is at this point that we set $t = 0$. Subsequently, the density is expected to vary with time and position in accordance with the equation

$$n(r,t) = \frac{N}{\pi^{3/2}(4Dt + r_0^2)^{3/2}} \exp\left(-\frac{r^2}{4Dt + r_0^2}\right) \quad (10)$$

where

$n(r,t)$ = number of particles/cm³ at distance, r, from the center at time, t,

N = total number of particles in cloud,

r_0 = half-width of Gaussian $\left(\frac{1}{e}\text{ value}\right)$ at $t = 0$ (cm),

D_n = diffusion coefficient for neutral species at cloud height (cm²/sec).

Table 5. Values Used for Obtaining Best Fit to Experimental *C*-3 Radar Data

Constituent	Altitude of release (km)	Photo-ionization probability k (sec^{-1})	Thermal efficiency c	Total number particles in cloud (N)	Initial release r_0 (m)	Neutral diffusion coefficient D_n (cm²/sec)	Ambipolar diffusion coefficient D_a (cm²/sec)
Cesium	128	$6{\cdot}5 \times 10^{-4}$	10^{-3}	$1{\cdot}0 \times 10^{24}$	300	$2{\cdot}5 \times 10^8$	$4{\cdot}2 \times 10^7$
Potassium	121	$1{\cdot}9 \times 10^{-5}$	5×10^{-4}	$3{\cdot}0 \times 10^{24}$	200	$6{\cdot}2 \times 10^7$	$9{\cdot}2 \times 10^6$

If luminosity is due to resonance-scattered sunlight and viewed in the back-scattering direction, light will therefore be scattered to the detector as a function of σ and in accordance with τ the number of atoms in the line of sight. The absorption cross-section, σ, of the sodium atom and its resonance level at 5890 Å is about 10^{-11} cm^2; hence, when the number of atoms in the line of sight is about 10^{11}, this portion of the cloud may be considered as being essentially optically dense. Since at these altitudes the collisional deactivation is negligible, the optically dense portion of the cloud will have a reflectivity of unity at the characteristic wave length. Further, the total number of alkali atoms will remain constant since the rate of chemical consumption by ambient oxygen is so slow. For example, the time for half-consumption, $t_{\frac{1}{2}}$ is $>10^7$ sec and $>10^5$ sec at 130 and 115 km, respectively (see Fig. 6 of Ref. 4).

The total number of particles in the line of sight (τ) at distance, d (cm) from center is given by

$$\tau = \frac{N}{\pi(4Dt + r_0^2)} \exp\left(-\frac{r^2}{4Dt + r_0^2}\right) \tag{11}$$

If it is assumed that the optical size of the cloud is determined by the distance from the center of that isophote for which $\tau = 1/\sigma$ (since the intensity drops rapidly for $\tau > \sigma$), we have

$$d^2 = -(4Dt + r_0^2) \ln \frac{\pi}{\sigma N}(4Dt + r_0^2) \tag{12}$$

$$d_{\max}^2 = \frac{N\sigma}{e\pi} \tag{13}$$

$$t_{d_{\max}} = \frac{1}{4D}\left(\frac{N\sigma}{e\pi} - r_0^2\right) \tag{14}$$

$$t_{d=0} = \frac{1}{4D}\left(\frac{N\sigma}{\pi} - r_0^2\right) \tag{15}$$

where

$d_{\max}$ = maximum radius of optical radius,

$t_{d_{\max}}$ = time to achieve this maximum radius, and

$t_{d=0}$ = time for cloud to disappear.

To effectively relate the optical model to the observed or photographed cloud size with the contaminant density and profile throughout the cloud requires consideration of the detector response to cloud luminosity under the varying twilight levels of background light. Many factors join to make quantitative measurements from a photographic image difficult, some of which are the following: (1) the maximum exposure time is limited by the background which varies over several decades during the twilight period, (2) the film is background-sensitive, that is, its sensitivity increases as a direct function of an increase in background light, which increase brings the level of intensity to a steeper part of the density versus exposure curve, and (3) the optically thin edges of the cloud do not provide a clear cut edge for measurement.

For quantitative work it is necessary, in practice, to combine careful instrument calibration with meticulous densitometry techniques to plot contour lines of constant density and relate these to a theoretical model before dimensions can be accurately ascertained. This was not accomplished in the present work and the absolute values derived suffered accordingly.

As an illustrative example of the optical model we shall analyse the Beattie-Coleman data for the 21 May flight. (Flight No. 3, item 7 in Table 4.) Here we are concerned with determining the parameters r_0 = the initial Gaussian half-width, N = the number of alkali atoms, and in this case D_n = the observed neutral diffusion coefficient, from the optical data. From equation (12) for $t = 0$ we obtain

$$d_0^2 = r_0^2 \ln \frac{\pi r_0^2}{\sigma N} \tag{16}$$

where d_0 = initial optical radius.

In order to solve equation (16) we need an estimate of N. We obtain this from equation (13) since $d_{\max}$ is an observable. Then from equation (16) we obtain r_0. Having obtained r_0 and N we can now obtain D from equation (14), since $t_{\max}$ is an observable.

These values are the first estimate for fitting equation (12) to our data. We subsequently adjust these parameters to obtain the best fit to the entire run of data since the initial values of r_0, D and N were obtained from two points, $t = 0$ and $t = t_{d_{\max}}$.

This fit is surprisingly accurate since small variations in both N and D cause large changes in our curve. This is indicated in Fig. 6 where the size ($2d$) is plotted against the theoretical

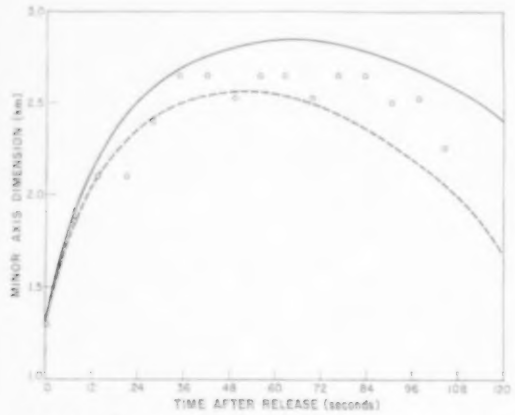

Fig. 6. The time variation of the minor axis optical diameter is indicated by the circles. The dashed and solid curves are theoretical curves for two different yields but the same diffusion coefficients.
—$N=1{\cdot}7\times10^{22}$ - - - - $N=1{\cdot}4\times10^{22}$
$D=7\times10^{7}$ cm²/sec
Beattie–Colman camera, 21st May, 1958.

curve for two closely spaced, different values of N.

The fit indicates a value of $D_n=7\times10^7$ cm²/sec and $N=1{\cdot}5\times10^{22}$ atoms or a sodium yield of approximately 3 per cent. The value of D_n is consistent with the theoretically extrapolated values of D_n at the altitude in question. Furthermore, since $t_{max}=1/D$, small changes in D shift the maximum and the curve along the t-axis in an extremely sensitive fashion.

Equation (15) for the disappearance of the contour line defining the optically dense cloud and the observed neutral diffusion coefficient, D_n, was used to determine the yield of the cesium vapor for the 21 May 1957 flight. For this purpose the cloud photographed in the second resonance line at 4557 Å was used and noted to last for about 130 sec. If the ratio of optical cross-sections for the first and second resonance lines of cesium is taken to be about 100 : 1, then the recorded contour line corresponds to about 3×10^{12} atoms/cm²-column. Thus the total number of cesium atoms released is about 10^{24} or about 3 per cent of the original. This value was not checked with a similar determination using the photographs of the first cesium line at 8521 Å since the cloud remained optically dense throughout the photographable time interval. The photographs at 5890 Å and 3300 Å taken with the six-camera bank were also used to determine the sodium yield in a similar manner. Although values obtained were in agreement with those established earlier, less credence was given them due to uncertainty as to the timing of the individual exposures. However, it is to be noted that, while sodium was used as a doping agent to determine yield by observation of the 5890 Å line, the assumption was made that the chemistry of sodium and cesium are similar. Here, the validity of this assumption was verified since the yields of both cesium and sodium were ascertained independently and found to agree.

3.5. *Wind determination: Velocity and shear data*

The formation of a small visible, photographable cloud at altitude can yield wind velocity data by means of simple optical triangulation techniques. A method of obtaining shear information from optical data is given below. In addition, a geometric method of extracting accurate horizontal wind velocity values from C-3 radar data is discussed.

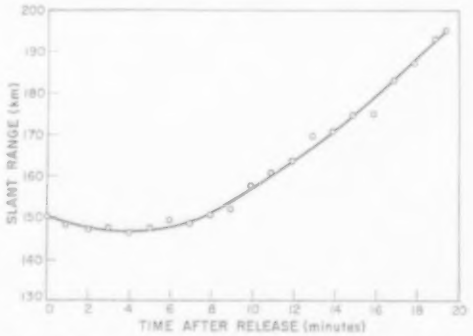

Fig. 7. The circles represent the C-3 radar slant range versus time for the 21 May experiment. The solid line is a best fit from equation (17) and a constant, horizontal wind velocity of 140 m/sec.

The pertinent radar data for obtaining horizontal wind velocities is the change in electron cloud slant range versus time. The data from the *C*-3 ionosonde are shown as circles in Fig. 7. The range points represent averages of the four soundings taken during each minute at 15 sec intervals and over a 20-min period. The smooth variation of the range with time for this 20-min period is strong support for the presence of a simple electron cloud. From the initial slant range of about 150 km, the subsequent change in slant range in time is presumably due to ionospheric winds. The character of the curve with a shallow minimum indicates the geometry depicted in Fig. 8 in which the positions of

Fig. 8. Schematic representation of geometrical determination of winds from C-3 slant range versus time plot.

cloud release and *C*-3 stations are included. Further, this situation can be described mathematically by the expression

$$S=[S_0^2+Vt(Vt-2S_0\cos\theta_0)]^{1/2} \qquad (17)$$

where

S_0 = initial slant range,

S = slant range between cloud trajectory and *C*-3 line of sight,

θ = initial angle,

V = wind velocity.

A best fit to the data was obtained for a V-value of 140 m/sec; the theoretical curve is shown as the solid line in Fig. 7. The excellent fit between the experimental points and the theoretical curve appeared to corroborate the notion of horizontal winds with a constant velocity of about 140 m/sec. This (140 m/sec) velocity is considerably greater than those previously determined in a similar manner, namely, 60 m/sec and 78 m/sec at 95 km[1] and 121 km[5], respectively. Concerning wind direction, it was clear from Fig. 8 that an ambiguity existed on the basis of these data alone. However, in this instance visual observations dictated the choice of direction as 87 degrees rather than 293 degrees. This case suffices to illustrate the geometric method of obtaining wind information via these and similar data.

Wind shear in the upper atmosphere has recently been measured by a technique in which a long sodium filament is ejected into the upper atmosphere (between 70 and 200 km)[11]. Careful analysis of the optical data leads to accurate shear data. Clearly, in a similar manner a point release can be utilized to determine the wind shear at the release altitude. For example, photographs of the contaminant cloud indicated an initially spherical cloud becoming ellipsoidal with time due to the prevailing wind shear at the cloud position.

The shear effect may be described by the following equation:

$$\frac{dn}{dt}=D\nabla^2 n-w\left(\frac{dn}{dx}\right) \qquad (18)$$

n = number of particles/cm^3,

D = diffusion coefficient, cm^2/sec,

w = wind velocity, taken parallel to x-axis, cm/sec.

The treatment of this equation will not be included in this discussion since it did not fall within the scope of this work. Rather, the present treatment is restricted to a more crude model, but one which gives a good qualitative fit to the data.

The photographed image of a cloud illuminated by resonance scattering is a complicated function of viewing angle, optical density of the cloud, film sensitivity and exposure time as well as background light intensity; for the purpose of determining shear it is convenient to consider only the relative values of the minor to the major axis of the elliptical image. Consider

that the cloud, in the absence of shear, would expand spherically with the diameter $2d_{\perp}(t)$ identical with the observed minor axis. If Y is the coefficient of shear, then a differential velocity of the cloud extremes (top edge to bottom edge) is given by

$$V_{diff} = 2Y d_{\perp}(t) \tag{19}$$

and the elongation L as viewed from below if the upper altitude winds are horizontal is given approximately by

$$L = \int V_{diff} dt \tag{20}$$

if the minor axis remains reasonably small compared to this elongation. This simplified model has the advantage of not being too dependent upon the absolute values of the cloud dimensions.

Our procedure has been to approximate the observed minor axis $d_{\perp}(t)$ by a linear expression

$$2d_{\perp}(t) = a + bt \tag{21}$$

In the case of the 35 mm camera data for 22 May 1958, we have

$$2d_{\perp}(t) = 1{\cdot}4 + \frac{4{\cdot}2}{200}t \tag{22}$$

We then have for the shear-produced elongation

$$L = Y(at + \tfrac{1}{2}bt^2) + \text{constant} \tag{23}$$

In Fig. 9 we have plotted the variation with time of the minor axis on the left hand graph and on the right hand graph the variation with time of the major axis together with the plot of equation (23). From these, a shear-value of $Y = 1{\cdot}1 \times 10^{-2}$ sec^{-1} was obtained.

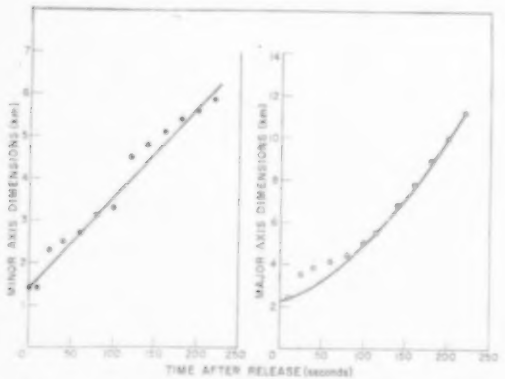

Fig. 9. The solid dots and circles represent the time variation minor and major axes optical diameters, respectively. The two curves show the best theoretical fit and indicate a wind shear of 1×10^{-2} sec^{-1}.
35 mm camera (5890 Å filter), 22nd May 1958.

Similar plots have been applied to the Lumicon data. It is recognized that the absolute cloud dimensions cannot be determined accurately from the Lumicon, due to the numerous changes in the Lumicon sensitivity control by the operator as well as a lack of calibration of the photographic film. However, it is felt that the errors involved are not as serious for simultaneously observed relative values for the minor and major axis. Data from the 22 May flight yielded a shear constant of 1×10^{-2} sec^{-1} in agreement with the above. The value obtained for 21 May was 6×10^{-3} sec^{-1}. These values were consistent with those obtained by sodium streamer experiments[11]. It was also recognized that the rate of diffusion will be a function of the cloud shape itself, but this effect is ignored in the above model whereas another assumption is that shear does not affect the growth of the minor axis. Yet, despite these limitations a reasonable plot was obtained for the concomitant variation of the major and minor axes.

3.6. *Low altitude data analysis: Chemical consumption, mutual neutralization and other electron decay processes*

In this section will be discussed a series of three experiments which were undertaken for the two-fold purpose of studying the effect of low altitudes (below 100 km) upon the formation of artificial electron clouds and the roles of a number of electron decay processes after the generation of these clouds. It was felt that the data required would afford not only an investigation of the effects of individual decay processes, but would allow further investigation of an earlier conclusion[4] that there probably existed some lower altitude below which the formation of detectable, high density, long-lived and solar-induced artificial electron clouds could not be achieved within the framework of the experimental techniques employed in this study. More pertinent to this conclusion, however, is the fact that several electron decay processes (e.g. chemical consumption, recombination

electron attachment, etc.) predominate at low altitudes in contra-distinction to other processes which exert maximum influence above the 100-km region.

For the present analysis, therefore, information was obtained concerning some of these decay processes. Of particular import was the derivation of coefficients for chemical consumption and mutual recombination.

Of the several radio-radar probes utilized in the cesium releases at 91, 82 and 69 km[8], a 40·7 pulsed radar located 15 miles east of the launch site yielded the most consistent—and therefore usable—data. The analysis applied to these data, indicated a total cloud duration of about 70 sec at 91 km, 4·3 sec at 82 km and 1·5 sec at 69 km.

The short lifetimes observed for the low-altitude generated clouds are due to at least two important effects: (1) the rapid destruction of cesium atoms by chemical consumption which prevents subsequent photoionization, and (2) rapid electron destruction through attachment followed by mutual neutralization. It was found, for the types of releases discussed in this paper, that the diffusion rate of the charged particles is much too slow to account for the observed cloud history. Also the photoionization production term remained relatively uninfluenced by diffusion of the neutrals except at about 90 km.

We present here a brief summary of the mathematical model. Details have been given in a previous paper[4]. We have

$$\frac{dn_e}{dt} = kn_0' e^{-bt} - \alpha n_e^2 \tag{24}$$

where

$n_e(0) = n_{e_0}$,

b = chemical consumption rate of consumption of the cesium by atmospheric oxygen (sec^{-1}), and

$$n_0' = \frac{n_0}{1+\lambda}$$

where λ = ratio of negative ions to electrons at equilibrium.
Finally,

$$\alpha = \alpha_e + \lambda \alpha_i \tag{25}$$

where

α_i is the coefficient of mutual neutralization

and

α_e is the cesium-ion recombination coefficient.

All other symbols are as previously defined.

Fortunately, this non-linear equation is susceptible to the complete formal solution* below.

$$n_e(t) = \frac{bl}{2\alpha}\,\xi \frac{[I_1(l)K_1(l\xi) - I_1(l\xi)K_1(l)] + \mu[I_0(l)K_1(l\xi) + I_1(l\xi)K_0(l)]}{[I_1(l)K_0(l\xi) + I_0(l\xi)K_1(l)] + \mu[I_0(l)K_0(l\xi) - I_0(l\xi)K_0(l)]} \tag{26}$$

where

$$l = \frac{2}{b}(2kn_0')^{1/2}$$

$$\mu = \frac{2\alpha n_e(0)}{lb}$$

$$\xi = e^{-\frac{1}{2}bt}$$

and where

$$y_1 = I_0(lZ)$$

$$y_2 = K_0(lZ)$$

where both expressions satisfy Bessels' zero order modified equation:

$$\frac{d^2y}{dZ^2} + \frac{1}{Z}\frac{dy}{dZ} - l^2 y = 0 \tag{27}$$

and where

$$I_0'(Z) = I_1(Z)$$

$$K_0'(Z) = K_1(Z)$$

Unfortunately, the solution of equation (26) is not susceptible to direct computation because of the large value of the arguments. However, numerical values have been obtained for equation (26) by the use of a variety of numerical approximations. These approximations and their range of validity are given elsewhere[8].

* This mathematical solution together with the approximations are due to Dr. H. K. Brown, Geophysics Corporation of America. The full details of this solution will appear in a forthcoming publication.

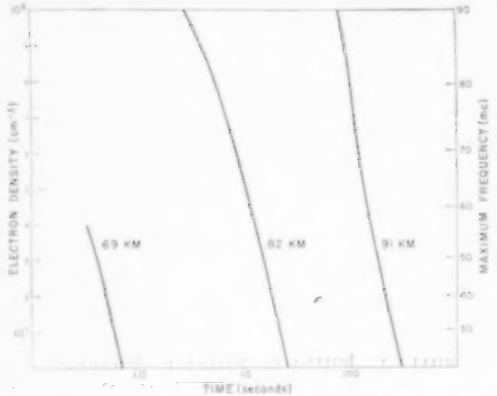

Fig. 10. Theoretical time variation of center-point electron density in accordance with equation (24) for 69, 82 and 91 km.

This solution for the parameters listed in Table 6 are given as Fig. 10. In general the solution reflects the altitude variation of the 40·7 Mc signal variation and gives order-of-magnitude agreement for the absolute times. The deviation between the theoretical and experimental data is greatest as expected at 91 km where no allowance was made for the effect of neutral diffusion on the photoionization term. Its direction is as expected[8].

From the analysis it is deduced that $\alpha_i = 10^{-7} - 10^{-8}$ cm^3 sec^{-1}, in rough agreement with estimates of Bates[12] for similar processes. The value of b is in reasonable agreement with the values computed in an earlier paper[8] using the sodum rate of consumption.

Using present techniques, the lowest altitude of effective cloud duration is about 70 km. A night-time, low-altitude experiment should give an independent measure of electron attachment rate to O_2 which can be meshed with the low altitude, daytime shots to obtain a more direct value of α_i.

4. CONCLUSIONS

The foregoing is intended as a review of some of the main points in the systematic study of the physics of artificial electron clouds. It has for its goal the elucidation of the basic electron creation and destruction processes.

This study has revealed that the theoretical photoionization cross-sections are consistent with the data contained, and that cesium is the most effective of the alkali metals used for this purpose. It has been shown that the chemical yields have been disappointingly small, namely, of the order of 2–3 per cent. Thermal ionization has been shown to be an effective process in the generation of artificial electron clouds, but here again, efficiencies of only about 0·1 per cent of the released number of atoms have been achieved.

An optical method has been devised for the successful determination of the cloud initial half-width, chemical yield, wind shear and neutral diffusion coefficients. A simple method has been used for determining (with one degree of ambiguity) the wind velocity from radar slant range data. A mathematical model has been applied to those experimental releases above 120 km in order to describe the observed electron decay history. The analysis gives measures of neutral and ambipolar diffusion, chemical yield, degree of thermal ionization and initial half-width. Reasonable correlation of radar data with the optical techniques employed has been demonstrated.

Another mathematical model has been devised and employed for the lower altitude (below 90 km) range which accounts for the dominant processes at these altitudes. These techniques

Table 6. Values of Basic Parameters Initially Used.

H (km)	n_h (cm^{-3})	D_n (cm^2 sec^{-1})	D_a (cm^2 sec^{-1})	r_0 (cm)	n_0 (cm^{-3})	ne_0 (cm^{-3})	λ	α (cm^3 sec^{-1})	b (sec^{-1})
91	$4{\cdot}0\times10^{13}$	$1{\cdot}7\times10^{5}$	$1{\cdot}8\times10^{4}$	$1{\cdot}17\times10^{4}$	$1{\cdot}1\times10^{11}$	$2{\cdot}2\times10^{8}$	0·009	2×10^{-7}	0·017
82	$2{\cdot}5\times10^{14}$	$4{\cdot}0\times10^{4}$	$4{\cdot}0\times10^{3}$	$6{\cdot}9\times10^{3}$	$5{\cdot}5\times10^{11}$	$1{\cdot}1\times10^{9}$	0·2	2×10^{-8}	0·2
69	$2{\cdot}0\times10^{15}$	$5{\cdot}4\times10^{3}$	$6{\cdot}5\times10^{2}$	$3{\cdot}8\times10^{3}$	$3{\cdot}3\times10^{12}$	$6{\cdot}6\times10^{9}$	2·0	2×10^{-7}	8·0

No.	Location	Equipment	Type*
1	Launch site—HAFB and Alamagordo, New Mexico	(A) 70 kW pulsed radar 23·1 Mc/s, 45 kW—40·7 Mc/s	B
		(B) Radars 100 kc—1·8 kW, 6 Mc/s—2·1 kW, 20·8 Mc/s 28 kW.	B
		(C) HAFB frequency monitor station—TV channels	F
2	White Sands Proving Gound, New Mexico	(A) C-3 vertical ionosonde 10 kW—1–25 Mc/s	B
		(B) Dovap net 1 kW—36·94 Mc/s, 125W—73·88 Mc/s	F
		Doran net 14 kW—132·48 Mc/s, 200 W—264·96 Mc/s	
		(C) Acoustical sounding	F
3	Sacramento Peak, New Mexico	(A) Cossor portable ionosonde 1 kW—1–20 Mc/s	B
4	Laredo, Texas to Durango, Colorado	Transmitter 1·2 mW—201 Mc/s	F
	Nevada site	(A) Receiver 201 Mc/s	F
	Utah site	(B) Receiver 201 Mc/s	F
	White's City, New Mexico	(C) Receiver 201 Mc/s	F
	Fort Stockton Texas	(D) Receiver 201 Mc/s	B
		(E) Receiver 201 Mc/s	B
5	Fort Huachuca, Arizona to Encino, New Mexico	Transmitter 10 kW—810 Mc/s, 50 W—13·56 Mc/s	F
	Lubbock, Texas	(A) Receivers 810 Mc/s and 13·56 Mc/s	F
	Williams A.F.B., Arizona	(B) Receivers 810 Mc/s and 13·56 Mc/s	F
		(C) Receiver 810 Mc/s	B
6	(Radio amateur 2– and 6–m net) Tucson, Arizona to Rosewell, New Mexico	Transmitter 50·01 Mc/s (6m) and 144·01 Mc/s (2m), 70 kW Radar 23·1 Mc/s	F
		(A) Receiver 50·01 Mc/s	B
	Austin, Texas	(B) Receiver 144·01 Mc/s	F
	El Paso, Texas	(C) Receiver 144·01 Mc/s	F
7	Phoenix, Arizona to Midland, Texas	Transmitter 100 kW—55·26 Mc/s	F
		(A) Receiver 55·26 Mc/s	F
8	Lubbock, Texas to Douglas, Arizona	Transmitter 216 kW—211·24 Mc/s	F
		(A) Receiver 211·24 Mc/s	F

*B = back scatter, F = forward scatter

also yield useful information on neutral and ambipolar diffusion, photoionization cross-sections, mutual neutralization, thermal ionization and the chemical consumption of the alkali contaminant by atmospheric oxygen. Information on electron attachment rates should be easily available by application of similar techniques. Additional work is in progress to solve the mathematical problems in the region 90–120 km where both diffusion and radiative recombination are important.

Finally, the foregoing summary has made obvious the possible usage of artificial electron clouds for radar propagation purposes. In particular, a significant potential for this application is indicated by the small chemical yields and thermal efficiencies experienced with the methods employed here. Clearly, these are capable of substantial increase. A systematic chemical engineering study is being currently pursued to this end and should yield substantial improvement towards realizing the full potential of the utilization of artificial electron clouds for radio-radar propagation.

REFERENCES

1. F. F. Marmo, J. Pressman, L. M. Aschenbrand, A. S. Jursa and M. Zelikoff, *J. Chem. Phys.* **25**, 187 (1956).
2. J. F. Bedinger, E. R. Manring and S. N. Ghosh, *J. Geophys. Res.* **63**, 19 (1958).
3. F. F. Marmo, L. M. Aschenbrand and J. Pressman, *Artificial Electron Clouds—I: Summary Report on the Creation of Artificial Electron Clouds in the Upper Atmosphere, Planet. Space Sci.* **1**, 227 (1959).
4. F. F. Marmo, J. Pressman and L. M. Aschenbrand, *Artificial Electron Clouds—II: General Considerations, Planet. Space Sci.* **1**, 291 (1959).
5. F. F. Marmo, L. M. Aschenbrand and J. Pressman, *Artificial Electron Clouds—III: Release of Atomic Potassium at 121 km, Planet. Space Sci.* **1**, 306 (1959).
6. J. Pressman, F. F. Marmo and L. M. Aschenbrand, *Artificial Electron Clouds—IV: Thermal Ionization Study, Nighttime Release of Cesium at 101 km, Planet. Space Sci.* **2**, 17 (1959).
7. F. F. Marmo, J. Pressman, E. R. Manring and L. M. Aschenbrand, *Artificial Electron Clouds—V: Morning Twilight Study, Release of Cesium and Sodium at 128 and 116 km, Planet. Space Sci.* **2**, 174 (1960).
8. J. Pressman, F. F. Marmo and L. M. Aschenbrand, *Artificial Electron Clouds—VI: Low Altitude Study, Release of Cesium at 69, 82 and 91 km, Planet. Space Sci.* In press (1960).
9. G. L. Weissler, *Handbuch der Physik* Bd. 21, 332 (1956).
10. A. Dalgarno, private communication.
11. E. R. Manring, J. F. Bedinger, H. B. Pettit and C. B. Moore, *J. Geophys. Res.* **64**, 587 (1959).
12. D. R. Bates, *The Physics of the Upper Atmosphere* in *The Earth as a Planet* (Edited by G. P. Kuiper) p. 618. University of Chicago (1954).

SPECTROSCOPIC MEASUREMENT OF THE TEMPERATURE OF SHOCK-HEATED OXYGEN

W. H. WURSTER
Cornell Aeronautical Laboratory, Buffalo, New York

Abstract—This paper presents the preliminary findings of experiments currently in progress in which the ultra-violet absorption of the Schumann–Runge band system of oxygen has been exploited as a means of determining the vibrational temperature of heated oxygen. The apparatus is described and results obtained to date are presented. These results demonstrate the usefulness of this device in measuring temperatures between 1500° and 3500°K for a limited range of optical thickness. Current work on the extension of the measurements to other densities and on the applicability of this technique to the temperature of air is discussed.

1. INTRODUCTION

One of the problems in the simulation of hypersonic flight situations, or even in basic studies of the properties of heated gases, is that of the determination of the thermodynamic state of the gas. This is reliably calculable only for the simplest of aerodynamic flows, and must in other cases be inferred from measurements. In most of these measurements it is essential that the flow remain unperturbed from an aerodynamic standpoint, making the use of optical probing desirable. Such is the case in the measurement of gas temperatures, where many methods have been reported which are based on spectroscopic techniques. They include the method of sodium line reversal[1] and the measurement of relative intensities of spectral lines of metals and of the bands of C_2 and CN[2]. These methods generally require additives to the gas and, further, the assumption of thermal equilibrium between the gas and the contaminants. In this paper is presented a discussion of the use of pure oxygen, always present in air below 5000°K, in the measurement of temperature by spectroscopic means.

2. ULTRA-VIOLET ABSORPTION OF OXYGEN

The radiative properties of oxygen at elevated temperatures have been studied at this laboratory[3, 4] under the sponsorship of the Air Force Office of Scientific Research (Contract AF 49 (638)-269). One of the outgrowths of this research was the undertaking of an experimental program aimed at making use of the spectral absorption of oxygen as an optical probe to determine oxygen temperatures. The description of such a probe is given, and the first calibration measurements made with this device are presented.

An examination of the pertinent potential energy curves for the oxygen molecule (Fig. 1) reveals that the absorption of radiation by oxygen molecules at room temperature is confined to transitions with energies in excess of 60,000 cm^{-1}. Such absorption produces the photo-dissociative continuum of oxygen in the vacuum ultra-violet at wave lengths below 2000 Å. It can be seen from Fig. 1 that at elevated temperatures the population of excited vibrational energy levels will result in absorptive transitions to selected vibrational levels of the upper $^3\Sigma_u^-$ electronic state. One thereby obtains the Schumann–Runge band spectrum in absorption.

A series of these spectra is shown in Fig. 2. These spectra were photographed in absorption with a large Littrow spectrograph, by passing the radiation from a high-speed argon flash-lamp through a sample of pure oxygen that had been heated by an incident and reflected shock

* This research was supported in whole or in part by the United States Air Force under Contract No. AF 18(603)-141, monitored by the Mechanics Division of the Air Force Office of Scientific Research of the Air Research and Development Command.

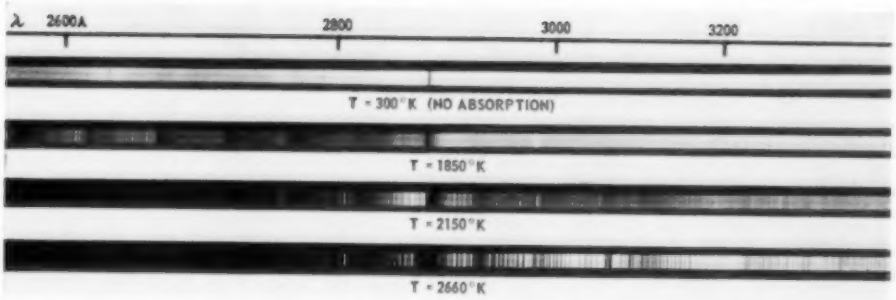

Fig. 2. Ultra-violet absorption spectra of oxygen at varying temperatures. Optical thickness ~ 50 cm-atmos (L = 6·4 cm, $\rho = 8\rho_0$).

Refer to page 160
(facing page 158)

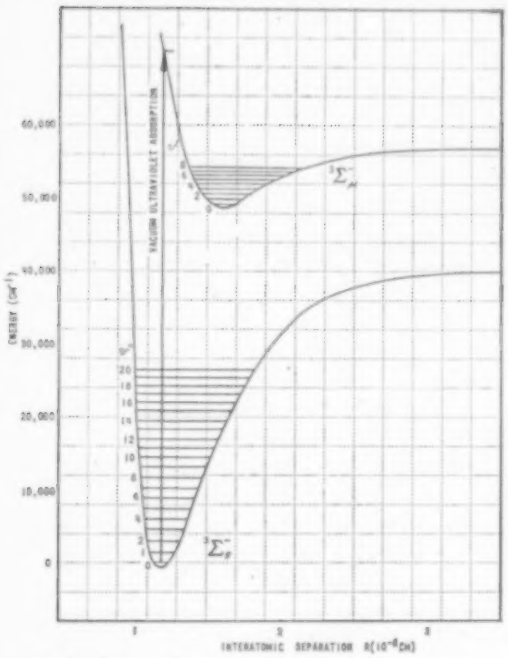

Fig. 1. Potential energy curves of the oxygen molecule.

wave in a closed shock tube. These spectra show the strong dependence of the oxygen absorption on the temperature; for example, at 2700 Å the gas undergoes a change from complete transparency, at room temperature, to almost total opacity at 2660°K. This strong temperature dependence is due to the exponential Boltzmann distribution of molecules in the respective excited energy levels. A method of temperature measurement based on the absorption of radiation in transitions from these various vibrational levels will therefore yield a measure of the vibrational temperature of the oxygen.

3. DESCRIPTION OF THE EXPERIMENTS

A schematic diagram of the apparatus is shown in Fig. 3. The optical system consists of a xenon flash-lamp, the collimating system through the shock tube and a Bausch and Lomb medium quartz spectrograph equipped with a photomultiplier adapter. The adapter is constructed as a unit to fit the plate-holder slide,

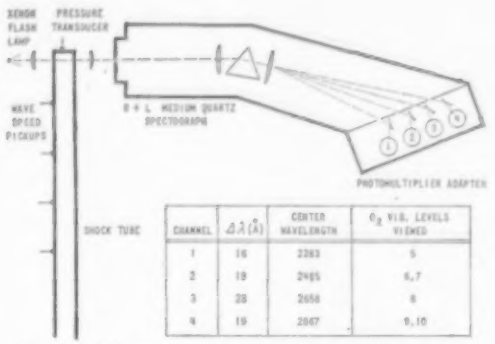

CHANNEL	$\Delta\lambda$ (Å)	CENTER WAVELENGTH	O_2 VIB. LEVELS VIEWED
1	16	2283	5
2	19	2495	6,7
3	20	2656	8
4	19	2867	9,10

Fig. 3. Schematic diagram of the radiation probe apparatus.

and contains a set of four variable exit slits placed in the focal plane of the spectrograph. Behind each slit is a plane mirror which directs the radiation from the slit to respective 1P28 photomultiplier tubes. The tube outputs are displayed and photographed on Tektronix 502 oscilloscopes. The time constant for the system was 2 μsec, and the size of the pencil of radiation through the shock tube was 4×4 mm. The pathlength through the test gas, equal to the inside dimension of the shock tube, was $2\frac{1}{2}$ in. Shock wave velocity was measured at five stations along the tube with the use of thin-film resistance gauges and oscillographic display. The measured velocity was used to calculate the temperature and density of the gas behind the reflected shock wave. In order to monitor the duration of the equilibrium testing time, the output of a fast-response pressure transducer, mounted in the reflecting wall of the shock tube, was also recorded. The testing time may be considered to be the interval of time between the passage of the reflected shock wave, and the arrival of other pressure disturbances caused by subsequent wave-interface phenomena.

The table included in Fig. 3 presents the wave lengths and the size of the wave length windows which each channel recorded, together with the vibrational quantum number of the transitions effective in each window. The wave lengths for channels 1, 3 and 4 were chosen so that minimum interference was to be expected by any NO gamma band absorption, which would be important in experiments with air as the test

gas. Also, for this reason, channel 2 was purposely set in the (0, 2) gamma bandhead of NO.

Typical oscillographic records for experiments in pure oxygen are shown in Fig. 4. In Fig. 4(a) the display of the flash lamp over its entire duration is shown, both in calibration, labelled (1), and in the experiment, labelled (2). The data were read from the expanded records of Fig. 4(b) which show the intensity attenuation by the gas at the time of the reflected shock wave arrival. The lamp was synchronized with the shock wave so that its maximum output coincided with the arrival of the wave. The flash-lamp output is reproducible to within the ability to read the records, and allows the transmission through the gas in terms of I/I_0 to be readily determined. Transmissions measured for as long as 100 μsec after shock wave arrival were constant, indicating the duration of the equilibrium testing time behind the reflected shock wave. The increased absorption in the record of Fig. 4(a) at $t = 0{\cdot}62$ msec was found to correlate exactly with a pressure increase recorded by the pressure transducer. It corresponds to subsequent heating of the gas by pressure waves resulting from the interaction of the reflected shock and the driver gas interface.

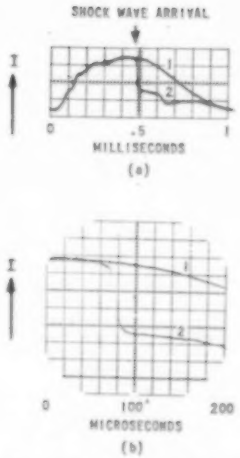

Fig. 4. Oscilloscope records of radiation intensity vs. time in channel 3, for the lamp flash in calibration (1) and during the experiment (2). The total lamp output is seen in the monitor-oscilloscope record (a) and the enlarged portion of interest, from which the data are taken, in (b).

4. RESULTS AND CONCLUSIONS

The data from a series of experiments in pure oxygen are presented in the graph of Fig. 5, where the transmission of the gas in each of the four wave length channels is plotted against the temperature of the oxygen for each experiment. These experiments were run at a constant molecular oxygen density of two times standard and with a pathlength of 6·4 cm.

As may be expected, the transmission in channels 3 and 4, which correspond to longer wave lengths and to transitions from higher-lying energy levels, does not decrease until higher temperatures are attained. Conversely, the transmission of the short-wave length channel 1 is attenuated at lower temperatures and rapidly reaches its minimum value. The advantage of using a series of channels is demonstrated in the broad range of temperatures (1500–3500°K) over which measurements, for these values of optical thickness, can be made. The vertical error bars on the graph reflect the ability to read the intensities from the oscilloscope records and the horizontal bars correspond to the error in temperatures introduced by an error of 1 per cent in the determination of the shock-wave velocity.

A few experiments have been performed at lower values of the molecular oxygen density. To obtain readable transmission values for a given pathlength, the lower density of absorbers

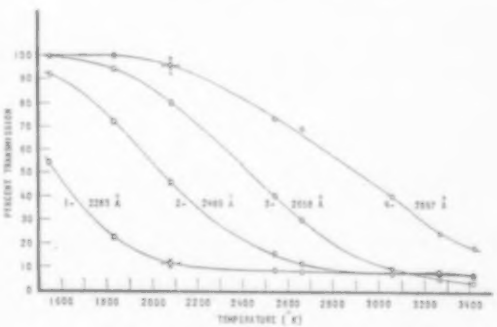

Fig. 5. Curves for the measured transmission vs. temperature in each of four wavelength "windows". Optical pathlength = 6·35 cm; $(\rho/\rho_0)_{O_2} = 2$.

must be compensated for by an increase in temperature, in order to maintain an observable number of molecules in a given vibrational energy level. The results indicate that, for the pathlength of 6·4 cm, densities of oxygen molecules of 0·1 standard can be conservatively measured at temperatures as low as 2500°K. For temperatures in the neighbourhood of 3200°K, densities as low as 0·05 standard can be measured. Other wave length windows may be used to extend the range of measurement, provided the flash-lamp intensity is sufficient to provide tolerable signal-to-noise ratios.

In terms of the application of this technique to other aerodynamic systems, such as tunnels and nozzles, it is of real importance to be able to predict the absorptions for densities and pathlengths other than those at which the calibrations are made. Such calculations require detailed knowledge of the number and spacings of the transitions effective in each window, the corresponding line strengths, and the dependence of the line shape on density and temperature. These parameters have been measured in the course of the study with the large Littrow spectrograph[4], and the calculations are presently being made. Preliminary calculations indicate that the shape of the transmission–temperature curve is reasonably predictable on the assumption of a smoothed absorption coefficient over the window wave length interval.

It would be most advantageous to obtain the temperature and density of the gas uniquely in a single measurement. At present, one or the other can be obtained if another independent measurement is available to give another relationship between temperature and density. Within the accuracy of the present system, the density dependence is too similar in the different channels, and allows only approximate values to be obtained for the density of the gas.

Experiments with the radiation probe currently in progress are aimed at establishing more closely the density–temperature–pathlength limitations of the probe in pure oxygen, which will allow better comparison to be made with the theoretical transmission calculations. In addition, experiments with air are being planned which will determine the effects of possible absorption by the gamma system of NO, and which will establish the practicability of the probe for the measurement of the temperature of air in hypersonic flow situations.

The author is pleased to acknowledge the contributions of Dr. C. E. Treanor and Miss Marcia Williams to this research.

REFERENCES

1. J. G. Clouston, A. G. Gaydon and I. I. Glass, *Proc. Roy. Soc.* A**248**, 429 (1958).
2. H. C. Wolfe, Editor, *Temperature—its Measurement and Control in Science and Industry*. Reinhold, New York (1955).
3. W. H. Wurster, C. E. Treanor and H. S. Glick, *J. Chem. Phys.* **29**, 250 (1958).
4. C. E. Treanor and W. H. Wurster, *Measured Transition Probabilities for the Schumann-Runge System of Oxygen*, to be published.

THE USE OF MODULATED ATOMIC-BEAM TECHNIQUES FOR THE STUDY OF SPACE-FLIGHT PROBLEMS*

G. S. HOLISTER,† R. T. BRACKMANN and W. L. FITE
General Atomic Division of General Dynamics Corporation, San Diego, California

Abstract—At altitudes in excess of 70 km, dissociation of the atmospheric gases occurs because of solar radiation. Above 120 km, atomic oxygen is a major constituent of the atmosphere, and in the exosphere and in interplanetary space the atmosphere is largely atomic hydrogen. The drag on satellites and other objects in the upper atmosphere is necessarily more complicated than in the lower atmosphere, which is composed of chemically stable systems, for in addition to thermal accommodation and the angular distribution of particles reflected by vehicle skins, it is necessary to consider (1) the reassociation of atoms into molecules at the surface, (2) the manner in which energy of reassociation is divided between kinetic energy of the newly formed molecules and surface heating and (3) the chemical reactions between the atomic atmosphere and the surface material of any vehicle. Under very-high-altitude flight conditions, the pressure is sufficiently low that the free molecular flow regime is realized, and the speed of the gas relative to the vehicle is of the order of 10^5 cm/sec.

For investigations of atom-surface interactions under these conditions, the use of beams of hydrogen and oxygen atoms is particularly appealing. However, a basic difficulty resides in tracing an atomic beam of number density of the order of 10^8 atoms/cm^3 through the residual gas of number density of the order of 10^{10} molecules/cm^3 (corresponding to a pressure of $2{\cdot}5\times10^{-7}$ mm Hg) in a laboratory vacuum system. This difficulty is overcome by modulating the atomic beam; in the present case, this is done by mechanically interrupting it at a frequency of 100 c/s. Under these conditions, any effect arising from the beam may be identified by its occurring at the modulation frequency and in a specified phase. Using this modulation technique, it becomes possible to use mass-spectrometric detection of the beam, since the electron-impact ionization cross-sections for hydrogen and oxygen atoms are known.

Two types of experiments will be discussed. In the first, an incident beam impinges on a surface and the particles leaving the surface are examined by means of a mass spectrometer. By varying the incident beam and/or the surface temperature, thermal accommodation coefficients are determined for a variety of surfaces and gases. Using an incident atomic beam, the probability that an atom will rebound from the surface as a free atom is measured, and from examination of the reflected molecular signal, information on the probability of reassociation at the surface is obtained.

In the second type of experiment, the atomic beam, which is monitored mass-spectrometrically, is allowed to strike a surface placed on a torsion balance, and a momentum transfer is measured directly. In these experiments, the atomic-beam apparatus is used as an atomic wind tunnel; when a hydrogen-atom beam from a furnace source operating at 3000°K is used, the case of a high-altitude satellite is fairly closely duplicated.

Results of a number of experiments using these techniques are presented.

* This research was supported by the United States Air Force through the Air Force Office of Scientific Research of the Air Research and Development Command under Contract No. AF49(638)-356. Reproduction in whole or in part is permitted for any purpose of the United States Government.

† Present address: The Budd Company, Instruments Division, Phoenixville, Pennsylvania.

1. INTRODUCTION

The recent achievements in the fields of upper-atmosphere and interplanetary flight have re-emphasized the need for a comprehensive analysis of the nature of the surface reactions which occur when atomic oxygen and hydrogen impinge on a solid surface. In this respect, an

apparatus which can reproduce the conditions of pressure, relative velocity and gas dissociation which will be met by a vehicle in the upper atmosphere must of necessity be a powerful research tool of great value in this field.

Such an apparatus is the modern atomic-beam machine—in particular, those types that use the modulation techniques which have been developed recently.

For the past 2 years, modulated-beam techniques have been used at General Atomic and have been found widely adaptable to a variety of problems. The specific problem which will be discussed here is the study of surface reactions of dissociated gases with surfaces. This problem has been under investigation at General Atomic for approximately 12 months on behalf of the Air Force Office of Scientific Research. The initial research was intended as a preliminary survey of the types of reactions which occur when a surface is travelling through a partially dissociated medium which is in a state of free molecular flow, as in the case of satellites. The investigation has therefore been concentrated (1) on developing techniques for the measurement and evaluation of data and (2) on obtaining a broad idea of the relative magnitude and importance of the types of phenomena which occur.

The following processes are representative of the problems amenable to investigation by atomic-beam techniques:

(1) The angular distribution of reflected particles.
(2) Energy interchange between neutral particles and the surface, as measured by the thermal accommodation coefficient.
(3) The reassociation of atoms into molecules at the surface.
(4) The manner in which energy of reassociation (of the order of 5 eV/molecule for H_2 and O_2) is divided between kinetic energy of the newly formed molecule and surface heating.
(5) Any chemical reactions which may occur.

2. APPARATUS

The fundamental problem in working with beams of chemically unstable particles, such as free atoms, is to distinguish clearly the effects arising from the particles in the beam from those associated with the molecules of the residual gas. Mass-spectrometric monitoring of beams of neutral particles both incident upon and reflected from a surface is obviously a very powerful technique, but a basic signal-to-noise difficulty is encountered. Since the neutral particles must be ionized by an atomic-collision process (ionization by electron impact), the signal is proportional to the *number density* of particles in the beam, and the number densities commonly encountered are of the order of 10^8 particles/cm^3. Although this is adequate to give workable signals, there is also a much larger signal arising from ionization of the residual gas in the vacuum chamber (a pressure of $2{\cdot}5 \times 10^{-7}$ mm Hg, corresponding to a number density of 10^{10} molecules/cm^3). The fact that a diffusion-pumped vacuum is subject to pressure drifts, bursts and low-frequency fluctuations all but precludes the use of d.c. beam techniques when normally gaseous substances are used.

However, because the pressure fluctuation spectrum in usual vacuum systems decreases rapidly with increasing frequency, the signal-to-noise ratio can be made quite favorable by the use of modulated-beam techniques. In the present study, the neutral beam was mechanically chopped at a frequency of 100 c/s and the ionizing electron beam was run d.c. Under these circumstances, the signal associated with the neutral beam occurs at the modulation frequency and in a specified phase, while the background signal is d.c. (plus some noise at the modulation frequency). The two signals can then be cleanly separated electronically, and effects due to the atomic beam become readily discernible.

Furthermore, since the cross sections for electron-impact ionization of the molecular gases are known[1] and the ionization cross sections for both atomic hydrogen[2] and atomic oxygen[3] have recently been determined, the mass-spectrometer signal strengths provide quantitative measurements of processes under study. Therefore, hydrogen and oxygen atoms may be used as readily as molecules.

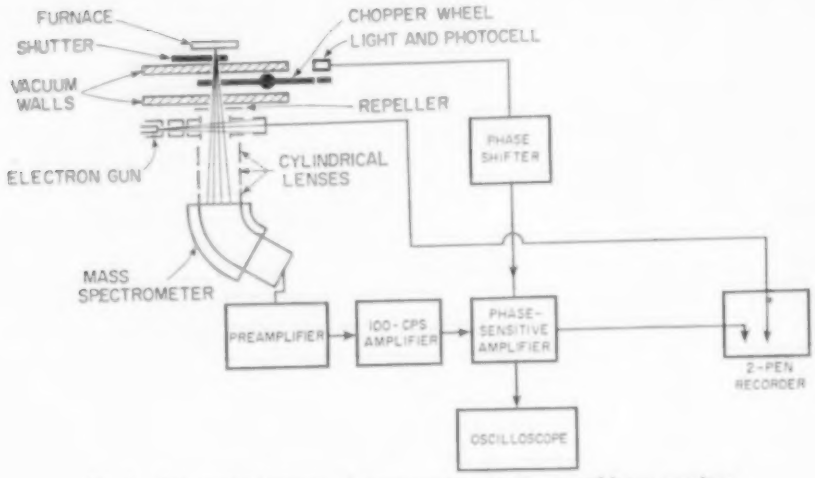

Fig. 1. Schematic diagram of mass-spectrometric neutral-beam monitor.

Fig. 1 shows schematically the experimental arrangement for the production and mass-spectrometric monitoring of a partially dissociated beam. The beam source is in the first of three differentially pumped chambers. After passing through a slit into the second chamber, the beam is interrupted by a rotating, toothed chopper wheel. It then proceeds into the third vacuum chamber, where any given experiment is carried out. For monitoring purposes, a d.c. electron beam crosses the neutral beam, ionizing about 1 particle in 10^6, and these ions are taken into a small sector-magnetic-field mass spectrometer. The mass spectrometer circuitry consists of (1) a preamplifier for lowering the impedence of the voltage signal developed by the ion current's passing throug a 10^{10}-Ω resistor, (2) a narrow band-pass amplifier, (3) a phase-sensitive detector and rectification stage, and (4) a d.c. recording potentiometer. The phase reference signal is derived from a light-and-photocell unit mounted at the chopper wheel.

Fig. 2 shows schematically a cross section through the machine. The atomic beam is produced by either a radiofrequency gas discharge source or a tungsten furnace. The largest section contains the experimental equipment and normally is pumped down to 10^{-7} mm Hg.

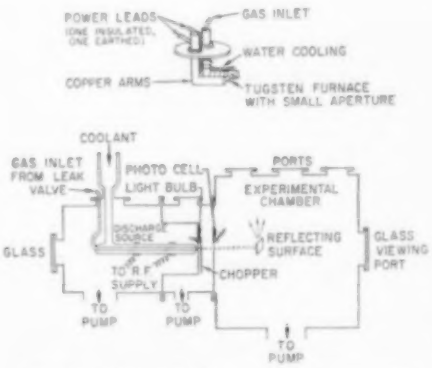

Fig. 2. Schematic of atomic-beam apparatus.

3. EXPERIMENTS

Generally, in using atomic beams to study the interaction of atoms with surfaces, each experiment requires a detector specific to the type of process under study. In this paper, experiments utilizing two types of detectors are described. The first detector is a mass spectrometer which monitors both the incident beam and the beam reflected from a solid surface. The second is a torsion balance, which is used to measure momentum transfer directly.

Experiments using mass-spectrometric detection

When mass-spectrometric detection of a

neutral beam is used, three types of information are obtained: (1) the chemical species in the beam; (2) the direction of travel of each chemical species, which is determined by moving the mass spectrometer; (3) the number density (n_i) of each neutral-particle species crossing the ionizing electron beam. If, in addition, the current density, J_i, or the mean velocity, v_i, of each species ($J_i = n_i v_i$) were measured simultaneously, all the most important information on the beam would be obtained. Even without knowledge of J_i or v_i, however, considerable information can be obtained from the mass spectrometer alone.

In our experiments using a mass spectrometer to detect reflected beams, the experimental arrangement shown in Fig. 3 was used. The

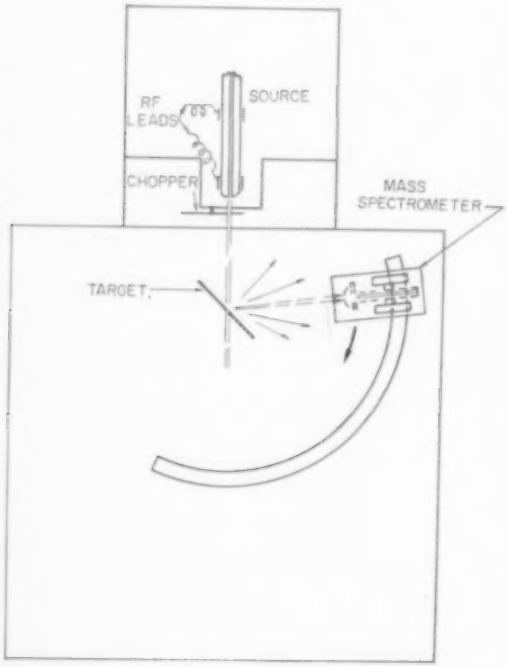

Fig. 3. Layout of experimental chamber for mass-spectrometric readings.

mass spectrometer moved on a circular arc about the point of impingement of the beam on the surface in question. To date, these surfaces have included the more common metals and plastics. In order to monitor the neutral incident beam, a small hole was made in the surface; when the mass spectrometer was placed directly behind the surface, the small fraction of the incident beam which passed through the aperture was detected and analysed. A corresponding analysis of the reflected beam could then be compared with that of the incident beam. By using this technique, the following representative results were obtained.

Angular distribution of reflected particles

Using common surfaces, the angular distribution of the reflected particles has been found in our experiments to approximate closely a distribution that varies as the cosine of the angle between the direction of observation and the normal to the surface, and that is independent of the angle of incidence. This agrees generally with the observations of others[4]. No specular bulges in the distribution have been observed, although on occasion a slight bulge in the direction of the incident beam, which may be instrumental in origin, has appeared. Most significant is the observation that reflected atoms and reflected molecules follow the same angular distribution under all experimental conditions used.

Mass analysis of reflected beams

When partially dissociated beams of both hydrogen and oxygen impinge on surfaces, the reflected beams have to date contained no discernible masses except the atoms and molecules of the incident gas. In particular, using surfaces in the vicinity of room temperature, no volatile oxides or hydrides of the surface material have been detected. From the noise level of the mass spectrometer, this implies that the probability of formation of volatile compounds with the surface material is less than or of the order of 1 per cent.

Thermal accommodation coefficients of molecules

In order to extract certain types of information on atom-surface interactions when the mean incident-atom speed differs from the mean particle speed associated with a particular target

surface temperature, and when some molecules accompany the atoms in the beam (which is always the case with oxygen from a gas-discharge source), it is necessary to know how energy is exchanged between the surface and the molecules. It is convenient in these experiments to define absolute temperature in terms of mean speed by the relation $T=\pi/8 \cdot m\bar{v}^2/k$, where m is the particle mass, $\bar{v}$ is the mean speed, and k is Boltzmann's constant. For a fixed current density of a single species in the beam, the mass-spectrometer signal is inversely proportional to the mean speed and therefore to the square root of the absolute temperature. Under these circumstances, the usual definition for the thermal accommodation coefficient, $\alpha=(T_B-T_R)/(T_B-T_S)$, where T_B and T_S are the temperatures of the incident beam and surface, respectively, and T_R is the effective temperature of the reflected beam, may be used as an index for energy exchange between a particle and a surface. By using a fixed beam temperature and a variable surface temperature and by noting the mass-spectrometer signal, this thermal accommodation coefficient may be readily determined. Fig. 4 shows the results of such a measurement using a room-temperature beam of H_2 incident on a copper surface. Results of this type of measurement using a variety of gases and surfaces have been generally in satisfactory agreement with results of other types of measurements, where these have been available. The wide range of independent variation of surface and beam temperatures is obvious.

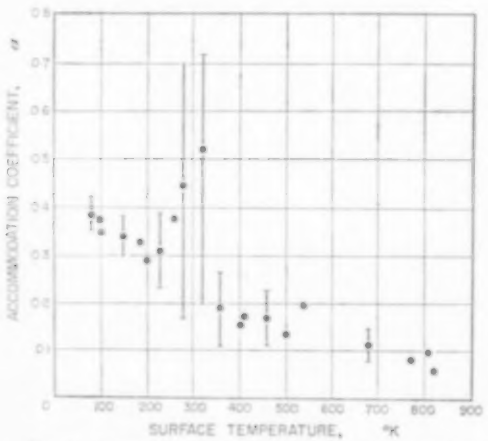

Fig. 4. Thermal accommodation coefficient of H_2 at 300°K on copper.

Probability of reflection of atoms striking surfaces

The probability that an atom will reflect as an atom after striking a surface when the beam and the surface are at the same temperature has been examined using the mass-spectrometer detector. In this experiment, a comparison of the reflected- and direct-beam signals, using a pure molecular beam, determines the necessary geometrical factor. By using this factor and the direct and reflected atomic beam signals, when the incident beam is dissociated, one obtains the "bouncing probability" immediately. This probability has ranged from 60 per cent to 80 per cent for room-temperature hydrogen and oxygen atoms reflected from a number of common laboratory surfaces. It is not possible from mass-spectrometric measurements alone to determine whether those atoms which do not reflect reassociate into molecules or combine chemically with or are adsorbed by the surface.

Branching of dissociation energy in reassociation

Although in experiments on the reflection of atoms from surfaces it is not possible to determine whether the atoms which are lost reassociate into molecules or combine with the surface, it is possible to set an upper limit on the fraction of the dissociation energy which appears as kinetic energy of the new molecules formed by reassociation at the surface, when identical beam and surface temperatures are used. From the measured degrees of dissociation of the incident and reflected beams and the geometrical factor determined in studies of the atom reflection probability, it is straightforward to determine the loss in molecular number density of the reflected gas that results from the impact of the atomic beam on the surface. Since this loss in number density occurs either because of sticking of some particles to the surface or increased speed of the newly formed molecules, and both processes decrease the mass-spectrometer reflected mole-

cular signal, an upper limit on the fraction of dissociation energy appearing as kinetic energy can be set. For atomic hydrogen on copper, this upper limit is 3 per cent. Evidently at least 97 per cent of the reassociation energy goes into heating the metal surface.

Experiments using torsion balances

In the measurement of transfer of momentum when atoms and molecules strike surfaces, it is convenient and most direct to use a torsion balance and measure force directly. Suspending actual models of space vehicles before the beam and using the apparatus as an atomic wind tunnel actually rather closely duplicates certain problems expected in space flight. This is particularly the case when a thermal-dissociation source for atomic hydrogen is used, because the mean speed of such atoms at 3000°K is almost identical to satellite speeds. For the purposes of this paper, it is appropriate to consider a simpler type of experiment, namely, the momentum transfer by atoms normally incident on surfaces.

When a gas beam with a current of the i^{th} species, I_i, having a molecular mass m_i and velocity v_i, strikes a surface, the momentum carried to the surface per unit time by the incident beam is $P_{inc} = \Sigma I_i m_i v_i$. The total force at the surface is this term plus a similar term describing the beam reflecting from the surface. The velocity $v_i \propto (T/m_i)^{1/2}$, where T is the absolute temperature of the beam and is normally the same for all particle species in the beam. Thus a parameter of interest is $P_{inc}/(T)^{1/2} \propto \Sigma I_i m_i^{1/2}$. In the absence of thermal accommodation and chemical rearrangement when the particles strike the surface, and using a single species in a beam of constant mass flow, $\theta/T^{1/2}$, where θ is the angular deflexion of the torsional pendulum, should be independent of temperature for fixed mass flow. Any deviations of this quantity from constancy are indicative of the surface collision phenomena.

In Fig. 5, two curves of $\theta/T^{1/2}$ are shown for hydrogen impinging on pyrex-glass and platinum surfaces at room temperatures. As the gas temperature increases above room temperature, the drop in the curve is indicative of thermal accommodation of the molecules. When the temperatures at which dissociation begins to occur are reached, a rise begins which continues up to the temperature at which the gas is almost completely dissociated (i.e. at least 98 per cent), where a plateau is reached. The fact that the plateau is somewhat higher with glass surfaces

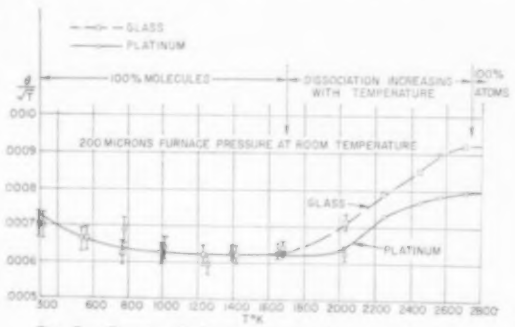

Fig. 5. Torsion-balance results (see text). Units on the ordinate are arbitrary.

than with platinum surfaces is consistent with platinum's being better able to catalyse the reassociation of the atoms at the surface. The fact that the value of $\theta/T^{1/2}$ using the glass surface is almost $2^{1/2}$ times larger for atomic than for molecular hydrogen is consistent with the assumption that the recombination probability and the thermal accommodation coefficient of 3000°K atoms striking room-temperature pyrex surfaces are quite small.

4. SUMMARY

Although the use of modulated-atomic-beam techniques for the study of the physical and chemical processes occurring when gaseous molecules and radicals interact with solid surfaces is in its infancy and considerable experimental refinement is required, it appears that these techniques offer a powerful method for such studies. Both the fact that a single macroscopic collision of a particle against a surface is under study and also the intrinsic cleanliness of atomic-beam techniques usually contribute to quite straightforward interpretation of experiments. With the addition of other detectors and sources complementing those

which are now in use, it appears likely that a number of complicated physical and chemical processes in atom-surface collisions can be isolated for experimental study.

Acknowledgement—We are indebted to Mr. David G. Hummer and Mr. J. A. Rutherford for their parts in the construction of the apparatus.

5. DISCUSSION

I. AMDUR: At the pressures in your target chamber, about 2×10^{-7} mm, one would expect your targets to have an adsorbed gas film, probably a monolayer, and that the observed accommodation coefficients would be more indicative of the beam particle–adsorbed gas system than of the beam particle–target substrata system.

G. HOLISTER: That is correct. The experiments were intended to simulate conditions of a surface covered by an absorbed gas layer subject to bombardment by thermal velocity atomic species.

It is interesting to note that at low temperatures where the adsorbed gas layer would be relatively undisturbed, the effective momentum accommodation coefficient for a glass and platinum surface are indistinguishable. This is consistent with certain free molecule thermal conductivity measurements which lead to essentially the same thermal accommodation coefficients on platinum, nickel and tungsten wires for a given gas when care has been exercised to retain an absorbed gas layer on the wires.

F. KAUFMAN: There is much information in the recent literature on the efficiency of various surfaces for the recombination of atomic oxygen, due mostly to the work of Linnett *et al.* at Oxford. For clean pyrex glass in particular, the efficiency is known to be between 10^{-4} and 10^{-3}. The value reported in this paper for the fraction of O atoms reflected from the surface, $0{\cdot}69 \pm 0{\cdot}20$, should therefore be 1·00, i.e. the errors are greater than estimated and there are few if any surfaces whose recombination efficiency is large enough to be measured with fair accuracy by this method.

W. FITE: It was very annoying that the apparent probability of reflection of both atomic hydrogen and atomic oxygen from pyrex surfaces, as determined in these experiments, is so low. It had been presumed that taking these values as 1·00, as suggested by the results of Linnett, Wise and a number of other investigators, would be a reasonable boundary condition on the whole series of experiments. However, not only were atoms missing from the reflected beam, but in the case of atomic hydrogen where the incident beam dissociation was sufficiently high to allow meaningful measurements on the molecules in the reflected beam, almost all of the atom loss showed up in an enhanced molecular content. Putting it another way, the dissociation fractions of the incident and reflected beams were markedly different, while the total mass flows in the two beams were not.

Perhaps the explanation of the differences in the results of sidearm discharge experiments of Linnett and others and those of this experiment lies in the fact that the absorbed gas layers were probably quite different. In the former experiments done at quite high pressures, the adsorbed gas was probably the species under study, while in our experiments the rate of surface impingement of gas from the beam is comparable to that from the background gas in the vacuum. Thus, it seems likely that the absorbed gas layer in our experiments was primarily nitrogen irrespective of the type of atom beam that was being run. At the present time we have no other hypothesis to offer.

In regard to accuracy of measurements of apparent reflection probabilities, the use of longer signal integration times can, we believe, reduce the experimental uncertainty in any given measurement to 1 or 2 per cent.

REFERENCES

1. J. T. TATE and P. T. SMITH, *Phys. Rev.* **39**, 270 (1932).
2. W. L. FITE and R. T. BRACKMANN, *Phys. Rev.* **112**, 1141 (1958).
3. W. L. FITE and R. T. BRACKMANN, *Phys. Rev.* **113**, 815 (1959).
4. F. C. HURLBUT, *J. Appl. Phys.* **28**, 844 (1957).

EXCITATION OF THE AURORAL GREEN LINE IN NITROGEN AFTERGLOW

R. A. YOUNG and K. C. CLARK
University of Washington, Seattle, Washington

Abstract—Production of the auroral green line of OI (^1D–^1S, 5577 Å) is observed during long (30 sec) afterglows in a static system containing nitrogen and small amounts of oxygen. Relative to the intensities of the N_2 1st positive bands, the measured intensities of 5577 Å and the NOβ bands increase with time. The long period of observation definitely eliminates the initial discharge as a possible source of the metastable oxygen atoms, and their chemical excitation in the afterglow volume is established. A probable process consistent with observations is that involving collision of N atoms with vibrationally excited NO molecules. This mechanism is discussed as a possible source of 5577 Å in the airglow.

Excitation in the airglow of the auroral green line of atomic oxygen (^1D–^1S, 5577 Å) is generally regarded as due to luminescent chemical reactions in the atmosphere. Possible excitation reactions have been proposed[1] involving atmospheric constituents known to exist at the observed heights of the airglow. Laboratory chemical excitation of this line has not been clearly distinguished from production in the initial discharge. Intense sources of this line, such as those of McLellan and Shrum[2] and of Noxon[3] undoubtedly rely upon electron collisions to excite the atomic oxygen. The 5577 Å line is often observed in active nitrogen generated in a flow system[4, 5], but these observations are limited to such an early portion of the decay that many of the observed ^1S atoms, whose radiative lifetime is about 1 sec[6], are those formed in the discharge by non-chemical processes.

The present observation of the auroral green line during the later portions of the nitrogen afterglow is the first verifiable instance of its chemical excitation. A production mechanism which is consistent with the results will be presented and its possible role in the upper atmosphere indicated.

1. EXPERIMENT

The experimental equipment is the same as that described in a previous paper[7] dealing with the 1st positive ($B^3\Pi - A^3\Sigma$) bands of the nitrogen afterglow. It employs a very fast spectrograph of low resolution, equipped with a servo-controlled aperture moving along the normal slit. This generates a time-resolved spectrum of uniform density but non-uniform time scale encompassing 30 sec of decay in a static gas system. This aperture arrangement effectively utilizes the afterglow radiation; more importantly, it emphasizes relative changes among the spectral components. Their explicit time dependence can be derived from continuous records of aperture position vs. time made throughout the long (1/2–12 hr) cyclic exposures. Observations were made in a 12 l. bulb coated internally with deliquescent phosphorous pentoxide to reduce surface reactions and externally with magnesium oxide to increase the light collection efficiency.

The 5577 Å line was emphasized by leaking oxygen into the system, already at about 1 mm Hg, at a rate corresponding to a pressure rise rate of 0·001 mm/hr. A liquid nitrogen trap was necessary to remove nitrogen oxides and other impurities from the gas volume during the long exposures.

Relative measurements of photographic exposure (intensity × time) along a spectral line were made using calibrated densitometer traces. The moving aperture was 1/20 of the full spectrum height. The spectrum was covered in ten separate densitometer sweeps of equally

spaced intervals, from which, on correlation with the continuously recorded aperture motion, curves of exposure vs. time were constructed. The servo system was adjusted to keep the integrated visible 1st positive band of nitrogen at constant exposure. Other bands observed deviating from uniform density are thus decaying in a manner different from the 1st positive system.

2. RESULTS

Figure 1 is a reproduction of a typical time-resolved afterglow spectrum of the N_2 1st positive system. The densities of the individual bands are approximately uniform along the path of the moving aperture[7] and collectively provide the reference curve for N_2 shown in Fig. 3.

Figure 2 is a reproduction of a typical spectrum made under the same conditions as before but with about 100 times the exposure in order to show weaker components. These features are the red and violet systems of CN, the β bands of NO and the auroral green line.

Results of densitometer measurements are displayed in Fig. 3. The photographic exposures are plotted logarithmically to permit arbitrary displacement into groups of similar time dependence. The slight variation for the N_2 1st positive bands is attributable to non-uniform illumination and can be taken into account when necessary. The NO bands decay more slowly than the N_2 bands. The 5577 Å line decays similarly with the NO bands, showing a definite growth relative to those of N_2. In this instance the CN bands also show a similar decay, but in other experiments their behavior was found variable.

The identification of the feature near 5577 Å as the auroral green line is based on the following groups of evidence: (1) Its strong occurence coincides critically and reasonably with the addition of suitable traces of oxygen. (2) From calibrations of the low resolution time-resolved spectrograms its wave length is measured to be 5577 ± 10 Å and its image width is less than that of any other afterglow features and corresponds to that of known line sources. Its position coincides with the green line produced by a Tesla discharge in the observation

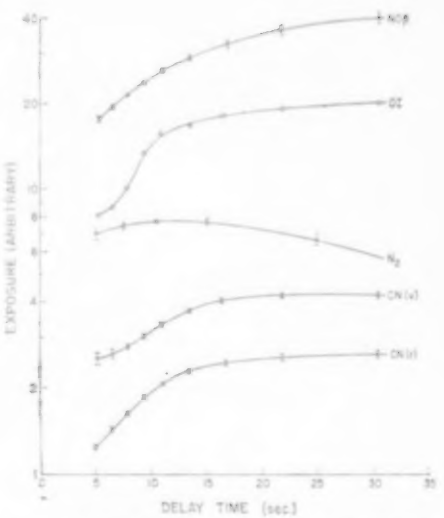

Fig. 3. Comparison of the time dependence of various afterglow emissions shown in Figs. 1 and 2. Curves represent groupings as to source, with the photographic exposures normalised within each group at $t = 10$ sec; the separation between groups is arbitrary. This is not a plot of intensity decay because of the common variation in length of exposure, but relative changes between groups are proportional to relative changes of intensity. All features identified in Figs. 1 and 2 except the very weak first positives were plotted and used to set the indicated deviations.

bulb. (3) From the spectrogram of Fig. 4 the wave length is found to be $5577{\cdot}4 \pm 0{\cdot}1$ Å, in agreement with the known value of 5577·35 Å. This corroborative spectrum was taken with crossed echelle and ordinary reflection gratings and a 2 in. $f/1{\cdot}4$ lens. It represents similar conditions to those of the previous spectrogram but is limited to that portion of the afterglow following the formative discharge by more than 20 sec in order to avoid any possibility of survival of original metastable oxygen atoms.

Evidence indicates that the green line is emitted from the volume and not the walls. Intensity measurements of the N_2 bands by suitably collimated photomultipliers show that little, if any, of this associated radiation comes from the wall. If the green line were produced at the wall, it might be highly perturbed, as is the green wall continuum observed by Noxon[3] in systems producing the green line in the

Licensed under CC BY 4.0

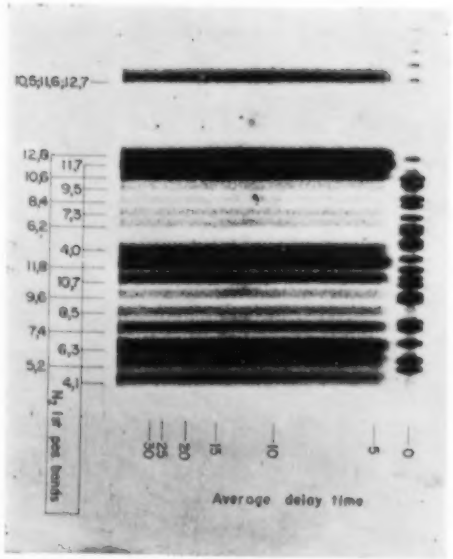

Fig. 1. Time-resolved spectrum of 1st positive bands in N_2 afterglow at 1 mm Hg pressure. Band identifications are marked, and wavelength increases to the right in all spectra. The non-uniform length of exposure is indicated by the scale of average elapsed time since the discharge, including an initial delay. This exposure time control produces the approximately constant density shown in Fig. 4.

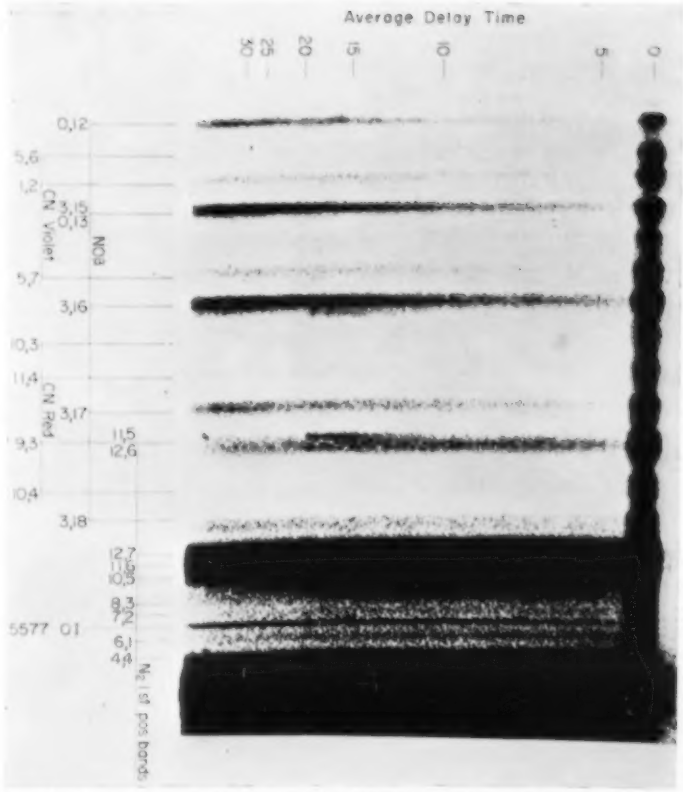

Fig. 2. Strongly exposed time-resolved spectrum showing the progressive increase of OI (5577 A) and weak NO_δ and CN band systems relative to those of N_2. The time scale is identical with that of Fig. 1.

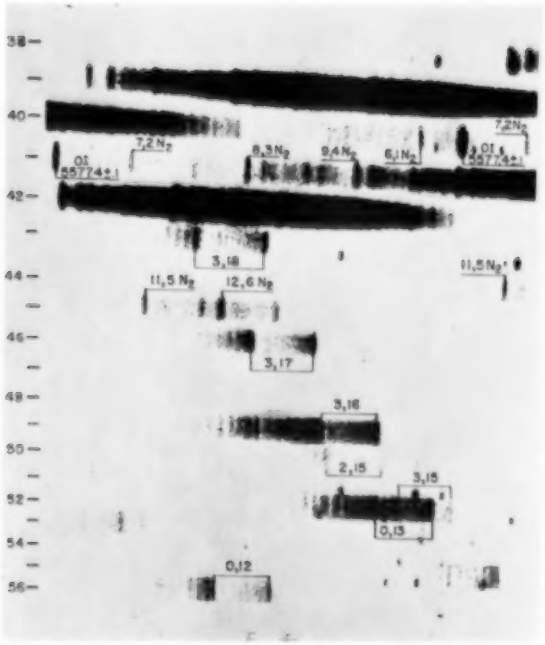

Fig. 4. Echelle spectrogram of nitrogen afterglow after 20 sec of decay, showing strong green line emission. Spectrum orders are numbered at the left margin, and bands of N_2 and NO_β are identified. Only those of N_2 are labelled. The 5577 Å line is shown in two orders.

volume and as are the shifted emission lines of afterglows condensed on extremely cold surfaces[6]. However, the absence of any observable wave length shift in Fig. 4 implies a volume emission.

3. INTERPRETATION

Since the radiative lifetime of the ^1S state of atomic oxygen is approximately 1 sec and Noxon[3] has found that approximately 10^8 collisions are necessary to deactivate this state, the ^1S state then has time to radiate; in any case, observations on the Tesla discharge experimentally establish this fact.

Several processes are conceivable as excitation mechanisms for the oxygen line. One may first consider the spin disallowed reaction

$$NO(^2\Pi, v \geqq 4) + N(^4S) \rightarrow N_2(^1\Sigma) + O(^1S). \quad (1)$$

Since the similar reaction

$$NO(^2\Pi) + N(^4S) \rightarrow N_2(^1\Sigma, v \text{ large}) + O(^3P) \quad (2)$$

occurs in almost every collision between the reactants[9], reaction (1), although inhibited by Wigner's spin conservation rule, still may occur with an observable rate when reactant populations are comparable. The relative importance of reactions (1) and (2) is set by the fixed specific reaction rates and by the ratio of concentrations of $NO(v \geqq 4)$ and $NO(v < 4)$. The following reaction, observed in the afterglow[10], produces the emission of NO β, γ bands, some of whose strongest transitions terminate on the $v \geqq 4$ levels required in reaction (1):

$$N(^4S) + O(^3P) + M \rightarrow NO(B^2\Pi \text{ or } A^2\Sigma) + M$$
$$NO(B^2\Pi \text{ or } A^2\Sigma) \rightarrow NO(X^2\Pi) + h\nu\,(\beta \text{ or } \gamma) \quad (3)$$

Published intensities of the β and γ bands of NO in active nitrogen given by Robinson and Nicholls[11] show that almost all of the total radiation populates the $v \geqq 4$ levels of the ground state of NO, with the $v = 5-9$ levels fairly uniformly populated.

In the cycle of reaction (3) followed by both (1) and (2), atomic oxygen acts as a catalyst for nitrogen recombination. Atomic nitrogen survives in these experiments only at very small concentrations of atomic oxygen, or, equivalently, of nitrogen oxides.

An alternative source of NO ($v = 6$) is offered by the reaction,

$$N(^4S) + O_2(^3\Sigma) \rightarrow NO(^2\Pi, v = 6) + O(^3P). \quad (4)$$

Although the rate of this two-body reaction is known to be small[9], it may become important compared to the three-body reaction (3) when sufficient molecular oxygen is present. The cyclic reactions (1), (2), and (3) lead to the following dependence of intensity ratios on concentrations:

$$I(O)/I(N_2) \sim [O]/[N] \sim I(NO\beta)/I(N_2). \quad (5)$$

If [O] is constant, these ratios should increase with time in inverse proportion to [N]. Between times 10 and 30 sec this concentration was measured to decrease by a factor of 4·5, using the square root of the 1st positive intensity recorded by a photomultiplier during the exposure. However, Fig. 3 shows an increase by a factor of only 1·7, indicating that [O] is slowly decreasing at a rate somewhat less than that of [N].

Equation (5) implies that the ratio $I(O)/I(NO\beta)$ remains fixed. However, if NO ($v = 4$–9) is depopulated by collision or radiation, then this intensity ratio will decrease during the afterglow decay because the relaxation time interval set by reaction (2) increases as [N] decreases. Between the times of 10 and 30 sec shown by Fig. 3, this ratio decreases by 20 per cent, while the interval during which relaxation can occur increases by a factor of 4·5. If one assumes the reasonable values of $[N] = 0{\cdot}001\,[N_2]$ at 10 sec and unity as the probability for reaction (2), the relaxation of NO can conveniently be described as exponential with a decay time of 2·6 msec. The radiative lifetime of NO ($v = 4$–9) is longer than that of the $v = 4$ level, which is 4·1 msec, as estimated from the $\Delta v = 1$ absorption bands[17]. Therefore, if the OI (5577 Å) line is excited by reactions (1) and (2), these results imply that at least 2×10^4 collisions with N_2 are needed to deactivate NO ($v = 4$–9).

Another possible excitation mechanism for the green line involves three-body atomic collisions, as suggested by Chapman[12],

$$O + O + O \rightarrow O_2 + O(^1S) \quad (6)$$
$$N + N + O \rightarrow N_2 + O(^1S). \quad (7)$$

The curves shown in Fig. 3 offer the possibility of ascertaining the relative importance of these reactions in the afterglow. Reactions (6) and (7)*, together with the known excitation mechanisms for the NOβ and N_2 1st positive bands, lead to the following relations respectively,

$$I(O) \propto [O]^3 \propto I^3(NO\beta)\, I^{-3/2}(N_2) \quad (8)$$

$$I(O) \propto [N]^2\,[O] \propto I(NO\beta)\, I^{1/2}(N_2). \quad (9)$$

One would expect because of the inequality [N]>[O] that reaction (7) would predominate over reaction (6) as, in fact, can be shown by forming the quantities indicated in equations (8) and (9). Thus, equation (8) predicts a much steeper rise of I(O) than is shown in Fig. 3, while equation (9) generates a curve which satisfactorily matches that of I(O) and also is congruent with that of I(CN red). The congruence with I(CN) is of unclear significance and emphasizes that I(O) may still arise not from reaction (9) but from another process common also to I(CN). This possibility is strengthened by the similarity of energies required for these excitations. If, however, reaction (7) does produce I(O), some transitory quenching of O(^1S) is required in the early stages of decay. This is not unreasonable in consideration of the known relaxation efficiency of N_2[15].

4. RELATION TO THE AIRGLOW

For many years the triple collision of oxygen atoms[14] has been accepted as the only energetically feasible excitation mechanism for 5577 Å in the airglow, although no corroborative measurements are available. The reaction sequence (4) followed by (1) may also contribute significantly to the observed green line intensity.

Results from recent rocket and sea level measurements of the green line in the airglow provide the following information: (1) Intensity of the 5577 Å radiation is[13] typically $300–600 \times 10^6$ photons/cm² sec. (2) The radiation occurs in a relatively thin layer[14] between about 95 and 105 km. (3) It has a patchy, inhomogeneous distribution. Recent investigations have also determined the kinetic temperature of 240°K at 100 km and the following concentrations of the reactants:

$$[N_2] = 1{\cdot}2 \times 10^{13}/\text{cm}^3, \quad [O_2] = 4 \times 10^{12}/\text{cm}^3.$$

Although the ratio $[N]/[N_2]$ is uncertain, a reasonable estimate is 10^{-2}, i.e. $[N] = 1{\cdot}2 \times 10^{11}/\text{cm}^3$. With the known rate of reaction (4) and the above values of concentrations, one can compute that NO ($v = 6$) is produced at the rate of $3 \times 10^6/\text{cm}^3$ sec. Wigner's spin conservation rule may inhibit reaction (1) relative to (2) by a factor of about 10^{-2}. Reaction (4) followed by reaction (1) would therefore lead to 200 photons/cm³ sec at 5577 Å. Uncertainties in [N] and in the effect of Wigner's rule permit flexibility in this estimate by an order of magnitude. If the green line is radiated uniformly from a 10-km layer, this rate produces 200×10^6 photons/cm² sec, in remarkable agreement with the value measured in airglow.

Nitrogen atoms present at 100 km have been transported by large-scale atmospheric motions from their source at heights near 150 km. Such turbulent transport could lead to considerably inhomogeneous distributions of [N] at the emission height, in agreement with the observed patchy emission of the green line.

While the distribution of 5577 Å emission within the 10-km thick radiating layer cannot be predicted because of the unknown distribution of N, its upper extent will be limited through (4) by the lack of O_2 above the 100–120 km dissociation region, and its lower boundary will be set through (1) by the diminishing [N].

Any mechanism energetic enough to produce the O(^1S) state should also produce O(^1D) from which the red line at 6300 Å is radiated. Because the radiative lifetime of the red line is 100 times that of the green line, non-radiative deactivation may be important in determining the intensity and distribution of the former. In fact, the observed non-correlation of the 5577 Å and 6300 Å intensity and their differing heights of emission are consistent with the proposed excitation mechanism of 5577 Å and the quenching reaction

$$O(^1D) + O_2(X^3\Sigma, v=0) \rightarrow O(^3P) + O_2(b^1\Sigma, v=2) \quad (6)$$

* Conversations with W. J. Schade and C. A. Barth concerning the feasibility of reaction (7) are gratefully acknowledged.

proposed by Bates and Dalgarno[16]. Reaction (6) is decisive in determining the behavior of the oxygen red line while reaction (4) followed by (1) determines the behavior of the green line.

It should be possible to measure the distribution of N throughout the emitting layer from rocket observations of the green line when current experiments determine the exact rate of reaction (1) and the effect of other atmospheric constituents on the relaxation of NO ($v=5$).

5. DISCUSSION

W. ZINMAN: Have you observed any glows beside the first positive? I am referring particularly to the work of Tanaka.

Reply: In answer to Dr. Zinman's question, we have not observed other band systems of nitrogen although we have observed those of CN and NO. It appears that the conditions under which the 2nd positive bands of nitrogen occur are representative of a shorter and more energetic afterglow than the late Lewis–Rayleigh afterglow.

C. A. BARTH: I would first like to comment on Dr. Zinman's suggestion. W. J. Schade, working in Professor Kaplan's laboratory at the University of California, Los Angeles, has found the 2nd positive bands of nitrogen in a room temperature Lewis–Rayleigh nitrogen afterglow. This extends Tanaka's work who found these bands in a low temperature afterglow. I would also like to report some other work that Schade has done which supports the very fine work that Dr. Young has presented here. Schade first produced a very pure nitrogen afterglow in which the 5577 Å atomic oxygen line was not present. He then added nitric oxide to the nitrogen afterglow and then found that the 5577 Å band did indeed appear. This result substantiates Dr. Young's finding that it is a chemical source that excites the 5577 Å line in the nitrogen Lewis–Rayleigh afterglow. It may also be noticed that the chemical species involved in Schade's experiment are the same as those involved in Dr. Young's explanation of this phenomena. I would also like to ask Dr. Young what the effect of temperature was on his intensity vs. time studies of the various afterglows.

R. A. YOUNG: The comments of Dr. Barth are most interesting. Temperature effects of a single pulsed discharge in a static system are of a much smaller order of magnitude than those common in flow systems using a continuous discharge. Any temperature effects produced in our observation volume are minor, and they would completely decay after a few seconds.

C. A. BARTH: It is also true that the effect of a temperature decrease would be to decrease the intensity of the various glows in a static system. You, of course, found an increase so this cannot be due to changing temperature.

REFERENCES

1. D. R. BATES, *The Earth as a Planet* (edited by G. P. KUIPER) Chap. 12. University of Chicago Press, Chicago, Illinois (1954). This volume reviews the observations and theoretical considerations pertinent to the upper atmosphere.
2. J. C. MCLELLAN and G. M. SHRUM, *Proc. Roy. Soc.* **A114,** 1 (1927).
3. J. F. NOXON, *Active Nitrogen at High Pressure.* Thesis, Harvard University (1957).
4. U. H. KURZWEG, A. M. BASS and H. P. BROIDA, *J. Mol. Spectr.* **1,** 184 (1957).
5. M. BROOK and J. KAPLAN, *Phys. Rev.* **96,** 1540 (1954).
6. R. H. GARSTANG, *The Airglow and the Aurorae* (edited by E. B. ARMSTRONG and A. DALGARNO) p. 324. Pergamon Press, New York (1955).
7. R. A. YOUNG and K. C. CLARK, *J. Chem. Phys.* **32,** 604 (1960).
8. H. P. BROIDA and O. S. LUTES, *J. Chem. Phys.* **24,** 484 (1956).
9. G. B. KISTIAKOWSKY and G. G. VOLPI, *J. Chem. Phys.* **28,** 665 (1958).
10. F. KAUFMAN and J. R. KELSO, *J. Chem. Phys.* **27,** 1209 (1957).
11. D. ROBINSON and R. W. NICHOLLS, *Proc. Phys. Soc., Lond.* **71,** 957 (1957).
12. S. CHAPMAN, *Proc. Roy. Soc.* **A132,** 353 (1931).
13. E. R. MANRING and H. B. PETTIT, *The Threshold of Space* (edited by M. ZELIKOFF) p. 58. Pergamon Press, London (1957).
14. M. J. KOOMEN, R. SCOLNIK and R. TOUSEY, Ref. 13, p. 217.

15. M. NICOLET, *The Earth as a Planet* (edited by G. P. KUIPER) Chap. 13. University of Chicago Press, Chicago, Illinois (1954).
16. D. R. BATES and A. DALGARNO, *J. Atmos. Terr. Phys.* **4**, 112 (1953).
17. S. S. PENNER and D. WEBER, *J. Chem. Phys.* **21**, 649 (1952); B. L. CRAWFORD, JR., and H. L. DINSMORE, *J. Chem. Phys.* **18**, 983 (1950).
18. BAUER, KNESER and SITTING, *J. Chem. Phys.* **30**, 1119 (1959).

A STUDY OF THE RECOMBINATION OF ATOMIC OXYGEN BY MEANS OF THE FLASH SPECTRA OF THE SCHUMANN–RUNGE SYSTEM*

J. A. GOLDEN and A. L. MYERSON†
General Electric Company, MSVD, Philadelphia, Pennsylvania

Abstract—The recombination of atomic oxygen has been studied at temperatures not exceeding several hundred degrees above room temperature. The process has been followed by obtaining flash absorption spectra in the vacuum ultra-violet of the entire Schumann–Runge system of molecular oxygen as a function of time.

A third-order specific reaction rate constant of $1{\cdot}2\times10^{15}$ $(cm^3)^2/mole^2$-sec. has been obtained, for the reaction $O+O+M$, and vibrationally excited oxygen has been observed in only the first level of the ground state.

1. INTRODUCTION

The process of the recombination of atomic oxygen, and its rate, have occupied a position of major interest among the physical chemical parameters which have concerned aerodynamicists working in the field of hypersonic flow. The uncertainty in the rate has been sufficient to preclude precise calculations of heat transfer in re-entry boundary layers and has left unanswered other questions relevant to such boundary layers.

In spite of this, no work has been reported which involves direct observations of the complete recombination process. In the present research, it has been our object to directly follow and study the oxygen recombination process under carefully defined and controlled conditions, by actually measuring spectroscopically the change in concentration of the product of the reaction.

Because of the complexity of the process, it was decided that it was vital to observe as much as possible of the absorption spectra of the oxygen molecule rather than suffer limitations of a very narrow band width of absorption such as is incurred in photomultiplier studies. Thus it was elected to follow the flash absorption spectra of the entire Schumann–Runge system. This necessitated the development of a technique for making gas phase chemical kinetics studies in the vacuum u.v. It is appropriate at this point to describe briefly the essential features of the flash spectroscopic technique. The method utilizes a flash lamp to produce an emission continuum in the spectral region of interest. The radiation thus produced is passed through the gases in a reaction cell and an absorption spectrum is obtained of the species present in the reaction system. It is desirable to use a spectrograph to record photographically the spectrum over an extended wave length increment; however, many investigators[1–3] have successfully used light filters in conjunction with a photomultiplier detector to measure the change in absorption of a particular species.

The most important advantage of the present method is that the flash lamps used are of such intensity that quantitative measurements can be made during the time required for a single flash—this time is less than 250 μsec. It is possible, then, to synchronize the lamp to fire at a particular time after time zero of the reaction process and thereby obtain the concentration of the species present at that time. By taking a series of spectra at various times, it is possible to obtain concentration vs. time data from which the kinetics of the process can be

* This work was performed under the auspices of the U.S. Air Force, Ballistic Missile Division, Contract No. AF04(647)-269.

† Present address: Cornell Aeronautical Laboratory Inc., Buffalo 21, N.Y.

analysed. In addition, the synchronized flash can be used to detect the growth or decay of many of the short-lived species which are important in gas phase reactions.

Two methods have been used extensively to initiate the chemical reactions studied by flash spectroscopy. These are photolysis and the ignition of explosive fuel–oxidant mixtures. Photolysis of oxygen was investigated in this laboratory as a source of oxygen atoms and found to be unsatisfactory because of the very small atom concentrations produced. The difficulty was that a photolysis cell, for use with lithium or calcium fluoride windows, could not be made sufficiently strong to withstand the energy required to dissociate a measurable amount of O_2. It is believed that flash spectroscopy has not previously been used in conjunction with gas reactions initiated in the field of an r.f. oscillator as described herein.

2. DEVELOPMENT OF EXPERIMENTAL TECHNIQUE

The most difficult problem is in the spectroscopic measurement. The band spectra of interest lie below 2000 Å; therefore a vacuum spectrograph and vacuum optics are required. In addition, the time required for atom recombination is short (10–100 msec). This means that a spectral flash of a few hundred microseconds duration must produce an emission continuum of sufficient intensity for quantitative photometric measurements.

A schematic drawing of the experimental arrangement is shown in Fig. 1. The oxygen was dissociated in a Pyrex tube of 38 mm inner diameter and 48 cm in length, by means of a 27 Mc/s r.f. oscillator using external parallel plates which capacitatively couple the reaction vessel to the tank circuit of the oscillator. The discharge could be quenched within 10 μsec, and the spectral flash triggered at any predetermined time thereafter using a standard pulse generator to produce the delayed signal. The radiation from the lamp was collimated using a spherical lithium fluoride lens. The collimated beam was passed through the reaction vessel and finally condensed on to the vacuum spectrograph entrance slit by means of a second spherical lithium fluoride lens. A spherical rather than cylindrical condensing lens was used because the vacuum spectrograph film racking mechanism allowed a small entrance slit image to produce a series of adjacent spectra from top to bottom on the film. Also, the "f" number of the condensing lens was chosen so that the cone of light at the spectrograph grating was only 1 to 2 cm larger than the usable portion of

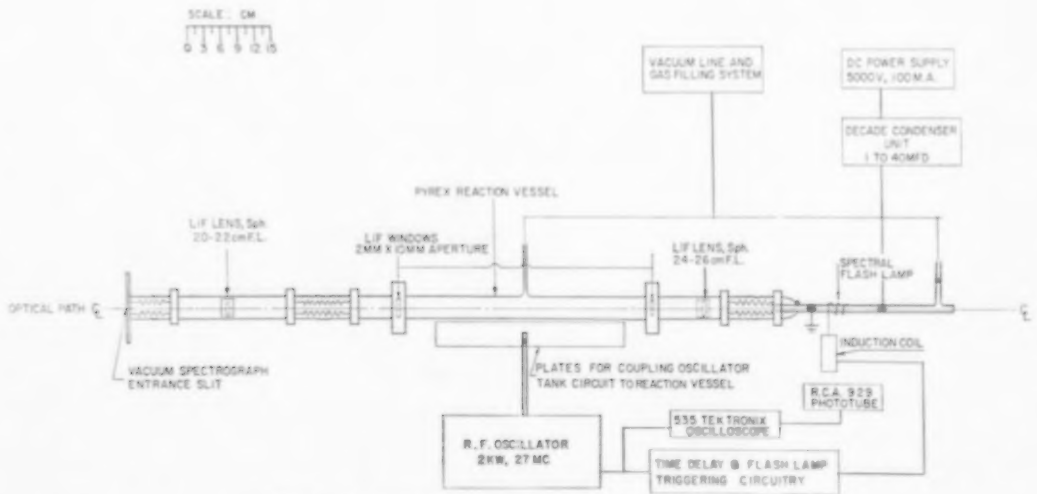
SCALE: CM
0 3 6 9 12 15
VACUUM LINE AND GAS FILLING SYSTEM
DC POWER SUPPLY 5000V, 100 M.A.
DECADE CONDENSER UNIT 1 TO 40MFD
PYREX REACTION VESSEL
LiF LENS, 5ph 20-22cmFL.
LiF WINDOWS 2MM X 10MM APERTURE
LiF LENS, 5ph 24-26cmFL.
SPECTRAL FLASH LAMP
OPTICAL PATH
VACUUM SPECTROGRAPH ENTRANCE SLIT
PLATES FOR COUPLING OSCILLATOR TANK CIRCUIT TO REACTION VESSEL
INDUCTION COIL
R.C.A. 929 PHOTOTUBE
535 TEKTRONIX OSCILLOSCOPE
R.F. OSCILLATOR 2KW, 27MC
TIME DELAY & FLASH LAMP TRIGGERING CIRCUITRY

Fig. 1. Schematic diagram of experimental arrangement.

the grating. These two considerations increased the film blackening by a factor of 3. Both lenses were mounted in iron holders to enable focusing to be made with the system under vacuum. The spectrum obtained at a given delay time was recorded on film by means of a custom-made vacuum spectrograph. The spectrum was quantitatively analysed by means of a densitometer and determination of O_2 densities made thereafter. The calibration involved the taking of flash absorption spectra of at least three known O_2 concentrations on the same film. It should be noted that the entire optical train external to the spectrograph ($1\frac{1}{2}$ meters in length) can be aligned while under vacuum. This was accomplished by using specially designed bellows and manipular assemblies. A vacuum of 5×10^{-6} mm Hg was maintained in the optical system and spectrograph.

An over-all photograph of the reaction and optical system is given in Fig. 2. The spectral flash lamp and collimating lens are located on the left. The reaction vessel is the portion of glass tubing in the center with white teflon flange compression at either end. The electrodes of the r.f. oscillator used to maintain the steady state concentration of oxygen atoms can be seen directly behind the reaction vessel. The section on the right contains the condensing lens. The slit of the vacuum spectrograph can barely be seen on the extreme right of the photograph.

In a recombination experiment a known pressure of gas was admitted to the reaction vessel and the r.f. oscillator turned on until a steady-state condition was attained*. Then the oscillator was turned off and, after a chosen delay time, an ignition coil was sparked. This served to ionize the gas between the electrodes in the flash tube, thus causing a 15 mF capacitor charged at 4000 V to be discharged in a few hundred μsec through the flash lamp. The resulting high current density through the lamp capillary produced a flash of high intensity radiation below 2000 Å. The time interval available in the time delay circuitry is between 10 μsec and 10 sec. Thus a series of spectra was taken at various times after cut-off of the oscillator.

The temperature of the system was checked carefully in recognition of the conditions which might have been created by the discharge. The total pressure was followed with the discharge "on" and, after cut-off, by means of a pressure transducer-oscilloscope apparatus from which the gas temperature was determined. The absorption spectra of molecular oxygen were then observed in a heated system at corresponding temperatures and pressures to correct for any change in the absorption coefficient. Wall effects were considered and minimized by observing only the inner 1-cm diameter of the reaction tube with the collimated beam. Changes in density during the cooling process, involving conductive and other effects, were also considered and found to be minor under these experimental conditions.

A modified commercial 2 kW 27 Mc/s dielectric heater was used as a source of r.f. power. A schematic diagram showing the oscillator revisions and time delay circuitry is given in Fig. 3. The oscillator consists of a vacuum tube unit of standard design using a full wave rectifier to supply the high voltage d.c. and a pair of flat copper plates in the "tank" circuit which capacitatively couple the r.f. power into the reaction vessel. However, there were several important changes in the original circuit. A cut-off switch was designed to collapse the r.f. field at the reaction vessel very rapidly. This was accomplished by a circuit which connects the high voltage transformer to ground by making a 5C22 thyratron conducting. When the switch *SI* was closed the power to the tank circuit was effectively short-circulated and the oscillator stopped after only a few cycles. The surge of current through the 5C22 caused an overload relay to open in the power section of the oscillator and thus prevented damage to the unit. The closing of switch *SI* also produced a voltage pulse to initiate the time delay circuitry by means of the two 10,000 Ω resistors and the 0·05 mF capacitor in the grid circuit of the 5C22.

* It was found using a transducer-oscilloscope measurement that the steady-state pressure was reached in less than 50 msec; however, the oscillator was usually run for 1-2 sec.

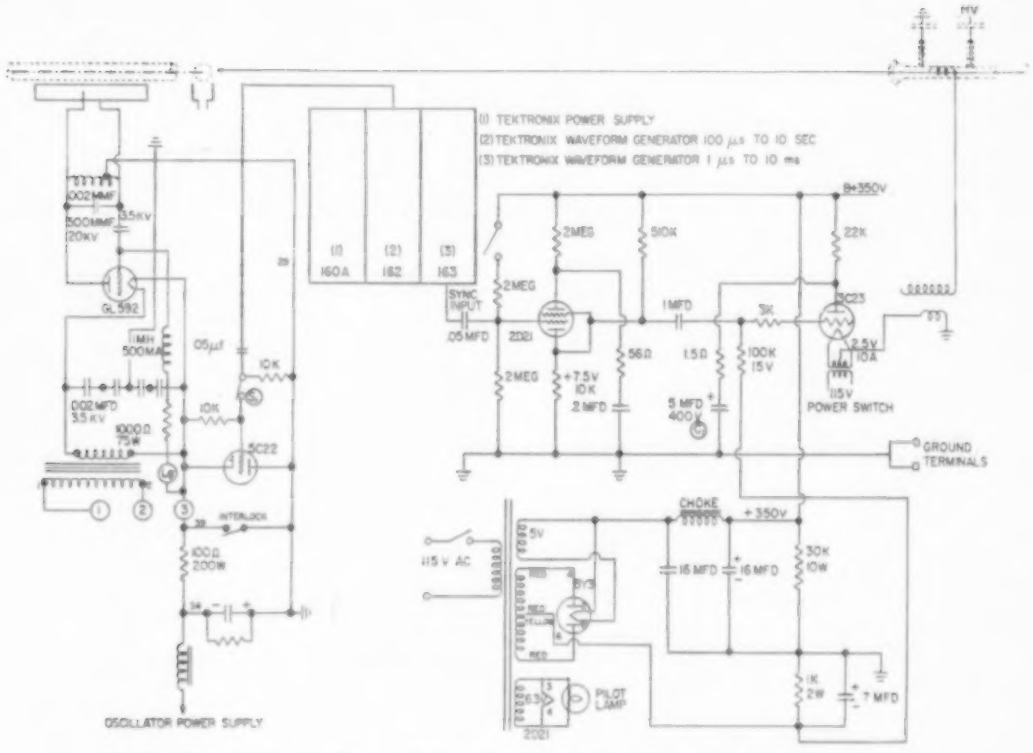

Fig. 3. Electrical circuit diagram of the r.f. oscillator cut-off and flash lamp triggering unit.

In order to eliminate the necessity of synchronizing the spectral flash with an r.f. output modulated by the 60 c/s house power, a filter was installed which produced a 27 Mc/s continuous wave with about 5 per cent ripple.

Oscilloscope trace photographs of the 27 Mc/s signal showed that the power decay time at the reaction vessel was less than 15 μsec. This fast cut-off gave an excellent "time zero" for the kinetics study because we had no overlap of the power decay with the atom recombination process. The three body recombination requires 10–100 msec. In fact, it is because these gas phase reactions are the slowest to decay that a valid kinetics measurement can be made with this technique. The deionization processes are complete in a few hundred microseconds.

The time delay units used were Tektronix no. 162 wave form generator (100 μsec–10 sec) and a Tektronix no. 163 pulse generator (1 μsec–10 msec). These were powered by a Tektronix no. 160 power supply. A specially designed triggering circuit was used in conjunction with these time delay boxes to cause the flash lamp to fire. The schematic diagram of this circuit is also given in Fig. 3. The input signal from the time delay units caused the 3C23 thyratron to become conducting and this served to discharge the 5 mF capacitor (*C1*) through the primary of an induction coil. A lead from the secondary of this coil, wound 2–3 times around the capillary section of the spectral flash lamp, carried the induced spark to the ground electrode through the low pressure gas in the capillary. This caused the flash lamp capacitor to discharge rapidly through the capillary to produce the spectral flash.

An accurate time delay measurement is important because the atom concentration undergoes large changes in a few milliseconds.

Therefore, a check was made of each delay time using the oscilloscope–phototube arrangement shown in Fig. 1. The signal which initiated the time delay circuits also triggered a single sweep on an oscilloscope. A phototube placed near the flash lamp produced a pulse on the scope trace from radiation picked up when the lamp flash occurred. This indicated the time between cut-off and lamp firing exclusive of any time constant in the electronic delay circuitry. The time delay settings were found to be accurate within 3 per cent in the range used in these experiments.

The most difficult problem was the development of the spectral source. Lipscomb *et al.*[1] in their flash photolysis technique had used a spectral flash source to about 2200 Å. Oldenberg[4], Frost[5] and others have used a Lyman type source for gas phase kinetics studies using a cycling technique to integrate the radiation from a number of flashes but also above 2000 Å. However, this required somewhere between 200 and 500 flashes to expose a film which could be used for quantitative work and therefore a difficult synchronization problem was encountered. In addition, the process under examination must be completely reversible. Recently Thrush[6] reported a far u.v. flash source. However, no quantitative studies were made with the lamp.

It is desirable to have a lamp with two features: first, that usable spectra can be taken in one or several flashes; second, that the lamp does not require any viewing window. The windows used for far u.v. transmission are made from lithium or calcium salt crystals and are very easily crazed and discolored. This causes serious scattering of the far u.v. radiation. The lamp we have developed for use here will give a single flash emission continuum to 1350 Å; also, the lamp is windowless. The lamp details are shown in Figs. 4 and 5. The discharge section consisted of a windowless*, 4 mm, quartz capillary with 1·5 mm tungsten electrodes

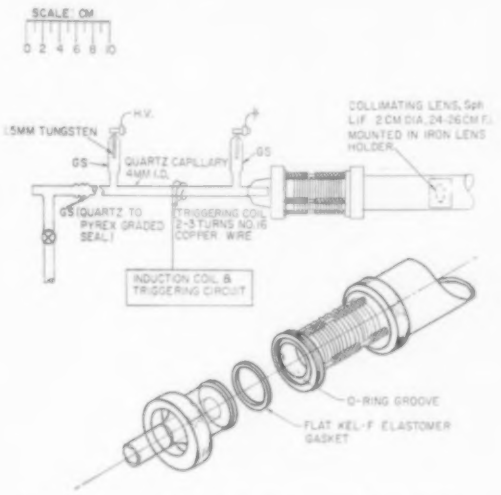

Fig. 4. Detailed drawing of spectral flash lamp.

sealed through graded glass sidearms spaced 15 cm apart. A vacuum stopcock was located 15 cm from the rear electrode to facilitate refilling. It was necessary to refill capillary flash tubes periodically because impurities eroded from the capillary wall during discharge made triggering difficult. Refilling is especially important in a lamp designed for the vacuum ultraviolet since oxygen and silicon, which absorb radiation below 2000 Å, are among the products of erosion. The lamp was attached to a collimating section through a brass bellows assembly which provided for adjustment of the capillary section by means of three threaded spacers 120° apart around the bellows. Each bellows flange contained an "*O*" ring groove and gasket as shown in Fig. 4. Connection to the flash lamp and collimating tube was made through flat glass flanges ground to a satin finish. Also, the lamp could be aligned while electrically "hot" using two rack and pinion mounts (see Fig. 5). The collimating section was 41 mm diameter Pyrex, 25 cm in length, with a LiF spherical lens of 24 cm focal length mounted in a movable iron holder. This allowed adjustment of the lens with a magnet from outside the lamp assembly. The lens position for the work reported here was such that the focal point was 3·5 cm behind the

* The lamp has also been used with a 2 mm thick CaF_2 window attached to the end of the capillary (using Kel-F no210 wax). The spectrum obtained (to 1750 Å) was approximately equal in intensity to that from the windowless lamp. However, the window becomes crazed after 150–200 flashes.

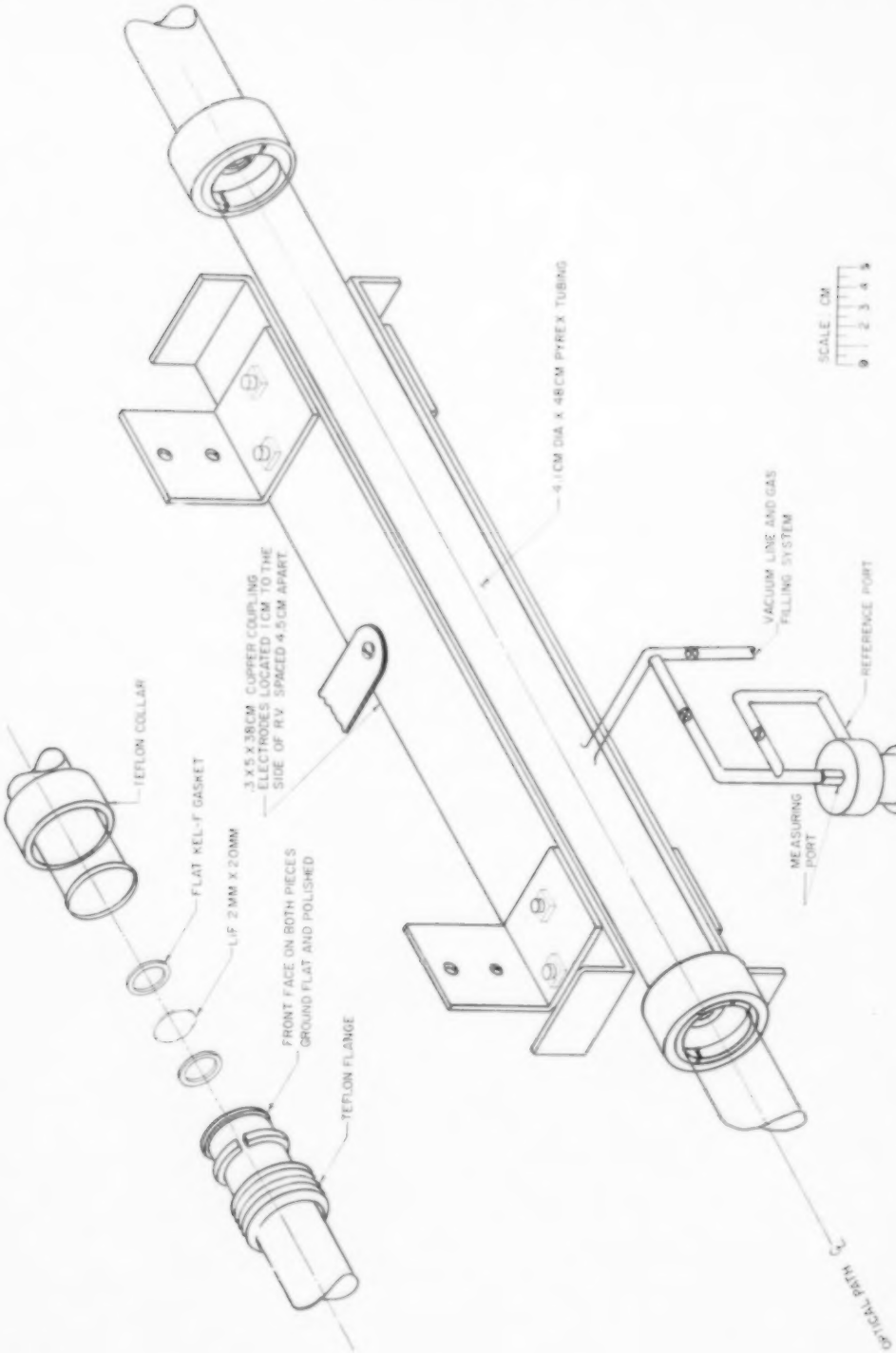
TEFLON COLLAR
FLAT KEL-F GASKET
LIP 2 MM X 2 MM
FRONT FACE ON BOTH PIECES GROUND FLAT AND POLISHED
TEFLON FLANGE
3 X 5 X 38 CM CUPPER COUPLING ELECTRODES LOCATED 1 CM TO THE SIDE OF R.V. SPACED 4.5 CM APART
4.1 CM DIA X 48 CM PYREX TUBING
VACUUM LINE AND GAS FILLING SYSTEM
REFERENCE PORT
DIAPHRAGM TYPE PRESSURE TRANSDUCER
MEASURING PORT
SCALE CM
0 1 2 3 4 5
OPTICAL PATH

Fig. 7. Reaction vessel and pressure transducer.

electrode nearest the lens. In operation, the lamp, including the collimating section, was filled with 10 cm of an inert gas. Xenon, krypton and argon were used interchangeably. However, we found that the krypton continuum is less overlaid with emission lines in the region of the Schumann–Runge system. A 15 mF capacitor attached to the HV electrode, charged to 4000 V, was discharged, as described above, to produce the radiation.

Several examples are shown in Fig. 6 of the spectra which have been obtained. At the top (a) is a single flash exposure of an emission continuum resulting from discharging through 10 cm Hg of krypton. The lamp was positioned 50 cm from the spectrograph entrance slit in this case. A part of the Schumann–Runge absorption system is shown in (b), (c) and (d). These spectra were obtained by flashing through the 48 cm reaction cell containing oxygen at 50, 20 and 10 mm Hg. Three flashes were used in each exposure to improve the reproduction here. However, single flash spectra were quite adequate for quantitative photometry.

The reaction vessel is shown in Fig. 7. A Pyrex tube, 3·8 cm inner diameter and 48 cm in length, was used in this work. The tube was made flat and ground to a satin finish at the ends and was closed except for two 1-cm diameter holes at either end. Since Pyrex is not transparent below 3000 Å, these holes served as apertures which defined a cylindrical beam of u.v. radiation of 1 cm diameter. This beam extended from the spectral flash along the cylindrical axis of the reaction vessel. This minimized the effect of wall recombination on the measurement. In addition, however, a calculation of the rate of diffusion of atomic oxygen at the pressures of these experiments showed that the concentration in this 1 cm concentric cylinder would remain essentially constant for the time required for recombination.

The tube was compartmented from the vacuum optical system by "sandwiching" lithium fluoride windows between Kel-F elastomer gaskets as shown in the figure. A vacuum tight seal was made using Teflon compression collars designed especially for this application. With this arrangement it was possible to obtain a vacuum of 10^{-6} mm Hg in the reaction vessel quite readily.

Oxygen was metered into the reaction vessel through a glass filling system which was also pumped to 10^{-6} mm before each experiment. Airco reagent grade gas was used and pressures were measured with a bellows type electromanometer (CEC no. 4-330 $\pm$ 1·5 lb/in² range). The pressure measurement accuracy was $\pm$0·1 mm Hg.

The location of the plate electrodes which couple the tank circuit of the r.f. oscillator to the reaction vessel can also be seen in Fig. 7. The electrodes were spaced 4·5 cm apart and were placed about 1 cm from the side of the vessel. The discharge obtained under these conditions is quite homogeneous. The color is a grey-white when undiluted oxygen is used in the reaction cell.

A pressure transducer (Schaevitz Engng. Co., Camden, N.J.) which measured differential pressure in the 0–180 mm range was attached to the reaction vessel as shown in Fig. 7. This instrument provided pressure data which were used to determine the gas temperature in the reaction vessel. The question of gas temperature is discussed further in Section III. At this point it is merely intended to show the location of the transducer in relation to the reaction vessel.

The vacuum spectrograph used for this work is the first of a new series designed by McPherson Precision Instruments Company (Acton, Mass). It is a 2-m normal incidence diffraction grating instrument which can be used as a spectrograph or a scanning monochromator in the 1000–6800 Å wave length range. In addition, several gratings can be used interchangeably with only minor mechanical adjustment. The spectra reported here were taken using the first order of a 600 1/mm original grating blazed for maximum intensity at 1550 Å in the first order using Eastman Kodak 103-0 u.v. sensitized film. With this grating it was possible to photograph a 2000 Å wave length span on an 11-in. film strip.

3. RESULTS AND CONCLUSIONS

In the initial rate measurements using 4 mm

of undiluted O_2, vibrationally excited oxygen (O_2*) appeared and was attributed to a high gas temperature in the discharge. It was estimated that the temperature in the reaction vessel could be 1000°C using the levels of O_2* which appeared, as a criterion. Further, in a mixture of 3 mm O_2 and 7 mm A there was no detectable amount of O_2*. Our initial interpretation of this was that the O_2* was produced thermally and that the argon served to absorb the heat released from oxygen recombination and thereby lower the gas temperature[7]. As a result of subsequent experimental work, it was found that the failure to observe excited oxygen in the oxygen-argon mixture was related to the limit of detection in our optical system rather than a lower gas temperature. That is, the amount of excited oxygen produced using an initial oxygen pressure of 3 mm Hg is just at the limit of detection in our system. Thus it is not possible to use unequivocally the absence of O_2* as a criterion for low gas temperature.

Although the increase in temperature in the reaction vessel should not seriously change the kinetics of recombination, the spectroscopic measurements could be difficult to interpret because of changes in absorption coefficient or shifts in maximum intensity within a band caused by changes in rotational distribution. Therefore, a more precise determination was made of the temperature at steady-state (with the oscillator in operation) since this condition represented the maximum gas temperature during an experiment. This measurement was made with a pressure transducer attached to the reaction vessel as shown in Fig. 7. A thin diaphragm type transducer was used. The instrument measured differential pressure in the 0–180 mm Hg range at any absolute level from 10^{-6} mm Hg to atmospheric pressure. The pressure increase with the oscillator "on" was interpreted in terms of temperature after taking into account the fraction resulting from O_2 dissociation.

The average temperature in the reaction vessel using oxygen in the 1–5 mm Hg pressure range was found to vary from 175°C at 1 mm Hg to 390°C at 5 mm Hg. These temperatures are in reasonable agreement with values determined by Oldenberg[5] and Kondratev[9] in a glow discharge. However, it should be noted that only qualitative comparison can be made since these investigations used internal electrodes and much lower frequency to obtain the discharge. From these data it was determined that the spectra of heated oxygen should be taken to about 400°C. Also, a calculation of the fractional population of the vibrational levels of oxygen at 400°C showed that less than 5 per cent of the initial concentration is in excited levels at this temperature. In addition, the change in rotational energy distribution within a vibrational band at this temperature was shown to have a negligible effect on the intensity of the absorption peaks which we use as a criterion for oxygen concentration. Films taken of heated oxygen in the 25–400°C temperature range were in good agreement with these calculations. The I/I_0 ratio at 400°C is still about 80 per cent of that measured at room temperature, whereas in a typical recombination experiment, this ratio is reduced to approximately 25 per cent of that given by the initial oxygen concentration.

The film reproduced in Fig. 8 is representative of the time delayed spectra taken during the recombination process. These data were obtained using 4·5 mm Hg O_2 + 5·5 mm Hg He in the reaction vessel. (The kinetics data reported here were taken with an initial O_2 concentration of 2·6 mm Hg, undiluted; however, these were not able to be reproduced with enough contrast for publication.) All the information necessary to obtain concentration vs. time data was included on each film so that difficulties in obtaining photographic reproducibility were minimized. At least three O_2 calibration exposures were obtained by first taking a single flash exposure through the initial oxygen pressure before the recombination experiment and subsequently repeating this by pumping out to two lower pressures of oxygen after taking the recombination exposures. The calibration exposures are designated (a), (h) and (i).

The time-delayed spectra are shown in exposures (b) through (g). The change in absorption with time can be readily seen from

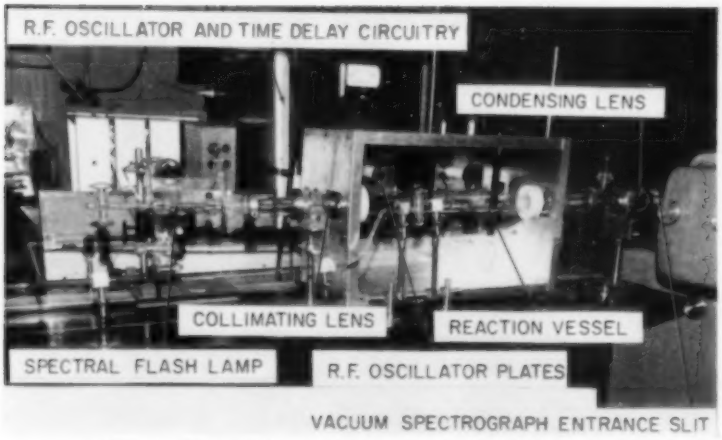

Fig. 2. Over-all view of the optical and reaction system.

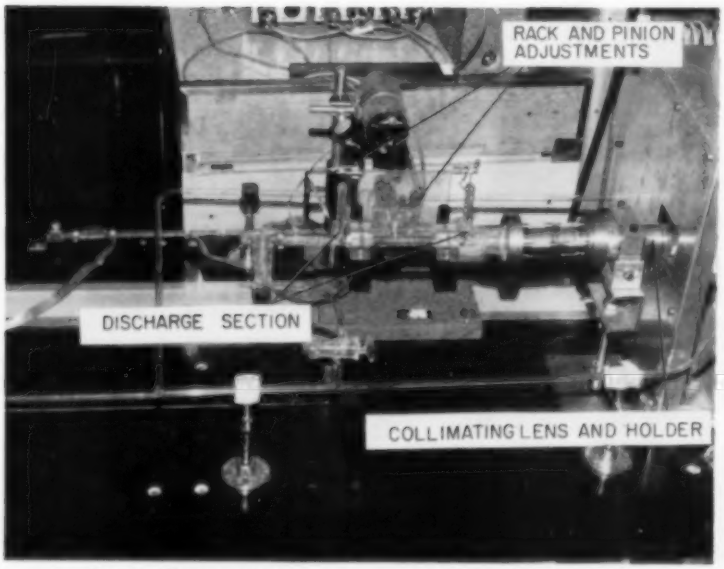

Fig. 5. Photograph showing spectral flash lamp in position.

Refer to page 176
(facing page 182*)*

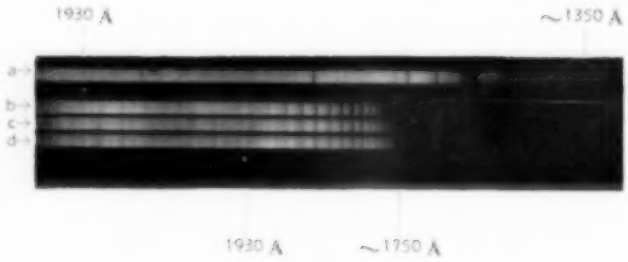

Fig. 6. Typical flash spectra obtained below 2000 Å.

(a) Single flash of emission continuum using 10 cm. Hg of krypton in the lamp.

(b), (c), (d) Schumann–Runge O_2 absorption using 50, 20 and 10 mm Hg in a 48-cm cell. Three flashes were superimposed to obtain each spectrum.

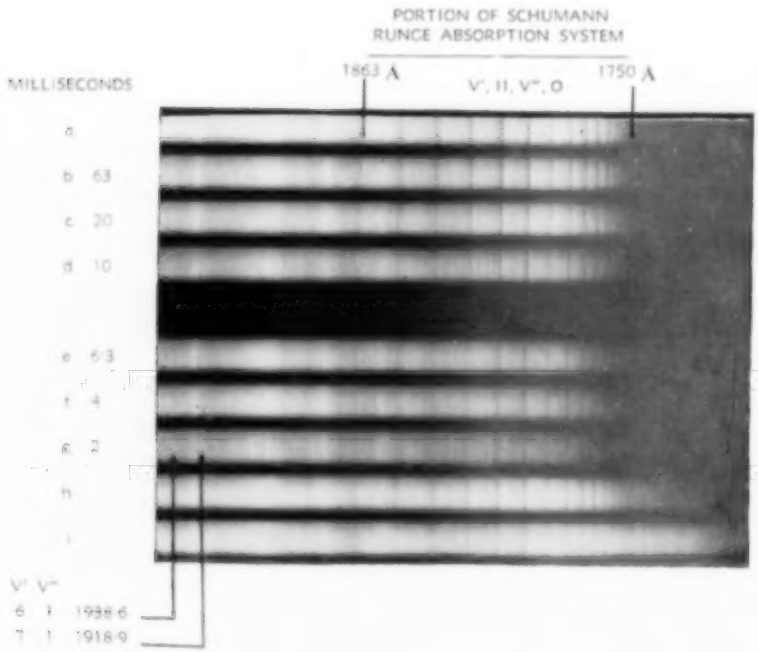

Fig. 8. Single flash absorption spectra showing growth of O_2 during recombination.

These data were obtained using a mixture of 4·5 mm Hg of O_2 and 5·5 mm Hg of He in the eraction vessel. (a), (h) and (i) are calibration spectra; the time delayed spectra are (b) through (g).

the photograph. The $V'=11$, $V''=0$ band head was used as a criterion for O_2 concentration in the data presented here. It was found empirically that this head gave the most reproducible calibration curve. A plot of O_2 concentration vs. time as obtained from the recombination films is shown by the solid line in Fig. 9. The

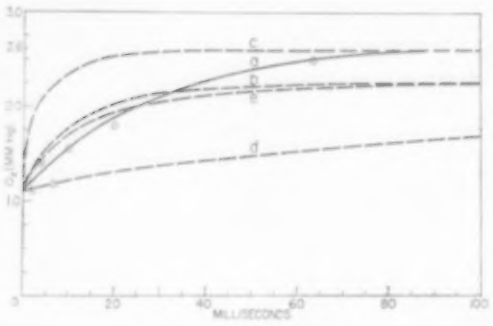

Fig. 9. Comparison of calculated with experimental values of oxygen concentration vs. time. (a) Experimental data; (b) calculated from equation (7) and experimental K_1; (c) and (d) calculated from equation (7) using $K_1=10^{16}$ and $K_1=10^{14}$ $(cm^3)^2$–moles^{-2}–sec^{-1}. (e) calculated from the computer analysis of equations (1)–(5).

data taken to date indicates that the accuracy of the experimental points is $\pm 0{\cdot}15$ mm Hg. A statistical analysis of the data will not be made until a more representative number of experiments have been carried out.

In addition to ground state oxygen, the spectra of several bands of the first excited level of oxygen can be seen in Fig. 8. It has been possible to identify the $V'=7$, $V''=1$ and the $V'=6$, $V''=1$ bands; these are indicated in the figure. No statement can be made at this time regarding the role of excited O_2 in the recombination process since our experiments do not distinguish among thermal, chemical or other excitation which could conceivably be caused by discharge processes. However, it is possible to follow the decay of excited oxygen from the spectra and, therefore, it should be possible to separate the two sources in subsequent experiments by adding substances with different efficiencies in effecting decay of O_2*.

It has been reported[10] that between 10 and 20 per cent of the oxygen in a gas discharge will be found in the $^1\Delta_g$ electronic level. This O_2 of course would be indicated as dissociated oxygen since the criterion for oxygen-atom concentration in our absorption measurement is the Schumann–Runge transition ($^3\Sigma_g^- \longrightarrow {}^3\Sigma_u^-$). However, it should be noted that the lifetime of the metastable oxygen will be much longer than the 50–60 msec recombination times which we observe. Thus by our measurement of the ground electronic state of oxygen at 60 msec, it is possible to estimate the concentration of metastable oxygen and determine whether the oxygen-atom concentration should be corrected. The spectra indicated that the amount of metastable O_2 is not greater than 10 per cent under the conditions of our experiment.

The following reactions were considered in our analysis of the gas phase recombination process:

$$O + O + M \xrightarrow{k_1} O_2 + M \qquad (1)$$

$$O_2 + M \xrightarrow{k_2} O + O + M \qquad (2)$$

$$O + O_2 + M \xrightarrow{k_3} O_3 + M \qquad (3)$$

$$O_3 + M \xrightarrow{k_4} O + O_2 + M \qquad (4)$$

$$O + O_3 \xrightarrow{k_5} 2O_2 \qquad (5)$$

where the third body M can be O, O_2 or O_3.

This system was treated analytically assuming that the percent dissociation at time zero was equal to the percent dissociation indicated in the experimental data. The rate constants k_3–k_5 were taken from Axworthy and Benson's[11] work on the thermal decomposition of O_3. A calculation was made of k_2 from k_1 and the equilibrium constant.

The constant k_1 was obtained from our O_2 concentration vs. time data using an expression for O_2 formation which assumes that O and O_2 have approximately the same third body efficiency and that a negligible amount of O_3 is formed during recombination.

Then from equation (1),

$$\frac{d(O_2)}{dt} = k_1 (O)^2 (M) \qquad (6)$$

However, under the conditions of our experiment, a large fraction of oxygen is dissociated

and M is not constant throughout the recombination process. The following expression takes into account this changing third body concentration:

$$(M) = [B + \tfrac{1}{2}(O)]$$

where:

B = the final (O_2) concentration.

Integration of the above gives:

$$\frac{1}{4B[B-(O_2)]} + \left. \frac{\ln[B-(O_2)] - \ln[2B-(O_2)]}{4B^2} \right|_{t_1}^{t_2} = k(t_2 - t_1) \tag{7}$$

The following tabulation gives typical k_1 values obtained using equation (7) and the experimental O_2 vs. time data:

Film no.	Initial O_2 concentration (mm Hg)	$k_1 \times 10^{-14}$ [(cm³)²/moles²/sec]	Temp. (°C)
314	2·6	5·5	175–200
321	↑	17·5	Determined
322	↕	17·5	from pressure
323	↓	11·5	transducer
324	2·6	8·5	measurements

The arithmetic average of the recombination rate constant obtained from the above tabulation was used in the integrated rate equation to calculate analytical concentration–time curves. In addition, similar curves were constructed assuming the rate constant to be an order of magnitude higher and an order of magnitude lower than the experimental value. These curves are shown in Fig. 9. The analytical curve constructed using our experimental k_1 values followed the experimental curves well enough to show that the experimental k_1

$$[10^{15}\,(\text{cm}^3)^2/\text{moles}^2/\text{sec}]$$

is accurate within a factor of 2 or 3. In addition, since this agreement was obtained using a constant k_1 throughout the recombination process, it is indicated that the third body efficiencies of O and O_2 are also within a factor of 2–3 of each other.

Reactions (1)–(5) were then programmed on a Royal McBee LGP-30 digital computer to follow the change in concentration with time of O, O_2, O_3 and M using an iterative process. The analysis showed that under the conditions of our experiment the O_3 concentration is from 2 to 3 orders of magnitude lower than any of the other species considered. This is also in agreement with our experimental observations, since it has not been possible to detect any absorption from the strong O_3 continuum between 2500 and 1750 Å. We have estimated that we should be able to detect 0·05 mm spectroscopically with our optical system. The O_2 vs. time data from the iteration is also plotted in Fig. 9.

An attempt was made to determine the importance of reaction (1) in the recombination process by comparing the O_2 production from (1) with that produced via (3) and (5). A calculation made, using concentrations from the computer analysis, showed the following:

Time (msec)	Rate of O_2 Production (moles/cm³/sec) × 10⁷	
	Reaction (1)	Reactions (3) and (5)
1·2	53	−1·3
10	17·2	−0·3
20	8·3	−0·1
40	3·2	−0·01
62	1·6	0

It is indicated from the above that, if our value of k_1 is accurate, then the oxygen atom recombination by way of reaction (1) is the important process except in systems in which the initial atom concentration is very small.

4. DISCUSSION

S. H. Bauer: It seems plausible, in view of the possibility that the actual concentration of O atoms is less than what you deduce by your difference measurement of the O_2 concentration, that you have generated a significant amount of ozone, particularly during the early times after turning off the discharge. This would have two effects: Ozone formation would further reduce

the O atom concentration, and this will provide an alternate mechanism for recombination.

$$\begin{aligned} O+O+O_2 &\longrightarrow O_3+O \\ O+O_2+O_2 &\longrightarrow O_3+O_2 \end{aligned} \quad (1)$$

$$O_3+O \longrightarrow 2O_2 \quad (2)$$

Thus, one would anticipate a lower than expected rate at first, going up as time increases.

A. L. MYERSON: The question of the importance of O_2 formation through the ozone mechanism

$$O+O_2+M \longrightarrow O_3+M \quad (1)$$

$$O_3+O \longrightarrow O_2+O_2 \quad (2)$$

has been considered in detail. The considerations are fully described in the preceding written article. The complete mechanism, including reactions not shown here, has been programmed on a LGP-30 computer. Our results are entirely compatible with the currently accepted set of specific reaction rate constants for (1) and (2) and our own value for k_1, for $O+O+M$. That is, it has been shown that, under our conditions of high O-atom concentration, the rate of formation of O_2 through the ozone mechanism is only a few per cent of that from the direct recombination.

F. KAUFMAN: Since this method measures the rate of formation of the ground state of O_2 rather than the disappearance of O, one must be extremely careful to rule out the presence of excited species. In O_2 discharges, the low-lying metastable $^1\Delta_g$ state is known to be formed in considerable concentration. It may be present in these experiments and this may also explain the abnormally high apparent dissociation of O_2 (40–60 per cent) reported here which we and other workers have not obtained with microwave or r.f. excitation.

Regarding the ozone mechanism for recombination, the steady-state concentration of O_3 will be quite small if the published values for k_2 are correct, and O_2 will be formed at twice the rate of k_1. This cannot be neglected since it accounts for about 20–50 per cent of the rate observed by Golden and Myerson.

R. A. YOUNG: Noxom has measured the collision efficiency of N_2 in deactivating both molecular and atomic metastable states: he finds approximately 10^5 collisions are needed to deactivate the metastable state of N, O and N_2 by N_2.

C. A. BARTH: I would like to further support the remarks that Drs. Kaufman and Young have made. In the oxygen molecule, the transition producing the atmospheric bands is of the magnetic dipole type. The lifetime of the upper state of this system, the $b^1\Sigma$, is of the order of 1 sec. This band is observed in emission from an oxygen afterglow at the same pressures used in Dr. Myerson's experiment. This observation shows that this metastable state survives some 10^7 collisions before radiation. The upper state of the infra-red atmospheric bands, the $a^1\Delta$, that Dr. Kaufman has suggested may be present under Dr. Myerson's experimental conditions, is even more metastable than these other states and, hence, it certainly may be expected to survive 10^7 or more collisions.

A. L. MYERSON: On the basis of the collision efficiencies stated, our experiments essentially eliminate the attachment of any importance to metastable oxygen molecules in so far as rates derived from our results are concerned. If 10^7–10^8 collisions are necessary to deactivate these excited oxygen molecules, as might be inferred from the work quoted by Drs. Barth and Young, then under our conditions these metastable species would survive for 100–1000 msec. Therefore, two conclusions can be drawn. One is that our rate measurements have been made long before the chemical kinetic process involving these species begins to occur. The second is that less than 10 per cent of the O_2 molecules are tied up in this form since, under conditions of an acceptable experiment, the concentration has returned to within this amount of the original concentrations long before 100 msec.

It does not seem to us that the concentrations of oxygen atoms obtained is abnormally high. The power of our source is 2000 W, a large fraction of which is coupled to the gas, and the frequency is 28 Mc/s which also must be considered in any comparison. An excellent example of this, which apparently has not been

noted in this case, is found in an article by K. R. Jennings and J. W. Linnett (*Nature* 182, 597, 1958). The latter describes a 350 W r.f. oscillator of 9·7 Mc/s frequency which provides atomic concentrations of 50–60 per cent in hydrogen. They then state that, "this compares favourably with most values quoted in the literature, and using microwave radiation from a Raytheon diathermy unit (250 W) at 0·12 mm Hg pressure, fewer than 10 per cent atoms are obtained".

R. E. DUFF: What about heterogeneous reactions?

A. L. MYERSON: With regard to heterogeneous reactions, only the central (1 cm diameter) portion of the 38 mm i.d. tube was used. Under these conditions, it was calculated that diffusion to the wall was too slow to effect the results significantly.

D. L. MATTHEWS: Byron's data showed that at the high temperature O was more efficient than O_2 as a collision partner in causing dissociation. Although I am not an expert on this question, it seems strange that this situation should be reversed at the lower temperature, since the recombination must be related to the dissociation for a specific reaction through the equilibrium constant.

A. L. MYERSON: Dr. Matthews' question brings up the matter of the effect of "sticky" collisions in accelerating three-body recombination. On the basis of the many articles on I atom recombination reported in the literature, the existence of an I_3 complex is quite important in this respect. At the low temperatures involved here, it would seem to us that an initial *two-body* collision, $O+O_2 \longrightarrow [O_3]$ (which would be followed by $O+[O_3] \longrightarrow O_2+O_2$ than normal duration which should decrease with increasing temperature.

Acknowledgement—The authors wish to thank Dr. M. H. Bortner of this laboratory for his helpful discussions and also Mr. R. L. Everett for his excellent performance of the laboratory experiments.

REFERENCES

1. F. J. LIPSCOMB, R. G. W. NORRISH, F. R. S. THRUSH and B. A. THRUSH, *Proc. Roy. Soc.* A**233**, 455 (1956).
2. R. L. STRONG, J. C. CHIEN, P. E. GRAF and J. E. WILLARD, *J. Chem. Phys.* **26**, 1287 (1957).
3. R. MARSHALL and N. DAVIDSON, *J. Chem. Phys.* **21**, 659 (1953).
4. A. A. FROST and O. OLDENBERG, *J. Chem. Phys.* **4**, 642 (1936).
5. A. A. FROST and O. OLDENBERG, *J. Chem. Phys.* **4**, 781 (1936).
6. B. A. THRUSH, *Proc. Roy. Soc.* A**243**, 555 (1958).
7. J. A. GOLDEN and A. L. MYERSON, *J. Chem. Phys.* **28**, 978 (1958).
8. O. OLDENBERG, *J. Chem. Phys.* **3**, 266 (1935).
9. V. N. KONDRAT'EV, *Acta phys.-chim. URSS* **5**, 301 (1936).
10. S. N. FONER and R. L. HUDSON, *J. Chem. Phys.* **25**, 601 (1956).
11. S. W. BENSON and A. E. AXWORTHY, *J. Chem. Phys.* **26**, 1718 (1957).

MOLECULAR STUDIES WITH A LOZIER ELECTRON IMPACT APPARATUS*

M. A. FINEMAN† and A. W. PETROCELLI‡
Providence College, Providence, Rhode Island

Abstract—The object of this paper has been to point out the potentialities of the Lozier electron impact apparatus for studying simple molecules. The several properties which may be determined with this instrument are first listed. Following a presentation of the various processes occurring on low energy electron bombardment, the manner of measuring a property related to the molecule is outlined by considering a polar dissociation process. The construction and operation of the Lozier apparatus is briefly described. Finally the results of our study of CO with this instrument are presented to demonstrate the utility of this technique of investigation.

Bombardment of molecules with low energy electrons to form ions is now a most fruitful method for investigating certain properties of molecules, free radicals, atoms and ions[1]. Although the most popular electron impact instrument for molecular studies is a mass spectrometer, other types are available. Some of the others, for instance the Lozier apparatus, which will be described later, have some features not present in mass spectrometers.

From electron impact studies with a Lozier apparatus it is possible to obtain, in principle, the following properties:

(1) Actual bond dissociation energies (not average bond energies) of molecules, ions and free radicals;
(2) Ionization potentials of molecules, free radicals and atoms;
(3) Electron affinities of atoms, and free radicals;
(4) Kinetic energy of ions and other fragments when formed;
(5) The kinetic energy distribution of ions formed under a given set of conditions;
(6) Cross sections for ionization as a function of the energy of the bombarding electrons;
(7) Energies of excited states of molecular ions;
(8) Heats of formation of ions and free radicals.

To study molecules by electron bombardment, an electron beam of known energy is allowed to collide with the gas molecules being investigated. By measuring and plotting the ion current produced as a function of the electron energy (i.e. an ionization efficiency curve), the minimum electron energy at which ions are formed can be deduced (i.e. the appearance potential of the ion). Furthermore, in some instruments, particularly in the Lozier apparatus, the kinetic energy of the ions formed can be measured by employing a stopping potential on the ion collector. From an analysis of such data, it is possible to determine one or more of the properties listed above.

It may be helpful at this point to summarize the several processes resulting in ions when a molecule is struck by an energetic electron[2]. In spite of the emphasis on the study of positive ions formed on electron bombardment, it is possible, and often very probable, that negative ions are also produced. Below are listed five processes leading to either negative or positive ions, or both, but limited to those where no

* This research was supported in part by a U.S. Atomic Energy Commission Contract AT(30-1)-1670.

† Presently at the National Bureau of Standards on leave from Providence College.

‡ Now at the Department of Chemistry, University of Rhode Island, Kingston, R.I.

more than two chemical fragments (not counting electrons) are formed.

Process I: Resonance electron capture

$$XY + e^- = XY^- \quad (1)$$

Process II: Dissociative electron attachment

$$XY + e^- = X + Y^- \quad (2)$$

Process III: Polar dissociation

$$XY + e^- = X^+ + Y^- + e^- \quad (3)$$

Process IV: Molecular ionization

$$XY + e^- = XY^+ + 2e^- \quad (4)$$

Process V: Dissociative ionization

$$XY + e^- = X^+ + Y + 2e^- \quad (5)$$

Note, there are three processes in which negative ions can be formed, and three in which positive ions can be produced. It should be emphasized that with larger molecules, with less symmetrical molecules, and/or with more energetic bombarding electrons, a greater number of different processes are possible[3].

In order to demonstrate how one of the molecular, ionic or atomic properties may be determined by an electron bombardment study[4], let us consider a polar dissociation process (Process III). The appearance potential of X^+ ions formed with kinetic energy, $A_k(X^+)$, in this process can be related to the dissociation energy of XY, $D(X-Y)$, the ionization potential of the radical (or atom X), $I(X)$, the electron affinity of Y, $EA(Y)$, the kinetic and excitation energies of both fragments, T and E_x respectively, by

$$A_k(X^+) = D(X-Y) + I(X) - EA(Y) + T + E_x \quad (6)$$

By setting a retarding potential, V_{ret}, on the ion collector, the appearance potential for X^+ ions observed is that for the formation of ions with kinetic energy equal to V_{ret}. The total kinetic energy of both fragments, T, can be related to that of the ion alone by applying the conservation of momentum principle, in which case it follows that

$$T = \left(\frac{M(X^+) + M(Y^-)}{M(Y^-)}\right) V_{ret} \quad (7)$$

where M (ion) is the mass of that ion. If T in equation (6) is replaced by its expression in equation (7) and at the same time $A_0(X^+)$ is equated to the constant terms in equation (6), that is

$$A_0(X^+) = D(X-Y) + I(X) - EA(Y) + E_x \quad (8)$$

the final relationship becomes

$$V_{ret} = \left(\frac{M(Y^-)}{M(X^+) + M(Y^-)}\right)\left(A_k(X^+) - A_0(X^+)\right). \quad (9)$$

A plot of the kinetic energy of the X^+ ion, V_{ret}, versus its appearance potential, $A_k(X^+)$, should be linear. The slope is the ratio of the mass of the fragment not being observed (Y^-) to the mass of the molecule itself. The intercept on the appearance potential axis is just $A_0(X^+)$. Thus, from a set of ionization efficiency curves obtained at various retarding potentials on the ion collector, it is possible to identify the ion being observed and determine the minimum energy needed to produce that ion in the given process with no kinetic energy, $A_0(X^+)$. Having determined $A_0(X^+)$, and assuming E_x can be evaluated in some way, it is then possible to find one of the three remaining terms if the other two are known.

In the case of diatomic molecules, the ionization potential of an atom is involved, and these are all known very accurately. If a monoenergetic electron beam is employed, it is generally possible to observe two or more processes in which a given ion is formed. If ions are observed from several different processes, it is possible not only to establish the excited states of the fragments, but also to determine values for the other quantities too.

In Table 1 are given the energy expressions for the appearance potentials of the five processes in terms of the properties mentioned above. The determination of one or more of the quantities involved in these expressions would be carried out in the same manner as indicated for the polar dissociation process.

From the example above, it is seen that one must establish the actual chemical process occurring, evaluate the kinetic energy of the fragments when formed and deduce the states of excitation of the fragment particles. In order

Table 1. Appearance Potential Expressions for Each of the Electron Impact Processes

Process	Appearance potential expression
I. $XY+e^-=XY^-$	$A_a(XY^-)=E_z(XY^-)-EA(XY)$
II. $XY+e^-=X+Y^-$	$A_k(Y^-)=D(X-Y)-EA(Y)+E_z+\frac{M_{XY}}{M_X}V_{ret}$
III. $XY+e^-=X^++Y^-+e^-$	$A_k(Y^-)=A_k(X^+)=D(X-Y)+I(X)-EA(Y)+E_z+T^*$
IV. $XY+e^-=XY^++2e^-$	$A_a(XY^+)=I(XY)+E_z$
V. $XY+e^-=X^++Y+2e^-$	$A_k(X^+)=D(X-Y)+I(X)+E_z+\frac{M_{XY}}{M_Y}V_{ret}$

* The total kinetic energy T would be expressed in terms of the kinetic energy of the ion (Y^- or X^+) being observed.

to establish the actual process, it is essential to determine the sign of the charge on the ion or ions formed, and to identify the particles themselves, usually by their mass.

The Lozier apparatus, a relatively inexpensive electron impact instrument, is ideal for investigations of simple molecules. With it, the formation of either positive or negative ions may easily be detected, their appearance potentials and initial kinetic energies readily determined, and by appropriate treatment of the data (if no more than two particles are formed) the masses of the fragments calculated. With this information one or more molecular or related properties can be deduced.

A brief description of the construction and operation of such an apparatus (see Fig. 1) follows. The Lozier apparatus consists of (1) a hot tungsten filament (*F*) as a source of electrons, (2) an anode (*A*) to pull out a constant electron current, (3) a set of electrodes to obtain an essentially monoenergetic electron beam[5] (*PBP'*), (4) an ionizing-analysing chamber, (5) an electrode to remove secondary electrons (*S*) and (6) an electron trap (*T*). The ionizing-analysing chamber is cylindrically symmetrical about the electron beam which is confined along the axis by a magnetic field of 160 G. The ions are formed in an electric field free region maintained by an electrode consisting of a set of tantalum washers (*M*) connected to the electron accelerating electrode (*E*). Another set of larger washers (*D*) around the first set makes it possible to discriminate between positive and negative ions by applying an appropriate voltage. The ions which are permitted to pass through the discriminator are collected by a cylindrical can (*C*) surrounding the other electrodes. Stray currents are prevented from leaking to the ion collector by a guard can (*G*).

Thus, with a Lozier apparatus, ionization efficiency curves at various fixed ion retarding

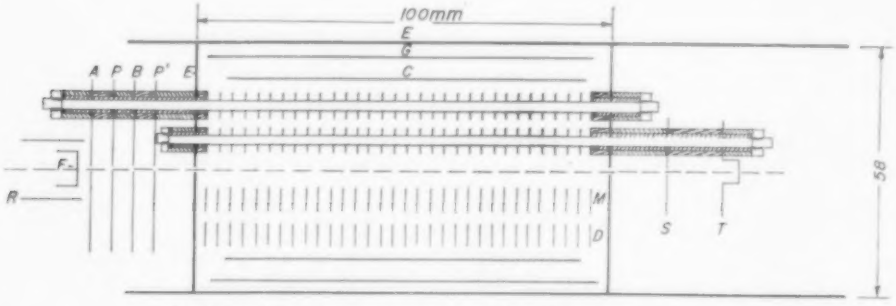

Fig. 1. Schematic diagram of the Lozier electron impact tube.

potentials are obtained from which the appearance potential of an ion with known kinetic energy can be determined. By plotting the kinetic energy of the ion versus its appearance potential, the mass of the ion formed can be deduced. With this information the process and the kinetic energy of the particles can be established. As mentioned earlier, the identification of the state of excitation of the fragments may be made if several different processes produce the same given ion.

A few words about the relative merits of a mass spectrometer and a Lozier apparatus might be interjected here. With the customary commercial mass spectrometers, only positive ions are examined. Custom built spectrometers can be adapted to observe negative ions and establish the kinetic energies of all the ions. If the energy levels of the fragments are desired, it is necessary to employ an essentially monoenergetic electron beam, and thereafter the data are treated in the same manner as data obtained via a Lozier apparatus. Thus, for simple processes, particularly those involving diatomic molecules, the only advantage a mass spectrometer has over a Lozier apparatus is that the mass of the ions are directly determined in a mass spectrometer while they are deduced from a set of data in a Lozier apparatus. On the other hand, the Lozier apparatus, unlike the commercial and custom built mass spectrometers, uses differential pumping between the filament and the ionizing chambers. The great advantage here is the fact that decomposition products and radicals formed by thermal decomposition on the hot filament wire are prevented from contaminating the sample gas in the ionizing-analysing chamber. Another advantage of a Lozier apparatus is that a calibration by means of positive ions of the electron energy scale can be used with confidence for studying negative ions. This is not the case for a mass spectrometer.

Carbon monoxide has been carefully investigated in our Lozier apparatus. The electron energy scale was calibrated by taking the appearance potential of the CO^+ ion as equal to the spectroscopic ionization potential[6]. A typical ionization efficiency curve for CO^+ is

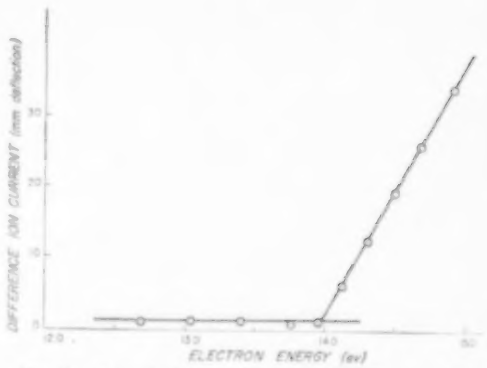

Fig. 2. A typical ionisation efficiency curve for CO^+ ion used for calibration of electron energy scale.

shown in Fig. 2. It should be noted that for this process, the difference ion current is linear with respect to electron energy above threshold. Four processes were recognized from the ionization efficiency curves for positive ions (Fig. 3). Negative ions were observed from a dissociative electron attachment process (Fig. 4) and by two polar dissociation processes (Fig. 5). The ion formed in each case and its appearance potential with zero kinetic energy were established, and it was shown that only five separate processes had been observed. These included a dissociative electron capture, two polar dissociation processes, and two dissociative ionization processes. A summary of the results of this investigation on CO is presented in Table 2.

By assuming that neither negative ion, O^- nor C^-, can exist in an excited electronic state and that the absolute errors are of the order of 0·3 eV or less, the states of excitation of all the fragments in each process can be established. By treating our data alone, we arrived at a dissociation energy of CO of $11{\cdot}23 \pm 0{\cdot}13$ eV, an electron affinity of oxygen of $1{\cdot}70 \pm 0{\cdot}22$ eV and an electron affinity of carbon between $1{\cdot}44 \pm 0{\cdot}30$ to $1{\cdot}59 \pm 0{\cdot}41$ eV. If the dissociation energy of CO is taken as that spectroscopic value closest to ours, i.e. 11·11 eV, the electron affinity of oxygen becomes $1{\cdot}58 \pm 0{\cdot}09$ eV and carbon becomes $1{\cdot}32 \pm 0{\cdot}17$ to $1{\cdot}47 \pm 0{\cdot}28$ eV. Using the EA(O) reported by Branscomb *et al.*[7] of 1·465 eV, the electron affinity of carbon is $1{\cdot}34 \pm 0{\cdot}13$ eV. This value is in good agree-

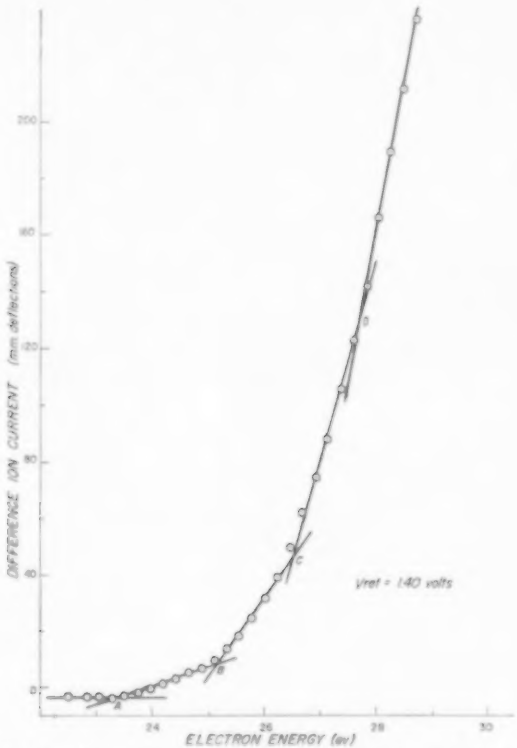

Fig. 3. An ionisation efficiency curve for positive ions from CO at a retarding potential of 1·40 V.

Table 2. Summary of Results of the Electron Impact Investigation of CO with a Lozier Apparatus

Process	Appearance potentials	
	$A_0(X^+)$ (eV)	$A_0(Y^-)$ (eV)
$CO+e^- = C^+(^2P^0)+O^-(^2P^0)+e^-$	20·89±0·09	20·92±0·05
$= C^+(^2P^0)+O\ (^3P)+2e^-$	22·57±0·20	
$= C^-(^4S^0)+O^+(^4S^0)+e^-$	23·41±0·17	22·97±0·07
$= C\ (^3P)+O^+(^4S^0)+2e^-$	24·78±0·23	
$= C\ (^3P)+O^-(^2P^0)$		9·39±0·05

ment, within experimental error, with that of Lagergren[8] of 1·1 eV.

It is hoped that this very brief review of our results on CO points out some of the potentialities of the Lozier electron impact apparatus in the study of simple molecules.

DISCUSSION

R. E. DUFF: What is the comparative usefulness of the Lozier apparatus and the mass spectrometer?

M. A. FINEMAN: Because of the importance of this question, the answer to it has been incorporated into the article itself.

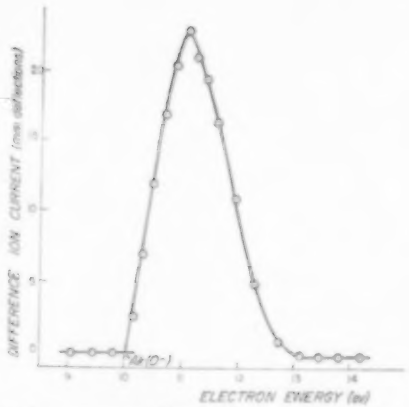

Fig. 4. An ionisation efficiency curve for negative oxygen ions formed from CO in a dissociative electron capture process at a retarding potential of 0·39 V.

C. W. BAULKNIGHT: What about the possibility of measuring ionization cross sections with the apparatus you described?

M. A. FINEMAN: Not only can positive ionization cross sections be measured with a Lozier apparatus, but also cross sections for negative ion formation. To measure cross sections with a Lozier apparatus, it is essential to use a comparative method. By doing so, parameters which would be difficult or impossible to assess cancel out in deriving the expression for calculating the cross sections. The specific ionization (I) (the ratio of ion current to electron current), the pressure (P) and the electron bombarding energy (E) are measured for both the gas under consideration (X) and the standard gas (S) of known cross sections. The cross section of the gas at a given electron energy, $Q(X)_E$, can be related to that of the standard gas in terms of the specific ionization currents and pressures.

$$Q(X)_E = Q(S)_{E'} \frac{I(X)_E P(S)}{I(S)_{E'} P(X)}$$

The subscripts E and E' show that the measurements on the unknown gas and the standard gas do not have to be made at the same electron energy. Even though the determination is obtained by a comparison of the unknown to a standard, some problems do arise when justifying the use of the above expression for measuring the cross section with a Lozier apparatus. Tozer[9] has analysed and discussed rather thoroughly the various problems in making cross section measurements with the Lozier apparatus. He concludes that values could, in some cases, be good to about 5 per cent.

T. C. PENG: Since the determination of the ionization potential is based on the discontinuity in the slope of the curve, drawn according to experimental data, and also since the velocity distribution in the test gas tends to round off the discontinuity into a smooth curvature, the

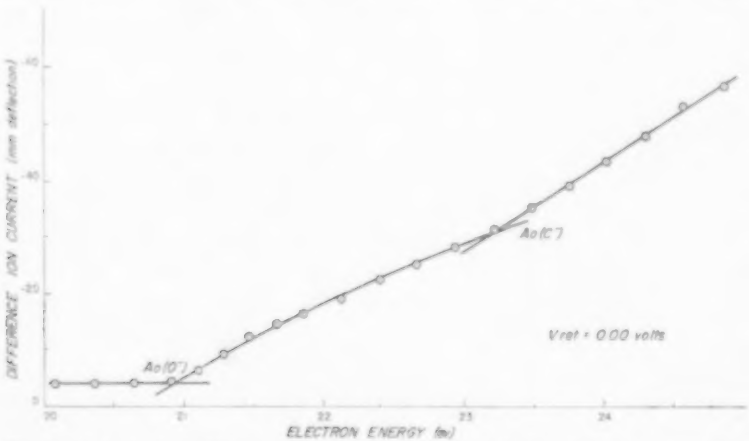

Fig. 5. An ionisation efficiency curve for negative ions from CO at zero retarding potential.

question then arises as to the accuracy of the ionization potential obtained in such an experimental procedure.

M. A. FINEMAN: The problem of accurately determining the appearance potential from an ionization efficiency curve has always been of great concern to those engaged in low energy electron impact studies. However, the energy distribution (or velocity distribution) of the test gas does not greatly contribute to the curvature (or tail) observed near the threshold for a given process. As the gas molecules are at room temperature, their average energy is only about 0·035 eV and so might contribute a small rounded portion of no more than 0·10 eV in the electron energy. The energy spread of the bombarding electrons (about 0·90 eV) is more serious in causing a rounded shoulder in the ionization efficiency curve. It is because of the influence of the electron energy spread on the ionization efficiency curve, that we (as well as many others) have employed a Fox electron gun. With this gun we have managed to use an essentially monoenergetic electron beam whose energy width was of the order of 0·10–0·20 eV. Using the method of Fox *et al.* to interpret the data, it is felt that with careful experimentation, ionization potentials of molecules can be determined to better than 0·10 eV.

REFERENCES

1. C. A. McDOWELL and J. D. CRAGGS, *Rep. Progr. Phys.* **18**, 374 (1955).
2. H. S. W. MASSEY, *Disc. Faraday Soc.* No. 12 (1952).
3. F. H. FIELD and J. L. FRANKLIN, *Electron Impact Phenomena.* Academic Press, New York (1957).
4. M. A. FINEMAN and G. F. MARTINS, *AEC Report* No. (NYO) 7237, O.T.S., Department of Commerce, Washington 25, D.C.
5. R. E. FOX, W. M. HICKAM, D. J. GROVE and T. KJELDAAS, Jr., *Rev. Sci. Instrum.* **26**, 1101 (1955).
6. R. E. FOX and W. M. HICKAM, *J. Chem. Phys.* **22**, 2059 (1954).
7. L. M. BRANSCOMB, D. S. BURCH, S. J. SMITH and S. GELTMAN, *Phys. Rev.* **111**, 504 (1958).
8. C. R. LAGERGREN, *Dissertation Abstr.* **16**, 770 (1956).
9. B. A. TOZER, *J. Electron Control*, **4**, 149 (1958).

ATOM CONCENTRATION MEASUREMENTS USING ELECTRON PARAMAGNETIC RESONANCE*

A. F. HILDEBRANDT, C. A. BARTH and F. B. BOOTH
Jet Propulsion Laboratory, Pasadena, California

Abstract—Atom concentration measurements were made of N (^4S) and H (^2S) produced by microwave discharges in gaseous N_2 and H_2. Spectrometer drifts and fluctuations were corrected by calibrating with the high field spectrum of O_2 at 1 mm Hg pressure. Atom surface recombination was prevented by conditioning the quartz tube with nitrogen atoms until the afterglow was plainly visible. Absolute comparisons were made with the intensity of a paramagnetic salt and with gas phase titrations. The EPR reproducibility is ±5 per cent or better, whereas the absolute measurements are ±25 per cent or better. The variation of atom density and concentration with pressure of each atomic species is given.

1. INTRODUCTION

In free radical stabilization work, flame studies and upper atmosphere research, there is an increasing need for absolute concentration measurements of atoms and other free radicals. Although atom concentrations have been measured by the heat of recombination on resistance thermometers[1, 2], and more recently by chemical titrations in gas flow systems[3, 11], these methods do not lend themselves readily to measurements of mixtures of free radicals.

Since the electron-paramagnetic-resonance (EPR) spectrometer can detect chemical species possessing a net magnetic moment with good sensitivity (10^{14} spins/cm^3), it seemed worthwhile to develop it into a quantitative instrument, for the measurement of radicals in gases. The results of such measurements in gases are summarized and discussed in detail in this report.

Atom-concentration measurements were made of N (^4S) and H (^2S) produced by microwave discharges in pure N_2 and H_2. The EPR spectrometer was calibrated by means of a standard 0·1 F $MnSO_4$ solution. The results for atomic nitrogen were confirmed by titration with NO[3].

* This work was performed under the auspices of the Department of the Army Ordnance Corps, Contract No. DA-04-495 ORD 18.

2. THEORY

It is desired to measure quantitatively the number of atoms of different species present in a gas by comparing the intensity of their electron-paramagnetic-resonance signals with the signal of a gravimetrically measured amount of paramagnetic salt. In order to relate the signal intensities of different paramagnetic species, it is necessary to determine the transition probabilities between Zeeman magnetic sublevels for the different atomic systems involved. This derivation will apply the method of Bloembergen, Purcell and Pound[4] to atomic systems, using the notation of Condon and Shortley[5]. The magnetic moment of an atom, **M**, is related to **L** and **S**, the orbital and spin angular-momentum operators, by

$$\mathbf{M} = -\frac{e}{2mc}(\mathbf{L}+2\mathbf{S}) \qquad (1)$$

where e, m and c are the electronic charge, mass and the velocity of light, respectively. The magnetic sublevels of an atom in a uniform magnetic field, H_0, are split by the energy $\Delta E = g\mu_0 M H_0$, where g is the Lande splitting factor, μ_0 the Bohr magnetron and M the magnetic quantum number. When the atom in the uniform magnetic field is subjected to electromagnetic radiation having a magnetic vector component perpendicular to H_0, transitions between the magnetic sublevels will be

induced at the resonant frequency with the transition probability, W, equal to

$$W=\frac{8\pi^3}{3h^2}(M\,|\,\mathbf{M}\,|\,M-1)^2\,\rho_\nu \qquad (2)$$

where ρ_ν is the radiation density and h is Planck's constant. The square of the matrix element is given in Ref. 5.

$$(\gamma, J, M\,|\,\mathbf{M}\,|\,\gamma, J, M-1)^2 = \\ =\tfrac{1}{2}g^2\mu_0{}^2\,(J+M)\,(J-M+1) \qquad (3)$$

where J is the total angular-momentum quantum number and γ describes all the quantum numbers except J and M. This relation is valid for any coupling scheme of the atom, provided the atom is in a weak magnetic field where only the pure Zeeman effect occurs.

An atom that has a nuclear spin has a total magnetic moment of

$$\mathbf{M}=-\frac{e}{2mc}(\mathbf{L}+2\mathbf{S})+\frac{eg_n}{2M_nc}\mathbf{I} \qquad (4)$$

where $\mathbf{I}$ is the nuclear angular momentum, $\mathbf{M}_n$ is the mass of the nucleus and g_n is the nuclear g factor. The contribution of the nuclear-spin part of the magnetic moment of the atom is of the order of 10^{-3} times the contribution from the electron spin part; hence, the nuclear spin does not significantly contribute to the intensity of the paramagnetic resonance absorption line. However, the coupling of the nuclear spin with the electron contribution does lead to a splitting of the EPR spectra into $2I+1$ lines. The intensity of each line is $1/(2I+1)$ times the intensity of the degenerate line and, hence, the total intensity is obtained from one of the hyperfine components, by multiplying the component intensity by $2I+1$.

The equivalent radiation density[4] may be taken as

$$\rho_\nu=\frac{3H_1{}^2G(\nu)}{4\pi} \qquad (5)$$

where H_1 is the amplitude of the oscillating r.f. magnetic field, $H=2H_1\cos 2\pi\nu t$ and $G(\nu)$ is the shape function of the absorption line. Combining equations (2), (3) and (5), the transition probability W of a single transition between magnetic sublevels is

$$W=\frac{g^2\mu_0{}^2H_1{}^2G(\nu)}{4h^2}(J+M)\,(J-M+1) \qquad (6)$$

where h is Planck's constant divided by 2π.

Since the Boltzmann factor for each of the magnetic sublevels may be approximated by $\exp[-(h\nu/kT]=1+(h\nu/kT)$ the population difference between adjacent sublevels is

$$N_m-N_{m-1}=\frac{h\nu}{kT}\frac{N}{2J+1} \qquad (7)$$

since there are $2J+1$ magnetic sublevels to each level where N is the number of spins.

The power, P, absorbed by a single transition between magnetic sublevels is equal to the product of the energy difference between the two sublevels, the population difference given by equation (7) and the transition probability given by equation (6):

$$P=\frac{N(h\nu H_1g\mu_0)^2G(\nu)}{4kTh^2}\left[\frac{(J+M)\,(J-M+1)}{2J+1}\right] \qquad (8)$$

For atoms that are subjected to the pure Zeeman effect (weak field or S states), the energy difference between the magnetic sublevels is equal and the lines are degenerate. To obtain the power absorbed by transitions between all the sublevels of a single level, equation (8) may be summed from $(-J+1)$ to J

$$P=\left[\frac{N(h\nu H_1g\mu_0)^2G(\nu)}{4kTh^2\,(2J+1)}\right]\sum_{M=-J+1}^{J}(J+M)\,(J-M+1)= \qquad (9)$$

$$=\frac{N(h\nu H_1g\mu_0)^2G(\nu)}{6kTh^2}J\,(J+1)$$

since

$$\sum_{M=-J+1}^{J}(J+M)\,(J-M+1)=\tfrac{2}{3}J\,(J+1)\,(2J+1)$$

For convenience, the power absorbed per unit volume may also be expressed in terms of χ'', the imaginary part of the complex magnetic susceptibility[6]:

$$P=4\pi\nu\chi''H_1{}^2 \qquad (10)$$

Comparing equations (9) and (10), χ'' is seen to be

$$\chi''=\frac{Ng^2\mu_0{}^2\nu G(\nu)}{6kT}J\,(J+1) \qquad (11)$$

Since the Varian EPR spectrometer employs low frequency modulation of the external magnetic field with phase sensitive detection, the recorder displays the derivative of the absorption mode, provided that the amplitude H_m of the low frequency modulation is small compared to the line width. For linear crystal detection, the amplitude of the signal displayed at the recorder, S, is proportional to the following expression:

$$S \propto H_m H_1 \frac{d\chi''}{dH}$$

where H is the external magnetic field[7]. If square-law detection were used, the recorder signal, S, would be proportional to H_1^2 instead of H_1. Since only the $G(\nu)$ part of χ'' in equation (11) varies with H, the following expression results for fixed frequency.

$$S \propto \frac{H_m H_1 N g^2 \mu_0^2 \nu J(J+1)}{6kT} \frac{dG(H)}{dH} \qquad (12)$$

A spectral absorption curve, where the line shape is produced by collisions, is given by the Lorentzian relation,

$$G(\nu) = \frac{2T_2}{1+4\pi^2 T_2^2 (\nu-\nu_0)^2} \qquad (13)$$

where T_2 is the lifetime of the state and ν_0 the resonant frequency[6]. Paramagnetic atoms in the gas phase have produced line shapes predicted by this theory[5]. Since $h\nu = g\mu_0 H$,

$$G(H) = \frac{T_2 g\mu_0/\hbar\pi}{1+\frac{g^2\mu_0^2}{\hbar^2}(H-H_0)^2 T_2^2}$$

Therefore,

$$\frac{dG(H)}{dH} = \frac{2T_2^3 g^2 \mu_0^3 (H-H_0)/\hbar^2\pi}{\left[1+\frac{g^2\mu_0^2}{\hbar^2}(H-H_0)^2 T_2^2\right]^2} \qquad (14)$$

The distance between the maximum and minimum points of the derivative curve, ΔH, is found by setting

$$d^2G(H)/dH^2 = 0: \qquad \Delta H = \frac{2\sqrt{3}\hbar}{3g\mu_0 T_2} \qquad (15)$$

since S has a maximum and a minimum value when

$$(H-H_0) = \pm \frac{\sqrt{3}\hbar}{3g\mu_0 T_2} \qquad (16)$$

The peak-to-peak signal height between S_{max} and S_{min} may be found by substituting equations (15) and (16) into equations (14) and (12),

$$S_{max} \propto \frac{H_m H_1 N g^2 \mu_0^2 \nu J(J+1)}{(\Delta H)^2 kT} \qquad (17)$$

To measure the number of paramagnetic atoms present with a fixed-frequency spectrometer, the following expression may be obtained from equation (17):

$$\frac{N_a}{N_b} = \frac{(S_{max})_a (\Delta H)_a^2 T_a g_b^2 J_b (J_b+1)(H_1)_b (H_m)_b}{(S_{max})_b (\Delta H)_b^2 T_b g_a^2 J_a (J_a+1)(H_1)_a (H_m)_a} \qquad (18)$$

Equation (18) applies to atoms undergoing the simple Zeeman effect. It may also be applied to atoms with a nuclear spin, provided that the signal intensity $(S_{max})(\Delta H)^2$ is summed for all the hyperfine components. This may be done by multiplying the signal intensity of one of these components by $2I+1$.

The atoms studied in this work were atomic nitrogen and atomic hydrogen. Nitrogen has a nuclear spin of 1 and, hence, has three hyperfine lines while hydrogen, with its nuclear spin of 1/2 has two hyperfine lines. Both of these atoms have Lande g factors of 2 and are thus centered near 3320 G. The paramagnetic salt $MnSO_4$, used as a standard, has a nuclear spin of 5/2 and a g factor of 2.

In order to verify the EPR measurements the nitrogen atoms were titrated with nitric oxide[3, 9].

For nitrogen atoms, the reaction is

$$N + NO \longrightarrow N_2 + O \qquad (19)$$

As the flow of NO is increased from zero to an equimolar amount of N, the afterglow changes from the characteristic orange of pure nitrogen to the blue of NO and then disappears at the end point. The blue color is characteristic of the γ, β and δ bands of NO produced by the reaction:

$$N + O + M \longrightarrow NO + M + h\nu \qquad (20)$$

where M is any third body. A slight excess of NO produces the pale green afterglow resulting from the reaction:

$$NO + O \longrightarrow NO_2 + h\nu$$

3. APPARATUS AND EXPERIMENTAL TECHNIQUE

The instrument used for paramagnetic resonance detection was a Varian 4500 spectrometer in conjunction with a Varian 4012-B high resolution electromagnet (see Fig. 1). Although the high-resolution magnet may not be necessary in most work, it proved quite valuable in this

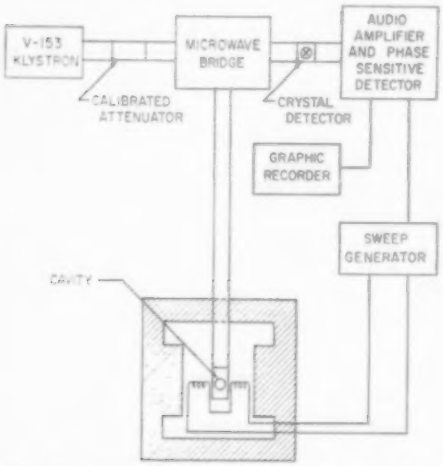

Fig. 1. Varian EPR spectrometer with 4012-B high resolution magnet.

research in which line widths are often limited by magnetic inhomogeneities; the limit being about 40 mG for a 0·5-in³ sample. The sensitivity of the spectrometer was sufficient to obtain usable measurements for atom densities of 10^{14} atom/cm³.

In order to observe such narrow lines quantitatively, i.e. without modulation broadening of the lines, it became necessary to modify the Varian 4205-A sweep unit with a continuous-decade potentiometer circuit (Fig. 2)*. This arrangement permitted a continuous variation of modulation field from 0 to the maximum value, whereas the previous variation was stepwise and had a minimum of about 35 mG.

Since it is desirable to study as wide a concentration range as possible, the spectrometer was further modified by adopting the large rect-

* The problem has recently been solved for large amplitudes of modulation.

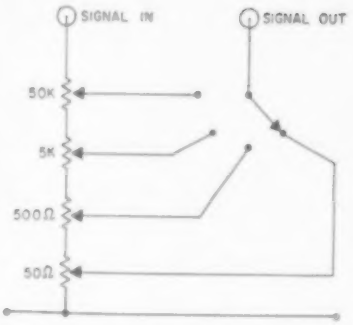

Fig. 2. Continuous decade potentiometer circuit for obtaining a continuous variation of field modulation amplitude.

angular sample cavity (Fig. 3). The choice of a rectangular over a cylindrical cavity was necessitated by the 1¾-in. gap of the high resolution magnet which, in turn, was necessary in order to observe the narrow lines. The large-diameter tubes perpendicular to the length of the cavity, as seen in Fig. 3, have a diameter of 14·5 mm (below cutoff), which prevents leakage of radiation out of the cavity. Because the sample tubes, having an I.D. of 12–13 mm, extend appreciably into the electric field of the cavity, only quartz, etched with HF to a wall thickness of ½ mm or less, is used. This procedure permits a high Q and reduces microphonics because of the small amount of glass in the cavity.

Because of the rigidity of the glass flow system and because of the inaccessibility of the standard iris screw in a 1¾-in. magnet gap, it became necessary to refine the iris screw to permit adjustment while in the magnet gap (Fig. 4). This construction permitted adjustment with the tip of a pencil eraser, which proved sufficiently sensitive for all adjustments.

A sketch of the flow system is seen in Fig. 5. The pressure could be measured upstream and downstream with a Consolidated Electrodynamics McLeod gauge or monitored constantly with Pirani gauges. The flow meters were either of the standard Fischer and Porter type, or were custom made and then calibrated with a gas buret at atmospheric pressure. The flow was controlled by Hoke stainless steel needle valves. The flow rates were the order of 0·1–3 cm³/sec

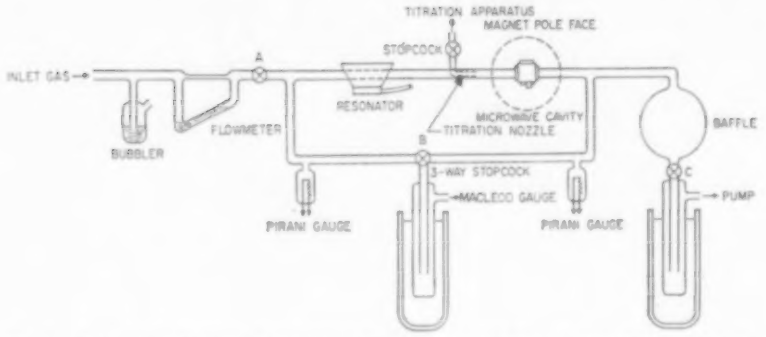

Fig. 5. Schematic diagram of apparatus for spin resonance and titration studies of discharge products.

s.t.p., corresponding to times of flight between 0·1 and 0·01 sec from the discharge to the cavity. The vacuum system consisted of a Welch 1397 E mechanical pump having a pumping rate of 13·5 ft^3/min with a Consolidated Electrodynamics VMF-21 air-cooled metal diffusion pump. The diffusion pump was used only for rapid pump down and cleanup and for leak testing. Fig. 6 is a photograph of the major portion of this system. Also seen in the photograph is the 2400-Mc microtherm unit used to maintain the gaseous discharge (the initiation of the discharge being accomplished by a tesla coil). The microtherm has a variable output with a maximum of 125 W. The antenna is fastened to an adjustable holder which is then adjusted until the microwaves are focused on the quartz tube in the proximity of the cavity; the holder also serves as an adjustment in studying the recombination as a function of the distance from the discharge. To prevent excessive heating of the quartz tube and to insure near-room-temperature gas in the cavity, a glass jacket is positioned over the quartz tube with O-rings and air forced through the annular space at a rate sufficient to maintain the exhaust air within a few degrees of room temperature.

Although equation (18) is linear in H_1 and does not include a general crystal law, the concentration measurements do depend upon the crystal-detection law. For a video crystal such as a Microwave Associates 408-B which was used here, one may obtain a square law or linear law, depending on the power level. In order to determine the power law, the signal intensity for DPPH was studied vs. calibrated microwave power for constant self-bias or constant microwave power incident on the crystal. These results are shown in the upper curve of Fig. 7. The crystal has a linear response within experimental error. The deviation from linearity apparent at the lower part of the curve is the result of signal loss caused by excessive insertion of the stub tuner, which is necessary for maintaining constant microwave power incident on the crystal. The lower curve is for the same range as before, except that the constant bias is no longer maintained by self-bias from the stub tuner but instead is maintained for a near-balance condition with the bias derived from a battery and potentiometer (Fig. 8). In the work described in this report, the self-bias, or constant-microwave-power condition, was used exclusively.

During the early part of the investigation, it became apparent that a systematic error was causing intensity variation outside the experimental error. After a careful study, it was found that for a particular crystal, the crystal sensitivity varied with crystal bias. A characteristic behavior is shown in Fig. 9. The reason for this behavior is the change of crystal impedance with crystal bias and the consequent change in the output power. Although Fig. 9 is representative, individual crystals vary as much as 50 per cent from this curve. One

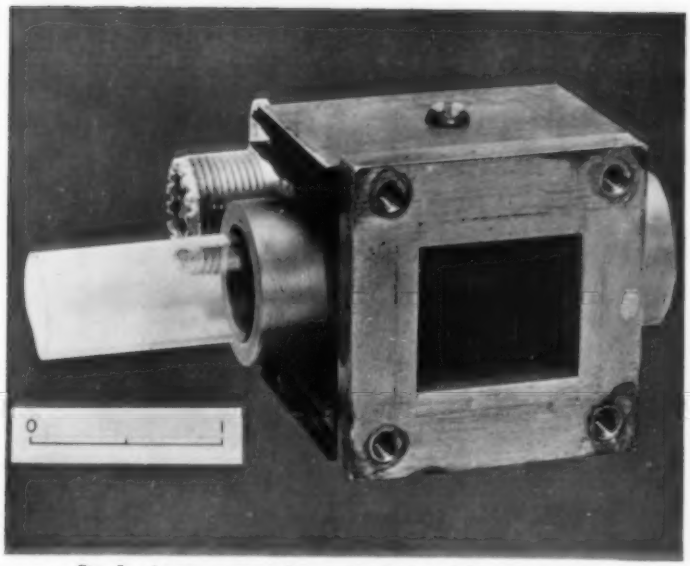

Fig. 3. Large rectangular cavity designed for gas studies.

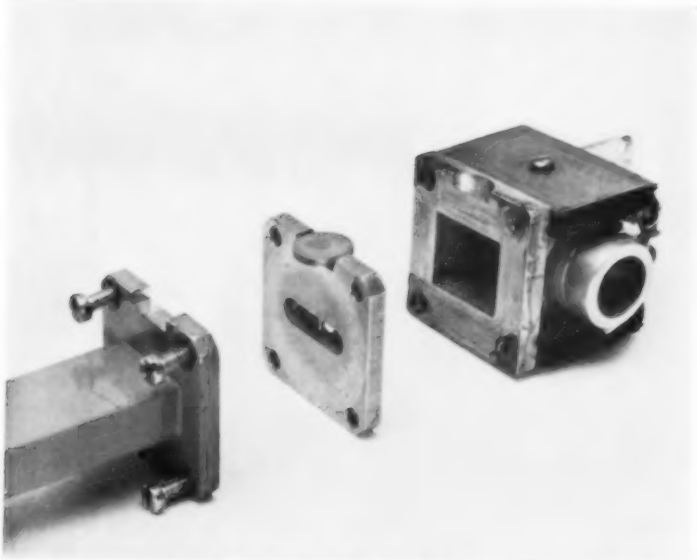

Fig. 4. Refinement of iris screw to permit adjustment while in magnet gaps.

(facing page 198)

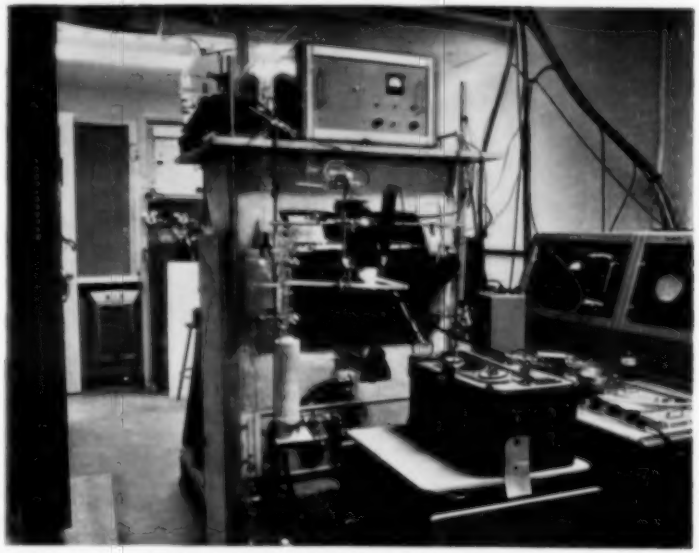

Fig. 6. Physical appearance of apparatus.

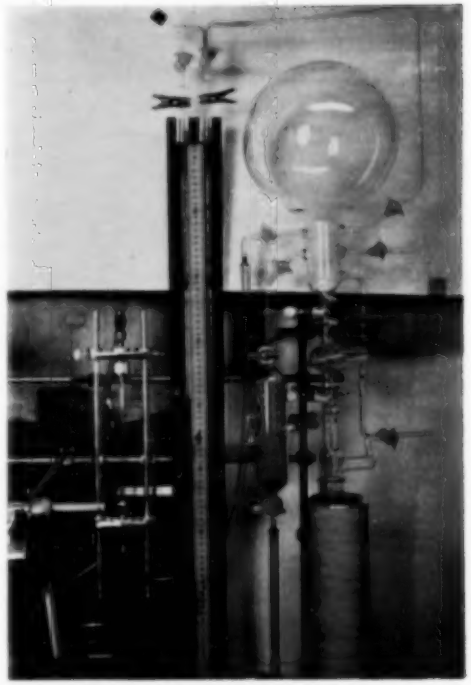

Fig. 11. Atom titration apparatus.

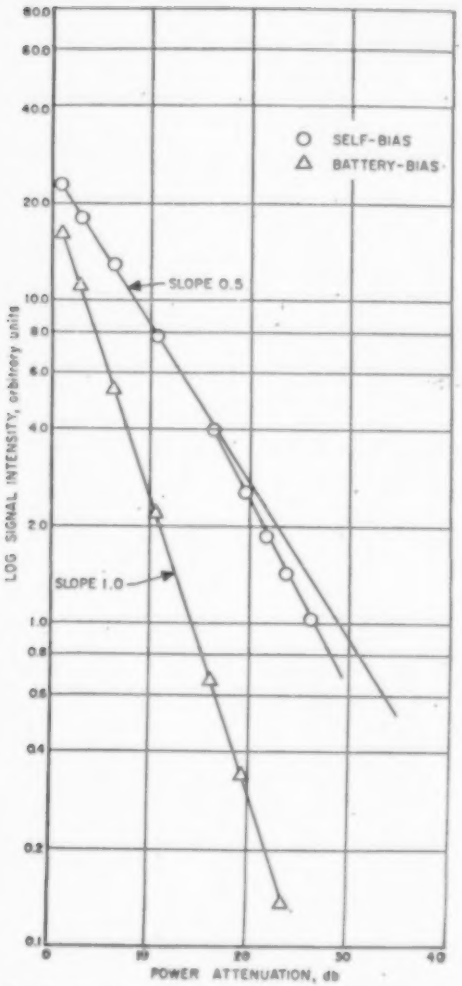

Fig. 7. Signal intensity vs. power delivered to solid DPPH.

rather disturbing feature of the system initially was that upon striking the discharge with a tesla coil, the crystal would always be affected and usually damaged if not destroyed. It was soon realized that the 2 Mc output of the leak tester would leak into the crystal via the crystal cable, with subsequent damage. This was eliminated by disconnecting the crystal while using the leak tester.

To prevent surface recombination, the quartz

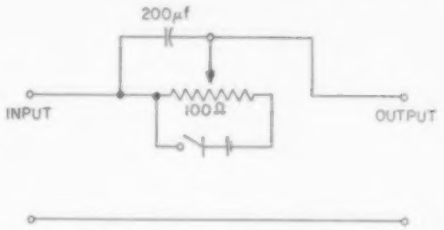

Fig. 8. Battery bias circuit.

tube between the discharge and cavity regions (up to 4 ft in length) was first cleaned rather thoroughly. This consisted of washing with soap and water, followed by a water rinse, which in turn was followed by a nitric-acid rinse. To ensure a fresh quartz surface, the surface was soaked in HF for about 15 min and then rinsed with water and dried in the vacuum system. If the system were now used under these conditions, one would still not see any appreciable nitrogen afterglow. In the past, workers have used a surface coating of metaphosphoric acid to prevent recombination.

It was found in the early phase of the investigation that this method of conditioning was not reproducible, that it varied from day to day and that it involved tedious preparation. Instead, a much simpler, reproducible method was discovered, which consisted of passing as high a density of nitrogen atoms as available through the quartz tube (after cleaning and evacuation) for a period of about 15 min. The afterglow, which would be evidence of the presence of atoms, was not noticeable at first, but soon would appear and continue to increase in length until it extended into the vacuum

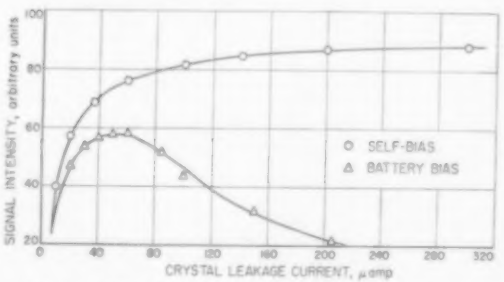

Fig. 9. Signal intensity vs. crystal leakage current for a given power level.

pump hose. After this conditioning, the atomic nitrogen concentration would be at a maximum value for the corresponding pressure and flow-rate conditioning. Also, when hydrogen was again introduced one could then observe large atomic hydrogen concentrations which were absent without the nitrogen "conditioning" or the use of metaphosphoric-acid coating. Eventually, the system would become contaminated, either because of impurities in the gases or inadvertent admission of atmospheric air. This contamination could easily be removed simply by reconditioning with the nitrogen discharge. The mechanism of the cleanup is still under investigation. The two most valuable features of the method were the ease of cleaning an assembled system and reproducibility.

The spectrometer is calibrated for the number of spins, using a known quantity of 0·1 F $MnSO_4$ in a 1½-mm I.D. capillary tube which is placed carefully along the H_1 field maximum. A representative spectrum is shown in Fig. 10. If either too large a conducting sample is placed at the maximum value of H_1 or a lossy dielectric

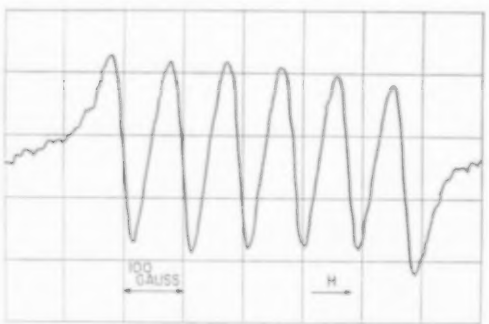

Fig. 10. Hyperfine spectra of Mn^{++} in 0·1 F $MnSO_4$.

is located in the region of the electric field, then the cavity Q will be affected adversely. Although the Q has been omitted in equation (18), it should, in general, be included. Also, the average of H_1^2 over the sample region is required in comparing the signal of a sample at the center of the tube with the signal of a sample filling the entire quartz tube. For the geometry used in this work, this value is calculated to be $H^2_{1\text{AVG}} = 0{\cdot}88\, H^2_{1\text{MAX}}$.

The titration apparatus for NO is shown schematically in the flow system of Fig. 5. The titrant is added between the discharge and cavity via a small nozzle. A 5l. storage flask is part of the gas-handling apparatus (Fig. 11). The flow rate of the titrants can be determined either by measuring the pressure drop in this storage flask or by calibrating a flow meter, the former being the one actually used. The pressure drop rate was measured with a differential oil manometer, using FS-5 Fluorlube (manufactured by Hooker Electrochemical Company), which is relatively inert to the corrosive NO gas.

Probably the most important single factor in obtaining accuracy was the normalization procedure using molecular oxygen. Because of the complexity of the overall instrument, it is impossible to obtain constant intensity measurements from day to day or even from experiment to experiment. This is aggravated by the difficult task of disassembling the flow system each day, obtaining a usable reading, and still accomplish some new work. By introducing 1 mm Hg of molecular oxygen into the sample tube, one can observe the complex molecular-oxygen-resonance structure starting at about 8000 G for the frequency of 9400 Mc. Because the lines are rather broad and are not limited by magnetic inhomogeneities which vary from day to day, any one of the oxygen lines is a suitable standard, provided it is readily identifiable and the temperature does not vary. Using this simple standard, the instrumental variables, such as gain variation due to aging, power line fluctuation, crystal degradation, etc., were soon understood and either eliminated or accounted for. After gaining confidence in the entire method, it was possible to continue taking data on the same experiment during the course of a week, during which a possible crystal-sensitivity change had occurred, and still have the results agree very well.

4. RESULTS

Applying equation (18) in intensity comparisons, it is assumed that all signals are characterized by a Lorentzian line shape or at least the same line shape. If this were not the case, the theory would have to be based on a

moment analysis of each spectrum. This assumption can readily be verified by examining the slope of the derivative curves. For the derivative of a Lorentzian absorption curve, the ratio of the maximum negative slope to the maximum positive slope would be 4·0 : 1. In this report, this ratio for H(^2S), N(^4S), and

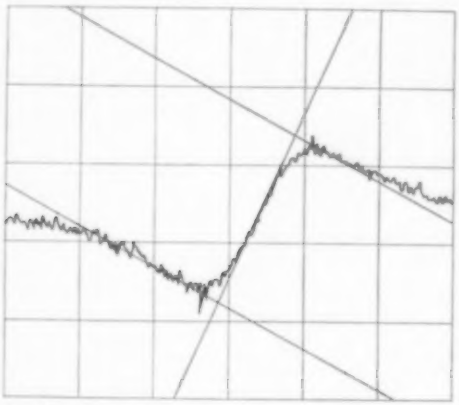

Fig. 12. The Lorentzian character of one of the lines of the H(^2S) spectrum.

Mn(^6S) was found experimentally to be 4·0 ± 0·3. A representative spectrum is seen in Fig. 12.

Another factor which must be considered in using equation (18) is the temperature of the gas in the cavity, room temperature being appropriate for the Mn standard. The EPR intensity of the gas varies with the square of the temperature at constant pressure, first because of a density factor and secondly because of a susceptibility variation.

An estimate of the temperature at 3 mm Hg was obtained by studying the molecular oxygen, at first without discharge and then with discharge. An intense line of the O_2 spectrum was first observed without discharge at room temperature. With discharge conditions, atmospheric air was first added to provide a poisoned wall for complete oxygen atom recombination within a few centimeters downstream. The fact that no atoms were present was verified by the addition of a minute quantity of NO_2, which was observed to produce no afterglow[11]. After obtaining equilibrium, it was found that the molecular oxygen signal at a distance of 35 cm from the discharge had decreased to a value appropriate to a temperature of about 50°C, whereas room temperature was 22°C. This is in fair agreement with other work[9].

At room temperature, the per cent atom concentration of high-purity dry nitrogen at 3-mm Hg pressure was found to be 2·0 ± 0·5 per cent. This result is shown in Fig. 13. The large error is due to the cavity-field-configuration estimate, pressure and temperature; the EPR reproducibility is better than ±5 per cent over the range shown.

The concentration at 3 mm Hg for the same discharge conditions and flow rate, was also measured independently by titration with NO. These results are also shown in Fig. 13. Since the apparatus was designed to observe the

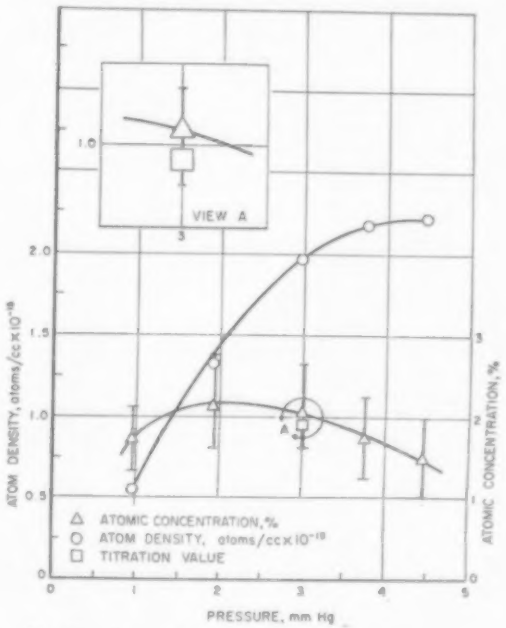

Fig. 13. Atom density and per cent atom concentration vs. pressure for atomic nitrogen.

titration products with the EPR, Fig. 5, there exists a systematic error between the EPR and titration results because of a small amount of wall recombination. To see how large this difference was, the discharge was moved from

the previous position by a factor of 2 away from the cavity. After equilibrium was attained, the signal was found to have decreased by about 5 per cent. Although there are two effects, namely increase of signal because of decreased temperature and decreased signal because of recombination, the recombination is relatively small for nitrogen. The reason titrations were not run at a lower pressure was because of the uncertainty in end point due to decreasing light intensity with decreasing atom density.

The curves in Fig. 13 are representative of the results obtained for nitrogen for a constant pump capacity, which was the case for all data except for one nitrogen experiment. In this case, it was found that for constant velocity of gas flowing through the cavity, the concentration curve was much more peaked and shifted to the left, but the maximum concentration was no greater. The pump capacity, exclusive of this case, was 5–13 ft^3/min, being constant within each experiment.

When approximately 10 per cent water vapor was added to the dry nitrogen, the atom density increased to a maximum of about 5 per cent. If more than 10 per cent water vapor was added, the N atom density was found to decrease markedly. There was never any difficulty in maintaining the discharge with dry nitrogen for pressure above 0·1 mm Hg. Also, it was found that the nitrogen atom density was rather insensitive to discharge power.

The hydrogen atom density and concentration at various pressures of molecular hydrogen are shown in Fig. 14.

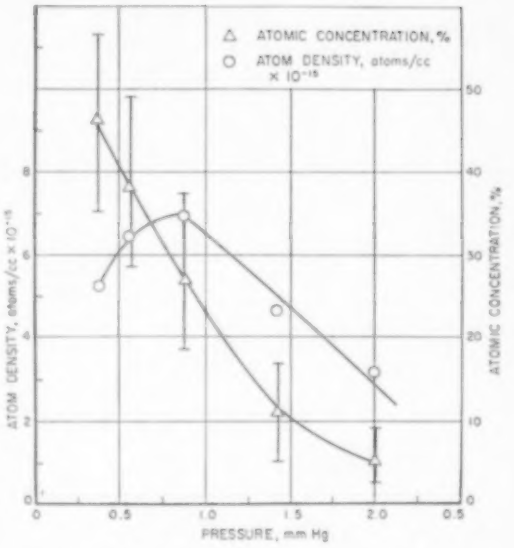

Fig. 14. Atom density and per cent atom concentration vs. pressure for atomic hydrogen.

5. CONCLUSIONS

Reproducible EPR intensity measurements can readily be made in the gas phase, provided a normalization standard such as molecular oxygen is used and there is sufficient homogeneity to retain a Lorentzian line shape. If the latter is not the case, a first moment analysis of each spectrum has to be made. For absolute intensity measurements, a better standard than Mn^{++} would be molecular oxygen with an N–NO titration, provided the titration is performed immediately after the cavity in a flow system to prevent recombination errors. The only difficult conversion factors are the temperature, which enters in as the square, and the pressure.

For atomic hydrogen in molecular hydrogen, a much simpler concentration measurement can be made; namely, measuring the line width and temperature, provided the line width is not determined predominantly by magnetic-field inhomogeneities[8]. Because of an inhomogeneity of about 40 mG over the sample in the present apparatus, the measurement by this technique is limited to a concentration of 10^{15} atoms/cm^3 or more. This may eventually be applied to a similar case, in which there is more than one species present, as in mixtures of oxygen atoms and molecular oxygen.

The atomic nitrogen and atomic hydrogen wall recombination can be reduced to a negligible value by passing nitrogen discharge products through the system at 4–5 mm Hg until the nitrogen afterglow extends throughout the system. The concentration for atomic hydrogen can be increased by adding a small amount of water vapor.

NOMENCLATURE

c = velocity of light in vacuo
d = symbol of differentiation
e = charge on the electron, e.s.u.
g = splitting factor for the electron
g_n = splitting factor for the nucleus
h = Planck's constant
$\hbar$ = Planck's constant divided by 2π
k = Boltzmann's constant
m = the mass of the electron
t = time
F = a formal-weight solution
$G(H)$ = normalized shape functions
H = magnetic field
H_0 = magnetic field corresponding to resonance
H_m = amplitude of the modulation field
$\mathbf{I}$ = nuclear angular momentum
I = nuclear quantum number
$\mathbf{J}$ = total angular momentum
J = atomic quantum number
H_1 = amplitude of the radio-frequency field
$\mathbf{L}$ = orbital angular momentum
$\mathbf{M}$ = the magnetic moment
M = magnetic quantum number
M_n = mass of the nucleus
N = number of spins per unit volume
N_J = number of spins per unit volume in the Jth state
P = power absorbed per unit volume of sample
Q = quality factor of an electrical circuit given by the energy stored per cycle divided by the energy lost per cycle
$\mathbf{S}$ = spin angular momentum
S = output of the phase sensitive detector
S_m = the peak to peak output of the phase sensitive detector
s.t.p. = standard temperature and pressure
T_a, T_b = absolute temperatures °K
T_2 = spin–spin relaxation time
W = transition probability
γ = all quantum numbers other than J, M
μ_0 = Bohr magneton
ν = frequency
ν_0 = resonant frequency
ρ_ν = radiation density
χ'' = imaginary part of magnetic susceptibility

REFERENCES

1. I. Langmuir, *Trans. Amer. Electrochem. Soc.* **20**, 2225 (1911).
2. H. Kroepelin and E. Vogel, in collaboration with G. Kremser, *Abh. Braunschw. Wiss. Ges.* **6**, 73 (1954).
3. F. Kaufman and J. R. Kelso, *J. Chem. Phys.* **27**, 1209 (1957).
4. N. Bloembergen, E. M. Purcell and R. V. Pound, *Phys. Rev.* **73**, 679 (1948).
5. E. U. Condon and E. H. Shortley, *The Theory of Atomic Spectra*. Cambridge University Press (1953).
6. E. R. Andrew, *Nuclear Magnetic Resonance*. Cambridge University Press (1955).
7. G. Feher, *Bell Syst. Tech. J.* **36**, 449 (1957).
8. A. F. Hildebrandt, F. B. Booth and C. A. Barth, *J. Chem. Phys.* **31**, 273 (1959).
9. G. B. Kistiakowsky and G. G. Volpi, *J. Chem. Phys.* **27**, 1141 (1957).
10. F. Kaufman and J. R. Kelso, *J. Chem. Phys.* **28**, 510 (1958).
11. F. Kaufman, *J. Chem. Phys.* **28**, 352 (1958).

INTRODUCTION TO SESSION ON THERMODYNAMICS AND TRANSPORT PROPERTIES OF GASES

C. F. CURTISS
University of Wisconsin, Madison, Wisconsin

The aerodynamic behavior of high-speed missiles moving through the atmosphere may be described by the hydrodynamic equations of change. These are the equations of continuity of each chemical species, the equation of motion of the mixture and the equation of energy balance. In these hydrodynamic equations of change appear a set of coefficients referred to as "transport coefficients". These coefficients are associated with the processes of diffusion, viscosity and thermal conductivity. Quantitatively, the solutions of the hydrodynamic equations depend upon the values of the various transport coefficients.

Quantitative predictions of the drag on a high-speed missile and the heat flux to a surface of such a missile, thus, depend on estimates of the values of the transport coefficients and the temperature and density variation of these coefficients. In this session the possibility of making such quantitative estimates is investigated and discussed.

For the simple nearly spherical uncharged molecules which occur in the atmosphere, kinetic theory has provided adequate expressions for the diffusion and viscosity coefficients in terms of the intermolecular potentials. The problem of estimating these transport coefficients is thus simply related to the problem of estimating the intermolecular potentials. The coefficient of thermal conductivity is complicated by the presence of energy in the internal degrees of freedom and the finite relaxation time required to equilibrate this energy with the translational energy of the molecules. The energy flux to the surface of a missile is also influenced by the rates of chemical reactions occurring in the gas. At sufficiently high temperatures some ionization of the atoms and molecules begins to occur, and new problems associated with the long range of the Coulomb potential arise.

The present status of our knowledge of intermolecular potentials and in particular the influence of small errors in intermolecular potentials on the transport properties is discussed in the first paper of the session.

THE PRESENT STATUS OF INTERMOLECULAR POTENTIALS FOR CALCULATIONS OF TRANSPORT PROPERTIES

R. A. BUCKINGHAM
University of London, London, England

Abstract—A review is given of the present state of knowledge of the interaction of systems having spherical symmetry, with special reference to the adequacy of analytic expressions used to represent such interactions, and to methods of deriving short range repulsive potentials. Some recent calculations of transport coefficients for "dissociated" atoms are briefly described. A bibliography of recent contributions to the subject is included.

1. INTRODUCTION

I should begin by saying that this discussion of intermolecular forces will be limited to systems which are more or less spherically symmetrical and non-polar. This is not to deny the great importance of investigating interactions which have angular dependence but of these, long-range forces accepted, we have relatively little knowledge as yet. The self-imposed restriction still leaves a considerable field for useful discussion.

The above title will be taken to mean "The present state of our knowledge of intermolecular potentials for calculations of transport properties". It is now a fact that for dilute gases at least, thanks to the theories of Chapman, Enskog and others, the calculations of transport properties presents no difficulty in principle, whenever the concept of an intermolecular potential is valid and the form of the potential is adequately known. At high temperatures in particular the calculation is often relatively simple, and in any case the availability of fast computers makes the task of deriving viscosity and diffusion coefficients easily acceptable. This I shall regard as sufficient excuse to concentrate on the problem of deducing the potentials we need.

It is not necessary for this purpose to dwell on the question of validity. This has been discussed in a recent paper by Hornig and Hirschfelder[1]. We are well aware of situations in which the concept of intermolecular potential is not very useful, but there is still a considerable range of phenomena for which it is, covering thermal energies up to 1 or 2 eV, for which many collisions are still effectively adiabatic.

As a preliminary we shall summarise some of the elementary facts concerning intermolecular forces and their evaluation. Many details can of course be found in the well known treatise on *Molecular Theory of Gases and Liquids* by Hirschfelder *et al.*[2].

First, Fig. 1 shows some of the commoner types of interaction:

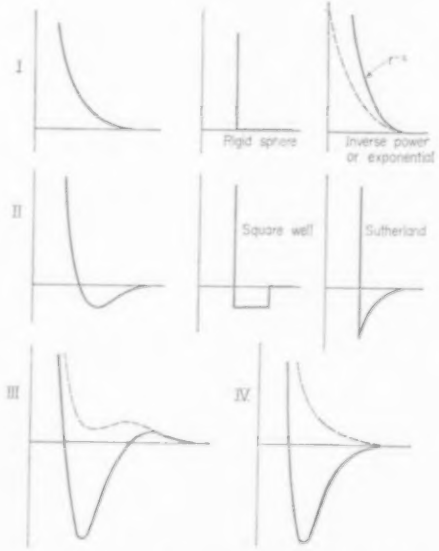

Fig. 1. Types of intermolecular potential.

(I) Simple repulsive potentials, such as may represent the interaction of two closed shell atoms in a gas at high temperature. Simple models are the rigid sphere potential, the inverse power potential or the exponential.

(II) A potential which is a combination of short-range repulsion and weak long-range attraction. This is typical of many interactions of closed shell systems when dispersive (van der Waals) forces are included. Crude models are the square well potential and the Sutherland potential.

(III) Potential with deep (or maybe shallow) well and repulsive barrier. This may occur in interactions involving metastable atoms (e.g. He′ and He), or in interactions between excited atoms as a result of "curve-crossing".

(IV) Potentials with deep potential well, characteristic of covalent (or perhaps ionic) bonding between atoms; often associated with repulsive potentials of type (I) or (III).

The derivation of potential energy functions may be carried out in a number of ways, including

(a) direct quantum mechanical calculations,

(b) direct experiments involving collision between atoms, ions or molecules,

(c) an inductive process, using known macroscopic properties of gases, liquids and solids to guide the choice of an analytic expression for the potential.

Other experimental techniques using for example vibrational relaxation times in molecular gases, also shock-wave and detonation phenomena, will no doubt prove useful, but the information derived from these at present is not very precise[4].

Table 1 shows some of the systems which have been treated theoretically. No doubt this list is incomplete, but it is intended to include only those systems for which both short range and long range interactions have been investigated. Even so there are very few cases in which the treatment has been "complete" in the sense that both first and second order effects have been included in the same calculations by choosing the unperturbed wave functions suitably. In any case only the simplest systems have so far yielded results of practical significance.

Table 1. Theoretical Calculations

Neutral		Ionic	
Ground states	Ref.	Ground states	Ref.
H + H	11, 23, 28	$H^+ + H, H_2^+$	8, 43
H + He	21, 35	$(He\,H)^{++}$	7, 13
H + Li	30	$H^+ + He$	17
H + Be	25	$H^- + H$	14
		$H^- + He$	39
$H + H_2, H_3$	See 2, 5, 82	$H_2^+ + H, H_3^+$	See 2
$H_2 + H_2$	15, 18, 19	$H^- + H_2$	40
He + He	16, 22, 24, 33, 34, 44, 45	$H_2^+ + He$	38
Li + Li	6, 12, 26, 27	$He^+ + He$	37, 41, 42
Ne + Ne	9	$Li^+ + H$	30
A + A	32	$Li^+ + He$	36
Excited states	Ref.	Excited states	Ref.
H + H′	29	$H^+ + H', (H_2^+)'$	8, 31
H′ + H′	55	$He^+ + He'$	
H + Be′	25		
He + He′	10		
Be + Be′	20		

I shall next discuss a few points concerned with the interaction potentials as a whole.

2. THE COMPLETE INTERACTION

There are various analytic expressions which have been in use for many years to represent interactions of the type shown in Fig. 2. These

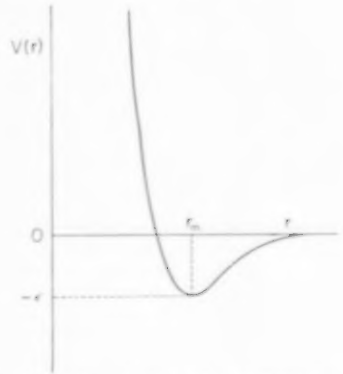

Fig. 2. Potential of type (2). Definition of parameters: $V(r)=\varepsilon v(\rho)$
$\rho=r/r_m$
$v(1)=-1,\ v'(1)=0$

are often written in the form

$$V=\varepsilon v(\rho), \quad \rho=r/r_m$$

where ε and r_m are convenient scaling factors and $v(\rho)$ is essentially a shape function which may itself contain one or more parameters. Some of these formulae are shown in Table 2, as follows:

The first, when $s=12$, gives the frequently used "Lennard–Jones potential". In the second, the exponential term would lead to a meaningless maximum at a very small value of ρ unless the function is arbitrarily made infinite at some point $\rho=\bar{\rho}$. In the third formula this difficulty is partly avoided by means of a suitable function $q(\rho)$, which eliminates the terms in ρ^{-6} and ρ^{-8} for small ρ. One form of $q(\rho)$ which has been used for this purpose[58,59] is $\exp[-4(1-\rho)^3/\rho^3]$, which has the effect of making these terms negligible for $\rho<0{\cdot}5$. It should be borne in mind that these inverse powers have significance only at intermediate and long ranges.

The results of using analytic expressions such as these to fit experimental data for virial coefficients, viscosities, etc., and thence to choose the best values for the parameters, have

Table 2. Intermolecular Potentials

$$V(r)=\varepsilon v(\rho)$$

with $\rho=r/r_m$, $v(1)=-1$.

$(s, 6)$	$v(\rho)=\left(\frac{6}{s-6}\right)\frac{1}{\rho^{12}}-\left(\frac{s}{s-6}\right)\frac{1}{\rho^6}$
$(\exp a, 6)$	$v(\rho)=\left(\frac{6}{a-6}\right)e^{-a(\rho-1)}-\left(\frac{a}{a-6}\right)\frac{1}{\rho^6}, \ \rho>\bar{\rho}$ $=\infty, \ \rho\leqslant\bar{\rho}.$
$(\exp a, 6, 8)$	$v(\rho)=v_2 e^{-a(\rho-1)}-v_1\frac{q(\rho)}{\rho^6}\left(1+\frac{b}{\rho^2}\right)$ where $v_1=\frac{a}{a(1+b)-6-8b}$ $v_2=\frac{6+8b}{a(1+b)-6-8b}$ $q(\rho)=1, \ \rho\geqslant 1$ $\longrightarrow 0, \ \rho\longrightarrow 0.$

not been uniformly successful. Even for helium, an apparently simple example, very discordant results have been published in recent years for the principal parameters, ε and r_m. This can be seen from Table 3 which contains several estimates of these parameters and in Fig. 3 which depicts the corresponding potentials.

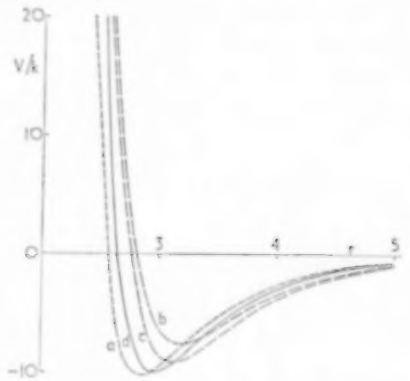

Fig. 3. Intermediate range interaction of normal helium atoms (V/k in °K; r in Å): (a) de Boer and Lunbeck[64,67]; (b) Kilpatrick, Keller and Hammel[66]; (c) Mason and Rice[69]; (d) Buckingham, Davies and Davies[59]. (For parameters, see Table 2).

This is surely contrary to theoretical expectations.

Likewise, though this is less important, the coefficient of the repulsive term may depend on a parameter such as b which is primarily a property of long range forces. A third disadvantage is that the curvature near the minimum is strongly influenced by the parameter associated with the inverse power or exponential term.

We are thus in the awkward position that a bend of the head of the curve makes the tail wag, and a twist of the tail causes the head to nod! However, if we are in earnest about deriving potentials which are physically significant and which correlate the widest variety of properties of the substance, it is very necessary to be able to vary the two ends of the curve independently of each other and independently of the position of the minimum.

Thus it is desirable to have three parameters to specify the radius and depth of the minimum and the curvature at the minimum; perhaps two more (e.g. van der Waals coefficients) to define the asymptotic variation for large r, and a further two to define the shape and magnitude

Table 3. Potential Parameters for He–He Interaction

Potential	ε/k (°K)	r_m Å	$c\,10^{60}$ (erg cm^6)	Λ_m	Authors
(12, 6)	10·22	2·869	1·573	2·385	de Boer[64], Lunbeck[67]
(exp 12·4, 6)	7·56	3·189	2·127	2·536	Kilpatrick, *et al.*[66]
(exp 12·4, 6)	9·16	3·135	2·325	2·305	Mason and Rice[69]
(exp 13·5, 6, 8)	9·97	2·976	1·50	2·33	Buckingham, *et al.*[59]
Theoretical			1·50		Dalgarno and Lynn[52]

c is the van der Waals coefficient of r^{-6}.

Λ_m is the quantal parameter $h/r_m\sqrt{(m\varepsilon)}$.

Similar uncertainties may be found in published results for most of the rare gases. These ambiguities may be due in part to different methods of fitting data, but the cause is perhaps more likely the fact that the shape functions $v(\rho)$ used are not flexible enough[57]. Thus if the van der Waals coefficient of r^{-6} is derived from any of the formulae shown, it is found to depend on the parameter associated with the repulsive term, either s if ρ^{-s} or a if $\exp(-a\rho)$. of the short range potential. This may mean using more than one function to represent the whole potential, but with computers becoming more easily available, there is no reason to shirk the extra computation which the large number of parameters will involve. It should be stressed that not all the parameters need be determined simultaneously; some will be derivable most effectively from one set of data, others from another set, and some guidance may be

obtainable from theoretical calculations. A piecemeal approach to this problem, governed by discretion and commonsense, may give the best results.

We shall now review rather briefly recent progress in connection with long range and intermediate range forces, and then discuss more fully the short range repulsive part of the potential.

3. LONG-RANGE FORCES

Not a great deal has been learned about the general properties of long-range forces between two atomic systems since the well known review by Margenau[3] in 1939. However, much notable progress in detail has been made in recent years, including a few calculations of the forces produced by quadrupole interactions.

The following developments should be briefly mentioned in passing:

(1) The work by Dalgarno[50–52] and his collaborators in improving the estimates of van der Waals coefficients from oscillator strengths, including the metastable states of helium; also the paper by Dalgarno and Lynn[136] on resonance interactions between hydrogen atoms.

(2) The progress, again by Dalgarno *et al.*[14,49,53], and also by Mason and Vanderslice[36–39,41,56], in understanding the mobilities of ions in gases.

(3) The calculations of Britton and Bean[47] on long-range forces between hydrogen molecules.

(4) Calculations by Linder and Hirschfelder[55] on the interactions between hydrogen atoms excited to $2s$ and $2p$ states, and also between oxygen and sulphur atoms in their ground states[54].

(5) On the experimental side, molecular beam experiments by Bernstein and Rothe[46] using beams of potassium and caesium atoms in a large number of gases.

4. INTERMEDIATE RANGE FORCES

Under this heading we shall include a large part of the work which has been done in the past on deriving parameters for various analytic potentials by fitting experimental data either for gases at moderate or low temperatures or for the crystalline state. A complete list of references to such work would be very long and only a few are given here.

Following the pioneer work of Lennard–Jones this approach was largely concerned with equation of state data and some crystal properties, although a few calculations of viscosity[61,64] were made prior to 1948. However, in that year the results of collision integral calculations for the Lennard–Jones potential published by Hirschfelder *et al.*[65] stimulated much further work using viscosity and other data on transport properties of gases. Thus their tabulations, which were based on classical mechanics, were followed by others using other forms of potential[59,66,69]. At the same time many calculations using quantum mechanics were carried out, mainly at two centres, London and Amsterdam, under the guidance of Massey[59,60] and de Boer[62] respectively. The quantal results were applied to the lighter gases (helium and hydrogen) and used low temperature data to derive the potential parameters. Interesting isotopic effects, as well as differences between quantal and classical mechanics were brought to light.

Crystal properties obviously provide a good means of obtaining information about the interaction in the neighbourhood of the potential minimum. This is particularly true of the rare gas crystals. Again the earlier work was carried out by Lennard–Jones, but the method of calculation has been refined from time to time, e.g. by Corner[63] and by Zucker[70]. Generally speaking these investigations together with the use of transport coefficients have provided the most reliable information on interactions in the intermediate range.

5. SHORT RANGE FORCES

One of the most fruitful sources of information about the short range repulsions between atoms and molecules has been the series of scattering experiments carried out by Amdur and his colleagues[73]. In these the effects of grazing collisions are observed, and an analysis of the results assuming a law of the form r^{-s} provides information about the interaction in

the range for which the energy lies between about 0·2 and 1·2 eV.

The analysis has shown that the exponent s tends to decrease as the nuclei approach closer, a result which we should expect because in the limit the electronic energy of the system tends to a finite value and the only infinite term arises from the Coulomb repulsion of the nuclei. The evidence on this softening effect is collected in Table 4.

Table 4 also contains some results derived from ion-scattering experiments by Cramer and Simons[78–81], which show a similar behaviour. There is a little doubt as to whether these interactions involved here are repulsive or attractive. Some care in interpretation is needed when there is a possibility of a molecular ion being formed (as in $He^+ + He$), and although the experimental data may be consistently represented on the basis of a single interaction potential being effective, there may in fact be more than one and the formal analysis merely leads to some averaged potential.

accurate when extrapolated to energies of 1 eV. The position has been well summarized in a recent paper by Amdur and Ross[75], when they state that these are "intermolecular potentials of a very restricted kind which may be used with some confidence as interpolation devices for predicting the property from which they were derived. They may be used as an interpolation device for predicting other properties with varying degrees of success depending on the analytical form of the potential, the number of parameters, and the specific properties involved". However, "the use of the intermolecular potential as an extrapolation device will lead to unreliable results".

Results for the interaction of normal helium atoms illustrate this very well (Fig. 4). Here the (12, 6) potential commonly used at larger separations rises far too steeply for $r < 4a_0$; and a potential with an exponential term also lies considerably above the curve which the scattering experiments indicate as most likely. Theoretical calculations have not yet wholly

Table 4. Potentials from Scattering Experiments

$V(r) \backsim r^{-s}$

Amdur, Mason *et al.*			Cramer and Simons		
	r (in A)	s		r (in A)	s
He + He	0·5–1·0	1·79			
	1·3–1·6	5·94			
H + He	1·2–1·7	3·29	$He^+ + Ne$	1·0–1·3	3·24
He + A	1·6–2·3	7·29		1·3–2·0	7·43
$He + N_2$	1·8–2·3	7·06	$Ne^+ + He$	0·5–1·4	4·28
Ne + Ne	1·7–2·1	9·99	$Ne^+ + A$	1·2–1·7	4·80
Ne + A	1·9–2·4	9·18		1·7–2·8	6·37
A + A	2·2–2·7	8·33	$A^+ + Ne$	1·0–1·3	4·40
$A + N_2$	2·3–2·8	7·79		1·3–1·7	7·16
$N_2 + N_2$	2·4–3·1	7·27		1·7–1·9	12.1
Kr + Kr	2·4–3·1	5·42			
Xe + Xe	3·0–3·6	7·97			

As indicated already most information about intermolecular potentials has until recently been derived from macroscopic properties, such as viscosities or virial coefficients, which involve thermal collision energies rarely in excess of 0·1 eV. It would be unreasonable to expect potentials derived by fitting such data to be

resolved this difficulty, even in the relatively simple case of helium. This can be seen more clearly from the variation of the electronic energy obtained by subtracting $4/r$ from the total interaction energy (Fig. 5). If for large r this electronic energy is assumed to tend to that of two separate He atoms, then as $r \longrightarrow 0$ it

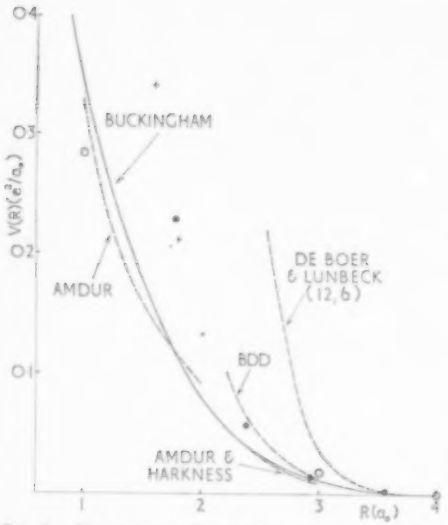

Fig. 4. Short range interaction of normal helium atoms: Total energy $V(R)$ as function of nuclear separation R.
Empirical potentials:
Amdur[71], Amdur and Harkness[72]—results of scattering experiments;
Buckingham[78]—potential based on equation (2);
de Boer, Lunbeck [64, 67]—extrapolated (12, 6) potential; Buckingham, Davies and Davies[59]—extrapolated (exp. 13·5, 6, 8) potential.
Theoretical estimates:
+ Griffing and Wehner[22], ° Sakamoto and Ishiguro[45]; · Rosen[44].

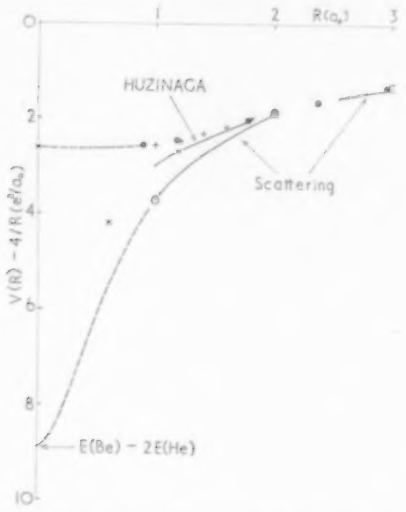

Fig. 5. Short range interaction of normal helium atoms: Electronic energy, $V(R) - 4/R$.
Theoretical estimates as in Fig. 4, with addition of points X by Eisenschitz and Crowe[16], and curve by Huzinaga[24].
The lower broken curve is based on equation (2).

should tend to the energy of a Be atom with a $(1s)^2(2s)^2$ configuration. A number of theoretical calculations have been unsuccessful for small r because the wave functions chosen were not consistent with this "united atom" configuration. Some recent calculations by Eisenschitz[16] and by Huzinaga[24] have largely avoided this pitfall and the results show a more satisfactory trend towards the ground state of Be.

There is clearly a need for some device which replaces the extrapolation problem of the short range potential by one which only requires interpolation. For two normal He atoms an obvious solution is to insert the known electronic energy of Be in a formula for the interaction energy which represents a Coulomb potential at very short range and then is rapidly diminished by an exponential factor. A simple expression of this type is that suggested by Frost and Woodson[86]:

$$V = \left(\frac{p_0}{r} + p_1\right) e^{-cr} \tag{1}$$

and a more elaborate function has been used by the author[78]:

$$V = \frac{1}{r}(p_0 + p_1 r + p_2 r^2 + p_3 r^3 + p_4 r^4)\, e^{-cr} \tag{2}$$

When r is small, equation (2) can be rewritten in the form

$$V = \frac{Z_1 Z_2}{r} + E_0 + [E_1 r] + E_2 r^2 + E_3 r^3 + E_4 r^4 + \ldots \tag{3}$$

where Z_1, Z_2 are the two nuclear charges and E_0 is the electronic energy of the "united atom". The coefficients in equations (2) and (3) are obviously related. Now perturbation theory shows that the term $E_1 r$ is likely to be absent, and the following relations then hold:

$$\begin{aligned} p_0 &= Z_1 Z_2 \\ p_1 &= E_0 + c p_0 \\ p_2 &= c E_0 + \tfrac{1}{2} c^2 p_0 \\ p_3 &= E_2 + \tfrac{1}{2} c^2 E_0 + \tfrac{1}{6} c^3 p_0 \\ p_4 &= E_3 + c E_2 + \tfrac{1}{6} c^2 E_0 - \tfrac{5}{12} c^4 p_0 \end{aligned}$$

Consequently if E_0 and E_2 are known all the coefficients up to p_3 are expressed in terms of a single adjustable parameter c. This may be chosen to give a potential which agrees best with the results of, say, scattering experiments. In one or two simple cases which have been investigated, it appears that E_3 depends only on nuclear attraction integrals and is therefore relatively easy to calculate. This would lead to an estimate of p_4 also. Alternatively p_4 may be chosen empirically so that V becomes zero for about the correct value of r.

A curve derived in this manner is shown in Fig. 5 and would seem to represent reasonably well all the information at present available about the short-range interaction of two helium atoms. Transport properties derived from this potential will shortly be available.

Some of the properties of the first few terms in expansion (3) have been investigated recently by Bingel[76, 77]. It should also be mentioned that theoretical calculations suggest the occurence of terms of the form $r^n \log r$ in the short-range interaction. However, as $n > 3$ the omission of terms such as these is not serious in a semi-empirical formula.

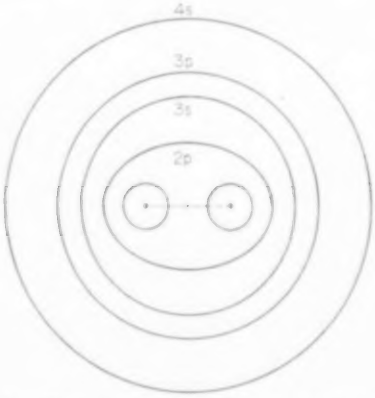

Fig. 6. Close interaction of two neon atoms (schematic).

For larger atoms it is not possible to use this technique without some modification. However, if for example we consider a system consisting of two neon nuclei in close proximity (at a distance of $\frac{1}{2}a_0$ or less) and surrounded by twenty electrons, it is clear that the system is similar to a calcium atom (Fig. 6). By using molecular orbitals perhaps of the LCAO type, for the four innermost electrons, and united atom orbitals centered on the midpoint between the two nuclei for the remaining closed shells, a good approximation to the energy of the system should be possible. Such a procedure has been suggested in the literature for calculations of equilibrium molecular structures and it would seem to be even more suitable here as a basis for calculating short-range interactions. Once the energy of the system has been determined for a few small values of the inter-nuclear distance it should be possible to derive a general expression of the shielded Coulomb type[2] to represent both this and any data obtained from scattering experiments.

Before leaving the subject of repulsive forces, it should be emphasized that, once the potential is known, fairly close estimates of viscosity may be obtained by means of the "equivalent hard sphere" approximation. It has been pointed out by Lefevre[55], and also by Hirschfelder and Eliason[57], that if the viscosity formula for a gas of rigid spheres is used to derive an equivalent rigid sphere diameter σ from a measured viscosity value and is plotted as a function of the thermal energy kT, the resulting curve lies very close to that representing the repulsive interaction potential. As an illustration of this, some recently calculated viscosities for the rare gases and also nitrogen, in the temperature range 1000°–15,000°K, have been converted to (σ, kT) plots and compared with the potentials from which they were derived by Amdur and Mason[74] (Fig. 7). Beyond about 0·2 eV ($0{\cdot}3 \times 10^{-12}$ erg) the agreement is good and would be still better if—as suggested by Hirschfelder and Eliason[57]—0·9 kT instead of kT were used for the ordinates of the crosses in Fig. 7.

Too much attention should not be placed on the divergences at the lower end of the curves, as other potential functions were used by Amdur and Mason[74] to continue the interactions to larger values of r.

Accordingly a known interaction potential can be used to give appropriate rigid sphere

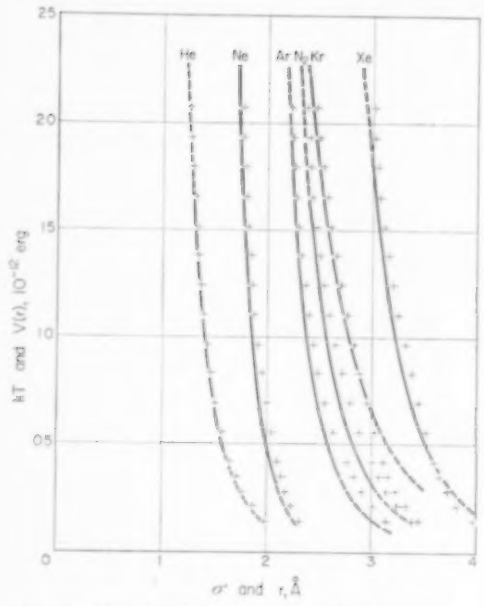

Fig. 7. The 'equivalent hard sphere' approximation. Comparison of short range potentials $V(R)$ from scattering experiments with hard sphere diameters corresponding to calculated viscosities (derived from paper by Amdur and Mason[74]). The temperature range is 1000–15,000 °K. Note that dashed portions at ends of curves represent extrapolations.

diameters for viscosity, which may be acceptable for a preliminary estimation and only improved later if a more precise calculation seems necessary. A similar procedure can be followed for estimates of diffusion coefficients.

6. "DISSOCIATED" ATOMS

In conclusion, brief reference must be made to the problem of deriving transport coefficients when the interaction has a deep minimum (several electron-volts), as in the case of two atoms which normally form a covalent bond but are in a free energy state as the result of molecular collisions or some other cause. This type of problem has not yet received a great deal of attention, but it is already important. The interactions are often quite well known; indeed when sufficient spectroscopic information is available to allow the Rydberg–Klein–Rees (RKR) method to be used, they can be determined with considerable accuracy[89, 90]. They may also be represented by various analytical expressions such as the familiar Morse potential:

$$V = D_e\left[e^{2b(\rho-1)} - 2e^{-b(\rho-1)}\right]$$

where $\rho = r/r_e$ and D_e is the energy at the equilibrium separation r_e, or by one of the forms suggested by Frost and his collaborators[85, 84]:

$$V = D_e\left[\frac{p}{\rho} - 1 - p\right]e^{-p(\rho-1)}$$

or

$$D_e\left[e^{-p(\rho-1)}\left(\frac{p}{\rho} - 1 - p\right) - \frac{d}{\rho^6}\phi_6(\rho)\right]$$

where

$$\phi_6(\rho) = 1 - e^{-\rho}\left(1 + \rho + \frac{\rho^2}{2!} + \ldots + \frac{\rho^5}{5!}\right)$$

In the latter expression the function ϕ_6 ensures that the term in ρ^{-6} makes a significant contribution well beyond the minimum.

A few calculations with interactions of this type have been made. Thus in 1954 Dalgarno[83] presented results for the diffusion coefficient and mobility of metastable helium atoms in normal helium. This was a semi-classical calculation of a kind which is often appropriate to such an interaction. More recently he has considered the transport coefficients of hydrogen atoms (in their ground states) at moderate to high temperatures*. The viscosity of hydrogen atoms up to room temperature has also been derived using quantal methods by Fox and the author, and the results related to some viscosity measurements on H–H_2 mixtures carried out at University College, London.

As mentioned already, Konowalow *et al.*[54] have derived interations of two O atoms, and two S atoms, in their ground states. This has involved estimates of first-order quadrupole interactions, varying as r^{-5}. From these they have been able to estimate, by semi-empirical rules, the viscosity and self-diffusion coefficients of O atoms up to 350°K and of S atoms up to 3000°K.

This type of problem becomes more difficult if one or both of the colliding species is in an

* Private communication.

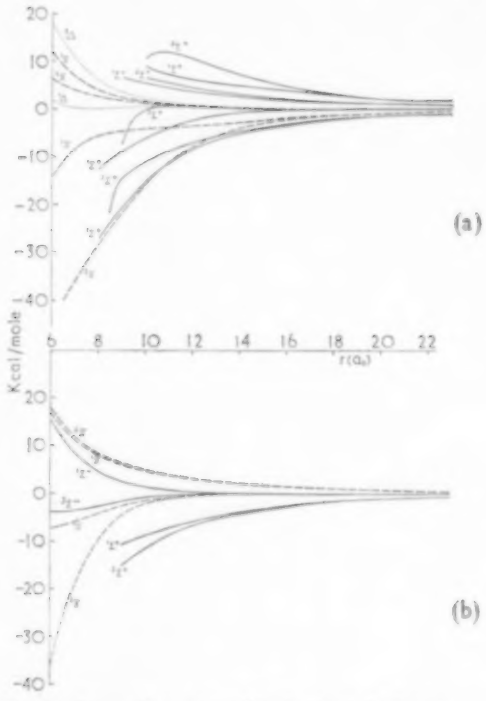

Fig. 8. Interaction potentials for two hydrogen atoms excited to 2*s* or 2*p* states (Linder and Hirschfelder[55]):
(a) Singlet *g* and triplet *u* states
(b) Singlet *u* and triplet *g* states.

excited state. Fig. 8 shows this clearly enough; it represents the possible interactions of two H atoms, in 2*s* or 2*p* states, as calculated by Linder and Hirschfelder[55]. All these modes of interactions must be allowed for in deriving transport coefficients. It is encouraging that a start has been made in this direction, and more progress can confidently be expected in the next few years.

Editor's Note

At the end of this presentation, the subject of charge–charge interactions was brought up by Mr. C. Baulknight. At that time, Dr. A. Dalgarno volunteered a rather extensive discussion on the subject. In the following pages, an elaboration of these interesting remarks is presented.

REFERENCES

General

1. J. F. Hornig and J. O. Hirschfelder, *Phys. Rev.* **103,** 908 (1956).
2. J. O. Hirschfelder, C. F. Curtiss and R. B. Bird, *Molecular Theory of Gases and Liquids*, Wiley, New York (1954).
3. H. Margenau, *Rev. mod. Phys.* **11,** 1 (1939).
4. T. L. Cottrell, *Disc. Faraday Soc.* **22,** 10 (1956).

Theoretical calculations

5. H. Aroeste and W. J. Jameson, Jr., *J. Chem. Phys.* **30,** 372 (1956).
6. J. Bartlett and W. Furry, *Phys. Rev.* **38,** 1615 (1931).
7. D. R. Bates and T. R. Carson, *Proc. Roy. Soc.* A**234,** 207 (1956).
8. D. R. Bates, K. Ledsham and A. L. Stewart, *Phil. Trans.* A**246,** 215 (1953).
9. W. E. Bleick and J. E. Mayer, *J. Chem. Phys.* **2,** 252 (1934).
10. R. A. Buckingham and A. Dalgarno, *Proc. Roy. Soc.* A**213,** 327 (1952).
11. A. S. Coolidge and H. James, *J. Chem. Phys.* **6,** 730 (1938).
12. C. A. Coulson and W. E. Duncanson, *Proc. Roy. Soc.* A**181,** 378 (1943).
13. A. Dalgarno and N. Lynn, *Proc. Phys. Soc., Lond.* A**70,** 223 (1957).

13a. A. Dalgarno and N. Lynn, *Proc. Phys. Soc., Lond.* A**69,** 821 (1956).

14. A. Dalgarno and M. R. C. McDowell, *Proc. Phys. Soc., Lond.* A**69,** 615 (1956).
15. J. de Boer, *Physica, s'Grav.* **9,** 363 (1942).
16. R. Eisenschitz and A. Crowe, *Nuovo Cimento Suppl.* **9,** 262 (1958).
17. A. A. Evett, *J. Chem. Phys.* **24,** 150 (1956).
18. A. A. Evett and H. Margenau, *Phys. Rev.* **90,** 1021 (1953).
19. A. A. Evett and H. Margenau, *J. Chem. Phys.* **21,** 958 (1953).
20. W. Furry and J. Bartlett, *Phys. Rev.* **39,** 210 (1932).
21. G. Gentile, *Z. Phys.* **63,** 795 (1930).
22. V. Griffing and J. F. Wehner, *J. Chem. Phys.* **23,** 1924 (1955).
23. J. O. Hirschfelder and J. W. Linnett, *J. Chem. Phys.* **18,** 130 (1950).
24. S. Huzinaga, *Progr. Theor. Phys.* **15,** 501 (1956); **17,** 169 and 512 (1957).
25. C. Ireland, *Phys. Rev.* **43,** 329 (1933).
26. H. James, *J. Chem. Phys.* **2,** 794 (1934).
27. H. James, *Phys. Rev.* **43,** 589 (1933).

28. H. M. James, A. S. Coolidge and R. D. Present, *J. Chem. Phys.* **4,** 187 and 193 (1936).
29. G. W. King and J. H. van Vleck, *Phys. Rev.* **55,** 1165 (1939).
30. J. Knipp, *J. Chem. Phys.* **4,** 300 (1936).
31. M. K. Krogdahl, *Astrophys. J.* **100,** 311 (1944).
32. M. Kunimune, *Progr. Theor. Phys.* **5,** 412 (1950).
33. N. Lynn, *Proc. Phys. Soc., Lond.* A**72,** 201 (1958).
34. H. Margenau, *Phys. Rev.* **56,** 1000 (1939).
35. E. A. Mason, J. Ross and P. N. Schatz, *J. Chem. Phys.* **25,** 626 (1956).
36. E. A. Mason, H. W. Schamp and J. T. Vanderslice, *Phys. Rev.* **112,** 445 (1958).
37. E. A. Mason and J. T. Vanderslice, *Phys. Rev.* **108,** 293 (1957).
38. E. A. Mason and J. T. Vanderslice, *J. Chem. Phys.* **27,** 917 (1957).
39. E. A. Mason and J. T. Vanderslice, *J. Chem. Phys.* **28,** 253 (1958).
40. E. A. Mason and J. T. Vanderslice, *J. Chem. Phys.* **28,** 1070 (1958).
41. E. A. Mason and J. T. Vanderslice, *J. Chem. Phys.* **29,** 361 (1958).
42. B. L. Moiseiwitsch, *Proc. Phys. Soc., Lond.* A**69,** 653 (1956).
43. P. D. Robinson, *Proc. Phys. Soc., Lond.* **71,** 828 (1958).
44. P. Rosen, *J. Chem. Phys.* **18,** 1182 (1950).
45. M. Sakamoto and E. Ishiguro, *Progr. Theor. Phys.* **15,** 37 (1956).

Long range forces

46. R. B. Bernstein and E. W. Rothe. Private communication.
47. F. R. Britton and D. T. W. Bean, *Canad. J. Phys.* **33,** 668 (1955).
48. J. S. Dahler and J. O. Hirschfelder, *J. Chem. Phys.* **25,** 986 (1956).
49. A. Dalgarno, *Phil. Trans.* A**250,** 426 (1958).
50. A. Dalgarno and A. E. Kingston, *Proc. Phys. Soc., Lond.* **72,** 1053 (1958).
51. A. Dalgarno and A. E. Kingston, *Proc. Phys. Soc., Lond.* **73,** 455 (1959).
52. A. Dalgarno and N. Lynn, *Proc. Phys. Soc., Lond.* A**70,** 802 (1957).
53. A. Dalgarno, M. R. C. McDowell and A. Williams, *Phil. Trans.* A**250,** 411 (1958).
54. D. D. Konowalow, B. Linder and J. O. Hirschfelder, *Univ. Wisconsin Nav. Res. Lab. Rep.* WIS-AEC-17 (1958).
55. B. Linder and J. O. Hirschfelder, *J. Chem. Phys.* **28,** 197 (1958).
56. E. A. Mason and J. T. Vanderslice, *Phys. Rev.* **114,** 497 (1959).

Intermediate range forces

57. I. Amdur and T. F. Schatzki, *J. Chem. Phys.* **27,** 1049 (1957).
58. R. A. Buckingham and J. Corner, *Proc. Roy. Soc.* A**189,** 118 (1948).
59. R. A. Buckingham, A. E. Davies and A. R. Davies, reported at *Conference on Thermodynamic and Transport Properties of Fluids, London, 1957.*
60. R. A. Buckingham, A. R. Davies and D. C. Gilles, *Proc. Phys. Soc., Lond.* **71,** 457 (1958).
61. R. A. Buckingham, J. Hamilton and H. S. W. Massey, *Proc. Roy. Soc.* A**179,** 103 (1941).
62. E. G. D. Cohen, M. J. Offerhaus, J. M. J. van Leeuwen, B. W. Roos and J. de Boer, *Physica, s'Grav.* **22,** 191 (1956).
63. J. Corner, *Trans. Faraday Soc.* **44,** 914 (1948).
64. J. de Boer, *Physica, s'Grav.* **10,** 348 (1943).
65. J. O. Hirschfelder, R. B. Bird and E. L. Spotz, *J. Chem. Phys.* **16,** 968 (1948).
66. J. E. Kilpatrick, W. E. Keller and E. F. Hammel, *Phys. Rev.* **97,** 9 (1955).
67. R. J. Lunbeck, Thesis, Amsterdam (1951).
68. E. A. Mason, *J. Chem. Phys.* **22,** 169 (1954).
69. E. A. Mason and W. E. Rice, *J. Chem. Phys.* **22,** 522 and 843 (1954).
70. I. J. Zucker, *J. Chem. Phys.* **25,** 915 (1956).

Short range forces

71. I. Amdur, *J. Chem. Phys.* **17,** 844 (1949).
72. I. Amdur and A. L. Harkness, *J. Chem. Phys.* **22,** 664 (1954).
73. I. Amdur and E. A. Mason, *J. Chem. Phys.* **25,** 632 (1956).
74. I. Amdur and E. A. Mason, *Phys. Fluids* **1,** 370 (1958).
75. I. Amdur and J. Ross, *Combustion and Flame* **2,** 412 (1958).
76. W. A. Bingel, *Z. Naturforsch.* **12**a, 59 (1957).
77. W. A. Bingel, *J. Chem. Phys.* **30,** 1250 and 1254 (1959).
78. R. A. Buckingham, *Trans. Faraday Soc.* **54,** 453 (1958).
79. W. H. Cramer and J. H. Simons, *J. Chem. Phys.* **26,** 1272 (1957).
80. W. H. Cramer, *J. Chem. Phys.* **28,** 688 (1958).
81. W. H. Cramer, *J. Chem. Phys.* **30,** 641 (1959).

Miscellaneous

82. S. F. Boys and I. Shavitt, *Univ. Wisconsin Nav. Res. Lab. Rep.* WIS-AF-13 (1959).
83. R. A. Buckingham and A. Dalgarno, *Proc. Roy. Soc.* A**213,** 506 (1952).
84. P. S. K. Chen and A. A. Frost, *J. Phys. Chem.* **61,** 828 (1957).

85. A. A. Frost and B. Musulin, *J. Chem. Phys.* **22**, 1017 (1954).
86. A. A. Frost and J. H. Woodson, *J. Amer. Chem. Soc.* **80**, 2615 (1958).
87. J. O. Hirschfelder and M. A. Eliason, *Ann. N.Y. Acad. Sci.* **67**, 451 (1957).
88. E. J. Lefevre, reported at *Conference on Thermodynamic and Transport Properties of Fluids, London, 1957.*
89. J. T. Vanderslice, E. A. Mason and E. R. Lippincott, *J. Chem. Phys.* **30**, 129 (1959).
90. J. T. Vanderslice, E. A. Mason, E. R. Lippincott and W. G. Maisch, *J. Mol. Spectrosc.* **3**, 17 (1959).

INTERMOLECULAR POTENTIALS FOR IONIC SYSTEMS

A. DALGARNO*
Geophysics Corporation of America, Boston

Abstract—A review is given of the present state of knowledge of the interaction potentials between ionic and atomic systems.

1. INTRODUCTION

Elsewhere in this volume, Buckingham has reviewed the present state of our knowledge of intermolecular potentials for calculations of transport properties and this paper, which deals with interaction potentials between atomic and ionic systems, should be read as a supplement to Buckingham's review.

If both the interacting particles are charged with excess charges ζ_1 and ζ_2 respectively, the interaction is dominated by the direct Coulomb interaction $\zeta_1\zeta_2/r$ and the collision integrals diverge. The divergence is (somewhat arbitrarily) avoided by either restricting the range of integration or by modifying the analytic form of the Coulomb term, the results being insensitive to the particular means adopted[1-3]. No complications are introduced by the ionic character, however, if one of the interacting particles is neutral, $\zeta_2=0$, say.

The interactions between a pair of neutral atoms and between an ion and a neutral atom are qualitatively very similar though at large distances of separation the interaction between an ion and an atom falls off more slowly because of the polarization of the atom by the inhomogeneous electric field due to excess charge ζ_1 on the ion. Thus in place of the asymptotic form $V(r)=-cr^{-6}$ appropriate to two neutral atoms, there occurs the asymptotic form

$$V(r)=-\zeta_1^2(ar^{-4}+br^{-6})-cr^{-6},$$

a and b being proportional to respectively the dipole and quadrupole polarizabilities of the neutral atom[4,5].

The derivation of interaction potentials for ion–atom pairs may be carried out in the ways Buckingham has described for atom–atom pairs though it should be noted that many of the experimental data on transport phenomena of ions in neutral gases refer to ions moving in their parent gas for which classical considerations may not suffice because of the symmetry of the colliding system[6,7].

Table 1. Quantal Calculations

Systems	Ref.	Systems	Ref.
H^+–H ($1s, 2s, 2p$)	8	H^+–He^+ ($1s, 2s, 2p$)	9
He^{++}–H	9	H^-–H	10, 11, 12
H^-–He	13	H^-–He^+	14
Li^+–H	15	Li^+–He	16
He^+–He	17	H^+–He	18, 19
He^{++}–He	20	Ca^{++}–Ne	50
K^+–A	50		

Table 1 lists those direct quantal calculations which are not restricted to the long-range part of the interaction. Apart from the cases H^+–H ($1s$, $2s$, $2p$), H^+–He^+ ($1s$, $2s$, $2p$) and He^{++}–H ($1s$), for which the results are essentially exact, the accuracy is not high.

2. ANALYTIC REPRESENTATIONS

Computations of collision integrals corresponding to analytic representations of the interaction potential for ionic systems are less extensive than for neutral systems. Langevin[21] and Hasse[22] used the interaction

$$V(r)=\infty \qquad r<r_0$$
$$=-ar^{-4} \qquad r>r_0$$

and Hasse and Cook[23] the interaction

$$V(r)=dr^{-8}-ar^{-4}.$$

* On leave of absence from the Department of Applied Mathematics, The Queen's University of Belfast, N. Ireland.

Some use has also been made of the representations[24, 25]

$$V(r) = \pm cr^{-s}$$

and of[19]

$$V(r) = A\exp(-br^{n}),$$

which have certain computational attractions, and Mason and Schamp[26] have recently presented an important and extensive tabulation of collision integrals corresponding to

$$V(r) = \frac{\varepsilon}{2}\left\{(1+\gamma)\left(\frac{r_m}{r}\right)^{12} - 4\gamma\left(\frac{r_m}{r}\right)^{6} - 3(1-\gamma)\left(\frac{r_m}{r}\right)^{4}\right\}.$$

Table 2. Analytical Representations

Systems	Ref.	Systems	Ref.
H^+–He	25, 19	H^-–HE	29, 13
He^+–He	27, 28	Ne^+–Ne	30, 49
H^-–Ne	29, 31, 32	H^-–A	31, 32
Li^+–He	33, 26	Na^+–He	26
Cs^+–He	26	K^+–A	26
Rb^+–Kr	26	Cs^+–Xe	26
He^+–Ne	49	Ne^+–He	49
Ne^+–A	52	A^+–Ne	52
A^+–A	52		

A partial list is given in Table 2 of those ionic systems, experimental data on which have been analysed using one of the representations specified. However, the criticisms Buckingham has made of the lack of flexibility of the representations adopted for neutral systems apply with rather more severity to ionic systems.

3. LONG RANGE INTERACTION

Because of the strength of the interaction potential when an ion and a neutral atom are widely separated, the transport properties of an ion moving in an unlike gas at temperatures below about 300°K depend in general only on the dipole polarizability of the gas atoms. For example, the mobility of an ion of mass m_1 moving in a gas composed of particles of mass m_2 is given at low temperatures by the formula

$$K = \frac{35{\cdot}9}{\sqrt{(\alpha\mu)}}\ \mathrm{cm^2\,V^{-1}\,sec^{-1}}$$

where α is the polarizability in atomic units (a_0^3) and μ is the reduced mass $m_1m_2/(m_1+m_2)$, measured in units of the proton mass. Thus the low temperature mobility depends upon the nature of the ion only through its mass.

Dipole polarizabilities can be obtained in a number of ways and Table 3 contains a list of recommended values for neutral atoms, from which the leading term of the long range interaction follows immediately.

Values of the second term of the interaction for a few ionic systems are available[4, 5] and the convergence of the series expansion has been discussed in some special cases for which

Table 3. Dipole Polarizabilities α in Units of $a_0^3 = 1{\cdot}48 \times 10^{-25}\ \mathrm{cm^3}$*

System	α	Ref.	System	α	Ref.
H	4·50	35	He	1·39	36
Ne	2·66	37	A	11·0	36
Kr	16·7	38	Xe	27·2	38
Li	165	5	Na	166	5
K	281	5	Rb	296	5
Cs	363	5	B	34	39
C	14	39	N	7·6	40
O	5·2	40	F	4·0	39
Ni	175	41	Ba	420	41, 42
Mo	60	42	Cu	150	42
Ta	115	42	W	65	42
			Be	50	48

* If energy is measured in rydbergs and the excess charge is unity, the leading terms of the interaction is $-\alpha r^{-4}$, r being in units of a_0 and α being as in the table.

the long range interaction can be calculated exactly[34]. The interaction of ions with atoms in excited states has also received attention[34, 51].

4. INTERACTIONS BETWEEN SIMILAR SYSTEMS

When two identical atoms with closed shell configurations (the inert gases) approach each other there is only one possible interaction potential and experimental data on such systems may be analysed in the usual way but when one of the interacting species does not have a closed shell configuration there are two possible modes of interaction, one $V^+(r)$ symmetrical with respect to interchange of the nuclei and the other $V^-(r)$ antisymmetrical[43]. The latter situation always occurs for example in the case of ions moving in their parent gases.

For such cases the usual analysis of data leads to an effective interaction potential which is some sort of average of V^+ and V^-. However, the average which is effective in controlling, say, direct elastic scattering is not the same as the average which is effective in controlling diffusion.

Unless direct quantal calculations are available, it is probably best to proceed under the assumption that V^+ and V^- have the forms

$$V^+ = V(r) - ar^{-4}$$

$$V^- = -V(r) - ar^{-4},$$

which represents qualitatively the expected behaviour.

In the case of diffusion (or mobility) data, it is useful to note that the diffusion cross section is roughly twice the cross section for the charge exchange process

$$X' + X \longrightarrow X + X'$$

or for the charge transfer process

$$X^+ + X \longrightarrow X + X^+.$$

5. NON-SPHERICAL SYSTEMS

In the treatment of non-spherical systems, collision cross sections should be calculated for particular orientations and then averaged over all orientations. In practice the average is usually taken before calculating the cross sections. The accuracy of this procedure is open to question[44] but for the sake of completeness, a list of references to interactions between non-spherical ionic systems is included in Table 4.

Table 4. Non-Spherical Systems

System	Ref.	System	Ref.
H^+–H_2	24, 45	H_3^+–H_2	24, 45
H_2^+–H_2	46, 45	H^+–H_2O	47
H_2^+–H_2O	47	H_3^+–H_2O	47
H_2^+–He	25, 19	H_3^+–He	25, 19
H^-–H_2	31, 32	He_2^+–He	26, 53
Ne_2^+–Ne	26		

REFERENCES

1. L. SPITZER, *The Physics of Ionized Gases*. Interscience Publishers, New York (1956).
2. O. THEIMER and H. HOFFMAN, *Astrophys. J.* **128**, 224 (1959).
3. R. L. LIBOFF, *Phys. of Fluids* **2**, 40 (1959).
4. H. MARGENAU, *Phil. of Sci.* **8**, 603 (1941).
5. A. DALGARNO and A. E. KINGSTON, *Proc. Phys. Soc., Lond.* **73**, 455 (1959).
6. H. S. W. MASSEY and C. B. O. MOHR, *Proc. Roy. Soc.* A**144**, 188 (1934).
7. A. DALGARNO, *Phil. Trans. Roy. Soc.* A**250**, 428 (1958).
8. D. R. BATES, K. LEDSHAM and A. L. STEWART, *Phil. Trans. Roy. Soc.* A**246**, 215 (1953).
9. D. R. BATES and T. R. CARSON, *Proc. Roy. Soc.* A**234**, 207 (1956).
10. A. DALGARNO and M. R. C. MCDOWELL, *Proc. Phys. Soc., Lond.* A**69**, 615 (1956).
11. B. K. GUPTA, *Physica s'Grav.* **25**, 190 (1959).
12. I. FISCHER-HJALMARS, *Arkiv för Fysik* **16**, 33 (1959).
13. E. A. MASON and J. T. VANDERSLICE, *J. Chem. Phys.* **28**, 253 (1958).
14. J. ROSS and E. A. MASON, *Astrophys. J.* **124**, 485 (1956).
15. O. PLATA, R. P. HURST and F. A. MATSEN, *J. Chem. Phys.* **31**, 501 (1959).
16. E. A. MASON, H. W. SCHAMP and J. T. VANDERSLICE, *Phys. Rev.* **112**, 445 (1958).
17. B. L. MOISEIWITSCH, *Proc. Phys. Soc.* A**69**, 653 (1956).
18. A. A. EVETT, *J. Chem. Phys.* **24**, 150 (1956).
19. E. A. MASON and J. T. VANDERSLICE, *J. Chem. Phys.* **27**, 917 (1957).
20. A. F. FERGUSON and B. L. MOISEIWITSCH, *Proc. Phys. Soc., Lond.*, **74**, 457 (1959).
21. P. LANGEVIN, *Ann. Chem. (Phys.)* **8**, 245 (1905).
22. H. R. HASSE, *Phil. Mag.* **1**, 139 (1926).
23. H. R. HASSE and W. R. COOK, *Phil. Mag.* **3**, 977 (1927); *Phil. Mag.* **12**, 554 (1931).

24. J. H. Simons, C. M. Fontana, E. E. Muschlitz and S. R. Jackson, *J. Chem. Phys.* **11**, 307 (1943).
25. J. H. Simons, E. E. Muschlitz and L. G. Unger, *J. Chem. Phys.* **11**, 322 (1943).
26. E. A. Mason and H. W. Schamp, *Ann. Phys.*, New York **4**, 233 (1958).
27. W. H. Cramer and J. H. Simons, *J. Chem. Phys.* **26**, 1272 (1957).
28. E. A. Mason and J. T. Vanderslice, *Phys. Rev.* **108**, 293 (1957); *J. Chem. Phys.* **29**, 361 (1958).
29. T. L. Bailey, C. J. May and E. E. Muschlitz, *J. Chem. Phys.* **26**, 1446 (1957).
30. E. A. Mason and J. T. Vanderslice, *J. Chem. Phys.* **30**, 599 (1959).
31. E. E. Muschlitz, T. L. Bailey and J. H. Simons, *J. Chem. Phys.* **26**, 711 (1957).
32. E. A. Mason and J. T. Vanderslice, *J. Chem. Phys.* **28**, 1070 (1958).
33. A. Dalgarno, M. R. C. McDowell and A. Williams, *Phil. Trans. Roy. Soc.* A**250**, 411 (1958).
34. A. Dalgarno and J. T. Lewis, *Proc. Phys. Soc., Lond.* A**69**, 57 (1956) and *Proc. Roy. Soc.* A**233**, 70 (1955); A. Dalgarno and A. L. Stewart, *Proc. Roy. Soc.* A**238**, 276 (1956) and A**240**, 274 (1957); A. Dalgarno and N. Lynn, *Proc. Phys. Soc.* A**70**, 233 (1957); P. D. Robinson, *Proc. Phys. Soc., Lond.* **71**, 828 (1958).
35. L. Pauling and E. B. Wilson, *Introduction to Quantum Mechanics.* McGraw-Hill, New York (1935).
36. L. Essen, *Proc. Phys. Soc., Lond.* B**66**, 189 (1953).
37. C. Cuthbertson and M. Cuthbertson, *Proc. Roy. Soc.* A**135**, 44 (1932).
38. C. Cuthbertson and M. Cuthbertson, *Proc. Roy. Soc.* A**84**, 13 (1911).
39. A. Dalgarno and D. Parkinson, *Proc. Roy. Soc.* A**250**, 422 (1959).
40. R. A. Alpher and D. R. White, *Phys. of Fluids* **2**, 153 (1959).
41. H. Liepack and M. Drechsler, *Naturwiss.* **3**, 52 (1956).
42. M. Drechsler and E. W. Müller, *Z. Phys.* **132**, 195 (1952).
43. *cf.* A. Dalgarno, this volume, p. 217.
44. A. M. Arthurs and A. Dalgarno, *Proc. Roy. Soc. A* in press (1960).
45. E. A. Mason and J. T. Vanderslice, *Phys. Rev.* **114**, 497 (1959).
46. J. H. Simons, C. M. Fontana, H. T. Francis and L. G. Unger, *J. Chem. Phys.* **11**, 313 (1943).
47. J. H. Simons, H. T. Francis, E. E. Muschlitz and G. C. Fryburg, *J. Chem. Phys.* **11**, 316 (1943).
48. D. Parkinson, *Proc. Phys. Soc., Lond.*, **75**, 169 (1960).
49. W. H. Cramer, *J. Chem. Phys.* **28**, 688 (1958).
50. D. W. Sida, *Phil. Mag.* ser. 8, **2**, 761 (1957).
51. C. A. Coulson and G. M. Gillam, *Proc. Roy. Soc. Edinb.* A**62**, 360 (1947).
52. M. K. Krogdahl, *Astrophys. J.* **100**, 311 and 333 (1944).
52. W. H. Cramer, *J. Chem. Phys.* **30**, 641 (1959).
53. S. Geltman, *Phys. Rev.* **90**, 808 (1953).

HIGH TEMPERATURE GASEOUS DIFFUSION EXPERIMENTS AND INTERMOLECULAR POTENTIAL ENERGY FUNCTIONS

R. E. WALKER, L. MONCHICK, A. A. WESTENBERG and S. FAVIN

Applied Physics Laboratory, The Johns Hopkins University, Silver Spring, Maryland

Abstract—A new method of measuring molecular diffusion coefficients of gases which makes use of precise sampling and gas analysis downstream of an essentially point source of trace gas in a uniform carrier gas has been recently described in several publications. The technique is especially adapted for determinations at elevated temperatures. The present paper is a discussion of binary diffusion data over the temperature range 300°–1150° K for all of the gas pairs studied at APL to date. These include He–N_2, CO_2–N_2, He–A, CO_2–O_2, CH_4–O_2, H_2–O_2, CO–O_2 and H_2O–O_2. The data cover a wide enough range in temperature and are of sufficient precision ($\sim \pm 2$ per cent) so that it is possible to examine them in terms of the kinetic theory of dilute gases and the intermolecular potential energy functions characterizing binary collision processes. The three functions used for which the necessary collision integrals had already been evaluated are the inverse power point center of repulsion potential, the Lennard–Jones (12–6) potential, and the modified Buckingham (Exp–6) potential. In addition, the collision integrals for the exponential point center of repulsion potential were evaluated by numerical means. The details of this calculation, which was performed on the Univac 1103 Digital Computer, will be published elsewhere. It is shown that while all four potentials can be fitted to the data about equally well, the actual potentials obtained in this way may be quite different. Conversely, however, the high temperature diffusion coefficients predicted from the four potentials fitted at lower temperatures agree rather well.

1. INTRODUCTION

In a recent publication[1] (paper I of a series) Walker and Westenberg have presented a detailed study of a new method for measuring molecular diffusion coefficients for gaseous systems. This method makes use of the change in concentration C downstream of a point source of trace gas emitted at a steady rate Q into a uniform (heated) jet of a second gas flowing at a constant velocity U (see Fig. 1). Under conditions of constant temperature and pressure, no chemical reactions or external forces, and where the source emits so little fluid that the density may be considered constant, the distribution of the trace component is given by

$$C = (Q/4\pi Dr)\exp[(x-r)U/2D] \qquad (1)$$

where $r = (x^2+y^2+z^2)^{1/2}$, and D is the binary diffusion coefficient. The stream velocity U is parallel to the x-axis. A detailed derivation of equation (1) has already been given in Ref. (1). By analysing a sample of the gas mixture removed from a point directly downstream of the source ($x=r$) and by measuring Q, D can be obtained. By heating the carrier gas,

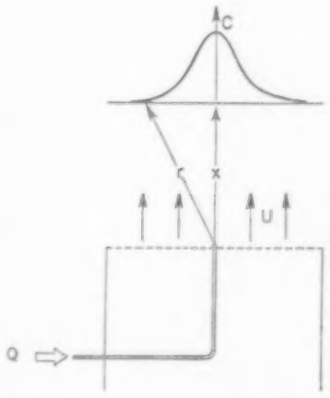

FIG. 1

Fig. 1. Schematic diagram of point source in a uniform flow.

measurements at high temperature can be made. The technique avoids placing moving parts in a high-temperature environment and free convection is not important—these problems have been the main drawbacks in extending the usual methods of measuring diffusion coefficients[3] to high temperatures. Details of the experimental equipment used in this work and a report on a systematic variation of parameters used in evaluating this method have been given in Ref. (1) together with data on the He–N_2 and CO_2–N_2 systems taken over a temperature interval 300°–1200°K and at 1 atm pressure. The precision of the method is shown to be ±1–2 per cent. Since the trace gas composition is small (<2 per cent), diffusion coefficients measured with this method are unambiguously defined at vanishing concentration of the trace gas. Reversing the respective roles of trace gas and carrier gas allows the maximum (small) effect of concentration to be measured.

The data cover a wide enough temperature range and are of sufficient precision so that it is possible to examine them in terms of the kinetic theory of dilute gases and the intermolecular potential energy functions characterizing binary collision processes. In paper II of the series[2] the He–N_2 and CO_2–N_2 diffusion measurements have been so interpreted to obtain intermolecular energy curves.

The point source method also has been used to measure diffusion coefficients for the gas pairs He–A, CO_2–O_2, CH_4–O_2, H_2–O_2, CO–O_2 and H_2O–O_2 over the nominal temperature range 300°–1150°K. These data and their interpretation in terms of intermolecular energies are given in papers III and IV of the series[4, 6].

2. KINETIC THEORY

The classical kinetic theory of transport properties has been described in the well known treatises of Chapman and Cowling[7], and Hirschfelder *et al.*[8] so that the details need not be reproduced here. In addition, paper II gives a brief account of how the kinetic theory is applied in the analysis of diffusion data for binary systems to obtain intermolecular forces between unlike molecular species. Measurement of molecular diffusion coefficients as a function of temperature is one of the best known methods of determining intermolecular forces between unlike molecules since, to a very good first approximation, unlike interactions alone determine this particular transport property.

The kinetic theory is meant to be used on molecules that are characterized by intermolecular potentials which are spherically symmetric and for which the collisions may be regarded as elastic. Strictly, of course, only monatomic gases with no internal degrees of freedom fulfil these requirements. However, since the transfer of mass is not appreciably affected by the fact that real molecules have internal degrees of freedom, and since the molecular interactions to be discussed do not depart too much from spherical symmetry*, we have accepted the theory as applying to them.

3. INTERPRETATION OF THE RESULTS

To obtain intermolecular potential energies from transport data, the procedure is to select a particular analytic function which approximates the actual (unknown) potential energy and to determine a set of parameters for the function that best reproduces the experimental data. This procedure is a necessary one since gas transport properties are given by a complicated set of collision integrals implicitly containing the potential energy[9]. These collision integrals are calculated by numerical means for all but the simplest potential functions. In the present work, four of the most realistic functions have been used to fit the data and then compared to each other.

The four potential functions used are the Lennard-Jones (12–6)

$$\phi(r) = 4\varepsilon[(\sigma/r)^{12} - (\sigma/r)^{6}], \tag{2}$$

the modified Buckingham (Exp–6)

$$\phi(r) = \frac{\varepsilon}{1-6/\alpha}\left[\frac{6}{\alpha}\exp\alpha(1-r/r_m) - \left(\frac{r_m}{r}\right)^{6}\right], \tag{3}$$

the point centers of repulsion

$$\phi(r) = d/r^{5} \tag{4}$$

* In one system to be considered, H_2O–O_2, a polar–nonpolar molecular interaction is involved. However, the effective potential energy of interaction still has the same form as for two non-polar molecules[5].

and the exponential repulsion

$$\phi(r) = A \exp(-r/\rho) \qquad (5)$$

In these expressions, r is the molecular separation distance, and the other quantities (ε, σ, α, r_m, d, δ, A, ρ) are constant parameters. For the potential functions given by (2), (3) and (4), the appropriate collision integrals have already been published[8, 10, 11]. Collision integrals for the exponential repulsion potential (5) have recently been computed by Monchick. The details of these calculations, which were performed on the Univac 1103 computer, will be published elsewhere. The Lennard–Jones (12–6) and the modified Buckingham (Exp–6) potentials are realistic potential functions to use in interpreting low temperature transport data since they include the London dispersion energy (attractive) term ($\phi \propto r^{-6}$), which has a reasonably firm theoretical basis and is important for low-energy molecular collisions. For high-temperature transport data (high-energy molecular collisions), the attractive forces are less important and the point centers of repulsion and exponential repulsion potentials are useful. Since molecular diffusion coefficients tend to be associated with more penetrating collisions than other transport properties at the same temperature[9], it would be expected that all of these potential functions would be more or less applicable in the analysis of the diffusion data. The potentials can be compared with each other and the results afford an interesting example of this type of procedure.

To determine the potential parameters that best fit the experimental data, a least squares method was used. Details of the method are presented in papers II and IV. To facilitate this rather tedious operation, the appropriate dimensionless collision integrals were fit to polynomial functions in $T^* (= kT/\varepsilon)$ and the entire procedure was programmed on an IBM 650 digital computer. As noted in paper II, high-temperature transport data are not especially sensitive to the choice of *compatible* potential parameters, so that the standard deviation of the measurements varies slowly at its minimum with respect to these parameters. For this reason, it was felt that the three parameters for the modified Buckingham (Exp–6) potential could not be unambiguously specified with the available data—rather, several choices of the parameters α were investigated and are reported below without discrimination. Actually, none of the reported parameters should be considered as being unique in view of the insensitivity of the standard deviation near its minimum.

A summary of the potentials fit to the diffusion measurements reported by us is given in Table 1. Also included are the Lennard–Jones (12–6) potential parameters determined from viscosity data on pure components and the usual combination rules. The range of r over which the determined potential can be expected to be valid (see paper II for a discussion of this rigid sphere range of validity) is also included. The classical method of computing the Lennard–Jones (12–6) potential parameters is seen to give results quite different from those parameters determined directly from the diffusion measurements. Actually, the viscosity data tend to emphasize a different portion of the potential energy curve than the diffusion data[9] so that agreement need not be expected.

It will be apparent from a survey of the standard deviations provided in this table that all of these intermolecular potentials are *about equally successful in fitting the diffusion data within the experimental error*. An equivalent compatibility does not exist, however, between the actual potential energies given by the fitted parameters of Table 1. Figs. 2 and 3 illustrate this important fact. Fig. 2 is a plot of the CO_2–O_2 potential energy of interaction where the range of validity extends into the "well" created by a combination of attractive and repulsive forces. It is obvious here that although the repulsive potentials (4) and (5) are quite adaptable to the analysis of the diffusion data, the corresponding potential energies so predicted do not include the attractive forces of the interaction, and hence differ significantly from the potential energies predicted through use of the Lennard–Jones (12–6) or modified Buckingham (Exp–6) models. In this case, the depth of the well ($\varepsilon/k \cong 200°K$) is of the same order of magnitude as the temperatures at which

Table 1. Summary of Potential Parameters for various Unlike Molecular Interactions Determined from Diffusion Data and Lennard–Jones (12–6) Viscosity Parameters of Pure Components (using Classical Combination Rules). Precision of Fit to the Experimentally Measured Diffusion Data and Range of Validity for the Potentials Determined from the Experimental Data are Included

Gas pair	Range of Validity		Point center of repulsion			Exponential repulsion			Modified Buckingham (Exp–6)				Lennard–Jones (12–6)			Lennard–Jones (12–6)	
	Min. (Å)	Max. (Å)	d (ergs Å^6 $\times 10^{10}$)	δ	Std. dev. (%)	A/k (°K $\times 10^{-3}$)	ρ (Å)	Std. dev. (%)	ϵ/k (°K)	rm (Å)	α	Std. dev. (%)	ϵ/k (°K)	σ (Å)	Std. dev. (%)	from viscosiy ϵ/k (°K)	σ (Å)
$He–N_2$	2·32	2·65	22·6	10·45	1·50	350	0·2414	1·58	85	3·069	17	1·49	69	2·87	1·49	28·6	3·163
$N_2–CO_2$	3·08	3·71	20·6	7·91	2·20	24·5	0·4319	2·36	110	4·309	12	1·82	154	3·520	1·72	130	3·823
									140	4·045	14	1·73					
									184	3·782	17	1·72					
He–A	2·21	2·58	1·81	8·12	2·22	26	0·3069	2·42	88	3·170	12	2·10	125	2·587	1·98	34·4	3·020
									114	2·971	14	1·99					
									150	2·777	17	1·98					
$CO_2–O_2$	3·09	3·76	3·75	6·54	2·60	6·5	0·5203	2·94	165	4·071	12	1·83	213	3·365	1·74	137	3·719
									202	3·846	14	1·78					
									255	3·616	17	1·74					
$H_2–O_2$	2·50	2·94	1·62	7·13	1·01	9·0	0·3948	1·22	117	3·421	12	0·58	152	2·825	0·63	57·8	3·228
									143	3·234	14	0·59					
									183	3·032	17	0·64					
$CH_4–O_2$	3·08	3·60	4·56	6·83	3·04	8·0	0·4915	3·30	145	4·061	12	2·37	182	3·367	2·25	113	3·668
									170	3·855	14	2·30					
									220	3·612	17	2·25					
$CO–O_2$	3·01	3·38	75·6	9·52	1·85	105	0·3392	1·87	40	4·525	12	2·03	91	3·480	1·73	88	3·624
									76	4·040	14	1·77					
									110	3·733	17	1·73					
$H_2O–O_2$	2·78	3·10	358	11·41	1·46	900	0·2610	1·50	55	4·154	12	2·50	80	3·335	1·40	163	3·148
									100	3·567	17	1·40					

the experiments were performed (300–1160°K), i.e. $1<T^*<5$. This marked difference between the various potentials does not prevail when the effective values of T^* are larger and the region of the well is avoided, which is the case for the He–A interaction graphed in Fig. 3. For the case of the He–A interaction, additional information on the potential energy of interaction for more penetrating collisions has been provided by the molecular beam scattering experiments of Amdur *et al.*[12]. The scattering potential is also included in Fig. 3. A comparison of Figs. 2 and 3 tends to show that for more penetrating collisions (i.e. higher temperatures) the particular choice of the potential function appears to be less critical. This feature prevails for all of the potential energy comparisons provided in Table 1. It should be emphasized that potentials determined in this way should not be extrapolated much beyond their ranges of validity—especially in the region of the "well". Even within the range of validity, it is impossible to state (without other evidence) which of the potentials are closest to the "true" potential, although it seems likely that potentials such as (2) and (3) which contain an attractive term would be more nearly correct for those cases that we have considered. Conversely, the errors introduced by extrapolation of a transport property to a higher temperature may not be excessive in spite of the disagreement between the various potentials, as is shown in the following section. This point has been made before[13], but it is well to stress it again.

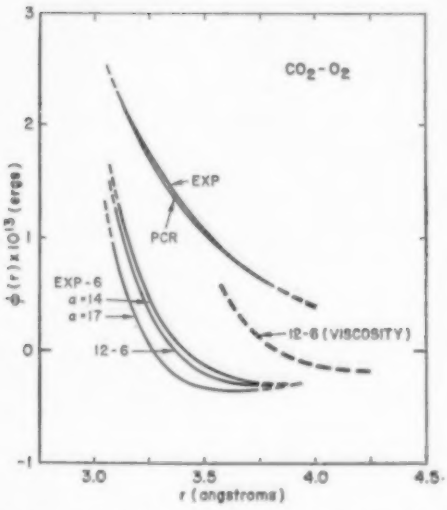

Fig. 2. Potential energy of interaction for CO_2–O_2 using potential parameters listed in Table 1.

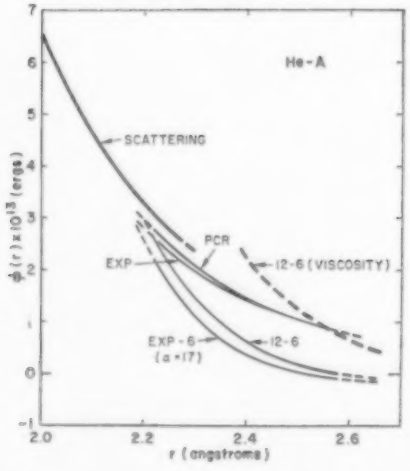

Fig. 3. Potential energy of interaction for He–A using the potential parameters listed in Table 1. The potential from molecular beam scattering experiments of Amdur, Mason and Harkness is included.

4. PREDICTION OF HIGH-TEMPERATURE DIFFUSION COEFFICIENTS

When available, intermolecular potentials determined from small-angle molecular beam scattering experiments provide an excellent foundation for predicting high temperature transport properties of unexcited species. Of those gas pairs that we have studied, scattering potentials for the He–A and He–N_2 interactions have been obtained by Amdur and his co-workers[12,14], and have previously been used to predict high-temperature diffusion coefficients[2,3,15]. For the other gas pairs studied, no additional intermolecular force data are available except as provided in Table 1. Since high-temperature diffusion data are often required in various problems, it is of interest to examine the error in extrapolating low temperature transport data to higher temperature. Table 2 gives values to 3000°K for the diffusion coefficients obtained by extrapolation using the rigorous kinetic theory and the various fitted intermolecular parameters given in Table 1. Also included in Table 2 are predictions of diffusion coefficients using parameters determined with the usual classical method of combining viscosity parameters. In addition, the scattering potentials have been used to compute high-temperature diffusion coefficients for the He–A and He–N_2 systems. Although the various intermolcular potentials for a particular interaction are, in general, quite different in themselves, the diffusion coefficients extrapolated from them are not necessarily so, as can be seen by examining Table 2. Errors (generally small) occur when diffusion coefficients are calculated from viscosity parameters. For those systems where additional potential energy information is lacking, it is impossible to state which of the extrapolated diffusion coefficients are more nearly correct.

REFERENCES

1. R. E. Walker and A. A. Westenberg, *J. Chem. Phys.* **29**, 1139 (1958).
2. R. E. Walker and A. A. Westenberg, *J. Chem. Phys.* **29**, 1147 (1958).
3. A. A. Westenberg and R. E. Walker, *ASME Symposium on Thermal Properties, Purdue University, Feb. 23–26 1959*, p. 314. McGraw-Hill, New York (1959).

Table 2. Predicted High-Temperature Diffusion Coefficients using the various Potential Functions given in Table I and the Scattering Potentials given in Refs. (12) and (14) (Trace of light Gas, p = 1 atm.)

Gas pair	Potential function	Temperature (°K)						
		300	500	1000	1500	2000	2500	3000
$He-N_2$	12-6	0·741	1·77	5·65	11·1	17·9	25·9	35·0
	Exp-6 (α = 17)	0·741	1·78	5·66	11·1	17·8	25·7	34·6
	p.c.r.	0·745	1·76	5·68	11·3	18·3	26·7	36·3
	exp	0·746	1·76	5·69	11·3	18·5	27·2	37·2
	12-6 (viscosity)	0·723	1·69	5·34	10·5	16·9	24·5	33·2
	p.c.r. (scattering)	—	—	5·54	11·4	19·1	28·4	39·3
CO_2-N_2	12-6	0·174	0·440	1·45	2·86	4·62	6·69	9·05
	Exp-6 (α = 17)	0·174	0·439	1·46	2·86	4·60	6·49	8·99
	p.c.r.	0·177	0·434	1·46	2·98	4·93	7·29	10·0
	exp	0·178	0·433	1·46	3·01	5·04	7·54	10·5
	12-6 (viscosity)	0·156	0·389	1·27	2·49	4·02	5·82	7·87
He–A	12-6	0·757	1·89	6·17	12·2	19·6	28·4	38·5
	Exp-6 (α = 17)	0·755	1·90	6·23	12·1	19·7	28·4	38·2
	p.c.r.	0·763	1·86	6·25	12·7	21·0	31·0	42·6
	exp	0·765	1·86	6·26	12·8	21·5	32·1	44·6
	12-6 (viscosity)	0·756	1·77	5·60	11·0	17·7	25·7	34·8
	p.c.r. (scattering)	—	—	5·98	12·3	20·5	30·6	32·1
CO_2-O_2	12-6	0·161	0·419	1·43	2·84	4·59	6·66	9·01
	Exp-6 (α = 17)	0·162	0·418	1·42	2·81	4·55	6·58	8·89
	p.c.r.	0·164	0·412	1·44	3·00	5·04	7·54	10·48
	exp	0·164	0·410	1·44	3·04	5·19	7·90	11·15
	12-6 (viscosity)	0·156	0·389	1·27	2·51	4·04	5·85	7·92
CH_4-O_2	12-6	0·226	0·581	1·95	3·86	6·23	9·03	12·22
	Exp-6 (α = 17)	0·230	0·593	2·00	3·95	6·38	9·23	12·45
	p.c.r.	0·229	0·574	1·99	4·11	6·88	10·26	14·23
	exp	0·230	0·570	1·99	4·18	7·11	10·77	15·18
	12-6 (viscosity)	0·225	0·554	1·79	3·52	5·67	8·21	11·1
H_2-O_2	12-6	0·821	2·09	6·93	13·7	22·2	32·1	43·4
	Exp-6 (α = 12)	0·818	2·07	6·99	14·1	23·1	34·0	46·6
	p.c.r.	0·828	2·06	7·06	14·5	24·3	36·1	50·0
	exp	0·830	2·05	7·10	14·9	25·2	38·1	53·6
	12-6 (viscosity)	0·830	1·97	6·27	12·3	19·8	28·7	38·8
$CO-O_2$	12-6	0·224	0·542	1·73	3·40	5·48	7·93	10·72
	Exp-6 (α = 17)	0·224	0·542	1·74	3·39	5·54	7·88	10·62
	p.c.r.	0·224	0·538	1·76	3·52	5·76	8·44	11·53
	exp	0·225	0·537	1·77	3·57	5·89	8·70	11·99
	12-6 (viscosity)	0·208	0·503	1·61	3·15	5·07	7·34	9·94
H_2O-O_2	12-6	0·288	0·692	2·21	4·32	6·96	10·09	13·65
	Exp-6 (α = 17)	0·286	0·691	2·20	4·31	6·93	10·00	13·48
	p.c.r.	0·294	0·691	2·21	4·35	7·05	10·24	13·90
	exp	0·294	0·690	2·21	4·37	7·11	10·38	14·16
	12-6 (viscosity)	0·260	0·660	2·19	4·32	6·98	10·1	13·7

4. R. E. WALKER and A. A. WESTENBERG, *J. Chem. Phys.* **31**, 519 (1959).
5. For a description, see W. JOST, *Diffusion in Solids, Liquids and Gases*, Chap. 10. Academic Press, New York (1952).
6. R. E. WALKER and A. A. WESTENBERG, *J. Chem. Phys.* **32**, 436 (1960).
7. S. CHAPMAN and T. G. COWLING, *The Mathematical Theory of Non-Uniform Gases*. Cambridge University Press, London (1939).

8. J. O. Hirschfelder, C. J. Curtiss and R. B. Bird, *The Molecular Theory of Gases and Liquids*. Wiley, New York (1954).
9. In a recent publication—J. O. Hirschfelder and M. A. Eliason, *Ann. N. Y. Acad. Sci.* **67**, 451 (1957)—a one-to-one correspondence between a transport property value and a point on a *particular* analytic potential function is shown to exist. As yet, it is impossible to unambiguously relate a value for a transport property to a point on the actual potential energy curve, especially in the low-temperature region.
10. E. A. Mason, *J. Chem. Phys.* **22**, 169 (1954).
11. E. A. Mason, *J. Chem. Phys.* **22**, 843 (1954).
12. I. Amdur, E. A. Mason and A. L. Harkness, *J. Chem. Phys.* **22**, 1071 (1954).
13. I. Amdur and J. Ross, *Combustion and Flame* **2**, 412 (1958).
14. I. Amdur, E. A. Mason and J. E. Jordan, *J. Chem. Phys.* **27**, 527 (1957).
15. I. Amdur and E. A. Mason, *Phys. Fluids* **1**, 370 (1958).

AN EXPERIMENTAL APPROACH TO THE DETERMINATION OF GASEOUS TRANSPORT PROPERTIES AT VERY HIGH TEMPERATURES*

I. AMDUR

Massachusetts Institute of Technology, Cambridge, Massachusetts

Abstract—Values of gaseous transport properties at elevated temperatures may be calculated from appropriate kinetic theory relations (or from statistical mechanics if equilibrium properties are of interest) provided that the correct intermolecular potential functions are known. It is pointed out that the potentials for this purpose may not be extrapolations of functions which are valid only for relatively large distances of separation, and therefore suitable only for calculation of low temperature properties, but must be ones which are valid at the smaller distances of separation of importance at elevated temperatures. The experimental procedure is described for determining such potentials from elastic scattering of neutral beam particles having kinetic energies of the order of 1000 eV. It is shown that meaningful potential energy information cannot be deduced from such experiments unless the shape and intensity distribution of the beam, as well as the geometry of the beam–detector system are taken into account. Results are tabulated for the potentials of a number of atom–atom and atom–molecule systems and a procedure for obtaining molecule–molecule interactions from such results is indicated.

The procedure is outlined for using appropriate interaction potentials for calculating transport properties over a wide range of temperature and the results are illustrated in terms of the viscosity of xenon between 1000° and 10,000°K. It is shown that the method may be applied to the calculation of properties of mixtures which require potentials between unlike particles. The criterion is given for determining the range of temperature over which all such calculations are valid, namely, that it is the magnitude of the *fraction* of the kinetic energy of the beam particles which is converted into *potential energy* at the distance of closest approach during a collision and not the kinetic energy itself, which determines the region of validity.

Possible experimental procedures are suggested which might be used to obtain intermolecular potentials for binary systems containing ions, dissociative atomic species, metastable and excited species.

In recent years there has been a greatly increased interest in the properties of gases at high temperatures, of the order of 1000°K, at very high temperatures, of the order of 10,000°K, and at extremely high temperatures, of the order of 10^5 °K and greater. Since direct accurate measurements of these properties at very high or extremely high temperatures is in general not feasible, an alternative approach is called for. One such approach is the combination of statistical mechanical theory with experimental determination of molecular properties, that is, forces of molecular interaction, to obtain calculated values of gas properties whose accuracy is comparable to that obtained at low temperatures by direct measurement[1, 2].

The present communication deals primarily with the direct experimental method for obtaining information about intermolecular forces in the range of interaction distance that is important for very high temperature gas properties. It will be assumed that the formal theoretical expressions for equilibrium and transport properties for dilute gases with spherically symmetric force fields (or force fields that may be treated as spherically symmetric)

* This research was supported in part by the U.S. Office of Naval Research under Contract Nonr 1841 (23).

are correctly given by statistical mechanics and kinetic theory[3,4].

The nature of the intermolecular potential $\phi(r)$ as a function of the interaction distance r for two non-polar atoms or molecules whose force fields or average force fields may be considered spherically symmetric, is shown in Fig. 1.

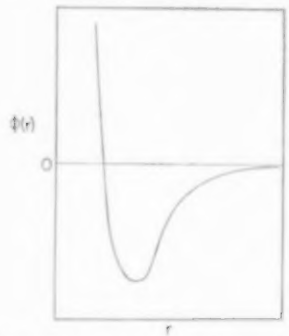

Fig. 1. Intermolecular potential as a function of separation distance.

Different gas properties such as the second virial coefficient, $B(T)$, the coefficient of viscosity, $\eta(T)$, or the self-diffusion coefficient, $D_{11}(T)$, are determined in effect by different portions of the $\phi(r)$ curve for a combination of three reasons:

(1) The analytical expressions which are used to represent $\phi(r)$ are empirical or semi-empirical relations whose functional forms are frequently chosen for mathematical convenience. The task of determining the parameters in these functions is, in effect, that of finding an approximate analytical representation of experimental results over a limited range.

(2) Although the integrals which relate $\phi(r)$ to the deflection angle θ in a collision extend from the distance of closest approach, $r=r_0$ to $r=\infty$, the extremely rapid decrease of $\phi(r)$ with r in effect makes $\phi(r)$ behave like a step function. For a given initial relative velocity, θ is actually determined by the trajectory of the colliding molecules very close to r_0.

(3) Since different types of collisions are involved in the transport of tangential momentum, normal momentum, mass, etc., different restricted regions of the $\phi(r)$ curve will be important for different transport and equilibrium gas properties.

The net result of the above considerations is that potential energy information derived from measurements of second virial coefficients over a limited range of temperature may not be really suitable for calculating other properties such as viscosity or diffusion coefficients in the same range of temperature. Moreover, and more important, potential parameters derived from measurements of a macroscopic property in a given range of temperature and which are therefore valid over a definite range of r, may not be extrapolated beyond this range without serious error. For example, parameters of the Lennard–Jones (12–6) potential for argon have been determined from the temperature dependence of the viscosity between 80° and 300°K. These parameters, which are valid over the approximate range $3{\cdot}60\,\text{Å} \leqq r \leqq 4{\cdot}80\,\text{Å}$ at 2·18 Å fail to reproduce by 700 per cent the potential as determined directly from molecular beam experiments in the range $2{\cdot}18\,\text{Å} \leqq r \leqq 2{\cdot}69\,\text{Å}$.

Since measurements of macroscopic gas properties at accessible temperatures, of the order of 1000°K and lower, almost always yield potential energy information at relatively large values of r (in the general region of the potential minimum), it is necessary to adopt a new experimental method to obtain directly, *without extrapolation*, such information at the small values of r required for calculation of high temperature gas properties.

This method and some of the results obtained with it have been described in detail in a series of published articles[5–17]. It may be summarized as follows:

Positive ions are produced by electron impact in a suitable positive ion source, for example, a low voltage arc. These ions are accelerated in an electric field to energies in the range 200–2000 eV. The accelerated ions are passed through gas of their own atomic or molecular species and are converted, without loss of energy, to high energy neutrals by resonant change transfer. The neutrals are collimated into a beam whose axis scattering yields total elastic cross sections, S, as a function of the energy, E, of the beam particles. Application

of classical scattering theory to two particles which have, or are assumed to have, spherically symmetric force fields, permits evaluation of $\phi(r)$ as a function of r from the measured variation of S with E.

If I_0 is the axis intensity of the unscattered high energy neutral beam and I, the corresponding axis intensity of the beam after it has passed through scattering gas, the experimental total elastic cross section is given by

$$\ln I_0/I = S \sum_i n_i l_i. \tag{1}$$

Here n_i refers to the number of scattering centers per unit volume along a length of scattering path l_i and S is a function of E and of θ, the *effective* average angular aperture of the detector–beam system. This effective aperture depends not only upon the size of the detector but upon the dimensions of the beam, the variation of unscattered particle intensity within the beam, and the law of force governing the interaction of beam particles and scattering particles. It may differ by several hundred per cent from the simple geometric aperture calculated only from the size of the detector and the distance of the detector from the region where scattering occurs. It is not possible to obtain reliable values of potential parameters unless θ is evaluated correctly[9] and unless the distribution of scattering particles along the scattering path is known so that $\sum_i n_i l_i$ may be calculated correctly[5].

To obtain numerical values of the potential parameters in an empirical potential function it is necessary to have a theoretical expression for $S = S(\theta, E)$ which contains these parameters. For a potential of the form $\phi(r) = K/r^s$, where K and s are the potential parameters, classical theory[15, 19] gives the following relation for the scattering angle θ (assumed to be small):

$$\theta = \frac{KC(s)}{r_0^s E} = \frac{\phi(r_0)C(s)}{E} \tag{2}$$

where r_0 is the distance of closest approach between the beam particle and the scattering particle and $C(s)$ is a constant which depends only on s. It is given by

$$C(s) = \sqrt{\pi}\,\Gamma\left(\frac{s}{2} + \frac{1}{2}\right)/\Gamma\left(\frac{s}{2}\right).$$

In the present case θ is to be identified with the average effective minimum angle through which a beam particle must be deflected in order to miss the detector. Since a coordinate system moving with the velocity of the center of mass is convenient for a two body scattering problem, θ in equation (2) stands for the *relative* average effective minimum angle of scattering and E stands for the initial kinetic energy of relative motion, $\frac{1}{2}\mu v^2$, where μ is the reduced mass of the beam particle–scattering particle system and v is the corresponding initial relative velocity. The classical total elastic scattering cross section for a system of energy E having an effective average angular aperture equal to θ in equation (2) is

$$S = S(\theta, E) = 2\pi \int_\theta^\pi G(\theta, E) \sin\theta d\theta =$$

$$= \pi b^2(\theta, E) = \pi r_0^2 [1 - \phi(r_0)/E] \tag{3}$$

where $G(\theta, E)$ is the angular distribution function for scattering and b the impact parameter characterizing the collision. The relation between them is

$$G(\theta, E) = \frac{b}{\sin\theta}\left|\frac{db}{d\theta}\right|.$$

If r_0 from equation (2) is substituted into equation (3), the desired theoretical relation for S is obtained:

$$S = \pi\left(\frac{KC}{\theta E}\right)^{2/s}\left(1 - \frac{\theta}{C}\right). \tag{4}$$

The parameters K and s can be obtained from the experimental cross sections by plotting $\ln S$ vs. $\ln E$. If $\phi(r) = K/r^s$ is an adequate representation of the potential over the range r equivalent to the range of r_0 in the experimental values of S, the plot will be a straight line of slope $-2/s$ and of intercept

$$\ln \pi (C/\theta)^{2/s}(1 - \theta/C) + \ln K^{2/s}.$$

If the inverse power potential is not an adequate empirical function, other potential forms may be assumed, to obtain relations corresponding to equations (3) and (4). For the type of experiments under discussion, θ/C is very much less than unity so that any error in determining the effective average angular aperture θ produces an equal error in K and thus in $\phi(r)$. Similarly,

errors in values of S calculated from equation (1), for example, by improper evaluation of $\Sigma n_i l_i$, will also lead to inaccurate values of $\phi(r)$ either through errors in s or in K, or in both.

Results of the procedure discussed above are illustrated in Figs. 2 and 3 for argon beams scattered in room temperature argon. In Fig. 2

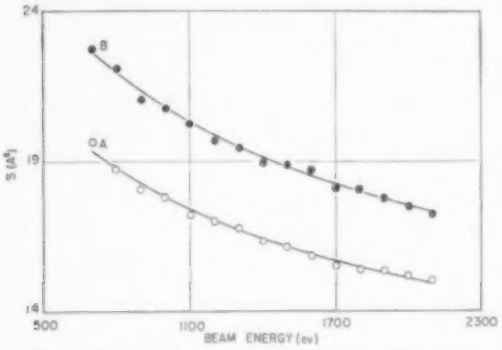

Fig. 2. Total elastic cross sections for argon scattered in argon: (a) wide detector; (b) narrow detector.

the two sets of experimental cross sections were measured with detectors of very different simple geometric relative apertures, 26·8 and 1·92 min. The effective relative average angular apertures of these detectors, for the Ar–Ar system, namely the values of θ in equation (4) were 12·7 and 7·94 min, respectively. Fig. 3, in which dashed portions of the curves represent extrapolations of the intermolecular potential beyond the actual region of its validity, shows the consistency of

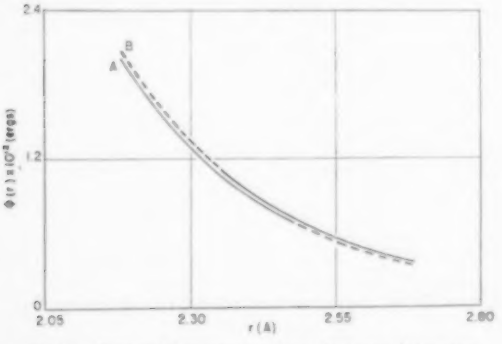

Fig. 3. Potential energy at close distances between two argon atoms: (a) wide detector results; b) narrow detector results.

the results for $\phi(r)$ which can be obtained from experimental measurements when correct values of θ are used in equation (4). Table 1 summarizes results for a number of systems involving only monatomic gases and Table 2 is a similar summary for systems involving diatomic scattering gases. In addition to the systems listed in these tables, measurements have been completed for: Ar–CO, Ar–O_2[20]; Ar–H_2[21]; He–CH_4, He–CH_3F, He–CH_2F_2, He–CHF_3, He–CF_4[22]. Although final calculations for these systems are in progress, it is apparent that Ar–CO and Ar–N_2 will have the same intermolecular potential as derived from scattering experiments in the same apparatus and approximately the same potential on the basis of measurements in different apparatuses. The Ar–O_2 potential will be somewhat lower than the Ar–N_2 potential and this difference in potentials will correspond to a difference of about 10 per cent, or less, in most high temperature transport properties. The results for He scattered by methane and its derivatives show an interesting systematic variation with increasing substitution. Measurements of this type may be helpful for predicting potentials for unknown systems on the basis of structural similarities to systems whose potentials are known.

Potentials such as those in Table 2 are averages with respect to all possible orientations in space of the scattering molecule relative to the beam particle. If it is assumed that interatomic forces are additive and that a single scattering molecule has an essentially fixed orientation in space during the brief period of a collision with the high velocity beam particle, it is possible to calculate *apparent interatomic* potentials which may then be used to calculate average molecule–molecule interactions. This procedure has been carried out for the He–N_2 and Ar–N_2 systems to obtain the following average N_2–N_2 potential[17]:

$$\phi(r) = 954 \times 10^{-12}/r^{7\cdot27}\,\text{ergs.}\quad (2\cdot43\,\text{Å} \leqq r \leqq 3\cdot07\,\text{Å})$$

Other atom–molecule scattering results mentioned above are being treated in the same manner to obtain average molecule–molecule interactions for the systems: CO–CO; O_2–O_2;

Table 1. Intermolecular Potentials for Atom–Atom Systems

System	$\phi(r) \times 10^{12}$ ergs (r in Å)	Range (Å)	Ref.
He–He	$4{\cdot}62/r^{1{\cdot}79}$ or $314\exp(-4{\cdot}21r^{1/2})$	0·52–1·02	6
	$7{\cdot}55/r^{5{\cdot}94}$	1·27–1·59	9
Ne–Ne	$500/r^{9{\cdot}99}$	1·76–2·13	12
Ar–Ar	$46{\cdot}1/r^{4{\cdot}52}$ or $3{\cdot}66\times10^{4}\exp(-6{\cdot}88r^{1/2})$	1·37–1·84	7
	$1360/r^{8{\cdot}33}$	2·18–2·69	10
Kr–Kr	$255/r^{5{\cdot}42}$	2·42–3·14	13
Xe–Xe	$1{\cdot}13\times10^{4}/r^{7{\cdot}97}$	3·01–3·60	14
He–Ar	$99{\cdot}5/r^{7{\cdot}25}$	1·64–2·27	11
Ne–Ar	$1010/r^{9{\cdot}15}$	1·91–2·44	16
H–He	$3{\cdot}75/r^{2{\cdot}29}$	1·16–1·71	15

Table 2. Intermolecular Potentials for Atom–Molecule Systems

System	$\phi(r) \times 10^{12}$ ergs (r in Å)	Range (Å)	Ref.
H–H_2	$70{\cdot}8\exp(-2{\cdot}99r^2)+6{\cdot}07\exp(-0{\cdot}942r^2)$	0·27–0·68	8
D–D_2	$45{\cdot}9\exp(-5{\cdot}17r^2)$	0·29–0·56	8
He–N_2	$119/r^{7{\cdot}06}$	1·79–2·29	17
Ar–N_2	$1210/r^{7{\cdot}78}$	2·28–2·83	17

H_2–H_2; CH_4–CH_4; CH_3F–CH_3F; CH_2F_2–CH_2F_2; CH_3F–CH_3F; CF_4–CF_4.

Once the intermolecular potential has been experimentally determined in the appropriate range of interaction distance, the calculation of high temperature gas properties for normal atomic and molecular species is relatively straightforward. A discussion of the fundamental statistical mechanical and kinetic theory relations, details of the calculation procedure and numerical results have been published[1,2]. The calculation procedure may be summarized as follows:

(a) Low temperature properties are calculated using potential energy functions which are valid at relatively large separation distances since it is these distances which are of major importance in determining the magnitude of the properties at low temperatures. Parameters of such functions, determined from experimental values of a variety of low temperature properties, have been tabulated by Hirschfelder *et al.*[3] and are satisfactory for calculations to about 1000°K.

(b) High temperature properties are calculated directly from beam potentials such as those listed in Tables 1 and 2. This high temperature region usually lies in the range 5000°–15,000°K, depending upon the property and the system.

(c) Intermediate range properties are calculated from potential functions which are blends or combinations of potentials valid at large separation distances with those valid at small separation distances (beam potentials). Such blended potentials, expressed in forms suitable for calculation of gas properties, reproduce reasonably well the characteristics of the beam potentials, at the same time retaining, as nearly as possible, the positions and magnitudes of the minima which appear in the potential functions appropriate for low temperature properties. The temperature range in which such blended potentials are used is approximately 1000°–5000°K.

(d) Final values of a given property are obtained by smoothing the values obtained in the separate ranges mentioned above. Fig. 4 shows the results of the calculation procedure for the viscosity of xenon. The curve has been arbitrarily terminated at 10,000°K to magnify

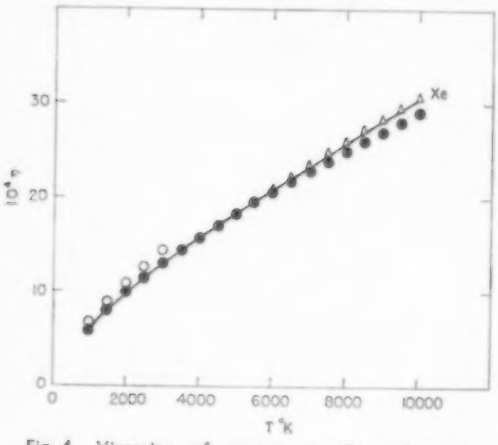

Fig. 4. Viscosity of xenon at elevated temperatures.

the features of the final smooth curve relative to the individual points. The low temperature points (open circles) have been deliberately extended to 3000°K to illustrate the error introduced by extrapolating the low temperature potential function beyond the range of its validity. The intermediate temperature points (closed circles) have been extended to 10,000°K for the same purpose. The deviation of these latter points from the smooth curve at the highest temperatures is a direct result of the procedure for blending potentials to obtain a function which is best suited for the intermediate range. The high temperature points (open triangles) would continue to fall on or close to the smooth curve if the figure were extended to 15,000°K. It is estimated that the smoothed viscosities are accurate to about 5 per cent over the entire temperature range and that the maximum error does not exceed 10 per cent. It is, perhaps, worth mentioning that xenon at moderate pressure would be extensively ionized and excited at 15,000°K and that there might be few instances in which the viscosity of ground state xenon at this temperature would be of interest. Nevertheless, the calculation procedures and principles are still applicable. In the case of gases such as helium or neon, ionization at this temperature (and even beyond) is slight and the viscosity of a system of ground state molecules has physical reality.

The calculation of gas properties which depend upon interactions between unlike particles is, in principle, similar to that for the properties of a pure gas described above. Such unlike particle interactions are required for calculating mutual and multicomponent diffusion coefficients, thermal diffusion factors, viscosities and thermal conductivities of binary and multicomponent mixtures. (There are, in addition, a number of equilibrium properties of gas mixtures which involve unlike particle interactions.) Interaction potentials for unlike particle systems can sometimes be measured directly, as in the case of the last three systems in Table 1 and the systems in Table 2, or, if this is not feasible, they can be obtained by combining potentials for systems of like molecules. Satisfactory experimental confirmation of combination rules for interactions at small distances has been obtained for several systems[11,16]. More general combination rules and expressions for transport properties of binary and multicomponent systems (the latter requiring potentials for all binary system combinations in a given multicomponent system) appear in references previously cited[3,4].

Numerical results based on considerations and procedures described in the present paper have been obtained by Amdur and Mason[1]. Equilibrium properties (virial coefficients), viscosity coefficients, translational thermal conductivity coefficients, self-diffusion coefficients and reduced isotopic thermal diffusion factors have been evaluated for temperatures between 1000° and 15,000°K. The He–Ar system was used to illustrate the character of the results which could be obtained for binary mixtures by calculating the following properties in the same temperature range: mutual diffusion coefficient; viscosity and thermal conductivity of an equimolar mixture; and the thermal diffusion factor for three compositions corresponding to mole fractions of He of 0, 1/2 and 1.

In making calculations of the type described in the present paper, it is extremely important to remember that the final values of the transport properties will be valid over a range of temperature that is determined by the range of the potential energy and *not* by the range of

kinetic energy of the beam particles. Otherwise expressed, it is the fraction of the kinetic energy of the beam particles which is converted into potential energy at the distance of closest approach during a collision and not the kinetic energy itself which determines the valid temperature range. For example, Le Fevre[23] has shown that if $\phi(r) = K/r^s$, the following relation is obtained between the potential energy and the absolute temperature for the coefficients of viscosity at elevated temperatures:

$$\phi(r_0) = kT \tag{5}$$

where r_0 is the equivalent hard sphere diameter which at the temperature T gives the same value of the viscosity as the actual inverse power potential. Moreover, this relation, which holds within 6 per cent, is not appreciably changed when other potential forms are assumed or when other transport properties at elevated temperatures are considered.

It follows from equation (5) that at 1000°K a potential energy of $1{\cdot}38 \times 10^{-13}$ ergs/molecule (0·086 eV) determines the magnitude of the viscosity and at 15,000°K the corresponding value is $2{\cdot}07 \times 10^{-12}$ ergs/molecule (1·29 eV). Most of the potential energy functions listed in Tables 1 and 2 are valid in this range and as shown in Figs. 2 and 3 were obtained from scattering of beam particles whose kinetic energies were of the order of 1000 eV. In principle, it is possible to obtain the same potential energy information from large angle scattering of beams with very much lower energies, of the order of 10 eV. It is very difficult in practice, however, to obtain such beams with sufficiently high intensities or with sufficiently small energy spreads. It is also harder to measure their intensities with the same precision as the high energy beams without using special detectors which are more difficult to construct and operate than the thermal detectors which have been used in the experiments described in this paper.

It is interesting, and quite possibly fruitful, to speculate on the possibilities of extending the present experimental method for calculating transport properties of neutral particles in their lowest internal energy states, since at elevated temperatures many systems of interest will contain, in addition to these ground state particles, excited species, ions, and dissociative atomic species. It would seem that if the proper potential functions for the species in question could be obtained, the difficulty of obtaining appropriate statistical mechanical or kinetic theory expressions might not be prohibitive.

In the case of ion–atom or ion–molecule interactions, the experimental procedure is probably simpler than for atom–atom or atom–molecule interactions. Ion beams of high intensity in the energy range of interest are relatively easy to produce and the problem of detection is even simpler than for high energy neutrals. Many experiments of this type have indeed been described in the literature[24].

Atom–atom interactions involving unstable atomic species could be obtained from scattering experiments in which atomic beam particles, such as H atoms, O atoms, etc., were scattered either by stable atoms or stable molecules. The H–He, H–H_2, and D–D_2 systems in Tables 1 and 2 are an example in point. By combining the results of such experiments with results for the appropriate stable particle systems, for example He–He, H_2–H_2, etc., it is possible to obtain interactions for the desired unstable atom–atom interactions. Incidentally, in many cases where such atom–atom interactions are of interest, the atom–molecule interactions which were obtained directly from the scattering experiments will also be important.

Interactions involving excited species are probably the most difficult to obtain. A suggested approach is to scatter a beam of stable ground state particles (He, Ar, etc.) through a layer of scattering gas which contains a known concentration of excited, metastable or, for that matter, dissociative atomic species. The concentrations of such species could be varied either by changing the temperature of the scattering gas or by irradiating the scattering gas with light of known intensity and spectral distribution. Experiments of this type would be quite difficult to interpret properly, but the importance of this type of interaction and the difficulty of obtaining quantitative experimental interaction information by other means would appear to justify serious consideration of the scheme.

REFERENCES

1. I. AMDUR and E. A. MASON, *Phys. of Fluids* **1**, 370 (1958).
2. I. AMDUR and J. ROSS, *Combustion and Flame* **2**, 412 (1958).
3. J. O. HIRSCHFELDER, C. F CURTISS and R. B. BIRD, *Molecular Theory of Gases and Liquids*. Wiley, New York (1954).
4. S. CHAPMAN and T. G. COWLING, *The Mathematical Theory of Non-Uniform Gases* (2nd Ed.). University Press, Cambridge (1952).
5. I. AMDUR, C. F. GLICK and H. PEARLMAN, *Proc. Amer. Acad. Arts Sci.* **76**, 101 (1948).
6. I. AMDUR, *J. Chem. Phys.* **17**, 844 (1949).
7. I. AMDUR, D. E. DAVENPORT and M. C. KELLS, *J. Chem. Phys.* **18**, 525 (1950).
8. I. AMDUR, M. C. KELLS and D. E. DAVENPORT, *J. Chem. Phys.* **18**, 1676 (1950).
9. I. AMDUR and A. L. HARKNESS, *J. Chem. Phys.* **22**, 664 (1954).
10. I. AMDUR and E. A. MASON, *J. Chem. Phys.* **22**, 670 (1954).
11. I. AMDUR, E. A. MASON and A. L. HARKNESS, *J. Chem. Phys.* **22**, 1071 (1954).
12. I. AMDUR and E. A. MASON, *J. Chem. Phys.* **23**, 415 (1955).
13. I. AMDUR and E. A. MASON, *J. Chem. Phys.* **23**, 2268 (1955).
14. I. AMDUR and E. A. MASON, *J. Chem. Phys.* **25**, 624 (1956).
15. I. AMDUR and E. A. MASON, *J. Chem. Phys.* **25**, 630 (1956).
16. I. AMDUR and E. A. MASON, *J. Chem. Phys.* **25**, 632 (1956).
17. I. AMDUR, E. A. MASON and J. E. JORDAN, *J. Chem. Phys.* **27**, 527 (1957).
18. E. H. KENNARD, *Kinetic Theory of Gases*, p. 115 McGraw-Hill, New York (1938).
19. M. C. KELLS, *J. Chem. Phys.* **16**, 1174 (1948).
20. J. E. JORDAN, Ph.D. Thesis, Massachusetts Institute of Technology (1958).
21. S. O. COLGATE, Ph.D. Thesis, Massachusetts Institute of Technology (1959).
22. I. AMDUR and M. S. LONGMIRE, *Bull. Amer. Phys. Soc.* ser. 2, **4**, 138 (1959).
23. E. J. LE FEVRE, *Proceedings of the Joint Conference on Thermodynamic and Transport Properties*, p. 124. The Institution of Mechanical Engineers, London (1958).
24. A series of papers by T. L. BAILEY, E. E. MUSCHLITZ, Jr., J. H. SIMONS and co-workers in *J. Chem. Phys.* (1943-1960) are of particular interest.

TRANSPORT PROPERTIES OF ATOMIC HYDROGEN

A. DALGARNO*

Geophysics Corporation of America, Boston, Massachusetts

Abstract—The effects of quantal symmetry requirements on the collision of two similar particles are discussed and it is pointed out that anomalously large values will occur for the cross section effective in diffusion but not for the cross section effective in viscosity and thermal conductivity. Quantitative data are reported for the diffusion cross sections associated with collisions of protons, neutral hydrogen atoms and negative hydrogen ions respectively with neutral hydrogen atoms at high temperatures.

1. INTRODUCTION

The quantitative prediction of transport phenomena for small departures from equilibrium can be reduced to the evaluation of collision cross sections Q^l defined according to

$$Q^l = 2\pi \int_{-1}^{+1} I(\theta)(1-\cos^l\theta)\, d(\cos\theta) \qquad (1)$$

where $I(\theta)$ is the differential cross section for elastic scattering through an angle θ measured in the center of mass system[1, 2]. The classical description of the elastic scattering of *unlike* particles is valid except at small angles of scattering which, however, do not contribute significantly to Q^l because of the factor of $(1-\cos^l\theta)$ in the integrand. Thus equation (1) can be written in the form

$$Q^l = 2\pi \int_0^\infty p(1-\cos^l\theta)\, dp, \qquad (2)$$

p being the impact parameter, and equation (2) can be computed straightforwardly using the expression for θ in terms of p derived from standard classical orbit theory:

$$\theta = \pi - 2\int_{r_0}^\infty dr/r \left\{ \frac{p^2}{r^2} - 1 - \frac{r^2 V(r)}{E} \right\}^{-\frac{1}{2}} \qquad (3)$$

where r is the separation of the two particles, r_0 is the distance of closest approach, $V(r)$ is the interaction potential and E is the energy of relative motion. There may be several possible interaction potentials and the actual cross section is then an appropriately weighted average of the individual cross sections associated with each interaction potential.

A more careful examination of the collision of two *similar* particles is required, for the theoretical description should take into account the requirements imposed by the symmetry of the collision.

2. COLLISIONS OF SIMILAR PARTICLES

For particles moving in their parent gas, it is necessary to use the quantal formula

$$Q^l = \frac{4\pi}{k^2} \sum_{s=0}^\infty f_l(s) \sin^2(\delta_s - \delta_{s+l}) \qquad (4)$$

where k is the wave number of the relative motion, δ_s is the elastic scattering phase shift of order s[3] and $f_l(s)$ is a rational function of s; in particular

$$f_l(s) = (s+1); \quad f_2(s) = \frac{(s+\frac{1}{2})(s+\frac{3}{2})}{(s+1)} \quad . \qquad (5)$$

In the unlike case it may be shown that the classical and quantal formulae become identical when Jeffreys' approximation is used for the phase shifts and the summation in equation (4) is replaced by an integration over

$$p = \sqrt{[s(s+1)/k]}.$$

In the like case there are in general two possible modes of interaction, one, $V^+(r)$, symmetric with respect to interchange of the nuclei and the other, $V^-(r)$, antisymmetric and if δ_s is associated with $V^\pm(r)$, δ_{s+1} is associated with $V^\mp(r)$. For most collisions of similar particles, one of $V^\pm(r)$ is attractive and the

* On leave from the Department of Applied Mathematics, The Queen's University of Belfast, N. Ireland.

other repulsive so that for most values of s

$$\delta_s^{\pm} - \delta_{s+l}^{\mp} \gg \delta_s^{\pm} - \delta_{s+l}^{\pm}. \tag{6}$$

Thus when l is odd, anomalously large values of Q^l are to be expected but not when l is even.

The case when l is unity is of particular interest. Since for most values of s

$$|\delta_s^+ - \delta_s^-| \gg |\delta_s^{\pm} - \delta_{s+1}^{\pm}|, \tag{7}$$

Q^1 can be written approximately as $2Q_e$ where

$$Q_e = \frac{\pi}{k^2} \sum_{s=0}^{\infty} (2s+1) \sin^2 (\delta_s^+ - \delta_s^-). \tag{8}$$

But equation (8) is just the quantal formula for the charge exchange or charge transfer cross section at low energies of impact[4], measurements of which are available for many cases. The accuracy of this relationship has been verified by comparison of measurements of Q_e with values of Q^1 derived from measurements of the mobilities of ions in their parent gases[5].

To demonstrate the magnitudes of Q^1 which may occur in cases of similar particles we reproduce in Table 1 the values for the collisions of protons, neutral hydrogen atoms and negative hydrogen ions respectively with neutral hydrogen atoms. The effect of the symmetry requirements is considerable and the cross sections are one or two orders of magnitude greater than for the collision of two unlike particles.

Table 1. Values of Q^1 in Units of 10^{-16} cm^2

Impact energy (eV)	H^+–H	H–H	H^-–H
0·1	124	41	647
1	100	33	435
10	75	26	275
100	50	19	155

REFERENCES

1. S. Chapman and T. G. Cowling, *The Mathematical Theory of Non-Uniform Gases*. Cambridge University Press (1952).
2. J. O. Hirschfelder, C. F. Curtiss and R. B. Bird, *The Molecular Theory of Gases and Liquids*. Wiley, New York (1954).
3. N. F. Mott and H. S. W. Massey, *The Theory of Atomic Collisions*. Clarendon Press, Oxford (1949).
4. D. R. Bates, H. S. W. Massey and A. L. Stewart, *Proc. Roy. Soc.* A**216**, 437 (1953).
5. A. Dalgarno, *Phil. Trans. Roy. Soc.* A**250**, 426 (1958).

ENERGY TRANSPORT IN HIGH TEMPERATURE AND REACTING GASES

R. S. BROKAW

Lewis Research Center, NASA, Cleveland, Ohio

Abstract—Methods presently available for estimating convective and conductive heat transfer in high temperature gases are reviewed, emphasizing the role of viscosity and thermal conductivity. Examination of engineering heat transfer correlations shows that large errors in thermal conductivity and viscosity lead to considerably smaller errors in heat transfer coefficient provided transport properties are obtained by techniques derived from rigorous kinetic theory. Because uncertainties in high temperature transport properties arise largely as a result of uncertainties in collision cross-sections, methods of estimating these cross-sections are considered; estimates show encouraging agreement with experiment for both stable and unstable species. Approximate formulas for viscosity and conductivity of mixtures are compared with rigorous formulas and with experiment.

Heat conduction in reacting gases is then considered; in such mixtures the diffusional transport of chemical enthalpy may lead to thermal conductivities an order of magnitude greater than in similar, but nonreacting gases. Theoretical predictions of the equilibrium conductivity compare favorably with experimental data for the nitrogen tetroxide and hydrogen fluoride systems. When chemical reaction rates are not high enough to maintain chemical equilibrium locally in a temperature gradient, theory shows that the effective thermal conductivity is related to the ratio of a diffusion time to the chemical relaxation time; low pressure data for the nitrogen tetroxide system are in accord with this analysis. Finally it is shown that experimental convective heat transfer in practical systems can be treated by these methods.

It is concluded that methods for calculating high-temperature heat transfer are in many respects well developed, so that rigorous calculations of the transport properties are often justified.

1. INTRODUCTION

Over the past several years a large effort has been expended in investigating energy transport in high temperature gases. The reasons for this interest are several-fold. The initial impetus came, perhaps, as a by product of the investigations of basic combustion processes which mushroomed with the advent of the jet age. The fundamental properties of flames involve a complex wedding of the transport processes with chemical kinetics—both unknowns at high temperatures. More recently the interest in high-temperature heat transport has been augmented by practical considerations of heat transfer from the reacting gases of rocket exhausts and, finally, the boundary layers of hypersonic aircraft and re-entering missiles.

It is the purpose of this paper to examine the tools which have been acquired for calculating high temperature heat transport. Heat transfer by conduction and convection will be treated; these processes involve the basic molecular transport coefficients of viscosity, thermal conductivity and mass diffusion. Emphasis will be placed on the basic transport properties rather than the heat transfer correlations as such. Heat transfer by radiation and in ionized gases lies outside the scope of this paper.

As a first step, engineering heat transfer correlations will be examined to determine the accuracies required of transport property estimates for calculations of practical systems. Next, the estimation of collision cross sections and calculation of the properties of gas mixtures will be discussed. A consideration of heat transport in reacting gases at chemical equili-

brium follows; the effects due to finite reaction rates will also be discussed. Finally, experimental and analytical data on convective heat transfer in reacting gases is examined.

2. ENGINEERING HEAT TRANSFER CORRELATIONS

Engineering heat transfer correlations are commonly expressions of the type

$$\mathrm{Nu} = f(\mathrm{Re}, \mathrm{Pr}) \tag{1}$$

This form is a consequence of dimensional analysis[1a]. The transport properties appear in the dimensionless groups

$$\mathrm{Nu} = \text{Nusselt number} = hd/\lambda$$
$$\mathrm{Re} = \text{Reynolds number} = \rho V d/\eta$$
$$\mathrm{Pr} = \text{Prandtl number} = c_p \eta/\lambda$$

where h is the heat transfer coefficient in the particular geometry under consideration (it is the heat flux through unit area with unit temperature difference), d is a characteristic dimension of the body (the diameter of a cylinder or pipe, the length of a flat plate), λ is the thermal conductivity and η the viscosity of the fluid, ρ and c_p are the fluid density and specific heat at constant pressure, and V is the velocity.

Two specific examples of equation (1) are

$$\mathrm{Nu} = 0{\cdot}662\,\mathrm{Re}^{1/2}\mathrm{Pr}^{1/3} \tag{2}$$

for a flat plate in laminar flow[1b] and

$$\mathrm{Nu} = 0{\cdot}036\,\mathrm{Re}^{0{\cdot}8}\mathrm{Pr}^{1/3} \tag{3}$$

for a flat plate in turbulent flow[2]. These expressions give average heat transfer coefficients; the Nusselt and Reynolds numbers are formulated using the length of the plate in the direction of the flow. High temperature correlations may be more complex to account for variations in fluid properties through the boundary layer (see, for example, the stagnation point heat transfer correlation of Fay and Riddell[3]). Nonetheless, equations (2) and (3) indicate typically the sensitivity of heat transfer predictions to uncertainties in the transports properties. Thus, in equation (2) the error in the heat transfer coefficient will be two thirds of the error in the thermal conductivity (through the Nusselt and Prandtl numbers) and one sixth of the error in the viscosity (through the Reynolds and Prandtl numbers).

However, when the viscosity and thermal conductivity are computed from the kinetic theory of gases, errors tend to be in the same direction, resulting in considerable cancellation. To illustrate this point, let us consider the case of a pure monatomic gas. (A similar cancellation will occur with mixtures of polyatomic gases, but the mathematical expressions are cumbersome.) For a monatomic gas the conductivity and viscosity are given by[4]

$$\lambda' = \frac{75}{64}\left[\frac{\sqrt{(\pi mkT)}}{\pi\sigma^2\Omega^{(2,2)^*}}\right]\left(\frac{k}{m}\right) \tag{4}$$

$$\eta = \frac{5}{16}\left[\frac{\sqrt{(\pi mkT)}}{\pi\sigma^2\Omega^{(2,2)^*}}\right] \tag{5}$$

where m is the molecular mass, k the Boltzmann constant and T is the absolute temperature. The quantity $\pi\sigma^2\Omega^{(2,2)^*}$ is a collision cross-section. (σ is the zero energy collision diameter while $\Omega^{(2,2)^*}$ accounts for the variation of collision cross-section with temperature for rigid elastic spheres $\Omega^{(2,2)^*} = 1$.) The uncertainties about the transport properties of gases at high temperature result mainly from uncertainties as to high temperature collision cross-sections. It is apparent that the Prandtl number, since it involves the ratio of the viscosity and conductivity, is independent of the collision cross-section; for a monatomic gas the Prandtl number is two thirds.

By rearranging, equation (2), the heat transfer coefficient for laminar flow is given as

$$\left.\begin{aligned} h &= 0{\cdot}662\,c_p(\rho V)^{1/2}\left(\frac{\eta}{d}\right)^{1/2}\mathrm{Pr}^{-2/3} \\ &\propto (\sigma^2\Omega^{(2,2)^*})^{-1/2} \end{aligned}\right\} \tag{6}$$

For turbulent flow, equation (3) yields,

$$\left.\begin{aligned} h &= 0{\cdot}036\,c_p(\rho V)^{0{\cdot}8}\left(\frac{\eta}{d}\right)^{0{\cdot}2}\mathrm{Pr}^{-2/3} \\ &\propto (\sigma^2\Omega^{(2,2)^*})^{-0{\cdot}2} \end{aligned}\right\} \tag{7}$$

Thus we see that a 10 per cent error in collision diameter, which would give rise to a 21 per cent error in viscosity or conductivity, causes a 10 per cent error in the heat transfer estimate

in laminar flow and only a 4 per cent error for turbulent flow.

Uncertainties in the absolute values of viscosity and conductivity at high temperatures often tempt workers to use crude and empirical methods to estimate these properties. Even if such methods are as accurate as the rigorous techniques for the individual properties, errors will be random rather than systematic. In this event 21 per cent errors in the transport properties would cause, on the average, 14 per cent errors in the laminar correlation and 17 per cent errors in the turbulent correlation†.

It is seen, then, that there is merit in rigorous transport property calculations despite uncertainty as to absolute magnitudes of the property values. Accordingly, the next two sections treat in turn, methods of estimating molecular diameters and approximate formulas for the viscosity and conductivity of gas mixtures.

3. ESTIMATION OF COLLISION DIAMETERS

As has already been stated, a major uncertainty in calculating high temperature transport properties is the uncertainty in collision diameters. This is particularly the case for unstable species—atoms and free radicals—which do not normally exist at moderate temperatures, but are abundant in high temperature gas equilibria.

Hirschfelder and Eliason[5] have developed a method for estimating collision diameters of atoms and molecules based on the mean radii of electrons in Slater orbitals. Their ideas form the basis of what follows.

The mean radius of an electron in a Slater orbital is

$$\bar{r} = \frac{n^*(2n^*+1)}{2(Z-S)} a_0$$

where Z is the atomic number, n^* is the effective principal quantum number of the electron, S is its screening constant, and a_0 is the Bohr radius = 0·5292 Å. Hirschfelder and Eliason note that in a diatomic molecule the internuclear distance, R_{ab}, is very nearly the sum of the Slater radii of the outermost electrons of the constituent atoms

$$R_{ab} = \bar{r}_a + \bar{r}_b \tag{8}$$

On the other hand, atoms in a thermal collision repel at much greater distances. By comparing collision diameters of the noble gases (derived from viscosity measurements) with the Slater radii Hirschfelder and Eliason established the empirical rule

$$\sigma_{ab} = \bar{r}_a + \bar{r}_b + 1{\cdot}8\ \text{Å} \tag{9}$$

Consider next the collision diameter of a homonuclear diatomic molecule. In two dimensions the diameter is the same as that of the constituent atom; in the third dimension, the diameter must be increased by the bond length. Assuming the diatomic molecule to be a spherocylinder, the average diameter, based on the mean cross-section of the molecule is

$$\sigma_{\text{molecule}} = \sqrt{[1{\cdot}849\,(r_a + r_b)^2 + 5{\cdot}13\,(r_a + r_b) + 3{\cdot}24]} \tag{10a}$$

$$= \sqrt{[1{\cdot}849\,R_{ab}^2 + 5{\cdot}13\,R_{ab} + 3{\cdot}24]} \tag{10b}$$

$$= \sqrt{[1{\cdot}849\,\sigma_{\text{atom}}^2 - 1{\cdot}528\,\sigma_{\text{atom}}]} \tag{10c}$$

(The average is based on area rather than diameter because cross-sections rather than diameters appear in the transport property formulas.)

For atoms, the following methods of estimating diameters are available:

$$\sigma_{\text{atom}} = 2\bar{r} + 1{\cdot}8\ \text{Å} \quad \text{(from equation 9)} \tag{11a}$$

$$= R_{aa} + 1{\cdot}8\ \text{Å} \quad \text{(from equations 8 and 9)} \tag{11b}$$

$$= 0{\cdot}413 + \sqrt{(0{\cdot}171 + 0{\cdot}540\,\sigma_{\text{molecule}}^2)} \quad \text{(from equation 10c)} \tag{11c}$$

These three techniques are compared with each other and with the available experimental data for atoms in Table 1. The agreement between prediction and experiment for the ground states of the noble gases is not surprising, as this is the basis of equation (9). Note, however, that the electronically excited states of neon, argon and xenon are expected to have enormous collision diameters; this is confirmed by the experimental values, derived from Molnar's[6] studies on the diffusion of these metastable atoms.

† This is so because the fractional error in a product is $\sqrt{\left(\sum_i \varepsilon_i^2\right)}$, where the ε_i are the fractional errors in the quantities forming the product.

Table 1. Calculated and Experimental Collision Diameters of Atoms

Atom	Collision diameter, (Å)			
	From Slater orbital radius (equaltion 11a)	From internuclear distance in diatomic molecule (equation 11b)	From collision diameter of diatomic molecule (equation 11c)	Experimental
Ground states				
H	3·4	2·5	2·6	2·7
He	2·7			2·6
N	3·2	2·9	3·2	
O	3·0	3·0	3·0	2·9
Ne	2·7			2·8
Cl	3·6	3·8	3·4, 3·7	
A	3·4			3·4
Br	4·0	4·1	3·5	
Kr	3·8			3·6
Xe	4·1			4·1
Excited states				
Ne	7·2			7·4
A	9·8			8·7
Xe	12·0			10·6

Table 2. Calculated and Experimental Collision Diameters of Diatomic Molecules

Molecule	Collision diameter, (Å)		
	From Slater orbital radii (equation 10a)	From internuclear distance (equation 10b)	Experimental
H_2	4·0	2·8	2·9
N_2	3·7	3·3	3·7
O_2	3·4	3·5	3·5
Cl_2	4·3	4·6	4·2, 4·4
Br_2	4·8	5·0	4·3
I_2	5·3	5·5	5·0
NO	3·6	3·4	3·5
CO	3·7	3·4	3·7
HCl	4·2	3·6	3·3
HI	4·6	4·0	4·1
OH	3·7	3·2	

The three methods of estimating diameters are generally in agreement, with the notable exception of the hydrogen atom where the Slater orbital treatment gives a high value†. In this case the methods based on internuclear distance or collision diameter of the hydrogen molecule are to be preferred.

Diameters of diatomic molecules may be computed by means of either equation (10a) or (10b); values so calculated are compared with experiment in Table 2. Agreement is again generally good; values computed from Slater radii are perhaps somewhat better except for molecules containing hydrogen. The Slater orbital radius for hydrogen seems too large; for molecules containing hydrogen atoms the method based on internuclear distance is to be preferred.

These techniques for estimating diameters show a probable error of 4·7 per cent from experiment, omitting Slater radius values for molecules with hydrogen atoms. While more accurate methods of estimating high temperature collision cross sections are certainly to be desired, the methods considered here are quite accurate enough to justify continuing with a rigorous treatment of the viscosity and thermal conductivity.

4. TRANSPORT PROPERTIES OF GAS MIXTURES

Rigorous kinetic theory expressions for the viscosity[9a] and thermal conductivity[10] have been developed by Hirschfelder, Curtiss and co-workers; recently an Eucken type expression for the diffusional transport of internal energy has been obtained[11]. These rigorous expressions generally describe the properties of gas mixtures very well, but are mathematically cumbersome. Somewhat simpler expressions, which are approximations derived from the rigorous relations, are presented here. These approximations are sufficiently accurate for practical purposes.

† The experimental diameter for the hydrogen atom was obtained from the ratio of the hydrogen atom and hydrogen molecule diameters computed by Amdur[7] from the viscosity data of Harteck[8].

Viscosity

The approximate formula for mixture viscosity is

$$\eta_{mix} = \sum_{i=1}^{v} \frac{\eta_i}{1 + \sum_{\substack{j=1 \\ j \neq i}}^{v} \Phi_{ij} \frac{x_j}{x_i}} \qquad (12)$$

where the η_i are the viscosities of the component gases and x_i, x_j are mole fractions.

Equation (12) is of the form originally proposed by Sutherland[12]. The author[13] has derived equation (12) as an approximation to the rigorous expression for viscosity. It is found that

$$\Phi_{ij} = \frac{\lambda_i'}{\lambda_{ij}'} \qquad (13)$$

where λ_i' is the monatomic or translational thermal conductivity of component i (calculable by equation 4) and λ_{ij}' is a ficticious conductivity characterizing the interaction between unlike molecules[9b]. By assuming rigid sphere formulas for viscosity and thermal conductivity the quantity λ_{ij}' may be eliminated from equation (13)[14], yielding

$$\Phi_{ij} = \frac{\left[1 + \left(\frac{\lambda_i'}{\lambda_j'}\right)^{1/2} \left(\frac{M_i}{M_j}\right)^{1/4}\right]^2}{2\sqrt{2}\left(1 + \frac{M_i}{M_j}\right)^{1/2}} \qquad (14a)$$

$$= \frac{\left[1 + \left(\frac{\eta_i}{\eta_j}\right)^{1/2} \left(\frac{M_j}{M_i}\right)^{1/4}\right]^2}{2\sqrt{2}\left(1 + \frac{M_i}{M_j}\right)^{1/2}} \qquad (14b)$$

The approximation involved in obtaining equations (12) and (13) leads to a systematic positive error in mixture viscosity. This is in a large measure counteracted by a systematic error in the opposite direction in the approximations leading from equation (13) to equations (14a) and (14b). Equations (12) and (14b) were first developed by Wilke[14] by an astute combination of empirical data fitting and intuitive reasoning.

Accordingly, the recommended approximations for calculating mixture viscosity are equations (12) and (14a) or (14b). Some calculations for binary systems with large differences in molecular weights (a severe test) are shown in Table 3. Note that the rigorous calculations reproduce the experimental values very well. For this discussion, however, the more important comparison is between the approximate and rigorous methods. The probable error of the approximate calculations is 1·9 per cent.

Table 3. Viscosity of Gas Mixtures

Gas Pair and temperature	Per cent of first gas	Viscosity ($P \times 10^5$)		
		Calculated		Experimental
		Approximate	Rigorous*	
He–Ar	0	22·23	22·23	22·11
20° C	34·05	22·92	—	22·78
	38·20	22·99	23·05	22·91
	49·06	23·15	23·19	22·96
	75·65	22·90	—	22·70
	100	19·26	19·26	19·73
H_2–Ar	0	22·23	22·23	22·11
20° C	29·42	21·82	21·40	21·40
	44·57	21·29	20·60	20·56
	65·15	19·75	18·60	18·57
	100	8·76	8·76	8·75
H_2–CO_2	0	14·93	14·93	14·93
23° C	19·93	15·10	15·07	15·01
	41·29	15·16	15·08	15·06
	78·50	14·15	13·72	13·70
	100	8·89	8·89	8·91

* Hirschfelder, Bird and Spotz, *Chem. Rev.* **44**, 205 (1949).

Thermal conductivity

The thermal conductivity of a mixture of unreacting polyatomic gases may be divided into two portions:

$$\lambda_{mix} = \lambda'_{mix} + \lambda''_{mix} \qquad (15)$$

Here λ'_{mix} represents the collisional transport of translational kinetic energy whereas λ''_{mix} accounts for the diffusional transport of internal energy. (The quantity λ'_{mix} completely accounts for the thermal conductivity of mixtures of the noble gases.)

The approximate formula for λ'_{mix} (of the same form as equation 12 for viscosity) is

$$\lambda'_{mix}=\sum_{i=1}^{v}\frac{\lambda'_i}{1+\sum_{\substack{j=1\\ j\neq i}}^{v}\psi_{ij}\frac{x_j}{x_i}} \tag{16}$$

where the λ'_i are the translational thermal conductivities of the component gases (equation 4). The coefficients ψ_{ij} are found to be[13]

$$\psi_{ij}=\Phi_{ij}\left\{1+\left(\frac{M_i-M_j}{M_i+M_j}\right)^2\left(\frac{15}{4A^*_{ij}}-1\right)\left[1+\left(\frac{12B^*_{ij}+5}{30-8A^*_{ij}}\right)\frac{M_j}{M_i-M_j}\right]\right\} \tag{17a}$$

$$\cong\Phi_{ij}\left[1+2{\cdot}41\frac{(M_i-M_j)(M_i-0{\cdot}142\,M_j)}{(M_i+M_j)^2}\right] \tag{17b}$$

since for many realistic intermolecular potentials $A^*_{ij}\simeq B^*_{ij}\simeq 1{\cdot}1$.

The formula for the internal thermal conductivity[11] is

$$\lambda''_{mix}=\sum_{i=1}^{v}\frac{\lambda''_i}{1+\sum_{\substack{j=1\\ j\neq i}}^{v}\frac{D_i}{D_{ij}}\frac{x_j}{x_i}} \tag{18}$$

where D_i is the self-diffusion coefficient of component i and D_{ij} is the binary diffusion coefficient between components i and j. It is convenient to approximate the ratio of diffusion coefficients as

$$\frac{D_i}{D_{ij}}\cong\Phi_{ij} \tag{19}$$

since the Φ_{ij} are in any event at hand for mixture viscosity calculation. The quantities λ''_i are the internal conductivities of the pure components; they may be calculated[15] as

$$\lambda''_i=\rho D_i c_{v_{i,\,int}}=\lambda'_i Le'\left(\frac{2}{5}\frac{C_{p_i}}{R}-1\right)$$

Here $c_{v_{i,\,int}}$ is the contribution of the internal degrees of freedom to the specific heat, C_{p_i} is the constant pressure heat capacity of component i and $Le=\rho c_p D/\lambda$ is the Lewis number. For a monatomic gas, $Le'=4A^*_i/5$, so that

$$\lambda''_i=\frac{4}{5}A^*_i\left(\frac{2}{5}\frac{C_{p_i}}{R}-1\right)\lambda'_i\cong 0{\cdot}88\left(\frac{2}{5}\frac{C_{p_i}}{R}-1\right)\lambda'_i \tag{20}$$

Approximate thermal conductivities, calculated via equations (15)–(19) are compared with rigorous calculations and with experiment in Table 4. Internal conductivities of the pure components were taken as the difference between the experimental thermal conductivity and the computed translational thermal conductivity. The agreement between the rigorous and approximate conductivities is very satisfactory; the probable error is 1·2 per cent. The benzene–

Table 4. Thermal Conductivity of Gas Mixtures

Gas pair and temperature	Per cent of first gas	Thermal conductivity, (cal/cm sec °C × 10⁵)		
		Calculated		Experimental
		Approximate	Rigorous[13]	
He–Ar	0	3·91	3·91	3·89
0° C	27·04	7·37	7·55	7·42
	45·37	10·78	11·02	10·77
	84·68	24·31	24·39	23·20
	94·61	30·45	30·46	29·39
	100	34·66	34·66	33·86
H_2–Ar	0	(3·90)	(3·90)	3·9
0° C	9	5·41	5·45	5·5
	18	7·11	7·15	7·3
	40	12·18	12·23	12·6
	60	18·44	18·44	18·7
	80·2	27·35	27·32	27·0
	100	(40·40)	(40·40)	40·4
H_2–CO_2	0	(3·60)	(3·60)	3·6
0° C	10	4·93	5·05	5·1
	25	7·34	7·63	7·7
	50	12·94	13·50	13·5
	75	22·49	22·91	22·7
	90·1	31·48	31·95	31·5
	100	(40·40)	(40·40)	40·4
C_6H_6–Ar	0	(4·85)	(4·85)	4·85
78° C	25	4·23	4·19	4·185
	50	3·85	3·83	3·795
	75	3·60	3·60	3·58
	100	(3·44)	(3·44)	3·44

argon mixtures are particularly interesting: although benzene and argon have molecular weights and thermal conductivities which are not too dissimilar, the mode of heat transport varies greatly. Argon transports heat as kinetic energy of translation only, whereas in benzene the internal conductivity accounts for three quarters of the total.

The approximate formulas for viscosity and thermal conductivity presented here describe well the behavior of gas mixtures and are adequate for all practical purposes, although the rigorous methods appear to be in slightly better agreement with experiment. The combined effect of these approximations is illustrated in Fig. 1 where calculated Prandtl numbers for

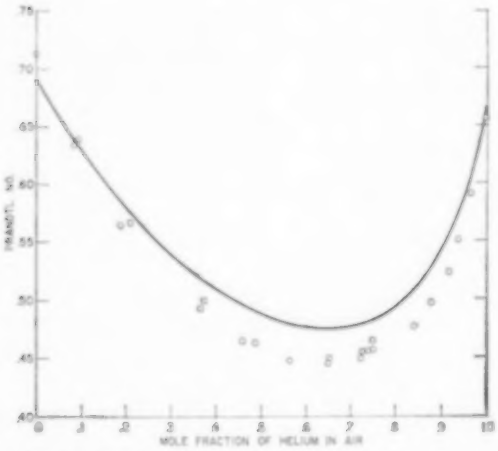

Fig. 1. Prandtl number of helium–air mixtures.

helium–air mixtures are compared with the direct experimental determinations of Eckert *et al.*[16]. (The calculations treated these gases as ternary mixtures of helium, oxygen and nitrogen.) Agreement is again good, the largest errors being about 5 per cent. Note the serious errors which would be incurred if it were naively assumed that Prandtl number varied linearly with mole fraction!

The most serious problem in treating the transport properties of gas mixtures arises in the case of mixtures involving polar molecules. The polar–nonpolar molecule interactions are essentially of a nonpolar nature and hence susceptible to treatments applicable to collisions of nonpolar molecules. On the other hand, when the polar molecules interact with one another they may interchange rotational energy over large distances; nonadiabatic collisions involving interchange between translational and rotational energy are perhaps the rule rather than the exception. This causes the thermal conductivity to be "abnormally" low relative to the viscosity. Further work, both theoretical and experimental, is needed to gain a sound understanding of the transport properties of polar gases.

5. HEAT CONDUCTION IN REACTING GASES

At high temperatures most gases of interest to aerodynamics and propulsion are partially dissociated, and hence undergo a variety of chemical reactions. In reacting gases, heat transport may be considerably higher than in "frozen" (nonreacting) mixtures. Large amounts of heat may be carried as chemical enthalpy of molecules which diffuse because of concentration gradients; these gradients exist because the gas composition varies with temperature. For example, in a gas which absorbs heat by dissociating as the temperature is raised, heat is transferred when a molecule dissociates in the high temperature region and the fragments diffuse toward the low-temperature region (there is a lower concentration of dissociated molecules at low temperature). In the low-temperature region the gas reassociates, releasing the heat absorbed from the high-temperature dissociation.

This phenomenon was first recognized by Nernst[17] who suggested that the high thermal conductivity of nitrogen tetroxide is caused by this effect. Another early worker in this field was Langmuir[18]; he observed a precipitous rise in the heat loss from tungsten wires in hydrogen in the temperature range from 2100° to 3300°K. No such effect was observed with nitrogen. Langmuir ascribed this effect to dissociation of the hydrogen at the tungsten followed by diffusion into and recombination in the surrounding cool gas. He presented a theoretical analysis, correct in its important features.

In what follows we shall consider first the

thermal conductivity of reacting gases assuming chemical equilibrium obtains locally throughout the gas. This assumes chemical reaction rates are very high. Effects due to reduced reaction rates will then be discussed.

Gas mixtures in equilibrium

When chemical equilibrium can be assumed to exist locally throughout a gas mixture, it becomes possible by differentiating the equilibrium relationships to relate the concentration gradients to the temperature gradient. The concentration gradients provide the driving force for the diffusional transport of chemical enthalpy. In this case one can define an equilibrium thermal conductivity, λ_e, independent of apparatus geometry.

$$\lambda_e = \lambda_f + \lambda_r \tag{21}$$

where λ_f is the thermal conductivity in the absence of chemical reactions (the "frozen" thermal conductivity) and λ_r is the augmentation due to the reactions.

The first treatment of this sort was due to Nernst[17] who derived an essentially correct formula for the nitrogen tetroxide dissociation. (The "diffusion coefficient" used by Nernst is not the usual binary diffusion coefficient; however, Nernst was alert to this possibility.) Another example of this type of analysis is the derivation of the Eucken type correction for the transport of internal energy in polyatomic gases. Eucken's original arguments were essentially intuitive[19]. Ubbelohde[20] took the decisive step of considering molecules with "excited" internal energy states as belonging to different chemical species; he pointed out that the flow of internal energy could be treated as energy transport due to diffusion of the "excited" molecules. This idea was elaborated by Chapman and Cowling[15], Hirschfelder[21] and others; it provides the basis for equation (20).

An explicit expression for the increase in thermal conductivity due to chemical reaction was developed in Ref. (22); this expression is applicable to gas mixtures involving any number of reactants, inert diluents, and chemical equilibria. This system of ν independent chemical reactions involving μ chemical species (both reactants and diluents) may be written in balanced form as

$$\sum_{k=1}^{\mu} n_{ik} X^k = 0 \qquad i = 1, 2 \ldots j \ldots \nu$$

Here X^k represent the chemical species and the n_{ik} are the stoichiometric coefficients for species k in reaction i. The heat of this reaction is

$$\Delta H_i = \sum_{k=1}^{\mu} n_{ik} H_k \qquad i = 1, 2 \ldots j \ldots \nu$$

where the H_k are the enthalpies of the species referred to a common base. For this system the thermal conductivity due to reaction is

$$\lambda_r = -\frac{1}{RT^2} \frac{\begin{vmatrix} A_{11} & \ldots & A_{1\nu} & \Delta H_1 \\ \cdot & & \cdot & \cdot \\ \cdot & & \cdot & \cdot \\ \cdot & & \cdot & \cdot \\ A_{1\nu} & \ldots & A_{\nu\nu} & \Delta H_\nu \\ \Delta H_1 & \ldots & \Delta H_\nu & 0 \end{vmatrix}}{\begin{vmatrix} A_{11} & \ldots & A_{1\nu} \\ \cdot & & \cdot \\ \cdot & & \cdot \\ \cdot & & \cdot \\ A_{1\nu} & \ldots & A_{\nu\nu} \end{vmatrix}} \tag{22}$$

where

$$A_{ij} = \sum_{k=1}^{\mu-1} \sum_{l=k+1}^{\mu} \frac{RT}{D_{kl} P} x_k x_l \left(\frac{n_{ik}}{x_k} - \frac{n_{il}}{x_l}\right)\left(\frac{n_{jk}}{x_k} - \frac{n_{jl}}{x_l}\right)$$
$$i, j = 1, 2 \ldots \nu$$

Here x_k, x_l are the mole fractions of components k and l, and P is the pressure. Any gas inert to reaction i or j is included, but has a zero stoichiometric coefficient for the reaction in which it does not participate. For a single reaction equation (22) reduces to

$$\lambda_r = \frac{\Delta H^2 / RT^2}{\sum_{k=1}^{\mu-1} \sum_{l=k+1}^{\mu} \frac{RT}{D_{kl} P} x_k x_l \left(\frac{n_k}{x_k} - \frac{n_l}{x_l}\right)^2} \tag{23}$$

(The index for the reaction has been dropped since there is but one reaction.)

Equation (23) has been subjected to extensive experimental testing for the pure nitrogen tetroxide–nitrogen dioxide system by Coffin and O'Neal[23]; more recently Coffin[24] has examined

the effects of inert diluents (argon or helium). Results at atmospheric pressure are shown in Figs. 2 and 3. The open symbols are for pure

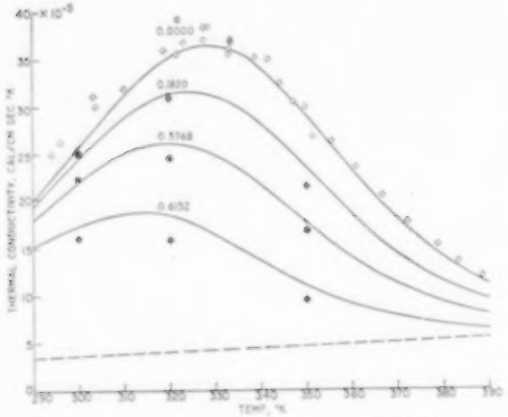

Fig. 2. Thermal conductivity of the N_2O_4–NO_2–Ar system.

N_2O_4–NO_2 (Ref. 23), the solid symbols are data for various "atom" fractions of diluent (Ref. 24). (The compositions are expressed in terms of the "atom" fraction of inert, considering the NO_2 group to be an "atom" since it survives this reaction. Then

$$a \equiv \frac{x_{\text{inert}}}{x_{\text{inert}} + x_{NO_2} + 2x_{N_2O_4}}$$

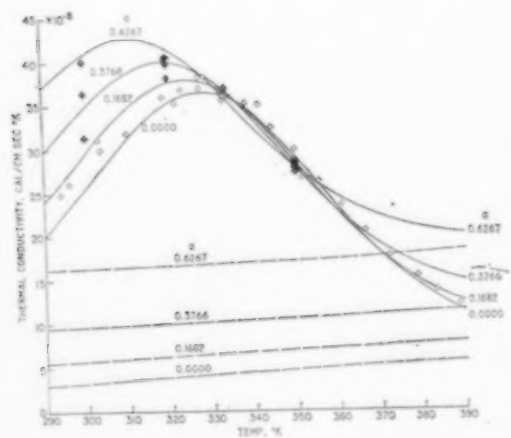

Fig. 3. Thermal conductivity of the N_2O_4–NO_2–He system.

For complete dissociation the atom and mole fractions of inert are identical.) Calculated equilibrium conductivities are shown as solid lines; frozen conductivities as dashed lines. (The frozen conductivities of the argon mixtures vary only slightly with argon atom fraction.)

The agreement between theory and experiment shown in Figs. 2 and 3 is generally satisfactory. The fact that the experimental data fall appreciably below the calculated values for high atom fractions of inert (most clearly seen in Fig. 2) is undoubtedly due to the reduction of the reaction rate at the lower reactant concentrations.

The application of equation (22) to a system of more than one reaction can be tested for the case of the thermal conductivity of hydrogen fluoride vapor. At moderate pressures the PVT behavior of hydrogen fluoride vapor can be described in terms of a monomer–hexamer equilibrium[25] although the date of Strohmeier and Briegleb[26] suggest a dimer at low pressures. The actual state of the vapor is not certain; there is spectroscopic evidence for a tetramer[27] and at higher pressure either higher polymers exist, or gas law deviations are appreciable.

Nonetheless, it appears that at low and moderate pressures the two equilibria

$$2HF \rightleftarrows (HF)_2; \qquad \Delta H_2 = 7{\cdot}4 \text{ kcal}$$
$$6HF \rightleftarrows (HF)_6; \qquad \Delta H_6 = 40{\cdot}5 \text{ kcal}$$

serve to specify the system rather well.

Computed and experimental[28] thermal conductivities of hydrogen fluoride vapor are compared in Fig. 4. The solid line was computed assuming both dimer and hexamer equilibria*, whereas the dashed line shows a previous calculation[22] which considered only the hexamer equilibrium. Note the extreme pressure dependence of the thermal conductivity. The maximum thermal conductivity is

* The compositions were calculated using the equilibrium constants $K_6 = 1{\cdot}27 \times 10^4$ atm^{-5}, $K_2 = 0{\cdot}542$ atm^{-1}; these values were estimated from PVT data in the literature[25, 26, 29] plus a low temperature spectroscopic value for K_6[27]. Diffusion coefficients were estimated from boiling point and liquid density; the values so obtained were increased 4 per cent to better fit the experimental data.

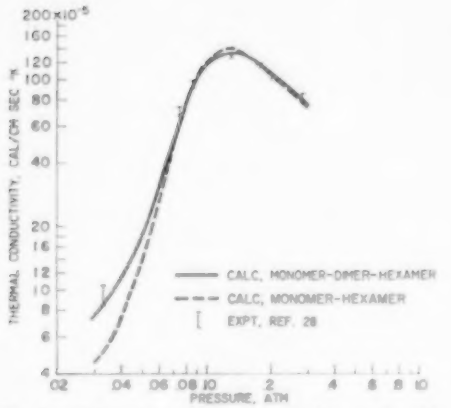

Fig. 4. Thermal conductivity of hydrogen fluoride vapor as a function of pressure at 267·7°K.

more than 3 times that of hydrogen at the same temperature and some 33 times the frozen conductivity expected in the absence of reaction. Inclusion of a dimer equilibrium markedly improves the agreement between theory and experiment in the low pressure region.

The experimental studies on nitrogen tetroxide and hydrogen fluoride serve to confirm the validity of the theoretical expressions for thermal conductivity of reacting gases in chemical equilibrium.

In the case of a simple dissociation of the type $A \rightleftarrows nB$ it is possible to relate equilibrium and frozen thermal conductivities to the corres- to the specific heat.)

$$\frac{\lambda_e}{\lambda_f} = 1 + \mathrm{Le}_{AB}\left(\frac{c_{p_e}}{c_{p_f}} - 1\right) \tag{24}$$

where c_{p_f} is the specific heat at constant pressure and composition and c_{p_e} is the specific heat with equilibrium attained. Le_{AB} is the Lewis number involving the frozen conductivity and specific heat and the binary diffusion coefficient between molecules A and B. (The modified Eucken expression for the conductivity in a polyatomic gas[21] can be obtained from this equation by substituting the monatomic gas specific heat and Lewis number). For a mixture of two gases the Lewis number varies with composition. For example, estimates for the dissociation of a diatomic molecule suggest that Le_{AB} varies from about 1·4 (gas composed entirely of molecules) to about 0·6 (gas composed entirely of atoms). For rough estimates, then, Le_{AB} is of the order of unity, so we may approximate

$$\frac{\lambda_e}{\lambda_f} \sim \frac{c_{p_e}}{c_{p_f}} \tag{25}$$

Mass transfer in gas mixtures containing more than two components cannot be characterized by a single diffusion coefficient so that there can be no simple relation between conductivity and specific heat such as equation (24). It seems likely, however, that the approximate expression of equation (25) is suitable for estimates of the order of magnitude of the thermal conductivity of multicomponent gas mixtures, such as rocket exhausts.

In analyses of convective heat transfer in atom–molecule mixtures (dissociating gases) the Lewis number is commonly introduced (e.g. Ref. 3). It appears reasonable to apply these analyses to multicomponent gas mixtures by regarding a rearrangement of equation (24)

$$\mathrm{Le} = \frac{\dfrac{\lambda_e}{\lambda_f} - 1}{\dfrac{c_{p_e}}{c_{p_f}} - 1} = \frac{\lambda_r}{\lambda_f}\frac{c_{p_f}}{c_{p_r}} \tag{26}$$

as a more general definition of Lewis number. (c_{p_r} is the contribution of the chemical reaction to the specific heat.)

It is instructive to consider the heat flux in a quiescent but reacting gas in terms of the enthalpy gradient

$$q = -\lambda_e \frac{dT}{dr} = -\frac{\lambda_e}{c_{p_e}}\frac{dH}{dr} \cong \frac{\lambda_f}{c_{p_f}}\frac{dH}{dr} \tag{27}$$

The portion of equation (27) which has been indicated as approximate for reacting gases at equilibrium is in fact correct for frozen mixtures. It seems likely that equation (27) is also a good approximation for intermediate reaction rates. This equation states that the driving force for heat transfer in reacting gases is the enthalpy gradient rather than the temperature gradient. Thus we can expect low heat transfer rates in a system of dissociated gases only if there is no recombination in the gas phase and the walls are noncatalytic.

Effects due to finite reaction rates

The discussion thus far has dealt with systems where the chemical reactions are presumed to be so rapid that chemical equilibrium prevails locally at all points in the gas mixture. Let us now consider the reduction in heat transport caused by reduced reaction rates. This problem was perhaps first considered by Dirac[30]; more recent treatments are to be found in Refs. (31)–(34). It should be noted that as these relaxation effects come into play heat transport cannot be described by a thermal conductivity which is solely a gas property. On the contrary, the "thermal conductivity" will depend on apparatus geometry.

Franck and Spalthoff[31] have considered the case of a dissociating dimer in the annulus of a hot wire thermal conductivity cell. They assume that equilibrium conditions obtain at the outer wall (radius r_a). Their expressions include terms to account for partial accommodation of the chemical reaction at the wire surface (radius r_i) as well as the more usual type of accommodation coefficient for translational and internal energy. Assuming that there is no accommodation of the reaction on the wire surface and that the departure from equilibrium is not great, Franck and Spalthoff's expression reduces to

$$\frac{\lambda^*}{\lambda_f} = \frac{1}{1 + \dfrac{\lambda_r}{\lambda_f \left(\dfrac{\lambda_e}{\lambda_f}\dfrac{l^2}{\tau_c D}\right)^{1/2}}} \tag{28}$$

where λ^* is the "thermal conductivity" in the particular cell geometry, D is the dimer-monomer diffusion coefficient, and τ_c is the relaxation time for the chemical reaction. l is a dimension characteristic of the apparatus; in this case it is

$$l = r_i \ln \frac{r_a}{r_i} \tag{29}$$

Meixner[32] derived an expression equivalent to equation (28) for the geometry of plane parallel plates. In this event $l = \Delta X/2$, where ΔX is the plate separation. If we expand equation (29) for the case where the inner and outer radii approach one another we find $l = r_a - r_i$. The apparent descrepancy between this result and the result obtained by Meixner is caused by the fact that Franck and Spalthoff assume accommodation of the reaction at one of the walls whereas Meixner did not.

It is instructive to consider the ingredients of the dimensionless group

$$\frac{\lambda_e}{\lambda_f}\frac{l^2}{\tau_c D} = \frac{\lambda_e}{\lambda_f}\frac{\tau_D}{\tau_c}$$

which describes the deviation of the effective "thermal conductivity" from the equilibrium value. In addition to the ratio of the equilibrium and frozen conductivities, there is the ratio of the quantity $l^2/D = \tau_D$ (a time characteristic of the diffusion process) to the relaxation time τ_c, characteristic of the chemical process.

Franck and Spalthoff applied their equations to their experimental data on the thermal conductivity of dissociating bromine and fluorine. The experimental results, which fell below calculated equilibrium conductivities, were explained in terms of the theory. Similarly, Prigogine and Waelbroeck[35] have demonstrated experimentally that rotational energy transfer in hydrogen and in oxygen decreases at low pressures; these decreases are consistent with theory and known rotational relaxation rates.

As was noted previously, the experimental data on the nitrogen tetroxide system fall appreciably below computed equilibrium values at low reactant concentrations. This effect has been calculated from the equations of Franck and Spalthoff and is compared with the low pressure experimental data of Coffin and O'Neal[23] in Figs. 5 and 6. The theoretical

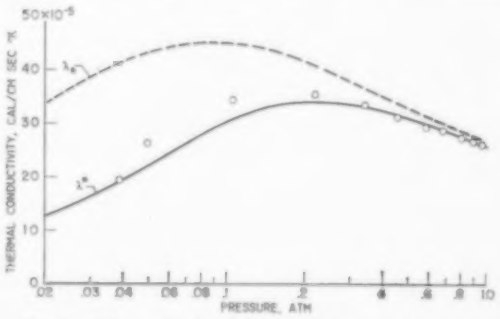

Fig. 5. Effect of chemical reaction rate on the thermal conductivity of the N_2O_4–$2NO_2$ system. $T = 296.0°K$.

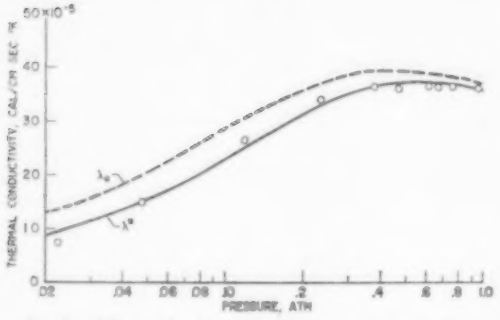

Fig. 6. Effect of chemical reaction rate on the thermal conductivity of the N_2O_4–$2NO_2$ system. $T = 318{\cdot}8°K$.

values have been adjusted to fit experiment at one atmosphere*.

The agreement between theory and experiment shown in Figs. 5 and 6 is indeed encouraging (although perhaps somewhat fortuitous, in view of uncertainties in gas phase and surface rates) and suggests that theory provides an adequate description of this phenomenon. In multicomponent mixtures involving several reactions it will no longer be possible to characterize the system by single relaxation and diffusion times. However, numerical extension of these analyses to more complex systems is undoubtedly possible as soon as the appropriate kinetics (both gas phase and surface) become known.

6. APPLICATIONS TO CONVECTIVE HEAT TRANSFER

Data on heat transfer from high temperatures and reacting gases for well defined geometries and gas flows are scarce. Some shock tube measurements on stagnation point heat transfer in dissociated air by Rose and Stark[38] are perhaps the most noteworthy data. These experimental results were shown to be consistent with the analysis of Fay and Riddell[3] for a Lewis number of 1·4. As noted in the previous section, a Lewis number of 1·4 appears reasonable for a slightly dissociated diatomic gas.

Low temperature data are available for turbulent heat transfer in a tube[39,40] for the nitrogen tetroxide system. These data have been correlated with the calculated equilibrium thermal conductivity and kinematic viscosity for this system[41] as shown in Fig. 7. In the case of

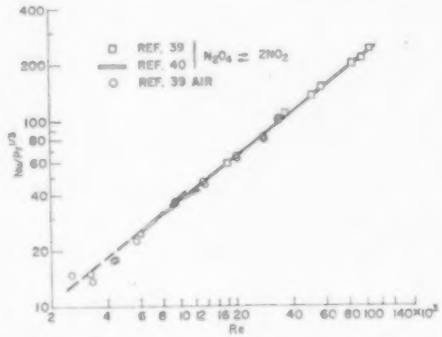

Fig. 7. Correlation of turbulent heat transfer in the nitrogen tetroxide system.

Schotte's work[40], there was a large variation in gas properties between tube entry and tube exit conditions; the terminal points of the bars in Fig. 7 represent calculation based on these extreme conditions. The transport properties used to formulate the Nusselt and Reynolds numbers were average values obtained by integration over the temperature difference between wall and stream. The Prandtl numbers were similarly averaged. Note that for this type of subsonic turbulent heat transfer mean values of the *kinematic* viscosities are required; poor correlation is obtained when absolute viscosities are averaged.

Approximate correlations which use frozen rather than equilibrium conductivities can be obtained by introducing equation (25), which is correct for a Lewis number of unity, into the definitions of Nusselt and Prandtl numbers. On this basis[22,41]

$$\mathrm{Nu}_e \cong \mathrm{Nu}_f \frac{c_{p_f}}{c_{p_e}} \cong \frac{\bar{c}_{p_f} \Delta T}{\Delta H}$$

$$\mathrm{Pr}_e \cong \mathrm{Pr}_f$$

Here $\bar{c}_{p_f}$ is a mean value of the frozen specific heat over the temperature difference ΔT and

* It was assumed that there was no accommodation of the chemical reaction on the surfaces. Corrections for the mean free path were omitted. Relaxation times were obtained from the rate data of Carrington and Davidson for the N_2O_4–NO_2–N_2 system[36]; these rate constants were increased threefold to account for the higher rates expected in the absence of nitrogen (see discussion by Davidson[37]).

ΔH is the corresponding enthalpy difference. A correlation of Beal and Lyerly[39] data based on frozen properties was also tested in Ref. (41). As expected, correlation was somewhat poorer than when equilibrium properties were used. (The standard deviation of nitrogen tetroxide data points increased from 3 to 5 per cent.)

When the group $Nu/Pr^{1/3}$ is correlated with Reynolds number, as in equations (2) and (3) and Fig. 7, the frozen property correlations can be improved by introducing a correction term involving the Lewis number and correlating

$$\frac{Nu_f}{Pr_f^{1/3}} \frac{\bar{c}_{p_f}\Delta T}{\Delta H}\left[1+(Le-1)\left(1-\frac{\bar{c}_{p_f}\Delta T}{\Delta H}\right)\right]^{-2/3}$$

as a function of Reynolds number. The correction term is reminiscent of similar corrections used in treatments of stagnation point heat transfer[3, 42]; indeed Rosner[43] has recently compared a correction term based on the relationship between equilibrium and frozen properties with the corrections Fay and Riddell[3] obtained empirically from their solutions of the stagnation point boundary layer equations. For a Lewis number of 1·4 these correction factors agreed within 3 per cent. We may conclude, then, that transport properties calculated for gas mixtures in chemical equilibrium may reasonably apply to computed convective heat transfer in equilibrium flows, using heat transfer correlations developed for nonreacting gases.

To this author's knowledge there is as yet no experimental data on convective heat transfer which demonstrates the effect of reduced reaction rate on heat flux. However, Fay and Riddell[3] have solved the boundary layer equations for a specific case of stagnation point heat transfer with a range of reaction rates for both catalytic and noncatalytic walls. Their results are shown as solid lines in Fig. 8, where the heat transfer parameter $Nu'/\sqrt{Re}$ is plotted for various values of a recombination rate parameter. This recombination parameter is a ratio of a diffusion time to a reaction time, evaluated at stream temperature. It should be noted that these Nusselt numbers are formulated from the computed heat transfer and the frozen thermal conductivity at the wall. For this reason they are indicated by primes.

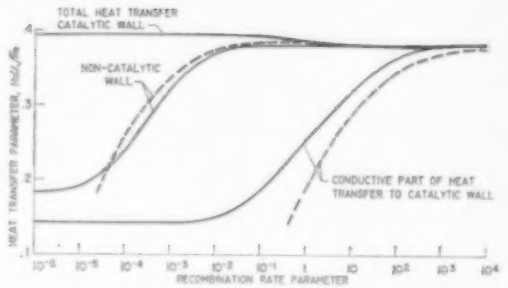

Fig. 8. Heat transfer for a boundary layer with finite recombination rates (Ref. 3).

It is tempting to try to apply equation (28), which was derived for heat transfer in quiescent gases, to the situation depicted in Fig. 8. To do this, we simply transform equation (28) as follows:

$$Nu'^{*} = \frac{Nu'_c}{1+\dfrac{Nu'_r}{Nu'_f\left(\dfrac{Nu'_r}{Nu'_f}\dfrac{\tau_D}{\tau_C}\right)^{1/2}}} \tag{30}$$

Values of the heat transfer parameter calculated from equation (30) are shown as dashed curves in Fig. 8. For the conductive part of the heat transfer to a catalytic wall, the atom concentrations are high only in the high temperature region. The approximate curve in this case was computed by identifying the recombination parameter with the ratio of diffusion and chemical times in equation (30).

Atom recombinations differ from most other chemical rate processes in that their rates are higher at lower temperatures. When the wall is noncatalytic, the atoms tend to diffuse into and recombine in the cooler region near the wall. The approximate curve in this case has been calculated by correcting the chemical time, τ_C, from stream to wall temperature. (The approximate curves have been terminated at the point the heat transfer parameter becomes equal to the frozen value.)

Note that the approximate curves for the temperature extremes bracket Fay and Riddell's exact calculations. The shapes of the approximate curves are similar to the exact curves at the higher values of the heat transfer parameter.

With the catalytic wall, the recombination must obviously occur at a temperature somewhat lower than the equilibrium stream temperature, and the direction of the difference between approximate and rigorous curves confirms this fact. On the other hand, with a noncatalytic wall recombination can occur in the gas phase right at the surface. For this reason the approximate and rigorous curves are in closer agreement for this case; again, however, the direction of the difference suggests reaction is occurring on the average somewhat away from the boundary of the system (in this case, the cold wall).

In a system where reaction rate increases with temperature, for example according to the Arrhenius expression, we would not expect any appreciable difference between the heat transfer to a noncatalytic wall and the conductive part of the heat transfer to a catalytic wall; in either case reaction would occur in the high temperature region. In this event the approximate curve should lie slightly above and to the left of an exact calculation.

Hence equation (30) provides us with a valuable tool for rapidly estimating the effects of finite reaction rate on convective heat transfer. The diffusion time may be estimated from a boundary layer thickness, δ, and a diffusion coefficient:

$$\tau_D = \frac{\delta^2}{\bar{D}}$$

This is consistent with Franck and Spalthoff's formulation for a system with equilibrium at one boundary. In a multicomponent mixture involving a single reaction the "diffusion coefficient" should probably be derived from the general definition of Lewis number (equation 26). This leads to

$$D = \frac{\lambda_r}{\rho c_{p_r}}$$

That is, for the "diffusion coefficient" one substitutes the thermal diffusivity associated with the chemical reaction.

Equation (30) should even be applicable to systems with more than one reaction provided the reactions are sufficiently different in rates so that they can be considered independently. There is as yet no simple analysis for a system of interlinking reactions—here is an area for future efforts.

7. SUMMARY AND CONCLUSIONS

This paper has examined the methods presently available of estimating convective and conductive heat transport in high temperature gases. The emphasis has been placed on methods of estimating the transport properties.

An examination of engineering heat transfer correlations has shown that large errors in thermal conductivity and viscosity lead to considerably smaller errors in heat transfer coefficient, provided high temperature properties are estimated by techniques derived from rigorous kinetic theory.

Uncertainties in high temperature conductivity and viscosity arise largely as a result of uncertainties in collision cross-section. Methods of estimating collision cross-sections have been considered, with particular emphasis on free radicals and other species not normally encountered at ordinary temperatures. Estimates show encouraging agreement with the scant experimental data for unstable species.

After a discussion of the properties of gas mixtures, heat conduction in reacting gases was considered. The theoretical expressions for the thermal conductivity of gas mixtures at chemical equilibrium have been presented. In such mixtures the diffusional transport of chemical enthalpy may lead to thermal conductivities an order of magnitude greater than in similar, but nonreacting gases. The theoretical predictions compare favorably with experimental data on the nitrogen tetroxide and the hydrogen fluoride systems.

The assumption of chemical equilibrium locally in a gas implies infinite reaction rates. Theory suggests that when rates are slower, the effective thermal conductivity is related to the ratio of a diffusion time (characteristic of the apparatus) and the relaxation time (characteristic of the chemical system). Low pressure data for the nitrogen tetroxide system are in accord with this analysis.

Finally, it has been shown that experimental convective heat transfer in practical systems can be treated by these methods. Equilibrium transport properties correlate experimental heat

transfer coefficients for the nitrogen tetroxide system. Simplified expressions obtained by assuming a Lewis number of unity were also tested and discussed. Exact calculations on the effect of reaction rate on stagnation point heat transfer may be approximated by a simple expression obtained by considering the effect of reaction rate on conductivity.

In conclusion, methods available for high temperature heat transfer calculations are well-developed in many aspects. In many cases rigorous calculations of transport properties are justified. Effects due to chemical reaction and relaxation seem to be understood, and applications for simple systems appear straightforward.

Large gaps in our understanding include the transport properties (particularly conductivity) of polar gases and gas mixtures containing polar gases. Expressions to treat relaxation effects in gases with multiple reactions would also be desirable. Of course, chemical kinetics of the appropriate reactions are largely lacking. Finally, additional data and calculations on high temperature collision cross-sections would be welcome.

REFERENCES

1. E. R. G. Eckert, *Introduction to the Transfer of Heat and Mass* (*a*) p. 136, (*b*) p. 92. McGraw-Hill, New York (1950).
2. A. P. Colburn, *Trans. Amer. Inst. Chem. Engrs.* **29**, 174 (1933).
3. J. A. Fay and F. R. Riddell, *J. Aero. Sci.* **25**, 73 (1958).
4. C. F. Curtiss, J. O. Hirschfelder and R. B. Bird, *Proceedings of the Second Biennial Gas Dynamics Symposium, Transport Properties in Gases* p. 3. North-Western University Press, Evanston, Illinois (1958).
5. J. O. Hirschfelder and M. A. Eliason, *Ann. N.Y. Acad. Sci.* **67**, 451 (1957).
6. J. P. Molnar, *Phys. Rev.* **83**, 940 (1951).
7. I. Amdur, *J. Chem. Phys.* **4**, 339 (1936).
8. P. Harteck, *Z. phys. Chem.* **139**, 98 (1928).
9. J. O. Hirschfelder, C. F. Curtiss and R. B. Bird, *Molecular Theory of Gases and Liquids*, (*a*) Equation 8.2–25, (*b*) Equation 8.2–34. Wiley, New York (1954).
10. C. Muckenfuss and C. F. Curtiss, *J. Chem. Phys.* **29**, 1273 (1958).
11. J. O. Hirschfelder, *Proceedings of the Joint Conference on Thermodynamic and Transport Properties of Fluids* p. 133. Institution of Mechanical Engineers, London (1958).
12. W. Sutherland, *Phil. Mag.* **40**, 421 (1895).
13. R. S. Brokaw, *J. Chem. Phys.* **29**, 391 (1958).
14. C. R. Wilke, *J. Chem. Phys.* **18**, 517 (1950).
15. S. Chapman and T. G. Cowling, *The Mathematical Theory of Non-Uniform Gases* p. 238. Cambridge University Press (1952).
16. E. R. G. Eckert, W. E. Ibele and T. F. Irvine, Jr., *Thermodynamic and Transport Properties of Gases, Liquids and Solids* p. 295. American Society of Mechanical Engineers, New York, and McGraw-Hill, New York (1959).
17. W. Nernst, *Festschrift Ludwig Boltzmann* p. 904, J. A. Barth, Leipzig (1904).
18. I. Langmuir, *J. Amer. Chem. Soc.* **34**, 860 (1912).
19. A. Eucken, *Phys. Z.* **14**, 324 (1913).
20. A. R. Ubbelohde, *J. Chem. Phys.* **3**, 219 (1935).
21. J. O. Hirschfelder, *J. Chem. Phys.* **26**, 282 (1957).
22. J. N. Butler and R. S. Brokaw, *J. Chem. Phys.* **26**, 1636 (1957); R. S. Brokaw, *J. Chem. Phys.* **32**, 1005 (1960).
23. K. P. Coffin and C. O'Neal, *Nat. Advis. Comm. Aero. Tech. Note* 4209 (Feb. 1958).
24. K. P. Coffin, *J. Chem. Phys.* **31**, 1290 (1959).
25. R. W. Long, J. L. Hildebrand and W. E. Morrell, *J. Amer. Chem. Soc.* **65**, 182 (1943).
26. W. Strohmeier and G. Briegleb, *Z. Elektrochem.* **57**, 662 (1953).
27. D. F. Smith, *J. Chem. Phys.* **28**, 1040 (1958).
28. E. U. Franck and W. Spalthoff, *Naturwiss.* **40**, 580 (1953).
29. K. Fredenhagen, *Z. anorg. Chem.* **218**, 161 (1934).
30. P. A. M. Dirac, *Proc. Cam. Phil. Soc.* **22**, 132 (1924).
31. E. U. Franck and W. Spalthoff, *Z. Elektrochem.* **58**, 374 (1954).
32. J. Meixner, *Z. Naturf.* **7a**, 553 (1952).
33. I. Prigogine and R. Buess, *Bull. Acad. Roy. Belg. cl. sci.* **38**, 711 (1952).
34. J. O. Hirschfelder, *J. Chem. Phys.* **26**, 274 (1957).
35. I. Prigogine and F. Waelbroeck, *Proceedings of the Joint Conference on Thermodynamic and Transport Properties of Fluids* p. 128. The Institution of Mechanical Engineers, London (1958).
36. T. Carrington and N. Davidson, *J. Phys. Chem.* **57**, 418 (1953).
37. N. Davidson, *J. Phys. Chem.* **57**, 427 (1953).
38. P. H. Rose and W. I. Stark, *J. Aero. Sci.* **25**, 86 (1958).
39. J. L. Beal and R. L. Lylerly, *WADC Tech. Rep.* 56-494 (Sept. 1956). (ASTIA No. AD 118074.)
40. W. Schotte, *Industr. Engng Chem.* **50**, 683 (1958).
41. R. S. Brokaw, *Nat. Advis. Comm. Aero. Res. Memo.* E57K19a (March 1958).
42. L. Lees, *Jet Propulsion* **26**, 259 (1956).
43. D. E. Rosner, *Amer. Rocket Soc.* **30**, 114 (1960).

MOLECULAR INTERACTIONS AT HIGH TEMPERATURES

C. E. TREANOR and G. T. SKINNER

Cornell Aeronautical Laboratory, Buffalo, New York

Abstract—An experimental and theoretical program concerning the interactions between gas particles having energies in the 1 to 10 eV range is discussed. A molecular beam has been constructed for the experimental work, using a shock tube as the source of high-energy atoms and molecules. In particular, the interest centers around those interactions characteristic of high-temperature air where considerable dissociation has occurred. The atom–molecule interactions, about which least is known, have been given first consideration because of their importance in estimating transport properties. A two-center potential has been used for preliminary investigation of the diatomic molecule as seen by an approaching atom.

1. INTRODUCTION

The most widely used method for study of the potential energy of interaction of atoms and molecules has been the measurement of virial coefficients and transport properties[1]. The potentials so obtained can be used to correlate the various experiments, but cannot be extrapolated reliably to determine the transport properties at higher temperatures, since, with the closer approach of the high-energy particles, a knowledge of the potential at smaller values of internuclear separation is required[2]. In addition, new molecules and atoms are often formed at the higher temperatures and the interaction energies for these new species are generally unknown.

A second method for the study of interactions is the use of a molecular beam to investigate the scattering of particles of known relative kinetic energy. Beams with kinetic energy of 500 eV/particle and greater have been used for this purpose, and the small-angle scattering yields information about the potential energies in the region of 1 eV[2, 3]. The data obtained from scattering of helium and argon from nitrogen molecules has been employed to infer N_2–N_2 potentials[4]. No direct experiments with nitrogen are as yet available, and atom–molecule interactions for the constituents of high-temperature air have not been measured.

In the present paper a method of producing a molecular beam in the energy range of 1–10 eV is described. This apparatus is being constructed at Cornell Aeronautical Laboratory with the support of the Air Force Office of Scientific Research. It is designed to produce neutral beams of both the molecular and atomic species of high-temperature air and to supply a measure of the differential scattering cross section for any such interaction. The description of atom–molecule interactions in terms of a two-center model for the molecule is also discussed.

2. MOLECULAR BEAM APPARATUS

The apparatus is essentially a molecular beam which uses as its source the gas heated behind a reflected shock in a shock tube. To form the molecular beam, the gas is expanded aerodynamically through an aperture at the end of the tube. A sharp-nosed body, containing an orifice in the nose, is placed in this flow. The

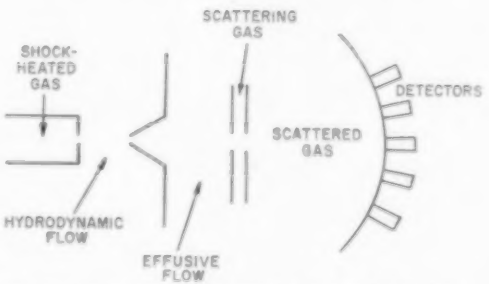

Fig. 1. Schematic of shock-tube molecular beam.

orifice serves as a collimating slit, so that effusive flow is obtained behind the slit. The schematic arrangement is shown in Fig. 1. This method of expansion was first introduced by Kantrowitz and Grey[5] as a means of obtaining a strong molecular beam from a conventional source. There are several additional advantages when a shock tube is used as the source of high-temperature gas. The aerodynamic expansion from the end of the shock tube cools and accelerates the gas. This procedure is commonly used to obtain high-speed flow for model testing, and the device is known as a shock tunnel[6].

In the present application, the expansion acts as an energy collimation, producing a nearly mono-energetic beam from the Maxwellian distribution in the shock tube. The calculated effect of the expansion on the energy distribution in the gas is shown in Fig. 2 for an initial

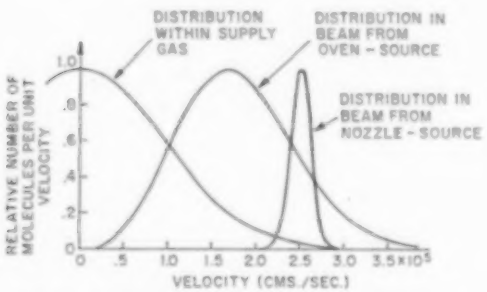

Fig. 2. Velocity Distribution 3,500° K oxygen supply.

temperature of 3500°K in the shock tube. A further advantage of this procedure lies in the fact that the beam can be formed of atomic species, so that the interaction of atoms and molecules can be studied. For example, if O_2 is used as a test gas, it is dissociated to its equilibrium composition of atoms and molecules in the shock tube, the mole fraction of atoms depending on the temperature and density behind the reflected shock. The expansion which cools the gas is much too rapid to permit recombination of the atoms, as has been demonstrated in nozzle-kinetics calculations[7]. Thus the degree of dissociation in the beam will be essentially that of the supply.

The beam is collimated at a point downstream where the mean-free path has increased to about 1 mm. The sides of the collimating orifice are conically shaped so that an attached shock occurs at the orifice. This is illustrated in Fig. 1. The container for the scattering gas serves as a second collimator, and the scattered beam is to be measured with detectors arranged on a 10-cm radius from the scatterer. The three sections of the apparatus are separately vacuum pumped. The first section is made with a 5-ft diameter to ensure that the large flow from the shock tube will not increase the pressure in this section during the experiment. A picture of the apparatus is shown in Fig. 3.

The total running time available for the experiment is of the order of 1 msec, the limitation being inherent in the shock tube source. This restriction places severe requirements on the detectors, which must be capable of both rapid response and high sensitivity. To this end an ionizing detector has been constructed and tested statically. This detector utilizes a cross flow of electrons, constricted by a magnetic field, to partially ionize the scattered beam. The ionized beam is then accelerated and collected and the collector current used as a measure of the strength of the original beam. An ionization efficiency of 1 in 10^3 would be sufficient for the measurement of that part of the beam scattered into a solid angle of 10^{-3} steradian. The electron current density for such an efficiency is not excessive, particularly if the electron steam is oriented such that the gas particles traverse about a centimeter of it. Static tests with the first detector built for this program indicate that approximately 1/10th of the calculated sensitivity is obtained. However, it is known that there is a serious ion loss in the system due to improper focussing. Ion bombardment patterns on the slit plate indicate that the ion beam suffered deflections from the static fields present. Shielding has now been introduced to correct this situation. Also from static tests, the rise time of the detector–electrometer arrangement falls in the neighbourhood of 20 μsec. Thus it appears that this instrument will be capable of detecting small fractions of the scattered beam. The design is

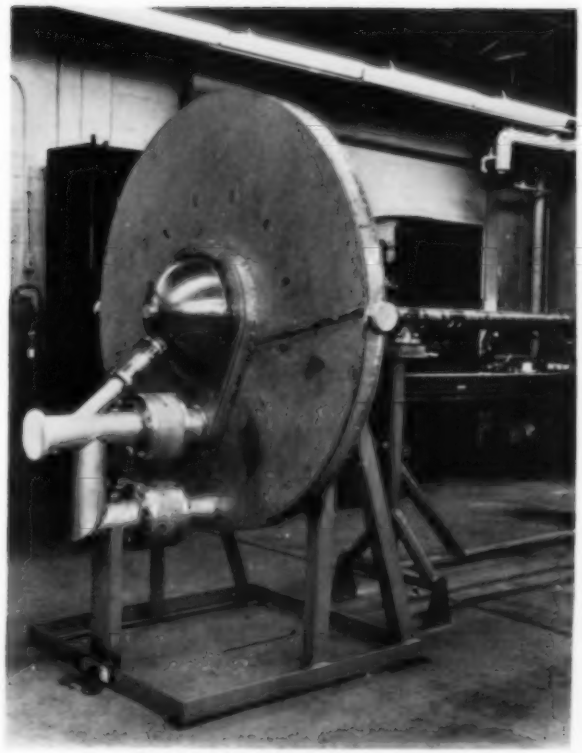

Fig. 3. Molecular beam apparatus.

(facing page 284)

such that an angular resolution of 1° is provided. Although not yet included in the detector, the design includes provision for a mass spectrometer magnet to separate particles, so that, for example, the scattering distribution for atoms on molecules can be studied.

3. METHOD OF CORRELATION OF RESULTS

The interaction of two molecules, or a molecule and an atom, is usually treated in terms of the interaction of two point centers, the two-center nature of the molecule being disregarded. Experimental data are then used to determine the constants involved in a phenomenological central potential. With experiments where the differential cross section is measured, the model must be capable of describing not only the total number of particles scattered, as a function of the energy of the incident particle, but also the angular distribution of these scattered particles. This additional requirement suggests the use of a two-center potential to provide a more complete description of the field of the molecule.

For the energy range and momentum range of the atoms and molecules of high-temperature air, the collisions can be considered from a completely classical viewpoint, once an interaction potential has been assumed. A spheroidal coordinate system (ξ, η, ϕ) provides a convenient method of describing a two-center force system, where

$$\xi \equiv \frac{r_1 + r_2}{2c}$$

r_1 and r_2 being the radial distances from the two foci and $2c$ the fixed separation of the force centers. The angle ϕ is measured relative to a plane containing the axis of the molecule. The Hamilton–Jacobi equations are separable in this coordinate system for any potential of the form

$$V = \frac{g(\xi)}{\xi^2 - \eta^2} \tag{1}$$

This form of the potential has been used to analyse experimental results for the scattering of low-energy electrons from molecules (where a quantum-mechanical calculation is required), using an attractive potential[6]. For atom–molecule interactions with relative kinetic energy of 1 eV or more, a purely repulsive potential is probably sufficient. If $g(\xi)$ is chosen of the form

$$g(\xi) = \frac{K}{(\xi^2 - 1)^n} \tag{2}$$

the potential behaves at large distances as a central potential of the form $\frac{1}{r^{2n+2}}$. For $n=1$ (Maxwellian at large distances) and for $n=2$, the solutions for the scattering can be obtained in terms of elliptic integrals. For higher values of n it is necessary to employ numerical integration, as is the case with a central potential. To illustrate the effect of the two-center nature of the potential, the scattering angle has been plotted in Fig. 4 as a function of impact parameter for $n=1$, for end-on collisions (where the potential is nearly central) and for the case where the direction of the molecular axis has been averaged over all orientations. The impact parameter is measured in units of c, one-half the separation of the force centers. The two-center repulsive potential described by equations (1) and (2) should be sufficiently flexible to provide a correlation with the experimental results for differential cross sections.

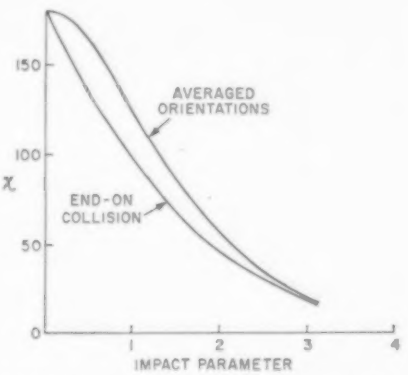

Fig. 4. Scattering from two-center potential.

REFERENCES

1. J. O. HIRSCHFELDER, C. F. CURTISS and R. B. BIRD, *Molecular Theory of Gases and Liquids*. Wiley, New York (1954).
2. I. AMDUR and J. ROSS, *Combustion and Flame* **2**, 412 (1958).

3. I. AMDUR and E. A. MASON, *Phys. of Fluids* **1**, 370 (1958).
4. I. AMDUR, E. A. MASON and J. E. JORDAN, *Scattering of High Velocity Neutral Particles; J. Chem. Phys.* **27**, 527 (1957).
5. A. KANTROWITZ and J. GREY, *Rev. Sci. Industrum.* **22** (1951).
6. C. E. WITTLIFF, M. R. WILSON and A. HERTZBERG, *The Tailored-Interface Hypersonic Shock Tunnel, Cornell Aero. Lab. Rep.* AD-1052-A-8 (AFOSR TN 59-31, AD 209203), Jan. 1959; also *J. Aero. Space Sci.* **26** (1959).
7. J. G. HALL, *Dissociation Nonequilibrium in Hypersonic Nozzle Flow*, presented at the 40th National Meeting, American Institute of Chemical Engineers, Kansas City, May 1959.
8. *Encyclopedia of Physics*, Vol. 37, part 1, p. 328. Springer, Berlin (1959).

THERMODYNAMIC EFFECTS OF COULOMBIC INTERACTIONS IN IONIZED GASES

H. MYERS and J. H. BUSS*
Douglas Aircraft Company, Santa Monica, California
and
S. W. BENSON†
University of Southern California, Los Angeles, California

Abstract—The deviations from ideality arising from the electrostatic interactions between charged particles in a plasma have been studied by an adaption of the Debye–Hückel theory. The results of the study for represenative systems are presented in the paper. The significant finding is that the composition of equilibrium mixtures shows large deviations from that calculated from ideal gas theory. At sufficiently high ion densities these deviations are large enough to alter the thermodynamic functions of the plasma.

1. INTRODUCTION

A plasma is distinguished from other gaseous systems by the presence of ions and electrons in the gas. The presence of these charged species gives rise to electrostatic interactions between the particles causing deviations from ideal gas behavior. The precise nature of these deviations from ideality for various representative gaseous systems is the subject of this paper. A theoretical development of the electrostatics, thermodynamics and composition of ionized gases is presented in the first three sections and provides a basis for the results contained in the section entitled "The Effect of the Coulombic Interations for Representative Systems".

2. ELECTROSTATICS OF IONIZED GASES

Basically the presence of charged particles in the vicinity of a given ion has the effect of altering the electric potential of the ion. The change in potential is determined by considering that each ion α is surrounded by an ionic atmosphere composed of all the other ions in the systems. The distribution of charges in the ionic atmosphere is assumed to be spherically symmetrical, obeying Poisson's equation relating charge density to potential. Furthermore the potential energy of the ions in the atmosphere is assumed to follow Boltzmann's law. The solution of the combined Poisson–Boltzmann equation for the electrostatic potential at the ion α leads to the result:

$$\psi(\alpha) = \frac{Z_\alpha e}{Dr} - \frac{Z_\alpha e}{D}\kappa \tag{1}$$

where

$$\kappa = \frac{4\pi e^2}{DkT}\Sigma N_i Z_i^2 \tag{2}$$

The overall electrostatic potential ψ consists of two terms, the potential at the ion due to its own charge and the potential at α due to the ionic atmosphere. The latter term is a direct consequence of the electrostatic interactions of the ions. The deviation of an ionized gas from the thermodynamics of an ideal gas is then related to the electrical work performed in changing each ion reversibly and isothermally to the additional potential $\psi(\alpha) = -Z_e\kappa/D$

$$W = \int_0^{\psi_\alpha} \Sigma_\alpha \psi_\alpha Z_\alpha e d\psi_\alpha = \int_0^{\psi_i} \Sigma_i \psi_i Z_i e d\psi_i = -\tfrac{1}{2}\frac{\Sigma_i N_i Z_i^2 e^2 \kappa}{D} \tag{3}$$

The total work expended in changing the ions represents the increase in the free energy of the system due to the electrostatic interaction of the particles.

* Present address, Space Technology Laboratories, Los Angeles, California.

† Consultant to the Douglas Aircraft Company Inc.

The method outlined above of relating the thermodynamic properties of an ionized system to the effect of Coulombic interactions on electrostatic potentials originated with Debye and Hückel[1]. The Debye–Hückel theory provides a successful explanation of the observed deviations of electrolytic solutions from ideality. In applying the Debye–Hückel theory to plasmas, there are several features of the theory which cause it to be more suitable to gaseous systems than to solutions. The charged species are assumed to be supported in a structureless, uniform dielectric medium, an over-simplification for electrolytic solutions, but quite valid for a plasma where the particles are considered to be in a vacuum. Therefore, precise results for plasmas do not depend on detailed considerations of solute–solvent interactions, and the dielectric constant can be taken as unity. A second aspect of the Debye treatment concerns the solution of the Poisson–Boltzmann equation. In obtaining the result of equation (3) Debye assumed that $Z_i e\psi(r) \ll kT$, expands the exponential $e^{-Z_i e\psi/kT}$ as a power series and neglects all terms higher than the second. For electrolytic solutions at room temperatures the above condition is satisfied when the solution is sufficiently dilute ($<10^{-5}$

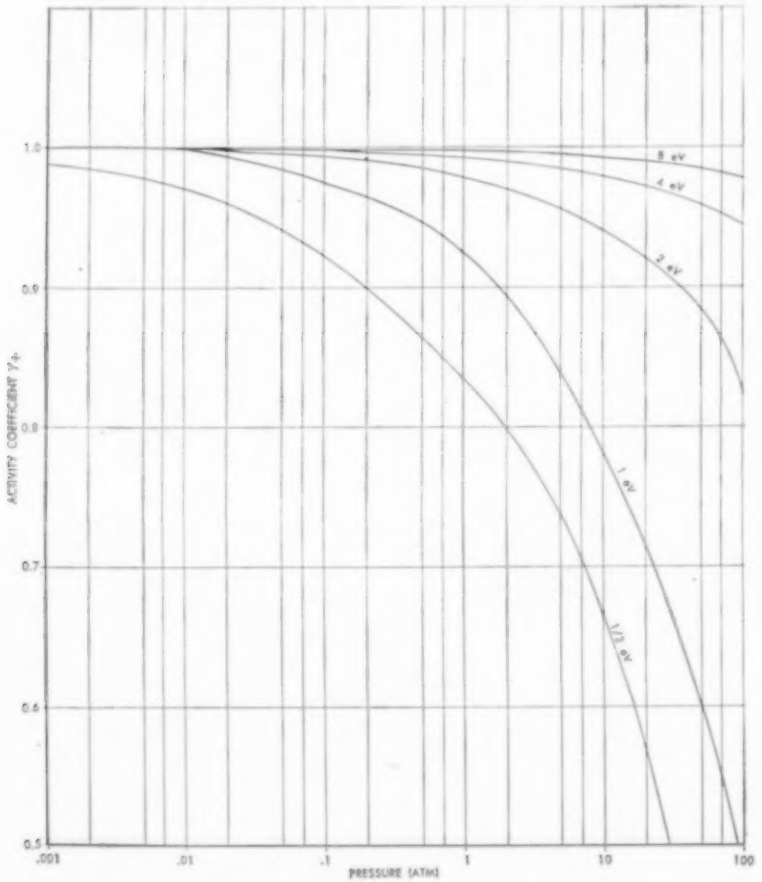

Fig. 1. Activity coefficient for sodium.

molar, which corresponds to 6×10^{20} particles/cm^3). For plasmas at temperatures where ionization is appreciable the condition that the thermal energy be very much greater than the interionic potential energy is more readily met. Therefore, we may expect the Debye–Hückel analysis to afford an excellent description of plasmas without resort to the extension of the theory by Gronwall[1] or the more elaborate cluster theory treatment of Mayer[2, 3].

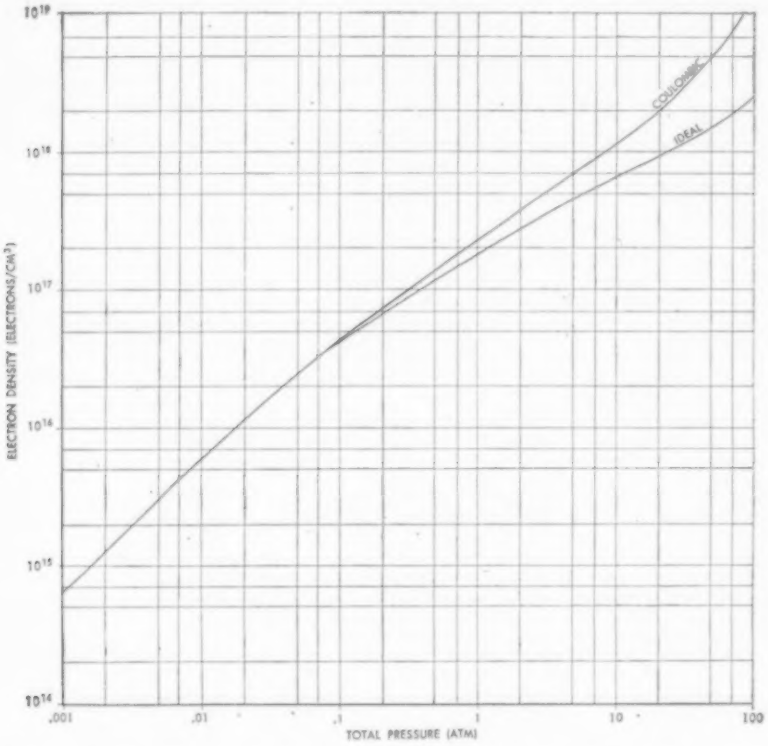

Fig. 2. Effect of electrostatic interactions on electron density, sodium at $\frac{1}{2}$ eV (5807°K).

3. THERMODYNAMICS OF IONIZED GASES

The deviation of the thermodynamic properties of a plasma from ideality is determined in terms of the work expended in the process of charging the particles to the potential induced by their mutual interactions. Because the electrical work is a function of the total number of ions, and thus a function of the ionic concentration, the charging process is best considered as occurring at constant volume. With the volume of the system held constant, the electrical work is equal to the total work and is equal to the Helmholtz free energy change. Expressing the Helmholtz free energy of the system in terms of the chemical potentials of the species present:

$$\mu_i = \left(\frac{\partial A}{\partial N_i}\right)_{T,V,N_j} = \mu_i^0 + kT \ln c_i \gamma_i \qquad (4)$$

The electrostatic contribution to the chemical potential of the i^{th} species μ_i^{El} is related to the activity coefficient,

$$\mu_i^{\text{El}} = \left(\frac{\partial A^{\text{El}}}{\partial N_i}\right)_{T,V,N_j} = kT \ln \gamma_i \qquad (5)$$

By this formulation the deviation of the ionic system from ideality is expressed completely by

the terms $kT \ln \gamma_i$. The standard state for species is the hypothetical state in which the interactions are negligibly small and γ equals unity. In terms of the activity coefficient, the deviation imposed by the electrostatic interactions is given by

$$\ln \gamma_i = -\frac{Z_i^2 e^2}{2DkT} \kappa \tag{6}$$

For dilute plasmas the dielectric constant may be taken as unity. Expressing the concentrations in moles/liter and introducing the ionic strength

$$s = 1/2 \Sigma_i c_i Z_i^2 \tag{7}$$

can now be derived in a straightforward manner. The excess partial molar Helmholtz free energy is given by:

$$\bar{A}_i^{EI} = RT \ln \gamma_i \tag{9}$$

For a system at constant volume, the excess partial molar Gibbs free energy is

$$\bar{F}^{EI} = \bar{A}_i^{EI} + P_i^{EI} V$$

Applying equations (8) and (9) and the relation:

$$P_i^{EI} = -\left(\frac{\partial \bar{A}_i^{EI}}{\partial V}\right)_T = -RT\left(\frac{\partial \ln \gamma_i}{\partial V}\right)_T = \tfrac{1}{2}\frac{\ln \gamma_i}{V} \tag{10}$$

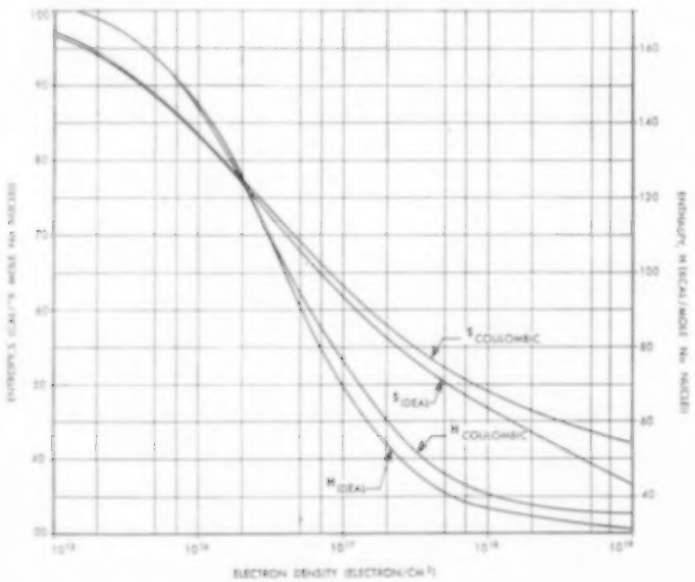

Fig. 3. Effect of electrostatic interactions on thermodynamic functions, sodium at ½ eV (5807°K).

Equation (6) can be written as

$$\ln \gamma_i = -\frac{Z_i^2 e^3}{(kT)^{3/2}} \left(\frac{\pi N}{500}\right)^{1/2} s^{1/2} = -\frac{AZ_i^2}{T^{3/2}} s^{1/2} \tag{8}$$

where the constant A is a universal constant for species equal to $4{\cdot}203 \times 10^6$ in the appropriate units.

Excess thermodynamic functions which express the effect of the electrostatic interactions we obtain

$$\bar{F}_i^{EI} = 3/2\, RT \ln \gamma_i \tag{11}$$

Similarly the excess partial molar entropy is determined by:

$$\bar{S}_i^{EI} = -\left(\frac{\partial \bar{A}_i^{EI}}{\partial T}\right)_V = -RT \ln \gamma_i - RT \frac{\partial \ln \gamma_i}{\partial T}_V$$

$$= 1/2\, R \ln \gamma_i \tag{12}$$

The excess partial molar enthalpy is then given by:

$$\bar{H}_i^{(2)} = \bar{F}_i^{(2)} + T\bar{S}^{(2)} = 2RT \ln \gamma_i \qquad (13)$$

4. COMPOSITION OF IONIZED GASES

In the temperature range in which ionization is appreciable, above 10,000°K for most gases, the important species present in the plasma are atoms, ions and electrons. The composition of the plasma may be calculated from the appropriate equilibrium constants determined from statistical mechanics. A serious conceptual difficulty arises, however, in the application of statistical mechanics to ionized gases[4]. This difficulty centers about a workable distinction between bound electronic states near the ionization threshold and a "free" ion–electron pair. There are an infinite number of bound states below the ionization limit and even worse the degeneracy $g_i \longrightarrow \infty$ as $\varepsilon_i \longrightarrow \varepsilon_{ion}$. We resolved this difficulty in calculating electronic partition functions by halting the summation at values of n corresponding to binding energies E_n of the order of kT. Bound states with values of n in excess of such a cut-off are then treated as weakly interacting ions and electrons by means of the Debye–Hückel formulation. The justification for this temperature dependent cut-off has been made in some detail by Bjerrum[5] and Fuoss[6] for electrolytic solutions and the arguments apply equally well to gases.

Consider a plasma consisting of the single component, A, which may possess n stages of ionization:

$$A = A^+ + e$$
$$A = A^{+2} + 2e$$
$$\cdots\cdots\cdots$$
$$A = A^{+n} + ne$$

For this system we define n equilibrium constants,

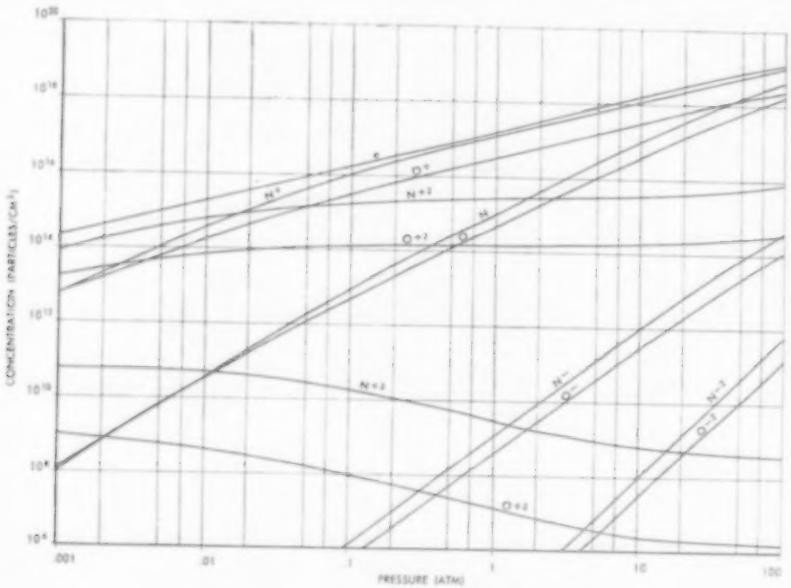

Fig. 4. Ionic distribution in air at 2 eV (23,228°K).

$$K_1 = \frac{(A^+)(e)}{(A)}, \quad K_2 = \frac{(A^{+2})(e)^2}{(A)}, \quad \ldots, \quad K_n = \frac{(A^{+n})(e)^n}{(A)} \qquad (14)$$

Additional relations between the constituents are provided by the conditions of electroneutrality and conservation of mass. With the values of the equilibrium constants specified by the choice of temperature and units of concentration, the choice of any one of the quantities A, A^+, A^{+2}, ..., A^{+n} or e is sufficient to uniquely

define the others. The selection of the concentration of electrons as the independent variable is particularly convenient because the concentration of the various species can be expressed directly in terms of (e) and the K's:

$$(\mathrm{A}) = \frac{1}{\frac{K_1}{(e)^2} + \frac{2K_2}{(e)^3} + \ldots + \frac{nK_n}{(e)^{n+1}}}$$

$$(\mathrm{A}^+) = \frac{K_1}{\frac{K_1}{(e)} + \frac{2K_2}{(e)^2} + \ldots + \frac{nK_n}{(e)^n}}$$

$$\ldots\ldots\ldots\ldots\ldots\ldots$$

$$(\mathrm{A}^{+m}) = \frac{K_m}{\sum_j jK_j (e)^{m-(n+1)}}, \quad m = 1, 2, \ldots, n \tag{15}$$

The equilibrium constants themselves are determined from the Gibbs free energies of the relevant processes. For the first stage of ionization, $\mathrm{A} = \mathrm{A}^+ + e$,

$$RT \ln K_1 = \Delta F_1^0 = -(\bar{F}_{\mathrm{A}^+} + \bar{F}_e - \bar{F}_{\mathrm{A}}) \tag{16}$$

where

$$\bar{F}_{\mathrm{A}^+} = \bar{F}_{\mathrm{A}^+}^0 + \bar{F}^{\mathrm{EX}} = -RT \ln (Q_{\mathrm{A}^+}/N) + 3/2\, RT \ln \gamma_+$$

$$\bar{F}_e = \bar{F}_e^0 + \bar{F}^{\mathrm{EX}} = -RT \ln (Q_e/N) + 3/2\, RT \ln \gamma_-$$

$$F_{\mathrm{A}} = F_{\mathrm{A}}^0 = -RT \ln (Q_{\mathrm{A}}/N) - E_0^0 \tag{17}$$

and Q_{A^+}, Q_e and Q_{A} are the molecular partition functions and E_0^0 is the ionization potential at absolute zero. Solving for K_1 we have

$$K_1 = \frac{\left(\frac{Q_{\mathrm{A}^+}}{\gamma_+^{3/2}}\right)\left(\frac{Q_e}{\gamma_-^{3/2}}\right)}{Q_{\mathrm{A}}} e^{-E_0/RT} \tag{18}$$

Since the γ's are themselves dependent on composition, there is no way to use equation (15) together with equation (18) to solve explicitly for the equilibrium compositions. The method we have chosen is one of iteration, in which we first calculate the ideal equilibrium compositions, neglecting Coulombic interactions, use the compositions in equation (8) to compute the γ's and then divide each of the K's by the appropriate product of the γ's to obtain

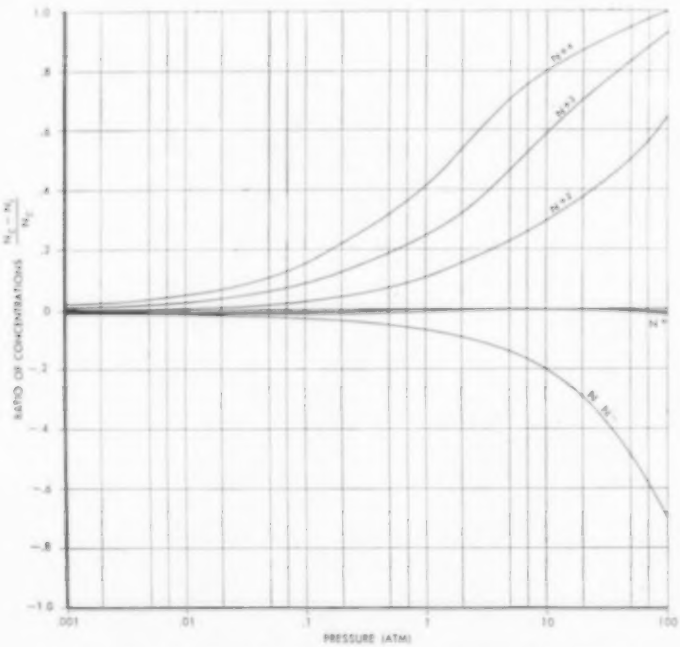

Fig. 5. Deviation from ideality, nitrogen in air at 2 eV (23,228°K).

"corrected" K's. The corrected K's are then used to obtain new equilibrium compositions. The procedure is repeated until convergence is attained.

The reduction in the free energy of the system due to electrostatic interactions therefore leads to a decrease in the effective ionization potentials and a corresponding increase in the degree of ionization. Moreover the concentration of the higher valence states is enhanced at the expense of the lower states.

components and therefore to their ionization potentials. We shall present the results of calculations for two contrasting cases and compare the effect of the Coulombic interactions on their properties.

The first class to be considered is the alkali metals. The thermodynamic properties of these plasmas are of practical interest in the design of ion propulsion devices. As a specific example of this class we consider the properties of sodium plasmas. Sodium does not have the

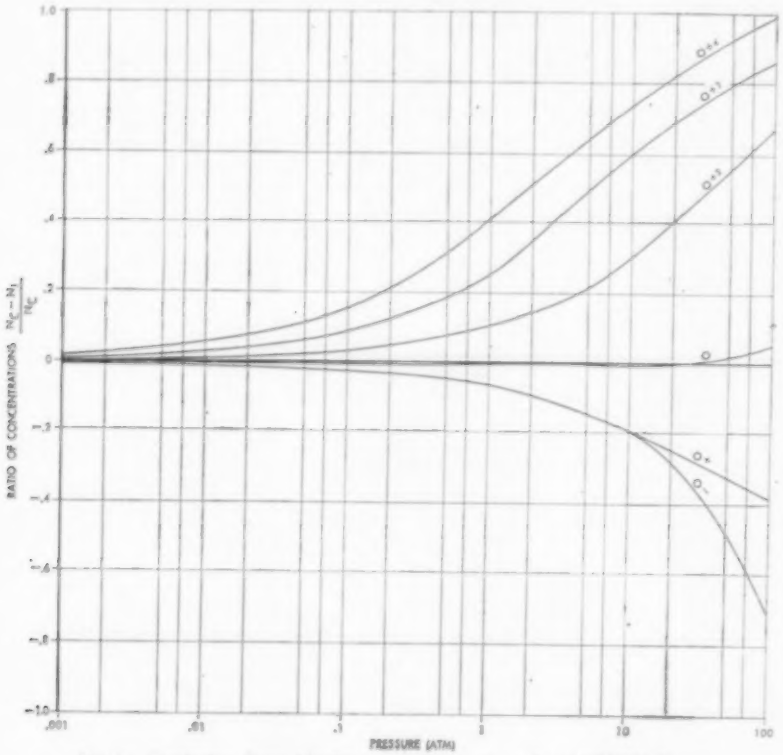

Fig. 6. Deviation from ideality, oxygen in air at 2 eV (23,228°K).

5. THE EFFECT OF THE COULOMBIC INTERACTIONS ON REPRESENTATIVE SYSTEMS

The precise influence of the electrostatic imperfections on the thermodynamic properties of plasmas is best appreciated by considering various representative systems in detail. The ionic properties of a particular plasma are closely related to the degree of ionization of its lowest ionization potentials of the alkali metals and therefore does not exhibit the largest deviation from ideality; on the other hand, its electronic levels are well established and its properties are representative of the group as a whole.

The deviation of sodium plasmas from ideality is best represented by the activity coefficient.

The behavior of the activity coefficient of sodium as a function of pressure at various temperatures is presented in Fig. 1. (Temperature is expressed in terms of equivalent thermal energy; a value of 1 eV corresponds to a temperature of 11,600°K.) At a given temperature the greatest deviations occur at the highest pressures, reflecting the influence of ion density on the activity coefficient. At first glance it would also appear that at a given pressure γ_+ is inversely proportional to temperature. This impression is misleading; in fact the relation between activity coefficient and temperature has a minimum value. The overall relation between temperature, pressure, and the minimum γ is complex, but at the higher pressures the minimum occurs at the temperature corresponding to $\frac{1}{6}$ the ionization potential.

to sodium atoms in the plasma. Consequently the density of sodium particles necessary to attain a given ion concentration is much less than that calculated when electrostatic effects are neglected. The extent of this effect is shown in Fig. 2 where the increased electron density resulting from the Coulombic interactions is evident. Generally this effect is sufficiently large that it must be taken into consideration in the calculation of the thermodynamic state of ionized gases from experimental values of electron densities. Indeed the phenomenon of "over-ionization" observed in shock tube experiments[7] can be explained in part in terms of the Coulombic effect of enhancing ionization.

The influence of electrostatic interactions on the thermodynamic properties of a sodium plasma is presented in Fig. 3. In the figure the

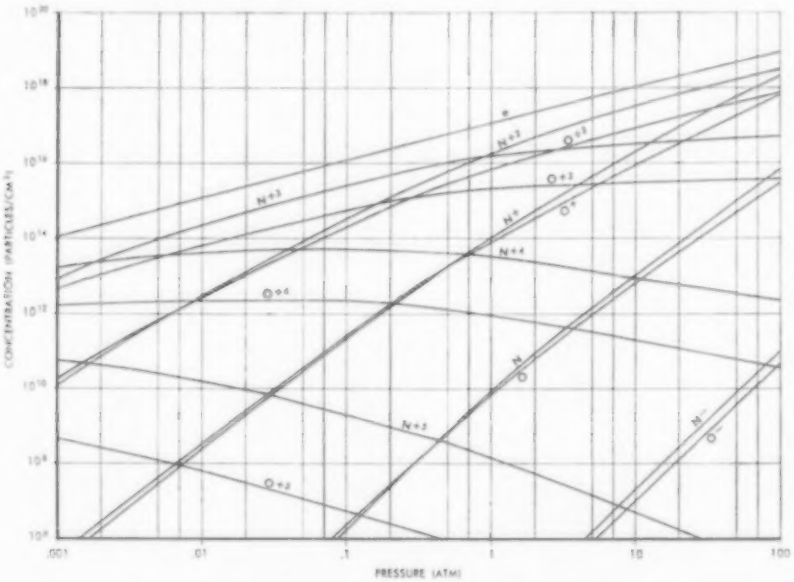

Fig. 7. Ionic distribution in air at 4 eV (46,456°K).

The greatest deviations from ideality in sodium plasmas occur at relatively low temperatures, where there is insufficient energy for ionization beyond Na^+. Under these conditions the Coulombic effect of enhancing ionization leads to an increase in the ratio of sodium ions

entropy and enthalpy of the ideal and Coulombic gas are compared on the common basis of electron density. The direct effect of the electrostatic interactions is to lower the entropy of the ionic constituents by $1/2\,R \ln \gamma_+$. For sodium at $\frac{1}{2}$ eV this may represent a

reduction of 5 per cent. However, the decrease in entropy due to the specific contribution of the Coulombic interactions is offset by the increase in entropy due to the lower pressure of the Coulombic gas (see Fig. 2.) Similar considerations pertain in the comparison of the enthalpies.

concentration of the upper valence states at the expense of the lower states.

The nature of the Coulombic effect for air and carbon dioxide at 2 and 4 eV are presented in Figs. 4–15. The first figure of each set presents the concentrations of the principal species in the gas when the electrostatic inter-

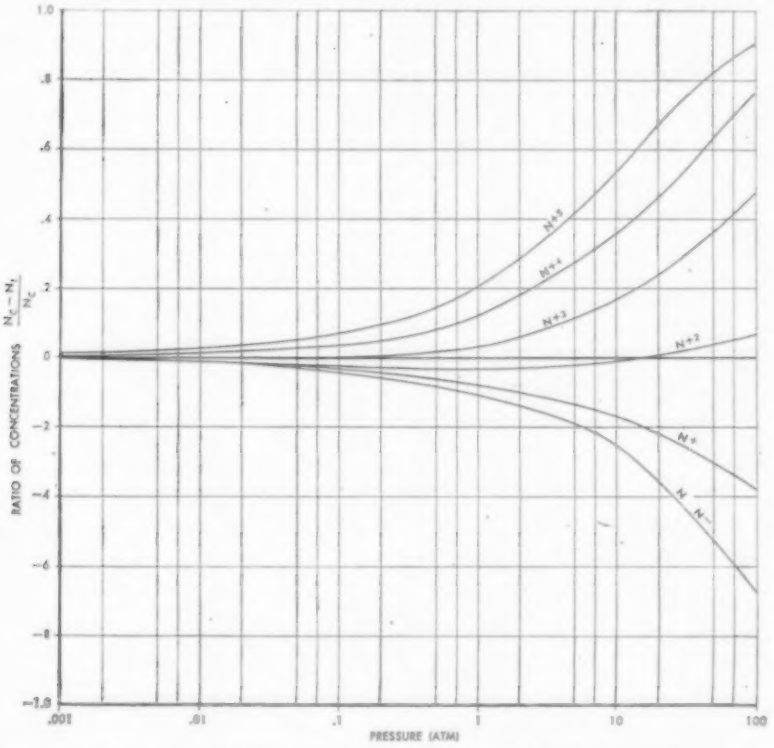

Fig. 8. Deviation from ideality, nitrogen in air at 4 eV (46,456°K).

The second class of plasmas to be considered are representative of planetary atmospheres: air for earth and carbon dioxide for Venus. In contrast to the alkali metal gases, the constituents of these gases have rather high first ionization potentials, 12–15 eV, and ionize appreciably only above 20,000°K. On the other hand, at these temperatures the upper valence states of the constituents are readily attainable. The effect of the electrostatic interactions in effectively reducing the ionization potentials therefore result in increasing the

actions between the particles are taken into account. The remaining two figures of the set then illustrate the deviation in the concentration of each constituent from the concentration calculated when the interactions are neglected. The deviations are expressed in terms of the concentration differences divided by the concentration in the Coulombic gas. It is seen that the largest deviations occur with the highest changed species and at the highest pressures. Furthermore the deviation from ideality is somewhat greater at 2 eV than 4 eV. These

trends reflect the inter-relation between temperature, concentration and valence expressed in equation (8). A reduction in the non-ideality of the gas at 4 eV due to temperature and ionic concentration is in part offset by the increased contribution to non-ideality of the high valence states.

The important finding of our analysis is that, while the thermodynamic functions of an ionized gas may or may not be effected by Coulombic interactions depending on the ionic density, the composition of equilibrium mixtures shows significant deviations from ideality. These deviations must be taken into account in any analysis which requires an accurate knowledge of concentrations such as the chemical kinetics of ionized gases. From the principle of detailed balancing, the Coulombic enhancement of ionization implies that rates of ionization are faster relative to rates of re-attachment in an interacting plasma. The detailed effect of the Coulombic interactions on reaction kinetics appears to be rather complex and comprises the next phase of our study of ionized gases.

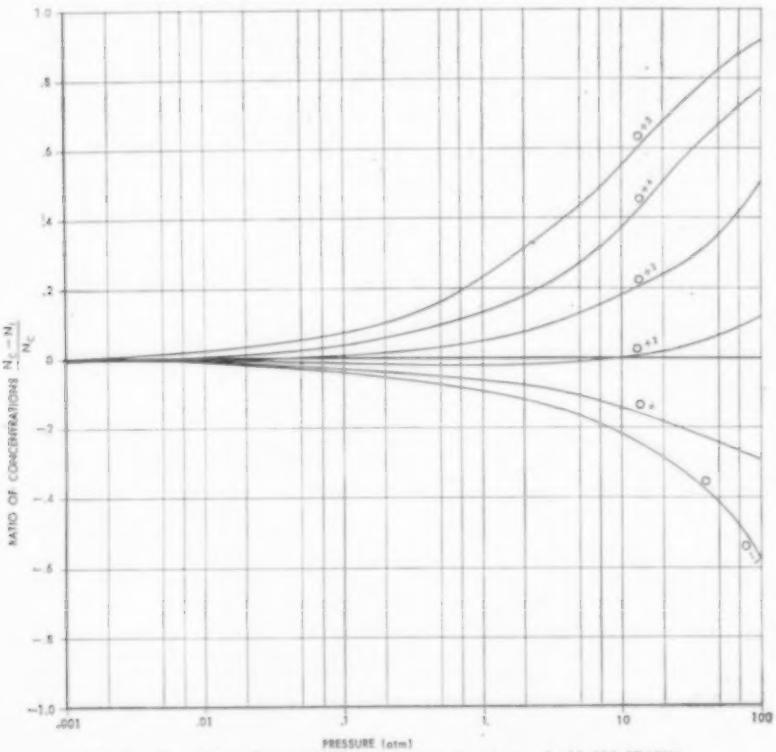

Fig. 9. Deviation from ideality, oxygen in air at 4 eV (46,456°K).

The effect of the Coulombic interactions on the thermodynamic functions of the atmospheric gases turns out to be rather small. At the temperatures and pressures considered, the first activity coefficients γ_+ of oxygen, nitrogen and carbon are usually larger than 0·85. Hence the direct effect on the electrostatic interactions, given by equations (11), (12) and (13), is small and the deviations from the ideal thermodynamic function that do occur result from the redistribution of the ionic concentrations.

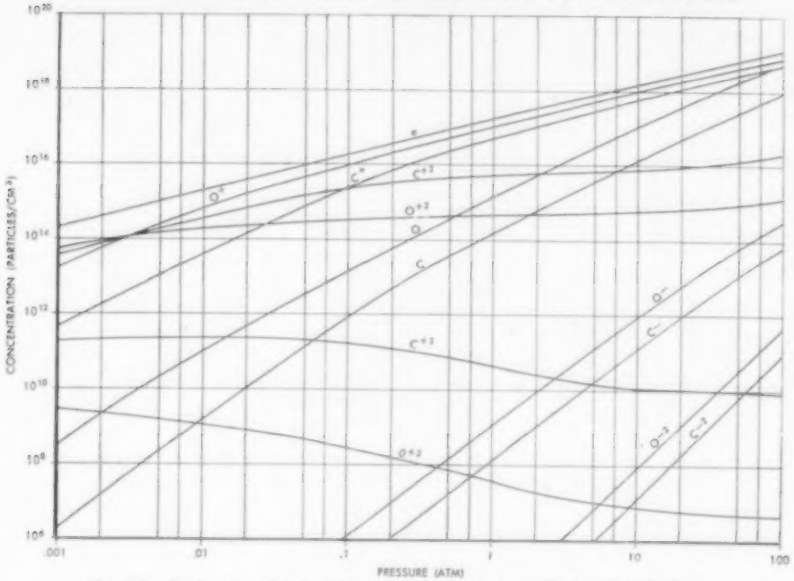

Fig. 10. Ionic distribution in carbon dioxide at 2e V (23,228°K).

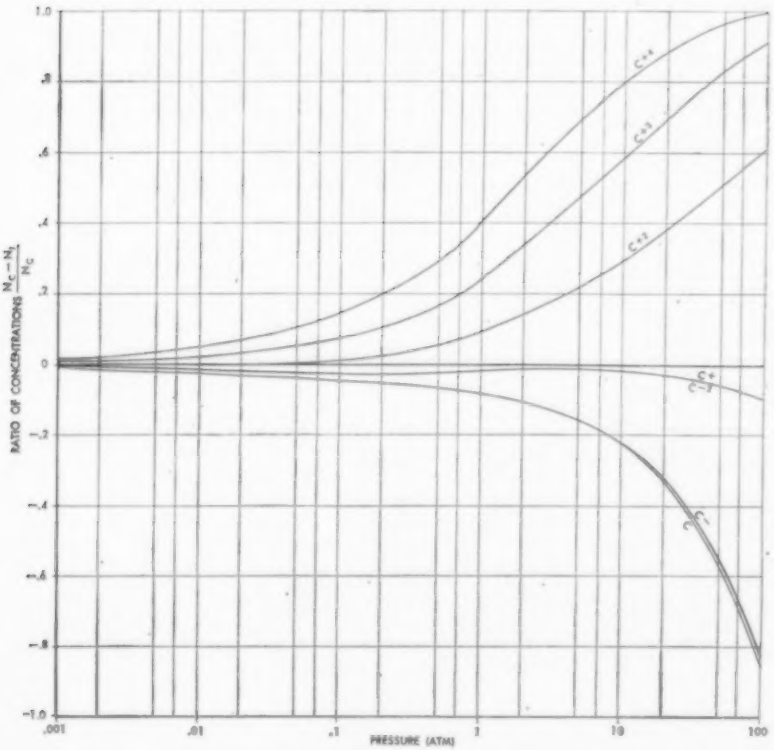

Fig. 11. Deviation from ideality, carbon in carbon dioxide at 2 eV (23,228°K).

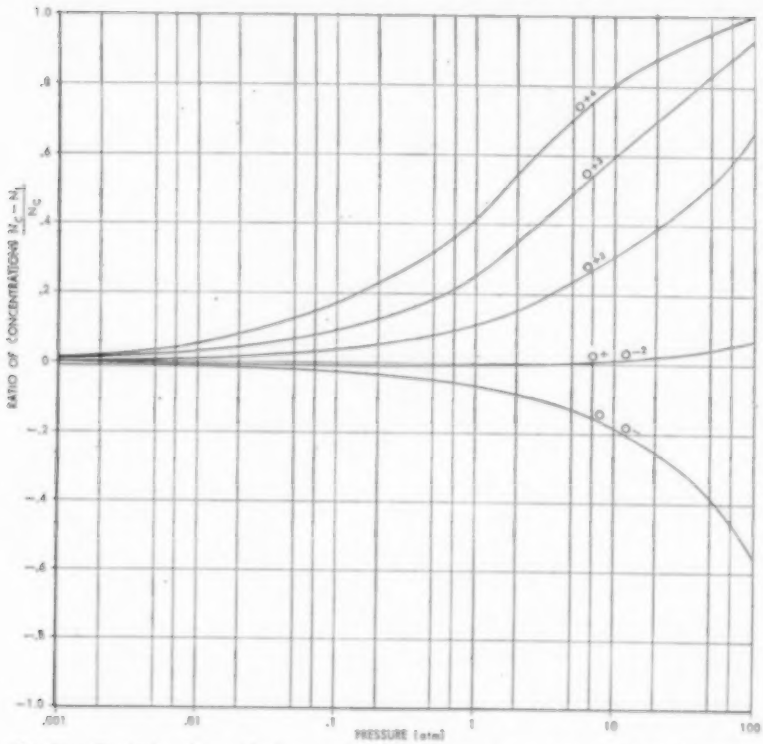

Fig. 12. Deviation from ideality, oxygen in carbon dioxide at 2 eV (23,228°K).

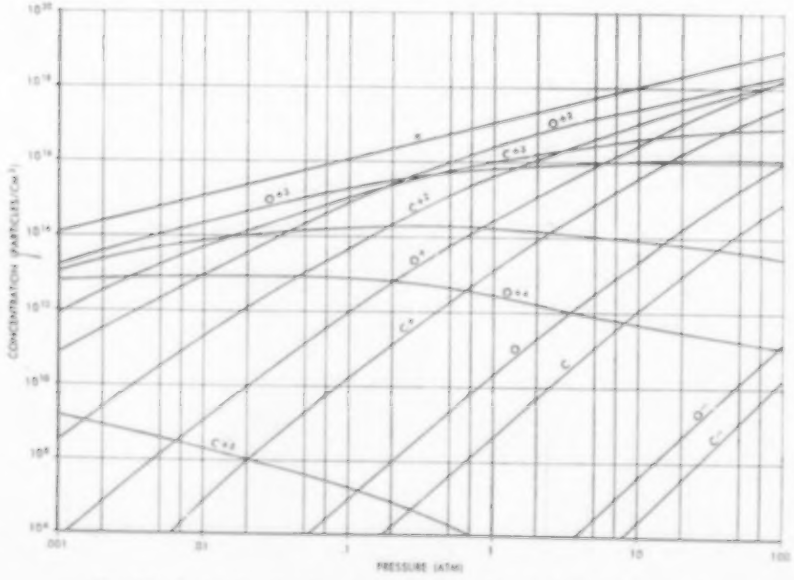

Fig. 13. Ionic distribution in carbon dioxide at 4 eV (46,456°K).

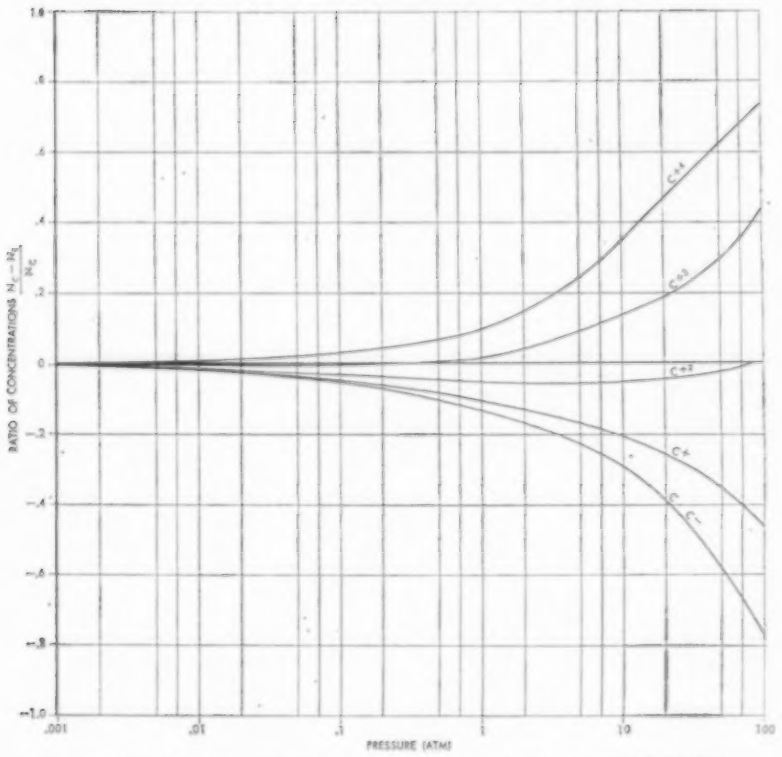

Fig. 14. Deviation from ideality, carbon in carbon dioxide at 4 eV (46,456°K).

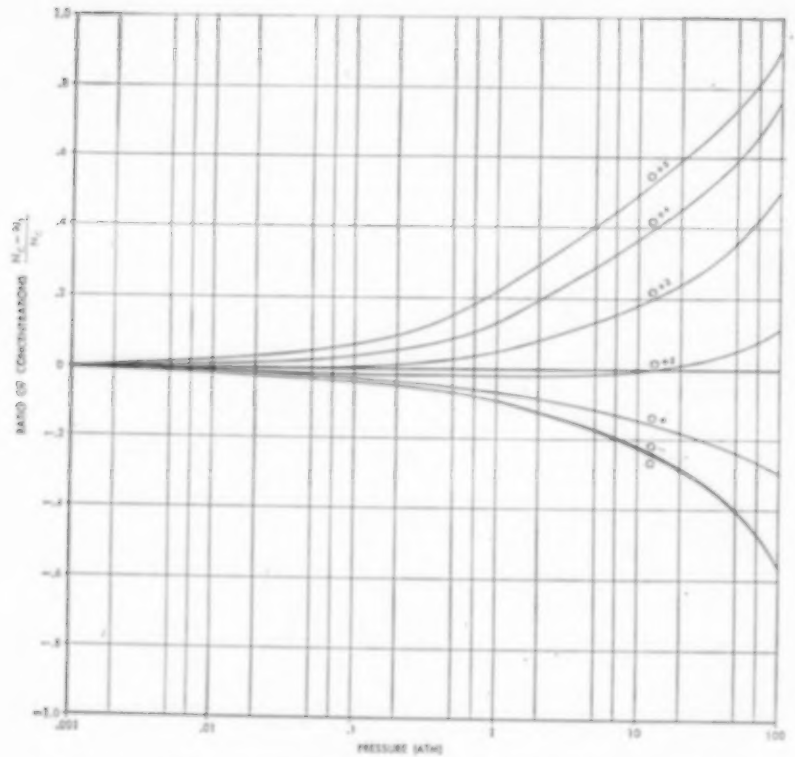

Fig. 15. Deviation from ideality, oxygen in carbon dioxide at 4 eV (46,456°K).

REFERENCES

1. For a detailed discussion of the Debye–Hückel Theory see H. S. HARNED and B. B. OWEN, *The Physical Chemistry of Electrolytic Solutions* (3rd Ed.) Reinhold, New York (1957).
2. W. B. MCMILLAN and J. E. MAYER, *J. Chem. Phys.* **13**, 276 (1954); J. E. MAYER, *J. Chem. Phys.* **18**, 1426 (1950); J. C. POIRIER, *J. Chem. Phys.* **21**, 965 (1953).
3. H. W. WOOLLEY, *Thermodynamic Functions for Atomic Ions*, Air Force Special Weapons Center Report AFSWC-TR-34 (1957); *J. Res. Nat. Bur. Stand.* **61**, 469 (1958).
4. S. W. BENSON, J. H. BUSS and H. MYERS, *Bull. Amer. Phys. Soc. ser.* 2, **4**, 375 (1959).
5. N. BJERRUM, *K. danske vidensk. Selsk., math. fys. Medd.* **7**, No. 9 (1926).
6. R. M. FUOSS, *Chem. Rev.* **17**, 27 (1935); *J. Amer. Chem. Soc.* **80**, 5059 (1958).
7. H. PETSCHEK and S. BYRON, *Ann. Phys.*, **1**, 270 (1957).

THE THERMODYNAMIC AND ELECTRICAL PROPERTIES OF MERCURY VAPOR AT PRESSURES BELOW ATMOSPHERIC AND HIGH TEMPERATURES

A. SHERMAN and F. MARTINEK
General Electric Company, FPLD, Cincinnati, Ohio

Abstract—The thermodynamic properties and electrical conductivity of mercury vapor have been calculated for temperatures between 1000°K and 15,000°K and pressures between atmospheric and 10^{-4} atm. The thermodynamic properties were determined by the methods of statistical mechanics. Account has been taken of the lowering of the ionization potential due to local electric fields and the number of terms employed in the electronic partition function has been limited in accordance with the theory of Ecker and Weizel. The electrical conductivity was computed on the basis of "free path" kinetic theory. It is shown that in the presence of a magnetic field the conductivity has directional properties. For a field of 10,000 G the change in conductivity is illustrated for a particular case.

1. INTRODUCTION

Recently, interest has been aroused in the behavior of high temperature gases as a result of studies in hypersonics and space propulsion. Since mercury vapor has been considered in various applications, it is the purpose of this paper to study some of its high temperature properties.

The degree of ionization, compressibility, mass, internal energy, enthalpy, entropy, specific heats and the ratio of specific heats have been obtained by the methods of statistical thermodynamics under the assumption of thermal equilibrium. The method of Ecker and Weizel[1] has been used to take account of the lowering of the ionization potential due to local electric fields as well as to limit the term series of the electronic partition function. The energy levels, their degeneracy as well as the ionization potential of the free atom are taken from *U.S. Dep. Comm., Nat. Bur. Stand. Circ.*, No. 467. No corrections were made to account for the Debye–Hückel ionic effect or for the presence of diatomic species.

The calculation of electrical conductivity is based on the "free path" kinetic theory. The electron neutral collision cross section is obtained from experimental data and the electron ion collision cross section is found from theoretical considerations. In addition, the presence of a magnetic field is shown to alter the conductivity (the Hall effect). A simple derivation, again based on "free path" kinetic theory, shows it to be a tensor. Upon the assumption that Hall currents are free to flow an example is presented for a field strength of 10,000 G which illustrates the reduction in conductivity that occurs in the presence of a magnetic field.

The computations were carried out on an IBM 704 digital computor at temperature and pressure intervals ensuring adequate reliability of data, especially in the region of chemical reactions. A temperature range from 1000°K to 15,000°K is covered for pressures between atmospheric and 10^{-4} atm.

2. PARTITION FUNCTIONS

The thermodynamic properties of a substance can be readily obtained from the partition function providing that the substance is in a state of thermal equilibrium. Under the conditions of thermal equilibrium the thermodynamic probability of a system will become a maximum and can be expressed as

$$P_{max} = \exp\left(\frac{E-F}{kT}\right) \tag{1}$$

where

E = internal energy of system
F = free energy of system
k = Boltzmann constant
T = temperature

The classical partition function Q, giving the sum of states or ensemble configurations, can be expressed in the non-quantized approach as a Gibbs phase integral for a mixture

$$Q = \frac{1}{\prod_{S_i}(N_{S_i}!)} \int\int \exp - \left(\frac{\varepsilon}{kT}\right) \prod_{S}^{N} (h^{-3} d^3 p_S d^3 r_S) \tag{2}$$

Where we have written for any quantity x

$$\prod_{i=1}^{n} x_i = x_1 x_2 x_3 \ldots x_n$$

and where

S_i = ith species
N = number of particles
ε = energy of a single particle
h = Planck's constant
p = momenta
r = length

The classical range of Lagrangian generalized momenta extend from $-\infty$ to $+\infty$ and the space coordinates from 0 to ∞.

The ordinary quantum mechanical partition function is of the form

$$Q = \sum_i g_i \exp - \left(\frac{\varepsilon_i}{kT}\right) \tag{3}$$

Where the summation of possible energies of the particle replaces the integration of a continuous energy function and where ε_i is the energy of the ith state of the particle and g_i is the degree of degeneracy of the ith state.

The partition function completely determines all thermodynamic properties of the substance. The accuracy of this basic function is, therefore, of decisive importance in the calculation of the properties of gases such as those which are partially ionized. The main difficulty lies in the correct and complete determination of the energy ε or ε_i in equations (2) or (3). The possible energies to be included are translational, rotational, vibrational, electronic and potential. Providing that these energies are independent of each other, the total partition function can be expressed as a product summation of individual partition functions associated with each mode of energy, i.e.

$$Q_{\text{tot}} = Q_{\text{tr}} \times Q_{\text{v+r}} \times Q_{\text{el}} \times Q_{\text{pot}}$$

(1) The *translational energy* partition function is given as

$$Q_{\text{tr}} = \frac{V}{h^3}(2\pi mkT)^{3/2} \tag{4a}$$

or substituting for V from the equation of state $pV = kT$

$$Q_{\text{tr}} = \left(\frac{2\pi mkT}{h^2}\right)^{3/2} \frac{kT}{p} \tag{4b}$$

where

m = particle mass
V = volume

The translational energy is always independent of the other possible energy forms.

(2) The *vibrational and rotational energies* present in polyatomic molecules are normally coupled. These energies are, however, absent in monatomic species, such as mercury, and do not warrant further consideration.

(3) The *electronic partition function* gives the contribution of energies associated with the excited electronic states of the atoms and charged particles. These contributions become more important with increasing temperature. In all cases such energies are quantized and the electronic partition function will be in the form of equation (3).

$$Q_{\text{el}} = \sum_i g_i \exp - \left(\frac{\varepsilon_i}{kT}\right)$$

The main difficult is the determination of the limit of the above series of terms without seriously impairing the accuracy of the electronic partition function. That is, the series diverges as the series limit is approached. Attempts have been made by several authors[1–5] to resolve these divergence difficulties. Of these, the most recent and complete treatise is the one by Ecker and Weizel[1] which gives the limit to the series of terms as

$$N_v^2 \leqq \sqrt{\left[\frac{Z^2 kT}{4\pi e^2 (1+Z)\, n_e a^2}\right]} \tag{5}$$

where

Z = positive charge
e = electronic charge
n_e = number density of electrons
a = Bohr radius

The limiting principle quantum number N_0 is the largest whole number that satisfies equation (5). This number (N_0) is plotted for mercury against the variable n_e/T (from Ref. 1) in Fig. 1. It shows that N_0 decreases with increasing n_e/T which is a function of the pressure, temperature and ionization potential. The electronic energy levels were derived from the analysis of optical spectra[6]. The degree of degeneracy of each level is

$$g_i = 2J_i + 1 \tag{6}$$

where J_i is the resultant of the total angular momentum of the ith level. The values of J_i were again taken from Ref. 6.

(4) The contributions of the *potential energies* have not been included in the partition function. The Debye–Hückel ionic effect, as well as the Lennard–Jones potential are more significant at higher pressures. The significance of such an omission for our pressure range remains to be evaluated.

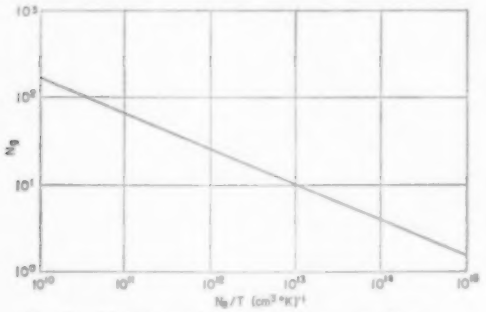

Fig. 1. Limiting principle quantum number.

3. THERMODYNAMIC PROPERTIES OF THE COMPONENTS

Once the partition function of each component has been established the thermodynamic properties of each can be determined from statistical mechanics:

Internal energy (caloric equation of state)

$$\frac{E - E_0}{RT} = T\left(\frac{\partial \ln Q}{\partial T}\right)_v \tag{7}$$

Enthalpy

$$\frac{H - E_0}{RT} = T\left(\frac{\partial \ln Q}{\partial T}\right)_p \tag{8}$$

Entropy

$$\frac{S}{R} = \ln Q + T\left(\frac{\partial \ln Q}{\partial T}\right)_p \tag{9}$$

Specific heat

$$C_v = \left(\frac{\partial E}{\partial T}\right)_v \qquad C_p = \left(\frac{\partial H}{\partial T}\right)_p \tag{10}$$

where E, H and S are respectively internal energy, enthalpy and entropy per mole while C_v and C_p are the specific heats per mole. The energy E_0 was chosen as the energy of the species at zero temperature and standard pressure.

For atomic mercury . . . Hg $E_0 = 0$
For the mercury ion . . . Hg^+ E_0 = energy of ionization
For electrons e^- $E_0 = 0$

4. CHEMICAL REACTION

The ionization reaction will proceed in such a way that the chemical potential of the mixture will be at a minimum, i.e.

$$\left(\frac{\partial \mu}{\partial x_i}\right)_{p,T} = 0 \tag{11}$$

where

μ = chemical potential
x_i = mole fraction

The reaction process will proceed as follows:

$$Hg \rightleftharpoons Hg^+ + e^-$$

Stoichiometric coefficients: $\nu_{Hg} = -1$, $\nu_{Hg^+} = 1$, $\nu_{e^-} = 1$

Sum of stoichiometric coefficients: $\Sigma\nu = 1$

Original composition: n_0 atoms/volume

Degree of ionization: ε

Composition during the process: $n_{Hg} = n_0(1 - \varepsilon)$
$n_{Hg^+} = n_0\varepsilon = n_{e^-}$

Total number of particles during the reaction:

$$\Sigma n = n_0(1 + \varepsilon)$$

Mole fractions of the mixture:

$$x_{Hg} = \frac{1-\varepsilon}{1+\varepsilon}$$

$$x_{Hg^+} = x_{e^-} = \frac{\varepsilon}{1+\varepsilon}$$

In order to evaluate the degree of ionization and, thereby, the mole fractions at a particular pressure and temperature, it is necessary to determine the equilibrium constant K_p for the ionization reaction. The equilibrium constant for an isothermal process in an ideal system at equilibrium (affinity = 0) is defined as

$$K_p = \prod_i p_i^{\nu_i} \tag{12}$$

where

p_i = partial pressure
ν_i = stoichiometric coefficient

For the mercury ionization reaction this gives

$$K_p = \frac{p_{Hg^+} p_{e^-}}{p_{Hg}} \tag{13}$$

For a mixture of perfect gases the partial pressure is expressed in terms of the total pressure as

$$p_i = \frac{n_i}{\sum_i n_i} p \tag{14}$$

where

n_i = number densities

Therefore, K_p can be written as

$$K_p = \frac{\varepsilon^2}{1-\varepsilon^2} p \tag{15}$$

Finally, the equilibrium constant for an ideal system is related to the partition functions of the reactants and products at standard pressure by

$$\ln K_p = -\left(\frac{\Delta E_0}{RT}\right) + \left(\sum_i \nu_i \ln Q_i\right)_{\text{products}} - \left(\sum_i \nu_i \ln Q_i\right)_{\text{reactants}} \tag{16}$$

and for mercury ionization we have

$$\ln K_p = -\frac{\Delta E_0}{RT} + \ln Q_{Hg^+} + \ln Q_{e^-} - \ln Q_{Hg} \tag{17}$$

The ΔE_0 is the difference between the energy of the products and the reactants in their standard state ($T = 0°K$, $p = 1$ atm) and represents the energy associated with the ionization of the mercury atom.

The ionization potential of a mercury atom is given[6] as 10·43 eV. Various experiments, however, have demonstrated that the work function for the renewal of an electron from an atom in an ionized gas is lower than the ionization energy of an isolated atom, and that it depends primarily on the electron density and the temperature. The reduction in the ionization potential is derived by Ecker and Weizel[1] to be

$$\Delta U_S = \Delta U_A + \Delta U_P = 0{\cdot}67 \sqrt[3]{\left(\frac{n_e}{10^{18}}\right)} + 0{\cdot}37 \sqrt{\left(\frac{n_e}{T \times 10^{14}}\right)} \tag{18}$$

ΔU_A is the reduction of the ionization energy due to the interaction with the electric potential of the unpolarized ionized gas.

ΔU_P is the reduction due to the polarization effect, i.e. the influence of the different average separations of like and unlike charged particles.

The present paper takes the above factor into account in the following way. To start with, ΔE_0 is set equal to 10·43 eV and n_e is calculated as a function of pressure and temperature. Then these values for n_e are used to calculate ΔU_S from equation (18) and n_e, as well as all other quantities, are recomputed using a new ΔE_0 as a function of pressure and temperature. This procedure is repeated until the correction of ΔE_0 becomes negligible. The degree of ionization, ε, is plotted in Fig. 2.

5. COMPRESSIBILITY

Each mole of atomic mercury will produce $(1+\varepsilon)$ moles of reacting mixture consisting of neutral atoms, ions and electrons if we consider the behavior of a fixed quantity (mass) of gas. For convenience we define Z to be the ratio of the number of moles of the reacting mixture to the original number of moles

$$Z = 1 + \varepsilon \tag{19}$$

or

$$Z = \frac{M_0}{M} \tag{20}$$

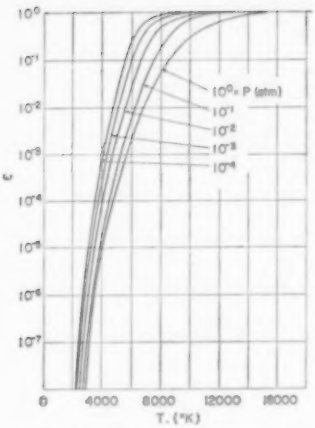

Fig. 2. Degree of ionization.

where M_0 is the original molecular weight and $\overline{M}$ is the mean molecular weight of the reactants. The compressibility is presented in Fig. 3 as a function of pressure and temperature.

It is worth while comparing at this point the results of calculating with a fixed ionization potential (10·43 eV) and an arbitrary cut off of the electronic term series (at $E=6kT$) with the calculations using termination of the series according to equation (5) and reduction of the ionization potential according to equation (18). An illustration of the difference is shown in Table 1 for 95 per cent degree of ionization.

It can be observed that the correction is most pronounced at higher pressures due to the higher electron density, n_e. At very low pressures, such as 10^{-4} atm, the effect is negligible. The thermodynamic properties of a substance undergoing a chemical reaction will be effected in a similar manner.

6. EQUATION OF STATE

Under the assumption that the reacting components behave as ideal gases, the mass after mixture can be obtained from the equation of state

$$\rho=\frac{pM_0}{ZRT} \tag{21}$$

as is shown in Fig. 4.

In addition, the electron and neutral atom number densities can be calculated from

$$n_e=\left(\frac{\varepsilon}{1+\varepsilon}\right)\frac{p}{kT};\quad n_n=\left(\frac{1-\varepsilon}{\varepsilon}\right)n_e \tag{21a), (21b}$$

and are shown in Figs. 5 and 6.

7. THERMODYNAMIC PROPERTIES OF THE MIXTURE

The thermodynamic properties of the mixture can be obtained by summation of the thermodynamic properties of the individual components weighted by the mole fractions. Thus, we find

Internal energy

$$ZE=Z\sum_i x_iE_i \tag{22}$$

Enthalpy

$$ZH=Z(E+RT) \tag{23}$$

Entropy

$$\frac{ZS}{R}=Z\left(\sum_i x_i\frac{S_i}{R}-\sum_i x_i\ln x_i-\ln\frac{p}{p_0}\right) \tag{24}$$

Specific heat

$$ZC_v=\left[\frac{\partial(ZE)}{\partial T}\right]_v$$
$$ZC_p=\left[\frac{\partial(ZH)}{\partial T}\right]_p \tag{25}$$

Table 1

Pressure	atm	10^{-4}	10^{-3}	10^{-2}	10^{-1}	1
Temperature (°K)	I.P. = 10·43 eV Series limit: $E=6kT$	$7{\cdot}7\times10^3$	$8{\cdot}7\times10^3$	$1{\cdot}02\times10^4$	$1{\cdot}21\times10^4$	$1{\cdot}48\times10^4$
Temperature (°K)	I.P. corrected by equation (18) Series limit: equation (5)	$7{\cdot}7\times10^3$	$8{\cdot}7\times10^3$	$1{\cdot}01\times10^4$	$1{\cdot}19\times10^4$	$1{\cdot}44\times10^4$

Ratio of specific heats

$$\gamma = \frac{C_p}{C_v} \tag{26}$$

These quantities are plotted versus pressure and temperature in Figs. 3–12.

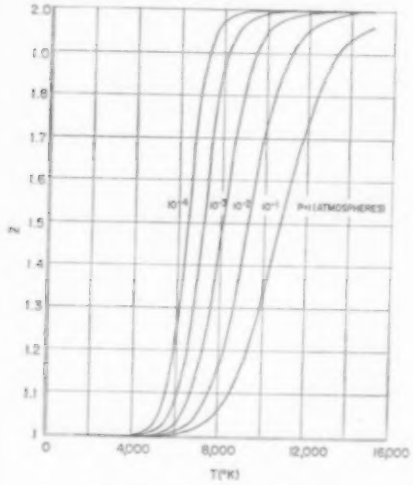

Fig. 3. Compressibility.

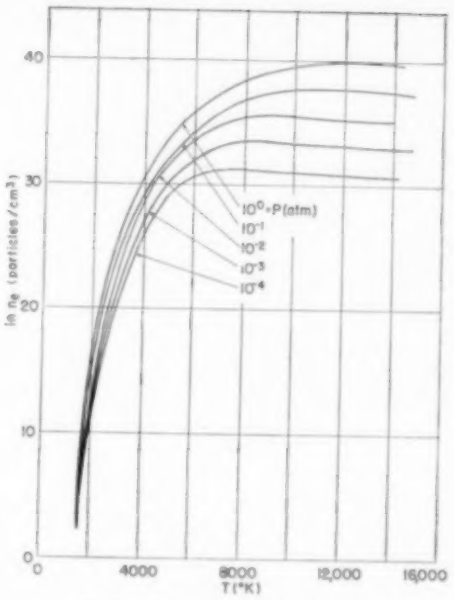

Fig. 5. Electron particle density.

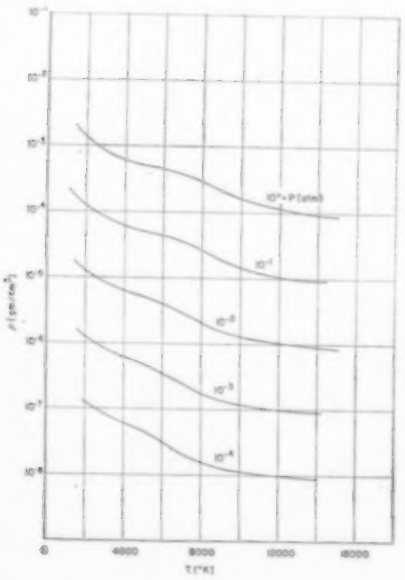

Fig. 4. Mass density.

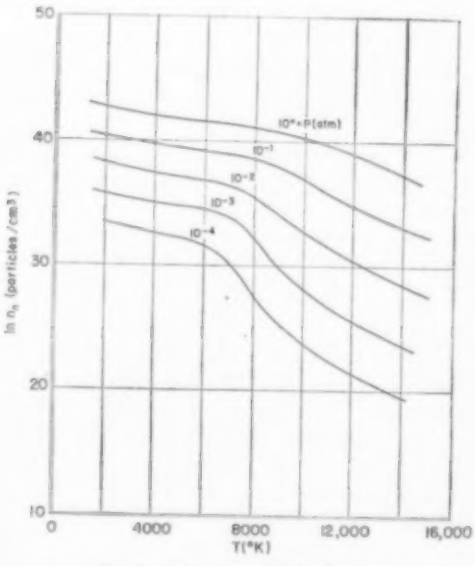

Fig. 6. Neutral particle density.

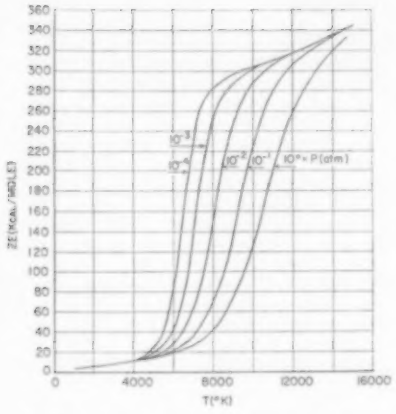

Fig. 7. Internal energy per original mole.

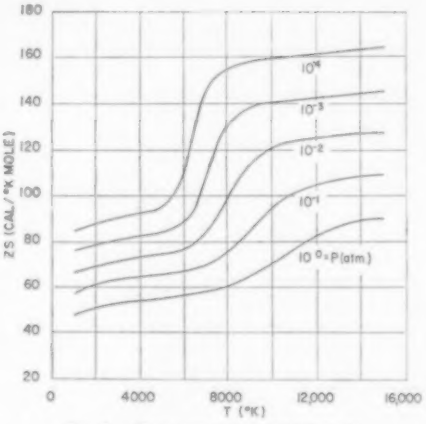

Fig. 9. Entropy per original mole.

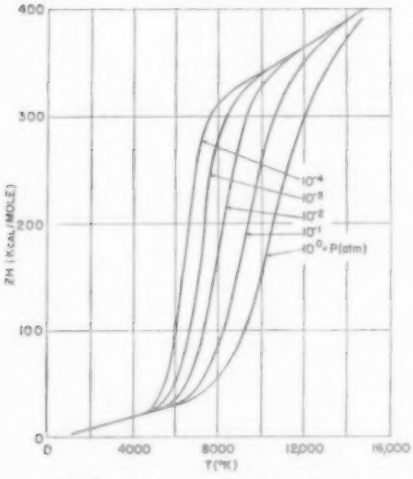

Fig. 8. Enthalpy per original mole.

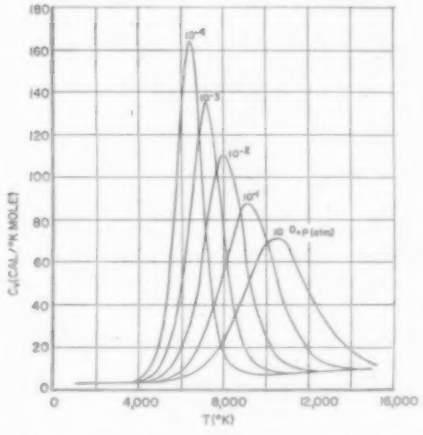

Fig. 10. Specific heat at constant volume per original mole.

8. ELECTRICAL CONDUCTIVITY

An accurate theoretical analysis of the electrical conductivity of a slightly ionized gas has been presented by Chapman and Cowling[7]. Similarly, accurate studies have been made for a fully ionized gas[8, 9]. Using less precise methods the "free path" kinetic theory leads to an expression for the conductivity valid for any degree of ionization.

$$\sigma = 0{\cdot}85 \frac{n_e e^2}{m_e} \bar{\tau}_e \tag{27}$$

where

n_e = number of electrons/volume
e = electronic charge
m_e = electron mass

The mean time between collisions of electrons with other particles $\bar{\tau}_e$ is given by

$$\bar{\tau}_e = \frac{1}{\sqrt{\left(\frac{8kT}{\pi m_e}\right)}(n_n Q_{en} + n_e Q_{ei})} \tag{28}$$

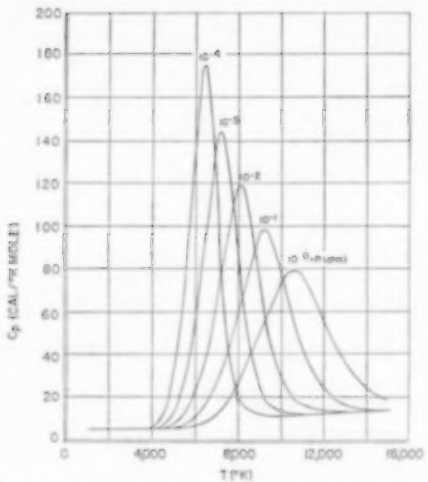

Fig. 11. Specific heat at constant pressure per original mole.

where

n_0 = number of atoms/volume
Q_{en} = electron–atom cross section
Q_{ei} = electron–ion cross section
k = Boltzmann constant
T = temperature

and an electrically neutral gas has been assumed.

The cross section for elastic collisions between electrons and atoms can be found from experimental measurements. Usually, the electron diffusion (Townsend) type of experiments are most useful for this type of data[10]. Unfortunately, no such data is available for mercury so that the data of Brode[11] which is obtained from a Ramsauer type experiment will be used. These results show no Ramsauer effect for electron energies down to 0·5 eV. Theoretical calculations[12] as well as some recent experimental measurements[13], however, indicate that at lower energies some of the effect should exist. Accordingly, Brode's data has been extrapolated, as shown in Fig. 13, down to zero energy. As the Ramsauer type of experiments only provide the cross section as a function of electron velocity, where all electrons are moving in the same direction and at the same velocity, it must be averaged over the electron velocity distribution to provide a cross section suitable for our needs. Again, using "free path" kinetic theory and assuming a Maxwellian distribution the average cross section as a function of temperature may be calculated from the following equation[10].

$$Q_{en} = \frac{kT}{m_e} \Big/ \int_0^\infty \frac{v}{Q_{en}(v)} \exp - \left(\frac{m_e v^2}{2kT}\right) dv \qquad (29)$$

where v is the electron velocity used in the Ramsauer type experiments. The resulting cross section, $Q_{en}(T)$, is shown in Figs. 13 and 14.

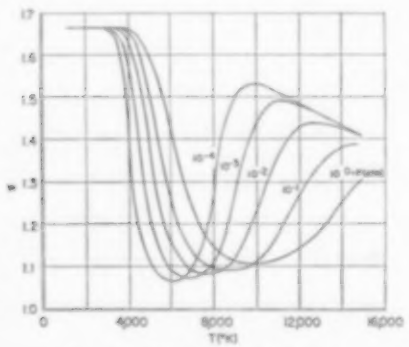

Fig. 12. Ratio of specific heats.

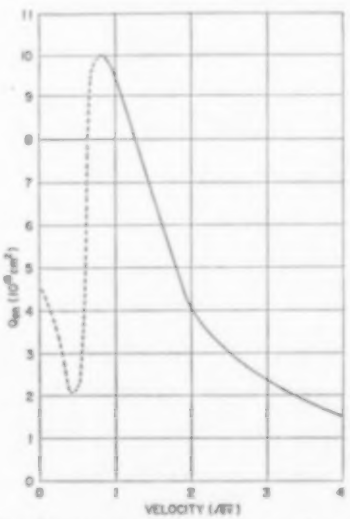

Fig. 13. Ramsauer collision cross section versus electron velocity.

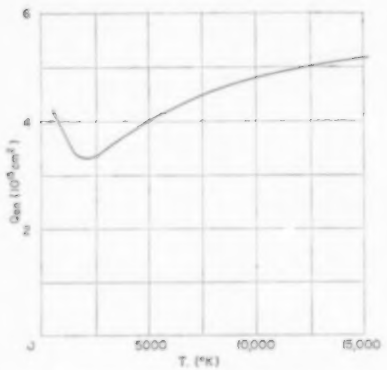

Fig. 14. Collision cross section versus temperature.

A collision cross section for electrons and ions, Q_{ei}, can be obtained if we consider the conductivity of a fully ionized gas[14] which is

$$\sigma = 0{\cdot}591 \frac{(kT)^{3/2}}{m_e^{1/2} e^2} \frac{1}{\ln \Lambda} \tag{30}$$

where

$$\Lambda = \frac{3}{\sqrt{(8)}\, e^3} \left(\frac{k^3 T^3}{\pi n_e} \right)^{\frac{1}{2}}$$

Equating this relation to equation (27), where equation (28) has been used for $\bar{\tau}_e$ with $n_n = 0$, we derive an expression for Q_{ei}

$$Q_{ei} = 0{\cdot}90 \left(\frac{e^2}{kT} \right)^2 \ln \left[\frac{1{\cdot}5}{\sqrt{(2)}\, e^3} \left(\frac{k^3 T^3}{\pi n_e} \right)^{\frac{1}{2}} \right] \tag{31}$$

Finally, combining equations (27), (28) and (31) gives us an equation for the calculation of the conductivity of a gas of arbitrary degree of ionization.

$$\sigma = 0{\cdot}85 \frac{n_e e^2}{m_e} \frac{1}{\sqrt{\left(\frac{8kT}{\pi m_e} \right)} \left(n_n Q_{en} + n_e \left\{ 0{\cdot}9 \left(\frac{e^2}{kT} \right)^2 \ln \left[\frac{1{\cdot}5}{\sqrt{(2)}\, e^3} \left(\frac{k^3 T^3}{\pi n_e} \right)^{\frac{1}{2}} \right] \right\} \right)} \tag{32}$$

The result of applying equation (32) to the calculation of σ is presented in Fig. 15. We note that in the very high temperature range, say above 9000°K, the conductivity increases with increasing pressure. In the low temperature range the reverse is true. The reason for this behavior is that the portion of each curve below the knee is essentially the conductivity of a slightly ionized gas, which increases with lower pressure (equation 27), while the portion above corresponds to the conductivity of a fully ionized gas which increases with higher pressure (equation 30).

Finally, it should be observed that no account has been taken of the collision of electrons with excited atoms. Although we expect this cross section to be larger than Q_{en} (Fig. 12) there is no data available with which to estimate it. As a result, we have used Q_{en} for our calculations and only point out that the resulting conductivity (Fig. 15) *may* be somewhat high for temperatures below 9000°K.

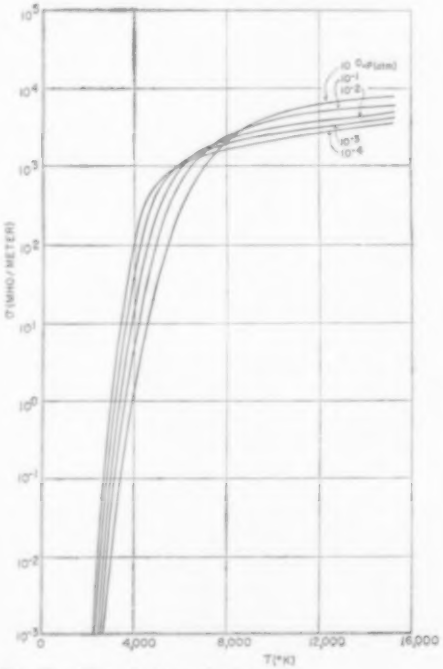

Fig. 15. Electrical conductivity.

9. INFLUENCE OF MAGNETIC FIELDS ON CONDUCTIVITY

Under normal circumstances the current density, $\bar{j}$, is related to the electric field strength,

$\bar{E}$, by a scalar conductivity, σ, as follows:

$$\bar{j}=\sigma\bar{E} \tag{33}$$

Or in a moving medium

$$\bar{j}=\sigma\,[\bar{E}+\bar{v}\times\bar{B}] \tag{34}$$

where

$\bar{B}$ = magnetic induction

$\bar{v}$ = velocity

Either of these expressions are referred to as Ohm's law and are normally valid for metals, liquids and gases.

In very low density gases subject to high magnetic field strengths, however, they are no longer correct and must be modified. Such a "generalized" Ohm's law can be derived by considering the ionized gas to be a mixture of three gases. That is, it may be thought of as a mixture of electrons, ions and atoms. If a momentum equation is written for the motion of each component and the collision terms evaluated by "free path" kinetic theory the desired relation can be derived[15].

$$n_e e\,(\bar{E}+\bar{v}\times\bar{B})+\left(1-\frac{f}{1+\dfrac{\omega_e\tau_{en}}{2\omega_i\tau_{in}}}\right)\nabla p_e=B\left(\frac{1}{\omega_e\tau_{ei}}+\frac{1}{\omega_e\tau_{en}+2\omega_i\tau_{in}}\right)\bar{j}+\left(1-\frac{2f}{1+\dfrac{\omega_e\tau_{en}}{2\omega_i\tau_{in}}}\right)\bar{j}\times\bar{B}+\frac{f^2/B}{\left(\dfrac{1}{\omega_e\tau_{en}}+\dfrac{1}{2\omega_i\tau_{in}}\right)}\left[\nabla p_e\times\bar{B}-(\bar{j}\times\bar{B})\times\bar{B}\right] \tag{35}$$

where

$\bar{v}$ = mass averaged velocity
f = fraction of atoms not ionized $= n_n/n_e+n_n$
p_e = electron partial pressure
B = magnitude of magnetic field
ω_e = electron cyclotron frequency $= eB/m_e$
ω_i = ion cyclotron frequency $= eB/m_i$
τ_{en} = electron–neutral mean collision time
τ_{in} = ion–neutral mean collision time
τ_{ei} = electron–ion mean collision time

For mercury, due to the large mass of the ion compared to the electron, we can assume that

$$\frac{\omega_e\tau_{en}}{2\omega_i\tau_{in}}\ll 1$$

and, as a result, simplify equation (35) to

$$\bar{j}=\frac{n_e e^2}{m_e\left(\dfrac{1}{\tau_{ei}}+\dfrac{1}{\tau_{en}}\right)}\left[\bar{E}+\bar{v}\times\bar{B}+\frac{\nabla p_e}{n_e e}-\frac{\bar{j}\times\bar{B}}{n_e e}-\frac{2f^2\tau_{in}}{m_i n_e}\left(\nabla p_e\times\bar{B}-(\bar{j}\times\bar{B})\times\bar{B}\right)\right] \tag{36}$$

For convenience we define

$$\sigma=\frac{n_e e^2}{m_e\left(\dfrac{1}{\tau_{ei}}+\dfrac{1}{\tau_{en}}\right)}$$

$$K=\frac{1}{n_e e}$$

$$\lambda=\frac{2f^2\tau_{in}}{m_i n_e}$$

and equation (36) can be written as

$$\bar{j}=\sigma\,[\bar{E}+\bar{v}\times\bar{B}+K\,(\nabla p_e-\bar{j}\times\bar{B})-\lambda\,(\nabla p_e\times\bar{B}-(\bar{j}\times\bar{B})\times\bar{B})] \tag{37}$$

The conductivity, σ, can be shown to be the same as in equation (27), apart from the constant, if we observe that

$$\tau_{ei}=\frac{1}{\sqrt{\left(\dfrac{8kT}{\pi m_e}\right)}n_e Q_{ei}}\quad;\qquad \tau_{en}=\frac{1}{\sqrt{\left(\dfrac{8kT}{\pi m_e}\right)}n_n Q_{en}}$$

from equation (28). In order to bring equation (37) into agreement with equation (27), numerically, we should redefine σ as

$$\sigma=0{\cdot}85\frac{n_e e^2}{m_e}\bar{\tau}_e \tag{38}$$

where

$$\bar{\tau}_e=\left(\frac{1}{\tau_{ei}}+\frac{1}{\tau_{en}}\right)^{-1}$$

The coefficient K is the "Hall coefficient" which is well known in solid state physics. The coefficient, λ, is the ion slip factor. When it is zero the mean velocity of the ions is equal to the mean velocity of the neutral atoms.

As equation (37) is written it does not express $\bar{j}$ as a function of $\bar{E}$ and $\bar{B}$, as for example equation (34) did, and is, therefore, not parti-

cularly convenient. A suitable equation can be derived by vector manipulation[16] but, for our purposes, another procedure will be more convenient. If we consider an x, y, z coordinate system and take $\bar{B}$ to be in the z direction we can define a "generalized" Ohm's law in the following form

$$\bar{j}=\bar{\bar{\sigma}}\cdot\bar{E}' \tag{39}$$

where an effective electric field has been defined as

$$\bar{E}'=\bar{E}+\bar{v}\times\bar{B}-\lambda\nabla p_e\times\bar{B}+K\nabla p_e \tag{40}$$

and the tensor conductivity is given by

$$\bar{\bar{\sigma}}=\sigma\begin{bmatrix} c_1 & -c_2 & 0\\ c_2 & c_1 & 0\\ 0 & 0 & 1\end{bmatrix}$$

where

$$c_1=\frac{1+1{\cdot}7f^2\omega_i\omega_e\tau_{in}\bar{\tau}_e}{(1+1{\cdot}7f^2\omega_i\omega_e\tau_{in}\bar{\tau}_e)^2+(0{\cdot}85\,\omega_e\bar{\tau}_e)^2}$$

$$c_2=\frac{0{\cdot}85\,\omega_e\bar{\tau}_e}{(1+1{\cdot}7f^2\omega_i\omega_e\tau_{in}\bar{\tau}_e)^2+(0{\cdot}85\,\omega_e\bar{\tau}_e)^2} \tag{41}$$

Equation (38) was used as the definition of σ. In order to illustrate the significance of $\bar{\bar{\sigma}}$ we will consider a simple example. If we apply an electric field $\bar{E}$ in the x direction and assume $E_y=0$ we obtain the following formula for the current flow in the x direction

$$j_x=\sigma\left[\frac{1+1{\cdot}7f^2\omega_i\omega_e\tau_{in}\bar{\tau}_e}{(1+1{\cdot}7f^2\omega_i\omega_e\tau_{in}\bar{\tau}_e)^2+(0{\cdot}85\,\omega_e\bar{\tau}_e)^2}\right]E'_x \tag{42}$$

The term in brackets will always be less than one and when multiplied by σ gives an "effective" conductivity, σ', which is always less than σ. Before the "effective" conductivity can be calculated we need to know τ_{in}. From "free path" kinetic theory it is

$$\tau_{in}=\frac{1}{4\sqrt{\left(\frac{kT}{\pi m_i}\right)}n_nQ_{in}} \tag{43}$$

Since there is no experimental data for Q_{in}, the cross section for scattering of mercury ions by neutral mercury atoms, we will use the value of 5×10^{-15} cm^2 as a first approximation. Normally, we would expect Q_{in} to be somewhat larger than Q_{en} so that the above choice will exaggerate the ion slip effect somewhat.

In Fig. 16 we plot the effective conductivity, σ', as a function of temperature for various pressures and a field of 10,000 G. It is apparent from these results that there can be an optimum temperature, depending on pressure, at which the conductivity is a maximum. At the lower pressures this optimum occurs at quite a low temperature and, as well, the conductivity is reduced by many orders of magnitude. In the example calculated the ion slip effect serves to increase the electrical conductivity. In other words, if it had been omitted conductivities lower than those shown in Fig. 16 would have been obtained. For other conditions, such as higher field strengths, the ion slip factor may reduce the electrical conductivity.

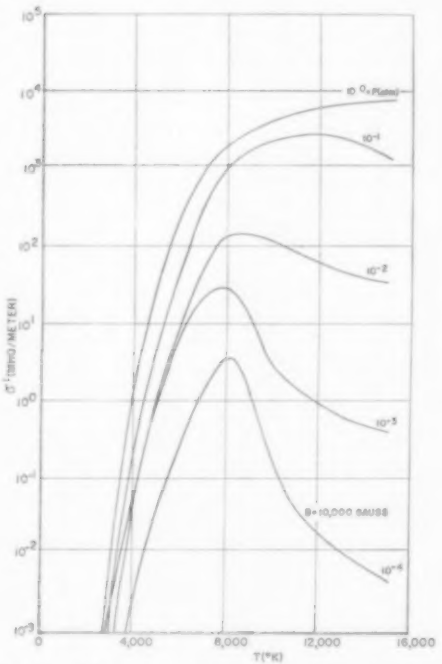

Fig. 16. Effective electrical conductivity at 10,000 G.

CONCLUSIONS

The thermodynamic properties of mercury vapor have been calculated for temperatures up to 15,000°K and pressures between 1 and 10^{-4} atmospheres. The first ionization is shown to be essentially complete at 15,000°K. At the lower pressures the ionization is completed earlier*. Corrections have been included to account for the lowering ionization potential and the finite limit of the electronic term series. The largest corrections occur at the higher pressures; the correction at 10^{-4} atmospheres being negligible. For example, the temperature required to give 95 per cent degree of ionization at 1 atm is corrected by approximately 2 per cent.

The electrical conductivity is calculated in the absence of a magnetic field as well as in the presence of one. The corrections due to a 10,000 G field, assuming Hall currents are free to flow, are found to be very important at low pressures. For example, at 10^{-4} atm and 15,000°K the conductivity has been lowered by 6 orders of magnitude. In addition, the conductivity, which previously rose monotonically, can now have a maximum at the lower pressures.

* However, only first degree ionization was considered.

Acknowledgements—The authors wish to acknowledge the many helpful discussions held with Dr. B. W. Harned of the Applied Research Operation. They would also like to acknowledge the assistance of Mrs. E. Thomas in performing the calculations.

This investigation has been partially supported by the Air Force Office of Scientific Research.

REFERENCES

1. G. Ecker and W. Weizel, *Ann. Phys., Lpz.* **17,** 126 (1956).
2. E. Fermi, *Z. Phys.* **26,** 54 (1924).
3. M. Planck, *Ann. Phys., Lpz.* **75,** 637 (1924).
4. Ch. Fuchtbauer, P. Schultz and A. Brandt, *Z. Phys.* **90,** 403 (1944).
5. K. Herzfeld, *Ann. Phys.* **51,** 261 (1916).
6. *Atomic Energy Levels* Vol 3. Nat. Bur. Stand. Circ. No. 467 (1958).
7. S. Chapman and T. G. Cowling, *The Mathematical Theory of Non-Uniform Gases.* University Press, Cambridge (1952).
8. T. G. Cowling, *Proc. Roy. Soc.* A**183,** 453 (1945).
9. L. Spitzer, Jr., *Physics of Fully Ionized Gases.* Interscience Publishers, New York (1956).
10. S. C. Lin, E. L. Resler and A. Kantrowitz, *J. Appl. Phys.* **26,** 95 (1955).
11. R. B. Brode, *Proc. Roy. Soc.* A**125,** 134 (1929).
12. W. P. Allis and P. M. Morse, *Z. Phys.* **70,** 567 (1931).
13. F. P. Adler and H. Margenau, *Phys. Rev.* **79,** 970 (1950).
14. L. Spitzer, Jr., and R. Harm, *Phys. Rev.* **89,** 997 (1953).
15. T. G. Cowling, *Magnetohydrodynamics.* Interscience Publishers, New York (1957).
16. N. H. Kemp and H. E. Petsheck, *J. Fl. Mech.* **4,** 553 (1958).

LIST OF PARTICIPANTS
IN THE CONFERENCE ON
PHYSICAL CHEMISTRY IN AERODYNAMICS AND SPACE FLIGHT

University of Pennsylvania, Philadelphia, Pennsylvania
September 1 – 3, 1959

ACKERMANN, R. J., Argonne National Laboratory, Lemont, Illinois
ADAMS, F. L., Bendix Aviation Corporation, Detroit, Michigan
AMDUR, I., Massachusetts Institute of Technology, Cambridge, Massachusetts
ANDERSON, A. D., NASA, Ames Research Center, Moffett Field, California

BACON, J. F., United Aircraft Corporation, East Hartford, Connecticut
BAICY, E. O., Ballistic Research Laboratory, Aberdeen, Maryland
BARRIAULT, R., AVCO Manufacturing Corporation, Wilmington, Massachusetts
BARTH, C. A., Jet Propulsion Laboratory, California Institute of Technology, Pasadena, California
BAUER, S. H., Cornell University, Ithaca, New York
BAULKNIGHT, C., General Electric Company, Missile and Space Vehicle Department, Philadelphia, Pennsylvania
BEAL, J. L., Cornell Aeronautical Laboratory, Buffalo, New York
BEECHER, N., National Research Corporation, Cambridge, Massachusetts
BENNETT, F. D., Ballistic Research Laboratory, Aberdeen, Maryland
BERKOWITZ, J., Arthur D. Little, Inc., Cambridge, Massachusetts
BIERLEIN, J. A., Wright Patterson Air Force Base, WADD, Dayton, Ohio
BIONDI, M. A., Westinghouse Research Laboratories, Pittsburgh, Pennsylvania
BLACKMAN, A. W., United Aircraft Corporation, East Hartford, Connecticut
BLEVISS, Z. O., Douglas Aircraft Company, Inc., Santa Monica, California
BOOBAR, M. G., Vidya, Inc., Palo Alto, California
BORTNER, M., General Electric Company, Missile and Space Vehicle Department, Philadelphia, Pennsylvania
BOWMAN, J. A., Martin Company, Denver, Colorado
BROKAW, R. S., NASA, Lewis Research Center, Cleveland, Ohio
BROOKS, M. S., Air Force Cambridge Research Center, ARDD, Hanscom Field, Bedford, Massachusetts
BUCKINGHAM, R. A., University of London Computer Unit, London, England
BURGERS, J. M., University of Maryland, College Park, Maryland

CHUAN, R. L., University of Southern California, Los Angeles, California
COHEN, A., Ballistic Research Laboratory, Aberdeen, Maryland
COHEN, J. B., Ballistic Research Laboratory, Aberdeen, Maryland

COLE, D. M., Martin Company, Denver, Colorado
COLWELL, J. E., Rocketdyne Corporation, Canoga Park, California
CONVERSE, A. O., Thiokol Chemical Corporation, Elkton, Maryland
CRAIN C. M., Rand Corporation, Santa Monica, California
CURTISS, C. F., University of Wisconsin, Naval Research Laboratory, Madison, Wisconsin

DALGARNO, A., The Queens University of Belfast, North Ireland
DOUGLAS, J. E., Stanford Research Institute, Menlo Park, California
DECKERS, G., Princeton University, Princeton, New Jersey
DUFF, R. E., Los Alamos Scientific Research Laboratory, Los Alamos, New Mexico

EFIMENKO, J., National Bureau of Standards, Washington, D.C.
EMBER, G., University of Delaware, Newark, Delaware
EVANS, M. W., Stanford Research Institute, Menlo Park, California
EYRING, H., University of Utah, Salt Lake City, Utah

FANNIN, R. M., University of Texas, Austin, Texas
FARBER, J., General Electric Company, Missile and Space Vehicle Department, Philadelphia, Pennsylvania
FAY, J. A., Massachusetts Institute of Technology, Cambridge, Massachusetts
FENN, J. B., Princeton University, Princeton, New Jersey
FERRON, J., University of Delaware, Newark, Delaware
FINEMAN, M. A., Providence College, Providence, Rhode Island
FOLEY, W. M., United Aircraft Corporation, East Hartford, Connecticut
FORD, H., Jet Propulsion Laboratory, California Institute of Technology, Pasadena, California
FOREMAN, K. M., Republic Aviation Corporation, Farmingdale, L.I., New York
FREEMAN M. P., American Cyanamid Company, Stamford, Connecticut
FRIEDMAN H., General Electric Company, Missile and Space Vehicle Department, Philadelphia, Pennsylvania

GAGGE, A., Air Force Office of Scientific Research, Washington, D.C.
GALOWIN, L. S., General Applied Science Laboratories, Inc., Hempstead, L.I., New York
GERHAUSER, J. M., Bendix Aviation Corporation, South Bend, Indiana
GILMORE, F. R., Rand Corporation, Santa Monica, California
GLASSMAN, I., Princeton University, Princeton, New Jersey
GOLDEN, J., General Electric Company, Missile and Space Vehicle Department, Philadelphia, Pennsylvania
GOLDSTEIN R., Lehigh University, Bethlehem, Pennsylvania
GOLDSTEIN, S., Harvard University, Cambridge, Massachusetts
GOLDSTONE, B. J., Radio Corporation of America, Camden, New Jersey
GORDON D. A., Stanford Research Institute, Menlo Park, California
GRASSE, F., Lehigh University, Bethlehem, Pennsylvania
GROSS, J. F., Rand Corporation, Santa Monica, California
GRUNTFEST, I. J., General Electric Company, Missile and Space Vehicle Department, Philadelphia, Pennsylvania

HACKER, D., Armour Research Foundation, Chicago, Illinois
HAMILTON, C. V., Martin Company, Denver, Colorado
HARSHBARGER, F. C., Convair—General Corporation, San Diego, California

HAUGHT, A. F., Princeton University, Princeton, New Jersey
HERTZBERG, A., Cornell Aeronautical Laboratory, Buffalo, New York
HIPSHER, H. F., National Aeronautics and Space Administration, Washington, D.C.
HOLISTER, G. S., Tatnall Measuring Systems Company, Phoenixville, Pennsylvania
HOURT, W., Atlantic Research Company, Alexandria, Virginia
HUFFMAN R. E., Air Force Cambridge Research Center, Geophysics Research Directorate, Hanscom Field, Bedford, Massachusetts
HULL, C. M., Harper College, Binghamton, New York

JORDAN, J. E., Massachusetts Institute of Technology, Cambridge, Massachusetts

KAPLAN, C., Air Force Office of Scientific Research, Washington, D.C.
KASKAN, W. E., General Electric Company, Research Laboratory, Schenectady, New York
KAUFMAN, F., Ballistic Research Laboratory, Aberdeen, Maryland
KILNER, S. B., Aerojet-General Corporation, Azusa, California
KIM, G., University of Pennsylvania, Philadelphia, Pennsylvania
KIVEL, B., AVCO Manufacturing Corporation, Wilmington, Massachusetts
KLEIN, M., National Bureau of Standards, Washington, D.C.
KNOX, B. E., Pennsylvania State University, University Park, Pennsylvania
KORMAN, S., Republic Aviation Corporation, Farmingdale, L.I., New York
KRIEGER, K. A., University of Pennsylvania, Philadelphia, Pennsylvania
KRULL, H. G., Marquardt Corporation, Van Nuys, California

LA VIER, E. C., Air Research and Development Command, Washington, D.C.
LEW, H. G., General Electric Company, Missile and Space Vehicle Department, Philadelphia, Pennsylvania
LIFSET, M. A., General Electric Company, Missile and Space Vehicle Department, Philadelphia, Pennsylvania
LIU, S. W., Martin Company, Baltimore, Maryland
LONG, M. E., General Electric Company, Missile and Space Vehicle Department, Philadelphia, Pennsylvania
LOPREST, F. J., Thiokol Chemical Corporation, Denville, New Jersey
LOZIER, W. W., National Carbon Company, Cleveland, Ohio

MACATICIAN, J., Thiokol Chemical Corporation, Denville, New Jersey
MACKAY, H. A., Sandia Corporation, Albuquerque, New Mexico
MARCUS, H., Wright Patterson Air Force Base, WADD, Dayton, Ohio
MARGRAVE, J., University of Wisconsin, Madison, Wisconsin
MARMO, F. F., Geophysics Corporation of America, Boston, Massachusetts
MARSHALL, F., Armour Research Foundation, Chicago, Illinois
MARTINEK, F., General Electric Company, Flight Propulsion Laboratory Department, Cincinnati, Ohio
MATTHEWS, D. L., Princeton University, Princeton, New Jersey
MATTRAW, H. C., General Electric Company, TEMPO, Santa Barbara, California
MAY, C. E., NASA, Lewis Research Center, Cleveland, Ohio
MCGREGOR, W. K., ARO, Inc., Tullahoma, Tennessee
MCINTOSH, D. L., McDonnell Aircraft Corporation, St. Louis, Missouri
MCMILLAN, F., Radiation Incorporated, Orlando, Florida
MEADOWS, E., NASA, Goddard Space Flight Laboratories, Washington, D.C.
MEDVED, D., Convair—General Corporation, San Diego, California

MILLER, J. G., University of Pennsylvania, Philadelphia, Pennsylvania
MIXER, R. Y., Stanford Research Institute, Menlo Park, California
MOFFATT, W. C., Massachusetts Institute of Technology, Cambridge, Massachusetts
MONCHICK, L., Applied Physics Laboratory, Johns Hopkins University, Silver Spring, Maryland
MONSON, P. R., Lockheed Aircraft Corporation, Sunnyvale, California
MOORE, F. K., Cornell Aeronautical Laboratory, Buffalo, New York
MORKOVIN, M. V., Martin Company, Baltimore, Maryland
MUCKENFUSS, C., General Electric Company, Research Laboratory, Schenectady, New York
MULLIKEN, R. S., University of Chicago, Chicago, Illinois
MURPHY, C. H., Ballistic Research Laboratory, Aberdeen, Maryland
MYERS, H., Douglas Aircraft Company, Inc., Santa Monica, California
MYERSON, A. L., General Electric Company, Missile and Space Vehicle Department, Philadelphia, Pennsylvania

NAGAMATSO, H. T., General Electric Company, Research Laboratory, Schenectady, New York
NELSON, L. S., Bell Telephone Laboratories, Inc., Murray Hill, New Jersey

OBERMAYER, A. S., Allied Research Associates, Boston, Massachusetts
OMAN, R. A., Grumman Aircraft Engineering Corporation, Bethpage, L.I., New York

PAI, S. I., University of Maryland, College Park, Maryland
PALMER, H. B., Pennsylvania State University, University Park, Pennsylvania
PARLIN, R. B., Operations Research Inc., Silver Spring, Maryland
PAYFER, G. E., Republic Aviation Corporation, Farmingdale, L.I., New York
PENG, T. C., NASA, Ames Research Center, Moffett Field, California
PENNER, S. S., California Institute of Technology, Pasadena, California
PERGAMENT, H., General Applied Science Laboratories, Inc., Hempstead, L.I., New York
PISANI, J. A., Thiokol Chemical Corporation, Denville, New Jersey
PROK, G. M., NASA, Lewis Research Center, Cleveland, Ohio

RAZELOS, P., Wright—Aeronautical Corporation, Wood Ridge, New Jersey
REID, J. W., General Electric Company, Missile and Space Vehicle Department, Philadelphia Pennsylvania
RIETHOF, T. R., General Electric Company, Missile and Space Vehicle Department, Philadelphia, Pennsylvania
RITMAN, H., Boeing Airplane Company, Seattle, Washington
ROCKMAN, C. M., Princeton University, Princeton, New Jersey
ROGERS, J. D., Los Alamos Scientific Research Laboratory, Los Alamos, New Mexico
ROGERS, M., Air Force Office of Scientific Research, Washington, D.C.
ROHAN, J. J., Air Force Cambridge Research Center, ARDC, Hanscom Field, Bedford, Massachusetts
ROSE, D. G., Los Alamos Scientific Research Laboratory, Los Alamos, New Mexico
ROSNER, D. E., AeroChem Research Laboratories, Inc., Princeton, New Jersey
ROTH, J. F., Franklin Institute, Research Laboratory, Philadelphia, Pennsylvania
ROTH, W., Armour Research Foundation, Chicago, Illinois
RUBY, S., AVCO Manufacturing Corporation, Wilmington, Massachusetts

SAFRAN, H., Radio Corporation of America, Burlington, Massachusetts
SALTZBURG, H., General Atomic, San Diego, California
SANCIER, K. M., Stanford Research Institute, Menlo Park, California

SCHELLER, K., Wright Patterson Air Force Base, WADD, Dayton, Ohio
SCHMIDT, D. L., Wright Patterson Air Force Base, WADD, Dayton, Ohio
SCHRYER, D. R., NASA, Langley Research Center, Hempstead, Virginia
SCOTT, J. E., University of Virginia, Charlottesville, Virginia
SEAMAN, R. J., McDonnell Aircraft Corporation, Chicago, Illinois
SEDNEY, R., Ballistic Research Laboratory, Aberdeen, Maryland
SETTLAGE, P. H., E. I. duPont de Nemours & Company, Experimental Station, Wilmington, Delaware
SHEPPARD, J. J., Convair Scientific Research Laboratory, San Diego, California.
SHOULETTE, W., University of Florida, Gainsville, Florida
SHULER, K. E., National Bureau of Standards, Washington, D.C.
SIEGLE, J. C., E. I. duPont de Nemours & Company, Experimental Station, Wilmington, Delaware
SIMHA, R., University of Southern California, Los Angeles, California.
SKRIVAN, J. F., American Cyanamid Company, Stamford, Connecticut
SMITH, A. C., Rand Corporation, Santa Monica, California
SQUIRE, C., Radio Corporation of America, Camden, New Jersey
STEG, L., General Electric Company, Missile and Space Vehicle Department, Philadelphia, Pennsylvania
STEINBERG, M., Armour Research Foundation, Chicago, Illinois
STEVERDING, B., Army Ballistic Missile Agency, Redstone Arsenal, Huntsville, Alabama
STOKES, C. S., Research Institutes of Temple University, Philadelphia, Pennsylvania
SULZMANN, K. G., Convair—General Corporation, San Diego, California
SUTTON, G. W., General Electric Company, Missile and Space Vehicle Department, Philadelphia, Pennsylvania
SZEGO, G. P., Space Technology Laboratories, Inc., Los Angeles, California

TALLEY, C. P., Experiment Incorporated, Richmond, Virginia
TANNENBAUM, S., Thiokol Chemical Corporation, Denville, New Jersey
THORN, R. J., Argonne National Laboratory, Lemont, Illinois
THORPE, M. L., Thermal Dynamics Corporation, Hanover, New Hampshire
TODD, F. C., Southwest Research Institute, San Antonio, Texas
TRACY, P. T., Convair—General Corporation, San Diego, California
TRAUGOTT, S. C., Martin Company, Baltimore, Maryland
TREANOR, C. E., Cornell Aeronautical Laboratory, Buffalo, New York
TSU, K., Princeton University, Princeton, New Jersey

UNGAR, E. W., Battelle Memorial Institute, Columbus, Ohio

VASTOLA, F. J., Pennsylvania State University, University Park, Pennsylvania
VIDALE, G., General Electric Company, Missile and Space Vehicle Department, Philadelphia, Pennsylvania

WACHMAN, H. Y., General Electric Company, Missile and Space Vehicle Department, Philadelphia, Pennsylvania
WACHTELL, G. P., Franklin Institute, Philadelphia, Pennsylvania
WAGNER, P., Los Alamos Scientific Research Laboratory, Los Alamos, New Mexico
WALKER, R. E., Applied Physics Laboratory, Johns Hopkins University, Silver Spring, Maryland
WARD, T. J., Radio Corporation of America, Camden, New Jersey
WEIMER, D., Lehigh University, Bethlehem, Pennsylvania
WESTENBERG, A. A., Applied Physics Laboratory, Johns Hopkins University, Silver Spring, Maryland
WHEELER, A., Aerojet-General Corporation, Azusa, California

WIEDERHORN, N. M., Arthur D. Little, Inc., Cambridge, Massachusetts
WRIGHT, H. M., Aeronutronics Systems, Inc., Newport Beach, California
WIKNER, E. G., General Atomic, San Diego, California
WILCOX, D., Southern Research Institute, Birmingham, Alabama
WINSLOW, G. H., Argonne National Laboratory, Lemont, Illinois
WOJTOWICZ, P., Radio Corporation of America, Princeton, New Jersey
WRAY, K. L., AVCO-Everett Research Laboratory, Everett, Massachusetts
WURSTER, W. H., Cornell Aeronautical Laboratory, Buffalo, New York

YOUNG, R. A., University of Washington, Seattle, Washington

ZELIKOFF, M., Geophysics Corporation of America, Boston, Massachusetts
ZINMAN, W. G., Republic Aviation Corporation, Farmingdale, L.I., New York

L.
61